Correlation Functions in Two-Dimensional Critical Systems with Conformal Symmetry

by

Steven Miguel Flores

A dissertation submitted in partial fulfillment
of the requirements for the degree of
Doctor of Philosophy
(Applied and Interdisciplinary Mathematics)
in The University of Michigan
2012

Doctoral Committee:

Professor Charles R. Doering, Co-chair
Professor Peter Kleban, Co-chair, University of Maine
Professor Robert M. Ziff
Professor Peter D. Miller

ACKNOWLEDGEMENTS

I would like to give special thanks to Peter Kleban, Robert M. Ziff, and Charles Doering for their mentorship during the writing of this thesis. I would also like to give special thanks to Jacob J. H. Simmons for many very insightful conversations that inspired much of the research presented in this thesis. Finally, I thank Jeffery B. Rauch for very helpful comments concerning the proofs presented in chapter two, and I thank Sergey Fomin for pointing out the connection of the work in chapter two with the Temperley-Lieb algebra which ultimately led me to some very useful results concerning the meander matrix that were discovered by P. Di Francesco, O. Golinelli, and E. Guitter.

TABLE OF CONTENTS

LIST OF FIGURES

Figure

LIST OF TABLES

Table

LIST OF APPENDICES

Appendix

LIST OF ABBREVIATIONS

BC boundary condition

BCC boundary condition change

FFBC free/fixed side-alternating boundary condition

BAC boundary arc connectivity

PDE partial differential equation

CFT conformal field theory

OPE operator product expansion

SLE Schramm-Löwner evolution

FK Fortuin-Kasteleyn

SW Swendsen-Wang

SCT special conformal transformation

CLE conformal loop ensemble

ABSTRACT

Correlation Functions in Two-Dimensional Critical Systems with Conformal Symmetry

by

Steven Miguel Flores

Co-Chairs: Charles R. Doering and Peter Kleban

This thesis presents a study of certain conformal field theory (CFT) correlation functions that describe physical observables in conformally invariant two-dimensional critical systems. These are typically continuum limits of critical lattice models in a domain within the complex plane and with a boundary. Certain clusters, called boundary clusters, anchor to the boundary of the domain, and many of their features are governed by a conformally invariant probability measure. For example, percolation is an example of a critical lattice model, and when it is confined to a domain with a boundary, clusters of connected, activated bonds that touch that boundary are the boundary clusters. This thesis is concerned with how the boundary clusters interact with each other according to that measure. One question that it considers are "how likely are these clusters to repel each other or to connect with one another in a certain topological configuration?" Chapter one non-rigorously derives an already well-known elliptic system of partial differential equations (PDE) closely tied to this matter by using standard techniques of CFT, chapters two and three rigorously infer certain properties concerning the solution space of this system, and chapter four uses

some of those results to predict an answer to this question. This thesis also considers local variations of this question such as "what regions of the domain do the perimeters of the boundary clusters explore," and "how often will several boundary clusters connect at just a single, specified point in the domain?" Chapter five predicts precise answers to these questions. All of these answers are quantitative predictions that we verify via high-precision computer simulation. Chapters four and five also present these simulation results. Further material that supplements chapter one is included in two appendices.

This thesis is a blend of research in mathematics and physics, and although mathematics is the language of physics, these two areas of study adhere to different standards of proof. Mathematics is inductive and based on rigorous proof while physics is deductive and based on agreement between prediction and observation. To emphasize this distinction, I have attempted to confine these two approaches to different chapters, although there is mixing in chapter three. Chapter one provides background material and context for the application of CFT to critical phenomena in two-dimensions, and it obviously belongs to the realm of physics. On the other hand, chapters two and three belong to the realm of mathematics as they rigorously prove certain theorems concerning a system of PDEs that arises in chapter one. Chapter four combines the results of the first three chapters to calculate observables called crossing probabilities, and chapter five, somewhat separate from all but chapter one, calculates other observables called pinch-point densities. Because these last two chapters rely on the results of chapter one, their results are predictive rather than rigorous. Thus, they belong to the realm of physics. To differentiate between these two approaches, definitions, lemmas, and theorems are typeset apart from the regular text in the mathematics sections, while definitions and predictive results are contained within the text of the physics sections. Also, I have reserved the word "conjecture" for a precise mathematical conjecture, and I have reserved the word "supposition"

for a more ambiguous guess that is not precisely defined in mathematical terms yet whose main idea is apparent.

CHAPTER I

Introduction

Two-dimensional lattice models are an important class of models in statistical mechanics used to describe two-dimensional crystals, ferromagnets, polymers, and more. Such models are typically defined on the lattice $a\mathbb{Z}^2$ with a the (very small) lattice spacing and with some collection of variables associated with each lattice site. These *lattice variables* interact via a Hamiltonian particular to the model, and the ensemble of possible system configurations is Boltzman-weighted. Often, these systems are simple enough for their quantitative properties to be exactly known and complicated enough to exhibit the macroscopic behavior of the real-world phenomena that they model. Many different lattice models are studied in the physics literature. Among them are the Q-state Potts model [1], the O(n) model [2], ice-type models, six-vertex and eight-vertex models, and more [3, 4, 5].

We suppose that the underlying lattice of the model under consideration has infinite size. In this situation, many lattice models, including all of those mentioned above, exhibit a (second-order) phase transition at a *critical temperature* (or *critical point*) T_c, and these models are of particular interest to this thesis. This critical point is often characterized by the divergence of the *correlation length* ξ measuring the average size of the largest *cluster* within a sample of the model [3]. A cluster is a collection of (usually) nearest-neighbor lattice sites that share some common

feature (such as an equal lattice variable). Above the critical point, large clusters are suppressed and ξ is finite. At the critical point, the size of every cluster is finite typically (this is proven true for percolation [6] and more recently for certain Ising model clusters [7]), but the supremum of the cluster size, and therefore ξ, is infinite. Below the critical point, an infinite-sized cluster exists, and ξ is redefined to be on the order of the largest finite cluster. This redefined ξ is finite. (These statements are true almost surely.) The distinctive behavior of the system is found at the critical point, which is loosely defined as the temperature for which ξ is infinite. The phenomenon of an infinite correlation length has meaning only for a model defined on an infinite lattice such as $a\mathbb{Z}^2$, and we typically call this the *thermodynamic limit* of the same model defined on a finite lattice.

Most lattice models of interest are defined via local interactions between lattice sites. As such, they are isotropic, so their observables must be invariant under translations and rotations. At the critical point, the infinite correlation length signals the vanishing of a length-scale, so these lattice models must also be invariant under dilations. However, there is another length scale, the lattice spacing a, that must be removed in order for this to be completely true. This is done by considering the *continuum limit* of the model. Though often difficult to capture mathematically, this limit has an intuitive definition: the continuum limit of a lattice with lattice spacing a is a process in which two simultaneous events transpire. First, the lattice spacing a is sent to zero, and second, new sites are constantly added to the lattice during this contraction so that the lattice does not eventually vanish but continues to fill the original domain $\mathcal{D} \subset \mathbb{C}$ that it occupied. The continuum limit is (conceptually) achieved when every point $z \in \mathcal{D}$ marks a lattice site of the resulting *continuum model.* Sometimes, the continuum model can be studied through a suitable limit of the observables of the corresponding discrete model [8, 9]. Also, the continuum limit may be viewed as an appropriate thermodynamic limit for a model contained within

a bounded domain since the number of lattice sites increases without bound.

Many critical continuum lattice models are supposed to exhibit an even stronger invariance property: conformal invariance [3, 9]. That is, the statistics of the system do not change when the system domain $\mathcal{D}$ is conformally mapped onto another domain $\mathcal{D}'$ in the complex plane. Conformal transformations are compositions of translations, rotations, dilations, all of which were mentioned above, and inversions, which are new. Taken together, the full conformal symmetry yields a powerful set of computational techniques that lead to many interesting exact results concerning scaling behavior and correlation functions of lattice variables at (or near) the critical point.

Several different methods have been used to calculate these quantities in two-dimensional critical models. One method, invented by physicists, is called *conformal field theory (CFT)* [10, 11]. CFT is essentially a quantum field theory in two-dimensional Euclidean space-time ($\mathbb{R}^2 \cong \mathbb{C}$ with a Euclidean metric) governed by a massless Lagrangian that endows the theory with conformal symmetry. CFT is not a rigorously developed mathematical theory, though representation-theoretic elements of it are rigorous and approaches to its axiomatization have been explored with success [12, 13]. Nonetheless, it provides many exact results with relatively little computation. (The price to pay is a serious detour into its formalism in order to understand it.) Furthermore, only certain CFTs, usually the minimal models, have been observed to possess the right structure to describe a critical lattice models. Because these theories are relatively few, models with the same macroscopic properties but different microscopic properties are presumed to have identical continuum limits in order to correspond with the same CFT. Physicists call this phenomenon *universality* and call a collection of models with identical continuum limits a *universality class.* For example, bond percolation and site percolation on the square lattice are different percolation models with different critical activation probabilities. Yet at their respective critical probabilities, their common observables are either proven or

observed through simulation to be equal in the continuum limit, so they belong to the same universality class.

A second and relatively new method called *Schramm-Löwner evolution (SLE)* has been used with recent success to prove many outstanding conjectures concerning various critical lattice models in their continuum limits. A subject of probability theory, SLE is a two-dimensional random growth process that generates planar curves with conformally invariant probability measures in a domain with a boundary [14, 15]. In many lattice models with conformally invariant continuum limits, cluster perimeters are conjectured, and in some cases proven, to have the statistics of SLE curves [8, 16]. In this thesis, we will primarily work within the CFT setting, frequently re-examining our results from the SLE point of view.

In this introduction, we present a survey of some critical lattice models that will be frequently mentioned in this work, and we present a brief introduction to the CFT, SLE, and Coulomb gas techniques that will give context to the research presented in this thesis.

1.1 Three critical lattice models

In this section, we briefly survey some classic lattice models with thermodynamic limits that exhibit a conformally invariant critical point. We will study the Ising model and two of its generalizations: the Q-state Potts model and the O(n) model. The observations that we make concerning these models will be essential to understanding many of the results in this thesis.

1.1.1 The Ising model

The two-dimensional *Ising model* approximates certain two-dimensional lattice models with short-range interactions. To define it, consider an $N \times N$ square lattice with lattice spacing a and with each site exhibiting one of two states: up (+) or

down ($-$). These states may be envisaged as the two spin states in a model for the magnetic moment of an atom. At the i-th lattice site, we represent these states by a *spin variable* σ_i that assumes one of two values:

$$\sigma_i = \begin{cases} +1 & \text{if spin up} \\ -1 & \text{if spin down.} \end{cases} \tag{1.1}$$

Two sites i and j are *nearest neighbors* if site i is either immediately right, left, above, or below site j, and their pairing is denoted by $\langle ij \rangle$. When two sites i and j are nearest neighbors, their proximity allows their spins to interact, introducing an energy $E_{ij} = -J\sigma_i\sigma_j/2$ into the system. Here, J is a coupling constant, and the interaction is called *ferromagnetic* when $J > 0$. (We assume ferromagnetic interactions throughout this thesis.) If an external magnetic field H is applied perpendicular to the lattice, then each spin couples to the field too, introducing an additional energy $E_i = -H\sigma_i$ into the system. If $\{\sigma\} = \{\sigma_i\}_{i=1}^{N^2}$ is a particular spin configuration, then the total energy of configuration $\{\sigma\}$ is

$$E[\{\sigma\}] = -\frac{J}{2}\sum_{\langle ij \rangle} \sigma_i\sigma_j - H\sum_i \sigma_i,$$

where the sum is taken over all nearest-neighbor pairs. The different spin configurations are weighted by the Boltzman distribution, so the probability of observing configuration $\{\sigma\}$ is given by

$$\mathbb{P}\{\sigma\} = \frac{e^{-\beta E[\{\sigma\}]}}{Z}, \quad Z = \sum_{\{\sigma\}} e^{-\beta E[\{\sigma\}]}, \tag{1.2}$$

where $\beta = 1/kT$, T is the temperature of the system, k is Boltzman's constant, and Z is the partition function for the system. The statistics implied by (1.2) define the two-dimensional Ising model on the $N \times N$ lattice. We note that the Boltzman distri-

bution favors configurations in which spins align with the magnetic field (i.e., $H > 0$ implies more $+$ spins than $-$ spins) and with their neighbors when the interactions are ferromagnetic (i.e., $J > 0$).

The Ising model may be defined on any lattice as long as the nearest neighbors of each site are clearly specified. For example, we will also consider the Ising model on the triangular lattice or on its dual, the honeycomb lattice. On either lattice, the nearest neighbors of a site are defined as the collection of sites closest to that particular site. Hence, each site of the triangular (resp. honeycomb) lattice (excluding boundary sites) has six (resp. three) nearest neighbors.

Also, we will need to specify a boundary condition (BC) for Ising models defined in domains with boundaries. If no BC is specified, then no conditioning is imposed on the spins of the boundary sites, and the boundary is said to be *free.* We may also condition a sequence of adjacent boundary sites to exhibit a particular spin state, and the segment of the boundary with this constraint is called *wired* or *fixed.* Other BCs are possible. For example, for a *periodic BC*, we topologically identify certain boundary segments with other boundary segments, thereby requiring the identified lattice sites to exhibit the same state.

Now we investigate the critical behavior of the thermodynamic limit of the Ising model. Critical points manifest themselves as singularities of thermodynamic observables, which are typically derivatives of the partition function. For example, we consider the average $M(T, H)$ of the mean spin-per-lattice-site $\bar{\sigma}$ over all possible configurations:

$$M(T,H) := \frac{1}{\beta Z} \sum_{\{\sigma\}} \bar{\sigma} e^{-\beta E[\{\sigma\}]} = \frac{1}{N^2 \beta} \frac{\partial}{\partial H} \log Z, \quad \bar{\sigma} := \frac{1}{N^2} \sum_i \sigma_i. \tag{1.3}$$

$M(T, H)$ is called the *average magnetization per site.* If $H > 0$, then samples with more $+$ spins than $-$ spins are favored, and $M > 0$. Next, we wish to know how

$M(T,H)$ behaves in the limit $H \downarrow 0$. To answer, we note that when $H = 0$, each configuration $\{\sigma\}$ and its opposite configuration, generated by flipping all of the spins in $\{\sigma\}$, have the same weight but opposite mean spin. Thus $M(T,0) = 0$, and because $M(T,H)$ is continuous when N is finite, we find that $M(T,H) \downarrow 0$ as $H \downarrow 0$. That is, no residual abundance of + spins remains as $H \downarrow 0$, and the system forgets its original + spin bias. The same is true with − spins if H starts out negative.

Now we take the thermodynamic limit $N \to \infty$. One can show that for each fixed pair (T,H) with $T > 0$, the limit of $M(T,H)$ as $N \to \infty$ exists, and we may study its behavior as H vanishes. This second limit follows the thermodynamic limit, and the two limits do not commute. With N infinite, we cannot suppose that the thermodynamic limit of $M(T,H)$ is continuous and conclude that it vanishes just as the magnetization of the finite system vanishes as H approaches zero. In fact, this will happen only if T is greater than a certain critical temperature T_c. If T is less than T_c, the system can remember its original spin bias:

$$\lim_{H\to 0\pm}\lim_{N\to\infty} M(T,H) = \begin{cases} 0 & \text{if } T \geq T_c \\ \pm M_0(T) & \text{if } T < T_c \end{cases}, \quad \text{where } M_0(T) > 0. \tag{1.4}$$

In the thermodynamic limit, the magnetization exhibits a jump discontinuity at $H = 0$ when the temperature is below the critical temperature [3]. Consequently, the system always (resp. never) remembers its spin up bias as H is decreased to zero when $T < T_c$ (resp. $T \geq T_c$). This phenomenon is called *spontaneous magnetization*. The discontinuity divides the system into two phases, positive H and negative H, and the discontinuous behavior of the magnetization as the strength of the magnetic field passes through zero when $T < T_c$ is called a *first order phase transition.* At the critical point $T = T_c$, the discontinuity vanishes, and the passage between these phases is called a *second order phase transition.* When $T > T_c$, the magnetization is a continuous function of the magnetic field, so we do not witness a phase transition. The

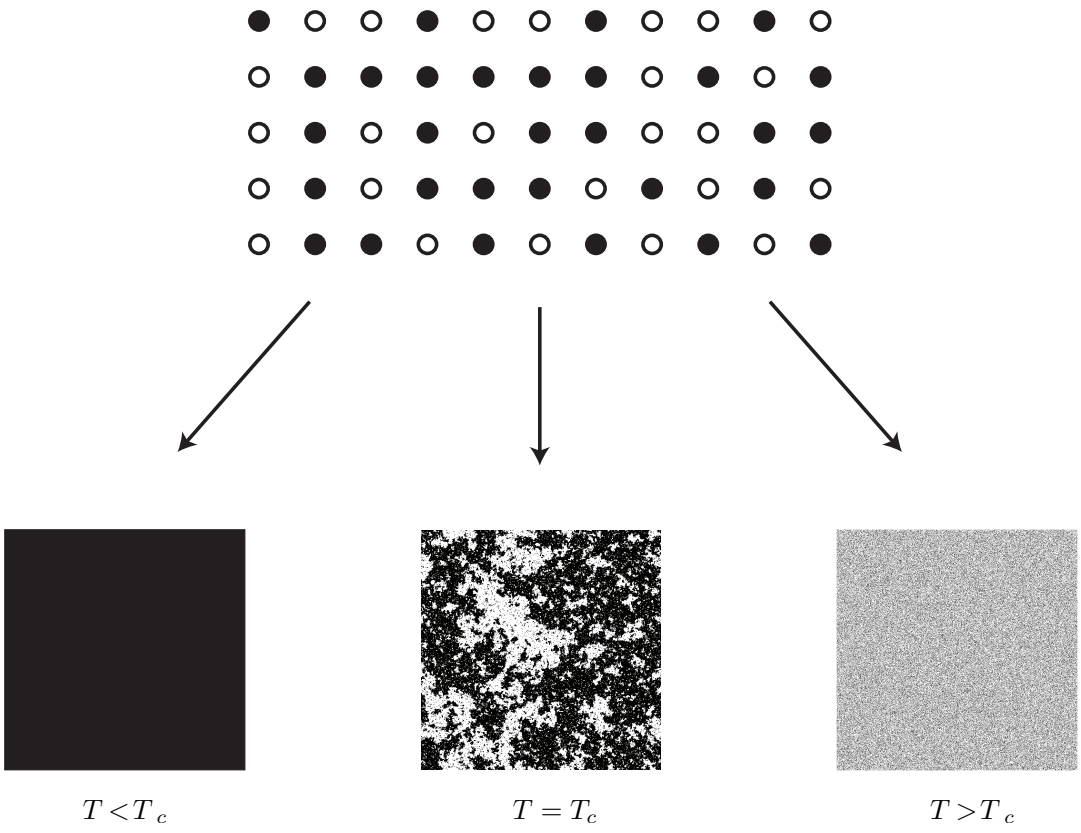

Figure 1.1: The thermodynamic limit of the ferromagnetic Ising model. Black (resp. white) disks represent sites in the + (resp. −) state. Below the critical temperature, samples with more + (resp. −) states scale away to a sea of + (resp. −) spin states. Above the critical temperature, samples scale away to a sea of uncorrelated + and − spin states with the appearance of white noise. At the critical temperature, finite clusters of either + or − spin states and of all sizes prevail.

passage from the lack of spontaneous magnetization to the exhibition of spontaneous magnetization indicates a phase transition within the zero-field (i.e. $H = 0$) Ising model at the critical point T_c. The first published derivation of these claims is given in [17]. They are also proven by relating the zeros of the partition function (1.2) as a function of a complex magnetic field with the magnetization [5]. These zeros, called Yang-Lee zeros, are determined in [18].

It is helpful to characterize this critical point in a way that does not initially require the magnetic field to be nonzero since we will generalize only the zero-field Ising model to other models below, and we want our understanding of the critical point to carry

over to these generalizations. This can be done in terms of the correlation length ξ. To define the correlation length, we first define the *spin cluster* of the i-th lattice site to be the set of lattice sites generated through the following recursion. We begin by including the i-th lattice site in the set, and presently, the set contains only this lattice site. Next, we add to the set those nearest neighbors of the i-th site that exhibit the same spin state as the i-th site. Next, we add to the set those nearest neighbors of any site in the set that exhibit the same spin state as that site, and so on. With spin clusters defined, we next define the correlation length ξ to be the average size of the largest finite-sized spin cluster. Now, we suppose that the magnetic field is zero. If the temperature is above the critical point, then the diameters of the spin clusters are finite, the magnetization is zero, and the correlation length is finite. On the other hand, if the temperature is at the critical point, then spin clusters of all finite sizes and spin types emerge, the magnetization is still zero, but the correlation length is infinite. Finally, if the temperature is below the critical point, then an infinite-size cluster exists and covers most of the system in each sample, the magnetization is nonzero, and the correlation length, now measuring the size of the largest finite-size cluster, is finite (figure 1.1). (These statements are true almost surely.)

The thermodynamic limit of the zero-field Ising partition function was calculated exactly in a landmark article by L. Onsager [19], and this result originally led to the discovery of the Ising model critical point in the thermodynamic limit. The article derives an expansion for the free energy per lattice site of the Ising model on a square lattice in a rectangle with doubly-periodic BCs (left/right sides identified and top/bottom sides identified). The expansion is [5]

$$f = \lim_{N\to\infty} \frac{\log Z}{N^2\beta} = \frac{4}{\pi\beta}(K - K_c)^2 \log|K - K_c| + \ldots, \tag{1.5}$$

where $K := \beta J$, $K_c = \log(\sqrt{2}+1)$, and the ellipsis stand for terms that are regular

in the limit $K \to K_c$. Although this quantity is continuous at $K = K_c$, the specific heat $C := \partial_K^2 f(K)$ is singular there, so K_c is a critical point. From knowing the thermodynamic limit partition function exactly, we further observe that the Ising model has a unique critical point, so $K_c = J/kT_c$ where T_c is the critical temperature for the spontaneous magnetization.

These characterizations of the critical point are supposed to be true for the Ising model on the triangular lattice and on the honeycomb lattice. Indeed, all of these models are supposed to belong to the same universality class. The critical points of the square, triangular, and honeycomb lattices are calculated in [20], and they are

$$K_c^{\text{sqr}} = \log(\sqrt{2}+1), \quad K_c^{\text{tri}} = \log\sqrt{3}, \quad K_c^{\text{hcb}} = \log[(\sqrt{3}+1)/(\sqrt{3}-1)]. \tag{1.6}$$

Many different observables characterize the physical attributes of the Ising model. For example, the two-point function of the spin variables

$$\langle \sigma_i \sigma_j \rangle := \mathbb{E}[\sigma_i \sigma_j] \tag{1.7}$$

measures the correlation of the spins between the lattice sites i and j. Also, the energy ε_i from interactions of the i-th lattice site with its neighbors,

$$\varepsilon_i = \frac{1}{4} \sum_{\langle ij \rangle} E_{ij}, \tag{1.8}$$

defines another lattice variable that quantifies energy distribution in the system. The two variables ε and σ are the fundamental lattice variables that characterize local properties of the Ising model. Together with a so-called "identity" $\mathbf{1}$, the collection of these three fields constitute a closed operator algebra in their corresponding CFT [3, 11]. We will delve deeper into the meaning of this statement in section 1.2.7.

1.1.2 The O(n) model

The two-dimensional $O(n)$ *model* is a natural extension of the Ising model [2]. To define it, we promote each spin variable σ_i of the Ising model to an n-component vector $\vec{\sigma}_i$ with Euclidean norm one, and we replace the product $\sigma_i\sigma_j$ in the nearest neighbor interaction with the dot product $\vec{\sigma}_i \cdot \vec{\sigma}_j$ (hence an obvious $O(n)$ symmetry). The new partition function defines the O(n) model:

$$Z_{\mathrm{O}(n)} = \int_{|\vec{\sigma}_1|=1} \dots \int_{|\vec{\sigma}_{N^2}|=1} e^{\beta J \sum_{\langle ij \rangle} \vec{\sigma}_i \cdot \vec{\sigma}_j / 2} \, d\sigma_1 \dots d\sigma_{N^2}. \tag{1.9}$$

The O(1) model is clearly the Ising model, and in this special case, the integrations in (1.9) are replaced by sums over the two possible spin states. In this special case, one may exactly represent each term in the O(1) partition function by a collection of non-crossing loops consisting of bonds between nearest-neighbor lattice sites [5]. To uncover this expansion, we insert $e^{x\sigma} = \cosh(x) + \sigma \sinh(x)$ for $\sigma = \pm 1$ into the partition function (1.9) with $n = 1$ and perform some elementary algebra to find

$$Z_{\mathrm{O}(1)} = \cosh^{2N^2}(K/2) \sum_{\{\sigma\}} \prod_{\langle ij \rangle} (1 + \tanh(K/2)\sigma_i\sigma_j), \tag{1.10}$$

where $K := \beta J$, and we expand the product out into 2^{2N^2} terms, where $2N^2$ is the number of nearest neighbor pairs when we impose doubly periodic BCs on the sides of the $N \times N$ lattice. Each term has the form $\tanh^m(K/2)(\sigma_{i_1}\sigma_{i_2}) \dots (\sigma_{i_{2m-1}}\sigma_{i_{2m}})$ for some positive integer m, where sites i_1 and i_2 are nearest neighbors, sites i_3 and i_4 are nearest neighbors, etc. Therefore, each pair of factors can be represented by a set $\{\beta\}$ of bonds $\beta_{i_j i_{j+1}}$ between nearest-neighbor sites i_j, i_{j+1}, with j odd, on the lattice.

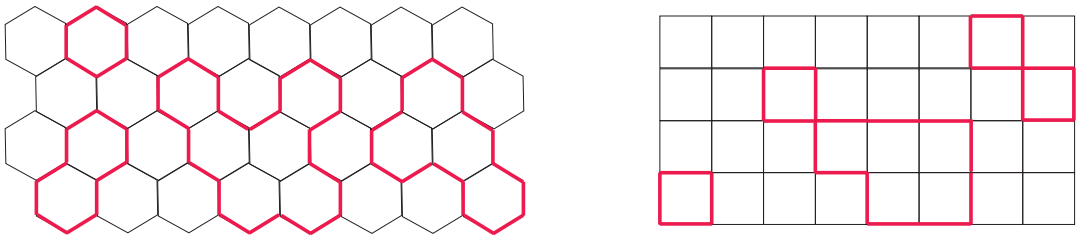

Figure 1.2: Illustration of loops (red) formed from bonds on the honeycomb lattice (left) and on the square lattice (right).

Next, we compute the the spin configuration sum over each term, and we find

$$\sum_{\{\sigma\}} (\sigma_{i_1}\sigma_{i_2})(\sigma_{i_3}\sigma_{i_4})\dots(\sigma_{i_{2m-1}}\sigma_{i_{2m}}) = \begin{cases} 2^{N^2} & \text{if } \{\beta\} \text{ consists of only loops} \\ 0 & \text{otherwise} \end{cases} \tag{1.11}$$

for the following reason. If the bonds in $\{\beta\}$ do not form only loops, then the sum will have the same number of $+1$ terms as -1 terms as a result of the $\pm$ symmetry, so it equals zero. However, if the bonds in $\{\beta\}$ form a loop (figure 1.2), then the indices of the spins may be arranged so that $\sigma_{i_2} = \sigma_{i_3}, \sigma_{i_4} = \sigma_{i_5}$, etc., and $\sigma_{i_{2m}} = \sigma_{i_1}$. With this rearrangement, we see that each term in the sum is one, so with $|\{\sigma\}| = 2^{N^2}$ terms, we arrive with (1.11). Similar reasoning leads to the same result when the collection of bonds $\{\beta\}$ consists of several non-crossing loops. Therefore we can write the partition function as

$$Z_{\mathrm{O}(1)}(K) = 2^{N^2}\cosh^{2N^2}(K/2)\sum_{\{\gamma\}} x^{\ell}, \quad x := \tanh(K/2), \tag{1.12}$$

where $\{\gamma\}$ is the collection of non-crossing loops, ℓ is the total number of bonds that comprise the loops of $\{\gamma\}$, and the sum is taken over all collections of non-crossing loops. This is the *high-temperature expansion* of the Ising model, so called because it is a power series in x centered at zero, or equivalently, in the temperature centered at infinity.

We momentarily digress to exploit the self-duality of the square lattice in order

to compute the unique critical point of the Ising model on the square lattice. (The calculation supposes doubly-periodic BCs, but the critical point is the same regardless of our choice of BC.) This technique was originally used in [21] to locate the critical point of the Ising model, assuming its existence and uniqueness, before Onsager's solution. By representing each spin configuration as a collection $\{\gamma^*\}$ of non-crossing loops surrounding the + spin clusters and formed from the bonds of the dual lattice (i.e., the lattice constituting the corners of square plaquettes that lie one-to-one on top of the original lattice sites and tesselate the plane), we find that

$$Z_{\mathrm{O}(1)}(K) = 2e^{KN^2} \sum_{\{\gamma^*\}} e^{-K\ell^*}, \tag{1.13}$$

where ℓ^* is the total number of bonds that comprise the loops of $\{\gamma^*\}$ and the sum is taken over all collections $\{\gamma^*\}$ of such non-crossing loops. This is the *low-temperature expansion* of the Ising model, so called because it is a power series in e^{-K} centered at zero, or equivalently, in the temperature centered at zero. Now, we define the *dual temperature* K^* relative to K through the relation

$$e^{-K^*} = \tanh K/2. \tag{1.14}$$

Then because the rectangular lattice is self-dual, the sum in (1.12) is identical to the sum in (1.13) upon replacing K with K^* in the latter. Therefore, we have

$$\frac{Z_{\mathrm{O}(1)}(K)}{2^{N^2}\cosh^{2N^2}(K/2)} = \frac{Z_{\mathrm{O}(1)}(K^*)}{2e^{K^*N^2}}, \tag{1.15}$$

so if K is a critical point, then K^* is also a critical point. But because the Ising model has a unique critical point K_c, we must have $K_c^* = K_c$. Plugging this relation into (1.14) gives $K_c = \log(\sqrt{2}+1)$.

Now we return to the O(n) model. When $n \neq 1$, such models do not have the

exact loop expansion (1.12) unless we modify the partition function (1.9) slightly to

$$Z_{\mathrm{O}(n)} = \int_{|\vec{\sigma}_1|=1} \dots \int_{|\vec{\sigma}_{N^2}|=1} \prod_{\langle ij \rangle} (1 + K\vec{\sigma}_i \cdot \vec{\sigma}_j/2)\, d\sigma_1 \dots d\sigma_{N^2}. \tag{1.16}$$

This modified partition function is found by expanding the exponential in (1.9) and dropping terms past first order. Although these two partition functions are only approximately equal in the high-temperature limit, the continuum limits of their respective models are supposed to belong to the same universality class [11], so we may identify them. Now, (1.16) has the following *loop expansion* that generalizes the expansion (1.12) for the case $n = 1$:

$$Z_{\mathrm{O}(n)} \propto \sum_{\{\gamma\}} x^{\ell} n^{N_l}, \quad x := \tanh(K/2). \tag{1.17}$$

Here, $\{\gamma\}$, ℓ, and the sum are defined identically to those in (1.12), and N_l is the number of loops in the particular collection $\{\gamma\}$ [22]. The proportionality constant is an irrelevant, lattice-dependent factor.

Equation (1.17) shows that the $\mathrm{O}(n)$ model furnishes an example of a more general lattice model called a *loop gas.* A loop gas is a lattice model for which each sample is a collection of non-crossing loops that visit the various lattice sites. The weight of each sample equals a product of *fugacity* factors, one for each loop, multiplying a "temperature" x raised to the power of the total length of the loops in the collection. Equation (1.17) shows that the $\mathrm{O}(n)$ model (1.16) is equivalent to a loop gas in which all loops have fugacity n. Because a loop fugacity does not necessarily have to be an integer, the expansion (1.17) extends the $\mathrm{O}(n)$ model to $n \notin \mathbb{Z}^+$.

A continuum limit description of the $\mathrm{O}(n)$ model with $n \in [-2, 2]$ may be formulated through its loop gas representation. This continuum limit is realized non-rigorously by shrinking the lattice and coarse-graining the loops in the sum (1.17) via

a renormalization group scheme. The renormalization is done in terms of the Coulomb gas in [22]. We find that the renormalization group flow has two fixed points in the positive temperature space with conformally invariant continuum limits, $x_c(n)$ and $\tilde{x}_c(n) > x_c(n)$. The former (resp. latter) fixed point is unstable (resp. stable, allowing us to identify the range $(x_c(n), \infty)$ with a common continuum limit). These fixed points are conjectured for the honeycomb lattice to be [22, 9]

$$x_c(n) = [2 + \sqrt{2-n}]^{-1/2}, \quad \tilde{x}_c(n) = [2 - \sqrt{2-n}]^{-1/2}. \tag{1.18}$$

These two fixed points correspond to two phases. A nice physical description of these phases is given in [23], and it goes as follows. First, if we start with a low temperature $x \in (0, x_c)$, the x will decrease under the renormalization group flow, suppressing long loops and encouraging short loops of finite length. Only the short loops survive almost surely, and they contract to points in the continuum limit, rendering the model trivial.

On the other hand, if we start with the critical temperature $x = x_c$, then x will not change under the renormalization group flow. Very long loops are encouraged, and in the continuum limit they become non-self-intersecting fractal loops almost surely. This nontrivial limit is called the *dilute phase* of the O(n) model (or of the loop gas). Because the diameters of the loops span all length scales, this limit exhibits dilation invariance, a prerequisite for conformal invariance. Since Ising spin cluster perimeters on the triangular lattice do not self-intersect almost surely, we identify the Ising model with the $n = 1$ dilute phase of the O(n) model. Using (1.18), we check that the Ising model critical point on the honeycomb lattice agrees with the critical temperature $x_c(1)$ of the dilute O(1) model:

$$x = \tanh(K_c^{\mathrm{hcb}}/2) = 1/\sqrt{3} = x_c(1). \tag{1.19}$$

Finally, if we start with a high temperature $x \in (x_c, \infty)$, then x will approach the fixed point $\tilde{x}_c$ under the renormalization group flow. Configurations with every site visited by very long loops dominate with high probability, and in the continuum limit they become self-intersecting (but still non-crossing) fractal loops almost surely. This nontrivial limit is called the *dense phase* of the O(n) model (or of the loop gas). In the dense phase, $n \in [0, 2]$, and in the dilute phase, $n \in [-2, 2]$.

1.1.3 The Q-state Potts model

The two-dimensional *Q-state Potts model* [1] exemplifies another natural extension of the Ising model with a loop gas representation. In the Potts model, the spin variable of each lattice site can assume any one of Q values, sometimes called *colors*, among the Q roots of unity:

$$\sigma_i \in \{\exp(2\pi i\theta/Q) \,:\, \theta \in \{0, 1, \ldots Q-1\}\}. \tag{1.20}$$

Only interactions between nearest-neighbor sites, say i and j, contribute an energy $E_{ij} = -J\delta_{\sigma_i,\sigma_j}$ to the system, and we again only consider ferromagnetic systems ($J > 0$). The total energy of a spin configuration is found by summing over all nearest-neighbor energies, and the Potts model is given by Boltzman-weighting the ensemble of all spin configurations. Thus, its partition function Z_Q is given by (1.2) with E_{ij} as defined above. We recover the Ising model partition function to within a factor when $Q = 2$.

The Potts model may also be viewed as a generalization of bond percolation [1]. Letting $\{\beta\}$ be a collection of activated bonds connecting nearest-neighbor sites of the lattice, we say that spin configuration $\{\sigma\}$ and bond configuration $\{\beta\}$ *agree* if all activated bonds join sites of like spin (figure 1.3), and we write $\{\sigma\} \sim \{\beta\}$. Then by expanding the partition function in a manner similar to that of the O(n) model

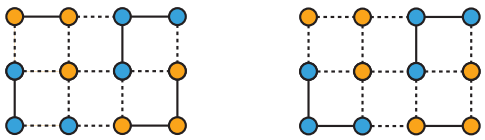

Figure 1.3: Two possible bond configurations that agree with a given spin configuration on a square lattice. Sites exhibit either the + (blue) or the − (orange) state. Bonds are activated (solid) only between nearest-neighbor sites of the same spin with probability $p = 1 - e^{-K}$.

in (1.10), one can show that to within a factor, the partition function is given by

$$\begin{aligned} Z_Q(p) &= (1-p)^{N_b} \sum_{\{\beta\}} \left(\frac{p}{1-p}\right)^{N_\beta} \sum_{\{\sigma\}} \mathbf{1}(\{\sigma\} \sim \{\beta\}) \\ &= \sum_{\{\beta\}} p^{N_\beta} (1-p)^{N_b - N_\beta} Q^{N_c} \qquad \text{with } e^K = 1/(1-p), \end{aligned} \tag{1.21}$$

where $K := \beta J$, $\mathbf{1}$ is the indicator function, N_b is the number of bonds on the lattice, and N_β and N_c are the number of activated bonds and *bond clusters* in configuration $\{\beta\}$ respectively. A bond cluster is a connected graph comprised of activated bonds, and N_c includes clusters of size zero, or lattice sites that do not touch activated bonds. If the system is confined to a domain with a boundary and a segment of the boundary is wired, then (1.21) sums exclusively over bond configurations in which all bonds between nearest-neighboring sites of that segment are activated.

The partition function (1.21) is identical to that of bond percolation with bond activation probability p, except with Q different colors uniformly distributed among the bond clusters (figure 1.4). This generalization of bond percolation is called the *random cluster model,* and the colored bond clusters are called *Fortuin-Kasteleyn (FK) clusters* [24]. When $Q = 1$, we recover percolation, and when $Q = 2$, the partition function (1.21) furnishes another representation of the Ising model. One can show that the correlation between two spins σ_i and σ_j, defined below, equals the probability that the two lattice sites i and j belong to a common FK cluster, which

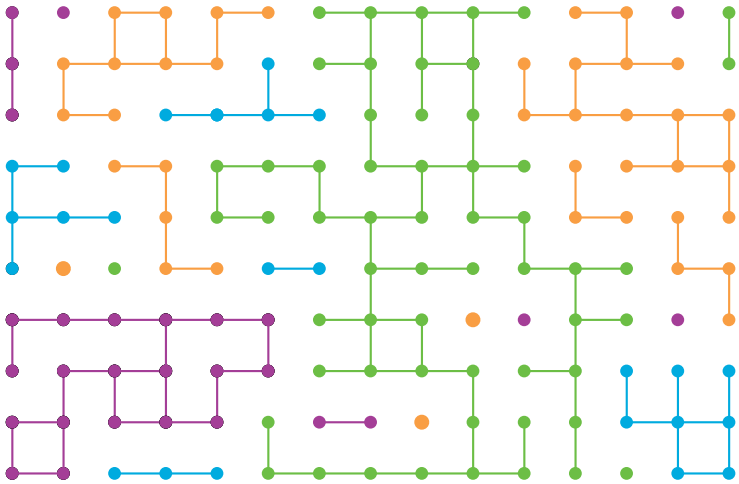

Figure 1.4: A sample bond configuration in the $Q = 4$ random cluster model. The four available colors are distributed with uniform probability across the bond clusters.

we write as $z_i \leftrightarrow z_j$:

$$\mathbb{E}[\sigma_i \sigma_j^* + \sigma_i^* \sigma_j] = \mathbb{P}\{z_i \leftrightarrow z_j\}. \tag{1.22}$$

(The star denotes the complex conjugate throughout this thesis unless stated otherwise in a particular instance.) Thus, we can compute spin correlation in the Potts model by calculating FK-cluster-connection probabilities in the corresponding random cluster model.

The absence of an exact solution for the Q-state Potts model with $Q > 2$ prevents us from rigorously establishing the existence of a unique critical point. However, strong numerical evidence suggests that a unique critical point does exist [1]. By coupling the Potts model to an external field and looking for spontaneous magnetization, one can show that such a critical point is first order for $Q > 4$ and second order for $Q \leq 4$ [25]. The $Q \leq 4$ zero-field critical Potts models is supposed to be conformally invariant, so we focus our attention on these models.

In spite of the lack of an exact solution, the critical point of the $Q \leq 4$ Potts model can be calculated exactly in certain cases by exploiting the symmetries of the lattice on which it is defined. In particular, we may exploit the self-duality of the square

lattice to compute the critical point [26] in a manner similar to the Ising model [21]. To begin, we consider a specific bond configuration $\{\beta\}$ together with the collection $\{\beta\}^*$ of dual bonds (bonds between nearest-neighbor dual sites) that do not cross the bonds of $\{\beta\}$. Now, the regular (resp. dual) bonds form N_ℓ (resp. N_ℓ^*) loops around the isolated dual (resp. regular) lattice sites. We let N_c^* be the number of dual bond clusters, and let N_β^* be the number of activated dual bonds. We therefore have

$$N_c = N_\ell^* + 1, \quad N_c^* = N_\ell + 1, \quad N_b = N_\beta + N_\beta^*. \tag{1.23}$$

We let N_s be the number of sites. Then the Euler relation for planar graphs says that

$$N_\ell = N_\beta + N_c - N_s. \tag{1.24}$$

We may use these relations to write the partition function (1.21) as

$$Z_Q(p) = (1-p)^{N_b} \left(\frac{p}{Q(1-p)}\right)^{N_b} Q^{N_s - 1} \sum_{\{\beta\}^*} \left(\frac{Q(1-p)}{p}\right)^{N_\beta^*} Q^{N_c^*}. \tag{1.25}$$

Now we define the dual activation probability p^* relative to p through the relation

$$\frac{p^*}{1-p^*} = \frac{Q(1-p)}{p}. \tag{1.26}$$

Because the square lattice is self-dual, we may reuse the reasoning that led to (1.15) to conclude from (1.21, 1.25) that $Z_Q(p)$ is proportional to $Z_Q(p^*)$, and therefore the unique critical point must satisfy $p_c^* = p_c$. Together with the requirement that $0 \leq p_c \leq 1$, this constraint gives the bond activation probability for the random cluster representation of the Potts model on the square lattice:

$$p_c^{\text{sqr}} = \frac{\sqrt{Q}}{1+\sqrt{Q}} \quad \Longleftrightarrow \quad K_c^{\text{sqr}} = \log(\sqrt{Q}+1). \tag{1.27}$$

We note that when $Q = 2$, $K_c^{\rm sqr}$ agrees with the critical point of the Ising model on the square lattice (1.6), and when $Q = 1$, $p_c^{\rm sqr} = 1/2$ is the bond-activation probability for critical bond percolation on the square lattice. A more complicated method using the "star-triangle transformation" [4] is used in [20] to calculate the critical bond activation probability for the random cluster model on the triangular lattice and on the honeycomb lattice. They are respectively

$$p_c^{\rm tri} = \frac{1}{1+Q\mu}, \qquad p_c^{\rm hcb} = \frac{\mu}{\mu+1}, \tag{1.28}$$

$$\mu := \frac{2}{\sqrt{Q}} \cos\left(\frac{1}{3}\arctan\sqrt{\frac{4}{Q}-1}\right). \tag{1.29}$$

Their respective critical temperatures K_c are given by the relation $e^{K_c} = 1/(1-p_c)$. We note that $K_c^{\rm tri}$ and $K_c^{\rm hcb}$ agree with (1.6) when $Q = 2$, as they must.

The random cluster representation of the Potts model on the square lattice has a loop gas representation [27]. An example of the loop configuration that corresponds with a particular bond configuration $\{\beta\} \cup \{\beta\}^*$ is shown in figure 1.5. The figure shows that each cluster of activated regular bonds or dual bonds is surrounded by a loop which may be generated through a *hull-walk* [28]. The hull-walk takes place on the *medial lattice*, another square lattice at angle $\pi/4$ to the original and formed from the midpoints of the regular and dual bonds of the original lattice. Starting at a specified medial lattice site, we walk along the bonds of the medial lattice so that our walk never steps backward or crosses an activated regular (resp. dual) bond of the regular (resp. dual) lattice, and our walk eventually returns to its starting point to form a loop. Each loop either traces the outer perimeter of a cluster of activated regular bonds (including clusters of size zero) or fills a hole within such a cluster. In a given bond configuration, there are respectively N_ℓ and N_c of each type, where N_ℓ and N_c are defined above, and the total number of loops N_l equals $N_\ell + N_c$. Exploiting the Euler relation (1.24), we find that the partition function (1.21) at the critical point

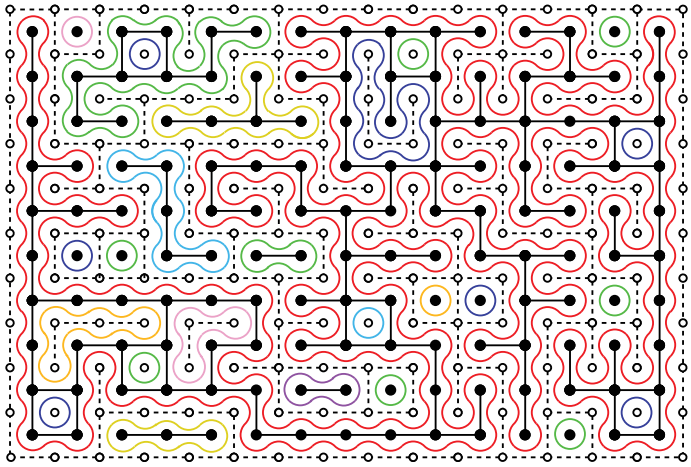

Figure 1.5: The loop configuration corresponding to a particular regular/dual bond configuration. The loops are generated through a hull-walk on the medial lattice. (The steps of the walk have been rounded into quarter-circles in the figure.)

p_c^{sqr} can be written as

$$Z_Q(p_c^{\text{sqr}}) = (1-p_c^{\text{sqr}})^{N_b} Q^{N_s/2} \sum_{\{\beta\}} (\sqrt{Q})^{N_l}. \tag{1.30}$$

Each bond configuration $\{\beta\}$ corresponds one-to-one with a unique loop configuration in which each side of an activated regular or dual bond is touched by a loop, so (1.30) is really a sum over all such loop configurations. At the critical point, the presence of clusters of all sizes implies loops of all lengths. Because every lattice site is visited by a loop, this partition function is supposed to flow onto a renormalized dense-phase loop gas with each loop enjoying a fugacity of $n = \sqrt{Q}$. We therefore call the random cluster representation of the Potts model the *dense phase* of the Potts model. Interestingly, this supposition provides a direct link between the continuum limits of the Potts model and the O(n) model. Such a relation is surprising since these generalizations of the Ising model initially appear to be quite different.

We have shown that the statistics of the Ising spin cluster perimeters have $n = 1$ dilute-phase loop gas descriptions thanks to (1.12) while the statistics of the Ising FK cluster perimeters have $n = \sqrt{2}$ dense-phase loop gas descriptions thanks to

(1.30). We might posit a similar dilute-versus-dense phase description for the spin-cluster versus FK-cluster perimeters respectively for $2 < Q \leq 4$. In particular, the loops for the dilute phase description of the $2 < Q \leq 4$ Potts model should be interfaces between clusters in which all spins exhibit some specific state, say, a, and clusters in which all spins exhibit any spin but a. The dense phase description is conveyed in (1.30), but the other, called the *dilute phase* of the Potts model has, to my knowledge, not been explicitly established by working with the discrete model. However, the relation between spin-cluster perimeters and FK-cluster perimeters is conjectured more easily by exploiting duality in SLE. We will describe this relation in more detail in section 1.2.8.

The terminology "dilute phase" and "dense phase" applied to the critical Q-state Potts model may seem odd. Indeed, the Q-state Potts model already has a high-temperature and a low-temperature phase separated by a unique critical point K_c. Now our terminology suggests that at the critical point, the Q-state Potts model itself has two different phases, dense and dilute, yet this assertion cannot be true since there is no adjustable parameter with its own critical point separating these so-called phases. Rather, the dense phase and the dilute phase are simply names for two different representations of the Potts model. The first is synonymous with the *spin-cluster representation*, that is, the original definition of the Potts model, and the second is synonymous with the random cluster representation. This terminology will become more natural when we introduce SLE in section 1.2.8.

1.1.4 Common features among lattice models

The Ising model and its generalizations that we have discussed have continuum limits that exhibit common special features at their critical points. The first feature is the emergence of conformally invariant observables at the critical point, which endows these models with CFT descriptions. The second is a connection to loop gases with

conformally invariant probability measures. The latter feature leads to an explicit construction of the minimal CFTs via the Coulomb gas formalism and, separately, the rigorous SLE/*conformal loop ensemble (CLE)* approach [29, 30].

We first investigate the emergence of conformal invariance in these models as we approach the critical point. Our treatment is similar to that in [3, 31]. We consider a Potts model on the infinite lattice $a\mathbb{Z}^2$ with small lattice spacing a. To measure the covariance of two spins, one at site i and the other at site j, we study the observable

$$\mathrm{Cov}[\sigma_j, \sigma_j] := \langle \sigma_i \sigma_j \rangle - \langle \sigma_i \rangle \langle \sigma_j \rangle. \tag{1.31}$$

Here, $\langle \ldots \rangle$ denotes averaging with respect to the Boltzman distribution. The one-point function $\langle \sigma_i \rangle$ is zero by the S_Q symmetry of the Potts model, so $\mathrm{Cov}[\sigma_j, \sigma_j]$ equals the *two-point correlation function* $\langle \sigma_i \sigma_j \rangle$. Because spins may be averaged over clusters of size on the order of the correlation length ξ, the correlation length sets a length-scale in the model that governs the long-distance decay of $\langle \sigma_i \sigma_j \rangle$. When the distance r between sites i and j is much greater than a, we typically find

$$\langle \sigma_i \sigma_j \rangle \sim C_\sigma^2 \left(\frac{a}{r}\right)^{2\Delta_\sigma} e^{-r/\xi}, \quad a \ll r. \tag{1.32}$$

Here, $\Delta_\sigma > 0$ is called the scaling weight of the spin variable σ, and it is one of several temperature-dependent *critical exponents* used to characterize a lattice model. Also, C_σ is a constant that depends on microscopic details of the model such as the lattice type. The two-point function (1.32) is clearly translation/rotation-invariant as it must be since the system is isotropic, but off of the critical point, the finite correlation length spoils dilation invariance. Also, we expect that correlation between sites i and j will vanish in the continuum limit ($a \to 0$, r fixed) since these sites grow more isolated from each other as more sites are added to the lattice, and equation (1.32) exhibits this presumption.

Now we examine the continuum limit. We let z be the location of the i-th lattice site in the complex plane, and we consider the spin density $\sigma(z)$, or the average of the spin variables at lattice sites in an ϵ-ball centered at z, in the limit $a \to 0$:

$$\frac{1}{\pi(\epsilon/a)^2} \sum_{|j-i|<\epsilon} \sigma_j \underset{a\to 0}{\longrightarrow} \sigma(z). \tag{1.33}$$

The sum on the left side contains $O(a^{-2})$ terms, so it is reasonable to suppose that this limit exists. Next, we let z_1 and z_2 be the respective locations of sites i_1 and i_2 in the complex plane, and we define the averaged two-point function

$$\langle \sigma(z_1)\sigma(z_2)\rangle := \lim_{a\to 0} \frac{1}{\pi^2(\epsilon/a)^4} \sum_{|j_1-i_1|<\epsilon} \sum_{|j_2-i_2|<\epsilon} \left(\frac{\epsilon}{a}\right)^{2\Delta_\sigma} \langle \sigma_{j_1}\sigma_{j_2}\rangle. \tag{1.34}$$

Then as $a \to 0$, the correlation length vanishes, so the original two-point function $\langle \sigma_{j_1}\sigma_{j_2}\rangle$, and therefore the averaged two-point function, vanishes exponentially fast. But at the critical point, the correlation length is infinite, so $\langle \sigma(z_1)\sigma(z_2)\rangle$ does not vanish. Instead, it behaves just as (1.32) with $a \mapsto \epsilon$ and $\xi \mapsto \infty$ when $\epsilon \ll |z_2 - z_1|$:

$$\langle \sigma(z_1)\sigma(z_2)\rangle \underset{\epsilon\to 0}{\sim} C_\sigma^2 \epsilon^{2\Delta_\sigma} \Upsilon(z_1, z_2), \quad \Upsilon(z_1, z_2) = |z_2 - z_1|^{-2\Delta_\sigma}. \tag{1.35}$$

Four important features of (1.35) are worth noting. First, the two-point function is dilation-invariant at the critical point. That is, it is invariant under the replacements $|z_2 - z_1| \mapsto \lambda|z_2 - z_1|$, and $\epsilon \mapsto \lambda\epsilon$.

Second, Υ is now a power law in the distance $|z_2 - z_1|$ between the lattice sites with exponent $-2\Delta_\sigma$. Power law decay, as opposed to exponential decay, typifies the behavior of correlation functions at the critical point.

Third, the asymptotic behavior of $\langle \sigma(z_1)\sigma(z_2)\rangle$ factors into one nonuniversal constant C_σ for each point times one scaling factor ϵ^{Δ_σ} for each point times a universal function Υ. In a given lattice model with a unique critical point, it is therefore natu-

ral to posit that for some set of lattice N not-necessarily-distinct variables $\{\alpha, \ldots, \zeta\}$ with respective universal scaling weights $\{\Delta_\alpha, \ldots, \Delta_\zeta\}$, the *$N$-point function*

$$\langle \alpha(z_1) \ldots \zeta(z_N) \rangle := \lim_{a \to 0} \frac{1}{\pi(\epsilon_1/a)^2} \ldots \\ \ldots \frac{1}{\pi(\epsilon_N/a)^2} \sum_{|j_1 - i_1| < \epsilon_1} \ldots \sum_{|j_N - i_N| < \epsilon_N} \left(\frac{\epsilon_1}{a}\right)^{\Delta_\alpha} \ldots \left(\frac{\epsilon_N}{a}\right)^{\Delta_\zeta} \langle \alpha_{j_1} \ldots \zeta_{j_N} \rangle, \quad (1.36)$$

with σ_i the value of the σ lattice variable at the i-th site located at $z_i \in \mathbb{C}$ (here, σ is a symbol for a generic lattice variable), exhibits the same factorized behavior as $\epsilon_1, \ldots, \epsilon_N \to 0$:

$$\langle \alpha(z_1) \ldots \zeta(z_N) \rangle \underset{\epsilon_i \to 0}{\sim} C_\alpha \ldots C_\zeta \epsilon_1^{\Delta_\alpha} \ldots \epsilon_N^{\Delta_\zeta} \Upsilon(z_1, \ldots, z_N). \quad (1.37)$$

Again, Υ is some universal function which we typically write as a correlation function of *local fields* $\phi_\sigma(z)$ defined in terms of the densities $\sigma(z)$ thus:

$$\sigma(z) \underset{\epsilon \to 0}{\sim} C_\sigma \epsilon^{\Delta_\sigma} \phi_\sigma(z). \quad (1.38)$$

The field ϕ_σ and its scaling weight are *universal*, or the same for all models within a universality class. On the other hand, the constant C_σ is *nonuniversal*, or depends on the microscopic details of the model such as the lattice type. For notational convenience, we write the universal function Υ as a correlation function of the fields,

$$\Upsilon(z_1, \ldots, z_N) = \langle \phi_\alpha(z_1) \ldots \phi_\zeta(z_N) \rangle, \quad (1.39)$$

to remind us of its relation to the true N-point function (1.37).

Fourth, (1.35) reveals more than dilation invariance. It also reveals (global) conformal invariance. Before we elaborate on this point, we state a few definitions. We let $\hat{\mathbb{C}} = \mathbb{C} \cup \{\infty\}$ be the one-point compactification of the complex plane with the

extra point ∞ called "infinity," and we bijectively map $\hat{\mathbb{C}}$ onto the Riemann sphere S^2 via a stereographic projection s so that infinity maps to the north pole. We let $\mathcal{D}$ be a connected subset of $\hat{\mathbb{C}}$, and we let $f : \mathcal{D} \to \hat{\mathbb{C}}$. Then s lifts f to the map $F : S^2 \to S^2$ given by $F = s \circ f \circ s^{-1}$. Given $z \in \mathcal{D}$, we let γ_1 and γ_2 be any two smooth curves in $s(\mathcal{D}) \subset S^2$ that intersect at $s(z)$, and we let $F(\gamma_1)$ and $F(\gamma_2)$ be the images of γ_1 and γ_2 respectively. These image curves necessarily intersect at $F(s(z))$. Furthermore, we let θ and θ' be the intersection angle of γ_1 with γ_2 and of $F(\gamma_1)$ with $F(\gamma_2)$ respectively. Then we say that f is *conformal at* z if $\theta = \theta'$. If f is conformal at a point $z \in \mathcal{D}$, then f is necessarily conformal in a neighborhood of that point, and we call f a *local conformal transformation.* If f is conformal at every point $z \in \mathcal{D}$, then we say that f is *conformal in* $\mathcal{D}$.

The stereographic map itself preserves angles between intersecting curves except when the intersection occurs at infinity, in which case the intersection angle is not defined. Therefore, if $z \in \mathcal{D}$ and $f(z)$ are finite, then we can streamline our definition to one that does not invoke the Riemann sphere as follows. We let γ_1 and γ_2 be any two smooth curves in $\hat{\mathbb{C}}$ that intersect at z, and we let $f(\gamma_1)$ and $f(\gamma_2)$ be their respective images under f which necessarily intersect at $f(z)$. We also let θ and θ' be the angle of intersection of γ_1 with γ_2 and of $f(\gamma_1)$ with $f(\gamma_2)$ respectively. Then we say that f is *conformal at* z if $\theta = \theta'$. This is the more conventional definition of conformality [32]. If z and $f(z)$ are finite, then it follows that f is conformal at z if and only if f is complex-differentiable (i.e., analytic or holomorphic as discussed in section A of the appendix) at z and the magnitude of its derivative at z is finite and nonzero. For instance, the maps $f(z) = z^{-1}$ and $f(z) = z^{-1/2}$ are not conformal at zero according to the latter definition. However (resp. Moreover), the map $f(z) = z^{-1}$ (resp. $f(z) = z^{-1/2}$) is (resp. is not) conformal at zero according to the former definition that invokes the Riemann sphere. We will use the former definition throughout this thesis because it gives a more elegant statement of the

following important fact.

A *global conformal transformation* is bijective map $f : \hat{\mathbb{C}} \to \hat{\mathbb{C}}$ that is conformal on $\hat{\mathbb{C}}$. A famous theorem from complex analysis [32] states that every global conformal transformation is a *Möbius transformation*, or a transformation of the form

$$f(z) = \frac{az + b}{cz + d}, \quad a, b, c, d \in \mathbb{C} \text{ with } ad - bc = 1, \tag{1.40}$$

and vice versa. It is straightforward to show that the set of all global conformal transformations forms a group, called the *global conformal group,* under composition that is isomorphic to $\mathrm{SL}_2(\mathbb{C})/\mathbb{Z}_2$.

These definitions set the stage for the following important observation. If f is a global conformal transformation and $z_i' = f(z_i)$, then under f, the right side of the two-point function (1.35) transforms into

$$C_\sigma^2 |\epsilon \partial f(z_1)|^{\Delta_\sigma} |\epsilon \partial f(z_2)|^{\Delta_\sigma} \Upsilon(z_1', z_2'). \tag{1.41}$$

On the other hand, we also observe that $\Upsilon(z_1, z_2) = |z_2 - z_1|^{-2\Delta_\sigma}$ satisfies the following functional equation:

$$\Upsilon(z_1', z_2') = |\partial f(z_1)|^{-\Delta_\sigma} |\partial f(z_2)|^{-\Delta_\sigma} \Upsilon(z_1, z_2). \tag{1.42}$$

After inserting (1.42) into the transformed two-point function (1.41), we find the original two-point function that preceded the transformation. We therefore conclude that the two-point function (1.35) is invariant under global conformal transformations, and we say that the two-point function is *conformally invariant.*

This observation leads us to posit that the N-point functions are also conformally invariant. According to the preceding discussion, if an N-point function of N lattice variables at respective sites $z_1, \ldots, z_N$ and with respective scaling weights $\Delta_1, \ldots, \Delta_N$

exhibits this symmetry, then its universal function $\Upsilon(z_1, \ldots, z_N)$ will satisfy the functional equation

$$\Upsilon(z'_1, \ldots, z'_N) = |\partial f(z_1)|^{-\Delta_1} \ldots |\partial f(z_N)|^{-\Delta_N} \Upsilon(z_1, \ldots, z_N) \tag{1.43}$$

for any global conformal transformation f. A function Υ satisfying property (1.43) is said to be *conformally covariant at z_i with scaling weight Δ_i* for each $i \in \{1, \ldots, N\}$. Conformal invariance of N-point functions has been observed in many critical lattice models [3], and when it is observed, it lays the foundation for nearly all continuum limit mathematical descriptions of these models.

The second common feature among the models discussed so far is the existence of their loop gas representations, which is useful for understanding their continuum limits. The continuum limit of a lattice model can be very elusive to capture directly. Some renormalization methods attempt to characterize it through coarse-graining the system and supposing that, with suitable modifications, the lattice variables flow onto a Gaussian free field (see [23, 33] and references therein), but these methods are non-rigorous, only give approximate results, and do not present a clear picture of the continuum limit. A more rigorous picture can be found not by studying the individual lattice variables but by studying the perimeters of their clusters which go to non-crossing fractal loops with conformally invariant probability measures in the continuum limit. These measures are conjectured, and in some cases proven, to be those of SLE/CLE [14, 15, 29, 30], and the loop gas representation of a model can often be used to identify a critical lattice model with one of these measures. Therefore, this second feature is very useful for developing rigorous constructions of the continuum limits of some of these critical systems, though proving the existence of the continuum limit and that this construction is indeed the correct description for it is technically very difficult. We will not pursue these matters in this thesis.

1.2 A Survey of conformal field theory

This section present a brief survey of the essential ingredients of conformal field theory (CFT), first proposed in [10]. Our treatment is similar to that in [3, 11, 34]. Our immediate goal is to develop a CFT description of the critical lattice models explored in the previous sections in bounded domains. Some basic familiarity with quantum field theory is assumed.

The philosophy behind our approach can be summarized as follows. In physics, one constructs a mathematical model of observed phenomena in order to predict further unobserved phenomena that can be verified in an experiment. For this reason, the development of the model proceeds heuristically rather than rigorously, and in spite of this, it often has compelling, unstudied mathematical structure. During or after the construction of the model, one may begin a new program to construct a rigorous mathematical theory that exhibits the same structure, giving the model rigorous footing and possibly even extending it. This description captures the evolution of CFT, which is loosely understood to be any mathematical structure with certain specific ingredients specified by its initial use in string theory, critical phenomena, and other topics. In this exposition, we will follow the more heuristic approach of CFT's early development. A more rigorous treatment can be found in [12] and the many references therein.

1.2.1 The continuum limit: from lattice variables to fields

One approach to constructing a continuum representation of a lattice model is to represent each lattice variable density $\sigma(z)$ at site z with a local field $\phi_\sigma(z)$ as in (1.38). The field $\phi_\sigma(z)$ is universal in the sense that it corresponds to a particular lattice variable density $\sigma(z)$ common to all models within a universality class. We will refer to a generic field as ϕ.

In a rigorous setting, the field ϕ is really a *field operator* which is a kind of

operator-valued distribution mapping a suitable space of test functions onto a set of self-adjoint operators acting on a Hilbert space of "states." This point of view is taken by some rigorous treatments of CFT. For now, we ignore these technicalities and suppose that ϕ is either a smooth function of $\hat{\mathbb{C}}$ (as treated in the path integral approach to quantum field theory) or an *operator* acting on some state space (as treated in the operator approach to quantum field theory), depending on which point of view is more convenient.

In section 1.1.4, we observed that correlation functions of fields are conformally covariant (1.43). We generalize (1.43) slightly to

$$\langle \phi'_1(z'_1, \bar{z}'_1) \dots \phi'_N(z'_N, \bar{z}'_N) \rangle_{\hat{\mathbb{C}}} = \partial f(z_1)^{-h_1} \bar{\partial} \bar{f}(\bar{z}_1)^{-\bar{h}_1} \dots \\ \times \dots \partial f(z_N)^{h_N} \bar{\partial} \bar{f}(\bar{z}_N)^{-\bar{h}_N} \langle \phi_1(z_1, \bar{z}_1) \dots \phi_N(z_N, \bar{z}_N) \rangle_{\hat{\mathbb{C}}}, \quad (1.44)$$

for any global conformal mapping $f : \hat{\mathbb{C}} \to \hat{\mathbb{C}}$. Again, $z'_i := f(z_i)$. For notational convenience, we treat z and $\bar{z}$ as independent holomorphic and antiholomorphic variables and f and $\bar{f}$ as independent holomorphic and antiholomorphic maps instead of complex conjugates. We discuss this point of view further in section A of the appendix. In (1.44), the numbers h and $\bar{h}$ are respectively called the *holomorphic conformal weight* and *antiholomorphic conformal weight* of the field ϕ, and they are not complex conjugates of each other. Rather, they are distinct numbers.

The primes on the fields on the left side of (1.44) indicate that the fields transform under the global conformal map too, and the nature of this transformation is discussed further in section B of the appendix. However, because the angled brackets $\langle \dots \rangle_{\hat{\mathbb{C}}}$ denote a thermal averaging over all possible fields with the common domain $\hat{\mathbb{C}}$ and weighted against a (globally) conformally invariant measure, the correlation function on the left side of (1.44) must equal the correlation function on the right side with z'_i replacing z_i for each $i \in \{1, \dots, N\}$. In other words, if we use the notation of the

previous section and define the N-point function

$$\Upsilon(z_1, \bar{z}_1, \ldots, z_N, \bar{z}_N) := \langle \phi_1(z_1, \bar{z}_1) \ldots \phi_N(z_N, \bar{z}_N) \rangle_{\hat{\mathbb{C}}}, \tag{1.45}$$

then (1.44) amounts to the functional relation

$$\Upsilon(z_1', \bar{z}_1', \ldots, z_N', \bar{z}_N') = \prod_{i=1}^{N} \partial f(z_i)^{-h_i} \bar{\partial} \bar{f}_i(\bar{z}_i)^{-\bar{h}_i} \Upsilon(z_1, \bar{z}_1, \ldots, z_N, \bar{z}_N). \tag{1.46}$$

We will explore the consequences of this equation further in the next section. Also, we will drop the subscript $\hat{\mathbb{C}}$ from the angled brackets for concision from now on.

We define the *scaling weight* and the *spin* of the field ϕ in terms of its conformal weights respectively as

$$\Delta := h + \bar{h}, \quad s := h - \bar{h}, \tag{1.47}$$

and if a field is *spinless,* that is $s = 0$, then the rule (1.44) reduces to the previous rule (1.43) when we set $\bar{z} = z^*$ and $\bar{f} = f^*$. All of the fields that we will encounter in this thesis are spinless.

Motivated by the transformation rule (1.44), we suppose that a field ϕ transforms according to the *conformal covariance law*

$$\phi(z, \bar{z}) \mapsto \phi'(z', \bar{z}') = \partial f(z)^{-h} \bar{\partial} \bar{f}(\bar{z})^{-\bar{h}} \phi(z, \bar{z}) \tag{1.48}$$

when f is a global conformal mapping. (We motivate this transformation rule in section B of the appendix.) We call such a field a *quasi-primary field.* The rule (1.48) is completely local, so to extend it to a local conformal transformation is natural. To this end, we call a field ϕ that transforms according to (1.48) for any transformation $f : \hat{\mathbb{C}} \to \hat{\mathbb{C}}$ and at any $z \in \hat{\mathbb{C}}$ where f is conformal a *primary field.* More informally, we say that a primary field transforms according to (1.48) under a local conformal transformation while a quasi-primary field transforms according to (1.48) under a

global conformal transformation. Clearly, a primary field is quasi-primary, but the converse is not necessarily true.

An N-point function Υ of quasi-primary (or primary) fields will obviously satisfy relation (1.46) for a global conformal mapping f. If all of the fields in the N-point function are primary, then we expect this constraint to strengthen since the transformation law (1.48) of a primary field holds for more than just global conformal transformations. However, to suppose that (1.46) is true for local conformal transformations which are conformal at $z_1, \ldots, z_N$ is incorrect. Indeed, the measure against which the N-point function averages the product of N fields is only invariant under global conformal transformations. So if f is conformal at $z_1, \ldots, z_N$ but is not a global conformal transformation, then the measure will change, and the correlation function on the left side of (1.44) will not equal that on the right side with z_i' replacing z_i. Instead, we find a prescription for calculating the new correlation function with the image measure. This is easiest to understand if f maps $\hat{\mathbb{C}}$ onto a region $\mathcal{D}$ that is a proper subset of $\hat{\mathbb{C}}$. In this case, the new correlation function $\Upsilon^{\mathcal{D}}$ is completely different from the original Υ. For one, they have different domains $\mathcal{D}^N$ and $\hat{\mathbb{C}}^N$ respectively. However, they are related through the transformation rule

$$\Upsilon^{\mathcal{D}}(z_1', \bar{z}_1', \ldots, z_N', \bar{z}_N') = \prod_{i=1}^{N} \partial f(z_i)^{-h_i} \bar{\partial} \bar{f}_i(\bar{z}_i)^{-\bar{h}_i} \Upsilon(z_1, \bar{z}_1, \ldots, z_N, \bar{z}_N). \tag{1.49}$$

For example, the map $f(z) = (L/2\pi) \log z$ sends the complex plane onto the infinite strip $(-\infty, \infty) \times [-L/2, L/2]$ with its top and bottom sides identified, or equivalently onto an infinite cylinder with circumference L. According to (1.49), the two-point function (1.35) of two spinless fields with scaling weight Δ transforms into

$$\langle \phi(z_1', \bar{z}_1') \phi(z_2', \bar{z}_2') \rangle_{\text{cyl.}} = \left(\frac{2\pi}{L} \right)^{2\Delta} \left[4 \sinh \frac{\pi(z_1' - z_2')}{L} \times \text{c.c.} \right]^{-\Delta}, \tag{1.50}$$

where we have set $\bar{z} = z^*$ and $\bar{z}' = f(z)^*$ and "c.c" stands for the complex conjugate

of the collection of factors that it multiplies. If the distance $r := |z_1' - z_2'|$ between the image points is much less than L, then the cylinder locally looks Euclidean, and we recover the original two-point function $r^{-2\Delta}$ on the plane. On the other hand, if r is much greater than L, then the image two-point function (1.50) behaves as $(2\pi/L)^{2\Delta} \exp(-\mathrm{Re}(r)/\xi)$ with a correlation length $\xi = L/2\pi\Delta$. The phenomenon of a finite correlation length occurs as a consequence of the finite length-scale intrinsic to the cylinder, namely its circumference.

A typical CFT consists of an infinite collection of fields organized into a hierarchy, and the top of this hierarchy B_0 comprises of a set of primary fields $\{\phi_\alpha\}_{\alpha \in B_0}$. If a CFT characterizes a critical lattice model, then these fields usually correspond with the fundamental lattice variables of the model, such as spin or energy density in the Ising model. The rest of the hierarchy B_1 consists of *secondary fields,* or fields $\{\phi_\alpha\}_{\alpha \in B_1}$ that are not primary but may be quasi-primary. Each secondary field depends on a primary field in some way, so the transformation law of a secondary field under a local conformal transformation, while not (1.48), is determined both by this law and the relation of the secondary field to its "parent" primary field. Usually, this law is (1.48) with correction terms added to it. These details will be discussed a little further in section 1.2.4.

1.2.2 Correlation functions in conformal field theory

Correlation functions serve as the principal observables of a critical lattice model. For this reason, the goal of a CFT is to calculate the correlation functions of all of its fields. These correlation functions are sometimes computed by using the *operator formalism,* in which the fields are promoted to quantum field operators that act on the sample space of the system. We let $|\Omega\rangle$ denote the configuration of lowest energy, called the *vacuum state.* Then we suppose that the CFT correlation function and its

quantum version are equivalent:

$$\langle \phi_1(z_1, \bar{z}_1) \dots \phi_N(z_N, \bar{z}_N) \rangle \quad \longleftrightarrow \quad \langle \Omega | \phi_N(z_1, \bar{z}_1) \dots \phi_1(z_N, \bar{z}_N) | \Omega \rangle. \tag{1.51}$$

The fields shown in the correlation function on the right side are operators, and they must typically be radially ordered, that is $|z_1| < \ldots < |z_N|$, in order for the correlation function on the right side to be well-defined. This detail is an artifact inherited from the time-ordering prescription of quantum field theory, and it usually does not concern us because the formulas for the N-point functions often can be analytically continued to the domain in $\mathbb{C}^N$ with $z_i \neq z_j$ for all indices $i \neq j$. We will survey a useful operator method called the Coulomb gas formalism in section 1.2.9.

To begin our study of correlation functions in CFT, we investigate how equation (1.46) restricts the form of an N-point function of quasi-primary operators. We let f be a global conformal transformation that is infinitesimal in a large disk $\mathcal{D}$ which is centered at some $\zeta \in \mathbb{C}$ and contains the points $z_1, \dots, z_N$. Such a transformation is necessarily of the form

$$f(z) = \frac{(1 + b/2)(z - \zeta) + a}{-c(z - \zeta) + 1 - b/2}, \quad z, \zeta \in \mathcal{D} \tag{1.52}$$

with $a, b, c \in \mathbb{C}$ sufficiently small, and has the following expansion to first order in a, b, and c:

$$f(z) = z + \epsilon(z), \quad \epsilon(z) = a + b(z - \zeta) + c(z - \zeta)^2 + \dots. \tag{1.53}$$

The first term in $\epsilon(z)$ signifies translation, the second term signifies rotation and dilation, and the third term signifies an special conformal transformation (SCT), which is essentially an inversion followed by a translation followed by another inversion. The infinitesimal versions of these three transformations constitute the infinitesimal

generators of the global conformal group. We break $\epsilon(z)$ into its three constituent pieces $\epsilon(z) = a$, $b(z-\zeta)$, or $c(z-\zeta)^2$, substitute each piece in (1.46), and expand to lowest order in these parameters to find the *conformal Ward identities:*

$$\sum_{i=1}^{N} \partial_i \Upsilon = 0, \quad \sum_{i=1}^{N} (z_i \partial_i + h_i)\Upsilon = 0, \quad \sum_{i=1}^{N} (z_i^2 \partial_i + 2h_i z_i)\Upsilon = 0. \tag{1.54}$$

By repeating these steps for the antiholomorphic sector with $\bar{\epsilon}(\bar{z}) = \bar{a}, \bar{b}(\bar{z}-\bar{\zeta})$, and $\bar{c}(\bar{z}-\bar{\zeta})^2$, we recover an identical set of partial differential equation (PDE)s in the antiholomorphic coordinates $\bar{z}_i$ and the conformal weights $\bar{h}_i$. When $N = 1, 2, 3$, we can solve the Ward identities to find explicit formulas for the one-point, two-point, and the three-point functions of quasi-primary operators:

$$\Upsilon(z_1, \bar{z_1}) = 0, \tag{1.55}$$

$$\Upsilon(z_1, \bar{z_1}, z_2, \bar{z}_2) = C_{12} \delta_{h_1, h_2} \delta_{\bar{h}_1, \bar{h}_2} (z_2 - z_1)^{-2h_1} \times \text{c.c.}, \tag{1.56}$$

$$\begin{aligned} \Upsilon(z_1, \bar{z_1}, z_2, \bar{z}_2, z_3, \bar{z}_3) = C_{123} \Big[& (z_2 - z_1)^{-h_1 - h_2 + h_3} \\ & \times (z_3 - z_2)^{-h_2 - h_3 + h_1} (z_1 - z_3)^{-h_3 - h_1 + h_2} \times \text{c.c.} \Big]. \end{aligned} \tag{1.57}$$

Here "c.c." stands for the antiholomorphic contribution which is identical to the holomorphic part except with antiholomorphic coordinates and conformal weights replacing their holomorphic counterparts. The normalization of the two-point function is arbitrary, but the normalization of the three-point function depends on that of the two-point function. We will briefly investigate this dependence later.

When $N \geq 4$, the conformal Ward identities may also be solved via the method of characteristics. We find that an N-point function of quasi-primary operators must always exhibit the ansatz

$$\Upsilon(z_1, \bar{z}_1, \ldots, z_N, \bar{z}_N)$$
$$= \prod_{1 \le i < j \le N} z_{ij}^{\mu_{ij}} \, G \left(\begin{array}{c} N-3 \text{ independent cross-ratios} \\ \text{formed from } \{z_i\}_{i=1}^N \end{array} \right) \times \text{c.c.}, \quad (1.58)$$

where $z_{ij} := z_i - z_j$, where G is an unspecified function with its i-th partial derivative existing everywhere except possibly when $z_i = z_j$ for some $j \neq i$, and where μ_{ij} is subject to the constraint

$$\sum_{j \neq i} \mu_{ij} = -2h_i \quad \text{for all } i \in \{1, \ldots, N\}. \quad (1.59)$$

A cross-ratio is a function $f(z_i, z_j, z_k, z_l) = z_{ij} z_{kl} / z_{ik} z_{jl}$ with i, j, k and l as distinct indices, and it is invariant under a global conformal transformation. The ansatz (1.58) explicitly exhibits the conformally covariant transformation law (1.46).

While an N-point function of quasi-primary operators must assume the form (1.58), the form of an N-point function of primary operators is even further constrained. We will examine these constraints later in section 1.2.5.

Typically, an additional condition is imposed on the N-point functions of primary operators. We require that when $N = 2, 3, 4$, such an N-point function Υ is invariant under the monodromy transformation induced by letting z_j (resp. $\bar{z}_j$) wind counterclockwise (resp. clockwise) around z_i (resp. $\bar{z}_i$) for all $j \neq i$. When $N = 2, 3, 4$, this condition is satisfied if the spin of each field in the correlation function is an integer [3]. With this condition imposed, we can use (1.46) with $f(z) = 1 - z$ and $f(z) = 1/z$ to uncover the *crossing relations*

$$G_{ij:kl}(\eta, \bar{\eta}) = G_{kj:il}(1 - \eta, 1 - \bar{\eta}), \quad G_{ij:kl}(\eta, \bar{\eta}) = \eta^{-2h_j} \bar{\eta}^{-2\bar{h}_j} G_{lj:ki}(1/\eta, 1/\bar{\eta}), \quad (1.60)$$

where $G_{ij;kl}(\eta,\bar{\eta})$ is defined by

$$G_{ij:kl}(\eta,\bar{\eta}) = \lim z_l^{2h_l}\bar{z}_l^{2\bar{h}_l}\Upsilon(z_1,\bar{z}_1,\ldots,z_4,\bar{z}_4), \tag{1.61}$$

with "lim" standing for the limit $(z_i,z_j,z_k,z_l) \to (0,\eta,1,\infty)$ and $(\bar{z}_i,\bar{z}_j,\bar{z}_k,\bar{z}_l) \to (0,\bar{\eta},1,\infty)$, and with the indices $\{i,j,k,l\}$ in one-to-one correspondence with $\{1,2,3,4\}$. The crossing relations are used to fix the coefficient of the three point function (1.57) and in some cases the explicit form of the four-point function.

1.2.3 The stress tensor and conformal families

In the next few sections, we investigate the extra constraints that local conformal invariance imposes on correlation functions of primary operators. These constraints are embodied in a special field called the *stress tensor.* In a quantum field theory, this is the conserved current associated with the translation invariance of the action. From this association, the stress tensor appears naturally in CFTs modeled by quantum field theories. In CFT, the stress tensor is always divergence-free, and it can be adjusted to be symmetric and traceless in space-time coordinates by exploiting the conformal symmetry of the theory. In holomorphic/antiholomorphic coordinates, the stress tensor is diagonal, and its 00 (resp. 11) component is holomorphic (resp. antiholomorphic). We call this component (modulo a conventional factor of -2π) $T(z)$ (resp. $\bar{T}(\bar{z})$). The two-point functions of these components are

$$\langle T(z_1)T(z_2)\rangle = \frac{c/2}{(z_1-z_2)^4}, \quad \langle \bar{T}(\bar{z}_1)\bar{T}(\bar{z}_2)\rangle = \frac{c/2}{(\bar{z}_1-\bar{z}_2)^4}, \quad \langle T(z_1)\bar{T}(\bar{z}_2)\rangle = 0, \tag{1.62}$$

with the *central charge* c some constant whose physical meaning we will discuss later.

Now we investigate how the stress tensor determines the variation $\delta\phi := \phi' - \phi$ of the field ϕ under an infinitesimal transformation $f(z) = z + \epsilon(z)$ that is conformal at

z. By using Nöther's theorem, one may show that this variation is given by [11]

$$\delta\phi(z,\bar{z}) = -\frac{1}{2\pi i}\oint_z dw\,\epsilon(w)T(w)\phi(z,\bar{z}) + \text{c.c.}. \tag{1.63}$$

This formula follows from the radial quantization scheme of CFT. The contour used for the integral is a simple loop of very small radius winding counterclockwise around the point z once. Letting X stand for a product of fields $\phi_1(z_1,\bar{z}_1)\ldots\phi_N(z_N,\bar{z}_N)$, the leading order contribution to the variation $\delta\langle X\rangle$ of $\langle X\rangle$ under the infinitesimal transformation f is given by

$$\delta\langle X\rangle = -\frac{1}{2\pi i}\oint_\Gamma dw\,\epsilon(w)\langle T(w)X\rangle + \frac{1}{2\pi i}\oint_{\bar{\Gamma}} d\bar{w}\,\bar{\epsilon}(\bar{w})\langle\bar{T}(\bar{w})X\rangle, \tag{1.64}$$

where Γ (resp. $\bar{\Gamma}$) is a contour that winds counterclockwise (resp. clockwise) around each point among $z_1,\ldots,z_N$ (resp. $\bar{z}_1,\ldots,\bar{z}_N$) once. This identity indicates that the holomorphic and antiholomorphic sectors of the theory are decoupled. Therefore, results pertaining to the antiholomorphic sector will be identical to those of the holomorphic sector except with anitholomorphic variables and conformal weights replacing their holomorphic counterparts. So for concision, we will only show the holomorphic sector in our calculations for now.

Now, if we suppose that any correlation function of the form $\langle T(w)\phi(z)X\rangle$, where X is a product of fields, has a Laurent series expansion $\sum_k A_k(z-w)^k$ for z near w, then upon inserting this expansion into (1.64), we find

$$\langle\delta\phi(z)X\rangle = -\frac{1}{2\pi i}\oint_z dw\,\epsilon(w)\sum_{k=-\infty}^{\infty} A_k(z-w)^k. \tag{1.65}$$

If ϕ is quasi-primary and $\epsilon(z) = (z-\zeta)^2$ for z sufficiently close to ζ, then the left side equals $-[(z-\zeta)^2\partial_z + 2(z-\zeta)h]\langle\phi X\rangle$ to lowest order in $z-\zeta$. This follows from the transformation rule (1.48). On the right side, we may evaluate the integral by the

method of residues, and after matching the result with the left side, we find two of the coefficients in the series expansion:

$$A_{-2} = h\langle\phi(z)X\rangle, \quad A_{-1} = \langle\partial\phi(z)X\rangle. \tag{1.66}$$

Here, h is the holomorphic weight of ϕ. Furthermore, if ϕ is primary, then we may repeat this calculation for $\epsilon(z) = (z-\zeta)^p$ with $p > 2$ to find that $A_k = 0$ for all $k < -2$. Therefore, the correlation function $\langle T(w)\phi(z)X\rangle$ has the expansion

$$\langle T(w)\phi(z)X\rangle = \frac{h\langle\phi(z)X\rangle}{(w-z)^2} + \frac{\langle\partial\phi(z)X\rangle}{w-z} + \text{terms regular as } w \to z, \tag{1.67}$$

when ϕ is primary. When ϕ is quasi-primary, the series is the same except that its singular part does not terminate with an order-two pole unless ϕ is primary too.

Of course, the variation of a correlation function of quasi-primary fields must vanish under an infinitesimal global conformal transformation such as $f(z) = z + (z-\zeta)^2$ with z very close to ζ. The Ward identities (1.54) already guarantee this symmetry. By expanding

$$\delta\langle X\rangle = -\sum_{i=1}^{N}[(z_i-\zeta)^2\partial_i + 2(z_i-\zeta)h_i]\langle X\rangle, \tag{1.68}$$

collecting like powers of ζ, and using the Ward identities, we find that $\delta\langle X\rangle = 0$. And also, by inserting (1.67) (including the higher order poles) and $\epsilon(z) = (z-\zeta)^2$ into (1.64) and evaluating the integral by the method of residues, we again find that $\delta\langle X\rangle = 0$, so our theory is consistent.

Because (1.67) is true for any string of fields X, we may drop these fields and write this relation in terms of just the stress tensor T and the primary field ϕ:

$$T(w)\phi(z) \underset{w\to z}{\sim} \frac{h\phi(z)}{(w-z)^2} + \frac{\partial\phi(z)}{w-z}, \quad \phi \text{ primary.} \tag{1.69}$$

This is an example of an *operator product expansion (OPE)*. An OPE is a kind of multiplication of two fields that equals the singular behavior of their composition within a correlation function as their respective points approach each other. Because the observables of CFT are the correlation functions, the OPE product and the composition product cannot be distinguished by any observable, so we denote both by $T(w)\phi(z)$. A similar OPE exists for $\bar{T}(\bar{w})\phi(\bar{z})$ as $\bar{w} \to \bar{z}$.

In explicit quantum-field-theoretic examples of CFT, the OPE of the stress tensor with itself has the following form that implies its two-point function (1.62):

$$T(w)T(z) \underset{w\to z}{\sim} \frac{c/2}{(z-w)^4} + \frac{2T(z)}{(z-w)^2} + \frac{\partial T(z)}{z-w}. \tag{1.70}$$

Examples include the massless free boson ($c = 1$) and the massless free fermion ($c = 1/2$). The OPE (1.70) indicates that the holomorphic part of the stress tensor is quasi-primary with holomorphic weight two. (The antiholomorphic weight is zero since $\bar{\partial}T = 0$.) By inserting this OPE into (1.63) and integrating, we can calculate the variation of the holomorphic part of the stress tensor under an infinitesimal mapping that is conformal at z. This leads to the transformation rule

$$T'(z') = \partial f(z)^{-2} \left(T(z) - \frac{c}{12}\{w; z\} \right), \tag{1.71}$$

where f is a map that is conformal at z. Here, $z' = f(z)$, and $\{w; z\}$ is the Schwarzian derivative [32]. This transformation law is perturbed from the transformation law of a primary field by a term proportional to the central charge. Because $\{w; z\}$ vanishes only if f is a global conformal transformation, we explicitly see that the holomorphic part of the stress tensor is quasi-primary with holomorphic weight two and antiholomorphic weight zero.

Now we suppose that the holomorphic part of the stress tensor admits a Laurent

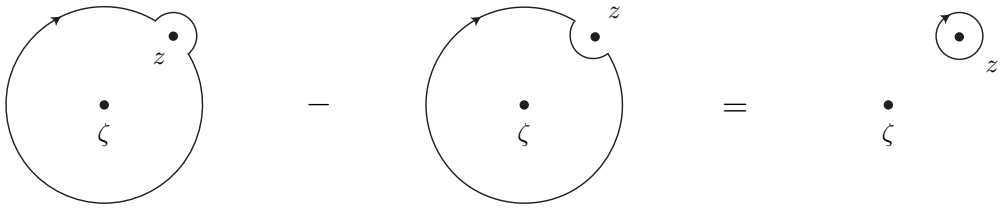

Figure 1.6: Illustration of the evaluation of the commutator appearing in (1.73).

expansion about a point ζ in the complex plane:

$$T(z) = \sum_{k=-\infty}^{\infty} (z-\zeta)^{-k-2} L_k(\zeta) \quad \Longleftrightarrow \quad L_k(\zeta) = \frac{1}{2\pi i} \oint_\zeta dw\, (w-\zeta)^{k+1} T(\zeta). \quad (1.72)$$

We call $L_k(\zeta)$ the k-th *mode* of the holomorphic part of the stress tensor. The k-th mode is analogous to the generator ℓ_k of the Witt algebra (B.30), presented in section B of the appendix, in that if we assume the point-of-view that ϕ is a quantum field operator acting on a Hilbert space of states, then the k-th mode is the infinitesimal generator of the transformation on these states under the map $f(z) = z + (z-\zeta)^{k+1}$.

A commutator may defined through the radial ordering prescription [11], mentioned at the beginning of section 1.2.2, so that the commutator $-[L_k(\zeta), \phi(z)]$ equals the field variation $\delta\phi$ when the map $f(z) = z + (z-\zeta)^{k+1}$ is conformal (i.e., when $k \geq -1$). For any integer k, this commutator is given by

$$\begin{aligned} [L_k(\zeta), \phi(z)] &= \frac{1}{2\pi i} \left[\oint_{\zeta,z} - \oint_\zeta \right] dw\, (w-\zeta)^{k+1} T(w)\phi(z) && (1.73) \\ &= \frac{1}{2\pi i} \oint_z dw\, (w-\zeta)^{k+1} T(w)\phi(z). && (1.74) \end{aligned}$$

Here, the contour of the first integral in (1.73) encircles ζ and z once while the contour of the second integral encircles ζ but not z once (figure 1.6). By substituting the OPE for the product $T(w)\phi(z)$ and integrating, we find that the commutator is given by

$$[L_k(\zeta), \phi(z)] = h(k+1)(z-\zeta)^k \phi(z) + (z-\zeta)^{k+1} \partial\phi(z). \quad (1.75)$$

After inserting $f(z) = z + (z-\zeta)^{k+1}$ with $k \geq -1$ into (1.48) and expanding to low order in $(z-\zeta)$, we find that the right side of (1.75) indeed equals $-\delta\phi$.

In the same manner, we can compute the commutator between two stress-tensor modes located at the same point ζ. Because these modes serve a role analogous to the generators of the Witt algebra (B.30) for scalar fields, we expect their commutators to be the same. Again, the radial ordering prescription gives

$$[L_n(\zeta), L_m(\zeta)] = \frac{1}{(2\pi i)^2}\left[\oint_\zeta dw_1 \oint_{\zeta,w_1} dw_2 - \oint_\zeta dw_2 \oint_{\zeta,w_2} dw_1\right] \times (w_2-\zeta)^{n+1}(w_1-\zeta)^{m+1}T(w_2)T(w_1). \quad (1.76)$$

Again, the subscripts on the integral sign indicate the variables encircled by the integration contours. The integration variable w_1 (resp. w_2) serves as w in the definition of $L_m(\zeta)$ (resp. $L_n(\zeta)$) in (1.72). The difference of integrals may be rewritten as an integration of w_2 around w_1 followed by an integration of w_1 around ζ (figure 1.7). After substituting the OPE (1.70) into the integrand, the integration may be explicitly performed to reveal

$$\begin{aligned} [L_n(\zeta), L_m(\zeta)] &= (n-m)L_{n+m}(\zeta) + \tfrac{c}{12}n(n+1)(n-1)\delta_{n,-m}, \\ [\bar{L}_n(\zeta), \bar{L}_m(\zeta)] &= (n-m)\bar{L}_{n+m}(\zeta) + \tfrac{c}{12}n(n+1)(n-1)\delta_{n,-m}, \\ [L_n(\zeta), \bar{L}_m(\zeta)] &= 0. \end{aligned} \quad (1.77)$$

(Now we are including the antiholomorphic sector.) That is, the holomorphic and anitholomorphic modes generate independent copies of the *Virasoro algebra*, an infinite-dimensional Lie algebra whose commutation relations are given by the top line of (1.77). The commutation relations (1.77) differ from those of the Witt algebra (B.30) by the addition of the second *conformal anomaly* term containing the central charge.

If the central charge is nonzero, then the set of generators $\{L_{-1}, L_0, L_1\}$ for the global conformal group spans the only subalgebra of the Virasoro algebra for which

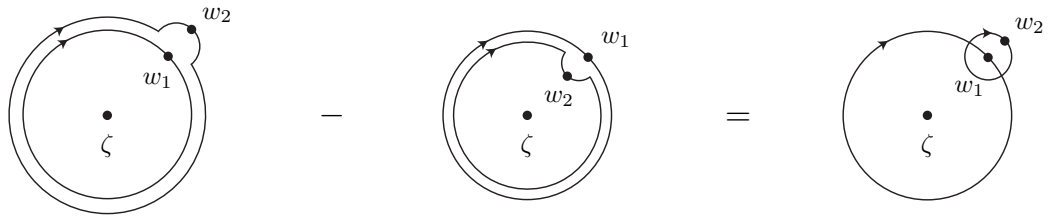

Figure 1.7: Illustration of the evaluation of the the stress-tensor-mode commutator in (1.73).

the conformal anomaly term vanishes. This indicates that while the global conformal symmetry (expressed through the covariance of correlation functions of quasi-primary fields under infinitesimal global conformal transformations) is preserved, the local conformal symmetry (expressed through the covariance of these same correlation functions under infinitesimal local conformal transformations) is broken. For example, if we map our CFT onto a cylinder of circumference L via $f(z) = (L/2\pi)\log z$, then the one-point function (or vacuum expectation value in the quantum-field-theoretic picture) of the stress tensor no longer vanishes as it does in the plane, but is proportional to $-c\pi^2/6L^2$, as can be verified from (1.71). This value is nonzero only when the central charge is nonzero and the conformal anomaly term of the Virasoro algebra is therefore present.

1.2.4 Verma modules

In this section, we investigate the representation theory of the Virasoro algebra from the physicist's point-of-view as a means to construct secondary fields from the primary fields of a CFT. A more mathematically rigorous account of the representation theory of the Virasoro algebra is given in [35].

The stress-tensor modes introduced in the previous section may be used to generate secondary fields from a parent primary field ϕ. In particular, we have from (1.75) with $k = -1, 0$ that

$$[L_0(\zeta), \phi(z)] = h\phi(z), \quad [L_{-1}(\zeta), \phi(z)] = \partial\phi(z). \tag{1.78}$$

The left commutator indicates that, in the adjoint representation, $\phi(z)$ is an eigenvector of $L_0(\zeta)$ with eigenvalue h. The right commutator produces a completely new field that is the derivative of the original primary field. After acting on it with $\operatorname{ad} L_0(\zeta)$, we find via the Jacobi identity that the new field satisfies

$$\begin{aligned} [L_0(\zeta), \partial\phi(z)] &= [L_{-1}(\zeta), [L_0(\zeta), \phi(z)]] + [[L_0(\zeta), L_{-1}(\zeta)]\phi(z)] && (1.79) \\ &= (h+1)\partial\phi(z). && (1.80) \end{aligned}$$

We thus conclude that $\partial\phi(z) = [L_{-1}(\zeta), \phi(z)]$ is another eigenvector of $L_0(\zeta)$ but with eigenvalue $h+1$ instead of h. We therefore interpret $L_{-1}(\zeta)$ as a *lowering operator.* The field $\partial\phi(z)$ is an example of a *descendant field* of $\phi(z)$.

In imitation of the quantum theory of angular momentum, we generate a representation of the Virasoro algebra through repeated application of *raising* ($k > 0$) and *lowering* ($k < 0$) operators $\operatorname{ad} L_k(\zeta)$ to a primary field $\phi(z)$ of conformal weight h. The representation $L_k(\zeta) \mapsto \operatorname{ad} L_k(\zeta)$ together with the infinite-dimensional vector space $V(c,h)$ on which it acts is called a *Verma module.* Here, $V(c,h)$ is spanned by the primary field and the descendent fields spawned by repeated application of the Virasoro generators to these fields, and c is the central charge of the theory. (In an abuse of terminology, we often call $V(c,h)$ the Verma module.) The descendent fields of the parent primary field are $[L_k(\zeta), \phi(z)]$ for some $k \in \mathbb{Z}$, and it is natural to send $\zeta \to z$ so that the descendent fields are local. Letting $\zeta \to z$ in (1.75), we find

$$[L_k(z), \phi(z)] = 0, \quad k \geq 1. \tag{1.81}$$

Thus a primary field is a *highest-weight vector* in a Verma module, and all other nonzero descendant fields in $V(c,h)$ are generated by applying lowering operators to it. Next, when $k = 0, -1$, $[L_k(\zeta), \phi(z)]$ is independent of ζ and is given by (1.78). Finally, when $k < -1$, the limit $\zeta \to z$ diverges, but morally, it should equal (1.74)

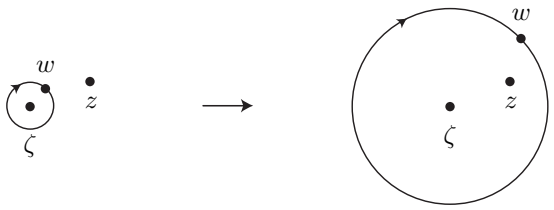

Figure 1.8: Illustration of the normal ordering prescription in (1.82). The point z is placed inside of the integration contour for the stress contour mode before sending $z \to \zeta$.

with the replacement $\zeta \mapsto z$. This direct replacement drops the divergent contribution that arises in the limit and in this sense can be viewed as a generalization of the normal ordering prescription in quantum field theory (figure 1.8). We define this normal ordering by

$$[L_k(\zeta), \phi(z)] \quad \mapsto \quad (L_k\phi)(z) := \frac{1}{2\pi i}\oint_z dw\,(w-z)^{k+1}T(w)\phi(z). \tag{1.82}$$

Repeated application of the lowering operators $\{L_k\}_{k<0}$ to the primary field $\phi(z)$ generates all of its descendants which span $V(c,h)$. Starting from (1.82), they may be defined recursively by

$$\begin{aligned}\phi^{(-k_n,-k_{n-1},\ldots,-k_1)}(z) &= (L_{-k_n}L_{-k_{n-1}}\ldots L_{-k_1}\phi)(z) &(1.83)\\ &:= \frac{1}{2\pi i}\oint_z dw\,(w-z)^{-k_n+1}T(w)\phi^{(-k_{n-1},\ldots,-k_1)}(z). &(1.84)\end{aligned}$$

We call such a field a *level l descendant* of the primary field $\phi(z)$, where $l := k_n + \ldots + k_1$. The collection of a primary field $\phi(z)$ and its descendants is called a *conformal family,* and it is denoted by $[\phi]$. The conformal family constitutes a basis for the infinite dimensional vector space $V(c,h)$, and the subspace $V_l(c,h)$ of level l descendants is spanned by the set of $\phi^{(-k_n,-k_{n-1},\ldots,-k_1)}$ with $l = k_n + \ldots + k_1$ and $1 \le k_n \le \ldots \le k_1$. Thus, the dimension of $V_l(c,h)$ equals the number of integer partitions of l.

We pause to introduce an alternative notation used by physicists. From the per-

spective of quantum field theory, the field is thought to act on a collection of elements in a Hilbert space containing the states of the system under study. In our application, these states are continuum limits of lattice model configurations. This state space is supposed to have a unique vacuum state $|\Omega\rangle$ that physically represents the state of lowest energy, and other states are generated by allowing the field operators of the theory to act on this state. In particular, a primary field $\phi(z)$ of conformal weight h acts on $|\Omega\rangle$ to produce a "state" $|h\rangle := \phi(z)|\Omega\rangle$. Furthermore, we write

$$|\{k_i\}; h\rangle := L_{-k_n} L_{-k_{n-1}} \dots L_{-k_1} |h\rangle := \phi^{(-k_n, -k_{n-1}, \dots, -k_1)}(z)|\Omega\rangle. \tag{1.85}$$

In this notation, (1.81) becomes $L_k|h\rangle = 0$ for $k \geq -1$. We require that the vacuum state is invariant under global conformal transformations, implying that the infinitesimal generators of these transformations, L_{-1}, L_0, and L_1, annihilate it. Using the commutation relations (1.77), we can show that this implies the more general rule

$$L_k|\Omega\rangle = 0, \quad k \geq -1. \tag{1.86}$$

This condition guarantees that the stress tensor one-point function vanishes, indicating that the energy of the vacuum state is zero, as desired.

We briefly describe the transformation properties of the descendant fields. Some descendant fields are quasi-primary, and because they transform identically to their parent primary field under global conformal transformations, $\operatorname{ad} L_1$ must annihilate them according to (1.81). This operator maps the subspace $V_l(c, h)$ of level l states in $V(c, h)$ onto the subspace $V_{l-1}(c, h)$ of level $l - 1$ states. Using (1.77), one can show that L_1 will not annihilate those pre-image states $L_{-k_n} \dots L_{-k_1}|h\rangle$ in $V_l(c, h)$ with $k_n = 1$, and there are exactly enough of these states for their images under L_1 to span $V_{l-1}(c, h)$. Thus, we can choose a basis for $V_l(c, h)$ consisting of these states and those states annihilated by L_1, the latter being quasi-primary. For example, at

the second level of a Verma module generated by the primary field $\phi(z)$, we find the quasi-primary operator

$$\phi^{(-2)}(z) = (L_{-2}\phi)(z) - \frac{3}{2(2h+1)}(L_{-1}L_{-1}\phi)(z). \tag{1.87}$$

Under a stronger restriction, this operator will play a central role in the work presented in this thesis. Now, a straightforward calculation using (1.77) shows that each descendant $|\{k_i\}; h\rangle$ of the highest-weight state $|h\rangle$ is an eigenvector of L_0:

$$L_0|\{k_i\}; h\rangle = (h + k_1 + \ldots + k_n)|\{k_i\}; h\rangle. \tag{1.88}$$

If the descendant field is quasi-primary, then the eigenvalue $h + k_1 + \ldots + k_n$ is its conformal weight. If a descendant field is not primary, then its transformation law under global conformal transformations is usually the holomorphic part of (1.48) with holomorphic weight $h + k_1 + \ldots + k_n$ plus additional correction terms.

Next, we endow the Verma module $V(c, h)$ with an inner product. The subspace $V_l(c, h)$ of level l states is spanned by $|\{k_i\}; h\rangle$ with $k_1 + \ldots + k_n = l$ and $1 \leq k_n \leq \ldots \leq k_1$. For example (figure 1.9),

$$\begin{gathered} V_1(c,h) = \mathrm{span}\{L_{-1}|h\rangle\}, \quad V_2(c,h) = \mathrm{span}\{L_{-1}^2|h\rangle, L_{-2}|h\rangle\} \\ V_3(c,h) = \mathrm{span}\{L_{-1}^3|h\rangle, L_{-1}L_{-2}|h\rangle, L_{-3}|h\rangle\} \end{gathered}. \tag{1.89}$$

If we can define an appropriate Hermitian conjugate for the stress tensor modes, then a Verma module has a natural inner product given by

$$\langle h\,; \{j_i\}|\{k_i\}; h\rangle = \langle h|L_{-j_1}^\dagger \ldots L_{-j_m}^\dagger L_{-k_n} \ldots L_{-k_1}|h\rangle. \tag{1.90}$$

Now, we wish for the spectrum of L_0 to be real since it consists of conformal weights of primary operators, and this is guaranteed if $L_0^\dagger = L_0$. For this and other physical

reasons, it is natural to define $L_k^\dagger := L_{-k}$. Using this definition and the commutators (1.77), we can compute the Gram matrix of the basis for $V(c,h)$ consisting of $|h\rangle$ and its descendent states by pushing all of the positive-index modes in (1.90) from left to right so that they annihilate the vacuum on the right side. We find that states at different levels of $V(c,h)$ are orthogonal to one another, so the Gram matrix is block-diagonal with each block corresponding to a different level subspace $V_l(c,h)$.

A Verma module is called *unitary* if it contains no negative-norm states. It has been shown that a Verma module with $c > 1, h > 0$ or with

$$c = 1 - \frac{6}{m(m+1)}, \quad m \in \mathbb{Z}^+, \tag{1.91}$$

$$h = h_{r,s} := \frac{[(m+1)r - ms)]^2}{4m(m+1)}, \qquad 1 \le r \le m, \quad 1 \le s \le r, \tag{1.92}$$

is unitary while all others are not [36]. In fact, the $h_{r,s}$ are the zeros of the determinant of the Gram matrix, called the *Kac determinant*. We will see that many of the critical lattice models surveyed in (1.1) are described by a CFT with a central charge among (1.91) and that their essential lattice variables are described by primary fields with conformal weights among (1.92).

There exists a simple relationship between a correlation function of primary fields $\phi_1(z_1), \ldots, \phi_N(z_N)$ and the same correlation function with one primary field $\phi_1(z_1)$ replaced by its descendant field $\phi_1^{(-k)}(z_1)$. The relation is

$$\langle \phi_1^{(-k)}(z_1)\phi_2(z_2)\ldots\phi_N(z_N)\rangle = \mathcal{L}_{-k}\langle \phi_1(z_1)\phi_2(z_2)\ldots\phi_N(z_N)\rangle \tag{1.93}$$

with $\mathcal{L}_{-k}$ the differential operator

$$\mathcal{L}_{-k} := \sum_{i=2}^{N}\left[\frac{(k-1)h_i}{(z_i - z_1)^k} - \frac{\partial_i}{(z_i - z_1)^{k-1}}\right], \quad k \ge 1. \tag{1.94}$$

This identity is found by replacing the descendent field $\phi^{(-k)}(z_1)$ on the left side of

(1.93) with its integral representation (1.82) and using the OPE (1.67) to perform the integration by the method of residues. This identity generalize further to

$$\langle \phi_1^{(-k_1,\ldots,-k_n)}(z_1)\phi_2(z_2)\ldots\phi_N(z_N)\rangle = \mathcal{L}_{-k_1}\ldots\mathcal{L}_{-k_n}\langle\phi_1(z_1)\phi_2(z_2)\ldots\phi_N(z_N)\rangle, \quad k_i \geq 1, \quad (1.95)$$

where $\phi_2(z_2),\ldots,\phi_N(z_N)$ are either primary fields or descendants of primary fields. Consequently, if we have an explicit formula for an N-point function of primary fields, then we effectively have an explicit formula for all N-point functions of the descendants of those primary fields too.

By invoking that the spectrum of L_0 is bounded from below, one can argue that a CFT consists of a collection of primary fields and their respective conformal families, and these families consist of quasi-primary fields and derivatives of primary and quasi-primary fields. Then a CFT is essentially a direct sum of the product of Verma modules $V(c,h)\otimes V(c,\bar{h})$ over all primary fields $\phi_{h,\bar{h}}$ in the theory. The second Verma module $V(c,\bar{h})$ in the tensor product pertains to the antiholomorphic sector.

Because the stress tensor is not primary, it must be the descendant of a primary field. Upon examining (1.82), it is apparent that T must be the $\phi^{(-2)}$ descendant of a nonlocal (i.e. independent of z) primary *identity field* $\mathbf{1}$ with the property $\mathbf{1}|\Omega\rangle = |\Omega\rangle$. Such a field necessarily has conformal weight zero and is nonlocal in the sense that its derivative vanishes everywhere.

1.2.5 Operator product expansions of primary fields

An OPE of two fields $\phi_1(z_1)$ and $\phi_2(z_2)$ is a formal series that, when inserted into any correlation function, gives a series representation of the correlation function in powers of the distance between the points for those fields. We have already seen two important examples of OPEs, (1.62) and (1.67).

The requirement of conformal covariance restricts the OPE of two primary fields to the general form (we now include the antiholomorphic sector)

$$\phi_1(z_1,\bar{z}_1)\phi_2(z_2,\bar{z}_2) \underset{z_2\to z_1}{\sim} \sum_{\alpha\in B_0} C_{12}^{\alpha} \sum_{l,\bar{l}\geq 0} z_{21}^{-h_1-h_2+h_\alpha+l}\bar{z}_{21}^{-\bar{h}_1-\bar{h}_2+\bar{h}_\alpha+\bar{l}} \times \sum_{\{k_i\}_l,\{\bar{k}_i\}_{\bar{l}}} \beta_{12}^{\alpha;\{k_i\}_l}\bar{\beta}_{12}^{\alpha;\{\bar{k}_i\}_{\bar{l}}}\phi_{\alpha}^{(-\{k_i\}_l;-\{\bar{k}_i\}_l)}(\zeta,\bar{\zeta}), \quad (1.96)$$

where the first sum is formally over all primary fields in the theory under consideration, the second sum is over all descendant levels, and the third sum is over all partitions $\{k_i\}_l$ of the positive integer l. The α index that appears of the first sum is sometimes called a *fusion channel*, and it has both holomorphic and antiholomorphic entries. Also, z_{21} is the difference $z_2 - z_1$ of the points, $\zeta = tz_1 + (1-t)z_2$ for some $t \in [0,1]$, and the unspecified coefficients β_{12}^{α} depend on t. We usually take $t = 0$ or $1/2$ or 1. Again, variables with bars over them simply pertain to the antiholomorphic sector and are not complex conjugates of the corresponding unbarred variables.

If we insert the OPE (1.96) into a two-point function, then the existence of a identity field among the primary fields appearing in the OPE ensures that the result does not vanish but gives the right side of (1.56). If we insert the OPE (1.96) into a three-point function and use (1.95), then because the conformal weights of two primary fields must be equal in order for their two-point function to not vanish, only one field in the first sum in (1.96) contributes to this series (if we identify all fields with equal conformal weights, which is a common practice but can have some pitfalls in logarithmic CFT). We thus find a series representation for the three-point function in terms of the two-point function. We can also find a similar series representation through straightforward algebra, which imposes a relatively weak constraint on the beta coefficients.

The observations of the previous paragraph illustrate the utility of the OPE. Its insertion into an N-point function of primary fields reduces that correlation function

to a series in derivatives of $(N-1)$-point functions. Repeating this process until a series in derivatives of two-point functions is reached, we find an explicit series representation of the original N-point function. If we do this for all N-point functions of primary fields and use (1.93), then we find series representations for all of the correlation functions in the CFT under consideration. Although this procedure works in principle, it is clearly impractical for large N from a computational point of view. Nonetheless, the OPE allows us to relate primary operators in a new way that will be necessary to describe the reducible structure of the unitary Verma modules in the next section.

In order for this method to be useful, the requirement of conformal invariance must be strong enough to determine the coefficients C_{12}^{α} and $\beta_{12\alpha}^{\alpha;\{k_n\}_l}$, and in fact, this is true. Demanding that both sides of (1.96) transform identically under the conformal transformation $f(z) = z + \epsilon_k (z-\zeta)^{k+1}$ that is infinitesimal at z_1 and z_2 for each integer $k \geq -1$ determines a system of $p(l)$ equations in the unkowns $\beta_{12}^{\alpha;\{k_n\}_l}$ for each level l, where $p(l)$ is the integer partition function. If $t = 1$ and the system is invertible, then the first few β_{12}^{α} are given by

$$\beta_{12}^{\alpha;\{1\}} = \Big((h_\alpha + h_1 - h_2)\beta_{12}^{\alpha;\{0\}}\Big)/2, \tag{1.97}$$

$$\begin{aligned}\beta_{12}^{\alpha;\{1,1\}} &= \Big(-12h_1h_\alpha + 6h_2h_\alpha - 6h_\alpha^2)\beta_{12}^{\alpha;\{0\}} + (c(1 + h_1 - h_2 + h_\alpha) \\ &+ 8(h_\alpha + h_1h_\alpha - h_2h_\alpha + h_\alpha^2))\beta_{12}^{\alpha;\{1\}}\Big)\Big(2(c + 2(c-5)h_\alpha + 16h_\alpha^2)\Big)^{-1},\end{aligned} \tag{1.98}$$

$$\begin{aligned}\beta_{12}^{\alpha;\{2\}} &= \Big(2h_\alpha(-h_2 + h_\alpha - 2h_2h_\alpha + 2h_\alpha^2 + 2h_1(1 + 2h_\alpha))\beta_{12}^{\alpha;\{0\}} \\ &- 6h_\alpha(1 + h_1 - h_2 + h_\alpha)\beta_{12}^{\alpha;\{1\}}\Big)\Big(c + 2(c-5)h_\alpha + 16h_\alpha^2\Big)^{-1}.\end{aligned} \tag{1.99}$$

The antiholomoprhic coefficients $\bar{\beta}_{12}^{\alpha;\{\bar{k}_i\}}$ are the same as their holomorphic counterparts after replacing the holomorphic weights with antiholomorphic weights. We note that the first coefficient $\beta_{12}^{\alpha;\{0\}}$ is not fixed by this method, but all other coefficients are multiples of it, so it can be absorbed into C_{12}^{α}. All of the systems of equations for

these coefficients are invertible whenever the Kac determinant is nonzero.

By inserting the OPE (1.96) into the three-point function (1.57), we immediately see that the OPE coefficient C_{12}^3 is simply the coefficient C_{123} of the three-point function. C_{12}^3 is usually computed by exploiting the so-called *crossing symmetry* of the four-point function. That is, within the four-point function, we let $z_2 \to z_1$ and $z_4 \to z_3$, and we substitute the OPE (1.96) for both limits to find (showing only the holomorphic sector for now)

$$\begin{aligned}&\langle\phi_1(z_1)\phi_2(z_2)\phi_3(z_3)\phi_4(z_4)\rangle \\ &\qquad \underset{\substack{z_2\to z_1\\ z_4\to z_3}}{\sim} \sum_{\alpha,\,\beta\in B_0} C_{12}^{\alpha} C_{34}^{\beta} z_{21}^{-h_1-h_2+h_\alpha} z_{43}^{-h_3-h_4+h_\beta} \langle\phi_\alpha(z_1)\phi_\beta(z_3)\rangle + \dots \end{aligned} \tag{1.100}$$

The structure of the two-point function (1.56) shows that only terms with $\alpha = \beta$ contribute to the expansion. This expansion prompts us to suppose that we may decompose $G_{ij:kl}$, defined in (1.61), into a sum of products of *conformal blocks* $\mathcal{F}_{ij:kl}^{\alpha}(\eta)$ and $\bar{\mathcal{F}}_{ij:kl}^{\alpha}(\bar{\eta})$ as follows:

$$G_{ij:kl}(\eta) = \sum_{\alpha\in B_0} C_{ij}^{\alpha} C_{kl}^{\alpha} \mathcal{F}_{ij:kl}^{\alpha}(\eta) \bar{\mathcal{F}}_{ij:kl}^{\alpha}(\bar{\eta}). \tag{1.101}$$

Here, $\mathcal{F}_{ij:kl}^{\alpha}(\eta)$ (resp. $\bar{\mathcal{F}}_{ij:kl}^{\alpha}(\bar{\eta})$) is the holomorphic (resp. antiholomorphic) part of the series in the OPE of $\phi_i(0)\phi_j(\eta)$ pertaining to the α conformal family. In this context, the crossing relations (1.60) become

$$\sum_{\alpha\in B_0} C_{ij}^{\alpha} C_{kl}^{\alpha} \mathcal{F}_{ij:kl}^{\alpha}(\eta) \mathcal{F}_{ij:kl}^{\alpha}(\bar{\eta}) = \sum_{\alpha\in B_0} C_{kj}^{\alpha} C_{il}^{\alpha} \mathcal{F}_{kj:il}^{\alpha}(1-\eta) \mathcal{F}_{kj:il}^{\alpha}(1-\bar{\eta}) \tag{1.102}$$

$$= \eta^{-2h_j} \bar{\eta}^{-2\bar{h}_j} \sum_{\alpha\in B_0} C_{lj}^{\alpha} C_{ki}^{\alpha} \mathcal{F}_{lj:ki}^{\alpha}(1/\eta) \mathcal{F}_{lj:ki}^{\alpha}(1/\bar{\eta}). \tag{1.103}$$

(The sums are only formal, as they make sense only when B_0 is finite. Such theories, called minimal models, will be examined in the next section.) These two conditions,

when considered over arbitrary choices of primary fields $i, j, k, l \in B_0$ are supposed to completely fix the three-point function coefficient C_{ij}^{α}.

Later, we will loosely refer to (the holomorphic or antiholomorphic part of) a $2N$-point function of primary fields in which these fields are collected into pairs whose respective OPEs pass through exactly one channel as a "conformal block."

1.2.6 Null states, fusion rules, and minimal models

Suppose that the Verma module $V(c,h)$ has a descendant field at level l that is primary. Such a descendant, called a *null-state,* is the highest-weight state of its own Verma submodule $V(c,h+l) \subset V(c,h)$ consisting of its own descendants. Because this submodule is invariant under the action of the stress tensor modes, its presence inside $V(c,h)$ deems the larger module reducible. A null-state earns its name from the fact that it has zero norm and a zero inner product with all other elements of $V(c,h)$. In this section, we investigate the reducibility of the Verma modules that contain null-states, and we will observe how the presence of null-states within a Verma module leads to new PDEs that govern certain correlation functions.

Because it is primary, a null-state $|h+l\rangle$ must be annihilated by the modes $\{L_k\}_{k\geq 1}$, and we can show that this property follows if $L_1|h+l\rangle = L_2|h+l\rangle = 0$ by using the commutation relations of the Virasoro algebra (1.77). These two conditions restrict h to particular values, and they lead to explicit expressions for the null-states. For example, in order for $|h+1\rangle = L_{-1}|h\rangle$ to be a level one null-state, we must have $L_1|h+1\rangle = L_2|h+1\rangle = 0$. By using (1.77), we can show that the conformal weight h of the highest-weight state $|h\rangle$ must be zero. We call this conformal weight $h_{1,1}$.

Next, we construct a level two null-state, which necessarily has the form $|h+2\rangle = (aL_{-1}^2 - L_{-2})|h\rangle$ for $a \in \mathbb{C}$. The condition that $L_1|h+2\rangle = 0$ makes this state quasi-primary and fixes $a = 3/2(2h+1)$ as in (1.87). The condition that $L_2|h+2\rangle = 0$ makes this state primary and fixes h to one of the following two functions of the

central charge:

$$\begin{cases} h = h_{1,2} := \frac{1}{16}\left[5 - c + \sqrt{(c-1)(c-25)}\right] \\ h = h_{2,1} := \frac{1}{16}\left[5 - c - \sqrt{(c-1)(c-25)}\right] \end{cases} . \tag{1.104}$$

Thus, the Verma modules $V(c, h_{1,2})$ and $V(c, h_{2,1})$ each contain a level two null-state.

We let $\phi_{1,2}$ denote a primary field of conformal weight $h_{1,2}$. Because its level two null-state is necessarily orthogonal to the other elements of its parent Verma module $V(c, h_{1,2})$, any N-point function that contains it must vanish. We therefore have

$$\left\langle \left[\frac{3}{2(2h_{1,2}+1)} \phi_{1,2}^{(-1,-1)}(z_1) - \phi_{1,2}^{(-2)}(z_1) \right] \phi_2(z_2) \dots \phi_N(z_N) \right\rangle = 0. \tag{1.105}$$

Using (1.93), we factor the stress tensor modes out into differential operators acting on the N-point function. In so doing, (1.105) becomes the following semi-elliptic PDE governing the correlation function $\langle \phi_{1,2}(z_1)\phi_2(z_2)\dots\phi_N(z_N)\rangle$:

$$\left[\frac{3\partial_1^2}{2(2h_{1,2}+1)} + \sum_{j=2}^{N} \left(\frac{\partial_j}{z_j - z_1} - \frac{h_j}{(z_j - z_1)^2} \right) \right] \langle \phi_{1,2}(z_1)\phi_2(z_2)\dots\phi_N(z_N)\rangle = 0. \tag{1.106}$$

Here, we have used translation invariance to write $\mathcal{L}_{-1} = -\partial_2 - \ldots - \partial_N = \partial_1$. This PDE is central to the work presented in this thesis. It will prove essential in studying interfaces between boundary clusters in lattice models. A similar PDE may be inferred from the level-two null-state in $V(c, h_{2,1})$ by replacing $(h_{1,2}, \phi_{1,2}) \mapsto (h_{2,1}, \phi_{2,1})$.

Equation (1.106) does not place new restrictions on the two-point function (1.56) with $h_1 = h_{1,2}$ or $h_{2,1}$. However, (1.106) restricts the conformal weight h_3 of the primary operator $\phi_3(z_3)$ in the three-point function $\langle \phi_1(z_1)\phi_2(z_2)\phi_3(z_3)\rangle$ with $h_1 = h_{1,2}$ or $h_{2,1}$ to one of two values depending on h_2:

$$h_1 = h_{1,2}, \quad \Longrightarrow \quad h_3 = h_{1,2} + h_2 + \Delta^{\pm}_{1,2}(h_2, c), \tag{1.107}$$

$$h_1 = h_{2,1}, \quad \Longrightarrow \quad h_3 = h_{2,1} + h_2 + \Delta^{\pm}_{2,1}(h_2, c). \tag{1.108}$$

Here, $\Delta^{\pm}_{1,2}$ and $\Delta^{\pm}_{2,1}$ are given by

$$\begin{aligned}
\Delta^{\pm}_{1,2}(h,c) &= \frac{1}{24}\left[c - 1 + \sqrt{(1-c)(25-c)} \pm |\sqrt{25-c} - \sqrt{1-c}|\sqrt{1-c+24h}\right], \\
\Delta^{\pm}_{2,1}(h,c) &= \frac{1}{24}\left[c - 1 - \sqrt{(1-c)(25-c)} \pm |\sqrt{25-c} + \sqrt{1-c}|\sqrt{1-c+24h}\right].
\end{aligned}$$

If the third conformal weight h_3 does not equal either of the two allowed values that are shown above, then the three-point function is necessarily zero. We note that $\Delta^{+}_{1,2}(h,c)$ is the famous KPZ formula from Liouville quantum gravity [37].

The rule (1.107, 1.108) is expressed more clearly if we define the variables

$$\alpha_{\pm} := \frac{\sqrt{1-c} \pm \sqrt{25-c}}{\sqrt{24}}, \quad \chi_0 := \frac{c-1}{24}, \tag{1.109}$$

and parameterize the conformal weight h in terms of a variable χ as

$$h(\chi) = \frac{\chi^2}{4} + \chi_0^2. \tag{1.110}$$

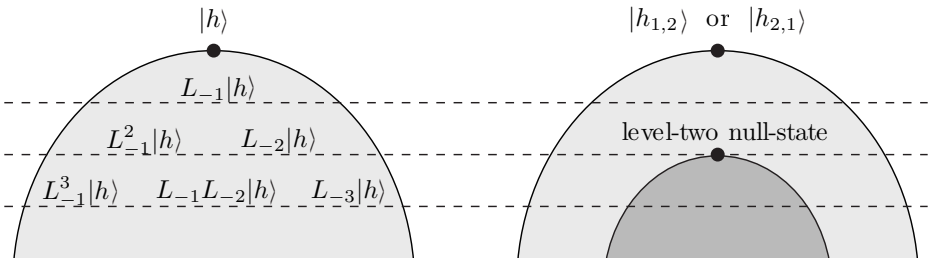

Figure 1.9: The graded structure of a generic Verma module (left), and the level-two null-state of either Verma module $V_{1,2}$ or $V_{2,1}$ and its submodule (right).

(In section 1.2.9, α_0 will serve as the background charge of the Coulomb gas.) Then the above results imply that in a three-point function $\langle\phi_1(z_1)\phi_2(z_2)\phi_3(z_3)\rangle$ with $h_1 = h_{1,2}$ or $h_{2,1}$, either the weights $h_3 = h(\chi_3)$ and $h_2 = h(\chi_2)$ are related by

$$h_3 = h(\chi_3), \quad \chi_3 = \begin{cases} \chi_2 + \alpha_- \text{ or } \chi_2 - \alpha_- & h_1 = h_{1,2} \\ \chi_2 + \alpha_+ \text{ or } \chi_2 - \alpha_+ & h_1 = h_{2,1} \end{cases}, \tag{1.111}$$

or else the three-point function is zero. This selection rule limits the number of channels that can appear in the OPE (1.96) of the primary fields $\phi_{1,2}$ or $\phi_{2,1}$ with ϕ_2 to two possibilities. Letting $\phi_{1,2}, \phi_{2,1}$, and ϕ_χ stand for fields with weights $h_{1,2}, h_{2,1}$, and $h(\chi)$ respectively, we express this rule as

$$\begin{aligned} [\phi_{1,2}] \times [\phi_\chi] &= [\phi_{\chi-\alpha_-}] + [\phi_{\chi+\alpha_-}] \\ [\phi_{2,1}] \times [\phi_\chi] &= [\phi_{\chi-\alpha_+}] + [\phi_{\chi+\alpha_+}] \end{aligned}. \tag{1.112}$$

This abuse of notation requires explanation. The $\times$ sign on the left side indicates a type of multiplication between conformal families called *fusion.* Meanwhile, the $+$ sign on the right side indicates not a literal sum but a statement of what conformal families appear in the OPE of $\phi_{1,2}$ or $\phi_{2,1}$ with ϕ_χ.

If we continue this analysis, then we ultimately find that a Verma module $V(c, h_{r,s})$ with highest-weight vector $\phi_{r,s}$ with conformal weight

$$h_{r,s} := \frac{1}{4}(r\alpha_+ + s\alpha_-)^2 - \alpha_0^2, \quad r, s \in \mathbb{Z}^+, \tag{1.113}$$

$$= \frac{1-c}{96}\left[\left(r + s + (r-s)\sqrt{\frac{25-c}{1-c}}\right)^2 - 4\right], \tag{1.114}$$

called a *Kac weight*, has a null-state at level rs. This is a consequence of the fact that the conformal weights of (1.113) exhaust the zeros of the Kac determinant. The primary field $\phi_{r,s}$ of conformal weight $h_{r,s}$ is called a *Kac operator.* Equation (1.112)

generalizes further to [11]

$$[\phi_{r,s}] \times [\phi_\chi] = \sum_{\substack{k=1-r \\ k+r=1 \,(\mathrm{mod}2)}}^{k=r-1} \sum_{\substack{l=1-s \\ l+s=1 \,(\mathrm{mod}2)}}^{l=s-1} [\phi_{\chi+k\alpha_++l\alpha_-}]. \tag{1.115}$$

(The summation index increments by two.) We note that $\phi_{1,1}$ serves as the identity field in this fusion rule, with conformal weight $h_{1,1} = 0$.

By exploiting the commutativity of the fusion operation, one can argue that the product of two Kac operators will exclusively contain Kac operators and consist of fewer fields than indicated in (1.115), a phenomenon called *truncation.* The new rule is

$$[\phi_{r_1,s_1}] \times [\phi_{r_2,s_2}] = \sum_{\substack{k=1+|r_1-r_2| \\ k+r_1+r_2=1 \,(\mathrm{mod}2)}}^{k=r_1+r_2-1} \sum_{\substack{l=1+|s_1-s_2| \\ l+s_1+s_2=1 \,(\mathrm{mod}2)}}^{l=s_1+s_2-1} [\phi_{k,l}], \tag{1.116}$$

and it exemplifies a CFT whose primary field content comprises of only a countable collection of Kac operators.

We might further speculate on the existence of a CFT comprised of a finite collection B_0 of conformal families of Kac operators. In such a theory, the other Kac operators in (1.116) that arise in the OPEs of the elements in B_0 appear as descendants of the other Kac operators in B_0. Indeed, this phenomenon is observed in CFTs with a central charge such that $p\alpha_- + p'\alpha_+ = 0$ for p, p' coprime. After isolating the central charge from this relation, we find that

$$c = 1 - 6\frac{(p-p')^2}{pp'}, \quad p', p \text{ coprime}, \tag{1.117}$$

and if we order the indices so that $p' < p$, then the Kac weights are

$$h_{r,s} = \frac{(pr - p's)^2 - (p-p')^2}{4pp'}. \tag{1.118}$$

Such a theory is called a (p, p') *minimal model,* and it is generated through fusions of

Kac operators among the finite set $B_0 = \{\phi_{r,s} \,:\, 1 \leq r < p', 1 \leq s < p\}$.

Now we verify the claims of the previous paragraph. To start, we divide the $\mathbb{Z}^+ \times \mathbb{Z}^+$ lattice, called the *conformal grid,* into the *boxes*

$$\{(r,s) \in \mathbb{Z}^+ \times \mathbb{Z}^+ \,:\, (m-1)p' < r < mp', (n-1)p < s < np\}, \quad m,n \in \mathbb{Z}^+. \tag{1.119}$$

Figure 1.11 shows part of the conformal grid divided into boxes for the $(4,3)$ minimal model. Each box contains $(p-1)(p'-1) = 6$ lattice points, and each Kac weight $h_{r,s}$ is represented by a colored disk at the lattice point (r,s), possibly with a slash passing through it. A disk of a particular color and with its slash (if it has one) pointing in a particular direction identifies a conformal weight that is unique within that box. From (1.118), we immediately see that

$$h_{r,s} = h_{r+p',s+p}, \quad h_{r,s} = h_{p'-r,p-s}. \tag{1.120}$$

The first property identifies all boxes that live on the same $\pi/4$ radian diagonal, and figure 1.11 indicates this property by using identical illustrations for these boxes. The figure also shows that Kac operators with either the r index equaling a multiple of p' or the s-index equaling a multiple of p are excluded from the theory since these operators are equivalent to Kac operators in the zeroth row or column. These operators lie outside of the conformal grid and thus outside of the theory. Consequently, the entire operator content of the theory belongs to the boxes in (1.119). The second property of (1.120) indicates that half of the conformal grid is redundant, and this redundancy is illustrated in figure 1.11 as follows. Two disks of the same color, with their slashes pointing in the same direction (if they both have a slash), and belonging to boxes with the same background shade of gray have equal conformal weights.

We call the bottom-left box in figure 1.11 the *Kac table.* Half of the Kac table is redundant as each point (r,s) on one side of the line connecting $(0,0)$ with (p,p') is

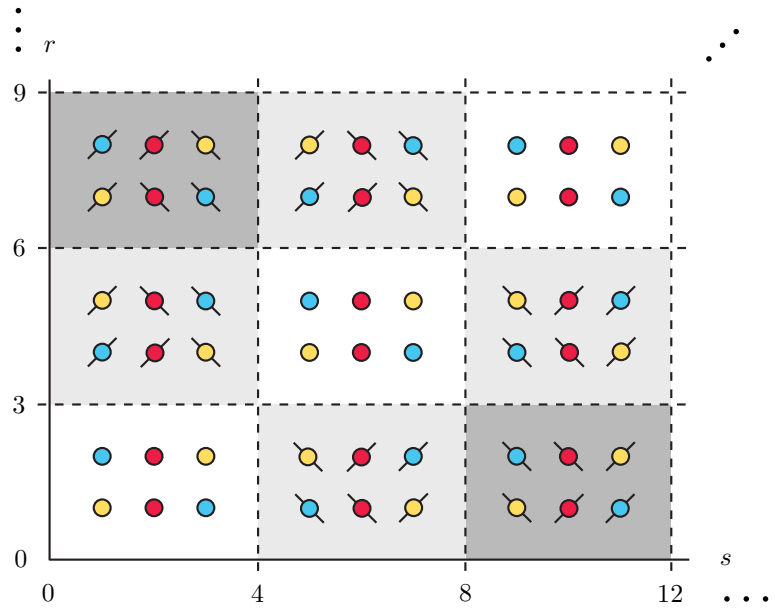

Figure 1.10: The conformal grid for the $(4, 3)$ minimal model. The bottom-left box is the Kac table. Boxes with the same shade of gray are identified with one another.

identified with another point $(p' - r, p - s)$ on the other side of the diagonal thanks to the reflection property $h_{r,s} = h_{p'-r,p-s}$ of (1.120). The disks corresponding to these two points in the Kac table are identified with each other in figure 1.11 by having both the same color and no slash passing through them. This reflection property also indicates that, in addition to its level rs null-state, the module $V_{r,s} := V(c_{p,p'}, h_{r,s})$, will harbor a null-state at level $(p' - r)(p - s)$. These two null-states have respective conformal weights

$$h_{r,s} + rs = h_{p'-r,p+s} = h_{p'+r,p-s}, \tag{1.121}$$

$$h_{r,s} + (p' - r)(p - s) = h_{r,2p-s} = h_{2p'-r,s}. \tag{1.122}$$

Remarkably, these conformal weights are Kac weights of the box immediately above or right of the Kac table. This is indicated by the gray background color of the plaquettes on the right side of (1.121-1.122). Therefore, these two null-states are also Kac operators which in turn generate their own Verma modules $V_{p'-r,p+s} \cong V_{p'+r,p-s}$

and $V_{r,2p-s} \cong V_{2p'-r,s}$, each with their own two null-states. The null-states of $V_{p'-r,p+s}$ are

$$h_{p'-r,p+s} + (p'-r)(p+s) = h_{r,2p+s} = h_{3p'-r,p-s}, \tag{1.123}$$

$$h_{p'-r,p+s} + (p'+r)(p-s) = h_{p'-r,3p-s} = h_{2p'+r,s}, \tag{1.124}$$

while the null-states of $V_{r,2p-s}$ are

$$h_{r,2p-s} + r(2p-s) = h_{p'-r,3p-s} = h_{2p'+r,s}, \tag{1.125}$$

$$h_{r,2p-s} + (2p'-r)s = h_{r,2p+s} = h_{3p'-r,p-s}. \tag{1.126}$$

The fact that weight (1.123) equals weight (1.126) (resp. weight (1.124) equals weight (1.125)) indicates that the corresponding null-states are identical and belong to the same box along the bottom or left side of the conformal grid. Therefore, the two null-states $\phi_{p'-r,p+s}$ and $\phi_{p'+r,p-s}$ generate the same two null-states $\phi_{r,2p+s}$ and $\phi_{p'-r,3p-s}$ which live in the intersection $V_{p'-r,p+s} \cap V_{r,2p-s}$. These null-states in turn spawn their own Verma modules $V_{r,2p+s} \cong V_{3p'-r,p-s}$ and $V_{p'-r,3p-s} \cong V_{2p'+r,s}$ which share two null-states (also with Kac weights) in their intersection, and so on. This pattern

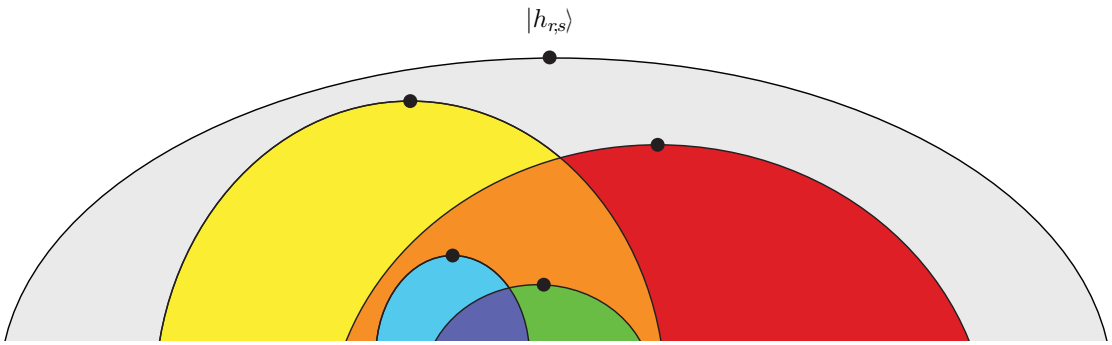

Figure 1.11: The infinite sequence of nested Verma submodules within the parent module $V_{r,s}$ in the (p,p') minimal model. The yellow and red submodules are $V_{p'-r,p+s} \cong V_{p'+r,p-s}$ and $V_{r,2p-s} \cong V_{2p'-r,s}$ respectively, and the blue and green submodules are $V_{r,2p+s} \cong V_{3p'-r,p-s}$ and $V_{p'-r,3p-s} \cong V_{2p'+r,s}$ respectively.

repeats indefinitely, and we find that $V_{r,s}$ contains a single infinite tower of pairs of Verma submodules with each of their intersections nesting yet another pair of Verma submodules. Each Verma module is generated by a null-state whose Kac weight belongs to a box along the bottom or left side of the conformal grid (figure 1.11). In fact, one can show that any Kac operator belonging to one of these boxes is a null-state descendant of a Kac operator in the Kac table. After identifying these boxes with their diagonals thanks to the left equation of (1.120), we see that each Kac operator generated by the OPE of two members of the conformal grid is a descendant of another member of the Kac table. In other words, the (p, p') minimal model comprises of a finite number of conformal families, namely those that belong to the Kac table.

Minimal models apparently exhibit very rich structure. With this structure now essentially understood, we can consider how to combine the holomorphic and anti-holomorphic minimal models into one theory. This question is typically answered by requiring this combination to be invariant under modular transformations [3, 11]. One possibility that achieves this goal is for all operators to be spinless. Such a theory is called a diagonal minimal model and is denoted by $\mathcal{M}(p, p')$. Modular invariant non-diagonal theories may be constructed too, and some of them give more authentic representations of continuum lattice models than any diagonal theory. However, we will not investigate such theories in this thesis.

The minimal model $\mathcal{M}(p, p')$ is unitary if each of its Verma modules $V_{r,s}$ with $1 \leq r < p', 1 \leq s < p$, are unitary. Because h must be positive in order for $V(c, h)$ to be unitary, a unitary minimal model contains no negative Kac weights. This condition is physically reasonable as it implies that all two-point functions decay with distance. An argument invoking Bezout's lemma indicates that only the $\mathcal{M}(p, p-1)$ minimal models are unitary [11], and upon letting $p = m + 1, p' = m$ in (1.117) and (1.118), we indeed recover the $c < 1$ unitary Verma modules of (1.91, 1.92).

1.2.7 Diagonal unitary minimal models and critical lattice models

The diagonal unitary minimal models $\mathcal{M}(m+1,m)$ describe many important critical lattice models, including many of those surveyed in section 1.1. In this section, we examine some of these descriptions.

The first diagonal unitary minimal model $\mathcal{M}(3,2)$ ($c=0$) describes the continuum limit of critical bond percolation via the FK bonds of a $Q=1$ Potts model. This minimal model consists of a single field $\phi_{1,2} \cong \phi_{1,1}$, the identity field, so this description is trivial in the same sense that a single-state Potts model is trivial. In reality, critical percolation is very rich with interesting observables that stem from fields that are not present in $\mathcal{M}(3,2)$ but are present in minimal model representations of Q-state Potts model with $Q>1$, and they are studied through a suitable $Q \to 1$ limit. We will study some of these observables later.

The smallest nontrivial diagonal unitary minimal model $\mathcal{M}(4,3)$ ($c=1/2$) describes the continuum limit of the Ising model [10]. It contains three conformal families, one corresponding with a spin density field σ, another corresponding with an energy density field ε, and a final corresponding with an identity field $\mathbf{1}$.

$$\phi_{1,1} \cong \phi_{2,3} \qquad \Longleftrightarrow \qquad \mathbf{1} \qquad \text{Identity,} \tag{1.127}$$

$$\phi_{1,2} \cong \phi_{2,2} \qquad \Longleftrightarrow \qquad \sigma \qquad \text{Spin Density,} \tag{1.128}$$

$$\phi_{1,3} \cong \phi_{2,1} \qquad \Longleftrightarrow \qquad \varepsilon \qquad \text{Energy Density.} \tag{1.129}$$

The fusion table follows from (1.116):

$$[\sigma]\times[\sigma]=[\mathbf{1}]+[\varepsilon], \quad [\sigma]\times[\varepsilon]=[\sigma], \quad [\varepsilon]\times[\varepsilon]=[\mathbf{1}]. \tag{1.130}$$

The identification of $\mathcal{M}(4,3)$ with the critical Ising model is made by comparing the scaling weights of the former with those calculated in the exact solution of the latter.

The result is

$$\begin{aligned} \langle \sigma(z_i)\sigma(z_j)\rangle &\propto \frac{1}{|z_i - z_j|^{2\Delta_\sigma}} \qquad \Longrightarrow \qquad h_\sigma = \Delta_\sigma/2 = 1/16 = h_{1,2}, \\ \langle \varepsilon(z_i)\varepsilon(z_j)\rangle &\propto \frac{1}{|z_i - z_j|^{2\Delta_\varepsilon}} \qquad \Longrightarrow \qquad h_\varepsilon = \Delta_\varepsilon/2 = 1/2 = h_{1,3}, \end{aligned} \tag{1.131}$$

which leads to the identification (1.127-1.129) above. With this identification, we find the three-point functions of these fields via (1.57). We can also calculate four-point functions of these fields by solving the $\phi_{1,2}$ and $\phi_{2,1}$ null-state PDEs, which reduce to hypergeometric ODEs in the unknown function G when the ansatz (1.58) is used. Certain details concerning how to join the holomorphic and antiholomorphic sectors must be addressed too, but we will not consider them here.

The next nontrivial diagonal unitary minimal model $\mathcal{M}(5,4)$ ($c = 7/10$) describes the tricritical Ising model [38], which may be realized as a generalization of the Ising model that allows site vacancies. This model contains a second "spin" variable τ_i, equaling zero (resp. one) if site i is vacant (resp. occupied) and that complements the usual spin variable σ_i which exists only for occupied sites. The energy of a spin configuration $\{(\sigma,\tau)\}$ is defined to be

$$E[\{(\sigma,\tau)\}] = -\sum_{\langle ij\rangle} \tau_i^2\tau_j^2(\delta_{\sigma_i,\sigma_j} + J) - \mu\sum_i \tau_i. \tag{1.132}$$

The first sum assigns energy $J+1$ (resp. J) to each pair of equal (resp. unequal) nearest-neighbor spins, and the second sum controls the number of vacancies via a chemical potential μ. Similar to the regular Ising model, one can associate an energy density with each of the three terms in (1.132). The identity, two spin densities, and three energy densities correspond one-to-one with the six conformal families of $\mathcal{M}(5,4)$. The correspondence is

$$\phi_{1,s} \cong \phi_{3,5-s}, \quad 1 \le s < 2 \qquad \Longleftrightarrow \qquad \text{Identity}, \tag{1.133}$$

$$\phi_{2,s} \cong \phi_{2,5-s}, \quad 1 \leq s < 3 \qquad \Longleftrightarrow \qquad \text{Spin Density}, \tag{1.134}$$

$$\phi_{3,s} \cong \phi_{1,5-s}, \quad 1 \leq s < 4 \qquad \Longleftrightarrow \qquad \text{Energy Density}, \tag{1.135}$$

and their respective weights and fusion rules given by (1.118) and (1.116) respectively.

The next unitary model $\mathcal{M}(6,5)$ ($c = 4/5$) comprises of ten conformal families with a sub-algebra of six families that closes under fusion. This sub-algebra describes the three-state Potts model [39], and it contains an identity field $\mathbf{1}$, a spin field σ, an energy field ε, and three additional fields X and Y related to the energy density and Z related to the spin density. However, it does not capture the entire three-state Potts model because it is not symmetric under the parity transformation $(\sigma, Z) \mapsto (-\sigma, -Z)$. A better description of this model is furnished by a modular-invariant non-diagonal minimal model [11].

For $Q \in \{1, 2, 3, 4\}$, the relation between m and Q is given by [3]

$$Q = 4\cos^2\left(\frac{\pi}{m+1}\right), \tag{1.136}$$

(The case $Q = 4$ corresponds with $m \to \infty$.) The spin density field and energy density field are respectively identified with the Kac operators

$$\sigma \cong \phi_{\frac{m+1}{2},\frac{m-1}{2}} \cong \phi_{\frac{m+1}{2},\frac{m+1}{2}} \cong \phi_{1/2,0}, \quad \varepsilon \cong \phi_{2,1} \cong \phi_{m-1,m-1}, \tag{1.137}$$

through their scaling exponents, which are computed in [40] using renormalization group methods.

All of the $\mathcal{M}(m+1,m)$ models represent a lattice model of some kind, for example the restricted solid-on-solid model when $m \geq 3$ [11]. In many of these examples, other operators outside of the Kac table have a physical interpretation in these theories, as can be seen in (1.137). We will describe some of these additional operators and the roles that they play in the next section.

1.2.8 Boundary conformal field theory and Schramm-Löwner evolution

The CFTs presented so far reside on the extended complex plane. It is also useful to formulate CFT in a simply connected domain $\mathcal{D} \subset \mathbb{C}$ with a (for now) smooth boundary $\partial\mathcal{D}$ such as the upper half-plane $\mathbb{H}$. In this section, we will investigate how to construct such a theory.

As usual, we suppose that the critical system under study is conformally invariant. By this, we now mean the following. Consider a conformal bijection taking a simply connected domain onto another simply connected domain, and suppose that a critical lattice model lives in the first domain. (For now, we assume that the BC is free.) Then in the continuum limit, the likelihood of any event of the image model in the second domain equals that of the original model in the first domain. This conjecture was originally supported by strong numerical evidence [41, 42] (resp. [43]) and subsequently proven for percolation and the Ising model in [16] and [44] respectively.

To be specific, we suppose that the first domain is the upper half-plane $\mathbb{H}$, and we let f be a conformal bijection taking $\mathbb{H}$ onto a simply connected domain $\mathcal{D}$. (Such a mapping always exists thanks to the Riemann mapping theorem.) Then conformal invariance implies the usual covariant transformation rule (1.49) relating an N-point function $\Upsilon^{\mathcal{D}}$ of primary fields with domain $\mathcal{D}$ to one $\Upsilon^{\mathbb{H}}$ with domain $\mathbb{H}$. This is

$$\Upsilon^{\mathcal{D}}(z_1', \bar{z}_1', \ldots, z_N', \bar{z}_N') = \prod_{i=1}^{N} \partial f(z_i)^{-h_i} \bar{\partial} \bar{f}(\bar{z}_i)^{-\bar{h}_i} \Upsilon^{\mathbb{H}}(z_1, \bar{z}_1, \ldots, z_N, \bar{z}_N). \tag{1.138}$$

Thus, calculating an N-point function $\Upsilon^{\mathcal{D}}$ of primary fields amounts to computing its half-plane version $\Upsilon^{\mathbb{H}}$ and transforming it to $\mathcal{D}$ using (1.138). (To simplify our notation, we will suppress the superscript $\mathbb{H}$ on all half-plane N-point functions from now on.) We presently think of the antiholomorphic section as a completely independent copy of the holomorphic sector, but later, we will set $\bar{z} = z^*$ and $\bar{f} = f^*$. If f is a global conformal bijection taking the upper half-plane onto itself (that is, a

Möbius transformation (1.40) with a, b, c, and d real), then we recover the functional equation (1.46). The usual conformal Ward identities (2.2) follow by considering the infinitesimal global conformal transformations $\epsilon(z) = a$, bz, or cz^2 that carry the half-plane onto itself (i.e., a, b, c are real and infinitesimal), and they restrict the half-plane N-point function Υ to the usual ansatz (1.58). Again, transformation law (1.138) motivates us to suppose that the transformation law for the primary fields is

$$\phi'_{h,\bar{h}}(z', \bar{z}') = \partial f(z)^{-h} \bar{\partial} \bar{f}_i(\bar{z})^{-\bar{h}} \phi_{h,\bar{h}}(z, \bar{z}). \tag{1.139}$$

Now we motivate a method, similar to the method of images in electrostatics, for computing the half-plane N-point function

$$\Upsilon^{\mathbb{H}}(z_1, \bar{z}_1, \ldots, z_N, \bar{z}_N) = \langle \phi_{h_1,\bar{h}_1}(z_1, \bar{z}_1) \ldots \phi_{h_N,\bar{h}_N}(z_N, \bar{z}_N) \rangle_{\mathbb{H}}. \tag{1.140}$$

This method was originally proposed by J. Cardy in [45]. Because the holomorphic and antiholomorphic coordinates live in different half-planes, and because we ultimately wish to set $\bar{z}_i = z_i^*$, it is convenient to position $z_1, \ldots, z_N$ in the upper half-plane $\mathbb{H}$ and $\bar{z}_1, \ldots, \bar{z}_N$ in the lower half-plane $\mathbb{H}^*$. We let $\mathcal{D}$ be a large, bounded domain containing $z_1, \ldots, z_N, \bar{z}_1, \ldots, \bar{z}_N$, and we let $\epsilon(z)$ (resp. $\bar{\epsilon}(\bar{z})$) be a conformal transformation of $\mathbb{H}$ (resp. $\mathbb{H}^*$) that is infinitesimal in $\mathcal{D}$. The variation law (1.64) is still true as long as the contour surrounding the holomorphic (resp. antiholomorphic) coordinates is in $\mathbb{H}$ (resp. $\mathbb{H}^*$). Because the contour surrounding the antiholomorphic coordinates is in the lower half-plane, its orientation is now counterclockwise. Next, we suppose that $\epsilon(z)$ and $\bar{\epsilon}(\bar{z})$ are real-valued and equal on $\mathbb{R} \cap \mathcal{D}$. Then in $\mathcal{D} \cap \mathbb{H}^*$, $\bar{\epsilon}$ must be the Schwarz-reflection of ϵ in $\mathcal{D} \cap \mathbb{H}$. We further require that the stress tensor satisfy $T(x) = \bar{T}(x)$ for $x \in \mathbb{R}$, which may be interpreted as the condition that energy does not cross the system boundary (the real axis). Thus, the integrands of the two integrals of the variation law (1.64) are identical, and their contours may be

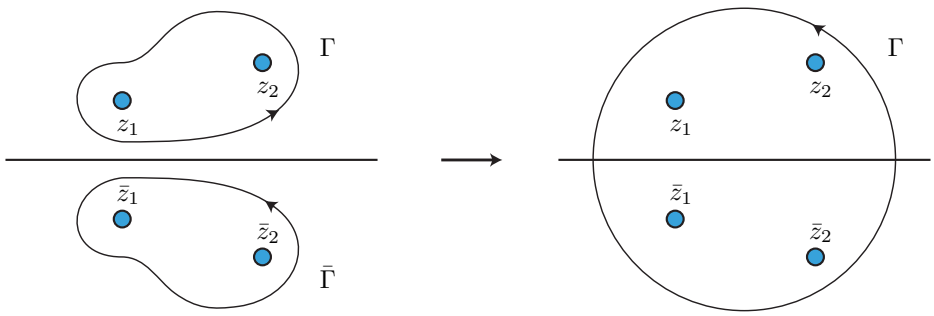

Figure 1.12: The method of images combines the N degrees of freedom of the holomorphic sector and the N degrees of freedom of the antiholomorphic sector of a boundary CFT in the upper half-plane into the holomorphic sector of a CFT over the complex plane and with $2N$ degrees of freedom.

fused into a single contour Γ winding around all of the points $z_1, \ldots, z_N, \bar{z}_1, \ldots, \bar{z}_N$ once to give the variation rule

$$\delta\langle X\rangle = -\frac{1}{2\pi i}\oint_\Gamma dw\, \epsilon(w)\langle T(w)X\rangle. \tag{1.141}$$

This happens to also be the variation law for a correlation function with $2N$ holomorphic variables $z_1, \ldots, z_N, \bar{z}_1, \ldots, \bar{z}_N$ of holomorphic weights $h_1, \ldots, h_N, \bar{h}_1, \ldots, \bar{h}_N$ and no antiholomorphic sector. With this interpretation, we posit that the half-plane correlation function (1.140) equals the whole-plane correlation function,

$$\langle \phi_{h,\bar{h}}(z_1,\bar{z}_1)\ldots\phi_{h,\bar{h}}(z_N,\bar{z}_N)\rangle_{\mathbb{H}} = \langle \phi_{h,0}(z_1)\phi_{\bar{h},0}(\bar{z}_1)\ldots\phi_{h,0}(z_N)\phi_{\bar{h},0}(\bar{z}_N)\rangle_{\hat{\mathbb{C}}}, \tag{1.142}$$

with $2N$ holomorphic variables $z_1, \ldots, z_N, \bar{z}_1, \ldots, \bar{z}_N$ of holomorphic weights $h_1, \ldots, h_N$, $\bar{h}_1, \ldots, \bar{h}_N$ and no antiholomorphic sector. This supposition has been used to successfully calculate many observables of systems in domains with boundary, including those presented in this thesis.

The introduction of a boundary invites the consideration of BCs. This possibility is realized when we consider the one-point function in the half-plane

$$\langle \phi(z)\rangle_{\mathbb{H}} = \langle \phi_h(z)\phi_h(\bar{z})\rangle_{\hat{\mathbb{C}}} = C(z-\bar{z})^{-2h}. \tag{1.143}$$

The one-point function over $\mathbb{H}$ vanishes only when $C = 0$. If ϕ is, for example, a spin-variable in a Potts model, then a one-point function averages over all possible spins that can occur at that point. A one-point function that vanishes regardless of proximity to the boundary indicates that the spin variables of the boundary sites in the real axis are *free,* or not constrained. But if $C \neq 0$, then the one-point function blows up since $h > 0$, indicating that these boundary sites are *fixed* to the same state. These BCs were previously considered for the Potts model in section 1.1.3. Other BCs may be considered with the condition that they be conformally invariant [46].

The BC of a system in the upper half-plane does not have to be homogeneous but may change at a point $x_0 \in \mathbb{R}$, and this change is induced by a *boundary condition change (BCC) operator* $\phi(x_0)$. BCC operators are examples of *boundary operators*, or boundary fields with the real axis as their domains. They are created by letting a *bulk operator,* that is, a field in *the bulk* (i.e. interior, in this case the upper half-plane), approach a boundary point in the real axis. In so doing, the bulk operator approaches its image in the lower half-plane and fuses with it to create a boundary operator. This process is called *bulk-image fusion.*

We suppose that the conformal bijection $f : \mathbb{H} \to \mathbb{D}$ extends continuously to the real axis and is real on an interval $I \subset \mathbb{R}$ so that its Schwarz reflection $\bar{f}$ analytically continues f to the lower half-plane. Now we let a spinless bulk field $\phi_{h,h}$ at $z \in \mathbb{H}$ approach $x \in I$ and fuse with its image to create a boundary field $\phi_{h_b}(x)$. Then in this limit, then the law (1.139) may be expanded into

$$|f(z) - \bar{f}(\bar{z})|^{-2h+h_b}\phi'_{h_b}(x') + \dots = |\partial f(x)|^{-2h}|z - \bar{z}|^{-2h+h_b}\phi_{h_b}(x) + \dots. \quad (1.144)$$

After isolating the boundary field $\phi'_{h_b}(x')$ on the right side and sending $z, \bar{z} \to x$, we

find a conformal covariance law for the boundary field:

$$\phi'_{h_b}(x') = |\partial f(x)|^{-h_b}\phi_{h_b}(x). \tag{1.145}$$

If we suppose that transformation law (1.145) is true even when the bulk point z approaches a point in the real axis not in I, then an $(N+M)$-point function Υ of N bulk operators and M boundary operators will obey the transformation law

$$\begin{aligned}\Upsilon^{\mathcal{D}}(z'_1, \bar{z}'_1, \ldots, z'_N, \bar{z}'_N; x'_{N+1}, \ldots, x'_{N+M}) &= \prod_{i=1}^{N} \partial f(z_i)^{-h_i} \bar{\partial} \bar{f}_i(\bar{z}_i)^{-\bar{h}_i} \\ &\times \prod_{i=1}^{M} |\partial f(x_{N+i})|^{h_{N+i}} \Upsilon^{\mathbb{H}}(z_1, \bar{z}_1, \ldots, z_N, \bar{z}_N; x_{N+1}, \ldots, x_{N+M}). \end{aligned} \tag{1.146}$$

Again, this rule reduces to a functional equation that restricts this $(N+M)$-point function to the ansatz (1.58) when $\mathcal{D} = \mathbb{H}$. Also, the OPE structure (1.96) is supposed to exist between a pair of boundary fields or a bulk field and a boundary field, but with only one sector instead of two. Typically, the OPE coefficients differ between bulk-bulk, bulk-boundary, and boundary-boundary fusion scenarios, but they are interrelated because boundary operators are appropriate limits of bulk operators.

The conformal weights of the BCC operators are inferred from a variety of heuristic arguments [47, 11]. Here, we quote the results in the case of the Q-state Potts model. We consider the fixed-to-free (resp. free-to-fixed) BCC first. A BCC at x_0 from the *fixed to state a* BC for $x < x_0$ (resp. $x > x_0$) to free for $x > x_0$ (resp. $x < x_0$) is induced by the $\phi_{1,2}(x_0)$ Kac operator, and we denote it by $\phi^{af}_{1,2}(x_0)$ (resp. $\phi^{fa}_{1,2}(x_0)$). If we fuse $\phi^{\alpha f}_{1,2}(x_1)$ with $\phi^{fb}_{1,2}(x_2)$ by sending $x_2 \to x_1$, then the fusion rule (1.116) shows that the OPE contains the identity family and the $\phi_{1,3}$ family. In our application, this is

$$\phi^{af}_{1,2}(x_1)\phi^{fb}_{1,2}(x_2) \underset{x_2 \to x_1}{\sim} \delta_{ab}\mathbf{1}^{aa} + \phi^{ab}_{1,3}(x_1), \tag{1.147}$$

with the following physical interpretation. If $a \neq b$, then in this limit, the two BCCs join into one BCC that takes us from fixed state a to fixed state b at x_1 as we pass rightward, and this fixed-to-fixed BCC is implemented by the boundary operator $\phi_{1,3}^{ab}(x_1)$. If $a = b$, then the lack of a BCC at x_1 is captured by the identity term in the OPE. The second term on the right side of (1.147) includes all configurations with an infinitesimal free segment (x_1, x_2) that abuts a fixed segment on either end so that the FK *boundary cluster* anchored to the left fixed segment is disconnected from that anchored to the right fixed segment. These configurations are also counted in the identity term. Of course, the order of the BCC may be switched so that we fuse $\phi_{1,2}^{fa}(x_1)$ with $\phi_{1,2}^{af}(x_2)$. Here, we need both BCC operators to involve the same fixed BC for physical consistency. We find a similar fusion rule:

$$\phi_{1,2}^{fa}(x_1)\phi_{1,2}^{af}(x_2) \underset{x_2 \to x_1}{\sim} \mathbf{1}^{ff} + \phi_{1,3}^{faf}(x_1). \tag{1.148}$$

Now, the second boundary operator $\phi_{1,3}^{faf}(x_1)$ on the right side conditions the existence of an infinitesimal segment at x_1 fixed to state a, and this forces a spin a FK boundary cluster to anchor to this infinitesimal segment.

In either of these cases, we may continue this fusion process an arbitrary number of times to create an arbitrary number of BCCs proximal to x_1. From (1.116), we have the fusion rule

$$\phi_{1,2}(x_1)\phi_{1,s+1}(x_2) \underset{x_2 \to x_1}{\sim} \phi_{1,s}(x_1) + \phi_{1,s+2}(x_1), \tag{1.149}$$

with the superscripts indicating the BCCs suppressed. In this rule $\phi_{1,s+1}(x_2)$ stands for s distinct BCCs clumped very near x_2, and fusing $\phi_{1,2}(x_1)$ with $\phi_{1,s+1}(x_2)$ either annihilates one of these BCCs or adds a new one. This explains product on the right side of (1.149).

Now we consider another BCC. The BCC from fixed to state a for $x < x_0$

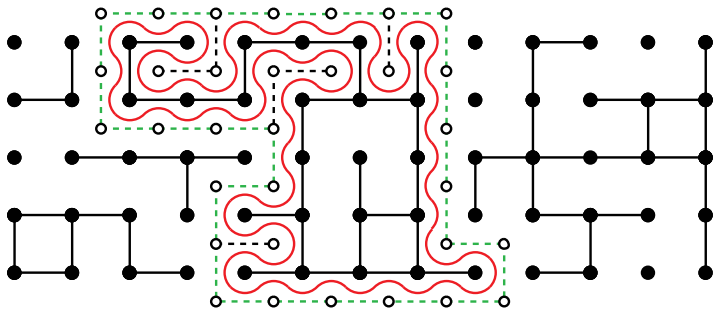

Figure 1.13: A boundary loop (red) surrounding an FK boundary cluster. If all sites inside (resp. outside) of the red curve are (resp. are not) in spin state a, then the green loop of activated dual bonds is a boundary loop surrounding a spin boundary cluster.

(resp. $x > x_0$) to *free but excluding state* a for $x > x_0$ (resp. $x < x_0$) is induced by the $\phi_{2,1}(x_0)$ Kac operator, and we denote it by $\phi_{2,1}^{a\not{a}}(x_0)$ (resp. $\phi_{2,1}^{\not{a}a}(x_0)$). By *free but excluding* a, we mean that boundary sites exhibit any spin state except a with uniform probability. If we fuse $\phi_{2,1}^{a\not{a}}(x_1)$ with $\phi_{2,1}^{\not{a}a}(x_2)$ by sending $x_2 \to x_1$, then the rule (1.116) shows that the OPE contains the identity family and the $\phi_{3,1}$ family. In our application, this is

$$\phi_{2,1}^{a\not{a}}(x_1)\phi_{2,1}^{\not{a}a}(x_2) \underset{x_2\to x_1}{\sim} \mathbf{1}^{aa} + \phi_{3,1}^{a\not{a}a}(x_1). \tag{1.150}$$

The interpretation of (1.150) is basically identical to that of (1.147) (except that $\phi_{3,1}^{a\not{a}a}(x_1)$ will now separate two disjoint boundary spin clusters with an infinitesimal free segment).

From now on, we will typically refer to the BCC at x_0 induced by either $\phi_{1,2}(x_0)$ or $\phi_{2,1}(x_0)$ as "fixed-to-free" or "free-to-fixed," even though this description is not completely accurate for $\phi_{2,1}(x_0)$.

The BCC operator $\phi_{1,2}(x_0)$ bears a second interpretation as a *boundary arc operator.* In the loop gas representation of the Potts model, a single loop, called a *boundary loop,* surrounds the FK boundary cluster anchored to the fixed segment at the side of x_0 and passes through x_0 (figure 1.13). The portion of the boundary loop in the upper half-plane, called a *boundary arc*, tightly wraps around the cluster's perimeter. Thus,

$\phi_{1,2}(x_0)$ earns its second name by conditioning a single boundary arc (resp. boundary loop) to anchor to (resp. pass through) x_0. The $\phi_{2,1}(x_0)$ BCC operator earns this name too by conditioning a boundary arc, the interface between a spin a boundary cluster and an adjacent boundary cluster that excludes spin a, to anchor to x_0.

Now we consider a four-point function $\langle \psi^{ab}(x_i)\psi^{bc}(x_j)\psi^{cd}(x_k)\psi^{da}(x_l)\rangle$ of BCC operators with $x_i < x_j < x_k < x_l$. Here, ψ^{ab} is a BCC operator taking us from BC a to BC b as we move rightwards along the real axis. Because the relative locations of the four points are constrained by their ordering on the real axis, only the functions $G_{ij:kl}$ and $G_{kj;il}$ of (1.61) are well-defined, and they satisfy the crossing relation (in just the variable η as there is only one sector)

$$G_{ij:kl}(\eta) = G_{kj:il}(1-\eta). \tag{1.151}$$

As is true with bulk correlation functions, the $G_{ij:kl}$ may be decomposed into conformal blocks $\mathcal{F}^{\alpha}_{ij;kl}(\eta)$, so the crossing relation (1.151) becomes

$$\sum_{\alpha\in B_0} C^{\alpha}_{ij}(a,c;b)C^{\alpha}_{kl}(c,a;d)\mathcal{F}^{\alpha}_{ij;kl}(\eta) = \sum_{\alpha\in B_0} C^{\alpha}_{kj}(b,d;c)C^{\alpha}_{il}(b,d;a)\mathcal{F}^{\alpha}_{kj;il}(1-\eta). \tag{1.152}$$

Our notation indicates that the boundary OPE coefficients may depend on the BCs. Some of these coefficients are computed in [48].

A rigorous mathematical theory called SLE captures the statistics of the boundary arcs described above. We give a brief description of SLE, and more information about it can be found in [14, 15, 49]. In the standard SLE setup, we condition our critical system in the upper half-plane to exhibit a free-to-fixed (resp. fixed-to-free) BCC at some $x_0 \in \mathbb{R}$ and a fixed-to-free (resp. free-to-fixed) BCC at infinity. Then a single boundary arc connects $x_0 \in \mathbb{R}$ with infinity and fluctuates in $\overline{\mathbb{H}}$ with the law of SLE, for which we now give a brief description. SLE is a conformally invariant stochastic process driven by Brownian motion that grows a fractal curve in $\overline{\mathbb{H}}$ from a

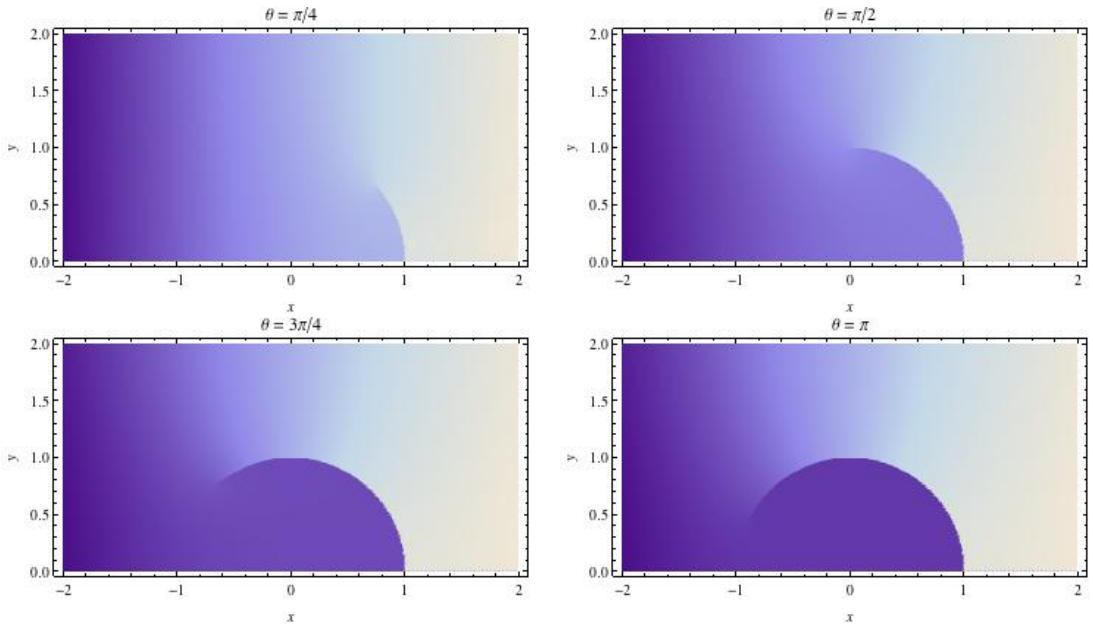

Figure 1.14: Density plot of $\mathrm{Re}[g_t(z)]$ with the deterministic driving function $\xi_t = 3\sqrt{1-2t} - 2$ and $t(\theta) = \frac{1}{2}\left(1 - \cos^4 \frac{\theta}{2}\right)$ at $\theta = \pi/4, \pi/2, 3\pi/4, \pi$. The semi-circular discontinuity $\{e^{i\phi} : 0 \leq \phi \leq \theta\}$ is the curve $\gamma[0, t(\theta)]$. All points in the unit disk intersected with $\mathbb{H}$ are swallowed, or mapped to -2, at their common swallowing time $\tau = 1/2$ ($\theta = \pi$).

specified boundary point $x_0 \in \mathbb{R}$. The curve explores $\overline{\mathbb{H}}$ without crossing itself or the real axis as the Brownian motion evolves, and in the long time limit, the tip of the curve approaches infinity. (By "conformally invariant," we mean that the probability measure is invariant under dilation about x_0 and the statistics of the completed SLE curve are invariant under the inversion $z \mapsto -1/(z - x_0)$.)

We assign a parameterization $\gamma : [0, \infty) \to \overline{\mathbb{H}}$ to the SLE curve (i.e., boundary arc) so that $\gamma(0) = x_0$ and $\gamma(t) \to \infty$ as $t \to \infty$. Then the curve is completely described by a random sequence of bijections $\{g_t\}_{t \geq 0}$ that conformally send the domain $\mathbb{H} \setminus H_t$ onto $\mathbb{H}$, where H_t is the connected component of $\mathbb{H} \setminus \gamma(0, t]$ containing infinity. If γ is a simple curve, then we may think of g_t as a "slit-mapping." Informally speaking, this slit-mapping cuts into the upper half-plane along γ from x_0 up to $\gamma(t)$ with scissors, conformally maps the part of the upper half-plane not touched by the scissors onto the upper half-plane, and in so doing melts the left and right "sides" of the curve $\gamma[0, t]$, now infinitesimally separated by the cut made by the scissors, into adjacent segments

of the real axis that touch at the image of the tip of the curve $\xi_t := g_t(\gamma(t)) \in \mathbb{R}$. The random real-valued stochastic process ξ_t is called the *driving function*, and a particular ξ_s specified for all $s \in [0,t]$ completely specifies the portion $\gamma[0,t]$ of the boundary arc. The maps $\{g_t\}_{t\geq 0}$ are uniquely determined when they are required to satisfy the *hydrodynamic normalization* at infinity,

$$g_t(z) \underset{z\to\infty}{\sim} z + \frac{b(t)}{z} + O\left(\frac{1}{z^2}\right), \tag{1.153}$$

where the differentiable function $b(t)$, called the *half-plane capacity of* H_t, is determined by our parameterization of γ. Conventionally, we use the parameterization that leads to $b(t) = 2t$. With this choice, one can show that $g_t(z)$ obeys the Löwner differential equation,

$$\partial_t g_t(z) = \frac{2}{g_t(z) - \xi_t}, \quad g_0(z) = z, \quad z \in \mathbb{H}. \tag{1.154}$$

Now, in order for γ to have the statistics of the lone boundary arc in the system described above, O. Schramm argues [14] that the driving function ξ_t must be a one-dimensional Brownian motion with *speed* κ and starting at x_0. That the driving function should be a Brownian motion in order to capture the law of a boundary arc is fixed by two special properties of SLE, conformal invariance, or the invariance of the probability measure under the scaling transformation $f : \mathbb{H} \to \mathbb{H}$ given by $f(z) = \lambda(z - x_0) + x_0$ for some $\lambda > 0$, and the "domain Markov property" [49, 15, 14].

As κ increases from zero, the roughness of the curves (i.e., their Hausdorff dimension, equaling $1 + \kappa/8$ [50]) increases, and there is a phase change at $\kappa = 4$. In the *dilute phase* $\kappa \in [0,4]$, the SLE curve $\gamma(0,\infty)$ does not intersect itself or the real axis, and in the *dense phase* $\kappa > 4$, γ intersects but does not cross itself and the real axis on all length scales. When $\kappa \geq 8$, γ is a space-filling curve in $\overline{\mathbb{H}}$. (These statements are true almost surely.) The results of this thesis will not extend to the $\kappa \geq 8$ regime.

Random walk or critical lattice model	κ	c	Current status
The loop-erased random walk [51]	2	-2	proven [52]
The self-avoiding random walk [53]	8/3	0	conjectured [54]
$Q = 2$ Potts spin cluster perimeters [1]	3	1/2	proven [44]
$Q = 3$ Potts spin cluster perimeters [1]	10/3	4/5	conjectured [9]
$Q = 4$ Potts spin/FK cluster perimeters [1, 24]	4	1	conjectured [9]
The level line of a Gaussian free field [55]	4	1	proven [55]
The harmonic explorer [55]	4	1	proven [55]
$Q = 3$ Potts FK cluster perimeters [24]	24/5	4/5	conjectured [9]
$Q = 2$ Potts FK cluster perimeters [24]	16/3	1/2	proven [44]
Percolation and smart-kinetic walks [6, 56]	6	0	proven [16]
Uniform spanning trees [52]	8	-2	proven [52]

Table 1.1: Models conjectured or proven to have conformally invariant continuum limits with SLE descriptions.

For each $z \in \mathbb{H}$, $g_t(z)$ is determined up to the *swallowing time* τ_z when $g_{\tau_z}(z) = \xi_{\tau_z}$ and the Löwner differential equation (1.154) is no longer well-defined. Since $g_t(\gamma(t)) = \xi_t$, the swallowing time may be the time when the boundary arc first touches the point $z \in \mathbb{H}$, an event with zero probability. This is always true in the dilute phase where $\tau_z = \infty$ almost surely since γ is simple. But in the dense phase, γ may lasso z and cut it off from infinity with an intersection with itself or the real-axis. At the moment of a self-intersection t_1, all points z enclosed by the loop $\gamma[t_0, t_1]$, where $t_0 < t_1$ is the biggest time such that $\gamma(t_0) = \gamma(t_1)$, are *swallowed,* or mapped to ξ_t, and $\tau_z = t_1$. A similar statement can be made when γ intersects the real axis. In the dense phase, all points are eventually swallowed this way (as opposed to touching γ), and H_t, defined above, is the half-plane complement of the set of point swallowed before or at time t. In the dilute phase, $H_t = \gamma(0, t]$. Again, these statements are true almost surely.

SLE accounts for a BCC induced by the insertion of a $\phi_{1,2}$ or $\phi_{2,1}$ operator at x_0, but it does not specify which side of x_0 is free and which side is fixed, as the growth of γ is symmetric about the $x = x_0$ axis. It also does not specify the precise state of the fixed side as this statement only has meaning in an appropriate lattice model.

Because boundary arcs are part of the boundary loops from the loop gas repre-

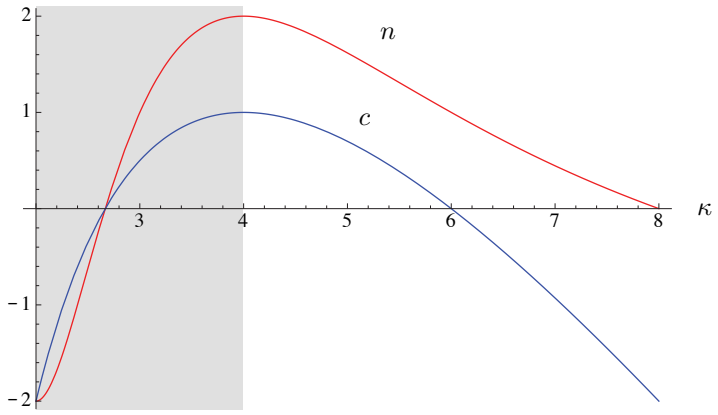

Figure 1.15: The O(n) loop fugacity (red) (1.155) and the central charge (1.170) (blue) as a function of κ over the range $\kappa \in (2, 8)$. We note that $n \in [-2, 0]$ corresponds with just the dilute phase (gray) while $n \in [0, 2]$ corresponds with both a dilute and dense κ value.

sentation of the O(n) model, we anticipate a relation between the parameters κ and n. This relationship is conjectured to be [9]

$$n(\kappa) = -2\cos(4\pi/\kappa), \quad \kappa \in [2, 8], \tag{1.155}$$

and it matches the dilute and dense phases of both models (figure 1.15). In particular, perimeters of boundary FK clusters in the Q-state Potts model must be SLE curves with their speed related to Q via $Q = \sqrt{n(\kappa)}$. An argument in the next paragraph will show that $\kappa > 4$ too.

Both FK and spin boundary cluster perimeters are conjectured, and in some cases proven, to approach SLE curves in the continuum limit, and the speeds of these two SLE curves are related through a property known as *duality.* By definition, each FK cluster sits within a spin cluster, and perimeters of either cluster are the same except that the FK-cluster perimeter will have fjords that cut into the spin cluster, making it rougher than the spin-cluster perimeter (figure 1.13). If these fjords are filled, then we recover the less-rough perimeter of the parent spin cluster. In the continuum limit, the fjords are the regions of the upper half-plane lassoed by a dense-phase SLE curve

as described above, and if we erase these fjords, then we should recover another SLE curve for some other speed $\hat{\kappa}$ in the dilute phase. Duality in SLE states that this is true with $\hat{\kappa} = 16/\kappa$, and we say that $\hat{\kappa}$ and κ are *dual* to each other.

With duality in mind, we collect the boundary arc operators $\phi_{1,2}$ and $\phi_{2,1}$ under a common name, *boundary one-leg operators,* and a common notation ψ_1:

$$\psi_1(x_0) := \begin{cases} \phi_{1,2}(x_0), & \kappa > 4 \\ \phi_{2,1}(x_0), & \kappa \leq 4 \end{cases} \quad \text{with weight} \quad \theta_1 := \begin{cases} h_{1,2}, & \kappa > 4 \\ h_{2,1}, & \kappa \leq 4 \end{cases}. \tag{1.156}$$

The conformal weight θ_1 is sometimes called the *boundary one-leg weight* or *SLE scaling exponent.* In this thesis, we adopt the convention that the boundary one-leg operator $\psi_1(x_0)$ sums over all possible BCCs that it may induce at x_0 after we commit the segment to its left to fixed and the segment to its right to free or vice versa. Also, we normalize its two-point function to

$$\Upsilon(x_1, x_2) = \langle \psi_1(x_1)\psi_1(x_2) \rangle = C_{11}^0 |x_2 - x_1|^{-2\theta_1}, \quad C_{11}^0 = n, \tag{1.157}$$

where n is the fugacity of the single boundary loop. (This two-point function corresponds to a modified SLE that starts at x_1 and ends at a second BCC located at x_2 instead of infinity.) This boundary loop surrounds the single boundary cluster anchored to either (x_1, x_2) or (x_2, x_1).

We may generalize the definition of a boundary one-leg operator ψ_1 with boundary one-leg weight θ_1 to a definition of a *boundary s-leg operator* ψ_s with *boundary s-leg weight* θ_1. These are given by

$$\psi_s(x_0) = \begin{cases} \phi_{1,s+1}(x_0) & \kappa > 4 \\ \phi_{s+1,1}(x_0) & \kappa \leq 4 \end{cases} \quad \text{with weight} \quad \theta_s := \begin{cases} h_{1,s+1} & \kappa > 4 \\ h_{s+1,1} & \kappa \leq 4 \end{cases}, \tag{1.158}$$

and they are so called because s distinct boundary arcs emanate from the BCC at x_0. Again, $\psi_s(x_0)$ sums over all possible BCCs that it may induce at x_0 after we commit the segment to its left to fixed and the segment to its right to free or vice versa. From (1.116), we have the fusion rules

$$\psi_1(x_1)\psi_s(x_2) \underset{x_2\to x_1}{\sim} \psi_{s-1}(x_1) + \psi_{s+1}(x_1), \tag{1.159}$$

$$\theta_{s\pm1} = \theta_1 + \theta_s + \Delta_1^{\pm}(\theta_s, \kappa) \tag{1.160}$$

where $\Delta_1^{\pm} := \Delta_{1,2}^{\pm}$ when $\kappa \geq 4$ and $\Delta_1^{\pm} := \Delta_{2,1}^{\pm}$ when $\kappa < 4$. Here, the KPZ formula [37] $\Delta_1^{\pm}$ (1.109) is written in terms of the SLE speed:

$$\Delta_1^{\pm}(h,\kappa) = \frac{\kappa - 4 \pm \sqrt{(\kappa-4)^2 + 16\kappa h}}{2\kappa}. \tag{1.161}$$

This rule may be interpreted as follows. If the boundary arc anchored to x_1 connects with the leftmost of the boundary arcs anchored to $x_2 > x_1$, then this boundary arc contracts to a point almost surely as $x_2 \to x_1$, leaving $s-1$ boundary arcs emanating from x_1. This explains the first term in (1.159). On the other hand, if these adjacent

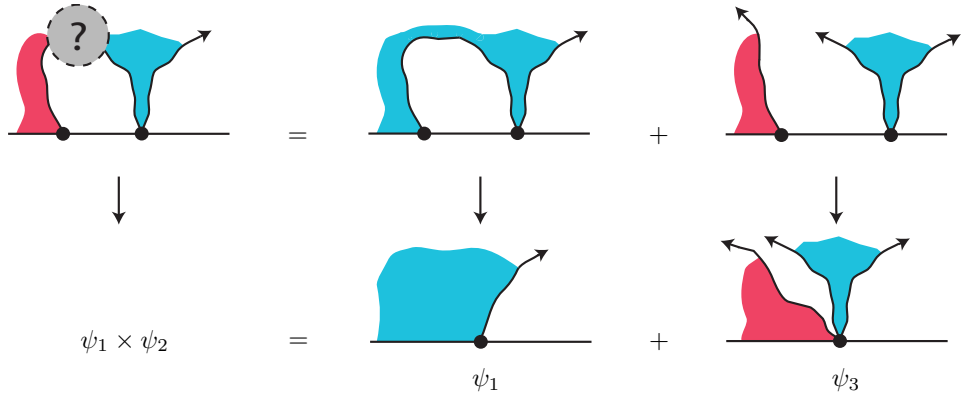

Figure 1.16: The fusion rule $\psi_1 \times \psi_2 = \psi_1 + \psi_3$. Each s-leg operator sums over all possible spin types of all boundary clusters anchored to it. Our use of different colors for the left versus right boundary cluster merely indicates this fact, and it does not indicate that these two clusters must exhibit different spins. However, the ψ_1 fusion channel is observed only for those samples in which both of these boundary clusters do exhibit the same spin state.

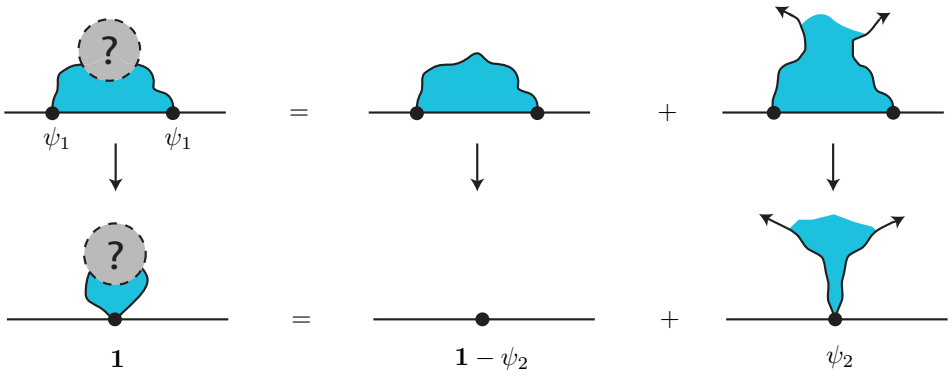

Figure 1.17: The fusion rule $\psi_1 \times \psi_1 = \mathbf{1} + \psi_2$. The identity family imposes no conditioning on the mutual connectivity of the two boundary arcs, and the two-leg family conditions the two boundary arcs to not mutually connect.

boundary arcs do not connect, then we find $s+1$ distinct boundary arcs emanating from x_2 as $x_2 \to x_1$. This explains the second term in (1.159). The case $s = 1$ is exceptional. On the right side of (1.159), we have a zero-leg operator (i.e., the identity) and a two-leg operator. The two boundary arcs of a pair of one-leg operators whose fusion contains only the identity (resp. two-leg) family are not (resp. are) conditioned to mutually connect.

Now we show how BCC operators are used to condition the BC of a system through an example. For an Ising model in the upper half-plane, we let the bulk spin field $\sigma \cong \phi_{1,2}$ approach the real axis and fuse with its image to create a *boundary spin field* $\phi_{1,3}$. According to (1.22), the correlation of the boundary spin field at $x_1 \in \mathbb{R}$ with the boundary spin field at $x_2 \in \mathbb{R}$ equals the probability that x_1 and x_2 are connected by a boundary FK cluster. In the latter situation, the part of the boundary $\mathbb{R} \setminus \{x_1, x_2\}$ is free with infinitesimal wired segments at x_1 and x_2. This exactly describes the BC induced by inserting boundary two-leg operators at x_1 and x_2, which invites us to reinterpret the boundary spin field as a (dense-phase) two-leg operator: $\psi_2 \cong \phi_{1,3}$ (figure 1.18). The probability of observing this BC event is therefore

$$\mathbb{P}(\mathrm{BC}) \underset{\epsilon_i \to 0}{\sim} c_2^2 \epsilon_1^{2\theta_2} \epsilon_2^{2\theta_2} \langle \psi_2(x_1) \psi_2(x_2) \rangle. \tag{1.162}$$

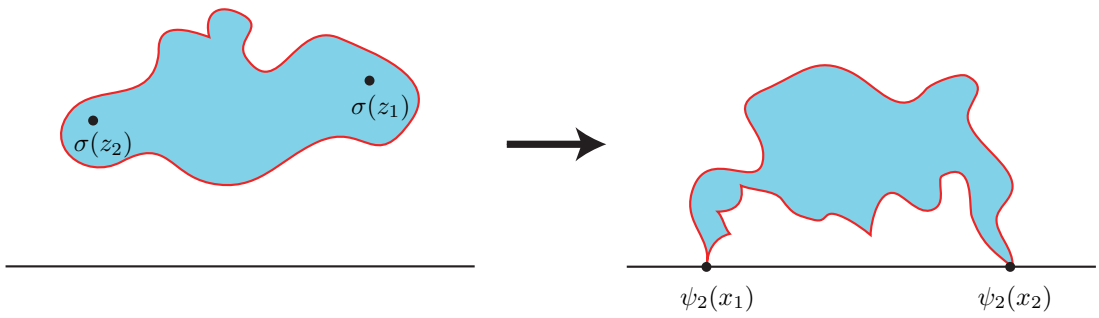

Figure 1.18: The bulk-image fusion of two bulk-spin operators (left) into two boundary-spin operators, or equivalently two (dense-phase) boundary two-leg operators (right). The shaded blue region is an FK cluster, and the red boundary in the right figure is a boundary loop.

This result requires some explanation. The BC event described above is really the collection of samples in which the i-th free-fixed-free BCC happens within a small distance ϵ_i from x_i. Also, c_2 is a nonuniversal constant that arises from the scaling limit of the boundary spin field.

Now we generalize (1.162). We posit that the probability that a system exhibits the particular BC event ς characterized by an s_1-leg BCC within distance ϵ_1 from x_1, an s_2-leg BCC within distance ϵ_2 from x_2, etc., is given by

$$\mathbb{P}(\varsigma) \underset{\epsilon_i \to 0}{\sim} c_{s_1} \dots c_{s_N} \epsilon_1^{2\theta_{s_1}} \dots \epsilon_N^{2\theta_{s_N}} \langle \psi_{s_1}(x_1) \dots \psi_{s_N}(x_N) \rangle, \tag{1.163}$$

where c_s is the nonuniversal scaling constant associated with ψ_s through (1.38). Furthermore, the expectation value of a product $\alpha(z_1) \dots \zeta(z_N)$ of lattice variable densities with $z_1, \dots, z_N \in \mathbb{H}$ and conditioned on the BC event ς is given by [57]

$$\mathbb{E}[\beta(z_1) \dots \zeta(z_M) \,|\, \varsigma] \underset{\epsilon_i \to 0}{\sim} c_\alpha \dots c_\zeta \epsilon_1^{2h_\alpha} \dots \epsilon_M^{2h_\zeta} \times \frac{\langle \alpha(z_1) \dots \zeta(z_M) \psi_{s_1}(x_1) \dots \psi_{s_N}(x_N) \rangle_{\mathbb{H}}}{\langle \psi_{s_1}(x_1) \dots \psi_{s_N}(x_N) \rangle_{\mathbb{R}}}. \tag{1.164}$$

With this understanding, we can infer a relationship between the SLE speed and the conformal weight of the one-leg operator. We follow the method used in [58]. We

let $N = 2$, $x_1 = 0$, and $x_2 = \infty$ in (1.164), we allow an SLE to evolve up to time t, and we define the random variable

$$X_t(z_1, \ldots, z_M) := \frac{\langle \alpha(z_1) \ldots \zeta(z_M) \psi_1(\gamma(t)) \psi_1(\infty) \rangle_{H_t}}{\langle \psi_1(\gamma(t)) \psi_1(\infty) \rangle_{\partial H_t}} = \partial g_t(z_1)^{h_1} \bar{\partial} \bar{g}_t(\bar{z}_1)^{\bar{h}_1} \ldots \\ \times \ldots \partial g_t(z_M)^{h_M} \bar{\partial} \bar{g}_t(\bar{z}_M)^{\bar{h}_M} \frac{\langle \alpha(g_t(z_1)) \ldots \zeta(g_t(z_M)) \psi_1(\xi_t) \psi_1(\infty) \rangle_{\mathbb{H}}}{\langle \psi_1(\xi_t) \psi_1(\infty) \rangle_{\mathbb{R}}}, \quad (1.165)$$

where $\bar{g}_t$ is the Schwarz reflection of g_t into the lower half-plane. X_t averages over all realizations of the SLE curve γ connecting zero to infinity conditioned on the event that the bottom segment $\gamma(0, t]$ is the particular curve determined by the specified sequence of conformal maps $\{g_s\}_{0 \leq s \leq t}$. By averaging X_t over all realizations of the bottom segment, we should recover X_0, so X_t must be a martingale. Thus, the drift term of its Itô derivative, which is proportional to

$$\left[\frac{\kappa}{4} \mathcal{L}_{-1}^2 - \mathcal{L}_{-2} \right] \left(\frac{\langle \alpha(g_t(z_1)) \ldots \zeta(g_t(z_M)) \psi_1(\xi_t) \psi_1(\infty) \rangle_{\mathbb{H}}}{\langle \psi_1(\xi_t) \psi_1(\infty) \rangle_{\mathbb{R}}} \right) \quad (1.166)$$

with the differential operators

$$\mathcal{L}_{-1} := \partial_{\xi_t}, \quad \mathcal{L}_{-2} := \sum_{i=1}^{M} \left(\frac{h_i}{(g_t(z_i) - \xi_t)^2} - \frac{\partial_i}{g_t(z_i) - \xi_t} + \text{c.c.} \right), \quad (1.167)$$

must vanish. The differential operator acting on the ratio of correlation functions in (1.166) is reminiscent of the differential operator in (1.106) that annihilates this ratio. They are matched by identifying the coefficients of their second derivative. We find

$$\frac{\kappa}{4} = \begin{cases} \frac{3}{2(2h_{1,2}+1)} & \Longrightarrow \quad h_{1,2} = (6 - \kappa)/2\kappa, \quad \kappa > 4 \\ \frac{3}{2(2h_{2,1}+1)} & \Longrightarrow \quad h_{2,1} = (6 - \kappa)/2\kappa, \quad \kappa \leq 4 \end{cases}, \quad (1.168)$$

and this leads to an explicit formula for the boundary one-leg weight in terms of κ:

$$\theta_1 = \frac{6-\kappa}{2\kappa}. \tag{1.169}$$

Using (1.104), (1.114), and (1.169), we can use (1.169) to derive formulas for the central charge c and Kac weights $h_{r,s}$ in terms of κ:

$$c(\kappa) = \frac{(6-\kappa)(3\kappa-8)}{2\kappa}, \quad h_{r,s} = \frac{1}{16\kappa}\begin{cases} (\kappa r - 4s)^2 - (\kappa-4)^2, & \kappa > 4 \\ (\kappa s - 4r)^2 - (\kappa-4)^2, & \kappa \leq 4 \end{cases}. \tag{1.170}$$

The boundary s-leg weight will be of particular use in this thesis, and now we see that in terms of κ it is given by

$$\theta_s = \frac{s(2s+4-\kappa)}{2\kappa}. \tag{1.171}$$

The result (1.170) is consistent with previously made claims. Except for the global maximum $c(4) = 1$ over $\kappa > 0$, exactly two positive κ values correspond with each value of c. If one value is κ, then the other is the dual speed $\hat{\kappa} = 16/\kappa$. Dual speeds must have the same central charge since they must correspond with the same critical system, so it is reassuring to see that this requirement is met by (1.170).

In this thesis, we study critical lattice models in simply connected domains and with a free/fixed side-alternating boundary condition (FFBC). This BC is comprised of an even number of free-to-fixed or fixed-to-free BCCs on the real axis, with the i-th BCC occurring within some small distance ϵ_i from a specified point x_i on the real axis, and with $x_1 < x_2 < \ldots < x_{2N-1} < x_{2N}$. Thus, the BC alternates from fixed to free to fixed, etc., or vice-versa, as we move rightward along the real axis (figure 1.19). Moreover, we can condition a pair of fixed sides to be *independently wired,* or not constrained to exhibit the same state, or we can condition them to be *mutually*

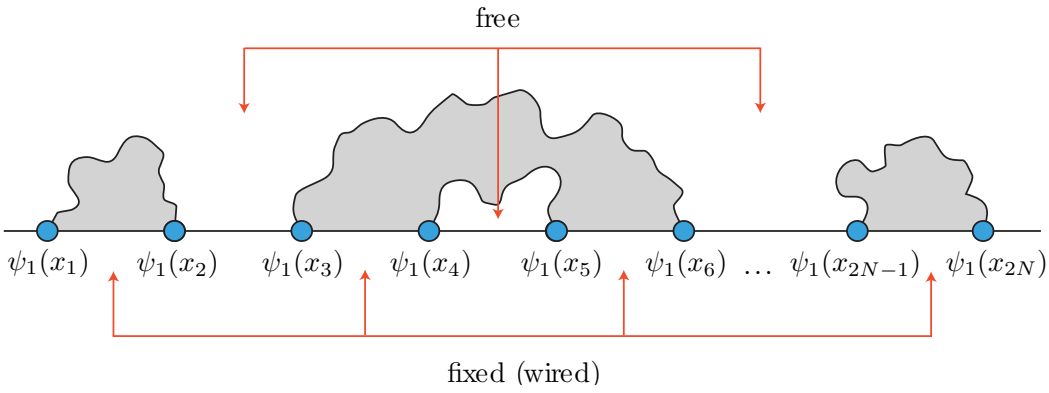

Figure 1.19: An illustration of the side-alternating free/fixed boundary condition.

wired, or constrained to exhibit the same state. Many different FFBC events can be considered by mutually wiring different collections of fixed segments with each other.

The likelihood of a observing a system configuration in the upper half-plane that exhibits the specified FFBC event ς is given by (1.163) with $N \mapsto 2N$ and $s_1, \dots, s_{2N} = 1$. This is

$$\mathbb{P}(\varsigma) \underset{\epsilon_i \to 0}{\sim} c_1^{2N} \epsilon_1^{2\theta_1} \dots \epsilon_{2N}^{2\theta_1} \Upsilon_\varsigma, \quad \Upsilon_\varsigma(x_1, \dots, x_{2N}) := \langle \psi_1(x_1) \dots \psi_1(x_{2N}) \rangle. \tag{1.172}$$

We call Υ_ς the *universal partition function* of the FFBC event ς.

In addition to the three Ward identities (1.54), Υ_ς must obey the null-state PDE (1.106) with the replacements $z_j \mapsto x_j \in \mathbb{R}$, $N \mapsto 2N$, $h_{1,2} \mapsto \theta_1$, and $h_j \mapsto \theta_1$. Because each BCC hosts a boundary one-leg operator, this $2N$-point function must also obey the $2N - 1$ distinct PDEs generated by cyclically permuting the indices $\{1, \dots, 2N\}$. Overall, this system is

$$\left[\frac{\kappa}{4} \partial_i^2 + \sum_{j \neq i}^{2N} \left(\frac{\partial_j}{x_j - x_i} - \frac{\theta_1}{(x_j - x_i)^2} \right) \right] \Upsilon_\varsigma(x_1, \dots, x_{2N}) = 0, \quad i \in \{1, \dots, 2N\}. \tag{1.173}$$

(This system is also derived from a multiple-SLE process modeling the same phenomena in [59, 60].) Remarkably, many classical solutions of the system (1.173) that also solve the Ward identities can be explicitly constructed through a method known as

the *Coulomb gas formalism* which we will survey in the next section. The primary goal of chapter two is to show that all classical solutions of (1.173) are given by this method.

1.2.9 The Coulomb gas formalism

To directly solve the composite system of null-state PDEs (1.173) and Ward identities (1.54) is very difficult. Another approach to finding solutions is to construct an explicit theory and use the computational techniques native to it to calculate the correlation functions. Though potentially simpler, this approach will only generate solutions of physical relevance in that particular theory. It could be that observables in other yet unknown theories solve the same system, implying the existence of another class of physically relevant solutions. So this approach does not address the extent to which known solutions that are particular to a theory fill out the complete solution space of the system. These issues will be addressed in the next chapter.

The explicit CFT that we will employ is called the *Coulomb gas* or *Liouville field theory*, and the methods born from it are called the *Coulomb gas formalism*. These methods were first presented in [61, 62]. Textbook treatments can be found in [3, 11].

To construct the Coulomb gas (non-rigorously), we begin with a massless bosonic free field $\varphi(z, \bar{z})$ over the complex plane. There is a rigorous mathematical theory called the *Gaussian free field* that captures many of the essential features of the bosonic free field [63]. Here, we will pursue the non-rigorous treatment used in the physics literature. The massless free boson has the conformally invariant action

$$S_0[\varphi] = \frac{1}{8\pi} \int_{\mathbb{C}} d^2x \, \partial\varphi(z, \bar{z}) \bar{\partial}\varphi(z, \bar{z}). \tag{1.174}$$

In the operator formalism, φ is quantized in terms of ladder operators that raise or lower the energy of the system. It may be broken into a sum of a holomorphic

component and an antiholomorphic component $\varphi(z,\bar{z}) = \varphi(z) + \bar{\varphi}(\bar{z})$ with respective two-point functions

$$\langle \varphi(z_1)\varphi(z_2)\rangle = -\frac{1}{2}\log z_{21}, \quad \langle \bar{\varphi}(\bar{z}_1)\bar{\varphi}(\bar{z}_2)\rangle = -\frac{1}{2}\log \bar{z}_{21}, \quad \langle \varphi(z_1)\bar{\varphi}(z_2)\rangle = 0, \tag{1.175}$$

where $z_{21} := z_2 - z_1$ (resp. $\bar{z}_{21} := \bar{z}_2 - \bar{z}_1$) and $|z_2| > |z_1|$ (resp. $|\bar{z}_2| > |\bar{z}_1|$). Thus, the complete two-point function $\langle \varphi(z_1,\bar{z}_1)\varphi(z_2,\bar{z}_2)\rangle$ equals $\log|z_{12}|$ which is the Coulomb potential in two-dimensional electrostatics. This justifies the name "Coulomb gas." The stress-tensor (i.e., the conserved current that follows from translation invariance of the theory) is

$$T(z) = -\frac{1}{2} : \partial\varphi(z)\partial\varphi(z) :, \quad \bar{T}(\bar{z}) := -\frac{1}{2} : \bar{\partial}\bar{\varphi}(\bar{z})\bar{\partial}\bar{\varphi}(\bar{z}) : \tag{1.176}$$

where ": ... :" indicates a normal-ordering of the ladder operators in the ladder operator expansion of $\partial\varphi$ and $\bar{\partial}\bar{\varphi}$ [11]. By using Wick's theorem to compute the OPE of T with itself and comparing with (1.70), we discover that the central charge of the theory is one.

We define a holomorphic (resp. antiholomorphic) field called a *chiral operator of charge α (resp. $\bar{\alpha}$)* by

$$V_\alpha(z) := : e^{i\sqrt{2}\alpha\varphi(z)} :, \quad \bar{V}_{\bar{\alpha}}(\bar{z}) := : e^{i\sqrt{2}\bar{\alpha}\bar{\varphi}(\bar{z})} : . \tag{1.177}$$

By investigating their OPE with the stress tensor and comparing with (1.69), we find that V_α (resp. $\bar{V}_{\bar{\alpha}}$) is a primary field with conformal weights $h = \alpha^2$ and $\bar{h} = 0$ (resp. $h = 0$ and $\bar{h} = \bar{\alpha}^2$). Using the ladder-operator expansion of φ and $\bar{\varphi}$, we can compute an N-point function of chiral operators, finding

$$\langle V_{\alpha_1}(z_1)\dots V_{\alpha_N}(z_N)\rangle = \delta_{\alpha_1+\dots+\alpha_N,\,0}\prod_{i<j} z_{ij}^{2\alpha_i\alpha_j}, \tag{1.178}$$

with a similar result for the antiholomorphic sector. The Kronecker delta shows that the total charge of the N-point function must be zero in order for the N-point function to be nonzero. This condition, called the *neutrality condition,* emerges naturally in the calculation, and it also emerges as a consequence of requiring the N-point function to satisfy the conformal Ward identities.

To broaden the scope of this theory to theories with central charge less than one, we add to the free action (1.174) a term that couples the free boson to the scalar curvature $\mathcal{R}$ of the Riemann sphere on which the theory is defined. (Now we are working with the one-point compactification of $\mathbb{C}$.) The action is now

$$S[\varphi] = S_0[\varphi] + \frac{\gamma}{4\pi}\int_{\mathbb{C}} d^2x\, \varphi(z,\bar{z})\mathcal{R}. \tag{1.179}$$

This additional term modifies the stress tensor to

$$T(z) = -\frac{1}{2} : \partial\varphi(z)\partial\varphi(z) : + \gamma\partial^2\varphi(z) \tag{1.180}$$

(with a similar modification to the antiholomorphic component), and by taking the OPE of $T(z)$ with itself, we find that the central charge of the theory has shifted to

$$c = 1 + 12\gamma^2. \tag{1.181}$$

We wish for c to be less than one since this range includes the minimal models and corresponds with SLE. Thus, we write $\gamma = i\alpha_0\sqrt{2}$ with $\alpha_0 > 0$ so that $c = 1 - 24\alpha_0^2$. By computing the OPE of a chiral operator $V_\alpha(z)$ with the modified stress tensor, we discover that the conformal weight of $V_\alpha(z)$ is shifted from $h = \alpha^2$ to

$$h(\alpha) = \alpha(\alpha - 2\alpha_0). \tag{1.182}$$

We say that the charges α and $2\alpha_0 - \alpha$ are *conjugate* because the conformal weights of the chiral operators V_α and $V_{2\alpha_0-\alpha}$ are equal.

Thanks to the Gauss-Bonnet theorem, the total scalar curvature $\frac{1}{8\pi}\int d^2x\,\mathcal{R}$ of the Riemann sphere is a topological invariant equaling one. Thus, we may distribute its scalar curvature $\mathcal{R}$ anywhere across the Riemann sphere without altering this quantity. To concentrate the curvature at infinity is the most natural choice, for then (1.179) reduces to (1.174) for almost all of $\mathbb{C}$ and we can compute correlation functions with this latter action. If we formally insert $\mathcal{R} = 8\pi\delta(x-\infty)$ into (1.179), then the action reduces to

$$S[\varphi] = S_0[\varphi] + i\sqrt{2}(2\alpha_0)\varphi(\infty). \tag{1.183}$$

A chiral N-point function equals an average over all possible field configurations φ weighted by the exponentiated action $e^{-S[\varphi]}$. In our case, this weight factors into

$$\exp(-S[\varphi]\,) = e^{i\sqrt{2}(-2\alpha_0)\varphi(\infty)}\exp(-S_0[\varphi]\,). \tag{1.184}$$

Thus, an N-point function in the Coulomb gas model with the modified action (1.179) equals an N-point function in the original Coulomb gas model (1.174) with a chiral operator of *background charge* $-2\alpha_0$ placed at infinity. At an infinite distance from the other points $z_1, \ldots, z_N$, this chiral operator does not interact with any of the other chiral operators. Its presence simply shifts the neutrality condition in (1.178) to $\alpha_1 + \ldots + \alpha_N = 2\alpha_0$. Therefore, an N-point function in this modified theory is given by

$$\langle V_{\alpha_1}(z_1)\ldots V_{\alpha_N}(z_N)\rangle = \delta_{\alpha_1+\ldots+\alpha_N,2\alpha_0}\prod_{i<j} z_{ij}^{2\alpha_i\alpha_j}, \quad \alpha_0 = \sqrt{\frac{1-c}{24}}. \tag{1.185}$$

Having extended our original $c = 1$ Coulomb gas theory to the $c < 1$ regime, we

seek a means to relax the neutrality condition in order to calculate some correlation functions that are not a-priori neutral. We begin by searching for chiral operators with conformal weight one. According to (1.182), these operators necessarily have charge $\alpha_\pm$, where the *screening charge* $\alpha_\pm$ is one of the two roots of the equation $\alpha_\pm(\alpha_\pm - 2\alpha_0) = 1$. Solving for these roots and using (1.170), we find

$$\alpha_\pm = \pm \begin{cases} (\sqrt{\kappa}/2)^\pm & \kappa > 4 \\ (\sqrt{\kappa}/2)^\mp & \kappa \leq 4 \end{cases}, \tag{1.186}$$

and because these charges are obviously conjugate to each other, we have $2\alpha_0 = \alpha_+ + \alpha_-$. Next, we construct a *screening operator* from the chiral operator $V^\pm(u) := V_{\alpha_\pm}(u)$, by integrating u along a closed contour Γ in the complex u-plane:

$$Q^\pm := \oint_\Gamma V^\pm(u)\, du. \tag{1.187}$$

Screening operators are non-local and have weight zero, so their insertion into a correlation function will not alter the latter's conformal properties. Consequently, if a correlation function has an $-m\alpha_+ - n\alpha_-$ charge deficit with $m, n \in \mathbb{Z}^+$, we may insert m copies of Q^+ and n copies of Q^- into the correlation function to neutralize it. Finally, we must determine an appropriate closed contour Γ for each screening charge, and these choices will depend on the specific fusion rules that we wish for the chiral operators in the correlation function to exhibit.

Now we apply these methods, i.e., the Coulomb gas formalism, to calculate a holomorphic four-point function with all four primary fields sharing the same conformal weight h. In this formalism, each field may be represented by either the chiral operator V_α or the chiral operator $V_{2\alpha_0-\alpha}$, both with conformal weight $h = \alpha(\alpha - 2\alpha_0)$.

We thus find five candidate correlation functions,

$$\langle V_\alpha V_\alpha V_\alpha V_\alpha \rangle, \quad \langle V_\alpha V_\alpha V_\alpha V_{2\alpha_0-\alpha} \rangle, \quad \langle V_\alpha V_\alpha V_{2\alpha_0-\alpha} V_{2\alpha_0-\alpha} \rangle, \tag{1.188}$$

$$\langle V_\alpha V_{2\alpha_0-\alpha} V_{2\alpha_0-\alpha} V_{2\alpha_0-\alpha} \rangle, \quad \langle V_{2\alpha_0-\alpha} V_{2\alpha_0-\alpha} V_{2\alpha_0-\alpha} V_{2\alpha_0-\alpha} \rangle, \tag{1.189}$$

none of which can be made neutral by inserting screening operators $Q^\pm$ unless 2α is an integer combination of α_+ and α_-. Therefore, we need α to assume one of the following values called *Kac charges*:

$$\alpha_{r,s}^\pm = \left(\frac{1 \pm r}{2}\right)\alpha_+ + \left(\frac{1 \pm s}{2}\right)\alpha_-, \quad r, s \in \mathbb{Z}. \tag{1.190}$$

We note that $\alpha_{r,s}^\pm$ and $\alpha_{r,s}^\mp$ are conjugate, and by using (1.182) and (1.113), we can show that the conformal weight of the chiral operator $V_{r,s}^\pm := V_{\alpha_{r,s}^\pm}$ is simply the Kac weight $h_{r,s}$ defined in (1.113):

$$h(\alpha_{r,s}^\pm) = \frac{1}{4}(r\alpha_+ + s\alpha_-)^2 - \alpha_0^2, \quad r, s \in \mathbb{Z}^+ = h_{r,s}. \tag{1.191}$$

Thus, we can use this method to compute the four-point function $\langle \phi_h \phi_h \phi_h \phi_h \rangle$ only if $h = h_{r,s}$ for some $r, s \in \mathbb{Z}$. It is interesting to witness the natural appearance of Kac operators in the Coulomb gas formalism.

As an example, we use this theory to calculate the holomorphic four-point function consisting of boundary one-leg operators:

$$\Upsilon(z_1, \ldots, z_4) := \langle \psi_1(z_1)\psi_1(z_2)\psi_1(z_3)\psi_1(z_4) \rangle. \tag{1.192}$$

In the dense phase ($\kappa > 4$), the chiral representation of this four-point function that requires the fewest screening operators is

$$\langle V^-_{1,2}(z_1)V^-_{1,2}(z_2)V^-_{1,2}(z_3)V^+_{1,2}(z_4)Q^-\rangle = \prod_{i<j}^{3}(z_i-z_j)^{2\alpha^-_{1,2}\alpha^-_{1,2}}$$
$$\times \prod_{i=1}^{3}(z_i-z_4)^{2\alpha^-_{1,2}\alpha^+_{1,2}} \oint_\Gamma \prod_{i=1}^{3}(u-z_i)^{2\alpha^-_{1,2}\alpha_-}(u-z_4)^{2\alpha^+_{1,2}\alpha_-}\,du. \quad (1.193)$$

Explicit formulas for the exponents appearing in (1.193) in terms of κ are found from (1.186, 1.190), and they are

$$2\alpha^-_{1,2}\alpha^-_{1,2} = \frac{2}{\kappa}, \quad 2\alpha^-_{1,2}\alpha^+_{1,2} = 1-\frac{6}{\kappa}, \quad 2\alpha^-_{1,2}\alpha_- = -\frac{4}{\kappa}, \quad 2\alpha^+_{1,2}\alpha_- = \frac{12}{\kappa}-2. \quad (1.194)$$

By replacing $V^\pm_{1,2} \mapsto V^\pm_{2,1}$ and $Q^- \mapsto Q^+$ in this example, we obtain the dilute phase ($\kappa \le 4$) version of this four-point function. But since none of the powers in (1.194) change as a result of this switch, the formula (1.193) is the same function in either phase. This is true for any N-point function of boundary s-leg operators, so we will always use notation consistent with the dense phase.

The closed contour Γ must wind around the branch points of the integrand in order for the integral in (1.193) to be nonzero, and in so doing, Γ will cross the branch cuts of the integrand and pass onto different Riemann sheets. Because the powers (1.194) are usually irrational, the winding number of Γ around each branch point must be zero in order to guarantee its closure. The simplest path that achieves this goal is a Pochhammer contour $\mathscr{P}(z_1, z_2)$ that entwines two of the branch points $\{z_i, z_j\}$ (figure 1.20). There are $\binom{4}{2} = 6$ possible contours, but as we will see in chapter two, at most two choices are linearly independent. In our present example, we choose Γ to be either $\mathscr{P}(z_1, z_2)$ or $\mathscr{P}(z_3, z_4)$.

If the respective exponents β_i and β_j of $(z_i - u)$ and $(z_j - u)$ in the integrand are greater than negative one, the Pochhammer contour $\mathscr{P}(z_1, z_2)$ can be replaced by a simple curve that starts at z_i and ends at z_j. By contracting $\mathscr{P}(z_i, z_j)$ so that it hugs the line segment $[z_i, z_j]$ and including the phases that the integrand accumulates with

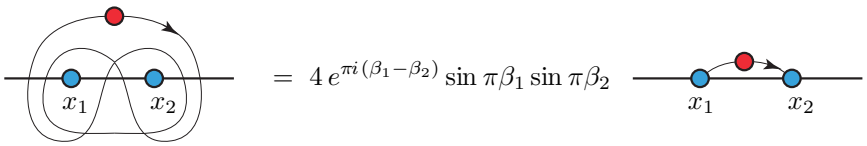

Figure 1.20: The Pochhammer contour $\mathscr{P}(x_1, x_2)$. If the numbers β_1 and β_2, where $e^{2\pi i\beta_1}$ and $e^{2\pi i\beta_2}$ are the monodromy factors associated with x_1 and x_2 respectively, are greater than negative one, then a Pochhammer contour may be replaced with the simple contour shown on the right.

each wind around these branch points, one can show that

$$\oint_{\mathscr{P}(z_1,z_2)} (z_i - v)^{\beta_i}(v - z_j)^{\beta_j} \dots\, dv$$
$$= 4 \exp \pi i(\beta_i - \beta_j) \sin\pi\beta_i \sin\pi\beta_j \int_{z_i}^{z_j} (z_i - v)^{\beta_i}(v - z_j)^{\beta_j} \dots\, dv. \quad (1.195)$$

If β_i or β_j is less than or equal to negative one, then the integral on the right side diverges, and this equality no longer holds. (The equality would hold if we kept the divergent endcap contributions that come from integrating around the tight loops of Γ that surround z_i and z_j, but the identity that would follow is not useful.) Equation (1.194) shows that we may replace the contours $\mathscr{P}(z_1, z_2)$ and $\mathscr{P}(z_3, z_4)$ for the integral in (1.193) with $[x_1, x_2]$ and $[x_3, x_4]$ respectively only in the dense phase.

The selection of integration contours affects some of the fusion rules of the chiral operators in a correlation function. The OPE of two chiral operators (1.177) of respective charges α_1 and α_2 contains only the conformal family of a chiral operator with charge $\alpha_1 + \alpha_2$. This is in direct analogy with the usual algebra rule $e^{i\sqrt{2}\alpha_1\varphi} e^{i\sqrt{2}\alpha_2\varphi} = e^{i\sqrt{2}(\alpha_1+\alpha_2)\varphi}$. To within a fusion constant, the leading term of the OPE is then

$$V_{\alpha_1}(z_1)V_{\alpha_2}(z_2) \underset{z_2\to z_1}{\sim} (z_2 - z_1)^{2\alpha_1\alpha_2} V_{\alpha_1+\alpha_2}(z_1) + \dots. \quad (1.196)$$

We note that the exponent $2\alpha_1\alpha_2$ equals $-h(\alpha_1) - h(\alpha_2) + h(\alpha_1 + \alpha_2)$ as it must in order for (1.196) to have the structure of an OPE of primary fields.

Now we look at how our choice of integration contours can change the fusion rule

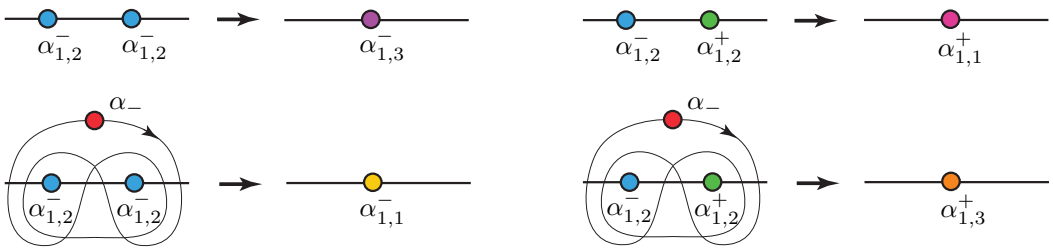

Figure 1.21: Fusion rules for pairs of boundary one-leg chiral operators both entwined and not entwined by a Pochhammer contour along which a screening charge is integrated.

(1.196) in example (1.193). The total charge of the chiral operators at the pairs of points $\{z_1, z_2\}$ (resp. $\{z_3, z_4\}$) is

$$\alpha^-_{1,2} + \alpha^-_{1,2} = \alpha^-_{1,3}, \quad (\text{resp. } \alpha^-_{1,2} + \alpha^+_{1,2} = \alpha^+_{1,1}), \tag{1.197}$$

which is that of a two-leg operator (resp. identity operator), so only the conformal family of this operator appears in the fusion of $V^-_{1,2}(z_1)$ with $V^-_{1,2}(z_2)$ (resp. $V^-_{1,2}(z_3)$ with $V^+_{1,2}(z_4)$). Now we suppose that $\Gamma = \mathscr{P}(z_1, z_2)$ (resp. $\Gamma = \mathscr{P}(z_3, z_4)$). Then because Γ is entwined with the two points, the screening charge α_- is pulled in with the fusion and adds to the total charge of the product. The new total charge is

$$\alpha^-_{1,2} + \alpha^-_{1,2} + \alpha_- = \alpha^-_{1,1}, \quad (\text{resp. } \alpha^-_{1,2} + \alpha^+_{1,2} + \alpha_- = \alpha^+_{1,3}). \tag{1.198}$$

The total charge has changed from that of a two-leg operator (resp. identity operator) to that of an identity operator (resp. two-leg operator) (figure 1.21).

So far, our calculations have pertained to only the isolated holomorphic or antiholomorphic sector. If $\psi_1(z)$ (resp. $\psi_1(\bar{z})$) is a holomorphic (resp. antiholomorphic) component of a spinless bulk field $\psi_1(z, \bar{z})$ with conformal weights $h = \bar{h} = \theta_1$, then we must sew the holomorphic and antiholomorphic sectors together to obtain the complete four-point function

$$\Upsilon(z_1, \bar{z}_1, \ldots, z_4, \bar{z}_4) \;:=\; \langle \psi_1(z_1, \bar{z}_1)\psi_1(z_2, \bar{z}_2)\psi_1(z_3, \bar{z}_3)\psi_1(z_4, \bar{z}_4)\rangle \tag{1.199}$$

$$= \quad z_{21}^{-2\theta_1} z_{43}^{-2\theta_1} \eta^{2\theta_1} \bar{z}_{21}^{-2\theta_1} \bar{z}_{43}^{-2\theta_1} \bar{\eta}^{2\theta_1} G_{12:34}(\eta, \bar{\eta}), \qquad (1.200)$$

with $G_{12:34}$, defined in (1.61), equaling a linear combination of the products of the conformal blocks pertaining to the holomorphic and antiholomorphic sectors:

$$G_{12:34}(\eta, \bar{\eta}) = \sum_{m,\bar{m}=0,2} C_{12}^{(m\bar{m})} C_{34}^{(m\bar{m})} \mathcal{F}_{12:34}^{m}(\eta) \mathcal{F}_{12:34}^{\bar{m}}(\bar{\eta}). \qquad (1.201)$$

We note that $C_{ij}^{(m\bar{m})} = C_{kl}^{(m\bar{m})}$ for all i, j, k, and l since all of the fields are ψ_1, and to reflect this, we write the OPE coefficient as $C_{11}^{(m\bar{m})}$. The fusion coefficient $C_{11}^{(m\bar{m})}$ is chosen so that $G_{12:34}(\eta, \bar{\eta})$ is single-valued for all $(\eta, \bar{\eta}) \in \mathbb{C}^2$. In particular, $G_{12:34}(\eta, \bar{\eta})$ must be invariant as η and $\bar{\eta}$ wind counterclockwise and clockwise respectively around the branch points zero, one, and infinity of $\mathcal{F}_{ij:kl}^{m}$. This condition requires $m = \bar{m}$ and fixes the ratio $(C_{11}^2/C_{11}^0)^2$, the denominator of which is simply the coefficient of the bulk two-point function $\langle \psi_1(z, \bar{z}) \psi_1(z, \bar{z}) \rangle$.

In this thesis, we will almost exclusively work with boundary operators, the correlation functions of which exhibit just one sector. Thus, the methods described in the previous paragraph cannot be used to calculate the boundary OPE coefficients, though other methods are available [48].

1.3 Summary

In this chapter, we have introduced several examples of lattice models with critical behavior and explained their relation with CFT. We have also proposed a method for studying these critical lattice models confined to domains with boundary and with a specified FFBC event, a setting in which we will work for the rest of this thesis. Using CFT, we argued that the universal partition function for such a system is governed by the system of differential equations (1.54, 1.173).

The remainder of this thesis investigates certain observables associated with the

critical systems and governed by the systems of PDEs described above. In chapter two, we begin this effort by seeking a complete description of the solution space of the system (1.54, 1.173). In chapter three, we reexamine special cases for which the solution space exhibits exceptional properties that are noted in chapter two. In chapter four, we apply the results of chapter two to calculate a fundamental set of observables called crossing probabilities for these critical systems. In chapter five, we use the techniques presented in chapter one to calculate another set of observables for these critical systems called pinch-point densities.

CHAPTER II

A solution space for a system of null-state differential equations

The goal of this chapter is to rigorously characterize the solution space of the system of PDEs that governs a $2N$-point function of boundary one-leg operators $\langle \psi_1(x_1) \dots \psi_1(x_{2N}) \rangle$. We achieve this goal modulo the proofs of two conjectures to be stated later. The first, conjecture II.7, seems to be a minor, technical detail, but the second, conejcture II.16, supports a major step in the proof of the results presented in this chapter. We propose an incomplete proof for the latter conjecture.

As we observed in chapter one, the system governing the $2N$-point function $\langle \psi_1(x_1) \dots \psi_1(x_{2N}) \rangle$ consists of the collection of $2N$ null-state PDEs (1.173),

$$\left[\frac{\kappa}{4} \partial_i^2 + \sum_{j \neq i}^{2N} \left(\frac{\partial_j}{x_j - x_i} - \frac{\theta_1}{(x_j - x_i)^2} \right) \right] F(x_1, \dots x_{2N}) = 0, \quad i \in \{1, 2, \dots, 2N\} \quad (2.1)$$

($\theta_1 := (6-\kappa)/2\kappa$ is the conformal weight (1.169) of the one-leg operator $\psi_1(x_i)$), and the three conformal Ward identities,

$$\begin{cases} \sum_{i=1}^{2N} \partial_i F(x_1, \dots x_{2N}) = 0 \\ \sum_{i=1}^{2N} (x_i \partial_i + \theta_1) F(x_1, \dots x_{2N}) = 0 \\ \sum_{i=1}^{2N} (x_i^2 \partial_i + 2\theta_1 x_i) F(x_1, \dots x_{2N}) = 0 \end{cases} . \quad (2.2)$$

We call the i-th null-state PDE among (2.1) *the null-state PDE centered on* x_i. This system is defined for $\kappa \neq 0$, and we will focus our attention on $\kappa \in (0, 8)$.

The subsystem of $2N$ null-state PDEs (2.1) is undefined on the locus of diagonal points, or points $(x_1, \ldots, x_{2N})$ with at least two of its coordinates equal. We let Ω be the complement of the locus of diagonal points in $\mathbb{R}^{2N}$. Then the diagonal points make up the boundary $\partial\Omega$, and together they divide Ω into connected components, each of the form

$$\Omega_\sigma := \{\boldsymbol{x} \in \Omega : x_{\sigma(1)} < x_{\sigma(2)} < \ldots < x_{\sigma(2N-1)} < x_{\sigma(2N)}\} \tag{2.3}$$

for some permutation $\sigma \in S_{2N}$. We will write $\boldsymbol{x}$ for the tuple $(x_1, \ldots, x_{2N}) \in \Omega_\sigma$. In this chapter and up through section 2.3, we will refer to $\boldsymbol{x}$ as a point and each x_i as a coordinate of that point, but in the rest of this thesis, we will refer to x_i as a point. By symmetry, it suffices to restrict the domain of our solutions to the component Ω_0 corresponding to the identity permutation.

Indeed, the subsystem (2.1) is elliptic, so all of its solutions exhibit strong regularity. After summing over the $2N$ null-state PDEs, we find that any solution obeys a linear, homogeneous, strictly elliptic PDE whose coefficients are analytic in Ω_0. (In fact, the principal part of this PDE is simply the Laplacian.) It follows from the theorem of Hans Lewy [64] that all of its solutions are analytic in Ω_0.

As we mentioned earlier, the Ward identities (1.54) can be solved by the method of characteristics. It follows that any solution F of these identities must have the form

$$F(\boldsymbol{x}) = G(\eta_1, \ldots, \eta_{2N-3}) \prod_{i=1}^{2N} |x_i - x_{\sigma(i)}|^{-\theta_1} \tag{2.4}$$

where σ is a pairing (i.e., a permutation $\sigma \in S_{2N}$ with $\sigma = \sigma^{-1}$) of the indices $\{1, \ldots, 2N\}$, where $\{\eta_1, \ldots, \eta_{2N-3}\}$ is any set of $2N-3$ independent cross-ratios that can be formed from $x_1, \ldots, x_{2N}$, and where $G(\eta_1, \ldots, \eta_{2N-3})$ is an analytic function

of $\boldsymbol{x}$ on Ω_0. The absolute value signs around the differences in (2.4) are included so that F is real. Without it, F would have a constant phase on Ω_0. The ansatz (2.4) implies that F satisfies the usual covariant transformation rule

$$F(\boldsymbol{x}') = |\partial f(x_1)|^{-\theta_1} \dots |\partial f(x_{2N})|^{-\theta_1} F(\boldsymbol{x}), \tag{2.5}$$

where f is a Möbius transformation taking the upper half-plane onto itself, $x_i' := f(x_i)$, and $\boldsymbol{x}' := f(\boldsymbol{x}) := (x_1' \dots, x_{2N}')$. (Actually, such transformations are compositions of translation by $a \in \mathbb{R}$, multiplication by $b > 0$, and the inversion $x \mapsto -1/x$, all of which have positive derivatives. Thus the absolute value signs in (2.5) are not necessary.) Some of these transformations may send Ω_0, the domain of F, onto another connected component of Ω. Transformation (2.108) gives such an example. In this case, $F(\boldsymbol{x}')$ is given by the right side of (2.4) with $x_i \mapsto x_i'$ and the cross-ratios unchanged since they are invariant under f. This function F over the different domain clearly solves the system (2.1-2.2) in the primed coordinates $(x_1', \dots, x_{2N}')$.

Before we begin our analysis, we state a prediction of the rank (i.e., dimension of the solution space) of the system (2.1-2.2) that is motivated by the discussion surrounding equation (1.173). The $2N$ boundary one-leg operators inserted at the points $x_1, \dots, x_{2N}$ introduce N noncrossing boundary arcs into the critical system in the upper half-plane that anchor to and connect these $2N$ points pairwise. These boundary arcs fluctuate in the upper half-plane according to the law of multiple-SLE [59, 60]. Similar to SLE, multiple-SLE is a stochastic process that evolves $2N$ curves in the upper half-plane from $2N$ origin-points $x_1, \dots, x_{2N}$ on the real axis until they join pairwise to form N distinct boundary arcs. But unlike regular SLE (or $2N$ multiple-SLE with $N = 1$), the law of $2N$ multiple-SLE with $N > 1$ is not uniquely determined by conformal invariance alone since the multiple-SLE curves of the latter process may be conditioned to join pairwise in more than one connectivity. Indeed, we must also

specify a function, called a "partition function" in [59], to drive the multiple-SLE process. [59, 60] argues that the partition function must solve the system (2.1-2.2) and that any solution of this system can serve as the partition function. Ref. [59, 60] also argue that our choice of partition function biases the boundary arcs to join pairwise in a certain *boundary arc connectivity (BAC)* and suppose the existence of a basis for the solution space of the system (2.1-2.2) in which each element conditions the boundary arcs to join in a particular BAC almost surely.

There are C_N possible BACs, where C_N is the N-th Catalan number. To prove this claim, we let C_N simply be the number of possible boundary arc connectivities for now. In each connectivity, an arc will connect x_1 with some other point x_j (where j is necessarily even) and divide $\overline{\mathbb{H}}$ into two simply connected domains. One domain will contain $(j-2)/2$ boundary arcs connecting the points $x_2, \ldots, x_{j-1}$ in one of $C_{j/2-1}$ connectivities, and the other will contain $N - j/2$ boundary arcs connecting $x_{j+1}, \ldots, x_{2N}$ in one of $C_{N-j/2}$ connectivities. Summing over all even j from $j = 2$ to $2N$, we find a recursive relation among the C_N, with the initial condition $C_1 = 1$.

$$C_N = \sum_{j=2,\,\text{even}}^{2N} C_{j/2-1} C_{N-j/2}, \quad C_1 = 1. \tag{2.6}$$

This is the recursion relation of the Catalan numbers, and it may be solved with a generating function to find the explicit formula

$$C_N = \frac{(2N)!}{N!(N+1)!}. \tag{2.7}$$

Thus, [60] predicts that the rank of the system (2.1-2.2) is C_N. A major goal of this chapter is to prove this statement.

2.1 The Coulomb gas solutions

Remarkably, many exact solutions of the system (2.1-2.2) are known, and they are constructed by using the Coulomb gas formalism outlined in section 1.2.9. We endow all but one coordinate x_c of $\boldsymbol{x} \in \Omega_0$ with the standard charge $\alpha^-_{1,2}$, we endow x_c with the conjugate charge $\alpha^+_{1,2}$, and we use $N-1$ screening operators. (When working with chiral operators, we will always use notation consistent with the dense phase of SLE for convenience, keeping in mind that the formulas are the same in both phases.) These choices give a neutral $2N$-point function of chiral operators,

$$\langle V^-_{1,2}(x_1)\dots V^-_{1,2}(x_{c-1})V^+_{1,2}(x_c)V^-_{1,2}(x_{c+1})\dots V^-_{1,2}(x_{2N})Q^-_1\dots Q^-_{N-1}\rangle, \tag{2.8}$$

that should satisfy the system (2.1-2.2). Using the results of section 1.2.9 and (2.132), we may write an explicit formula for (2.8). The formula is

$$\begin{aligned} F(\{\Gamma_m\}_{m=1}^{N-1}|\boldsymbol{x}) &:= \prod_{\substack{i<j\\ i,j\neq c}}(x_j-x_i)^{2/\kappa}\prod_{i\neq c}(x_c-x_i)^{1-6/\kappa} \\ &\times \mathcal{I}_{N-1}\left(\beta_{kl}=\left\{\begin{array}{ll} -4/\kappa, & k\neq c \\ 12/\kappa-2, & k=c\end{array}\right\}; \gamma_{pq}=\frac{8}{\kappa}\;\middle|\;\{\Gamma_m\}_{m=1}^{N-1}\;\middle|\;\boldsymbol{x}\right), \end{aligned} \tag{2.9}$$

where $c\in\{1,\dots,2N\}$, $\mathcal{I}_M$ with $M\in\mathbb{Z}^+$ is the M-fold *Coulomb-gas integral*

$$\begin{aligned} &\mathcal{I}_M(\{\beta_{kl}\};\{\gamma_{pq}\}\,|\,\{\Gamma_m\}_{m=1}^M\,|\,x_1,\dots,x_{2N}) := \\ &\int_{\Gamma_1}\int_{\Gamma_2}\dots\int_{\Gamma_M}\left(\prod_{k=1}^{2N}\prod_{l=1}^{M}(x_k-u_l)^{\beta_{kl}}\right)\left(\prod_{p<q}^{M}(u_p-u_q)^{\gamma_{pq}}\right)du_M\dots du_2\,du_1, \end{aligned} \tag{2.10}$$

and $\{\Gamma_m\}$ is a collection of closed contours in $\mathbb{C}$. Throughout this thesis, we will use the branch of the logarithm such that $\arg(z)\in[-\pi,\pi)$ for $z\in\mathbb{C}$. This determines the orientations of the branch cuts of the integrand for $\mathcal{I}_M$.

Definition II.1. A linear combination of the functions given in (2.9) is called a *Coulomb gas solution.*

The Coulomb gas formalism is non-rigorous, so we must prove that the candidate solution (2.9) indeed solves the system (2.1-2.2). This proof was originally given in [60], and we give the same proof here with a slightly different presentation.

Theorem II.2. *Every Coulomb gas solution solves the system (2.1-2.2).*

Proof. In the proof, we will use the notation $x_{2N+k} := u_k$ and from (1.186, 1.190),

$$\alpha_+ = \sqrt{\kappa}/2, \quad \alpha_- = -2/\sqrt{\kappa}, \quad 2\alpha_0 = \alpha_+ + \alpha_-, \tag{2.11}$$

$$\alpha_{1,2}^- = -\alpha_-/2 = 1/\sqrt{\kappa}, \quad \alpha_{1,2}^+ = \alpha_+ + 3\alpha_-/2 = (\kappa - 6)/2\sqrt{\kappa}. \tag{2.12}$$

These are the dense-phase values of the Kac and screening charges to be used in this proof.

We begin with a different construction of the Coulomb gas solution (2.9) that suggests how it will solve the null-state PDEs (2.1). For a collection of real "charges" $\{\alpha_i\}_{i=1}^{2N+M}$, we define the function

$$\Phi(x_1, \dots, x_{2N+M}) := \prod_{i<j}^{2N+M} (x_j - x_i)^{2\alpha_i\alpha_j}. \tag{2.13}$$

In the Coulomb gas formalism, α_i is the charge associated with chiral operator located at the coordinate x_i. Our strategy is to choose the α_i such that for each $i \in \{1, \dots, 2N\}$, we have

$$\left[\frac{\kappa}{4}\partial_i^2 + \sum_{j\neq i}^{2N}\left(\frac{\partial_j}{x_j - x_i} - \frac{(6-\kappa)/2\kappa}{(x_j - x_i)^2}\right)\right]\Phi = \sum_{k=2N+1}^{2N+M} \partial_k(\ \dots\ ), \tag{2.14}$$

where "..." stands for some analytic function. Once done, we integrate the coordinates $x_{2N+1}, \dots, x_{2N+M}$ on both sides of (2.14) around closed, nonintersecting con-

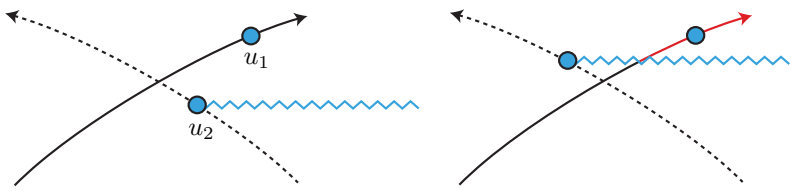

Figure 2.1: The integration of u_1 along a contour Γ_1 that crosses the contour Γ_2 of u_2. The integrand for the u_1 integration restricted to $\Gamma_1 \times \Gamma_2$ is not a continuous function of u_2 since whether or not Γ_1 crosses the u_2 branch cut depends on the location of u_2.

tours $\{\Gamma_1, \ldots, \Gamma_M\}$ (such as non-intersecting Pochhammer contours). Because either side of (2.14) is absolutely integrable on each path, we can perform these integrations in any order. Integrating the right side of (2.14) will therefore give zero. Finally, because the contours do not intersect (figure 2.1), we have sufficient continuity to use the Leibniz rule of integration to exchange the order of differentiation and integration on the left side of (2.14). We therefore find that $F := \oint \Phi$ solves the null-state PDEs (2.1). We note that M counts the number of screening charges to be used in the Coulomb gas construction (2.8).

With some algebra, we find that for any collection of real "conformal weights" $\{h_j\}$, "charges" $\{\alpha_j\}$, a positive integer M, and each $i \in \{1, 2, \ldots, 2N+M\}$,

$$\begin{aligned}
&\left[\frac{\kappa}{4}\partial_i^2 + \sum_{j\neq i}^{2N+M}\left(\frac{\partial_j}{x_j - x_i} - \frac{h_j}{(x_j-x_i)^2}\right)\right]\Phi \\
&= \left[\sum_{\substack{j,k\neq i\\ j\neq k}}^{2N+M} \frac{\alpha_j\alpha_k(\kappa\alpha_i^2 - 1)}{(x_j-x_i)(x_k-x_i)} + \sum_{j\neq i}^{2N+M}\frac{\alpha_i\alpha_j(\kappa\alpha_i\alpha_j - \kappa/2 + 2) - h_j}{(x_j-x_i)^2}\right]\Phi. \qquad (2.15)
\end{aligned}$$

If $h_j = (6-\kappa)/2\kappa$ for $1 \leq j \leq 2N$ and $h_j = 1$ for $j > 2N$ (the conformal weight of a boundary one-leg operator and screening operator respectively), then for $1 \leq i \leq 2N$, (2.15) can be written as

$$\left[\frac{\kappa}{4}\partial_i^2 + \sum_{j\neq i}^{2N}\left(\frac{\partial_j}{x_j - x_i} - \frac{(6-\kappa)/2\kappa}{(x_j-x_i)^2}\right)\right]\Phi = \sum_{k=2N+1}^{2N+M}\partial_k\left(-\frac{\Phi}{x_k - x_i}\right)$$

$$+\left[\sum_{\substack{j,k\neq i\\ j\neq k}}\frac{\alpha_j\alpha_k(\kappa\alpha_i^2-1)}{(x_j-x_i)(x_k-x_i)}+\sum_{j\neq i}\frac{\alpha_i\alpha_j(\kappa\alpha_i\alpha_j-\kappa/2+2)-h_j}{(x_j-x_i)^2}\right]\Phi. \quad (2.16)$$

We recognize the differential operator of the null-state PDE centered on x_i (2.1) on the left side of (2.16). Now we choose a particular $i \neq 2N$. One way to obtain the form (2.14) for this particular i is by choosing the α_i and $\{\alpha_j\}_{j\neq i}$ such that

$$\alpha_i = \alpha_{1,2}^- = 1/\sqrt{\kappa}, \quad \alpha_j^{\pm} = \alpha_0 \pm \sqrt{\alpha_0^2 + h_j}, \quad j \neq i, \quad (2.17)$$

so that the term in brackets on the right side of (2.16) vanishes. Note that for $j \in \{1, \ldots, i-1, i+1, \ldots, 2N\}$, $h_j = (6-\kappa)/2\kappa$ implies $\alpha_j^{\pm} = \alpha_{1,2}^{\pm}$, and for $j > 2N$, $h_j = 1$ implies $\alpha_j^{\pm} = \alpha_{\pm}$. If we choose the $-$ sign for all α_j, then the bracketed term will vanish again for the other $2N-1$ null state PDEs, and for $1 \leq i \leq 2N$ we find

$$\left[\frac{\kappa}{4}\partial_i^2 + \sum_{j\neq i}^{2N}\left(\frac{\partial_j}{x_j-x_i} - \frac{(6-\kappa)/2\kappa}{(x_j-x_i)^2}\right)\right]\Phi = \sum_{k=2N+1}^{2N+M}\partial_k\left(-\frac{\Phi}{x_k-x_i}\right). \quad (2.18)$$

As previously discussed, the function $F = \oint \Phi$ is annihilated by the differential operator on the left for all $1 \leq i \leq 2N$ provided that none of the M integration contours intersect.

However, the function F as prescribed above does not obey the Ward identities (2.2), so we cannot use this choice of signs for (2.17). The Ward identities dictate that F must have the form (2.4). This is equivalent to requiring that the function

$$\begin{aligned} G(x_1, \ldots, x_{2N}) &:= \prod_{j=1,\ \text{odd}}^{2N}(x_{j+1}-x_j)^{2\theta_1}F(x_1, \ldots, x_{2N}) \\ &= \prod_{j=1,\ \text{odd}}^{2N}(x_{j+1}-x_j)^{6/\kappa-1}\oint_{\Gamma_1}\ldots\oint_{\Gamma_M}\Phi(x_1, \ldots, x_{2N+M})\,dx_{2N+1}\ldots dx_{2N+M} \end{aligned} \quad (2.19)$$

is invariant under Möbius transformations, or equivalently, depends on only a set of

$2N-3$ independent cross-ratios that can be formed from $\{x_1, \ldots, x_{2N}\}$. We choose these cross-ratios to be

$$\eta_i = f(x_i) \quad \text{with} \quad f(x) := \frac{(x-x_1)(x_{2N}-x_{2N-1})}{(x_{2N-1}-x_1)(x_{2N}-x)}, \tag{2.20}$$

so that $\eta_1 = 0 < \eta_2 < \eta_3 < \ldots < \eta_{2N-2} < f(x_{2N-1}) = 1 < f(x_{2N}) = \infty$. Then this condition amounts to requiring that G satisfy

$$G(x_1, x_2, x_3, \ldots, x_{2N-2}, x_{2N-1}, x_{2N}) = G(0, \eta_1, \eta_2, \ldots, \eta_{2N-3}, 1, \infty). \tag{2.21}$$

Now we seek sign choices for (2.17) that may lead to this identity. Because the right side is necessarily finite, we momentarily ignore its infinite factors. Using (2.19), we see that the k-th integral on the right side of (2.21) has the form

$$\int \eta_k^{\beta_1} (1-\eta_k)^{\beta_{2N-1}} \prod_{i=2}^{2N-2} (\eta_i - \eta_k)^{\beta_i} \prod_{\substack{j=2N+1 \\ j\neq k}}^{2N+M} (\eta_j - \eta_k)^{\beta_j} \, d\eta_k \tag{2.22}$$

while the k-th integral on the left side of (2.21) has the form

$$\int \prod_{i=1}^{2N} (x_i - x_k)^{\beta_i} \prod_{\substack{j=2N+1 \\ j\neq k}}^{2N+M} (x_j - x_k)^{\beta_j} \, dx_k. \tag{2.23}$$

We note that the integrand of (2.23) contains an extra factor that was dropped in (2.22) when x_{2N} was sent to infinity. The simplest condition that achieves the equality in (2.21) is for the integrals (2.22) and (2.23) to be the same up to algebraic prefactors. After the change of variables $\eta_i = f(x_i)$, the first integral (2.22) transforms into

$$\mathcal{P}(x_1, \ldots, x_{2N}) \int \prod_{i=1}^{2N-1} \left(\frac{x_i - x_k}{x_{2N} - x_k} \right)^{\beta_i} \prod_{\substack{j=2N+1 \\ j\neq k}}^{2N+M} \left(\frac{x_j - x_k}{x_{2N} - x_k} \right)^{\beta_j} \frac{dx_k}{(x_{2N} - x_k)^2}, \tag{2.24}$$

where $\mathcal{P}(x_1, \ldots, x_{2N})$ is an algebraic prefactor whose explicit formula is presently unimportant. To match the integral in (2.24) with that in (2.23), we must have

$$\beta_{2N} = \sum_{j \neq k, 2N} \beta_j - 2. \tag{2.25}$$

In other words, the sum of the powers in the integrand of each integral (2.23) appearing in $\oint \Phi$ must equal negative two. (We note that this is achieved if all of the α_i in (5.119) sum to the background charge $2\alpha_0$. This is the Coulomb gas neutrality condition discussed in section 1.2.9:

$$-2 = \sum_{j \neq k} \beta_j = 2\alpha_k \sum_{j \neq k} \alpha_j = 2\alpha_k \left(\sum_j \alpha_j - \alpha_k \right) = 2\alpha_\pm \left(\sum_j \alpha_j - \alpha_\pm \right) \tag{2.26}$$

$$\iff \qquad \sum_j \alpha_j = 2\alpha_0. \tag{2.27}$$

To arrive with (2.27), we use the identities $\alpha_+ + \alpha_- = 2\alpha_0$ and $\alpha_+ \alpha_- = -1$.)

Let σ_k be the sum of the powers of the k-th integral in $\oint \Phi$. The results of the previous paragraph suggest that we should choose the signs in (2.17) so that $\sigma_k = -2$ for all $k \in \{2N+1, \ldots, 2N+M\}$. If we choose

$$\begin{cases} \alpha_j = \alpha_{1,2}^- & j \in \{1, \ldots, p\} \\ \alpha_j = \alpha_{1,2}^+, & j \in \{p+1, \ldots, 2N\} \\ \alpha_j = \alpha_-, & j \in \{2N+1, \ldots, 2N+q\} \\ \alpha_j = \alpha_+, & j \in \{2N+q+1, \ldots, 2N+M\} \end{cases}, \tag{2.28}$$

and let $p' := 2N - p$ and $q' := M - q$, then the condition $\sigma_k = -2$ for all $k \in \{2N+1, \ldots, 2N+M\}$ becomes

$$\sigma_k \;\; = \;\; [2p\alpha_{1,2}^- + 2p'\alpha_{1,2}^+ + 2(q-1)\alpha_- + 2q'\alpha_+]\alpha_- \tag{2.29}$$

$$= -2, \quad k \in \{2N+1, \ldots, 2N+q\} \quad \text{if } q \neq 0, \tag{2.30}$$

$$\sigma_k = [2p\alpha_{1,2}^- + 2p'\alpha_{1,2}^+ + 2q\alpha_- + 2(q'-1)\alpha_+]\alpha_+ \tag{2.31}$$

$$= -2, \quad k \in \{2N+q+1, \ldots, 2N+M\} \quad \text{if } q' \neq 0. \tag{2.32}$$

Equation (2.31) implies that $p' + q' - 1 = 0$, which is impossible for $p', q' \in \mathbb{Z}^+$. Thus, $q' = 0$, $q = M$, and requirement (2.31) vanishes. Equation (2.29) gives

$$p' = 1, \quad p = 2N - 1, \quad M = N - 1. \tag{2.33}$$

To satisfy these requirements, we choose the $-$ (resp. $+$) sign in (2.17) for the α_j with $j \neq 2N$ (resp. $j = 2N$).

With the charges and number of integrals set, we see that (2.18) is true for $M = N - 1$ and $i < 2N$. Now we must also show that when $i = 2N$ the term in brackets on the right side of (2.16) with $M = N - 1$ is a sum of derivatives with respect to $x_{2N+1}, \ldots, x_{3N-1}$. This amounts to tedious algebra that is explicitly done in [60] with the result

$$\left[\frac{\kappa}{4}\partial_{2N}^2 + \sum_{j\neq 2N}\left(\frac{\partial_j}{x_j - x_{2N}} - \frac{(6-\kappa)/2\kappa}{(x_j - x_{2N})^2}\right)\right]\Phi = \sum_{k=2N+1}^{3N-1}\partial_k\left(-\frac{\Phi}{x_k - x_{2N}}\right)$$
$$+ \frac{1}{2}\sum_{k=2N+1}^{3N-1}\partial_k\left[\frac{8-\kappa}{x_k - x_{2N}}\left(\prod_{l=1}^{2N-1}\frac{x_k - x_l}{x_{2N} - x_l}\prod_{\substack{m=2N+1\\ m\neq k}}^{3N-1}\left(\frac{x_{2N} - x_m}{x_k - x_m}\right)^2\right)\Phi\right]. \tag{2.34}$$

Thus, $\oint \Phi$ solves the null-state PDEs (2.1).

To finish, we need to prove that $\oint \Phi$ solves the Ward identities (2.2) too. This is equivalent to showing that G, as defined in (2.19), satisfies the condition (2.21). We can prove this condition by changing integration variables on the right side of (2.21) from x_i to η_i via f (2.20) as described above, and doing some straightforward but tedious algebra. We omit the details. This proves that linear combinations of

the functions (2.9) with $c = 2N$ solve the system (2.1-2.2). Because the system is invariant under permutation of the coordinates, we see that (2.9) with c equaling any index among $\{1, \ldots, 2N-1\}$ solves this system too. $\square$

As we discussed in section 1.2.9, all of the integration contours must wind non-trivially around some of the branch points of the integrand in order for the solution to not be zero, and the winding number of each contour around each branch point must zero in order for the contour to close. Finally, the contours must not intersect for the reason mentioned in the proof (figure 2.1). For large N, there are many choices of contours that satisfy these criteria, and by carefully choosing the correct contours, we may construct different solutions with important physical interpretations in various critical lattice models of interest. These choices will be explored in chapter four.

2.2 Some low dimensional cases

Before considering the system (2.1-2.2) for general N, we examine the cases $N = 1, 2$, and 3 with $\kappa = 6$ for which the solution space is known exactly. In each case, the solution space is finite dimensional with dimension equaling the N-th Catalan number C_N (2.7).

We begin with the case $N = 1$. The first Ward identity of (2.2) implies that any solution is only a function of the difference $x_2 - x_1$. Using this ansatz, the two null-state PDEs (2.1) become the same Euler differential equation, the general solution of which has two characteristic powers: $1 - 6/\kappa$ and $2/\kappa$. The second and third Ward identities exclude the second power. Thus, the solution space has dimension $C_1 = 1$ and is spanned by

$$\Pi_1(\boldsymbol{x}) = (x_2 - x_1)^{1-6/\kappa}. \tag{2.35}$$

This is the familiar two-point function of CFT for two boundary one-leg operators with identity fusion coefficient C_{11}^0 chosen to equal one.

Next, we consider the case $N = 2$. The Ward identities demand that our solutions have the form (2.4). We write

$$F(\boldsymbol{x}) = x_{42}^{-2\theta_1} x_{31}^{-2\theta_1} G(\eta), \tag{2.36}$$

where $x_{ij} := x_i - x_j$ and $\eta = x_{21}x_{43}/x_{31}x_{42}$. By substituting (2.36) into any one of the null-state PDEs, we find that $[\eta(1-\eta)]^{-2/\kappa} G(\eta)$ solves a second order hypergeometric differential equation. Upon solving it, we find that the solution space has dimension $C_2 = 2$ and is spanned by

$$\Pi_k(\boldsymbol{x}) = \frac{\Gamma(12/\kappa - 1)\Gamma(4/\kappa)}{\Gamma(8/\kappa)\Gamma(8/\kappa - 1)} (x_{42}x_{31})^{1-6/\kappa} G_k(\eta), \quad k = 1, 2, \tag{2.37}$$

where

$$G_1(\eta) = G_2(1-\eta) = \eta^{2/\kappa}(1-\eta)^{1-6/\kappa}\, {}_2F_1\left(\frac{4}{\kappa}, 1 - \frac{4}{\kappa}; \frac{8}{\kappa} \,\middle|\, \eta\right), \tag{2.38}$$

with ${}_2F_1$ the Gauss hypergeometric function. The solutions (2.37) may also be found by using the Coulomb gas formalism. We define

$$\begin{aligned} \mathcal{I}_1(\Gamma \,|\, x_1, \ldots, x_4) &:= \beta(-4/\kappa, -4/\kappa)^{-1} \\ &\quad \times \int_\Gamma \mathcal{N}[(x_1 - u)^{-4/\kappa}(x_2 - u)^{-4/\kappa}(x_3 - u)^{-4/\kappa}(x_4 - u)^{12/\kappa - 2}]\, du\,, \end{aligned} \tag{2.39}$$

where β is the Euler beta function, Γ is a line segment with endpoints at branch points of the integrand, and $\mathcal{N}$ orders the differences in the integrand so that $\mathcal{I}_1$ is real. Then one can show that

$$\Pi_1(\boldsymbol{x}) = n(x_{21}x_{31}x_{32})^{2/\kappa}(x_{41}x_{42}x_{43})^{1-6/\kappa} \mathcal{I}_1([x_3, x_4] \,|\, \boldsymbol{x}), \tag{2.40}$$

$$\Pi_2(\boldsymbol{x}) = n(x_{21}x_{31}x_{32})^{2/\kappa}(x_{41}x_{42}x_{43})^{1-6/\kappa} \mathcal{I}_1([x_4, x_1] \,|\, \boldsymbol{x}), \tag{2.41}$$

where n is the loop fugacity (1.155) of the O(n) model. By integrating along $[x_1, x_2]$

and $[x_2, x_3]$ instead, we find another pair of linearly independent solutions,

$$F_1(\boldsymbol{x}) = n^2(x_{21}x_{31}x_{32})^{2/\kappa}(x_{41}x_{42}x_{43})^{1-6/\kappa}\mathcal{I}_1([x_2,x_3]\,|\,\boldsymbol{x}), \tag{2.42}$$

$$F_2(\boldsymbol{x}) = n^2(x_{21}x_{31}x_{32})^{2/\kappa}(x_{41}x_{42}x_{43})^{1-6/\kappa}\mathcal{I}_1([x_1,x_2]\,|\,\boldsymbol{x}). \tag{2.43}$$

These solutions are related as follows:

$$F_1 = n^2\Pi_1 + n\Pi_2, \quad F_2 = n\Pi_1 + n^2\Pi_2. \tag{2.44}$$

Both the Π_k, the F_k, and their interrelation (2.44) will bear important physical interpretations in chapter four, and the F_k will serve a useful purpose later in this chapter.

Although the integration in (2.39) converges only for $\kappa > 4$, $\mathcal{I}_1$ may be analytically continued to $\kappa \leq 4$ by replacing the contour Γ with a Pochhammer contour that entwines the endpoints of Γ. The relation between these latter contours and the simple contours used above is captured by (1.195).

Finally, we consider the case $N = 3$. These solutions are easily constructed through the Coulomb gas formalism. We define

$$\mathcal{I}_2(\Gamma_1,\Gamma_2\,|\,\boldsymbol{x}) = \beta(-4/\kappa,-4/\kappa)^{-2}\int_{\Gamma_1}\int_{\Gamma_2}\mathcal{N}\Big[(u_2-u_1)^{8/\kappa}\ldots \\ \ldots\times(x_6-u_1)^{12/\kappa-2}(x_6-u_2)^{12/\kappa-2}\prod_{i=1}^{5}\prod_{j=1}^{2}(x_i-u_j)^{-4/\kappa}\Big]\,du_1\,du_2, \tag{2.45}$$

where Γ_1 and Γ_2 are line segments with endpoints at the branch points of the integrand and $\mathcal{N}$ orders the differences of the integrand so that $\mathcal{I}_2$ is real. Then the linearly independent set of five functions

$$F_1(\boldsymbol{x}) = n^3\,\mathcal{P}(\boldsymbol{x})\,\mathcal{I}_2([x_1,x_2],[x_3,x_4]\,|\,\boldsymbol{x}), \tag{2.46}$$

$$F_2(\boldsymbol{x}) = n^3\,\mathcal{P}(\boldsymbol{x})\,\mathcal{I}_2([x_2,x_3],[x_4,x_5]\,|\,\boldsymbol{x}), \tag{2.47}$$

$$F_3(\boldsymbol{x}) = n^3\,\mathcal{P}(\boldsymbol{x})\,\mathcal{I}_2([x_1,x_2],[x_4,x_5]\,|\,\boldsymbol{x}), \tag{2.48}$$

$$F_4(\boldsymbol{x}) = n^3\,\mathcal{P}(\boldsymbol{x})\,\mathcal{I}_2([x_1,x_4],[x_2,x_3]\,|\,\boldsymbol{x}), \tag{2.49}$$

$$F_5(\boldsymbol{x}) = n^3\,\mathcal{P}(\boldsymbol{x})\,\mathcal{I}_2([x_2,x_5],[x_3,x_4]\,|\,\boldsymbol{x}), \tag{2.50}$$

with the prefactor

$$\mathcal{P}(\boldsymbol{x}) = (x_{61}x_{62}x_{63}x_{64}x_{65})^{1-6/\kappa}(x_{21}x_{31}x_{41}x_{51}x_{32}x_{42}x_{52}x_{43}x_{53}x_{54})^{2/\kappa}, \tag{2.51}$$

solve the system (2.1-2.2) with $N = 3$. If these solutions are linearly independent, then the dimension is at least $C_3 = 5$. Later, we will see that these five solutions are indeed linearly independent for most values of κ. The dimension can be shown to equal five exactly when $\kappa = 6$ by converting the system (2.1-2.2) into a hypergeometric system whose solution space is spanned by four Lauricella functions F_D [60]. We believe that this process can be repeated for $\kappa \neq 6$ too, which would prove that the dimension of the solution space is indeed $C_3 = 5$.

Computing the dimension of the solution space clearly becomes very difficult for $N > 3$. For this reason, we will rely on a different approach to be developed in the next section.

2.3 A solution space $\mathcal{S}_N$ for the system (2.1-2.2)

To glean a deeper understanding of the system (2.1-2.2), we investigate the behavior of solutions near $\partial\Omega_0$. This approach is motivated by interpreting the solutions of the system as $2N$-point functions of boundary one-leg operators. We choose an $i \in \{1,\ldots,2N-1\}$ and send $x_{i+1} \to x_i$ so that operators $\psi_1(x_i)$ and $\psi_1(x_{i+1})$ fuse into some combination of an identity operator $\psi_0(x_i)$ (which is actually independent of x_i necessarily) and a boundary two-leg operator at $\psi_2(x_i)$. Inserting their OPE

into the $2N$-point function, we find

$$\begin{aligned}
&\langle \psi_1(x_1)\dots\psi_1(x_i)\psi_1(x_{i+1})\dots\psi_1(x_{2N})\rangle \\
&\quad = \; C_{11}^0 (x_{i+1}-x_i)^{-2\theta_1+\theta_0}\langle \psi_1(x_1)\dots\psi_0(x_i)\psi_1(x_{i+2})\dots\psi_{2N}(x_{2N})\rangle + \dots \qquad (2.52)\\
&\quad + \; C_{11}^2 (x_{i+1}-x_i)^{-2\theta_1+\theta_2}\langle \psi_1(x_1)\dots\psi_2(x_i)\psi_1(x_{i+2})\dots\psi_{2N}(x_{2N})\rangle + \dots . \qquad (2.53)
\end{aligned}$$

Equations (2.52) and (2.53) correspond to the identity and two-leg fusion channel respectively, and for our present purposes, C_{11}^0 and C_{11}^2 are arbitrary real constants. We recall that θ_s is the conformal weight (1.171) of the boundary s-leg operator.

Motivated by this fact from CFT, we might suppose that a generic solution F of the system (2.1-2.2) has a Frobenius series expansion in $(x_{i+1}-x_i)$ as $x_{i+1}\to x_i$ with one of two indicial powers. If we suppose this to be true, then for x_{i+1} near x_i, we may write

$$\begin{aligned}
F(x_1,\dots,x_{2N}) &= (x_{i+1}-x_i)^p F_0(x_1,\dots,x_i,x_{i+2},\dots,x_{2N}) \\
&+ (x_{i+1}-x_i)^{p+1} F_1(x_1,\dots,x_i,x_{i+2},\dots,x_{2N}) \\
&+ (x_{i+1}-x_i)^{p+2} F_2(x_1,\dots,x_i,x_{i+2},\dots,x_{2N}) + \dots . \qquad (2.54)
\end{aligned}$$

Plugging this expansion into null-state PDEs centered on x_i and x_{i+1} and collecting the leading order contributions, we find from either equation that

$$\left[\frac{\kappa}{4}p(p-1)+p-\frac{6-\kappa}{2\kappa}\right]F_0 = 0. \qquad (2.55)$$

Solving this equation for p, we find the two exponents $p_1 = -2\theta_1+\theta_0 = 1-6/\kappa$ and $p_2 = -2\theta_1+\theta_2 = 2/\kappa$ that appear in (2.52) and (2.53) respectively. At next order, the null-state PDEs centered on x_i and x_{i+1} respectively imply that

$$-\kappa p\partial_i F_0 + \left[\frac{\kappa}{4}(p+1)p+(p+1)-\frac{6-\kappa}{2\kappa}\right]F_1 \;=\; 0 \qquad (2.56)$$

$$-2\partial_i F_0 + \left[\frac{\kappa}{4}(p+1)p + (p+1) - \frac{6-\kappa}{2\kappa}\right] F_1 \;\; = \;\; 0. \tag{2.57}$$

Taking their difference when $p = 1-6/\kappa$ gives $\partial_i F_0 = 0$, so $F_1 = 0$. In the language of CFT, the condition $\partial_i F_0 = 0$ is equivalent to the identity operator being nonlocal, and the condition that $F_1 = 0$ is equivalent to the vanishing of the level-one descendant of the identity operator. After comparing (2.54) with (2.52), we interpret F_0 as a $(2N-2)$-point function of boundary one-leg operators. If this supposition is true, then F_0 must solve the system (2.1-2.2) in the coordinates $\{x_j\}_{j\neq i,i+1}$ and with $N \mapsto N-1$. When $p = 2/\kappa$, the equations (2.56) and (2.57) are identical, and $\partial_i F$ is typically not zero.

These heuristic calculations suggest that we investigate the behavior of solutions F of (2.1-2.2) near $\partial\Omega$. To this end, we let a point $\boldsymbol{x} \in \Omega_0$ approach $\partial\Omega_0$ along a path in Ω_0 such that only two adjacent coordinates x_i and x_{i+1} approach each other, while the other coordinates remain bounded away from each other and from x_i and x_{i+1}. As this happens, we also require that the sign of F does not change infinitely often as we follow this path. This condition rules out behavior that would otherwise be physically inconsistent with the applications that we have in mind. We will investigate these applications in chapter four.

Lemma II.3. *Let $F : \Omega_0 \to \mathbb{R}$ solve the system (2.1-2.2), and let $\kappa \in (0,8)$. Suppose that for every $\boldsymbol{x}_0 \in \partial\Omega_0$ with only two coordinates equal, say $x_i = x_{i+1}$, there exists a region $V \subset \Omega_0$ of the form*

$$V \;\; := \;\; \{\boldsymbol{x} \in \Omega_0 \,:\, x_i < x_{i+1} < x_i + \delta\} \cap U, \tag{2.58}$$

$$\textit{with} \quad U \;\; := \;\; \bigcap_{j\neq i+1} \{\boldsymbol{x} \in \Omega_0 \,:\, (\boldsymbol{x}_0)_j - \delta < x_j < (\boldsymbol{x}_0)_j + \delta\}, \tag{2.59}$$

for some small $\delta(\boldsymbol{x}_0) > 0$ such that F restricted to V is nonpositive or nonnegative.

(Here, $(\boldsymbol{x}_0)_j$ is the j-th coordinate of $\boldsymbol{x}_0$.) Then (with $\theta_1 := (6-\kappa)/2\kappa$), we have

$$\left\{ \begin{array}{l} F(\boldsymbol{x}) = O((x_{i+1}-x_i)^{-2\theta_1}) \\ \partial_j F(\boldsymbol{x}) = O((x_{i+1}-x_i)^{-2\theta_1}) \\ \partial_j\partial_k F(\boldsymbol{x}) = O((x_{i+1}-x_i)^{-2\theta_1}) \end{array} \right\} \quad \begin{array}{c} \text{as } x_{i+1} \to x_i \\ \text{for all } j,k \neq i, i+1, \end{array} \tag{2.60}$$

for all $\boldsymbol{x} \in V$.

Proof. Let $\boldsymbol{x}_0 = (x_1, \ldots, x_{i-1}, x_i, x_i, x_{i+2}, \ldots, x_{2N})$ with the i-th and $(i+1)$-th coordinates being the only two coordinates that are equal. We let $\epsilon := x_{i+1} - x_i < \delta(\boldsymbol{x}_0)$, we let $x := x_i$, we relabel the variables $\{x_j\}_{j\neq i,i+1}$ as $\{\xi_1, \xi_2, \ldots, \xi_{2N-3}, \xi_{2N-2}\}$ in ascending order, and we let $\boldsymbol{\xi} := (\xi_1, \ldots, \xi_{2N-2})$. For $(\boldsymbol{\xi}, x, \epsilon) \in V$, we define

$$\tilde{F}(\boldsymbol{\xi}; x, \epsilon) := F(\xi_1, \ldots, \xi_{i-1}, x, x+\epsilon, \xi_i, \ldots, \xi_{2N-2}). \tag{2.61}$$

In these variables, we must prove that for fixed $\boldsymbol{\xi}$ and x, $\tilde{F}(\boldsymbol{\xi}; x, \epsilon), \partial_j \tilde{F}(\boldsymbol{\xi}; x, \epsilon)$ and $\partial_j\partial_k \tilde{F}(\boldsymbol{\xi}; x, \epsilon)$ are $O(\epsilon^{1-6/\kappa})$ as $\epsilon \downarrow 0$.

Using the first Ward identity (2.2), we write the null-state PDE centered on x_i as $\mathcal{L}[\tilde{F}] = \mathcal{M}[\tilde{F}]$, where

$$\mathcal{M} := \sum_j \left(\frac{(6-\kappa)/2\kappa}{(\xi_j - x - \epsilon)^2} - \frac{(\xi_j - x)\partial_j}{\epsilon(\xi_j - x - \epsilon)} \right), \quad \mathcal{L} := \frac{\kappa}{4}\partial_\epsilon^2 + \frac{\partial_\epsilon}{\epsilon} - \frac{(6-\kappa)/2\kappa}{\epsilon^2}. \tag{2.62}$$

Thinking of ϵ as a time variable propagating backwards from an initial condition at some $b \in (0, \delta)$ to zero, we can invert the Euler differential operator $\mathcal{L}$ with a Green function that solves the adjoint problem

$$\mathcal{L}^*[G](\epsilon, \eta) := \left[\frac{\kappa}{4}\partial_\eta^2 - \frac{\partial_\eta}{\eta} - \frac{(6-\kappa)/2\kappa - 1}{\eta^2} \right] G(\epsilon, \eta) = \delta(\eta - \epsilon) \tag{2.63}$$

with $\epsilon > 0$ a parameter. We choose the initial conditions $G(\epsilon, 0) = \partial_\eta G(\epsilon, 0) = 0$. Also, G must be continuous at $\eta = \epsilon$, and $\partial_\eta G$ must have a jump discontinuity of $4/\kappa$

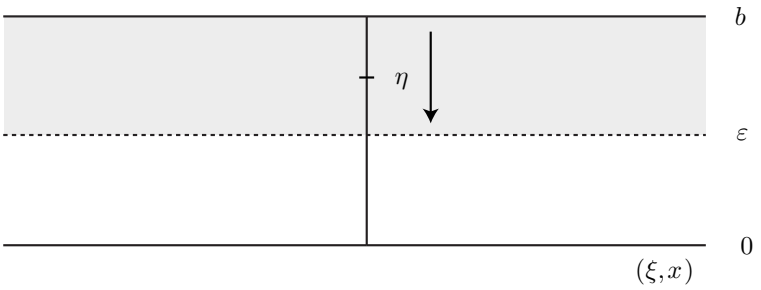

Figure 2.2: The setup for the inversion of the Euler operator $\mathcal{L}$ in (2.62). The integration variable propagates from its initial condition at $b > \epsilon$ to $\epsilon > 0$. The Green function is zero outside of the gray region.

at $\eta = \epsilon$ in order to solve the adjoint equation (2.63). The unique solution to this initial value problem is

$$G(\epsilon, \eta) = \frac{4\eta}{8-\kappa}\Theta(\eta - \epsilon)\left[\left(\frac{\epsilon}{\eta}\right)^{1-6/\kappa} - \left(\frac{\epsilon}{\eta}\right)^{2/\kappa}\right], \quad 0 < \epsilon, \eta < b. \tag{2.64}$$

The Heaviside function Θ enforces causality ($G(\epsilon, \eta) = 0$ when $\eta \leq \epsilon$). Using the usual Green identity [65]

$$\begin{aligned}\int_0^b &[\mathcal{L}[\tilde{F}](\boldsymbol{\xi}; x, \eta)G(\epsilon, \eta) - \tilde{F}(\boldsymbol{\xi}; x, \eta)\mathcal{L}^*[G](\epsilon, \eta)]\, d\eta \\ &= \frac{\kappa}{4}\left[G(\epsilon, \eta)\,\partial_\epsilon \tilde{F}(\boldsymbol{\xi}; x, \eta) - \partial_\eta G(\epsilon, \eta)\tilde{F}(\boldsymbol{\xi}; x, \eta)\right]_0^b + \frac{1}{b}G(\epsilon, \eta)\tilde{F}(\boldsymbol{\xi}; x, \eta)\Big|_0^b,\end{aligned} \tag{2.65}$$

we find that for all $b \in (0, \delta)$, $\tilde{F}$ solves the integral equation

$$\begin{aligned}\tilde{F}(\boldsymbol{\xi}; x, \epsilon) = &\int_\epsilon^b G(\epsilon, \eta)\mathcal{M}[\tilde{F}](\boldsymbol{\xi}; x, \eta)\, d\eta \\ &- \frac{\kappa}{4}\left[G(\epsilon, b)\,\partial_\epsilon \tilde{F}(\boldsymbol{\xi}; x, b) - \partial_\eta G(\epsilon, b)\tilde{F}(\boldsymbol{\xi}; x, b)\right] - \frac{1}{b}G(\epsilon, b)\tilde{F}(\boldsymbol{\xi}; x, b).\end{aligned} \tag{2.66}$$

All of the terms on the right side except the integral are manifestly $O(\epsilon^{1-6/\kappa})$, so we only need to bound the integral. After estimating the coefficients in the integrand and estimating G for $\kappa < 8$, we find

$$|\tilde{F}(\boldsymbol{\xi};x,\epsilon)| \le \frac{8}{8-\kappa}\int_\epsilon^b \left(\frac{\epsilon}{\eta}\right)^{1-6/\kappa} \sum_j \left[\sup_{0\le\eta\le b}\left|\frac{\xi_j - x}{\xi_j - x - \eta}\right| |\partial_j \tilde{F}(\boldsymbol{\xi};x,\eta)| \right.$$
$$\left. + \sup_{0\le\eta\le b}\left|\frac{\eta(6-\kappa)/2\kappa}{(\xi_j - x - \eta)^2}\right| |\tilde{F}(\xi;x,\eta)| \right] d\eta + O(\epsilon^{1-6/\kappa}). \quad (2.67)$$

It is natural to define $H(\boldsymbol{\xi};x,\epsilon) := \epsilon^{6/\kappa-1}\tilde{F}(\boldsymbol{\xi};x,\epsilon)$ so that proving the lemma amounts to showing that $H(\boldsymbol{\xi};x,\epsilon), \partial_j H(\boldsymbol{\xi};x,\epsilon)$, and $\partial_j\partial_k H(\boldsymbol{\xi};x,\epsilon)$ are bounded as $\epsilon \downarrow 0$. Then for sufficiently small ϵ, there are positive functions $c_0(\boldsymbol{\xi},x,b)$ and $c_1(\boldsymbol{\xi},x,b)$ such that

$$|H(\boldsymbol{\xi};x,\epsilon)| \le c_1 + c_0\int_\epsilon^b \left(|H(\boldsymbol{\xi};x,\eta)| + \sum_j |\partial_j H(\boldsymbol{\xi};x,\eta)|\right) d\eta. \quad (2.68)$$

Next, we bound terms in (2.68) that contain derivatives of H. For $j \ne i, i+1$, the null-state PDE centered on x_j becomes

$$\left[\frac{\kappa}{4}\partial_j^2 + \sum_{k\ne j}\left(\frac{\partial_k}{\xi_k - \xi_j} - \frac{(6-\kappa)/2\kappa}{(\xi_k-\xi_j)^2}\right) + \frac{\partial_x}{x-\xi_j} - \frac{\epsilon\partial_\epsilon}{(x-\xi_j)(x+\epsilon-\xi_j)}\right.$$
$$\left. - \frac{(6-\kappa)/2\kappa}{(x-\xi_j)^2} - \frac{(6-\kappa)/2\kappa}{(x+\epsilon-\xi_j)^2} + \frac{6/\kappa - 1}{(x-\xi_j)(x+\epsilon-\xi_j)}\right] H = 0, \quad (2.69)$$

now for $j \in \{1,\dots,2N-2\}$, while that centered on x_i becomes

$$\left[\frac{\kappa}{4}(\partial_x - \partial_\epsilon)^2 + \frac{\partial_\epsilon}{\epsilon} + \frac{(6-\kappa)(\partial_x - \partial_\epsilon)}{2\epsilon} + \sum_k\left(\frac{\partial_k}{\xi_k - x} - \frac{(6-\kappa)/2\kappa}{(\xi_k - x)^2}\right)\right] H = 0 \quad (2.70)$$

and that centered on x_{i+1} becomes

$$\left[\frac{\kappa}{4}\partial_\epsilon^2 - \frac{(\partial_x - \partial_\epsilon)}{\epsilon} - \frac{(6-\kappa)\partial_\epsilon}{2\epsilon} + \sum_k\left(\frac{\partial_k}{\xi_k - x - \epsilon} - \frac{(6-\kappa)/2\kappa}{(\xi_k - x - \epsilon)^2}\right)\right] H = 0. \quad (2.71)$$

Also, the three Ward identities (2.2) are (again with $\theta_1 := (6-\kappa)/2\kappa$)

$$\sum\nolimits_k \partial_k H + \partial_x H = 0 \quad (2.72)$$

$$\sum\nolimits_k (\xi_k \partial_k + \theta_1) H + x \partial_x H + \epsilon \partial_\epsilon H = 0 \tag{2.73}$$

$$\sum\nolimits_k (\xi_k^2 \partial_k + 2\theta_1 \xi_k) H + x^2 \partial_x H + \epsilon^2 \partial_\epsilon H + 2x\epsilon \partial_\epsilon H = 0. \tag{2.74}$$

Summing over (2.69) and using (2.72-2.73), we find that $H(\boldsymbol{\xi}; x, \epsilon)$ obeys a uniformly elliptic linear PDE in the coordinates of $\boldsymbol{\xi}$ and with x and ϵ as parameters:

$$\begin{aligned} \sum_j \Bigg[\frac{\kappa}{4} \partial_j^2 + \sum_{k \neq j} \left(\frac{\partial_k}{\xi_k - \xi_j} - \frac{(6-\kappa)/2\kappa}{(\xi_k - \xi_j)^2} \right) - \sum_k \frac{\partial_k}{x - \xi_j} \\ - \sum_k \frac{(x - \xi_k)\partial_k}{(x - \xi_j)(x + \epsilon - \xi_j)} + \frac{(N-1)(6/\kappa - 1)}{(x - \xi_j)(x + \epsilon - \xi_j)} \\ - \frac{(6-\kappa)/2\kappa}{(x - \xi_j)^2} - \frac{(6-\kappa)/2\kappa}{(x + \epsilon - \xi_j)^2} + \frac{6/\kappa - 1}{(x - \xi_j)(x + \epsilon - \xi_j)} \Bigg] H \quad = 0. \end{aligned} \tag{2.75}$$

Now let $\mathcal{B} = (\tilde{\xi}_1 - b, \tilde{\xi}_1 + b) \times \ldots \times (\tilde{\xi}_{2N-2} - b, \tilde{\xi}_{2N-2} + b)$. We may use the Schauder interior estimates [66] to find that for all $j, k \in \{1, \ldots, 2N-2\}$ and $\boldsymbol{\xi} \in \mathcal{B}$,

$$\operatorname{dist}(\boldsymbol{\xi}, \partial\mathcal{B}) |\partial_j H(\boldsymbol{\xi}; x, \epsilon)| \leq C \sup_{\boldsymbol{\psi} \in \mathcal{B}} |H(\boldsymbol{\psi}; x, \epsilon)|, \tag{2.76}$$

$$\operatorname{dist}(\boldsymbol{\xi}, \partial\mathcal{B}) |\partial_j \partial_k H(\boldsymbol{\xi}; x, \epsilon)| \leq C \sup_{\boldsymbol{\psi} \in \mathcal{B}} |H(\boldsymbol{\psi}; x, \epsilon)|, \tag{2.77}$$

where the positive function $C(\boldsymbol{\xi}, x, \epsilon)$ depends on ϵ implicitly through the supremums of the coefficients of (2.75) over $\mathcal{B}$. Because these supremums are bounded as $\epsilon \downarrow 0$, it follows that C is bounded by a function C' independent of ϵ for all $\epsilon \in (0, b)$, and we may replace C by C' in (2.76-2.77). Thus, (2.68) becomes

$$|H(\boldsymbol{\xi}; x, \epsilon)| \leq c_1 + c_2 \int_\epsilon^b \sup_{\boldsymbol{\psi} \in \mathcal{B}} |H(\boldsymbol{\psi}; x, \eta)| \, d\eta \tag{2.78}$$

where $c_2 = c_0(1 + C'(N-2)/\operatorname{dist}(\boldsymbol{\xi}, \partial\mathcal{B}))$. Because $\tilde{F}$ is nonpositive or nonnegative

on V which contains $\mathcal{B}$, the elliptic PDE (2.75) implies the Harnack inequality [66]

$$\begin{aligned}\sup_{\boldsymbol{\psi}\in\mathcal{B}}|H(\boldsymbol{\psi};x,\eta)| &\leq c\inf_{\boldsymbol{\psi}\in\mathcal{B}}|H(\boldsymbol{\psi};x,\eta)| \\ &\leq c\,|H(\boldsymbol{\xi};x,\eta)|, \quad \eta\in(0,b). \end{aligned} \tag{2.79}$$

where the positive function $c(\boldsymbol{\xi},x,\eta,\delta,b)$ depends on η only through the supremums of the coefficients in (2.75) over V, which are bounded as $\eta\downarrow 0$ since the coordinate of $\boldsymbol{\xi}$ are bounded away from each other. Thus, this function may be replaced by a function $c_3(\boldsymbol{\xi},x,\delta,b)$ independent of η in (2.79), and (2.68) with $t=1/\epsilon, s=1/\eta$ becomes

$$|H(\boldsymbol{\xi};x,1/t)|\leq c_1+c_2c_3\int_{1/b}^{t}\frac{1}{s^2}|H(\boldsymbol{\xi};x,1/s)|\,ds. \tag{2.80}$$

Using the Gronwall inequality, we conclude from (2.80) that $|H(\boldsymbol{\xi};x,\epsilon)|\leq c_1e^{c_2c_3(b-\epsilon)}$ and is thus bounded as $\epsilon\to 0$. From (2.76-2.77) and the boundedness of H, we also conclude that all $\partial_jH(\boldsymbol{\xi};x,\epsilon),\partial_j\partial_kH(\boldsymbol{\xi};x,\epsilon)$ are bounded as $\epsilon\downarrow 0$ too. □

A main step in our proof of lemma II.3 involves bounding the magnitudes of the derivatives $\partial_jF(\boldsymbol{x})$ and $\partial_j\partial_kF(\boldsymbol{x})$ with $j,k\neq i,i+1$ by $C|F(\boldsymbol{x})|$ when $x_{i+1}\to x_i$, where C does not depend on x_{i+1}. Our approach involves summing over the null-state PDEs centered on x_j with $j\neq i,i+1$ to obtain a strictly elliptic PDE and using the interior Schauder estimates and the Harnack inequality. This step holds only if $F(\boldsymbol{x})$ does not change sign infinitely often as $x_{i+1}\to x_i$ in some $V\subset\Omega_0$ whose boundary contains the boundary point of interest with only the two coordinates x_{i+1} and x_i equal. This requirement on $F(\boldsymbol{x})$ is physically reasonable, but we currently do not know how to prove it.

Now, we expect $F(\boldsymbol{x})$ to be comparable with its derivatives with respect to x_j with $j\neq i,i+1$ as $x_{i+1}\to x_i$ because we anticipate that $F(\boldsymbol{x})$ behaves like a product of powers of the differences of pairs of the coordinates of $\boldsymbol{x}$. And we anticipate this latter property by noting the resemblance of the null-state PDE centered on x_j (2.1)

to a second order Euler differential equation in the j-th coordinate. But by summing over the null-state PDEs in our proof, we discard this important information. This effect suggests that elliptic PDE theory is not sufficient to prove lemma II.3 with the positivity condition on V omitted.

We will encounter a similar situation when we state conjecture II.16. Elliptic PDE theory will suggest an obvious proof, but the proof is incomplete without supposing another seemingly reasonable but less apparent condition to be true. We will propose a different partial proof of this conjecture that bypasses these shortcomings by working with the individual null-state PDEs. This latter proof seems to be the better avenue for proving this conjecture (II.16), to be stated later.

Lemma II.4. *Let $F : \Omega_0 \to \mathbb{R}$ solve the system (2.1-2.2), let $\kappa \in (0, 8)$, and suppose that F satisfies (2.60) for all $\boldsymbol{x} \in \Omega_0$. Then for all $i \in \{1, \ldots, 2N-1\}$, the limit*

$$F'(\boldsymbol{x}') := \lim_{x_{i+1} \to x_i} (x_{i+1} - x_i)^{2\theta_1} F(\boldsymbol{x}) \tag{2.81}$$

exists for all points in $\boldsymbol{x}' \in \mathscr{D} := \{\pi(\boldsymbol{x}) \in \mathbb{R}^{2N-1} : \boldsymbol{x} \in \Omega_0\}$ where π projects away the $(i+1)$-th coordinate (that is, $\mathscr{D}$ is the part of $\partial\Omega_0$ with only the two coordinates x_i and x_{i+1} equal). Furthermore, $F'(\boldsymbol{x}')$ solves the system (2.1-2.2) with $N \mapsto N-1$ in the coordinates $\{x_j\}_{j \neq i, i+1}$ and does not depend on x_i. Lastly, $(x_{i+1} - x_i)^{2\theta_1} F(\boldsymbol{x})$ extends continuously to $\mathscr{D}$.

Proof. We let $H, \boldsymbol{\xi}, x$, and ϵ be defined as in the proof of lemma II.3. First, we show that $H(\boldsymbol{\xi}; x, \epsilon)$ has a limit as $\epsilon \downarrow 0$. Since $H(\boldsymbol{\xi}; x, \epsilon)$ is bounded as $\epsilon \downarrow 0$, it suffices to show that its superior limit and inferior limit are equal. From (2.66), we have that for any $b \in (0, \xi_i - x)$ and $\epsilon \in (0, b)$ that

$$H(\boldsymbol{\xi}; x, \epsilon) = H(\boldsymbol{\xi}; x, b) - \frac{\kappa}{4} J(\epsilon, b) \partial_\epsilon H(\boldsymbol{\xi}; x, b) + \int_\epsilon^b J(\epsilon, \eta) \mathcal{M}[H](\boldsymbol{\xi}; x, \eta)\, d\eta, \tag{2.82}$$

where $\mathcal{M}[H](\boldsymbol{\xi}; x, \eta)$ is given in (2.62), and where J is the modified Green function

$$J(\epsilon, \eta) = \frac{4\eta}{8-\kappa}\Theta(\eta - \epsilon)\left[1 - \left(\frac{\epsilon}{\eta}\right)^{8/\kappa - 1}\right], \quad 0 < \epsilon, \eta < b. \tag{2.83}$$

The bracketed factor in $J(\epsilon, \eta)$ is bounded by two since $\kappa < 8$, and $\eta\mathcal{M}[H](\boldsymbol{\xi}; x, \eta)$ is a bounded function of η over $(0, b)$ according to previous arguments. Thus, we may replace the lower limit of integration in (2.82) with zero and take the supremum of both sides over $\epsilon \in (0, b)$ to find

$$\sup_{0<\epsilon<b} |H(\boldsymbol{\xi}; x, \epsilon) - H(\boldsymbol{\xi}; x, b)| \leq \frac{2\kappa}{8-\kappa}\left[|b\partial_\epsilon H(\boldsymbol{\xi}; x, b)| + \frac{4b}{\kappa}c_4(b)\right], \tag{2.84}$$

where $c_4(\boldsymbol{\xi}, x, b) := \sup_{0<\eta<b} |\eta\mathcal{M}[H](\boldsymbol{\xi}; x, \eta)|$. Next, we show that $b\partial_\epsilon H(\boldsymbol{\xi}; x, b)$ vanishes as $b \downarrow 0$. We can differentiate (2.82) with respect to ϵ to find a similar integral equation governing $\epsilon\partial_\epsilon H(\boldsymbol{\xi}; x, \epsilon)$. We find

$$\epsilon\partial_\epsilon H(\boldsymbol{\xi}; x, \epsilon) = \left(\frac{\epsilon}{b}\right)^{8/\kappa - 1} b\partial_\epsilon H(\boldsymbol{\xi}; x, b) - \frac{4}{\kappa}\int_\epsilon^b \left(\frac{\epsilon}{\eta}\right)^{8/\kappa - 1} \eta\mathcal{M}[H](\boldsymbol{\xi}; x, \eta)\, d\eta. \tag{2.85}$$

Reusing the same argument that justified the second term on the right side of (2.84), it follows from (2.85) that

$$\begin{aligned} |\epsilon\partial_\epsilon H(\boldsymbol{\xi}; x, \epsilon)| \leq \left(\frac{\epsilon}{b}\right)^{8/\kappa - 1} & |b\partial_\epsilon H(\boldsymbol{\xi}; x, b)| \\ & + \frac{2c_4(\boldsymbol{\xi}, x, b)}{|\kappa - 4|}\epsilon^{8/\kappa - 1}|b^{2-8/\kappa} - \epsilon^{2-8/\kappa}| \longrightarrow 0 \quad \text{as } \epsilon \downarrow 0 \end{aligned} \tag{2.86}$$

since $\kappa < 8$. Because $c_4(\boldsymbol{\xi}, x, b)$ is obviously nonincreasing as $b \downarrow 0$, we find from (2.84) that

$$\lim_{b\downarrow 0} \sup_{0<\epsilon<b} |H(\boldsymbol{\xi}; x, \epsilon) - H(\boldsymbol{\xi}; x, b)| = 0, \tag{2.87}$$

and we conclude that the inferior and superior limits of $H(\boldsymbol{\xi}; x, \epsilon)$ as $\epsilon \downarrow 0$ are equal.

Furthermore, we can show that the limit of $H(\boldsymbol{\xi}; x, \epsilon)$ as $\epsilon \downarrow 0$ is approached

uniformly over any sufficiently small neighborhood $U \subset \mathscr{D}$. By replacing ϵ with zero and then b with ϵ in (2.82) and taking a supremum over all $(\boldsymbol{\xi}, x) \in U$, we find

$$\begin{aligned} \sup_U |H(\boldsymbol{\xi}; x, \epsilon) - H(\boldsymbol{\xi}; x, 0)| &\leq \frac{\kappa}{8-\kappa} \sup_U |\epsilon \partial_\epsilon H(\boldsymbol{\xi}; x, \epsilon)| \\ &+ \frac{4}{8-\kappa} \int_0^\epsilon \sup_U |\eta \mathcal{M}[H] \boldsymbol{\xi}; x, \eta)| d\eta. \end{aligned} \tag{2.88}$$

After taking the supremum of both sides of (2.86) over all $(\boldsymbol{\xi}, x) \in U$, we see that $\sup_U |\epsilon \partial_\epsilon H(\boldsymbol{\xi}; x, \epsilon)|$ vanishes as $\epsilon \downarrow 0$. Furthermore, the integrand in (2.88) is bounded as $\eta \downarrow 0$ according to previous arguments, so the integral vanishes in this limit. Thus, the supremum on the left side of (2.88) vanishes as $\epsilon \downarrow 0$, so the convergence is uniform over U. From this, we infer that the limit of $H(\boldsymbol{\xi}; x, \epsilon)$ as $\epsilon \downarrow 0$ is continuous on $\mathscr{D}$, and furthermore, that $H(\boldsymbol{\xi}; x, \epsilon)$ extends continuously to $\Omega_0 \cup \mathscr{D}$.

We can recycle these arguments to show that $\partial_j H(\boldsymbol{\xi}; x, \epsilon)$ and $\partial_j^2 H(\boldsymbol{\xi}; x, \epsilon)$ uniformly approach limits as $\epsilon \downarrow 0$ for all $j \in \{1, \ldots, 2N-2\}$. By taking the j-th partial derivative of (2.82) (because $H(\boldsymbol{\xi}; x, \epsilon)$ is analytic in Ω_0, we can exchange the order of integration and differentiation), we find an equation similar to (2.82) but with a few changes. First, the integrand, though slightly changed from that of (2.82), will still be a bounded function of η on $(0, b)$ since each of the first two derivatives of $H(\boldsymbol{\xi}; x, \epsilon)$ is bounded in the coordinates of $\boldsymbol{\xi}$. Second, $\epsilon \partial_\epsilon H(\boldsymbol{\xi}; x, \epsilon)$ in the first term of (2.82) will be replaced with $\epsilon \partial_\epsilon \partial_j H(\boldsymbol{\xi}; x, \epsilon)$. By taking the j-th partial derivative of (2.85) and following the reasoning that led to (2.86), we find that $\epsilon \partial_\epsilon \partial_j H(\boldsymbol{\xi}; x, \epsilon)$ vanishes as $\epsilon \downarrow 0$. Thus, we may reuse all of the reasoning presented above to show that $\partial_j H(\boldsymbol{\xi}; x, \epsilon)$ approaches a limit as $\epsilon \downarrow 0$ uniformly in sufficiently small neighborhoods of $\mathscr{D}$. It follows immediately from (2.69) that each $\partial_j^2 H(\boldsymbol{\xi}; x, \epsilon)$ approaches a limit as $\epsilon \downarrow 0$ uniformly in sufficiently small neighborhoods of $\mathscr{D}$ too.

Now we show that this limit of $H(\boldsymbol{\xi}; x, \epsilon)$ solves the system (2.1-2.2) in the coordinates of $\boldsymbol{\xi}$ and with $N \mapsto N-1$. We prove this by showing that (2.69, 2.72-

2.74) approaches this system as $\epsilon \downarrow 0$. Upon inspection, it is evident that we need $\epsilon\partial_\epsilon H(\boldsymbol{\xi}; x, \epsilon)$ and $\partial_x H(\boldsymbol{\xi}; x, \epsilon)$ to vanish as $\epsilon \downarrow 0$. Having proven the former statement in (2.86), we now prove the latter. Upon subtracting (2.71) from (2.70), we find the following PDE:

$$\begin{aligned}\left[\frac{\kappa}{4}\partial_x - \frac{\kappa}{2}\partial_\epsilon + \frac{8-\kappa}{2\epsilon}\right]\partial_x H(\boldsymbol{\xi}; x, \epsilon) \\ = \sum_j \left[\frac{\epsilon\partial_j}{(\xi_j - x)(\xi_j - x - \epsilon)} + \frac{[\epsilon + 2(x-\xi_j)]\epsilon(6-\kappa)/2\kappa}{(\xi_j - x)^2(\xi_j - x - \epsilon)^2}\right] H(\boldsymbol{\xi}; x, \epsilon). \quad (2.89)\end{aligned}$$

We choose an $a > 0$ less than $\min\{x - \xi_{i-1}, (b-\epsilon)/2\}$, and we let $Z(t) := \partial_x H(\xi; x - t, \epsilon + 2t)$ for $t \in [0, a]$. Upon evaluating (2.89) at $(\boldsymbol{\xi}; x, \epsilon) \mapsto (\boldsymbol{\xi}, x - t, \epsilon + 2t)$ and multiplying both sides by $-4(\epsilon + 2t)^{1-8/\kappa}/\kappa$, we find

$$\begin{aligned}\frac{d}{dt}\left[(\epsilon + 2t)^{1-8/\kappa} Z(t)\right] = -\frac{4}{\kappa}(\epsilon + 2t)^{2-8/\kappa} \sum_j \left[\frac{\partial_j}{(\xi_j - x + t)(\xi_j - x - \epsilon - t)}\right. \\ \left. + \frac{[\epsilon + 2(x-\xi_j)](6-\kappa)/2\kappa)}{(\xi_j - x + t)^2(\xi_j - x - \epsilon - t)^2}\right] H(\xi; x - t, \epsilon + 2t). \quad (2.90)\end{aligned}$$

Integrating both sides with respect to t from 0 to a, we have

$$\begin{aligned}\partial_x H(\boldsymbol{\xi}; x, \epsilon) = \left(\frac{\epsilon}{\epsilon + 2a}\right)^{8/\kappa - 1} \partial_x H(\boldsymbol{\xi}; x - a, \epsilon + 2a) \\ + \frac{4}{\kappa}\epsilon^{8/\kappa - 1} \int_0^a dt\, (\epsilon + 2t)^{2-8/\kappa} \sum_j \left[\frac{\partial_j}{(\xi_j - x + t)(\xi_j - x - \epsilon - t)}\right. \\ \left. + \frac{[\epsilon + 2(x-\xi_j)](6-\kappa)/2\kappa)}{(\xi_j - x + t)^2(\xi_j - x - \epsilon - t)^2}\right] H(\boldsymbol{\xi}; x - t, \epsilon + 2t).\end{aligned} \quad (2.91)$$

Because the sum inside of the integrand is a function of t bounded over $(0, a)$ uniformly in $\epsilon \in (0, b)$, we have that for some positive function $c_5(\boldsymbol{\xi}, x, a)$

$$|\partial_x H(\boldsymbol{\xi}; x, \epsilon)| \leq \left(\frac{\epsilon}{\epsilon + 2a}\right)^{8/\kappa - 1} |\partial_x H(\boldsymbol{\xi}; x - a, \epsilon + 2a)|$$

$$+ c_5 \epsilon^{8/\kappa - 1} \int_0^a dt \, (\epsilon + 2t)^{2 - 8/\kappa}. \quad (2.92)$$

We therefore have

$$\partial_x H(\boldsymbol{\xi}; x, \epsilon) = O(\epsilon^{8/\kappa - 1}) + O(\epsilon^2) \to 0 \quad \text{as } \epsilon \downarrow 0. \quad (2.93)$$

So by sending $\epsilon \downarrow 0$ in (2.69) and (2.72-2.74), we find equations almost identical to the $(2N-2)$ null-state PDEs and the three Ward identities in the coordinates of $\boldsymbol{\xi}$:

$$\frac{\kappa}{4} \lim_{\epsilon \downarrow 0} \partial_k^2 H + \sum_{j \neq k} \left(\frac{1}{\xi_j - \xi_k} \lim_{\epsilon \downarrow 0} \partial_j H - \frac{(6-\kappa)/2\kappa}{(\xi_j - \xi_k)^2} \lim_{\epsilon \downarrow 0} H \right) = 0 \quad (2.94)$$

$$\sum_j \lim_{\epsilon \downarrow 0} \partial_j H = 0 \quad (2.95)$$

$$\sum_j \xi_j \lim_{\epsilon \downarrow 0} \partial_j H + \theta_1 \lim_{\epsilon \downarrow 0} H = 0 \quad (2.96)$$

$$\sum_j \xi_j^2 \lim_{\epsilon \downarrow 0} \partial_j H + 2\theta_1 \xi_j \lim_{\epsilon \downarrow 0} H = 0. \quad (2.97)$$

Because the limit of each derivative is approached uniformly in a sufficiently small neighborhood of $\mathscr{D}$, we may commute the limit with each differentiation in (2.94-2.97) to find that H solves the $(2N-2)$ null-state PDEs and the three Ward identities in the coordinates of $\boldsymbol{\xi}$.

Equation (2.72) shows that we may also commute the limit $\epsilon \downarrow 0$ with a single derivative with respect to x. Because $\partial_x H(\boldsymbol{\xi}; x, \epsilon)$ vanishes as $\epsilon \downarrow 0$, it therefore immediately follows that the limit of $H(\boldsymbol{\xi}; x, \epsilon)$ does not depend on x.

□

We note some facts that are implied by the proof of lemma II.4. First, this proof leads to some interesting integral equations that $H(\boldsymbol{\xi}; x, \epsilon)$ and $\tilde{F}(\boldsymbol{\xi}; x, \epsilon)$ must satisfy.

After replacing ϵ with zero and replacing b with ϵ in (2.82), we find

$$H(\boldsymbol{\xi}; x, \epsilon) = H(\boldsymbol{\xi}; x, 0) + \frac{\kappa\epsilon}{8-\kappa}\partial_\epsilon H(\boldsymbol{\xi}; x, \epsilon) - \frac{4}{8-\kappa}\int_0^\epsilon \eta \mathcal{M}[H](\boldsymbol{\xi}; x, \eta)\, d\eta. \quad (2.98)$$

This integral equation is interesting because it integrates over all $\eta \in (0, \epsilon)$ instead of over all $\eta > \epsilon$ up to some positive cutoff b. By moving the middle term on the right side to the left side, rewriting the left side as a derivative, and integrating up to some cutoff b (sufficiently small so that the integral is not improper), we further find that

$$H(\boldsymbol{\xi}; x, \epsilon) = \left(\frac{\epsilon}{b}\right)^{8/\kappa-1} H(\boldsymbol{\xi}; x, b) + \left[1 - \left(\frac{\epsilon}{b}\right)^{8/\kappa-1}\right] H(\boldsymbol{\xi}; x, 0) - \frac{4\epsilon^{8/\kappa-1}}{\kappa}\int_\epsilon^b \int_0^\beta \beta^{-8/\kappa}\eta \mathcal{M}[H](\boldsymbol{\xi}; x, \eta)\, d\eta\, d\beta. \quad (2.99)$$

In terms of $\tilde{F}(\boldsymbol{\xi}; x, \epsilon)$, this is

$$\tilde{F}(\boldsymbol{\xi}; x, \epsilon) = \left(\frac{\epsilon}{b}\right)^{2/\kappa} \tilde{F}(\boldsymbol{\xi}; x, b) + \left[\left(\frac{\epsilon}{b}\right)^{1-6/\kappa} - \left(\frac{\epsilon}{b}\right)^{2/\kappa}\right] b^{1-6/\kappa} H(\boldsymbol{\xi}; x, 0) - \frac{4\epsilon^{2/\kappa}}{\kappa}\int_\epsilon^b \int_0^\beta \beta^{-8/\kappa}\eta^{6/\kappa} \mathcal{M}[\tilde{F}](\boldsymbol{\xi}; x, \eta)\, d\eta\, d\beta. \quad (2.100)$$

We will use these integral equations later.

Second, because the limit $F'(\boldsymbol{x}')$ in (2.81) does not depend on x_i, we may take the trivial limit $x_i \to x_{i-1}$ after sending $x_{i+1} \to x_i$ so that the domain of F' is

$$\Omega_0' := \{(x_1, \ldots, x_{i-1}, x_{i+2}, \ldots, x_{2N}) \in \mathbb{R}^{2N-2} \,:\, x_1 < \ldots < x_{i-1} < x_{i+2} < \ldots < x_{2N}\}.$$

Definition II.5. We call $F' : \Omega_0' \to \mathbb{R}$ in lemma II.4 a *limit solution*.

Definition II.6. Let $\kappa \in (0, 8)$. Define $\mathcal{S}_1$ be the one-dimensional vector space spanned by the solution (2.35) for the system (2.1-2.2) when $N = 1$. Let $\mathcal{S}_N$ be the subspace of solutions for the system (2.1-2.2) that satisfy the conditions (2.60) for all

$\boldsymbol{x} \in \Omega_0$, the equivalent condition at infinity,

$$\begin{cases} F(-t, x_2, \ldots, x_{2N-1}, t) = O(t^{-2\theta_1}) \\ \partial_j F(-t, x_2, \ldots, x_{2N-1}, t) = O(t^{-2\theta_1}) \qquad \text{as } t \to \infty \\ \partial_j \partial_k F(-t, x_2, \ldots, x_{2N-1}, t) = O(t^{-2\theta_1}) \end{cases} \tag{2.101}$$

for all $x_2 < x_3 < \ldots < x_{2N-2} < x_{2N-1}$ and all $j, k \in \{2, \ldots, 2N-1\}$, and have all of their limit solutions in $\mathcal{S}_{N-1}$.

The new condition at infinity will be used below. The space $\mathcal{S}_N$ is defined recursively, which is somewhat awkward. The low-dimensional examples of section 2.2 and the discussion following lemma II.3 suggest the following conjecture.

Conjecture II.7. *Let $\kappa \in (0, 8)$. Then $\mathcal{S}_N$ constitutes the entire solution space of the system (2.1-2.2).*

We can prove the conjecture if we can prove lemma II.3 with the condition that the solution not change sign infinitely often as $x_{i+1} \to x_i$ dropped, since this gives (2.60). The condition at infinity is then proven by mapping $-t$ and t to adjacent points $f(-t)$ and zero via the mapping (2.108), to be used below, and using the proven lemma II.3. Further details are presented in the discussion following (2.108).

The discussion preceding (2.7) suggests that the dimension of $\mathcal{S}_N$ equals the N-th Catalan number C_N. Next, we show that $\dim \mathcal{S}_N \leq C_N$ if a certain conjecture, conjecture II.16, is true. We obtain this upper bound by studying the dual space $\mathcal{S}_N^*$ for which lemma II.4 suggests a construction. We start with an element of $\mathcal{S}_N$, take the limit shown in (2.81), and arrive with an element of $\mathcal{S}_{N-1}$. Then we repeat this process $N-1$ more times until we arrive with an element of $\mathcal{S}_0 = \mathbb{R}$. Because it is a linear map of $\mathcal{S}_N$ into the real numbers, this sequence of limits is an element of $\mathcal{S}_N^*$. This leads us to the notion of a consistently ordered sequences of limits.

Definition II.8. Let $M \leq N$, and let $S = \{x_{i_1}, \ldots, x_{i_{2M}}\} \subset \{x_1, \ldots, x_{2N}\}$ be a subset of coordinates such that for all $j, k \in \{1, \ldots, M\}$,

- $x_{i_{2j-1}} < x_{i_{2j}}$,
- if $x_{i_{2j-1}} < x_{i_{2k-1}} < x_{i_{2j}}$, then $x_{i_{2j-1}} < x_{i_{2k-1}} < x_{i_{2k}} < x_{i_{2j}}$,
- if $x_{i_{2j-1}} < x_{i_{2k}} < x_{i_{2j}}$, then $x_{i_{2j-1}} < x_{i_{2k-1}} < x_{i_{2k}} < x_{i_{2j}}$,
- the set $\{x_1, \ldots, x_{2N}\} \backslash S$ is in either in the interval $(x_{i_{2j-1}}, x_{i_{2j}})$ or is in the interval $(x_{i_{2j}}, x_{i_{2j-1}}) := (-\infty, x_{i_{2j-1}}) \cup (x_{i_{2j}}, \infty)$ with the two infinities identified.

Let the symbols $\bar{\ell}_j$ and $\underline{\ell}_j$ stand for the limits

$$\bar{\ell}_j := \{x_{i_{2j}} \to x_{i_{2j-1}}\}, \quad \underline{\ell}_j := \{x_{i_{2j}} \to \infty, x_{i_{2j-1}} \to -\infty\},$$

and let ℓ_j stand for either. Let $\mathscr{L}$ be the ordered collection $\{\ell_1, \ldots, \ell_M\}$. Then $\mathscr{L}$ is said to be a *consistently ordered sequence of limits involving the coordinates in* S if the following are true for all $j, k \in \{1, \ldots, M\}$:

- Either $\bar{\ell}_j \in \mathscr{L}$ or $\underline{\ell}_j \in \mathscr{L}$, but not both.
- If $M < N$, then which of either $\bar{\ell}_j$ or $\underline{\ell}_j$ is in $\mathscr{L}$ is determined as follows:

$$\{x_1, \ldots, x_{2N}\} \setminus S \subset (x_{i_{2j}}, x_{i_{2j-1}}) \quad \Longrightarrow \quad \bar{\ell}_j \in \mathscr{L}, \tag{2.102}$$

$$\{x_1, \ldots, x_{2N}\} \setminus S \subset (x_{i_{2j-1}}, x_{i_{2j}}) \quad \Longrightarrow \quad \underline{\ell}_j \in \mathscr{L}. \tag{2.103}$$

- If $x_{i_{2j-1}} < x_{i_{2k-1}} < x_{i_{2k}} < x_{i_{2j}}$, then we say that ℓ_j *nests* ℓ_k, and

$$\bar{\ell}_j \in \mathscr{L} \quad \Longrightarrow \quad \bar{\ell}_k \in \mathscr{L}, \quad \text{and} \quad k < j, \tag{2.104}$$

$$\underline{\ell}_k \in \mathscr{L} \quad \Longrightarrow \quad \underline{\ell}_j \in \mathscr{L}, \quad \text{and} \quad j < k. \tag{2.105}$$

- If $x_{i_{2j-1}} < x_{i_{2j}} < x_{i_{2k-1}} < x_{i_{2k}}$ or $x_{i_{2k-1}} < x_{i_{2k}} < x_{i_{2j-1}} < x_{i_{2j}}$, then we say that ℓ_j *does not nest* ℓ_k, and

$$\underline{\ell}_j \in \mathscr{L} \quad \Longrightarrow \quad \bar{\ell}_k \in \mathscr{L}, \quad \text{and} \quad k < j. \tag{2.106}$$

If $M = N$, then the above rules may not determine which of $\bar{\ell}_j$ or $\underline{\ell}_j$ is in $\mathscr{L}$. If this is true, then either $\bar{\ell}_j$ or $\underline{\ell}_j$ may be in $\mathscr{L}$. We call M the *length* of $\mathscr{L}$. Now let F be some function of $x_{i_{2j-1}}$ and $x_{i_{2j}}$. We promote the symbols $\bar{\ell}_j$ and $\underline{\ell}_j$ to transforms that act on F by

$$\bar{\ell}_j F := \lim_{x_{i_{2j}} \to x_{i_{2j-1}}} (x_{i_{2j}} - x_{i_{2j-1}})^{2\theta_1} F(x_{i_{2j-1}}, x_{i_{2j}}), \quad \underline{\ell}_j F = \lim_{t\to\infty} (2t)^{2\theta_1} F(-t, t), \tag{2.107}$$

provided that these limits exist, and we say that $\bar{\ell}_j$ (resp. $\underline{\ell}_j$) *collapses* the interval $(x_{i_{2j-1}}, x_{i_{2j}})$ (resp. $(x_{i_{2j}}, x_{i_{2j-1}})$). We define the action of $\mathscr{L} = \{\ell_1, \ldots, \ell_M\}$ on $F : \Omega_0 \to \mathbb{R}$ as $\mathscr{L}F = \ell_M \ell_{M-1} \ldots \ell_2 \ell_1 F$ when this limit exists.

According to theorem II.4, the limit $\bar{\ell}F$ with $\bar{\ell} = \{x_{i+1} \to x_i\}$ exists and is in $\mathcal{S}_{N-1}$ for all $F \in \mathcal{S}_N$ and all $i \in \{1, \ldots, 2N-1\}$ when $\kappa \in (0, 8)$. This definition tackles the issue of how to take several of these limits in sequence in a way that is well-defined. For example, if $x_1 < x_2 < x_3 < x_4$, then the limit $x_4 \to x_1$ must follow the limit $x_3 \to x_2$. Definition II.8 prescribes the necessary conditions to ensure that this happens.

Next, we show that the limit $\underline{\ell}F$ exists for $\underline{\ell} = \{x_{2N} \to \infty, x_1 \to -\infty\}$ and is in $\mathcal{S}_{N-1}$ for all $F \in \mathcal{S}_N$ and all $i \in \{1, \ldots, 2N-1\}$ when $\kappa \in (0, 8)$. We also call this limit a limit solution of F, naturally extending definition II.5. To show that $\underline{\ell}F$ exists, we employ the Möbius transformation

$$f(x) = \frac{(x_{2N-1} - x_{2N-2})(x - x_{2N})}{(x_{2N} - x_{2N-2})(x - x_{2N-1})}, \tag{2.108}$$

and we write $x' = f(x)$ in the computations that follow. A straightforward calculation shows that f cyclically permutes the coordinates rightward along the real axis so that $x'_{2N} = 0 < x'_1 < x'_2 < \ldots < x'_{2N-2} = 1 < x'_{2N-1} = \infty$. From (2.5), we find

$$(2t)^{2\theta_1} F(-t, x_2, \ldots, x_{2N-1}, t) \underset{t\to\infty}{\sim} |\partial f(x_2)|^{\theta_1} \ldots |\partial f(x_{2N-1})|^{\theta_1} x_1'^{2\theta_1} F(x'_1, \ldots, x'_{2N}). \quad (2.109)$$

We note that the point $\boldsymbol{x}' := (x'_1, \ldots, x'_{2N})$ is not in Ω_0 since $x'_{2N} < x'_1$, yet if we write $F(\boldsymbol{x})$ in the form (2.4) with $\sigma(1) = 2N$, then $F(\boldsymbol{x}')$ is defined by the right side of (2.4) and solves the system (2.1-2.2) in the primed coordinates. Moreover, the condition at infinity (2.101) implies that $F(\boldsymbol{x}')$ satisfies the condition (2.60) in the primed coordinates with $i \mapsto 2N$ and $i+1 \mapsto 1$. The limit $t \to \infty$ is equivalent to $x'_1 \to x'_{2N}$, so if we let $\bar{\ell} = \{x'_1 \to x'_{2N}\}$, then we have

$$\underline{\ell} F(x_2, \ldots, x_{2N-1}) = |\partial f(x_2)|^{\theta_1} \ldots |\partial f(x_{2N-1})|^{\theta_1} \bar{\ell} F(x'_2, \ldots, x'_{2N-1}). \quad (2.110)$$

According to lemma II.4, the limit on the right side exists and, upon transforming back to the unprimed coordinates (which eliminates the derivative prefactors), solves the system (2.1-2.2) in the unprimed coordinates $x_2, \ldots, x_{2N}$. It is therefore in $\mathcal{S}_{N-1}$. Thus, an "underbar" limit $\underline{\ell}$ is essentially equivalent to an "overbar limit" $\bar{\ell}$. This result together with lemma II.4 proves the following lemma.

Lemma II.9. *Let $\kappa \in (0, 8)$, and let $\mathscr{L} = \{\ell_1, \ldots, \ell_M\}$ be a consistently ordered sequence of limits of length M. Then the limit $\mathscr{L}F$ exists for all $F \in \mathcal{S}_N$ and is in $\mathcal{S}_{N-M}$. In particular, if $M = N$, then the limit is a real number.*

Proof. We let $S_M = \{x_{i_1}, \ldots, x_{i_{2M}}\} \subset \{x_1, \ldots, x_{2N}\}$, and we let $\mathscr{L} =: \mathscr{L}_M = \{\ell_1, \ell_2, \ldots, \ell_M\}$ be a consistently ordered sequence of limits involving the coordinates in S_M. If the first element of $\mathscr{L}_M$ is $\bar{\ell}_1 = \{x_{i_2} \to x_{i_1}\}$, then according to definition II.8,

$\bar{\ell}_1$ cannot nest any other element of $\mathscr{L}_M$, and no coordinate among $\{x_1, \ldots, x_{2N}\} \setminus S_M$ is in (x_{i_1}, x_{i_2}). It follows that $x_{i_1} = x_i$ and $x_{i_2} = x_{i+1}$ for some $i \in \{1, \ldots, 2N-1\}$. According to lemma II.4, the limit $\bar{\ell}_1 F$ exists and is in $\mathcal{S}_{N-1}$. Or, if the first element of $\mathscr{L}_M$ is $\underline{\ell}_1 = \{x_{i_2} \to \infty, x_{i_1} \to -\infty\}$, then according to definition II.8, no other element of $\mathscr{L}_M$ can nest $\underline{\ell}_1$, and all coordinates among $\{x_1, \ldots, x_{2N}\} \setminus S_M$ must be in (x_{i_1}, x_{i_2}). It follows that $x_{i_1} = x_1$ and $x_{i_2} = x_{2N}$. According to the calculation presented before lemma II.9, the limit $\underline{\ell}_1 F$ exists and is in $\mathcal{S}_{N-1}$. We are now left with showing that the limit $\mathscr{L}_{M-1}\ell_1 F$ with $\mathscr{L}_{M-1} = \{\ell_2, \ldots, \ell_M\}$ exists. It is straightforward to check that $\mathscr{L}_{M-1}$ is a consistently ordered sequence of limits involving the coordinates in $S_{M-1} = \{x_{i_1}, \ldots, x_{i_{2M}}\}$ as a subset of $\{x_1, \ldots, x_{2N}\} \setminus \{x_{i_1}, x_{i_2}\}$. But because $\ell_1 F \in \mathcal{S}_{N-1}$, we can repeat the reasoning presented above to conclude that $\ell_2 \ell_1 F$ exists and is in $\mathcal{S}_{N-2}$. We may repeat this reasoning $M-2$ more times until we find that $\ell_M \ldots \ell_1 F$ exists and is in $\mathcal{S}_{N-M}$. □

The set of consistently ordered sequences of limits forms a vector space with a natural partition into equivalence classes given by the following definition.

Definition II.10. We say that two consistently ordered sequences of limits $\mathscr{L} = \{\ell_1, \ldots, \ell_M\}$ and $\mathscr{L}' = \{\ell'_1, \ldots, \ell'_M\}$ involving the same coordinates $\{x_1, \ldots, x_{2M}\}$ are *equivalent* if at least one of the following are true.

- There exists a permutation $\sigma \in S_{2M}$ on $\{1, \ldots, M\}$ such that $\ell'_j = \ell_{\sigma(j)}$ for all $j \in \{1, \ldots, M\}$.
- For any $j \in \{1, \ldots, M\}$, $\bar{\ell}_j$ (resp. $\underline{\ell}_j$) in $\mathscr{L}$ is replaced by $\underline{\ell}_j$ (resp. $\bar{\ell}_j$) in $\mathscr{L}'$.

This defines an equivalence relation on the set of all consistently ordered sequences of limits of length M, and we let $[\mathscr{L}]$ stand for the equivalence class containing $\mathscr{L}$. When $M = N$, we let $\mathscr{B}^*_N := \{[\mathscr{L}_1], [\mathscr{L}_2], \ldots\}$ be the set of all equivalence classes.

Lemma II.11. *The cardinality of $\mathscr{B}^*_N$ equals the N-th Catalan number C_N.*

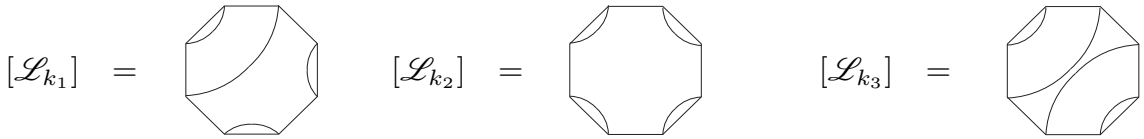

Figure 2.3: Polygon diagrams for three different equivalence classes of consistently ordered sequences of limits of length $N = 4$. The other $C_4 - 3 = 11$ diagrams are found by rotating one of these three.

Proof. To each $[\mathscr{L}]$ of length M, we associate a unique *interior arc connectivity diagram* via the following recipe. If $\{x_{i_{2j}} \to x_{i_{2j-1}}\} \in [\mathscr{L}_k]$, then we connect $x_{i_{2j}}$ to $x_{i_{2j-1}}$ with an *interior arc* in the upper half-plane. We do this for each limit ℓ_j in $[\mathscr{L}]$, taking care to ensure that the arcs do not intersect (which is possible if and only if the sequences of limits are consistently ordered). Thus, each $[\mathscr{L}]$ corresponds to a unique arc connectivity diagram, and vice versa. But in the discussion surrounding (2.7), we proved that the number of such diagrams equals the M-th Catalan number. Now set $M = N$. □

Definition II.12. We define the *half-plane diagram of* $[\mathscr{L}]$ to be the diagram described in the proof of lemma II.11. We define the *polygon diagram* of $[\mathscr{L}]$ to be the image of the half-plane diagram under the conformal map sending the coordinates $x_1, \ldots, x_{2N}$ and the upper half-plane to the vertices and interior of a $2N$-sided polygon respectively (figure 2.3). Often, we will refer to both of these diagrams simply as the *diagram of* $[\mathscr{L}]$, or more generally, as *interior arc connectivity diagrams.* When $M = N$, we call the interior arc connectivity exhibited by the diagram for $[\mathscr{L}_k]$ *the k-th arc connectivity.*

Lemma II.13. *Let $F \in \mathcal{S}_N$, let $\kappa \in (0, 8)$, and let $[\mathscr{L}]$ be an equivalence class of consistently ordered sequences of limits of length $M \leq N$. Then $[\mathscr{L}]F$ is well-defined.*

Proof. We let $F \in \mathcal{S}_N$, and we let $[\mathscr{L}]$ be an equivalence class of consistently ordered sequences of limits of length $M \leq N$. The proof of the lemma is by induction on M.

To begin, we suppose that $[\mathscr{L}]$ has length two. If the arcs for ℓ_1 and ℓ_2 in the half-plane diagram of $[\mathscr{L}]$ are un-nested, we let $\bar{\ell}_1 = \{x_{i+1} \to x_i\}$ and $\bar{\ell}_2 = \{x_{j+1} \to x_j\}$. We must show that $\bar{\ell}_1\bar{\ell}_2 F = \bar{\ell}_2\bar{\ell}_1 F$, or

$$\lim_{x_{i+1}\to x_i}\lim_{x_{j+1}\to x_j}(x_{i+1}-x_i)^{2\theta_1}(x_{j+1}-x_j)^{2\theta_1}F(\boldsymbol{x}) \\ = \lim_{x_{j+1}\to x_j}\lim_{x_{i+1}\to x_i}(x_{i+1}-x_i)^{2\theta_1}(x_{j+1}-x_j)^{2\theta_1}F(\boldsymbol{x}). \quad (2.111)$$

If the arc for ℓ_2 nests the arc for ℓ_1, then by transforming (2.111) via (2.110), we will have proven the equivalent statement $\bar{\ell}_1\underline{\ell}_2 F = \underline{\ell}_2\bar{\ell}_1 F$.

We let $x := x_i, x' := x_j, \epsilon := x_{i+1} - x_i, \epsilon' := x_{j+1} - x_j$ with $j \neq i-1, i, i+1$, we relabel the other $2N-4$ coordinates $\{x_k\}_{k\neq i,i+1,j,j+1}$ in ascending order by $\{\xi_1, \ldots, \xi_{2N-4}\}$, and we let $\boldsymbol{\xi} = (\xi_1, \xi_2, \ldots, \xi_{2N-5}, \xi_{2N-4})$. (This definition of $\boldsymbol{\xi}$ is not the same as that in the proof of lemma II.3). We restrict to $\epsilon \in (0, b], \epsilon' \in (0, b']$ where b and b' are small enough to ensure that x_{i+1} and x_{j+1} are respectively less than x_{i+2} and x_{j+2}. We let $I(\boldsymbol{\xi}; x', \epsilon'; x, \epsilon)$ equal $\epsilon'^{2\theta_1}\epsilon^{2\theta_1}F$. Now for all $\epsilon \in (0, b']$, (2.82) gives

$$I(\boldsymbol{\xi}; x', \epsilon'; x, \epsilon) = I(\boldsymbol{\xi}; x', \epsilon'; x, b) - \frac{\kappa}{4}J(\epsilon, b)\partial_\epsilon I(\boldsymbol{\xi}; x', \epsilon'; x, b) \\ + \int_\epsilon^b J(\epsilon, \eta)\mathcal{N}[I](\boldsymbol{\xi}; x', \epsilon'; x, \eta)d\eta, \quad (2.112)$$

where $J(\epsilon, \eta)$ is defined in (2.83) and where we have

$$\mathcal{N} := \frac{\partial_x}{\eta} - \sum_k\left(\frac{\partial_l}{\xi_l - x - \eta} - \frac{(6-\kappa)/2\kappa}{(\xi_l - x - \eta)^2}\right) - \frac{\partial_{x'} - \partial_{\epsilon'}}{x' - x - \eta} \\ - \frac{\partial_{\epsilon'}}{x' + \epsilon' - x - \eta} + \frac{(6-\kappa)/2\kappa}{(x' - x - \eta)^2} + \frac{(6-\kappa)/2\kappa}{(x' + \epsilon' - x - \eta)^2}. \quad (2.113)$$

Now we fix $\boldsymbol{\xi}, x$, and x' to different values, and we let $I_\epsilon : [0, b'] \to \mathbb{R}$ be such that $I_\epsilon(\epsilon') = I(\boldsymbol{\xi}; x', \epsilon'; x, \epsilon)$ for $\epsilon' \in (0, b']$ and $I_\epsilon(0)$ equals the limit of $I_\epsilon(\epsilon')$ as $\epsilon' \downarrow 0$ (which is guaranteed to exist when $\kappa \in (0, 8)$ thanks to lemma II.3) so that each I_ϵ

is continuous on $[0, b']$. By taking the supremum over all $\epsilon' \in [0, b']$, we find

$$\sup_{\epsilon' \in [0,b']} |I_\epsilon(\epsilon') - I_\epsilon(0)| \leq \frac{\kappa}{8-\kappa} \sup_{\epsilon' \in [0,b']} |\epsilon \partial_\epsilon I(\epsilon')| + \frac{4}{8-\kappa} \int_0^\epsilon \sup_{\epsilon' \in [0,b']} |\eta \mathcal{N}[I_\eta](\epsilon')| \, d\eta. \quad (2.114)$$

It is evident from (2.113) and previous arguments in the proof of lemma II.3 that the integrand is bounded over $[0, b] \times [0, b']$, so the integral vanishes in the limit $\epsilon \downarrow 0$. Furthermore, we can use this former fact and (2.86) to show that $\sup_{\epsilon' \in [0,b]} |\epsilon \partial_\epsilon I(\epsilon')|$ vanishes as $\epsilon \downarrow 0$. Thus, the right side of (2.114) vanishes as $\epsilon \downarrow 0$, $I_\epsilon(\epsilon')$ approaches its limit $I_0(\epsilon')$ uniformly over $[0, b']$, and we may exchange the order of the limits as demonstrated in (2.111). Consequently, we have shown that $[\mathscr{L}]F$ is well-defined when the length of $[\mathscr{L}]$ is two.

Now we suppose that for all $F \in \mathcal{S}_N$ and all $[\mathscr{L}']$ of length less than M, $[\mathscr{L}']F$ is well-defined. We choose an $F \in \mathcal{S}_N$ and an $[\mathscr{L}] = \{\ell_1, \ldots, \ell_M\}$. (Unlike in definition II.8, this set is not ordered. It becomes ordered when we specify an element $\mathscr{L} \in [\mathscr{L}]$, and in this proof, the subscript of ℓ_n does not indicate this ordering. Rather the subscript labels the arcs in the diagram for $[\mathscr{L}]$.) Each element of $[\mathscr{L}]$ equals $\ell_m \mathscr{L}_m$ for some $m \in \{1, \ldots, M\}$ and some $\mathscr{L}_m \in [\mathscr{L}_m] = \{\ell_k\}_{k \neq m}$ of length $M - 1$. We let A be the set of all indices m for which there is an element of $[\mathscr{L}]$ that ends with ℓ_m. For fixed $m \in A$, all elements of $[\mathscr{L}]$ of the form $\ell_m \mathscr{L}_m$ are equivalent by definition, and we represent their equivalence sub-class by $\ell_m[\mathscr{L}_m]$. By the induction hypothesis, $[\mathscr{L}_m]F$ is well-defined for all $m \in A$, so to finish the proof, we must show that $\ell_m[\mathscr{L}_m]F = \ell_n[\mathscr{L}_n]F$ for each pair $(m, n) \in A \times A$.

If we suppose that $M < N$, then the condition that $m, n \in A$ and $m \neq n$ places constraints on the arc connectivities in the half-plane diagram of $[\mathscr{L}]$. In this diagram, the arc for ℓ_m (resp. ℓ_n) connects the coordinates $x_{i_{2m-1}}$ and $x_{i_{2m}}$ (resp. $x_{i_{2n-1}}$ and $x_{i_{2n}}$). We let $S := \{x_{i_1}, \ldots, x_{i_{2M}}\}$ be the set of coordinates involved in $[\mathscr{L}]$ (or the set of

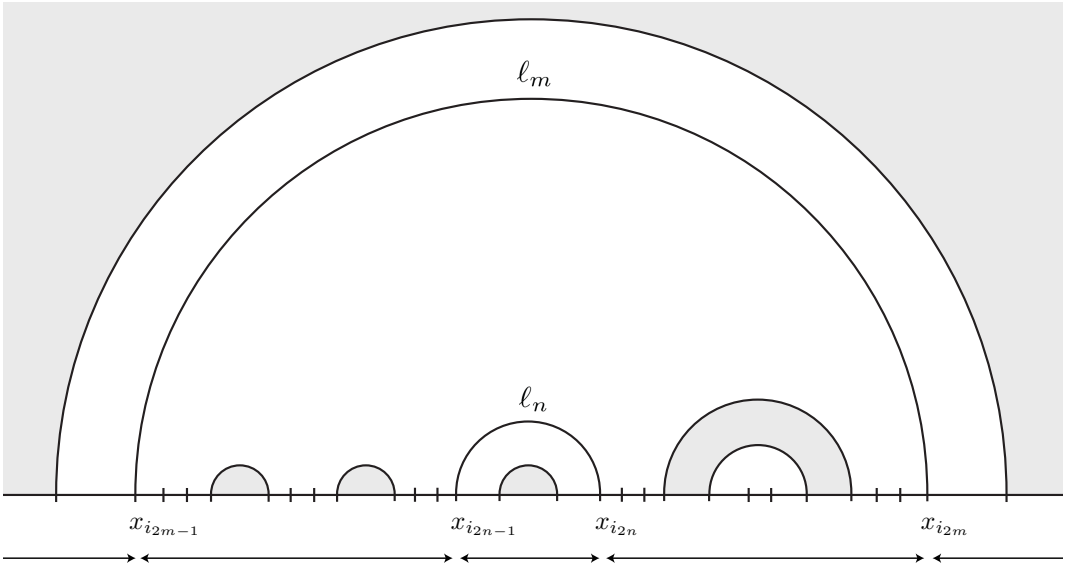

Figure 2.4: A possibile interior arc connectivity for an $[\mathscr{L}]$ that can be decomposed as $\ell_m[\mathscr{L}_m]$ and $\ell_n[\mathscr{L}_n]$. The arcs for ℓ_n and ℓ_m are shown while the other $M-2$ arcs, not shown, are in the gray regions. The tick marks locate the coordinates in $\{x_1, \ldots, x_{2N}\} \setminus S$.

coordinates connected together by arcs in the diagram for $[\mathscr{L}]$), and we suppose that the arc for ℓ_m nests the arc for ℓ_n. We recall that $m \in A$ if there is an element of $[\mathscr{L}]$ in which the limit ℓ_m is taken last. Then if $m, n \in A$, one can show that since $M < N$,

1. all coordinates in $\{x_1, \ldots, x_{2N}\} \setminus S$ must be in $(x_{i_{2m-1}}, x_{i_{2n-1}}) \cup (x_{i_{2n}}, x_{i_{2m}})$, or else it will not be possible to collapse either ℓ_m or ℓ_n last (a contradiction), and

2. no arc in the half-plane diagram of $[\mathscr{L}]$ may connect an $x_i \in (x_{i_{2m-1}}, x_{i_{2n-1}})$ with an $x_j \in (x_{i_{2n}}, x_{i_{2m}})$, or else it will not be possible to collapse either ℓ_m or ℓ_n last (a contradiction).

The last restriction follows from the first restriction. Figure 2.4 gives an example diagram for such an $[\mathscr{L}]$. As a consequence of these two restrictions, the coordinates $x_{i_{2m-1}}$,$x_{i_{2n-1}}$,$x_{i_{2n}}$, and $x_{i_{2m}}$ divide the $M-2$ arcs in the half-plane diagram for $[\mathscr{L}]$ not associated with ℓ_m or ℓ_n into four "bins." The first bin contains arcs whose two endpoints are in $(-\infty, x_{i_{2m-1}}) \cup (x_{i_{2m}}, \infty)$, the second in $(x_{i_{2m-1}}, x_{i_{2n-1}})$, the third

in $(x_{i_{2n-1}}, x_{i_{2n}})$, and the fourth in $(x_{i_{2n}}, x_{i_{2m}})$. Because these arcs are isolated into bins, there exists a consistently ordered sequence of limits $\mathscr{L}_{m,n}$ that collapses all of the intervals of these arcs, leaving only the arc for ℓ_m and the arc for ℓ_n. Because, $\mathscr{L}_{m,n} \subset \mathscr{L}$, lemma II.9 implies that $\mathscr{L}_{m,n}F \in \mathcal{S}_{N-M+2}$. We have already proven that $\underline{\ell}_m \bar{\ell}_n \mathscr{L}_{m,n}F = \bar{\ell}_n \underline{\ell}_m \mathscr{L}_{m,n}F$ in (2.111). But also, $\bar{\ell}_n \mathscr{L}_{m,n} \in [\mathscr{L}_m]$ and $\underline{\ell}_m \mathscr{L}_{m,n} \in [\mathscr{L}_n]$, so this equality and the induction hypothesis imply that $\underline{\ell}_m[\mathscr{L}_m]F = \bar{\ell}_n[\mathscr{L}_n]F$ for $m, n \in A$. Thus, $[\mathscr{L}]F$ is well-defined when $M < N$. The proof for the case where the arcs for ℓ_m, ℓ_n are un-nested proceeds similarly.

When $N = M$, the two constraints mentioned above no longer apply. First, the set $\{x_1, \ldots, x_{2N}\} \setminus S$ is empty, and second (supposing again that the arc for ℓ_m nests the arc for ℓ_n), an arc may connect an $x_i \in (x_{i_{2m-1}}, x_{i_{2n-1}})$ with an $x_j \in (x_{i_{2n}}, x_{i_{2m}})$. If the latter possibility is not exhibited, then the argument of the previous paragraph proves that $[\mathscr{L}]F$ is well-defined when $M = N$. If it is exhibited, then we let $\ell_{k_1}, \ldots, \ell_{k_l}$ label the l arcs connecting an $x_i \in (x_{i_{2m-1}}, x_{i_{2n-1}})$ with an $x_j \in (x_{i_{2n}}, x_{i_{2m}})$ from outermost at ℓ_{k_1} to innermost at ℓ_{k_l}. When $M = N$, it is easy to see that all elements of $[\mathscr{L}]$ are in A. Thus, we may use the previous result to conclude that $\underline{\ell}_m[\mathscr{L}_m]F = \bar{\ell}_{k_1}[\mathscr{L}_{k_1}]F$, then (because $\{x_1, \ldots, x_{2N}\} \setminus S$ is empty) $\underline{\ell}_{k_1}[\mathscr{L}_{k_1}]F = \bar{\ell}_{k_2}[\mathscr{L}_{k_2}]F$, etc., until we reach $\underline{\ell}_{k_l}[\mathscr{L}_{k_l}]F = \bar{\ell}_n[\mathscr{L}_n]F$. Thus, $\ell_m[\mathscr{L}_m]F = \ell_n[\mathscr{L}_n]F$, so $[\mathscr{L}]F$ is well-defined when $M = N$. The proof for the case where the arcs for ℓ_m and ℓ_n are un-nested proceeds similarly. □

Now we define an *identity interval,* a *two-leg interval,* and a *mixed interval,* and these definitions will clearly be motivated by CFT considerations. Namely, if each endpoint of an interval (x_i, x_{i+1}) host a one-leg operator, then upon sending $x_{i+1} \to x_i$, these operators will fuse into a combination of an identity operator and a two-leg operator. As previously discussed, these two fusion channels are observed in the Frobenius series expansions of the correlation function in x_{i+1} about x_i. A series with indicial power $p = -2\theta_1 + \theta_0 = 1 - 6/\kappa$ (resp. $p = -2\theta_1 - \theta_2 = 2/\kappa$) corresponds with

the identity (resp. two-leg) family of the OPE. Lemma II.4 allows us to capture this phenomenon in a slightly more general way that applies to any element of $\mathcal{S}_N$.

Definition II.14. Let $F \in \mathcal{S}_N$, let $\kappa \in (0,8)$, let $i \in \{1,\dots,2N-1\}$, and let $\boldsymbol{x} \in \Omega_0$. We call the open interval (x_i, x_{i+1})

- a *two-leg interval* if $\lim_{x_{i+1}\to x_i}(x_{i+1}-x_i)^{2\theta_1}F(\boldsymbol{x}) = 0$,
- an *identity interval* if $\lim_{x_{i+1}\to x_i}(x_{i+1}-x_i)^{2\theta_1}F(\boldsymbol{x}) \neq 0$ and $(x_{i+1}-x_i)^{2\theta_1}F(\boldsymbol{x})$ (continuously extended to $\Omega_0 \cup \mathscr{D}$) is analytic at $x_{i+1} = x_i$ for all $\kappa \in (0,8)$,
- a *mixed interval* if $\lim_{x_{i+1}\to x_i}(x_{i+1}-x_i)^{2\theta_1}F(\boldsymbol{x}) \neq 0$ and $(x_{i+1}-x_i)^{2\theta_1}F(\boldsymbol{x})$ (continuously extended to $\Omega_0 \cup \mathscr{D}$) is not analytic at $x_{i+1} = x_i$ for some $\kappa \in (0,8)$.

In fact, the Green function (2.64) that we used in the proof of lemma II.3 gives the power law for the rate of decay of the limit in the two-leg interval definition. This is simply the two-leg exponent $2/\kappa = -2\theta_1 + \theta_2$, as we expect.

Lemma II.15. *Let $F \in \mathcal{S}_N$, let $\kappa \in (0,8)$, and let $\mathscr{D}$ be as defined in lemma II.4. If (x_i, x_{i+1}) is a two-leg interval, then $F(\boldsymbol{x}) = O((x_{i+1}-x_i)^{-2\theta_1+\theta_2})$ as $x_{i+1} \to x_i$ for all $\boldsymbol{x}' \in \mathscr{D}$, where $\theta_2 := 8/\kappa - 1$ is the conformal weight (1.171) of the boundary two-leg operator. Furthermore, the limit*

$$F_2(\boldsymbol{x}') := \lim_{x_{i+1}\to x_i}(x_{i+1}-x_i)^{2\theta_1-\theta_2}F(\boldsymbol{x}) \tag{2.115}$$

exists for all $\kappa \in (0,8)$ and all points $\boldsymbol{x}' \in \mathscr{D}$ and is not zero if F is not zero. Finally, for each $j \in \{1,\dots,i-1,i+2,\dots,2N\}$, $F_2(\boldsymbol{x}')$ solves the modified null-state PDE centered on x_j,

$$\left[\frac{\kappa}{4}\partial_j^2 + \sum_{k\neq j,i,i+1}^{2N}\left(\frac{\partial_j}{x_k-x_j} - \frac{\theta_1}{(x_k-x_j)^2}\right) + \frac{\partial_i}{x_i-x_j} - \frac{\theta_2}{(x_i-x_j)^2}\right]F_2(\boldsymbol{x}') = 0, \tag{2.116}$$

and the modified Ward identities

$$\begin{cases} \sum_{j=1}^{2N} \partial_j F_2(\boldsymbol{x}') = 0 \\ \left[\sum_{j\neq i}^{2N}(x_j\partial_j + \theta_1) + \partial_i + \theta_2\right] F_2(\boldsymbol{x}') = 0 \\ \left[\sum_{j\neq i}^{2N}(x_j^2\partial_j + 2\theta_1 x_j) + x_i^2\partial_i + 2\theta_2 x_i\right] F_2(\boldsymbol{x}') = 0 \end{cases} . \tag{2.117}$$

Proof. Because $F \in \mathcal{S}_N$, the integrand for the η integration in (2.100) is bounded as $\eta \downarrow 0$. Thus, the complete term in (2.100) with the double integral is $O(\epsilon^{2-6/\kappa})$. Furthermore, $H(\boldsymbol{\xi}; x, 0) = 0$ since (x_i, x_{i+1}) is a two-leg interval, so $\tilde{F}(\boldsymbol{\xi}; x, \epsilon) = O(\epsilon^p)$ for $p = \min\{2/\kappa, 2-6/\kappa\}$. If $p = 2-6/\kappa$, then we insert this result back into (2.100) and repeat these steps to find that $\tilde{F}(\boldsymbol{\xi}; x, \epsilon) = O(\epsilon^p)$ for $p = \min\{2/\kappa, 3-6/\kappa\}$. We continue this process until we have $p = 2/\kappa = -2\theta_1 + \theta_2$.

Now we show that the limit (2.115) exists and is approached uniformly over small neighborhoods of $\mathscr{D}$. The reasoning follows the proof of lemma II.4. We let $K(\boldsymbol{\xi}; x, \epsilon) := \epsilon^{-2/\kappa}\tilde{F}(\boldsymbol{\xi}; x, \epsilon)$. Then (2.100) shows that

$$K(\boldsymbol{\xi}; x, \epsilon) - K(\boldsymbol{\xi}; x, b) = -\frac{4}{\kappa}\int_\epsilon^b \frac{1}{\beta}\int_0^\beta \left(\frac{\eta}{\beta}\right)^{8/\kappa-1} \eta\mathcal{M}[K](\boldsymbol{\xi}; x, \eta)\, d\eta\, d\beta. \tag{2.118}$$

According to previous arguments, the integrand of the η integral is bounded for all $\eta \in (0, b)$. Thus, the integral vanishes as $\epsilon, b \downarrow 0$, we have

$$\lim_{b\downarrow 0} \sup_{0<\epsilon<b} |K(\boldsymbol{\xi}; x, \epsilon) - K(\boldsymbol{\xi}; x, b)| = 0, \tag{2.119}$$

and the limit $F_2(\boldsymbol{\xi}; x)$ of $K(\boldsymbol{\xi}; x, \epsilon)$ as $\epsilon \downarrow 0$ exists. Letting $b = 0$ in (2.118) and letting U be a sufficiently small neighborhood of $(\boldsymbol{\xi}, x)$ in $\mathscr{D}$, we have

$$\sup_U |K(\boldsymbol{\xi}; x, \epsilon) - K(\boldsymbol{\xi}; x, 0)| \le \frac{4}{\kappa}\int_0^\epsilon \frac{1}{\beta}\int_0^\beta \sup_U |\eta\mathcal{M}[K](\boldsymbol{\xi}; x, \eta)|\, d\eta\, d\beta \longrightarrow 0 \quad \text{as } \epsilon \downarrow 0. \tag{2.120}$$

The limit follows because the supremum of the integrand of the η integral is bounded for all $\eta \in (0, b)$. Hence, the limit $F_2(\boldsymbol{\xi}; x)$ is approached uniformly in U and is therefore continuous. The same is shown to be true of its first and second derivatives with respect to the coordinates of $\boldsymbol{\xi}$ by following the same procedure.

Next, we show that the limit $F_2(\boldsymbol{\xi}; x) = K(\boldsymbol{\xi}; x, 0)$ is not zero. To the contrary, we suppose that $K(\boldsymbol{\xi}; x, 0)$ is zero while $\tilde{F}$ is not zero. Letting $b = 0$ in (2.118) and recalling that $|\eta \mathcal{M}[K](\boldsymbol{\xi}; x, \eta)|, |\eta \partial_j \mathcal{M}[K](\boldsymbol{\xi}; x, \eta)| \leq C_0(\boldsymbol{\xi}; x)$ for all $\eta \in (0, \epsilon)$ and some positive function $C_0(\boldsymbol{\xi}; x)$, we find that there is a positive function $C(\boldsymbol{\xi}; x)$ such that

$$|K(\boldsymbol{\xi}; x, \epsilon)| \leq C_0(\boldsymbol{\xi}; x) C(\boldsymbol{\xi}; x) \epsilon. \tag{2.121}$$

A similar $O(\epsilon)$ bound exists for the first partial derivatives of $K(\boldsymbol{\xi}; x, \epsilon)$ with respect to the coordinates of $\boldsymbol{\xi}$, and we may choose the function $C(\boldsymbol{\xi}; x)$ to be the same for all of them. By inserting this estimate back into (2.118) and iterating this process $p - 1$ times, we find that

$$|K(\boldsymbol{\xi}; x, \epsilon)| \leq C_0(\boldsymbol{\xi}; x) \frac{C(\boldsymbol{\xi}; x)^p}{p!} \epsilon^p \quad \text{for all } p \in \mathbb{Z}^+. \tag{2.122}$$

Letting $p \to \infty$, we conclude that the left side is zero, implying that $\tilde{F}(\boldsymbol{\xi}; x, \epsilon)$ is zero, a contradiction.

To show that $F_2(\boldsymbol{\xi}; x)$ solves (2.116-2.117), we insert $\tilde{F}(\boldsymbol{\xi}; x, \epsilon) = \epsilon^{-2\theta_1 + \theta_2} K(\boldsymbol{\xi}; x, \epsilon)$ into the null-state PDEs centered on x_j with $j \neq i, i+1$ and into the three Ward identities, multiply through by $\epsilon^{2\theta_1 - \theta_2}$, and send $\epsilon \downarrow 0$. That this limit is uniform in sufficiently small neighborhoods of $\mathscr{D}$ allows us to commute the limit with the derivatives appearing in these PDEs. Thus, we recover the PDEs (2.116-2.117). The details are identical to those for the similar task presented at the end of the proof of lemma II.4. □

In the language of CFT, F_2 is, to within a factor, a $(2N - 1)$-point function

with a boundary two-leg operator at x_i and a boundary one-leg operator at each $x_1, \ldots, x_{i-1}, x_{i+2}, \ldots, x_{2N}$. This $(2N-1)$-point function follows from the OPE of the boundary one-leg operators $\psi_1(x_i)$ and $\psi_1(x_{i+1})$. Because (x_i, x_{i+1}) is a two-leg interval, this OPE leads with a boundary two-leg operator:

$$\overbrace{\langle \psi_1(x_1) \ldots \psi_1(x_{i-1}) \psi_1(x_i) \psi_1(x_{i+1}) \psi_1(x_{i+2}) \ldots \psi_1(x_{2N}) \rangle}^{F} \underset{x_{i+1} \to x_i}{\sim} (x_{i+1} - x_i)^{-2\theta_1 + \theta_2} \underbrace{C_{11}^2 \langle \psi_1(x_1) \ldots \psi_1(x_{i-1}) \psi_2(x_i) \psi_1(x_{i+2}) \ldots \psi_1(x_{2N}) \rangle}_{F_2}. \tag{2.123}$$

CFT therefore implies that F_2 solves the null-state PDEs (2.116) associated with the $2N-2$ boundary one-leg operators on the right side of (2.123). Because x_i now hosts a boundary two-leg operator whose conformal weight is θ_2 rather than θ_1, the original null-state PDEs (2.1) centered on x_j with $j \neq i, i+1$ are modified to (2.116) to account for this change.

With this understanding, we anticipate an adaptation of lemmas II.3, II.4, and II.15 into lemmas concerning the limiting behavior of F_2 as $x_{i+2} \to x_i$. For example, by studying the null-state PDE (2.116) with $j = i+2$, we can show that

$$F_2(x_1, \ldots, x_i, x_{i+2}, \ldots, x_{2N}) = O((x_{i+2} - x_i)^{-\theta_1 - \theta_2 + \theta_1}), \quad \text{as } x_{i+2} \to x_i. \tag{2.124}$$

The proof is identical to the proof of lemma II.3. Again, we assume that F_2 does not change sign infinitely often as $x_{i+2} \to x_i$, a condition that we believe is ultimately unnecessary although we currently do not how to prove this. Furthermore, we can also prove that the limit of $(x_{i+2} - x_i)^{\theta_1 + \theta_2 - \theta_1} F_2$ as $x_{i+2} \to x_i$ exists, and if it is zero, then the limit F_3 of $(x_{i+2} - x_i)^{\theta_1 + \theta_2 - \theta_3} F_2$ as $x_{i+2} \to x_i$ exists and is not zero. Here, $\theta_3 := 3(10-\kappa)/2\kappa$ is the weight of the boundary three-leg operator. The proof of these two claims are respectively identical to the proofs of lemmas II.4 and II.15, and

the latter situation is consistent with an OPE of $\psi_2(x_i)$ with $\psi_1(x_{i+2})$ that leads with the boundary three-leg operator:

$$\overbrace{C_{11}^2\langle\psi_1(x_1)\dots\psi_1(x_{i-1})\psi_2(x_i)\psi_1(x_{i+2})\psi_1(x_{i+3})\dots\psi_1(x_{2N})\rangle}^{F_2}$$
$$\underset{x_{i+2}\to x_i}{\sim}(x_{i+2}-x_i)^{-2\theta_1+\theta_2}\underbrace{C_{11}^2C_{21}^3\langle\psi_1(x_1)\dots\psi_1(x_{i-1})\psi_3(x_i)\psi_1(x_{i+3})\dots\psi_1(x_{2N})\rangle}_{F_3}. \tag{2.125}$$

We mention that F_2 solves another PDE not included among (2.116-2.117). This is the null-state PDE associated with the boundary two-leg operator $\psi_2(x_i)$, and it is given by the Benoit-Saint-Aubin formula [67]. This PDE is not used to prove any of the claims made in the previous paragraph, so we do not show it. (In fact, the null-state PDE centered on x_i is only used to prove that the limit solution (2.81) does not depend on x_i in the original situation of lemma II.4. This is obviously not a feature of F_2.)

We can continue this generalization further. We let F_s be the $(2N-s+1)$-point function

$$F_s(x_1,\dots,x_i,x_{i+s},\dots,x_{2N})=\prod_{k=2}^{s}C_{k-1,1}^k \times\langle\psi_1(x_1)\dots\psi_1(x_{i-1})\psi_s(x_i)\psi_1(x_{i+s})\dots\psi_1(x_{2N})\rangle. \tag{2.126}$$

Here, $C_{s,1}^{s+1}$ is the OPE coefficient of the fusion $\psi_s\times\psi_1=\psi_{s+1}$. CFT says that F_s must solve the system of $(2N-s)$ null-state PDEs

$$\left[\frac{\kappa}{4}\partial_j^2+\sum_{k\neq j,i,\dots,i+s-1}^{2N}\left(\frac{\partial_j}{x_k-x_j}-\frac{\theta_1}{(x_k-x_j)^2}\right)+\frac{\partial_i}{x_i-x_j}-\frac{\theta_s}{(x_i-x_j)^2}\right]F_s=0, \tag{2.127}$$

with $j \in \{1, \ldots, i-1, i+s, \ldots, 2N\}$, and the modified Ward identities

$$\begin{cases} \sum_{j\neq i,\ldots i+s-1}^{2N} \partial_j F_s = 0 \\ \left[\sum_{j\neq i,\ldots i+s-1}^{2N} (x_j\partial_j + \theta_1) + x_i\partial_i + \theta_s\right] F_s = 0 \\ \left[\sum_{j\neq i,\ldots i+s-1}^{2N} (x_j^2\partial_j + 2\theta_1 x_j) + x_i^2\partial_i + 2\theta_s x_i\right] F_s = 0 \end{cases} . \tag{2.128}$$

Here, θ_s is the conformal weight of the s-leg operator (1.171)

$$\theta_s = \frac{s(2s+4-\kappa)}{2\kappa}. \tag{2.129}$$

This system of PDEs implies the growth condition

$$F_s(x_1, \ldots, x_i, x_{i+s}, \ldots, x_{2N}) = O((x_{i+s} - x_i)^{-\theta_1-\theta_s+\theta_{s-1}}), \quad \text{as } x_{i+s} \to x_i. \tag{2.130}$$

The proof is identical to the proof of lemma II.3, with a few slight alterations. After letting $\epsilon := x_{i+s} - x_i$ and relabeling the variables $\{x_j\}_{j\neq i,\ldots,i+s}$ as $\{\xi_1, \ldots, \xi_{2N-s-1}\}$ in ascending order, we find that the differential operator $\mathcal{L}_s$ of (2.62) is now

$$\mathcal{L}_s := \frac{\kappa}{4}\partial_\epsilon^2 + \frac{\partial_\epsilon}{\epsilon} - \frac{\theta_s}{\epsilon^2}, \tag{2.131}$$

while $\mathcal{M}$ does not change (except that the number of coordinates for $\boldsymbol{\xi}$ decreases to $2N-s-1$). The characteristic exponents of $\mathcal{L}_s$ are

$$p_1 = -\theta_1 - \theta_s + \theta_{s-1} = 1 - 2(s+2)/\kappa, \quad p_2 = -\theta_1 - \theta_s + \theta_{s+1} = 2s/\kappa, \tag{2.132}$$

and the Green function (2.64) is altered to

$$G_s(\epsilon, \eta) = \frac{4\eta}{\kappa(\theta_{s+1} - \theta_{s-1})}\Theta(\eta - \epsilon)\left[\left(\frac{\epsilon}{\eta}\right)^{-\theta_1-\theta_s+\theta_{s-1}} - \left(\frac{\epsilon}{\eta}\right)^{-\theta_1-\theta_s+\theta_{s+1}}\right]. \tag{2.133}$$

Again, to prove (2.130), we assume that F_s does not change sign infinitely often as $x_{i+s} \to x_i$, a condition that we believe is ultimately unnecessary although we currently do not know how to prove it. Furthermore, we may also prove that the limit of $(x_{i+s} - x_i)^{\theta_1+\theta_s-\theta_{s-1}} F_s$ as $x_{i+s} \to x_i$ exists, and if it is zero, then the limit F_{s+1} of $(x_{i+s} - x_i)^{\theta_1+\theta_s-\theta_{s+1}} F_s$ as $x_{i+s} \to x_i$ exists, is not zero, and solves the system (2.127-2.136) with $s \mapsto s+1$. The proof of these two claims are respectively identical to the proofs of lemmas II.4 and II.15, and the latter situation is consistent with an OPE of $\psi_s(x_i)$ with $\psi_1(x_{i+s})$ that leads with the boundary $(s+1)$-leg operator:

$$\begin{aligned}
&\overbrace{C_{11}^2 \dots C_{s-1,1}^s \langle \psi_1(x_1) \dots \psi_1(x_{i-1}) \psi_s(x_i) \psi_1(x_{i+s}) \psi_1(x_{i+s+1}) \dots \psi_1(x_{2N}) \rangle}^{F_s} \\
&\qquad \underset{x_{i+s} \to x_i}{\sim} (x_{i+s} - x_i)^{-\theta_1-\theta_s+\theta_{s+1}} \\
&\qquad \times \underbrace{C_{11}^2 \dots C_{s1}^{s+1} \langle \psi_1(x_1) \dots \psi_1(x_{i-1}) \psi_{s+1}(x_i) \psi_1(x_{i+s+1}) \dots \psi_1(x_{2N}) \rangle}_{F_{s+1}} .
\end{aligned} \tag{2.134}$$

The case $s = 1$ reproduces lemmas II.3, II.4, and II.15 with $F_1 := F \in \mathcal{S}_N$.

These observations serve as a significant part of the proof that $\dim \mathcal{S}_N \leq C_N$ for the following reasons. First, it is reasonable to suppose that the two possibly different power laws that $F \in \mathcal{S}_N$ exhibits as $x_{i+1} \to x_{i+1}$ or $x_{i+2} \to x_{i+1}$ determines which of the two power laws among (2.132) that F_2 will exhibit as $x_{i+2} \to x_i$. For instance, we suppose that the adjacent intervals (x_i, x_{i+1}), and (x_{i+1}, x_{i+2}) are two-leg intervals. In chapter one, we noted that boundary arcs anchored to the endpoints of a two-leg interval are conditioned to not mutually connect. Therefore, none of x_i, x_{i+1}, and x_{i+2} may be connected by a common boundary arc, and the limit $x_{i+1} \to x_i$ followed by the limit $x_{i+2} \to x_i$ should produce a boundary three-leg operator at x_i. Consequently, we expect that we can prove that if (x_i, x_{i+1}), and (x_{i+1}, x_{i+2}) are two-leg intervals, then $F_2(x_1, \dots, x_i, x_{i+2}, \dots, x_{2N}) = O((x_{i+2} - x_i)^{-\theta_1-\theta_2+\theta_3})$.

Next, we suppose that each of $(x_i, x_{i+1}), \dots, (x_{i+s-1}, x_{i+s})$ is a two-leg interval.

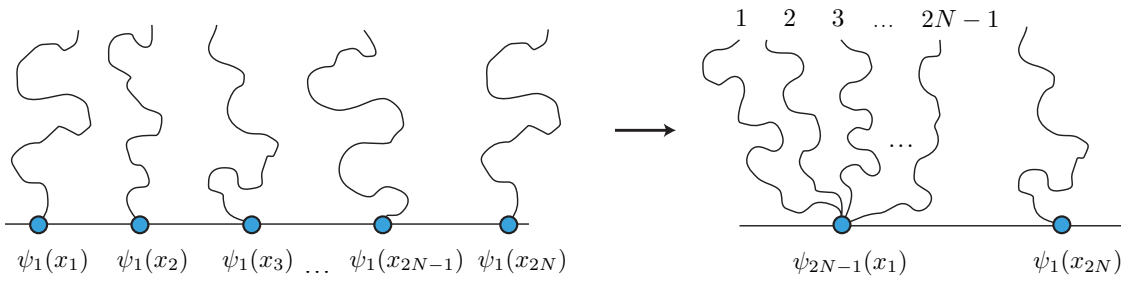

Figure 2.5: The existence of a solution with all intervals among (x_1, x_2), ..., (x_{2N-1}, x_{2N}) as two-leg intervals implies the existence of a nonzero two-point function of a boundary $(2N-1)$-leg operator and a boundary one-leg operator, an impossibility.

Again, this implies that none of $x_i, \ldots, x_{i+s}$ may be connected by a common boundary arc, for otherwise a pair x_j, x_{j+1} among them must be mutually connected through a boundary arc, contradicting that (x_j, x_{j+1}) is a two-leg interval. Then the same argument of the previous paragraph suggests that

$$F_s(x_1, \ldots, x_i, x_{i+s}, \ldots, x_{2N}) = O((x_{i+s} - x_i)^{-\theta_1 - \theta_s + \theta_{s+1}}). \tag{2.135}$$

Again, we expect that we can prove (2.135) and that the proof will be a straightforward generalization of the proof for the case $s = 2$.

Finally, we choose an $F \in \mathcal{S}_N$ not equal to zero, we let $i = 1$, and we suppose that each of $(x_1, x_2), \ldots, (x_{2N-1}, x_{2N})$ is a two-leg interval. Then according to the preceding arguments, F_{2N-1} is not zero and solves the three modified Ward identities (2.117) with $s = 2N - 1$. This system is

$$\begin{cases} [\partial_1 + \partial_{2N}] F_{2N-1}(x_1, x_{2N}) = 0 \\ [x_1 \partial_1 + x_{2N} \partial_{2N} + \theta_{2N-1} + \theta_1] F_{2N-1}(x_1, x_{2N}) = 0 \\ [x_1^2 \partial_1 + x_{2N}^2 \partial_{2N} + 2x_1 \theta_{2N-1} + 2x_{2N} \theta_1] F_{2N-1}(x_1, x_{2N}) = 0 \end{cases} . \tag{2.136}$$

It is straightforward to show that only zero solves this system. This implies that F_{2N-1} is zero, a contradiction. (Or in terms of CFT, F_{2N-1} is a two-point function

with a boundary $(2N-1)$-leg operator and a boundary one-leg operator (figure 2.5), and because these operators have different conformal weights, this two-point function is zero.) Thus, we have motivated the following conjecture.

Conjecture II.16. *Let $F \in \mathcal{S}_N$, and let $\kappa \in (0,8)$. If each of $(x_1,x_2),\ldots,(x_{2N-1},x_{2N})$ are two-leg intervals, then F is zero.*

We expect that the proof of this conjecture follows from the preceding discussion and is most straightforwardly completed by proving (2.135) for all $s \in \{1,\ldots,2N-2\}$ (and by proving, or finding a way to drop, the supposition that the sign of F_s does not change infinitely often as we send $x_{i+s} \to x_i$ for all $s \in \{1,\ldots,2N-1\}$, a condition that we strongly suspect is true anyway).

It is interesting to note that conjecture II.16 is not true if we omit the Ward identities (2.2) and only consider the $2N$ null-state PDEs (2.1). Then (as long as the notion of a "two-leg interval" is well-defined for a solution of this reduced system), the conjecture is false, as the following counterexample shows:

$$F(\boldsymbol{x}) = \prod_{i<j}^{2N} (x_j - x_i)^{2/\kappa}. \tag{2.137}$$

This function, for which each of the intervals $(x_1,x_2),\ldots,(x_{2N-1},x_{2N})$ are two-leg intervals, solves the $2N$ null-state PDEs and the first Ward identity, but it does not solve the other two Ward identities.

The weak maximum principle might seem to lend a more straightforward proof of conjecture II.16, but this approach encounters technical difficulties. Such a proof would proceed as follows. We fix $x_1 = a, x_{2N} = b$ with $a < b$, we let $F \in \mathcal{S}_N$, we let

$$\Omega_{a,b} = \{(x_2,\ldots,x_{2N-1}) \in \mathbb{R}^{2N-2} \,:\, a < x_2 < \ldots < x_{2N-1} < b\}, \tag{2.138}$$

and we let $F_R : \Omega_{a,b} \to \mathbb{R}$ be given by $F_R(x_2,\ldots,x_{2N-1}) = F(a,x_2,\ldots,x_{2N-1},b)$.

After using the first two Ward identities of (2.2) to eliminate all derivatives in x_1, x_{2N}, the null-state PDE centered on x_j with $j \in \{2, \ldots, 2N-1\}$ becomes

$$\left[\frac{\kappa}{4}\partial_j^2 + \sum_{k\neq j,1,2N}\left(\frac{\partial_k}{x_k - x_j} - \frac{(6-\kappa)/2\kappa}{(x_k-x_j)^2}\right) - \sum_{k\neq 1,2N}\frac{(x_k-a)\partial_k}{(b-x_j)(x_j-a)}\right.$$
$$\left. + \sum_{k\neq 1,2N}\frac{\partial_k}{x_j-a} - \frac{N(6/\kappa-1)}{(b-x_j)(x_j-a)} - \frac{(6-\kappa)/2\kappa}{(x_j-a)^2} - \frac{(6-\kappa)/2\kappa}{(b-x_j)^2}\right] F_R = 0. \quad (2.139)$$

If we sum (2.139) over $j \in \{2, \ldots, 2N-1\}$, then we find a strictly elliptic PDE with a nonpositive constant term if $\kappa \in (0, 6]$. Because all of its intervals are two-leg intervals, F_R continuously extends to and equals zero on $\partial\Omega_{a,b} \setminus E$, according to lemma II.4, where E is the set of points $(a, x_2, \ldots, x_{2N-1}, b) \in \partial\Omega_0$ with three or more coordinates equal. If we show that F_R continuously extends to and equals zero on E too, then we can invoke the weak maximum principle to prove conjecture II.16 for $\kappa \in (0, 6]$. However, we have not found a way to justify this claim, nor have we found bounds on the growth of F_R near E for which we could use a Phragmén-Lindelöf maximum principle to skirt this issue. Furthermore, such a principle would be difficult to apply since the coefficients of (2.139) are not bounded as the points in E are approached.

Supposing that conjecture II.16 is true, the proof that $\dim \mathcal{S}_N \leq C_N$ follows immediately.

Lemma II.17. *Let $F \in \mathcal{S}_N$, let $\kappa \in (0, 8)$, and suppose that conjecture II.16 is true. Let $v : \mathcal{S}_N \to \mathbb{R}^{C_N}$ be the map with the k-th coordinate of $v(F)$ equaling $[\mathscr{L}_k]F$ for $[\mathscr{L}_k] \in \mathscr{B}_N^*$. Then v is a linear injection, so $\dim \mathcal{S}_N \leq C_N$.*

Proof. The map v is clearly linear. To show that it is injective, we argue that its kernel is trivial. Suppose that F is not zero. We construct a consistently ordered sequence of limits $\mathscr{L}$ such that $\mathscr{L}F \neq 0$ as follows. By conjecture II.16, F has at least one mixed interval or identity interval $(x_{i_1}, x_{i_2}) = (x_i, x_{i+1})$. We let $\bar{\ell}_1$ collapse

this interval. Then according to lemma II.3, $\bar{\ell}_1 F \in \mathcal{S}_{N-1}$. Also, $\bar{\ell}_1 F$ is not zero since (x_{i_1}, x_{i_2}) is not a two-leg interval, so it must have at least one identity interval or mixed interval (x_{i_3}, x_{i_4}). Repeating this process $N-1$ times leaves us with a nonzero number $\mathscr{L}F$, where $\mathscr{L} = \{\ell_1, \ell_2, \ldots, \ell_N\}$. Thus, $v(F) \neq 0$, and $\ker v = \{0\}$. The dimension theorem of linear algebra then implies that $\dim \mathcal{S}_N \leq C_N$. □

In the next section, we will show that $\dim \mathcal{S}_N = C_N$, assuming conjecture II.16. Before we do this, we state a corollary that justifies our exclusive consideration of the system (2.1-2.2) with an even number of independent variables. Up until now, the results of this section have not required this number to be even, so they hold even when it is odd (though M should always be even in definition II.8). We therefore let $\mathcal{S}_{N+1/2}$ be defined exactly as $\mathcal{S}_N$ for the system (2.1-2.2) with $2N+1$ independent variables.

Corollary II.18. *Let $F \in \mathcal{S}_{N+1/2}$, and suppose that conjecture II.16 is true. If $\kappa \in (0,6) \cup (6,8)$, then $\mathcal{S}_{N+1/2} = \{0\}$.*

Proof. We suppose that $F \in \mathcal{S}_{N+1/2}$ is not zero. Then as noted in the proof of lemma II.17, there exists a consistently ordered sequence of limits $\mathscr{L}$ of length N such that $F' := \mathscr{L}F$ is not zero. Lemma II.3 shows that F' is a function of only one $x_k \in \{x_1, \ldots, x_{2N+1}\}$ and solves the system

$$\frac{\kappa}{2}\partial_k^2 F' = 0, \quad \partial_k F' = 0, \quad [x_k \partial_k + \theta_1] F' = 0, \quad [x_k^2 \partial_k + 2x_k \theta_1] F' = 0. \tag{2.140}$$

If $\kappa \neq 6$, then $\theta_1 \neq 0$ and F' is zero, a contradiction.

□

We conjecture a similar corollary for the case $\kappa = 6$, for which $\theta_1 = 0$, and we propose a proof of this conjecture that is similar to the proposed proof of conjecture II.16.

Conjecture II.19. *Let $F \in \mathcal{S}_{N+1/2}$. If $\kappa = 6$, then $\mathcal{S}_{N+1/2} = \mathbb{R}$.*

We expect the proof of this conjecture to ultimately proceed as follows. If we differentiate the three conformal Ward identities and the null-state PDEs centered on $x_1, \ldots, x_{2N}$ with respect to x_{2N+1} and let $G = \partial_{2N+1} F$, then we find the system of $2N$ null-state PDEs,

$$\left[\frac{\kappa}{4}\partial_i^2 + \sum_{j\neq i}^{2N+1} \frac{\partial_j}{x_j - x_i} - \frac{1}{(x_{2N+1} - x_i)^2}\right] G(x_1, \ldots, x_{2N+1}) = 0, \quad i \in \{1, \ldots, 2N\}, \tag{2.141}$$

together with the system of three conformal Ward identities:

$$\begin{cases} \sum_{i=1}^{2N+1} \partial_i G(x_1, \ldots x_{2N+1}) = 0 \\ \sum_{i=1}^{2N+1} x_i \partial_i G(x_1, \ldots x_{2N+1}) + G(x_1, \ldots x_{2N+1}) = 0 \\ \sum_{i=1}^{2N+1} x_i^2 \partial_i G(x_1, \ldots x_{2N+1}) + 2x_{2N+1} G(x_1, \ldots x_{2N+1}) = 0 \end{cases} . \tag{2.142}$$

We note that relative to G, the coordinates $x_1, \ldots, x_{2N}$ have conformal weight zero while the anomalous coordinate x_{2N+1} has weight one. Now we argue that if G is not zero, then at least one of the intervals among $(x_1, x_2), \ldots, (x_{2N-1}, x_{2N})$ is not a two-leg interval by reusing the proposed proof for conjecture II.16. We describe the general idea using CFT and omit further details. If we assume the contrary, then it should be possible to fuse the boundary one-leg operators at the coordinates $x_1, \ldots, x_{2N}$ into a single boundary $2N$-leg operator, leaving us with a two-point function of a boundary $2N$-leg operator and a derivative of a boundary one-leg operator. The conformal weights of these operators are different, so this two-point function vanishes, implying that G is zero. This is a contradiction.

We continue to assume that G is not zero. Having established the existence of an interval (x_i, x_{i+1}) among $(x_1, x_2), \ldots, (x_{2N-1}, x_{2N})$ that is not a two-leg interval, we collapse it to find a nonzero limit. Then the arguments of the pre-

vious paragraph can be reused to prove the existence of another interval among $(x_1, x_2), \ldots, (x_{i-1}, x_i), (x_i, x_{i+2}), \ldots, (x_{2N-1}, x_{2N})$ that is not a two-leg interval, and we collapse that interval too. We repeat the process indefinitely until all intervals among $(x_1, x_2), \ldots, (x_{2N-1}, x_{2N})$ have been collapsed. The limit of this sequence of interval collapses is a function not equal to zero and also a conformally covariant function of just x_{2N+1} with conformal weight one there. However, the only function with this latter property is trivially zero, a contradiction. We therefore conclude that G is indeed zero.

The conclusion of the previous paragraph that $G := \partial_{2N+1} F = 0$ may be inserted into the null-state PDE for F centered on x_{2N+1} to find

$$\sum_{j=1}^{2N} (x_{2N+1} - x_j)^{-1} \partial_j F(x_1, \ldots, x_{2N}) = 0. \tag{2.143}$$

We fix the coordinates $x_1, \ldots, x_{2N}$ to arbitrary values, and we fix x_{2N+1} to $2N$ distinct arbitrary values greater than x_{2N} to create an invertible system of $2N$ equations in the unknowns $\partial_1 F(x_1, \ldots, x_{2N}), \ldots, \partial_{2N} F(x_1, \ldots, x_{2N})$. The one unique solution of this system is the zero solution, so all of the unknowns equal zero. Finally, because $x_1, \ldots, x_{2N}$ were chosen arbitrarily, we conclude that $\partial_1 F, \ldots, \partial_{2N} F$ are zero too. Thus F must be a constant. This concludes our proposed proof of conjecture II.19.

2.4 A basis $\mathcal{B}_N$ for $\mathcal{S}_N$ and the meander matrix

Having found an upper bound on the dimension of $\mathcal{S}_N$ in lemma II.17 (under the assumption of conjecture II.16), we next prove that $\dim \mathcal{S}_N = C_N$ (again, assuming this conjecture) by selecting a certain subset $\mathcal{B}_N \subset \mathcal{S}_N$ of cardinality C_N and showing that this set is linearly independent. Such a set $\mathcal{B}_N$ therefore serves as a basis for $\mathcal{S}_N$ which proves the claim. In this section and in the rest of this thesis, we will refer to the coordinates $x_1, \ldots, x_{2N}$ of $\boldsymbol{x}$ as "points."

Definition II.20. For $k \in \{1, \ldots, C_N\}$, let F_k be the Coulomb gas solution (2.9), with $c = 2N$, times

$$n(\kappa)^N \beta(-4/\kappa, -4, \kappa)^{1-N}, \tag{2.144}$$

where $n(\kappa)$ is the O(n) loop fugacity (1.155), where $\beta(a, b)$ is the Euler beta function, and with the integration contours $\{\Gamma_m\}$ chosen as follows. Each pair of points $\{x_i, x_j\}$ linked by an arc in the half-plane diagram for $[\mathscr{L}_k]$ is connected by a simple contour among $\{\Gamma_m\}$ and starting and ending at x_i and x_j respectively, except for the pair with the point x_{2N}. Each contour resides in $\overline{\mathbb{H}}$, and they bend in $\mathbb{H}$ so that no two integration contours intersect. Furthermore, we order the differences in the factors of the integrand for each F_k so that each is real. (This is always possible, as we show in the discussion following the proof of lemma II.22 below.) Let $\mathcal{B}_N = \{F_1 \ldots, F_{C_N}\}$. Let the *polygon (resp. half-plane) diagram of* F_k be the diagram of $[\mathscr{L}_k]$ except with *exterior arcs* drawn on the outside of the $2N$-sided polygon (resp. drawn inside the lower half-plane). We call either diagram an *exterior arc connectivity diagram*.

The calculations that we present below make evident the fact that $\mathcal{B}_N \subset \mathcal{S}_N$. In particular, we indirectly prove that $F_k(\boldsymbol{x}) = O((x_{i+1} - x_i)^{-2\theta_1})$ by directly showing that limit of $(x_{i+1} - x_i)^{2\theta_1} F_k(\boldsymbol{x})$ as $x_{i+1} \to x_i$ exists. We can also prove this statement for first and second partial derivatives of $F_k \in \mathcal{B}_N$ not with respect to x_i or x_{i+1} by differentiating the explicit formula for F_k, and this proves (2.60). Moreover, we will show that the limit of $(x_{i+1} - x_i)^{2\theta_1} F_k$ as $x_{i+1} \to x_i$ is a multiple of an element in $\mathcal{B}_{N-1}$, so it follows that $F_k \in \mathcal{S}_N$. (The condition (2.101) at infinity can be proven similarly by using transformation rule (2.5) with the mapping (2.108).)

If $\kappa \leq 4$, then the integrations prescribed in this definition will diverge. Convergence is restored by replacing each integration contour connecting the pair of points x_i and x_j with the Pochhammer contour $\mathscr{P}(x_i, x_j)$, taking care to ensure that no two such contours intersect. To keep the same normalization as used for when $\kappa > 4$, we

divide by one factor of $4\sin^2(4\pi/\kappa)$ for each contour. Thus, when $\kappa \leq 4$, we use the prefactor

$$n(\kappa)^N \left[4\sin^2\left(\frac{4\pi}{\kappa}\right)\beta(-4/\kappa,-4,\kappa)\right]^{1-N} \tag{2.145}$$

instead of the original prefactor (2.144). The arguments that follow presume the integration contours to be simple curves described in definition II.20, but they hold for either type of contour for reasons that will be given below.

We will prove that $\mathcal{B}_N$ is linearly independent (assuming conjecture II.16) for all but the following SLE speeds and is linearly dependent otherwise.

Definition II.21. An SLE speed is called an *exceptional speed* if it equals any of

$$\kappa_{q,q'} := 4q/q', \quad \kappa_{q,2mq\pm q'}, \quad m \in \mathbb{Z}^+, \tag{2.146}$$

where (q, q') are a pair of coprime integers with $1 \leq q' < q$.

To prove the linear independence of $\mathcal{B}_N$, we will show that the set $v(\mathcal{B}_N) := \{v(F_k)\}_{k=1}^{C_N}$ is linearly independent and invoke lemma II.17. To calculate the vectors in $v(\mathcal{B}_N)$, we must compute $[\mathscr{L}_k]F_{k'}$ for all $F_{k'} \in \mathcal{B}_N$ and all $[\mathscr{L}_k] \in \mathscr{B}_N^*$. As each computation involves taking N somewhat complicated limits, this task might seem tedious. However, it can be simplified by using the diagrams for $[\mathscr{L}_k]$ and $F_{k'}$.

We start with a sample calculation. We choose an $F_{k'} \in \mathcal{B}_N$, an $[\mathscr{L}_k] \in \mathscr{B}_N^*$, and an arc in the diagram for $[\mathscr{L}_k]$ linking a pair of adjacent points x_i and x_{i+1}. Topological considerations show that at least one such arc with neither endpoint being x_{2N} exists, and we choose this arc to represent the first limit $\bar{\ell}_1 = \{x_{i+1} \to x_i\}$ taken in $[\mathscr{L}_k]$. Now the value of $\bar{\ell}_1 F_{k'}$ depends on how the integration contours interact with the interval (x_i, x_{i+1}) to be collapsed. The limit $\bar{\ell}_1 F_{k'}$ is

$$\begin{aligned} \bar{\ell}_1 F_{k'} &= \lim_{x_{i+1}\to x_i} (x_{i+1}-x_i)^{2\theta_1} F_{k'} \\ &= \lim_{x_{i+1}\to x_i} (x_{i+1}-x_i)^{6/\kappa-1} n(\kappa)^N \beta(-4/\kappa,-4/\kappa)^{1-N} \end{aligned} \tag{2.147}$$

$$\times \quad \left((x_{i+1} - x_i)^{2/\kappa} \dots \int_{\Gamma_1} du_1 \, (x_{i+1} - u_1)^{-4/\kappa} (u_1 - x_i)^{-4/\kappa} \dots \right). \quad (2.148)$$

The ellipses stand for the additional factors and integrations in $F_{k'}$ that appear in (2.9). Some of these factors contain x_i and x_{i+1} and are therefore affected by the limit. But none of them have zero or infinite limits, so they do not matter in the present calculation. Now we suppose that no contour among $\{\Gamma_m\}$ has its endpoints at x_i or x_{i+1}. (This is actually not possible, but we consider this case anyway because it will come up as a consequence of deforming the integration contours later.) Then the limit of the integrand approaches a finite value uniformly in u_1, the limit of the integral is finite, and $\bar{\ell}_1 F_{k'} = 0$ if $\kappa < 8$. Evidently, (x_i, x_{i+1}) is a two-leg interval.

Now we suppose that $\Gamma_1 = [x_i, x_{i+1}]^+$. (The plus sign indicates that the contour bends up into the upper half-plane with endpoints still at x_i and x_{i+1}.) In this case, the limit of the integrand is not approached uniformly in $u_1 \in \Gamma_1$. The substitution $u(t) = (1-t)x_i + t x_{i+1}$ factors the $(x_{i+1} - x_i)$-dependence out of the integral, and we find that the limit $\bar{\ell}_1 F_{k'}$ is not zero. In fact, the limit is $F_{k'}$ but with factors containing x_i, x_{i+1}, and u_1 dropped, the integration along Γ_1 dropped, and a factor of $\beta(-4/\kappa, -4/\kappa)^{-1}$ dropped. To within an extra factor of n, this limit is clearly in $\mathcal{B}_{N-1}$, and (x_i, x_{i+1}) is evidently an identity interval.

In addition, Γ_1 may have just one of its endpoints equal x_i or x_{i+1}, and in this case (x_i, x_{i+1}) is a mixed interval as a more careful calculation in section 2.5 will show. These observations point to a certain fact: by touching x_i and/or x_{i+1} (or crossing (x_i, x_{i+1})), an integration contour converts a two-leg interval (x_i, x_{i+1}) into an identity interval or a mixed interval.

Lemma II.22. *Let $\kappa \in (0, 8)$, and suppose that conjecture II.16 is true. If κ is not (resp. is) an exceptional speed with $q \leq N+1$, then $\mathcal{B}_N$ is linearly independent (resp. linearly dependent).*

Proof. To prove the lemma, we will show that $\{v(F_1), \dots, v(F_{C_N})\}$ is linearly inde-

pendent when κ is not an exceptional speed with $q \leq N+1$ by computing $[\mathscr{L}_k]F_{k'}$ for all $F_{k'} \in \mathcal{B}_N$. In the calculation, we make sure to never collapse an interval that has x_{2N} for an endpoint so that the conjugate charge remains upon taking the limit. This is always possible since any diagram for any consistently ordered sequence of limits has at least two distinct arcs connecting either a pair of adjacent points or x_1 with x_{2N}.

We choose a first limit $\bar{\ell}_1 = \{x_{i+1} \to x_i\}$ in $[\mathscr{L}_k]$. As we noted earlier, when we collapse an interval in the domain of $F_{k'} \in \mathcal{B}_N$, the outcome depends on whether the endpoints of that interval are endpoints of an integration contour. There are four different cases to consider (figure 2.6). The explicit computations that pertain to each are deferred to section 2.5. We simply summarize the results.

In the first case, neither x_i nor x_{i+1} is an endpoint of a contour, (x_i, x_{i+1}) is a two-leg interval, and the limit $\bar{\ell}_1 F_{k'}$ is zero (2.147).

In the second case, both x_i and x_{i+1} are endpoints of the same contour Γ_1, (x_i, x_{i+1}) is an identity interval, and the limit $\bar{\ell}_1 F_{k'}$ is $nF'_{k'}$, with $F'_{k'} \in \mathcal{B}_{N-1}$ as described above.

In the third case, only one of the endpoints among $\{x_i, x_{i+1}\}$ is the endpoint of a contour Γ_1. This situation requires more care. We suppose that one endpoint of Γ_1 is at x_i but the other endpoint is not at x_{i+1}. We break Γ_1 into a contour Γ'_1

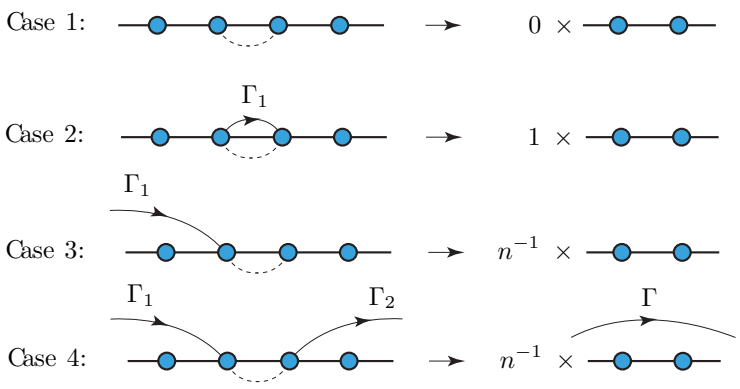

Figure 2.6: The four cases of interval collapse. The dashed curve connects the endpoints of the intervals to be collapsed, and the solid curves indicate the integration contours. (Case four is shown in more detail in figure 2.7.)

that terminates at x_{i-1} and another along $[x_{i-1}, x_i]^+$. Now we must take the limit of $(x_{i+1} - x_i)^{6/\kappa - 1}$ times

$$\begin{aligned} F_{k'} = \prod_{\substack{m<j \\ (m,j)\neq(i,i+1)}}^{2N-1} & (x_j - x_m)^{2/\kappa}(x_{2N} - x_m)^{1-6/\kappa} \int_{\{\Gamma_{m>1}\}} du_2 \dots du_{N-1} \\ & \times \left(\prod_{\substack{m\geq 1 \\ k>1}} (u_k - x_m)^{-4/\kappa}(u_k - x_{2N})^{12/\kappa - 2} \right) \left(\prod_{1<k<l} (u_k - u_l)^{8/\kappa} \right) \\ & \times \left[(x_{i+1} - x_i)^{2/\kappa} \left(\int_{\Gamma_1'} + \int_{x_{i-1}}^{x_i} du_1 \right) \left(\prod_{k>1} (u_k - u_1)^{8/\kappa} \right) \right. \\ & \qquad \left. \times (u_1 - x_{2N})^{12/\kappa - 2} \prod_{m=1}^{2N-1} (u_1 - x_m)^{-4/\kappa} \right] \end{aligned} \tag{2.149}$$

as $x_{i+1} \to x_i$. (Although we have not explicitly done this here, the differences in the integrand of (2.149) should be ordered so that F_k is real. Below, we argue that this is always possible.) In the bracketed factor spanning the last two lines of (2.149), the u_1 integral along Γ_1' falls under the first case and vanishes in the limit, and the u_1 integral along (x_{i-1}, x_i) is identical to that in (2.167) with $\beta_i = \beta_{i+1} = -\gamma/2 = -4/\kappa$. The asymptotic behavior of this integral is given in (2.172) in section 2.5.3, so this limit equals that of the second case multiplied by an extra factor of n^{-1} accumulated from deforming Γ_1. Therefore, in the third case, the limit $\bar{\ell}_1 F_{k'} = F'_{k'}$ is an element of $\mathcal{B}_{N-1}$. Also, (x_i, x_{i+1}) is a mixed interval.

In the fourth and most complicated case, x_i is an endpoint of Γ_1 and x_{i+1} is an endpoint of a different contour Γ_2. Similar to case three, we separate the u_1 and u_2 integrals from the other $N-3$ integrals, and we break Γ_1 (resp. Γ_2) into a contour Γ_1' (resp. Γ_2') that terminates at x_{i-1} (resp. x_{i+2}) and another along $[x_{i-1}, x_i]^+$ (resp. $[x_{i+1}, x_{i+2}]^+$) (figure 2.7). This results in four terms. The first integrates u_1 and u_2 along Γ_1' and Γ_2' respectively, and because neither of these contours terminates at x_i or x_{i+1}, we are in the first case. The limit is thus zero. The second term

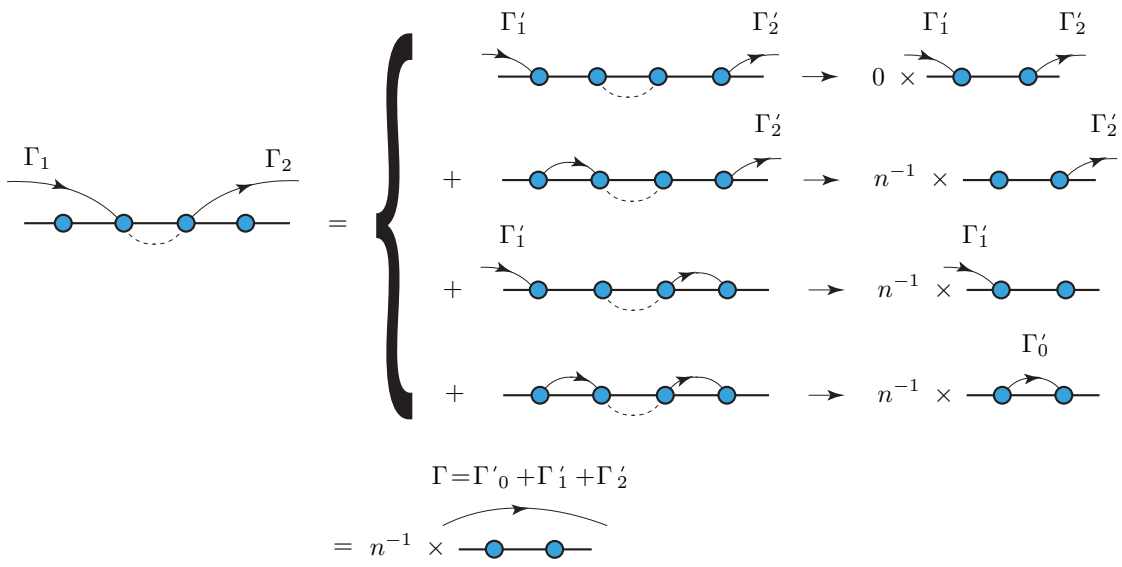

Figure 2.7: The decomposition of the fourth case into the first three cases. The top and middle terms fall in the first and third cases respectively.

integrates u_1 along $[x_{i-1}, x_i]^+$ and u_2 along Γ_2'. This term falls under the third case, and its limit is the element of $\mathcal{B}_{N-1}$ with contours $\{\Gamma_2', \Gamma_3, \ldots, \Gamma_{N-1}\}$. The third term integrates u_1 along Γ_1' and u_2 along $[x_{i+1}, x_{i+2}]^+$. It also falls under the third case, and its limit is the element of $\mathcal{B}_{N-1}$ with contours $\{\Gamma_1', \Gamma_3, \ldots, \Gamma_{N-1}\}$. The fourth and most complicated term integrates u_1 along $[x_{i-1}, x_i]^+$ and u_2 along $[x_{i+1}, x_{i+2}]^+$. Its asymptotic behavior as $x_{i+1} \to x_i$ is computed in section 2.5.4, and the result is (2.188). Its limit is the element of $\mathcal{B}_{N-1}$ with contours $\{\Gamma_0', \Gamma_3, \ldots, \Gamma_{N-1}\}$, where $\Gamma_0' := [x_{i-1}, x_{i+2}]^+$. Summing all four terms gives the element of $\mathcal{B}_{N-1}$ with contours $\{\Gamma, \Gamma_3, \ldots, \Gamma_{N-1}\}$, where $\Gamma := \Gamma_0' + \Gamma_1' + \Gamma_2'$ is the contour generated by the joining of Γ_1 with Γ_2 induced by pinching their respective endpoints x_i and x_{i+1} together.

These calculations are facilitated by a diagrammatic method. We draw the poly-

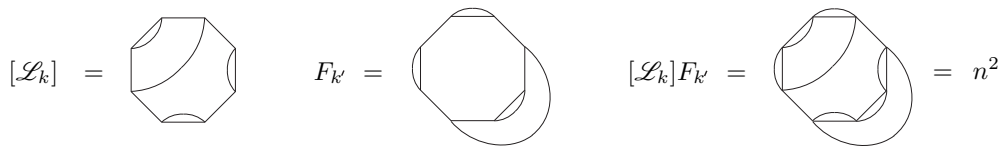

Figure 2.8: A example of the diagram for an $[\mathscr{L}_k] \in \mathscr{B}_N^*$, the diagram for an $F_{k'} \in \mathcal{B}_N$, and the diagram for their product $[\mathscr{L}_k]F_{k'} = n^2$.

gon diagram for $[\mathscr{L}_k]$ and that for $F_{k'}$ on the same polygon (figure 2.8) and call this the diagram for $[\mathscr{L}_k]F_{k'}$. The interior and exterior arcs respectively represent the limits of $[\mathscr{L}_k]$ to be taken and the integration contours of $F_{k'}$ (except for the exterior arc with an endpoint at x_{2N}, which has no associated integration contour). These arcs join to form loops that dodge in and out of the $2N$-sided polygon through its vertices. We suppose that vertices x_i and x_{i+1}, neither of which are x_{2N}, are connected by an interior arc, so we can take the limit $x_{i+1} \to x_i$ first. Topological considerations show that at least one such interior arc exists in the diagram of each $[\mathscr{L}_k]$. Then either one of two cases may occur. First, x_i and x_{i+1} may also be connected through an exterior arc that joins with the interior arc to form a loop intersecting the polygon at just x_i and x_{i+1}. This limit falls under the second case. Collapsing the interval (x_i, x_{i+1}) amounts to deleting this side and the loop that surrounds it from the polygon, creating a $(2N-2)$-gon (after dropping the leftover vertex x_i since the limit does not depend on it), and the limit is n times the element of $\mathcal{B}_{N-1}$ whose diagram is given by the remaining interior and exterior arcs. Or second, x_i and x_{i+1} are not connected by a single exterior arc. This limit falls under the third or fourth case. Collapsing the interval (x_i, x_{i+1}) amounts to deleting this interval and its interior arc while joining the two exterior arcs into one, and the limit is the element of $\mathcal{B}_{N-1}$ whose diagram is given by the remaining interior and exterior arcs. We perform this process N times so that each loop is eventually contracted away and leaves a factor of n in its wake. If the number of loops in the diagram for $[\mathscr{L}_k]F_{k'}$ (with the polygon deleted) is $l_{k,k'}$, then we have

$$[\mathscr{L}_k]F_{k'} = n^{l_{k,k'}}. \tag{2.150}$$

This result establishes a natural inner product on the space of diagrams for the elements of $\mathscr{B}_N^*$ identical to the inner product on Temperley-Lieb algebras studied in [68]:

$$\langle\, [\mathscr{L}_k], [\mathscr{L}]_{k'} \rangle := [\mathscr{L}_k]F_{k'} = n^{l_{k,k'}}. \tag{2.151}$$

The Gram matrix $M_N(\kappa)$ of this inner product is called the *meander matrix* [68], and it is clearly symmetric. In our application, the rows (or columns) of this matrix are $\{v(F_1), \ldots, v(F_{C_N})\}$. Assuming that conjecture II.16 is true, we conclude from lemma II.17 that $\mathcal{B}_N$ is linearly independent if and only if $\det M_N(\kappa) \neq 0$.

The determinant of the meander matrix is computed in [68], and it is

$$\begin{aligned} \det M_N(\kappa) &= \prod_{q=1}^{N} U_q(n(\kappa))^{a(N,q)} && (2.152) \\ &= \prod_{1 \leq q' < q \leq N+1} (n(\kappa) - n_{q,q'})^{a(N,q-1)}, \quad n_{q,q'} = -2\cos\left(\frac{\pi q'}{q}\right), && (2.153) \end{aligned}$$

where U_q is the q-th Chebychev polynomial of the second kind, and the power $a(N,q)$ is given by

$$a(N,q) = \binom{2N}{N-q} - 2\binom{2N}{N-q-1} + \binom{2N}{N-q-2}. \qquad (2.154)$$

Because (2.153) only depends on the ratio q'/q, we adopt the convention that the pair (q,q') labeling $n_{q,q'}$ is coprime. Table 2.1 shows a list of the first few $n_{q,q'}$. Because $\kappa' = \kappa_{q,q'}$ or $\kappa_{q,2mq\pm q'}$ for any positive integer m are the only SLE speeds such that $n(\kappa') = n_{q,q'}$, and $n(\kappa_{q,2mq\pm q'}) = n_{q,q'}$, the lemma follows. (All of the other zeros of $\det M_N(\kappa)$ are $\kappa_{q,-q'}$ and $\kappa_{q,2mq\pm q'}$ with m a negative integer. They are negative and therefore cannot be SLE speeds, so we do not consider them.) □

It is always possible to order the differences of the factors that are outside and inside of the integrand of each $F_k \in \mathcal{B}_N$ so that F_k is real. The correct ordering of the differences of the factors that are outside of the integrand is obvious, and we assume that this is ordering is already used. The correct ordering of the differences of the factors that are inside of the integrand may be found by considering the action of $[\mathscr{L}_k]$ on F_k. Topological considerations show that there exists at least one interval (x_i, x_{i+1}) of F_k whose endpoints are connected by an integration contour Γ_1. Then

$\bar{\ell}_1 = \{x_{i+1} \to x_i\}$ is a limit of $[\mathscr{L}_k]$ which we may choose to take first. Furthermore, it is always possible to deform all of the contours that arc over (x_i, x_{i+1}) so that they do not pass over this interval but pass over infinity instead. We let u_m be the integration variable for the contour Γ_m, and recalling that all contours are in $\overline{\overline{\mathbb{H}}}$, we flatten the contours so that each is arbitrarily close to the real axis. Then u_m with $m > 1$ couples with x_i, x_{i+1}, and u_1 only through the product of factors

$$(u_m - x_{i+1})^{-4/\kappa}(u_m - x_i)^{-4/\kappa}(u_m - u_1)^{8/\kappa}. \tag{2.155}$$

As long as we order the differences in the factors as in (2.155), this product is real for all $u_m \in \Gamma_m$ with $m > 1$. This statement is true even if Γ_m arcs over (x_i, x_{i+1}) since, after deforming Γ_m so that it passes over infinity instead of (x_i, x_{i+1}), either $u_m < x_i, x_{i+1}, u_1$ or $u_m > x_i, x_{i+1}, u_1$ for all $u_m \in \Gamma_m$ and $m > 1$. Consequently, we can order the differences in the factors of the integrand for the u_1 integration so that this integration is real for all $x_i < x_{i+1}$ and $u_m \in \Gamma_m$ with $m > 1$. Next, we take the limit $\bar{\ell}_1 F_k$, which equals n times an element of $\mathcal{B}_{N-1}$, and we repeat the previous step. The integration variable, previously u_1, is now labeled u_2. Performing the second step determines how to order the differences in the factors of the integrand for the u_2 integration in $\bar{\ell}_1 F_k$ so that this integration is real for all $u_m \in \Gamma_m$ with $m > 2$. We repeat this process until we reach $[\mathscr{L}_k]F_k = n^N$. Altogether, these steps determine an ordering of the differences in all of the factors in the complete integrand of F_k. Because $[\mathscr{L}_k]F_k$ is real and because none of the limits alter the phase, we conclude that F_k, with this ordering imposed on the integrand, is real. We let "$\mathcal{N}$" be the operator that orders the differences in the factors of the integrand this way, and we indicate that this ordering is done by placing the integrand within the brackets of $\int_{\Gamma_1} \dots \int_{\Gamma_{N-1}} \mathcal{N}[\,\dots\,]\, du_1 \dots du_{N-1}$.

Lemma II.17 establishes an interesting corollary. We choose an $F_k \in \mathcal{B}_N$ and

$c \in \{1, \ldots, 2N-1\}$, and we let $F_k^{(c)}$ be the Coulomb gas solution (2.9) with the same normalization and integration contours as F_k, except that the contour with an endpoint at x_c is omitted and a contour with endpoints at x_{2N} and the coordinate x_i connected to x_{2N} in the half-plane diagram for F_k is included. As usual, the new contour is simple, is in $\overline{\mathbb{H}}$, does not intersect the other contours, and if $\kappa < 4$, is replaced by a Pochhammer contour that entwines x_i with x_{2N}. Clearly, $F_k^{(2N)} = F_k$. Also, when $c \neq 2N$, we still order the differences in the factors of the integrand of $F_k^{(c)}$ so that $F_k^{(c)}$ is real by following the recipe prescribed in the previous paragraph. If we follow this procedure, then because $c \neq 2N$, at one of the steps the interval to be collapsed might not be of the form (x_i, x_{i+1}) for some $i \in \{1, \ldots, 2N-1\}$ but rather may be (x_{2N}, x_1), so the limit $\bar{\ell} = \{x_{i+1} \to x_i\}$ is replaced with $\underline{\ell} = \{x_1 \to -\infty, x_{2N} \to \infty\}$. We represent $F_k^{(c)}$ with the same diagram as that for $F_k \in \mathcal{B}_N$.

The proof of lemma II.22 shows that $[\mathscr{L}_k]F_{k'}^{(c)} = [\mathscr{L}_k]F_{k'}$ for all $k, k' \in \{1, \ldots, C_N\}$. Therefore, lemma II.17 implies the following corollary.

Corollary II.23. *Let $\kappa \in (0, 8)$, let $F_k^{(c)}$ be defined relative to $F_k \in \mathcal{B}_N$ as described above, and suppose that conjecture II.16 is true. Then $F_k^{(c)} = F_k^{(c')}$ for all $c, c' \in \{1, \ldots, 2N\}$.*

This corollary may be explained in terms of CFT as follows. We may think of F_k as a $2N$-point conformal block in the sense that only the identity fusion channel propagates between each pair of operators $\psi_1(x_i)$ and $\psi_1(x_j)$ whose coordinates x_i and x_j are connected by an arc in the diagram for F_k. For good reasons (related to a physical interpretation for the elements of $\mathcal{B}_N$ to be presented in chapter four), we expect these conformal blocks to correspond one-to-one with the C_N arc connectivity diagrams. On the other hand, the Coulomb gas formalism gives seemingly different formulas for conformal blocks, F_k and $F_k^{(c)}$, with the same diagram. These formulas differ only by the placement of their conjugate charge. Corollary II.23 shows that they are all equal (if we assume that conjecture II.16 is true). Therefore, the correspondence between

the conformal blocks and the C_N arc connectivity diagrams is indeed one-to-one.

The proof of lemma II.22 establishes another useful corollary that we will use in chapter three.

Corollary II.24. *Let $\kappa \in (0,8)$, and suppose that conjecture II.16 is true. Then the rank of $\mathcal{B}_N$ equals the rank of the meander matrix $M_N(\kappa)$.*

In [69], the nullity of the meander matrix is shown to equal the multiplicity $d_N(q,q')$ of the root $n_{q,q'}$ in its determinant formula (2.153), so by the dimension theorem, we have

$$\operatorname{rank} M_N(\kappa) = \left\{ \begin{array}{ll|l} C_N, & \kappa \neq \kappa_{q,q'} \text{ or } \kappa_{q,2mq\pm q'} & 1 \leq q < q' \leq N+1, \\ C_N - d_N(q,q'), & \kappa = \kappa_{q,q'} \text{ or } \kappa_{q,2mq\pm q'} & q,q' \text{ coprime}, m \in \mathbb{Z}^+ \end{array} \right. . \quad (2.156)$$

In [68], the following summation formula for the rank of $M_N(\kappa)$, is computed and shown to equal an integer, a fact that is not immediately apparent from the formula:

$$\operatorname{rank} M_N(\kappa_{q,q'}) = \operatorname{rank} M_N(\kappa_{q,2mq\pm q'}) = \frac{1}{2q} \sum_{l=1}^{q-1} \left(2 \sin \frac{\pi l}{q}\right)^2 \left(2 \cos \frac{\pi l}{q}\right)^{2N} . \quad (2.157)$$

We use lemma II.22 to prove most of the following theorem. This is the main result of this chapter.

Theorem II.25. *Let $\kappa \in (0,8)$, and suppose that conjecture II.16 is true. Then $\dim \mathcal{S}_N = C_N$, and $\mathcal{S}_N$ is spanned by the Coulomb gas solutions (2.9). If κ is not an exceptional speed with $q \leq N+1$, then $\mathcal{B}_N$ is a basis for $\mathcal{S}_N$.*

Proof. The theorem follows immediately from lemma II.22 when κ is not an exceptional speed. To prove the theorem when κ is an exceptional speed, we will construct a linearly independent set $\mathcal{B}'_N$ of cardinality C_N from the linearly dependent set $\mathcal{B}_N$ by perturbing κ away from the exceptional speed.

Let κ' be an exceptional speed corresponding to the root $n_{q,q'}$ of $\det M_N$. We see from (2.156) that $\mathcal{B}_N$ has rank $C_N - d_N(q,q')$. Therefore, the solutions in $\mathcal{B}_N$ will satisfy exactly $l = d_N(q,q')$ different linear dependences, which we write as

$$\sum\nolimits_k a_{j,k} F_k(\kappa') = 0, \quad j \in \{1,\dots,l\}, \tag{2.158}$$

where the vectors $a_j := (a_{j,1},\dots,a_{j,C_N})$ are linearly independent and span the kernel of $M_N(\kappa')$.

Next, we construct a new linearly independent set $\mathcal{B}'_N$ of cardinality C_N. We let A be any $C_N \times C_N$ invertible matrix whose first k rows are a_j, and for arbitrary κ, we consider the set of solutions

$$\Big\{ \sum\nolimits_k a_{1,k} F_k(\kappa), \dots, \sum\nolimits_k a_{l,k} F_k(\kappa), \\ \sum\nolimits_k a_{l+1,k} F_k(\kappa), \dots, \sum\nolimits_k a_{C_N,k} F_k(\kappa) \Big\}. \tag{2.159}$$

For $\kappa \neq \kappa'$, this new set is also linearly independent since $\det A \neq 0$, but when $\kappa = \kappa'$, the first l entries are zero while the others form a linearly independent set. Because each $F_k(\kappa)$ is analytic at κ', the j-th entry vanishes at rate $O((\kappa-\kappa')^{m_j})$ as $\kappa \to \kappa'$ for each $j \in \{1,\dots,l\}$, with m_j a positive integer. So we adjust the set (2.159) so that all of its entries are $O(1)$ as $\kappa \to \kappa'$:

$$\mathcal{B}'_N := \Big\{ (\kappa-\kappa')^{-m_1} \sum\nolimits_k a_{1,k} F_k(\kappa), \dots, (\kappa-\kappa')^{-m_l} \sum\nolimits_k a_{l,k} F_k(\kappa), \\ \sum\nolimits_k a_{l+1,k} F_k(\kappa), \dots, \sum\nolimits_k a_{C_N,k} F_k(\kappa) \Big\}. \tag{2.160}$$

We let $\Lambda_j(\kappa)$ be the j-th element of $\mathcal{B}'_N$, as they are ordered in (2.160). To show that $\mathcal{B}'_N$ is linearly independent when $\kappa = \kappa'$, we check that the determinant of the matrix

$M'_N(\kappa)$ whose j-th column is $v(\Lambda_j)$ is not zero. This determinant equals

$$\begin{aligned} \det M'_N(\kappa) &= (\kappa - \kappa')^{-m_1 - \ldots - m_l} \det A \det M_N(\kappa) \\ &= O((\kappa - \kappa')^{d_N(q,q') - m_1 - \ldots - m_l}). \end{aligned} \tag{2.161}$$

Now, $\det M'_N(\kappa')$ is finite since all of its entries are finite, and $d_N(q, q') = l$ [69]. So because all of the exponents m_j are positive integers, each must equal one. Thus, $\det M'_N(\kappa) = O(1)$ as $\kappa \to \kappa'$. □

We look more closely at the exceptional speeds κ' corresponding to $n(\kappa') = n_{2,1} = 0$. In this case, $\mathcal{B}_N$ exhibits $l = d_N(2,1) = C_N$ distinct linear dependences. That is, each of its elements equals zero when $\kappa = \kappa'$. In the proof of theorem II.25, we therefore have $a_{j,k} = \delta_{j,k}$. The proof shows that each element is $O(\kappa - \kappa')$ as $\kappa \to \kappa'$, and it prescribes that we multiply each by $(\kappa - \kappa')^{-1}$ before sending $\kappa \to \kappa'$ to construct a linearly independent set $\mathcal{B}'_N$ that spans $\mathcal{S}_N$.

This observation invites us to look more closely at the normalization of the elements of $\mathcal{B}_N$. We begin with the exceptional speeds $\kappa' \in (0, 8)$ corresponding to $n_{2,1} = 0$, all of which equal $8/m$ for some odd positive integer $m > 1$ according to (2.146). Since $\kappa' \leq 4$ in each case, each $F_k \in \mathcal{B}_N$ will bear the full prefactor (2.145):

$$n(\kappa) \left[\frac{n(\kappa)\Gamma(2 - 8/\kappa)}{4 \sin^2(4\pi/\kappa)\Gamma(1 - 4/\kappa)^2} \right]^{N-1}. \tag{2.162}$$

The bracketed factor and the integral that it multiplies to give $F_k(\kappa)$ are $O(1)$ as $\kappa \to \kappa'$. If we include the leftmost factor of $n(\kappa) = O(\kappa - \kappa')$ in (2.162), then $F_k(\kappa)$ is $O(\kappa - \kappa')$, but if we drop it, then $F_k(\kappa)$ is $O(1)$. This is just the renormalization of $\mathcal{B}_N$ described in the previous paragraph. Also, dropping the factor of $n(\kappa)$ amounts to dividing $\det M_N(\kappa)$ by $n(\kappa)^{C_N}$, and because $n(\kappa') = 0$ is a zero of $\det M_N(\kappa')$ with multiplicity C_N, this division adjusts the determinant so it is $O(1)$.

The previous paragraph covers half of the singularities of the prefactor (2.162). All of the other singularities occur at $\kappa' = 8/m$ for some even positive integer m. These speeds are not exceptional, and because each is less than or equal to four, each $F_k(\kappa) \in \mathcal{B}_N$ is again endowed with the full prefactor in (2.162) when $\kappa = \kappa'$. For these cases, one can check that (2.162) is $O((\kappa - \kappa')^{1-N})$ as $\kappa \to \kappa'$. But also, the set $\{\kappa' = 8/m \,:\, m > 0, \text{ even}\}$ is exactly the set of speeds for which the points entwined by the Pochhammer contours of the $N-1$ integrals in $F_k(\kappa')$ are poles rather than branch points. In this event, each Pochhammer contour $\mathscr{P}(x_i, x_j)$ in each $F_k \in \mathcal{B}_N$ decomposes into four loops. Two loops encircle x_i in opposite directions, two loops encircle x_j in opposite directions, so the integration around $\mathscr{P}(x_i, x_j)$ is zero. Further, one can check that each of the $N-1$ integrals in $F_k(\kappa)$ is $O(\kappa - \kappa')$ as $\kappa \to \kappa'$. So when multiplied by the prefactor (2.162), we have that $F_k(\kappa)$ is $O(1)$ as $\kappa \to \kappa'$ as needed.

The composite set $\{\kappa' = 8/m \,:\, m \in \mathbb{Z}^+ \setminus \{1\}\}$ combining the cases of the previous two paragraphs covers all cases in which the prefactor (2.162) for $F_k(\kappa)$ may vanish or blow up and in which branch points of the integrals in $F_k(\kappa)$ become poles. Interestingly, these are exactly the SLE speeds for which the two characteristic powers $2/\kappa$ and $1 - 6/\kappa$ of the Euler differential operator $\mathcal{L}$ in (2.62) differ by a positive integer. Now we explore the consequences of this observation.

It is easy to show that each element of $\mathcal{B}_N$ as a function of x_{i+1} with $i \in \{1, \ldots, 2N-1\}$ equals a linear combination of two Frobenius series centered on x_i, each with coefficients that depend on x_j with $j \neq i+1$. With theorem II.25, this fact leads to the following corollary.

Corollary II.26. *Let $F \in \mathcal{S}_N$, let $\kappa \in (0, 8)$ not be an exceptional speed with $q \leq N+1$, and let $i \in \{1, \ldots, 2N-1\}$. Then F as a function of x_{i+1} equals a linear combination of at most two distinct Frobenius series centered at x_i, with coefficients depending on x_j with $j \neq i+1$, and with respective indicial powers $1 - 6/\kappa$ and $2/\kappa$.*

We anticipated this corollary earlier in the discussion surrounding (2.54), and we note that the indicial powers stated in the corollary agree with the powers (2.55) predicted in this discussion. If $\kappa = \kappa'$ is an exceptional speed with $q \leq N+1$, then $\mathcal{B}_N$ is linearly dependent, and in the proof of theorem II.25 we find a new basis for $\mathcal{S}_N$ by expanding the linear combinations of $\mathcal{B}_N$ that vanish to first order in κ near κ' and keeping only the first order contribution with $\kappa = \kappa'$. Because κ appears only in the powers of the elements of $\mathcal{B}_N$, this first order term will have factors of logarithms in the distances between the points. This invites the consideration of logarithmic conformal field theory [70].

Now when κ is in the set $\{\kappa' = 8/m \,:\, m \in \mathbb{Z}^+ \setminus \{1\}\}$, the two indicial powers $1-6/\kappa$ and $2/\kappa$ differ by a positive integer, and the two Frobenius series coalesce into one. If m is even, then κ' is not an exceptional speed, $\mathcal{B}_N$ is linearly independent, and corollary II.26 is true. But if m is odd, then κ' is an exceptional speed with $q = 2 \leq N+1$, $\mathcal{B}_N$ is linearly dependent, and some solutions in $\mathcal{S}_N$ will equal logarithms multiplying Frobenius series expansions. This is reminiscent of similar phenomena in the Frobenius theory of second order, linear, homogeneous differential equations. Near a regular singular point x_0, solutions of such differential equations typically equal linear combinations of two Frobenius series centered at x_0 and with different indicial powers. But if these two powers differ by an integer, then just one of the two linearly independent solutions may not have such a Frobenius series expansion. Instead, that second solution equals a logarithm of the distance to x_0 multiplying a Frobenius series plus another Frobenius series. Interestingly, when $\kappa = 8/m$ with $m > 1$ an odd integer, the elements of $\mathcal{S}_N$ seem to generalize this phenomenon.

Corollary II.26 allows us to reinterpret the definition II.14 of "identity," "two-leg," and "mixed" intervals in a way that is more native to CFT. Namely, an interval (x_i, x_{i+1}) of $F \in \mathcal{S}_N$ is a mixed interval if F equals a linear combination of two

Frobenius series in x_{i+1} centered on x_i with respective indicial powers $1-6/\kappa$ and $2/\kappa$, an identity interval if it equals just one such Frobenius series with indicial power $1-6/\kappa$, and a two-leg interval if it equals just one such Frobenius series with indicial power $2/\kappa$ or if F is zero. In CFT, these three cases respectively imply that the OPE of $\psi_1(x_i)$ with $\psi_1(x_{i+1})$ has both the identity and the two-leg fusion channel, the identity fusion channel exclusively, and the two-leg channel exclusively (if F is not zero in this last case).

We end our discussion about exceptional speeds with some remarks on the special O(n) loop fugacities $n_{q,q'}$ of (2.153) and the minimal models. The correspondence between the O(n) model and SLE captured by (1.155) holds only for $\kappa \geq 2$. When $n_{q,q'} \geq 0$, two exceptional speeds correspond with $n_{q,q'}$, and they are

$$\kappa_{q,q'} = 4q/q', \quad \kappa_{q,2q-q'} = 4q/(2q-q'), \tag{2.163}$$

in the dense and dilute phases of SLE and the O(n) model respectively. We note that these two speeds are not dual to one another. When $n_{q,q'} < 0$, one exceptional speed $\kappa_{q,2q-q'}$ corresponds with $n_{q,q'}$. Some well known examples are $n_{2,1} = 0$ corresponding to $\kappa_{2,1} = 8$ (the uniform spanning tree) and $\kappa_{2,3} = 8/3$ (the self-avoiding walk), and $n_{3,2} = 1$ corresponding to $\kappa_{3,2} = 6$ (percolation cluster perimeters) and $\kappa_{3,4} = 3$ (Ising spin cluster perimeters). More generally, we can show from (1.170) that $c(\kappa_{q,q'})$ is the central charge $c_{q,q'} = 1 - 6(q-q')^2/qq'$ of the (q,q') minimal model in CFT. We explore the connection between exceptional speeds and minimal models further in chapter three.

We end this section with a result that completes our understanding of the dual space $\mathcal{S}_N^*$.

Lemma II.27. *Let $\kappa \in (0,8)$, and suppose that conjecture II.16 is true. Then $\mathscr{B}_N^*$ is a basis for $\mathcal{S}_N^*$.*

q' \ q	1	2	3	4	5	6
1	$\times$	0	-1	$-\sqrt{2}$	$-\frac{1+\sqrt{5}}{2}$	$-\sqrt{3}$
2	$\times$	$\times$	1	0	$\frac{1-\sqrt{5}}{2}$	-1
3	$\times$	$\times$	$\times$	$\sqrt{2}$	$\frac{-1+\sqrt{5}}{2}$	0
4	$\times$	$\times$	$\times$	$\times$	$\frac{1+\sqrt{5}}{2}$	1
5	$\times$	$\times$	$\times$	$\times$	$\times$	$\sqrt{3}$

Table 2.1: The first few zeros $n_{q,q'}$ of the meander determinant. From left to right, the superdiagonal harbors the dense phase O(n) loop fugacities of the uniform spanning tree, percolation, the Ising model, the tri-critical Ising model, and the three-state Potts model respectively.

Proof. If conjecture II.16 is true, then lemma II.17 shows that $\dim \mathcal{S}_N < \infty$, so $\dim \mathcal{S}_N^* = \dim \mathcal{S}_N = C_N$. We let $\mathcal{M} = \{[\mathscr{L}_k]\}_{k=1}^{M}$ be a maximal linearly independent subset of $\mathscr{B}_N^*$. We will prove the lemma by showing that $M = C_N$.

First, we show that $\mathcal{M}$ is nonempty. If If $n(\kappa) \neq 0$, then no $[\mathscr{L}_k]$ can be the zero-functional since $[\mathscr{L}_k]F_{k'} = n(\kappa)^{l_{k,k'}} \neq 0$. If $n(\kappa) = 0 = n_{2,1}$, then the discussion following theorem II.25 shows that we must drop a factor of $n(\kappa)$ from each element of $\mathcal{B}_N$ so that the meander determinant is not zero after this adjustment. This implies the existence of at least one $F_{k'} \in \mathcal{B}_N$ for each $[\mathscr{L}_k] \in \mathscr{B}_N^*$ such that $[\mathscr{L}_k]F_{k'} \neq 0$. So when $n(\kappa) = 0$, no $[\mathscr{L}_k]$ is the zero-functional either. Thus, $\mathcal{M}$ is nonempty.

Now suppose that $M < C_N$. Then $\mathcal{S}_N^*$ has a finite basis for which $\mathcal{M}$ can serve as a proper subset. We let

$$\begin{aligned} B_N^* &= \{[\mathscr{L}_1], \ldots, [\mathscr{L}_M], f_{M+1}, \ldots f_{C_N}\} \\ B_N &= \{\Pi_1, \ldots \Pi_M, \Pi_{M+1}, \ldots, \Pi_{C_N}\} \end{aligned}$$

be dual bases for $\mathcal{S}_N^*$ and $\mathcal{S}_N$ respectively. Then we have $[\mathscr{L}_k]\Pi_{k'} = 0$ for all $k \leq M$ and all $k' > M$. Moreover, the elements $\{[\mathscr{L}_{M+1}], \ldots, [\mathscr{L}_{C_N}]\}$ of $\mathscr{B}_N^*$ that are not in $\mathcal{M}$ must be linear combinations of those in $\mathcal{M}$ since $\mathcal{M}$ is maximal, so they also

annihilate $\Pi_{k'}$ for all $k' > M$. Then $v(\Pi_{k'}) = 0$, so $\Pi_{k'}$ is zero for all $k' > M$, according to lemma II.17. But this contradicts the fact that each $\Pi_{k'}$ is an element of a basis. We therefore conclude that $M = C_N$. □

This lemma allows us to define a basis $\mathscr{B}_N$ for $\mathcal{S}_N$ that is dual to $\mathscr{B}_N^*$. In chapter four, we present a physical interpretation for the elements of $\mathscr{B}_N$ in terms of cluster crossing probabilities in a $2N$-sided polygon with a specified FFBC.

2.5 Asymptotic behavior of Coulomb-gas integrals under interval collapse

The purpose of this section is to calculate the asymptotic behavior of the Coulomb gas integral $\mathcal{I}_M$ (2.10) when the interval (x_i, x_{i+1}) is collapsed, under certain conditions placed on the powers β_{kl} and γ_{pq} that are consistent with the application in this chapter. The results of this calculation were used to prove lemma II.22. There, we alluded to these results, but we postponed their justification to this section. In what follows, we will assume that the collection $\{\Gamma_m\}$ of nonintersecting contours connecting the various branch points of the integrand of $\mathcal{I}_M$ pairwise are simple curves. The results remain true when these simple curves are replaced by nonintersecting Pochhammer contours entwining the endpoints of those curves, and we will explain why below.

There are four different cases to consider (figure 2.9). In the first case, no contour among $\{\Gamma_m\}$ ends at either x_i or x_{i+1}. In the second case, one contour Γ_1 follows along and just above (x_i, x_{i+1}) with endpoints at x_i and x_{i+1}. In the third case, one contour Γ_1 will end at one, but not both, of x_i and x_{i+1}, and no contour will end at the other point. In the fourth case, a contour Γ_1 terminates at x_i, and a different contour Γ_2 terminates at x_{i+1}.

In order to compute the asymptotic behavior of $\mathcal{I}_M$ in each of these cases, we will

typically need to deform one or two of the integration contours. In order to do this correctly, we must specify a choice of branch for the logarithm function. We choose the branch so that $\arg z \in [-\pi, \pi)$ for all $z \in \mathbb{C}$. Thus the integrand of (2.10), viewed as a function of the integration variable u_j, has several branch cuts with each starting at a branch point, following along the real axis, and terminating at x_{2N}. (These statements are not quite true and need refinement when κ is an exceptional speed. We will consider these special cases in the next chapter.) With this convention set, we have the following identitiy which will prove useful later. Suppose that $x, u, \beta \in \mathbb{R}$ with $x < u$. Then for positive $\epsilon \ll u$, we have

$$(x - (u \pm i\epsilon))^{\beta} = e^{\mp \pi i \beta}(u \pm i\epsilon - x)^{\beta}. \tag{2.164}$$

2.5.1 The first case

In the first case, no contour among $\{\Gamma_m\}$ in $\mathcal{I}_M$ ends at either x_i or x_{i+1}. In this case, the result is trivial. The integrand approaches a limit as $x_{i+1} \to x_i$ uniformly in the integration variables, and the limit is found by simply setting $x_{i+1} = x_i$ in $\mathcal{I}_M$.

2.5.2 The second case

In the second case, the contour Γ_1 in $\mathcal{I}_M$ follows just above (x_i, x_{i+1}) with its endpoints at x_i and x_{i+1}. The factors of the integrand of $\mathcal{I}_M$ approach a limit as $x_{i+1} \to x_i$ uniformly in u_1, except for $(u_1 - x_i)^{\beta_i}$ and $(u_1 - x_{i+1})^{\beta_{i+1}}$ which must be treated with care since u_1 is drawn in with the limit. Therefore, we only need

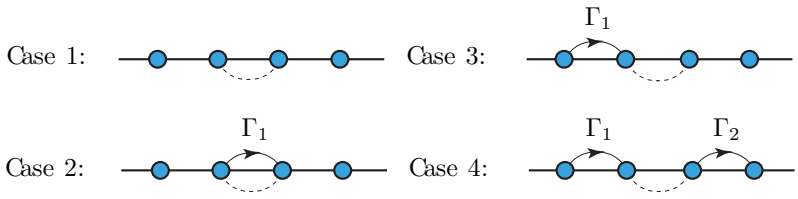

Figure 2.9: The four cases of interval collapse. The dashed curves connect the endpoints of the interval to be collapsed, and the solid curves indicate the integration contours.

to study the integration with respect to u_1. This integral has the form of $\mathcal{I}_1$ with arguments $\{x_j\}_{j\neq i,i+1} \cup \{u_k\}_{k>1}$, where each u_k is fixed to some value in Γ_k (which we may take to be real by forcing Γ_k to touch the real axis there). If we relabel the variables $x_1, \ldots, x_{2N}, u_2, \ldots, u_M$ in ascending order as $x_1, x_2, \ldots$ (and adjust the values of $i-1, i$, and $i+1$ so that they are still the indices of the original points x_{i-1}, x_i and x_{i+1} respectively before the relabeling), then the integration with respect to u_1 is

$$\mathcal{I}_1(\{\beta_j\} \,|\, [x_i, x_{i+1}] \,|\, x_1, \ldots) = \int_{x_i}^{x_{i+1}} \mathcal{N}\left[\prod_j (u_1 - x_j)^{\beta_j}\right] du_1. \tag{2.165}$$

The operator $\mathcal{N}$ orders the differences in the integrand so that they are positive. By using the substitution $u(t) = (1-t)x_i + t x_{i+1}$ and factoring the dependence on $x_{i+1} - x_i$ out of the integral, we find the asymptotic behavior of $\mathcal{I}_1$ under the interval collapse $x_{i+1} \to x_i$:

$$\begin{aligned} \mathcal{I}_1 \underset{x_{i+1}\to x_i}{\sim} & (x_{i+1} - x_i)^{\beta_i + \beta_{i+1} + 1} \mathcal{N}\left[\prod_{j\neq i} (x_{i+1} - x_j)^{\beta_j}\right] \int_0^1 t^{\beta_i} (1-t)^{\beta_{i+1}}\, dt \\ = & \frac{\Gamma(\beta_i + 1)\Gamma(\beta_{i+1} + 1)}{\Gamma(\beta_i + \beta_{i+1} + 2)} (x_{i+1} - x_i)^{\beta_i + \beta_{i+1} + 1} \mathcal{N}\left[\prod_{j\neq i} (x_{i+1} - x_j)^{\beta_j}\right]. \end{aligned} \tag{2.166}$$

If $\beta_i \leq -1$ or $\beta_{i+1} \leq -1$, then the integral diverges. In this case, we analytically continue the result by replacing Γ_1 with the Pochhammer contour $\mathscr{P}(x_i, x_{i+1})$ (figure 1.20) and dividing by $4e^{\pi i(\beta_i - \beta_{i+1})} \sin \pi\beta_i \sin \pi\beta_{i+1}$ so that $\mathcal{I}_1$ exists.

2.5.3 The third case

In the third case, one contour Γ_1 of $\mathcal{I}_M$ ends at either one, but not both, of x_i and x_{i+1}, and no contour ends at the other point. Without loss of generality, we suppose that the endpoint of Γ_1 is x_i, and we assume that Γ_1 follows just above (x_{i-1}, x_i) with its other endpoint at x_{i-1}. This assumption is accommodated by the proof of lemma

II.22. The factors of the integrand of $\mathcal{I}_M$ approach a limit as $x_{i+1} \to x_i$ uniformly in u_1, except for $(u_1 - x_{i+1})^{\beta_{i+1}}$. Therefore, we only need to study the integration with respect to u_1. If we relabel the $K = 2N + M - 1$ variables $x_1, \ldots, x_{2N}, u_2, \ldots, u_M$ in ascending order as $x_1, x_2, \ldots$ (and adjust the values of $i-1, i$ and $i+1$ so that they are still the indices of the original points x_{i-1}, x_i, and x_{i+1} respectively before the relabeling), then the integration with respect to u_1 is

$$I_i := \mathcal{I}_1(\{\beta_j\} \,|\, [x_{i-1}, x_i] \,|\, x_1, \ldots, x_K) = \int_{x_{i-1}}^{x_i} \mathcal{N} \left[\prod_j (u_1 - x_j)^{\beta_j} \right] du_1. \tag{2.167}$$

We require the sum $\sum_j \beta_j$ to equal an integer so that infinity is not a branch point. We also require the sum to be less than negative one so that the integral converges if one of its bounds is infinite. This is consistent with our application in section 2.4. There, the exponents $\beta_i, \beta_{i+1}, \gamma$, and β_j with $j \neq i, i+1$ satisfy

$$\begin{aligned} &\textstyle\sum_j \beta_j = -2, \quad \beta_i = \beta_{i+1} = -4/\kappa, \\ &\qquad \beta_j = -4/\kappa \quad \text{or} \quad 8/\kappa \quad \text{or} \quad 12/\kappa - 2 \quad \text{for } j \neq i, i+1 \text{ and } \kappa \in (0, 8). \end{aligned} \tag{2.168}$$

If $\beta_{i-1} \leq -1$ or $\beta_i \leq -1$, then the integral diverges, and we analytically continue it by replacing Γ_1 with $\mathscr{P}(x_{i-1}, x_i)$ and dividing by $4e^{\pi i(\beta_{i-1} - \beta_i)} \sin \pi\beta_{i-1} \sin \pi\beta_i$.

To calculate the asymptotic behavior of I_i as $x_{i+1} \to x_i$, we rewrite it as a linear combination of the $\{I_k\}_{k \neq i-1, i+1}$, with I_k defined as in (2.167) except with its limits of integration at x_{k-1} and x_k. An integration along a large semicircle of radius R with

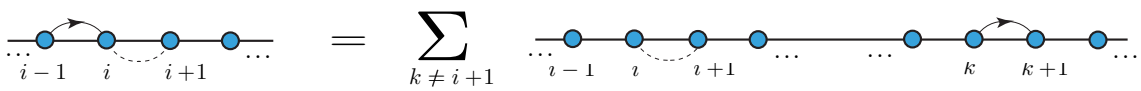

Figure 2.10: The third case. The dashed curve connects the endpoints of the interval to be collapsed. The integration contour is pushed from $[x_{i-1}, x_i]$ onto any interval except $[x_{i+1}, x_{i+2}]$.

counterclockwise (resp. clockwise) orientation in the upper (resp. lower) half-plane with its base on the real axis gives zero according to Cauchy's theorem. As $R \to \infty$, the integration along the circular part of the semi-circle vanishes as $R^{-\sum_j \beta_j + 1}$, and we find (with the $-$ (resp. $+$) sign corresponding with the upper (resp. lower) half-plane setting)

$$\sum_{k=1}^{K} e^{\pm \pi i \sum_{l=1}^{k} \beta_l} I_{k+1} = 0. \tag{2.169}$$

(Here, we identify x_{K+1} with x_1.) Now, we can solve for I_i (2.167) in terms of I_{k+1} with $k \neq i+1$ (figure 2.10). The solution is

$$I_i = -\sum_{k=1}^{i-2} \frac{\sin \pi \sum_{l=k+1}^{i+1} \beta_l}{\sin \pi(\beta_i + \beta_{i+1})} I_{k+1} + \sum_{k=i+2}^{K} \frac{\sin \pi \sum_{l=i+2}^{k} \beta_l}{\sin \pi(\beta_i + \beta_{i+1})} I_{k+1} - \frac{\sin \pi \beta_{i+1}}{\sin \pi(\beta_i + \beta_{i+1})} I_{i+1}. \tag{2.170}$$

(If any of these integrals diverge, then we analytically continue it as prescribed above, and (2.170) is still true for the analytic continuation.) The integral I_{k+1} with $k \neq i$ (resp. $k = i$) falls under the first (resp. second) case, so we find the asymptotic behavior

$$\begin{aligned} I_i \underset{x_{i+1} \to x_i}{\sim} & -\sum_{k=1}^{i-2} \frac{\sin \pi \sum_{l=k+1}^{i+1} \beta_l}{\sin \pi(\beta_i + \beta_{i+1})} \int_{x_k}^{x_{k+1}} \mathcal{N} \left[(u - x_i)^{\beta_i + \beta_{i+1}} \prod_{j \neq i, i+1} (u_1 - x_j)^{\beta_j} \right] du_1 \\ & + \sum_{k=i+2}^{K} \frac{\sin \pi \sum_{l=i+2}^{k} \beta_l}{\sin \pi(\beta_i + \beta_{i+1})} \int_{x_k}^{x_{k+1}} \mathcal{N} \left[(u - x_i)^{\beta_i + \beta_{i+1}} \prod_{j \neq i, i+1} (u_1 - x_j)^{\beta_j} \right] du_1 \\ & - \frac{\sin \pi \beta_{i+1} \, \Gamma(\beta_i + 1) \Gamma(\beta_{i+1} + 1)}{\sin \pi(\beta_i + \beta_{i+1}) \Gamma(\beta_i + \beta_{i+1} + 2)} \\ & \times (x_{i+1} - x_i)^{\beta_i + \beta_{i+1} + 1} \mathcal{N} \left[\prod_{j \neq i, i+1} (x_{i+1} - x_j)^{\beta_j} \right]. \end{aligned} \tag{2.171}$$

If $\beta_i + \beta_{i+1} \geq -1$, then all terms are finite and I_i has a limit. If $\beta_i + \beta_{i+1} < -1$, then the last term will blow up while the others remain finite, and we have

$$I_i \underset{x_{i+1}\to x_i}{\sim} -\frac{\sin\pi\beta_{i+1}\,\Gamma(\beta_i+1)\Gamma(\beta_{i+1}+1)}{\sin\pi(\beta_i+\beta_{i+1})\Gamma(\beta_i+\beta_{i+1}+2)} \times (x_{i+1}-x_i)^{\beta_i+\beta_{i+1}+1}\mathcal{N}\left[\prod_{j\neq i,i+1}(x_{i+1}-x_j)^{\beta_j}\right], \quad \beta_i+\beta_{i+1}<-1. \quad (2.172)$$

This latter case is consistent with our application (2.168). We note that (2.172) is identical to (2.166) except for the ratio of sine functions and factor of negative one multiplying the former. This ratio equals the negative reciprocal of the O(n) fugacity factor (1.155) in our application (2.168).

It is straightforward to check that the asymptotic behavior of I_{i+2} is also given by the right side of (2.172). Both of these situations exhaust the third case.

2.5.4 The fourth case

In the fourth case, one contour Γ_1 of $\mathcal{I}_M$ ends at x_i, and a different contour Γ_2 ends at x_{i+1}. The factors of the integrand of $\mathcal{I}_M$ approach a limit as $x_{i+1}\to x_i$ uniformly in $(u_1,u_2)\in\Gamma_1\times\Gamma_2$, except for the factors $(u_1-x_{i+1})^{\beta_{i+1}}$, and $(u_2-x_i)^{\beta_i}$. Therefore, we only need to study the integrals with respect to u_1 and u_2. This double integral has the form of $\mathcal{I}_2$, and without loss of generality, we suppose that Γ_1 (resp. Γ_2) follows just above (x_{i-1},x_i) (resp. (x_{i+1},x_{i+2})) with its other endpoint at x_{i-1} (resp. x_{i+2})). This assumption is accommodated by the proof of lemma II.22. If we relabel the $K=2N+M-2$ variables $x_1,\ldots,x_{2N},u_3,\ldots,u_M$ in ascending order

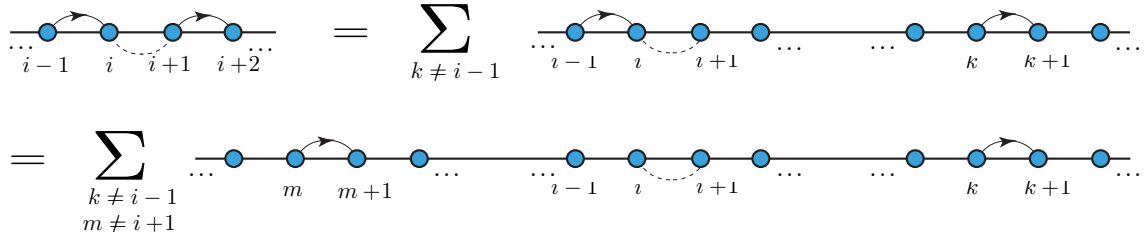

Figure 2.11: The fourth case. The dashed curve connects the endpoints of the interval to be collapsed. The left (resp. right) integration contour is pushed from $[x_{i-1},x_i]$ (resp. $[x_{i+1},x_{i+2}]$) onto any interval except $[x_{i+1},x_{i+2}]$ (resp. $[x_{i-1},x_i]$).

as $x_1, x_2, \ldots, x_K$ (and adjust the values of $i-1, i, i+1$, and $i+2$ so that they are still the indices of the original points x_{i-1}, x_i, x_{i+1}, and x_{i+2} respectively before the relabeling), then the integration with respect to u_1 and u_2 is

$$\begin{aligned} I_{i,i+2} &:= \mathcal{I}_2(\{\beta_j\}; \gamma \,|\, [x_{i-1}, x_i], [x_{i+1}, x_{i+2}] \,|\, x_1, \ldots) \\ &= \int_{x_{i-1}}^{x_i} \int_{x_{i+1}}^{x_{i+2}} \mathcal{N}\bigg[\prod_j (u_1 - x_j)^{\beta_j} (u_2 - x_j)^{\beta_j} (u_2 - u_1)^{\gamma} \bigg] \, du_2 \, du_1. \end{aligned} \quad (2.173)$$

Here, we assume that the sum $\sum_j \beta_j + \gamma$ is an integer less than negative one so that infinity is not a branch point and so that integrating from end to end of and just above or below the real axis gives zero. In our application in section 2.4, the exponents $\beta_i, \beta_{i+1}, \gamma$, and β_j with $j \neq i, i+1$ satisfy

$$\begin{aligned} &\sum\nolimits_j \beta_j + \gamma = -2, \quad \beta_i = \beta_{i+1} = -4/\kappa, \quad \gamma = 8/\kappa, \\ &\qquad \beta_j = -4/\kappa \quad \text{or} \quad 8/\kappa \quad \text{or} \quad 12/\kappa - 2 \quad \text{for } j \neq i, i+1 \text{ and } \kappa \in (0, 8). \end{aligned} \quad (2.174)$$

Again, if $\beta_{i-1} \leq -1$ or $\beta_i \leq -1$ (resp. $\beta_{i+1} \leq -1$ or $\beta_{i+2} \leq -1$), then the integral diverges, and we analytically continue it by replacing Γ_1 (resp. Γ_2) with $\mathscr{P}(x_{i-1}, x_i)$ (resp. $\mathscr{P}(x_{i+1}, x_{i+2})$) and dividing by $4e^{\pi i(\beta_{i-1} - \beta_i)} \sin \pi\beta_{i-1} \sin \pi\beta_i$ (resp. $4e^{\pi i(\beta_{i+1} - \beta_{i+2})} \sin \pi\beta_{i+1} \sin \pi\beta_{i+2}$). As in the third scenario, this replacement analytically continues all of the linear dependences that we will derive below to these cases.

To calculate the asymptotic behavior of $I_{i,i+2}$, we pursue the strategy used in the third case. We rewrite $I_{i,i+2}$ as a linear combination of the elements of $\{I_{j,k}\}_{j,k \neq i,i+2}$ where $I_{j,k}$ is defined as in (2.173) except with its u_1 (resp. u_2) limits of integration at x_{j-1} and x_j (resp. x_{k-1} and x_k). All integrals in the linear combination will fall under the first or second case, so their asymptotic behavior is already understood.

Now a subtlety arises that we must address. Due to the factor $(u_2 - u_1)^{\gamma}$ appearing in the integrand of $I_{j,k}$, it is impossible to arrange the integrand of any $I_{j,j}$ so that

the double integral is real. This issue can be corrected by noting that

$$\int_{x_j}^{x_{j+1}} \int_{x_j}^{u_1} \mathcal{N}\Big[\prod_j (u_1 - x_j)^{\beta_j}(u_2 - x_j)^{\beta_j}(u_1 - u_2)^{\gamma}\Big]\, du_2\, du_1$$
$$= \int_{x_j}^{x_{j+1}} \int_{u_1}^{x_{j+1}} \mathcal{N}\Big[\prod_j (u_1 - x_j)^{\beta_j}(u_2 - x_j)^{\beta_j}(u_2 - u_1)^{\gamma}\Big]\, du_2\, du_1. \quad (2.175)$$

Because these integrals are real, we redefine $I_{j,j}$ to be either of them.

We now repeat the steps of case three, and the work that follows is straightforward but tedious. Because the complete result is complicated and unnecessary for our purposes, we will specialize to cases with certain conditions imposed on $\{\beta_j, \gamma\}$ that are consistent with (2.174). By integrating u_2 just along the top and bottom of the real axis and using Cauchy's theorem, we find

$$\sum_{k=1}^{i-2} e^{\pm\pi i \sum_{l=1}^{k}\beta_l} I_{i,k+1} + e^{\pm\pi i \sum_{l=1}^{i-1}\beta_l}(1 + e^{\pm\pi i\gamma}) I_{i,i}$$
$$+ \sum_{k=i}^{K} e^{\pm\pi i(\sum_{l=1}^{k}\beta_l + \gamma)} I_{i,k+1} = 0. \quad (2.176)$$

(Here, we identify x_{K+1} with x_1.) We solve this system of equations for $I_{i,i+2}$ in terms of $I_{i,k+1}$ with $k \neq i-1$. The result is (figure 2.11)

$$I_{i,i+2} = \sum_{k=1}^{i-2} \frac{\sin\pi(\sum_{l=k+1}^{i-1}\beta_l + \gamma/2)}{\sin\pi(\beta_i + \beta_{i+1} + \gamma/2)} I_{i,k+1} - \frac{\sin\pi(\beta_i + \gamma/2)}{\sin\pi(\beta_i + \beta_{i+1} + \gamma/2)} I_{i,i+1}$$
$$- \sum_{k=i+2}^{K} \frac{\sin\pi(\sum_{l=i}^{k}\beta_l + \gamma/2)}{\sin\pi(\beta_i + \beta_{i+1} + \gamma/2)} I_{i,k+1}. \quad (2.177)$$

Now, if the asymptotic behavior of $I_{i,i+2}$ for general $\{\beta_j, \gamma\}$ with $\sum_j \beta_j + \gamma$ an integer less than negative one is desired, one must isloate the remaining $I_{i,k+1}$ in terms of $I_{j,k+1}$ with $j \neq i+2$ using the same method. This task is very difficult to do in complete generality. If $\beta_i + \beta_{i+1} < -1$, as it is in our application (2.174), then the

$I_{i,i+1}$ term will give many terms that blow up as $(x_{i+1}-x_i)^{\beta_i+\beta_{i+1}+1}$ while each of the other terms will only give one such term. To avoid this complication, we assume $\beta_i+\gamma/2=0$ so that this term vanishes. Overall, we have assumed the conditions

$$\sum\nolimits_j \beta_j+\gamma\in\mathbb{Z}^-\setminus\{-1\},\quad \beta_i+\gamma/2=0 \tag{2.178}$$

which are consistent with our application (2.174). To address the other terms in (2.177), we integrate u_1 just along the top and bottom of the real axis to find that

$$\sum_{m=1}^{k-1} e^{\pm\pi i\sum_{n=1}^m\beta_n} I_{m+1,k+1}+e^{\pm\pi i\sum_{n=1}^k\beta_n}(1+e^{\pm\pi i\gamma})I_{k+1,k+1} + \sum_{m=k+1}^{K} e^{\pm\pi i(\sum_{n=1}^m\beta_n+\gamma)} I_{m+1,k+1}=0. \tag{2.179}$$

Now we isolate each $I_{i,k+1}$ with $k\neq i-1,i,i+1$ in terms of all $I_{m+1,k+1}$ with $m\neq i+1$ and substitute the result into (2.177). This process, though straightforward, is tedious. However, if we add a third condition $\beta_i+\beta_{i+1}<-1$ to (2.178),

$$\sum\nolimits_j \beta_j+\gamma\in\mathbb{Z}^-\setminus\{-1\},\quad \beta_i+\gamma/2=0,\quad \beta_i+\beta_{i+1}<-1, \tag{2.180}$$

then we see from (2.172) that $I_{i+1,k+1}$ will dominate over all $I_{m+1,k+1}$ with $m\neq i+1$, so we only concern ourself with the former integral. Condiditons (2.180) are consistent with our application (2.174). Thus we find

$$I_{i,k+1}\underset{x_{i+1}\to x_i}{\sim}-\frac{\sin\pi\beta_{i+1}}{\sin\pi(\beta_i+\beta_{i+1})}I_{i+1,k+1}. \tag{2.181}$$

The asymptotic behavior of the integral from x_i to x_{i+1} inside of $I_{i+1,k+1}$ as $x_{i+1}\to x_i$ falls under the second case and can be computed using the results of section 2.5.2. Under the assumptions of (2.180), substituting (2.181) into (2.177) gives

$$I_{i,i+2} \underset{x_{i+1}\to x_i}{\sim} \left[-\sum_{k=1}^{i-2} \frac{\sin\pi(\sum_{l=k+1}^{i-1}\beta_l + \gamma/2)}{\sin\pi(\beta_i+\beta_{i+1}+\gamma/2)} + \sum_{k=i+2}^{K} \frac{\sin\pi(\sum_{l=i}^{k}\beta_l + \gamma/2)}{\sin\pi(\beta_i+\beta_{i+1}+\gamma/2)} \right]$$
$$\times \int_{x_k}^{x_{k+1}} \mathcal{N}\left[(u_2-x_i)^{\beta_i+\beta_{i+1}+\gamma} \prod_{j\neq i,i+1} (u_2-x_j)^{\beta_j} \right] du_2$$
$$\times \frac{\sin(\pi\beta_{i+1})\Gamma(\beta_i+1)\Gamma(\beta_{i+1}+1)}{\sin\pi(\beta_i+\beta_{i+1})\Gamma(\beta_i+\beta_{i+1}+2)} (x_{i+1}-x_i)^{\beta_{i+1}+\beta_i+1}$$
$$\times \mathcal{N}\left[\prod_{j\neq i,i+1} (x_j-x_i)^{\beta_j} \right]. \quad (2.182)$$

This is the asymptotic behavior of $I_{i,i+2}$ as $x_{i+1} \to x_i$ under the conditions (2.180).

Equation (2.182) can be simplified considerably if we introduce a fourth condition that is consistent with our application (2.174). First, we consider the integral

$$I'_{i+2} := \int_{x_{i-1}}^{x_{i+2}} \mathcal{N}\left[\prod_{j\neq i,i+1} (u_2-x_j)^{\beta_j} \right] du_2. \quad (2.183)$$

The prime signifies that the points x_j with $j \neq i, i+1$ are in the domain of I'_{i+2} while x_i and x_{i+1} are not. If we add the condition $\beta_{i+1} = \beta_i$ to (2.180) so that we have assumed overall that

$$\sum\nolimits_j \beta_j + \gamma \in \mathbb{Z}^- \setminus \{-1\}, \quad \beta_i + \gamma/2 = 0, \quad \beta_i + \beta_{i+1} < -1, \quad \beta_i = \beta_{i+1}, \quad (2.184)$$

then the sum of the powers in (2.183) $\sum_{j\neq i,i+1}\beta_j$ is an integer less than negative one. So by integrating u just across the top and bottom of the real axis, we find

$$A^{\pm} := \sum_{k=1}^{K}{}' e^{\pm\pi i \sum_{l=1}^{\prime k}\beta_l} I'_{k+1} = 0, \quad (2.185)$$

where the prime indicates summation over indices except $k, l = i, i+1$. Conditions (2.184) are consistent with our application (2.174). Now after isolating I'_{i+2} from the

linear combination

$$A^{+}e^{-\pi i\sum_{l=1}^{'i-1}\beta_l}e^{\pi i(\beta_i+\beta_{i+1}+\gamma/2)}-A^{-}e^{\pi i\sum_{l=1}^{'i-1}\beta_l}e^{-\pi i(\beta_i+\beta_{i+1}+\gamma/2)}=0, \tag{2.186}$$

we find

$$I'_{i+2}=\left[\sum_{k=1}^{i-2}\frac{\sin\pi(\sum_{l=k+1}^{i-1}\beta_l-\beta_i-\beta_{i+1}-\gamma/2)}{\sin\pi(\beta_i+\beta_{i+1}+\gamma/2)}\right.$$
$$\left.-\sum_{k=i+2}^{K}\frac{\sin\pi(\sum_{l=i}^{k}\beta_l+\gamma/2)}{\sin\pi(\beta_i+\beta_{i+1}+\gamma/2)}\right]\int_{x_k}^{x_{k+1}}\mathcal{N}\left[\prod_{j\neq i,i+1}(u_2-x_j)^{\beta_j}\right]du_2. \tag{2.187}$$

With the condition that $\beta_{i+1}=\beta_i$ in (2.184), the right side of (2.187) equals the product of the first bracketed factor with the integral on the right side of (2.182). We can use this fact to write (2.182) is a simpler form. Overall, we find

$$I_{i,i+2}\underset{x_{i+1}\to x_i}{\sim}-\frac{\sin(\pi\beta_{i+1})\Gamma(\beta_i+1)\Gamma(\beta_{i+1}+1)}{\sin\pi(\beta_i+\beta_{i+1})\Gamma(\beta_i+\beta_{i+1}+2)}(x_{i+1}-x_i)^{\beta_{i+1}+\beta_i+1}$$
$$\times\mathcal{N}\left[\prod_{j\neq i,i+1}(x_j-x_i)^{\beta_j}\right]\int_{x_{i-1}}^{x_{i+2}}\mathcal{N}\left[\prod_{j\neq i,i+1}(u_2-x_j)^{\beta_j}\right]du_2. \tag{2.188}$$

Remarkably, under the conditions (2.184), the interval collapse $x_{i+1}\to x_i$ appears to have joined contours Γ_1 and Γ_2 of (2.173) into a single contour Γ connecting the leftmost endpoint x_{i-1} of Γ_1 with the rightmost endpoint x_{i+2} of Γ_2. The points x_i and x_{i+1} do not participate in the remaining integral. We note that the ratio of the sine functions equals the negative reciprocal of the O(n) fugacity factor (1.155) in our application (2.174).

A summary of the nontrivial asymptotic behaviors of the integrals studied in cases two, three, and four are presented in figure 2.12.

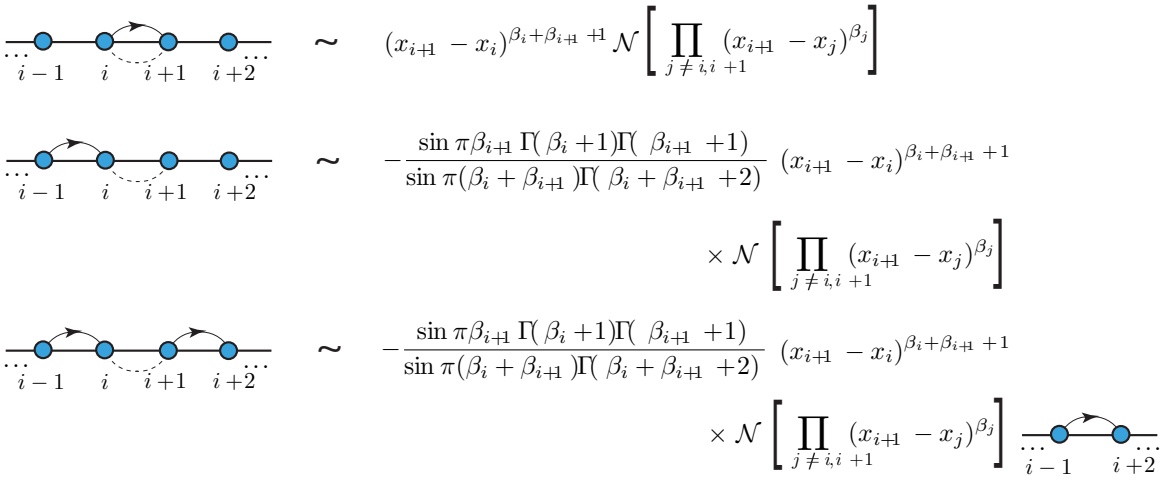

Figure 2.12: A summary of the asymptotic behaviors of the Coulomb gas integrals studied in this section under the interval collapse of cases two, three, and four. The dashed curve connects the endpoints of the interval to be collapsed.

2.6 Summary

We summarize the main results of this chapter and suggest extensions of this research. The principal result is theorem II.25, which says that, if conjecture II.16 is true, then the solution space $\mathcal{S}_N$ (definition II.6) for the system (2.1-2.2) of $2N$ null-state PDEs and three Ward identities has dimension C_N, with C_N the N-th Catalan number (2.7). Still assuming this conjecture, $\mathcal{B}_N$ of definition II.20 serves as a basis for $\mathcal{S}_N$ when κ is not an exceptional speed (2.146) with $q \leq N+1$. This latter fact was proven by establishing an isomorphism between the elements of $\mathcal{B}_N$ and the columns of the meander matrix $M_N(\kappa)$ whose k, k'-th entry is given by (2.150) with $n(\kappa)$ given by (1.155). When κ is an exceptional speed with $q \leq N+1$, the determinant of the meander matrix is zero, so $\mathcal{B}_N$ is linearly dependent. In this case, an "adjusted" set $\mathcal{B}'_N$, whose construction from $\mathcal{B}_N$ is given in the proof of theorem II.25, serves as a basis for $\mathcal{S}_N$.

The principal goal of proving that the solution space of the system (2.1-2.2) has dimension C_N and is spanned by the Coulomb gas solutions is still unfinished, although most of the work towards this end is done in this chapter. Conjecturers II.7

and II.16 must be proven in order to achieve this ultimate goal, and we have devoted some discussion about how this might be done. We feel that these two matters are technical rather than monumental and that a complete proof can be formed from the work presented in this chapter.

Another extension of this work is to extend these results to systems of PDEs that govern correlation functions of an arbitrary number of boundary multiple-leg operators (or any correlation function of fields belonging exclusively to either the first row or the first column, but not both, of the conformal grid). These PDEs are explicitly given by the Benoit-Saint-Aubin formula [67]. We recall from chapter one that a boundary s-leg operator is created by fusing together s distinct boundary one-leg operators. Thus, the correlation functions studied in this chapter are building blocks for these more complicated correlation functions in that we can, in principal, study the latter as a suitable limit of the former. As such, it should be possible to glean information about them by looking at the results of this chapter in this limit.

CHAPTER III

Exceptional SLE speeds and CFT minimal models

We recall that the Verma module $V(c,h)$ is reducible when the conformal weight h is that of a Kac operator $\phi_{r,s}$ due to the existence of a level rs null-state. CFT translates this reducibility into a differential equation that governs any correlation function containing this Kac operator. For example, a correlation function including the Kac operator $\phi_{1,2}$ satisfies the differential equation (1.106). Now, the (p,p') minimal model, or a CFT with central charge

$$c_{p,p'} = 1 - \frac{6(p-p')^2}{pp'}, \quad p < p' \text{ coprime}, \tag{3.1}$$

has additional structure described in section 1.2.6. The operator content of the theory is comprised of the conformal families of the Kac operators $\phi_{r,s}$ with $1 \leq r < p'$ and $1 \leq s < p$. The Verma module $V_{r,s}$ with $\phi_{r,s}$ as its highest-weight vector has not just one null-state at level rs, but an infinite tower of null-states at levels $(p'-r)(p-s), rs+(p'-r)(p+s), rs+(p'+r)(p-s)$, etc., which implies that a correlation function containing $\phi_{r,s}$ must satisfy an infinite system of null-state PDEs, including the original null-state PDE that follows from the level rs null-state.

In chapter two, we focused our attention on $2N$-point functions with all fields either $\phi_{1,2}$ or $\phi_{2,1}$. Such correlation functions are governed by the system of $2N$ $\phi_{1,2}$ null-state PDEs (2.1) and three Ward identities (2.2). In chapter two, we observed

that the set $\mathcal{B}_N$ of particular Coulomb gas solutions is linearly independent, and thus serves as a basis for the solution space $\mathcal{S}_N$ for this system, only when κ is not an exceptional speed (2.146) with $q \leq N+1$ and is linearly dependent otherwise (if we assume conjecture II.16). As this linear dependence may be indicative of additional constraints imposed on the $2N$-point functions, we speculate that this phenomena and that of the previous paragraphs are related, so the additional constraints are these extra PDEs that complement the original system. This speculation is supported by the fact that each exceptional speed corresponds with the central charge of a minimal model. From (1.114) and (1.117), we have

$$\begin{aligned} c(\kappa_{q,q'}) &= 1 - \frac{6(q-q')^2}{qq'} = c_{p,p'} \qquad & p &:= \max\{q,q'\} \\ h_{r,s}(\kappa_{q,q'}) &= \frac{(pr-p's)^2-(p-p')^2}{4pp'} \quad , & p' &:= \min\{q,q'\} \end{aligned} \quad . \tag{3.2}$$

That is, $c(\kappa_{q,q'})$ is the central charge of the (p,p') minimal model with $p = \max\{q,q'\}$ and $p' = \min\{q,q'\}$.

In this chapter, we will use the explicit form of the Coulomb gas solutions (2.9) to investigate why $\mathcal{B}_N$ is linearly dependent and how these linear dependences appear only when κ is an exceptional speed with $q \leq N+1$. By answering these questions, we will witness how the elements of $\mathcal{B}_N$ exhibit the truncation of the first row/column of the conformal grid to the Kac table in a minimal model. Moreover, we will conjecture that if κ is an exceptional speed with $q \leq N+1$, then $\mathcal{B}_N$ is a basis for the solution space of the infinite tower of null-state PDEs governing the $2N$-point function $\langle \psi_1(x_1) \dots \psi_1(x_{2N}) \rangle$ in the corresponding minimal model. If this is true, then the dimension of the solution space of this infinite system is immediately given by the rank of $\mathcal{B}_N$ (2.157).

Throughout this chapter, we will assume that conjecture II.16 is true, and the term "solution" will mean an element of $\mathcal{S}_N$. This semantic matter is irrelevant if conjecture II.7 is true. Also, we will use the Coulomb gas notation consistent with

the dense phase ($\kappa > 4$).

3.1 Linear dependences of s-leg solutions

In this section, we study a collection of solutions called *s-leg solutions* which arise through a natural selection of integration contours. These solutions will provide a framework for most of the results of this chapter.

The s-leg solutions are found among a relatively simple choice of integration contours $\{\Gamma_m\}$ for the Coulomb-gas integral $\mathcal{I}_{N-1}$ defined in (2.10). As mentioned in chapter two, each contour must wind around the branch points, its winding number around each branch point must be zero, and different contours may not intersect each other. With no other contours specified, we choose the contour Γ_1 first. The simplest choice that satisfies the necessary criteria is a Pochhammer contour $\mathscr{P}(x_i, x_j)$ (figure 1.20) entwining the pair of branch points x_i and x_j. Because the next contour Γ_2 cannot cross Γ_1, we identify the closure of the interior of Γ_1 with a point p and let Γ_2 be a Pochhammer contour entwining any pair of points in the set $\{p\} \cup \{x_k\}_{k \neq i,j}$. By repeating this process $N-3$ more times, we generate a collection $\{\Gamma_m\}$ of $N-1$ nonintersecting, nested, closed contours that wind around the branch points and each other. We call such a collection a *simple configuration.*

Definition III.1. A *simple configuration* is a collection of Pochhammer contours $\{\Gamma_m\}$ in $\mathbb{C}$ such that both loops of each Pochhammer contour nest either one branch point among $x_1, \ldots, x_{2N}$ or one sequence of nested Pochhammer contours in $\{\Gamma_m\}$. A Coulomb gas solution of the form (2.9) is called a *simple solution* if its set of integration contours $\{\Gamma_m\}$ is a simple configuration.

Of course, not all solutions are simple since a loop of a Pochhammer contour may encircle more than one branch point or other closed contour and since a contour can be something more complicated than a Pochhammer contour. However, if conjecture

II.16 is true, then all solutions are linear combinations of simple solutions, namely those in $\mathcal{B}_N$. This is a consequence of lemma II.22 and theorem II.25.

In this chapter, we use identity (1.195) to replace some of the Pochhammer contours $\mathscr{P}(x_i, x_j)$ with integration along the arc $[x_i, x_j]^+$ as long as this latter integral does not diverge. The arc $[x_i, x_j]^+$ is formed by bending $[x_i, x_j]$ into the upper half plane while keeping the endpoints fixed at x_i, x_j. If κ is such that the integration along $[x_i, x_j]^+$ does diverge ($\kappa \leq 4$), then this replacement is not possible, but we can use an analytic continuation in κ (as demonstrated in section 2.5.3) to show that the results of this chapter extend to such κ in spite of this.

For many choices of simple configurations, $\mathcal{I}_{N-1}$ is zero as a result of a special property involving a charge-neutral-pair.

Definition III.2. A *charge-neutral pair* is a pair of adjacent points x_i and x_{i+1} among $x_1, \ldots, x_{2N}$, each with charge $\alpha^-_{1,2}$ (as defined by the Coulomb gas construction that gives the solutions (2.9)), and a Pochhammer contour $\mathscr{P}(x_i, x_{i+1})$ (or a bent contour $[x_i, x_{i+1}]^+$ replacing it when $\kappa > 4$).

The term "charge-neutral pair" originates from the fact that, in the Coulomb gas formalism, the total charge of such a configuration is $2\alpha^-_{1,2} + \alpha_- = 0$, where the screening charge α_- is the charge of the integration variable.

Now we suppose that $\mathcal{I}_{N-1}$ with $N > 2$ has a charge-neutral pair at, say, x_1 and x_2, and one of its contours Γ is a simple loop that winds once around the charge-neutral

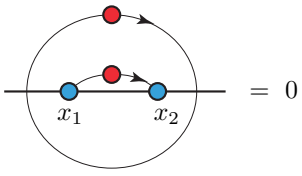

Figure 3.1: The integration of a screening charge around a simple loop surrounding a charge-neutral pair equals zero.

pair. (We note that Γ closes in this special case.) Then $\mathcal{I}_{N-1}$ is zero since

$$\oint_\Gamma \oint_{[x_1,x_2]^+} (u_1-x_1)^{-4/\kappa}(x_2-u_1)^{-4/\kappa}(u_2-x_1)^{-4/\kappa} \times (x_2-u_2)^{-4/\kappa}(u_2-u_1)^{8/\kappa}\ldots\, du_2\, du_1 = 0. \quad (3.3)$$

(The ellipsis stands for the other factors that appear in the integrand of $\mathcal{I}_{N-1}$.) This identity is verified as follows. After fixing u_2 to a specific value in $[x_1, x_2]$, we decompose the portion of Γ above (resp. below) $[x_1, x_2]$ into the segments $[x_1, u_2]^+$ and $[u_2, x_2]^+$ (resp. $[x_1, u_2]^-$ and $[u_2, x_2]^-$). Then the total integration around Γ gives

$$I_1(u_2) + e^{-8\pi i/\kappa} I_2(u_2) - I_2(u_2) - e^{-8\pi i/\kappa} I_1(u_2), \quad (3.4)$$

where we have defined

$$I_1(u_2) := \int_{x_1}^{u_2} (u_1-x_1)^{-4/\kappa}(x_2-u_1)^{-4/\kappa}(u_2-u_1)^{8/\kappa}\ldots\, du_1, \quad (3.5)$$

$$I_2(u_2) := \int_{u_2}^{x_2} (u_1-x_1)^{-4/\kappa}(x_2-u_1)^{-4/\kappa}(u_1-u_2)^{8/\kappa}\ldots\, du_1, \quad (3.6)$$

with the ellipsis standing for the same omitted factors as in (3.3). Upon multiplying both sides of (3.4) by $(u_2-x_1)^{-4/\kappa}(x_2-u_2)^{-4/\kappa}$, integrating u_2 from x_1 to x_2, and using identity (2.175), we prove (3.3).

Identity (3.3) restricts the number of nonzero simple solutions. In particular, we see that if any charge-neutral pair is nested by a Pochhammer contour, then (3.3) implies that $\mathcal{I}_{N-1}$ is zero. However, if one of the two points x_i and x_j entwined by $\mathscr{P}(x_i, x_j)$ bears the conjugate charge $\alpha^+_{1,2}$, then $\mathscr{P}(x_i, x_j)$ can be nested within another Pochhammer contour to give a nonzero simple solution (as long as the other loop of the outer Pochhammer contour does not nest a charge-neutral pair). In our Coulomb gas solutions (2.9), we have chosen x_c to bear the conjugate charge.

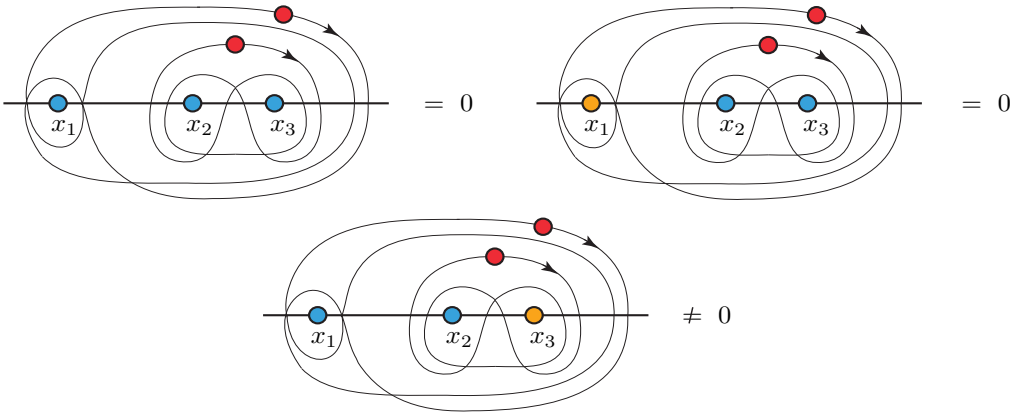

Figure 3.2: Various nestings allowed in a simple configuration. If a Pochhammer contour surrounds a charge-neutral pair, then integration around such a contour gives zero. (In the figures of chapters three and four, a blue (resp. orange, resp. red) circle marks a point of charge $\alpha^-_{1,2}$ (resp. $\alpha^+_{1,2}$, resp. α_-) in the dense phase.)

Therefore, the set of contours for a nonzero simple solution consists of a set of $s-1 \leq N-1$ nested Pochhammer contours encircling a collection of s points $x_{i_1}, \ldots, x_{i_s}$, with x_c one of the two most deeply nested points, and $N-s$ un-nested Pochhammer contours, each entwining its own unique pair of points among $x_{i_{s+1}}, \ldots, x_{i_{2N}}$ into a charge-neutral pair (figure 3.3). This observation leads to the following definition.

Definition III.3. Let $1 < s \leq N$. A simple solution other than zero is an *s-leg solution* if its unique sequence of nested Pochhammer contours consists of $s-1$ contours entwining s adjacent points and the most deeply nested contour encircles the point that bears the conjugate charge. (The points x_{2N} and x_1 are considered to be adjacent in the sense that they are adjacent to each other when the real axis is mapped onto a circle.) If a simple solution other than zero has no Pochhammer contour that entwines the point bearing the conjugate charge with another point, then it is called a *zero-leg solution*. If an s-leg solution $F(\kappa)$ goes to zero as $\kappa \to \kappa'$ for some κ' then $F(\kappa) = O((\kappa - \kappa')^p)$ for some $p \in \mathbb{Z}^+$ since F is analytic at κ', and in this case, we define the s-leg solution to be the limit of $(\kappa - \kappa')^{-p} F(\kappa)$ as $\kappa \to \kappa'$.

We note that every element of $\mathcal{B}_N$ is a zero-leg solution by definition and that, according to corollary II.23, every zero-leg solution is an element of $\mathcal{B}_N$ too.

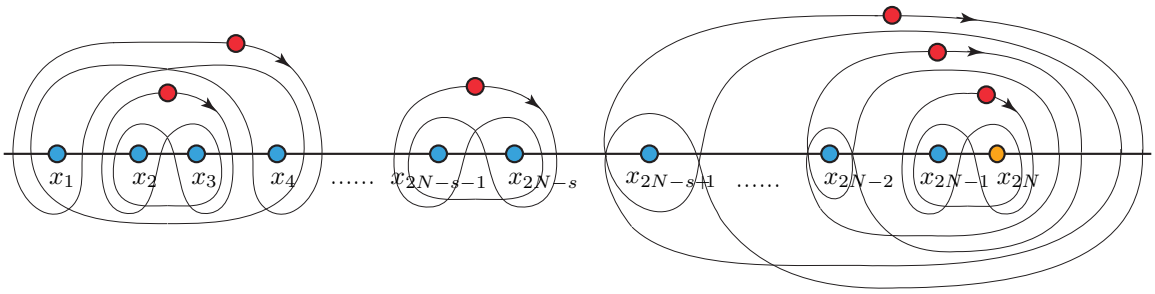

Figure 3.3: A simple configuration with $s-1$ nested contours corresponding to an s-leg solution. The ellipses denote additional points not shown in the picture. We note that the charge-neutral pair entwining x_2 with x_3 can be un-nested from the contour that surrounds it by using identity (3.3).

The term "s-leg solution" derives from terminology used in CFT. The total charge of the collection of s points entwined by the sequence of $s-1$ nested contours is

$$(s-1)\alpha_{1,2}^{-} + \alpha_{1,2}^{+} + (s-1)\alpha_{-} = \alpha_{1,s+1}^{+}, \tag{3.7}$$

which is the charge of a chiral operator with the conformal weight θ_s of an s-leg operator (1.171). So if all of these nested points are brought together, then all of the $s-1$ screening charges are drawn in, and the fusion product will contain just the conformal family of the s-leg operator. (A process in which we bring more than two points together at a time is not well-defined in the sense of an OPE. It may still be achieved in a certain sense by pulling the two points nested by the deepest contour together, say $x_{2N} \to x_{2N-1}$, and omitting the descendant terms and the factor of $(x_{2N} - x_{2N-1})^{-2\theta_1+\theta_2}$ on the leading term. In the leading term, which is now equivalent to a $(2N-1)$-point function with a two-leg operator at x_{2N-1}, the point x_{2N-1} is entwined with the next point, say x_{2N-2}, by what was the second most deeply nested contour in the original s-leg solution. This contour is now the most deeply nested contour. We repeat this process $s-2$ times until all $s-1$ nested contours are contracted away and we are left with an s-leg operator.)

We suppose that κ is not an exceptional speed with $q \leq N+1$. Because $\mathcal{B}_N$ spans

$\mathcal{S}_N$ (if we assume conjecture II.16), the s-leg solutions are linear combinations of the zero-leg solutions. Now we demonstrate how to uncover these linear dependences from the explicit forms of the s-leg solutions. This is a first step towards our ultimate goal of understanding why $\mathcal{B}_N$ becomes linearly dependent when κ equals an exceptional speed with $q \leq N+1$. We will specialize to the arrangement illustrated in figure 3.3 where the points $x_{2N-s+1}, \ldots, x_{2N}$ are entwined by the sequence of $s-1$ nested contours and where x_{2N} bears the conjugate charge.

Starting with $N = 2$, we decompose a two-leg solution into a linear combination of the zero-leg solutions. We let $F(\Gamma)$ be the Coulomb gas solution (2.9) with $N = 2$, $c = 4$, and integration contour Γ. Next, we choose Γ to be a clockwise-oriented, simple, closed curve that tightly wraps around $[x_1, x_4]$, and for $j = 1, 2, 3$, we let $[x_j, x_{j+1}]^+$ (resp. $[x_j, x_{j+1}]^-$) be the part of Γ just above (resp. below) $[x_j, x_{j+1}]$. Because the branch points x_1, x_2, and x_3 have a monodromy factor of $\exp(-8\pi i/\kappa)$, the integrand I_1 of $\mathcal{I}_1$ restricted to $[x_j, x_{j+1}]^+$ differs by a factor of $\exp(-8\pi ij/\kappa)$ from I_1 restricted to $[x_j, x_{j+1}]^-$ (figure 3.4), and they combine into a real-valued integral along $[x_j, x_{j+1}]^+$ times $2i\sin(4\pi j/\kappa)$. By Cauchy's theorem, $\oint_\Gamma I_1 = 0$, so by using

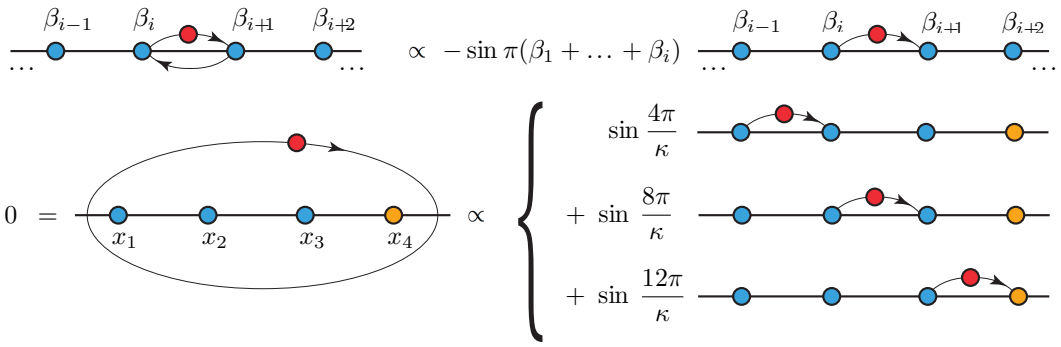

Figure 3.4: The decomposition of a two-leg solution into a linear combination of two zero-leg solutions when $N = 2$. The illustration at the top illustrates the combination of integrations above and below an interval into a single integration above that interval. The monodromy factor of a point with β_i marked above it is $\exp(2\pi i\beta_i)$.

(2.164), we have

$$\sin\left(\frac{4\pi}{\kappa}\right)|F([x_1,x_2]^+)| + \sin\left(\frac{8\pi}{\kappa}\right)|F([x_2,x_3]^+)| \\ = -\sin\left(\frac{12\pi}{\kappa}\right)|F([x_3,x_4]^+)|. \quad (3.8)$$

(The absolute value sign merely eliminates a constant phase that is already accounted for in the factors with the sine function.) Equation (3.8) has the linear relation we sought since the left side is a linear combination of zero-leg solutions while the right side is just a two-leg solution. This decomposition is illustrated in figure 3.4. With small modifications, it is equivalent to the crossing relation (1.152). In general, linear dependences among simple solutions with $N > 2$ may be interpreted as generalizations of crossing relations.

Next with $N = 3$, we decompose a three-leg solution into a linear combination of two-leg solutions, and then we decompose each of those two-leg solutions into a linear combination of the zero-leg solutions. We let $F(\Gamma_1, \Gamma_2)$ be a Coulomb gas solution (2.9) with $N = 3, c = 6$, and integration contours Γ_1 and Γ_2 with $\Gamma_2 = [x_5, x_6]^+$, and we let Γ be a clockwise-oriented, simple, closed curve that tightly wraps around $[x_1, x_6]$. By pinching the top and bottom halves of Γ together at x_4, we divide Γ into two clockwise-oriented loops anchored to x_4. The left loop Γ_l surrounds $[x_1, x_4]$, and the right loop Γ_r surrounds Γ_2 (figure 3.5). Γ_l can be decomposed similarly to the $N = 2$ case, and we have

$$2i\sin\left(\frac{4\pi}{\kappa}\right)|F([x_1,x_2]^+,[x_5,x_6]^+)| + 2i\sin\left(\frac{8\pi}{\kappa}\right)|F([x_2,x_3]^+,[x_5,x_6]^+)| \\ + 2i\sin\left(\frac{12\pi}{\kappa}\right)|F([x_3,x_4]^+,[x_5,x_6]^+)| + F(\Gamma_r,[x_5,x_6]^+) = 0. \quad (3.9)$$

The right contour Γ_r is not closed since the integrand I_2 of $\mathcal{I}_2$ acquires a monodromy factor of $\exp(-32\pi i/\kappa)$ as it is traced clockwise. To close Γ_r, we add

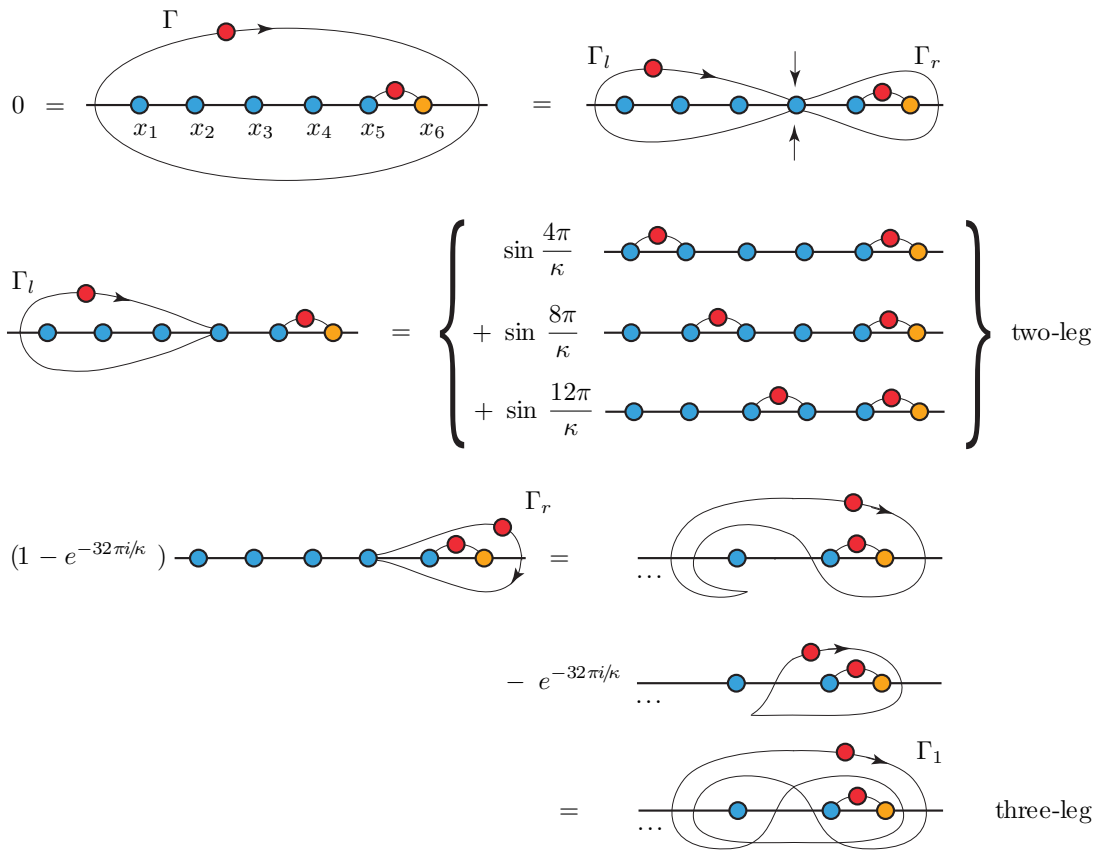

Figure 3.5: The decomposition of a three-leg solution into three two-leg solutions when $N = 3$.

$-\exp(-32\pi i/\kappa)F(\Gamma_r, [x_5, x_6]^+)$ to $F(\Gamma_r, [x_5, x_6]^+)$. In this combination, two copies of Γ_r live on different Riemann sheets of I_2, are oriented in opposite directions, and join to form the Pochhammer contour $\Gamma_1 = \mathscr{P}(x_4, \Gamma_2)$ that entwines x_4 with Γ_2 (figure 3.5). We find that

$$2\sin\left(\frac{4\pi}{\kappa}\right)|F([x_1,x_2]^+,[x_5,x_6]^+)| + 2\sin\left(\frac{8\pi}{\kappa}\right)|F([x_2,x_3]^+,[x_5,x_6]^+)| + 2\sin\left(\frac{12\pi}{\kappa}\right)|F([x_3,x_4]^+,[x_5,x_6]^+)| = i(1-e^{-32\pi i/\kappa})^{-1}F(\Gamma_r,[x_5,x_6]^+). \quad (3.10)$$

This is the linear dependence that we seek since the left side is a linear combination of two-leg solutions while the right side is just a three-leg solution.

Next, we decompose each of the two-leg solutions appearing on the left side of

(3.10) into a linear combination of the zero-leg solutions. We explicitly show how to do this for the two-leg solution $F([x_2, x_3]^+, [x_5, x_6]^+)$, and the procedure may be used with the other two-leg solutions. The procedure is identical to that used for the $N = 2$ case except for one subtlety. If we replace $[x_5, x_6]^+$ in the two-leg solution $F([x_2, x_3]^+, [x_5, x_6]^+)$ by a clockwise-oriented, simple, closed curve Γ that tightly wraps around $[x_1, x_6]$ and decompose Γ into smaller contours along the segments $[x_j, x_{j+1}]^+$, then some of these contours risk touching the other contour $[x_2, x_3]^+$ at its endpoints. (We recall from the proof of theorem II.2 that $F(\Gamma_1, \Gamma_2)$ is a solution of the system (2.1-2.2) if the contours Γ_1 and Γ_2 do not touch.) Using identity (3.3), we avoid this issue by letting the bottom half of Γ cross $[x_1, x_2]$ to above the real axis, pass above the contour $[x_2, x_3]^+$, and cross $[x_3, x_4]$ to below the real axis as we move from left to right (figure 3.6). The entire section on the lower half of Γ that now passes above the real axis differs from the corresponding section on the upper half of Γ by only the monodromy factor of x_1. Thus, we find a linear dependence between zero-leg solutions in $\mathcal{B}_3$ and a two-leg solution:

$$-\sin\left(\frac{4\pi}{\kappa}\right)|F(\{[x_2, x_3]^+, [x_1, x_4]^+\})| - \sin\left(\frac{8\pi}{\kappa}\right)|F(\{[x_2, x_3]^+, [x_4, x_5]^+\})| = \sin\left(\frac{12\pi}{\kappa}\right)|F(\{[x_2, x_3]^+, [x_5, x_6]^+\})|. \quad (3.11)$$

We can find similar linear dependences for the other two two-leg solutions on the left side of (3.10), and when all of these relations are combined, we have decomposed the three leg solution into a linear combination of zero-leg solutions.

The "invisibility" of a charge neutral pair to this mitotic process indicates a useful

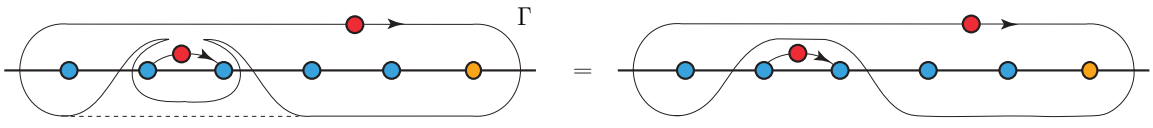

Figure 3.6: The deformation of an integration contour around a charge-neutral pair.

fact. We suppose that we have some linear relation between a collection of s-leg solutions in $\mathcal{S}_N$. Then by splicing a common collection of M charge-neutral pairs into each solution that appears in the linear relation, we promote this relation to one between s-leg solutions in $\mathcal{S}_{N+M}$. This fact might seem obvious from the Coulomb gas point-of-view. In this case, we add a charge-neutral pair by multiplying the collection of chiral operators on both sides of the linear relation by the three chiral operators that comprise the pair. But when correlations of these chiral operators are taken, those belonging to the charge-neutral pair become entwined with the other chiral operators in the formulas that follow, and this "multiplication" interpretation of their insertion is obfuscated.

When κ is not an exceptional speed with $q \leq N+1$, this process can be repeated for arbitrarily large N and $1 < s \leq N$. We start by replacing the outermost contour of the $s-1$ nested contours in an s-leg solution F by a clockwise-oriented, simple, closed curve that tightly wraps around $[x_1, x_{2N}]$. This leads to a linear dependence of F on several $(s-1)$-leg solutions. Next, we replace the outermost contour of the $s-2$ nested contours in each of these $(s-1)$-leg solutions by a clockwise-oriented, simple, closed curve that tightly wraps around $[x_1, x_{2N}]$. This leads to a linear dependence of each $(s-1)$-leg solution on several $(s-2)$-leg solutions. We repeat this process until we reach the zero-leg solutions, thereby finding a direct (though tedious) way to express any s-leg solution as a linear combination of the zero-leg solutions.

As previously mentioned, the conclusion of the previous paragraph is false only when κ is an exceptional speed κ' (2.146) with $q \leq N+1$, in which case $\mathcal{B}_N$ is linearly dependent. To understand the failure of the method in these cases, we consider an s-leg solution $F_0(\kappa)$ with $s = q-1$ and q the larger index of the exceptional speed κ'. We replace the outermost nested contour of $F_0(\kappa)$ with a clockwise-oriented, simple, closed curve Γ that wraps around $[x_1, x_{2N}]$ and the other $s-2$ nested contours. As usual, the integration around Γ gives zero. Next, we pinch the upper and lower halves

of Γ together along $I := [x_{2N-s+1}, x_{2N-s+2}]$, and we perform the integration around Γ before any of the other $s-2$ integrations. The integrand changes by a phase of

$$\exp[\underbrace{2\pi i(2N-s+1)(-4/\kappa)}_{1.} + \underbrace{2\pi i(N-s)(8/\kappa)}_{2.}] = \exp[-8\pi i(s+1)/\kappa] \tag{3.12}$$

as we move from the part of Γ just above I to the part just below I. The first term of the exponential arises from the $2N-s+1$ points x_j to the left of I, and the second term arises from the $N-s$ screening charges to the left of I. When $\kappa = \kappa'$ and $s = q-1$, this phase equals one, so the integrations along the part of Γ just above and below I sum to zero. Consequently, Γ splits into a left, clockwise-oriented, closed contour Γ_l that wraps around $[x_1, x_{2N-s+1}]$ and a right, clockwise-oriented, closed contour Γ_r

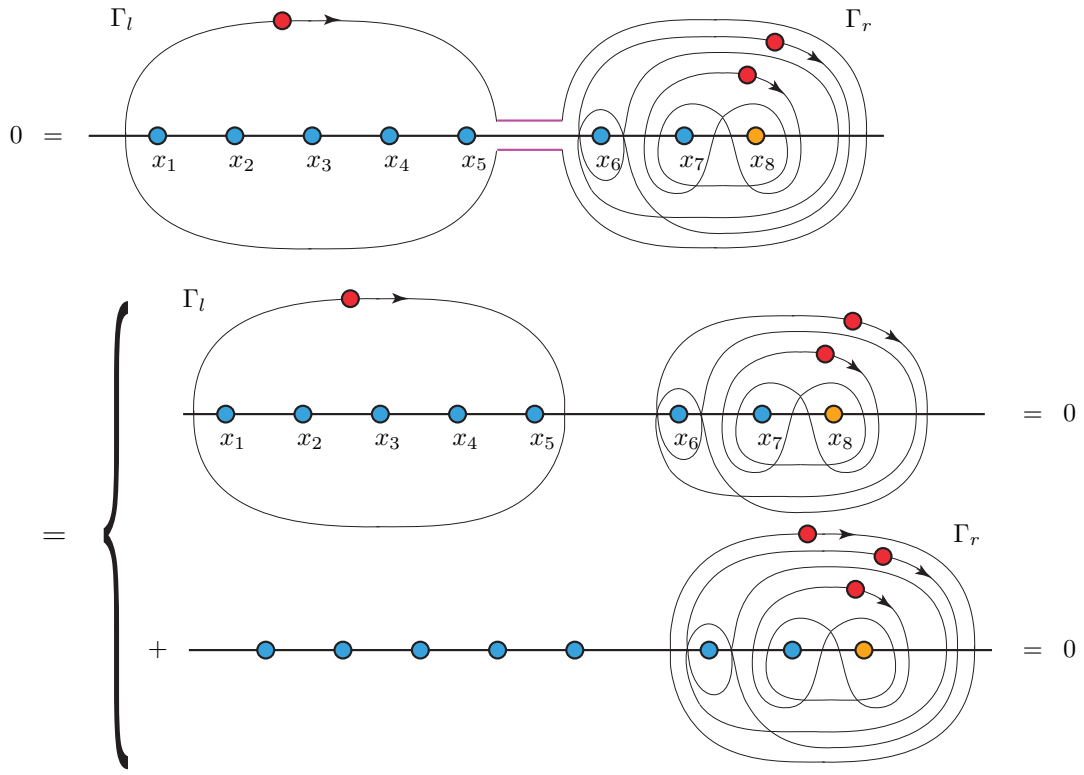

Figure 3.7: The linear dependency involving three-leg solutions when $N = 4$ and $\kappa = \kappa_{5,q'}$. In the top line, the integration along the upper purple segment cancels that of the lower purple segment because there is no branch cut along $[x_5, x_6]$. This breaks the integration along the outer loop into integration along Γ_l and Γ_r. Integration around the latter, and therefore also the former, contour equals zero.

that is totally separated from Γ_l and that wraps around both $[x_{2N-s+2}, x_{2N}]$ and the other $N-2$ nested contours. The sum of the integration around Γ_l and the integration around Γ_r equals zero. Figure 3.7 illustrates an example with $s = N = 4$ and $q = 5$.

Now we argue that the integration around Γ_r equals zero. Earlier, we observed that for generic κ, the integration around Γ_r is proportional to the s-leg solution $F_0(\kappa)$ (figure 3.5). However, when $\kappa = \kappa'$, the lack of a branch cut along I allows Γ_r to cross this interval and close into a simple loop that separates $[x_{2N-s+2}, x_{2N}]$ from $[x_1, x_{2N-s+1}]$. Consequently, the integration around Γ_r delivers a solution to the system (2.1-2.2). If this integration gives an s-leg solution in $\mathcal{S}_N$, then eliminating the charge-neutral pairs with a sequence of limits must leave an s-leg solution Π in $\mathcal{S}_s$. However, after taking this sequence of limits, all s intervals to the left of I are two-leg intervals of Π. Each diagram of every element of $\mathscr{B}_s^*$ has an arc that mutually connects the endpoint of one of these intervals, so every element of $\mathscr{B}_s^*$ annihilates Π. Lemma II.17 implies that Π is thus zero, so the integration around Γ_r is zero too.

The integration along Γ_l can be decomposed into a linear combination of $(s-1)$-leg solutions, then $(s-2)$-leg solutions, etc., by following the process described above. Next, we argue that this process indeed can be continued until we reach a linear combination of the zero-leg solutions. At each step, we encounter several s'-leg solutions for some $s' < s = q - 1$. Such a solution consists of $s' - 1$ nested contours, entwining the points $x_{2N-s'+1}, \ldots, x_{2N}$ together, and $N - s'$ charge-neutral pairs. Now we consider the integration around $\Gamma_r^{s'}$, the outermost of the $s' - 1$ nested contours, before all other integrations in this s'-leg solution. Its integrand will change by the phase (3.12) with $s \mapsto s'$ as we cross the interval $I_{s'} := [x_{2N-s'+1}, x_{2N-s'+2}]$. Because $s' < s = q - 1$, this phase never equals one, so $\Gamma_r^{s'}$ does not close into a simple loop that crosses $I_{s'}$. Rather, $\Gamma_r^{s'}$ entwines $x_{2N-s'+1}$ with the other $s'-2$ nested contours of the s'-leg solution in the usual way shown in figure 3.5. Therefore, we can decompose each s'-leg solution that arises into a linear combination of $(s'-1)$-leg solutions when

$s' \in \{3, \ldots, s-1\}$. And when we reach $s' = 2$, we can decompose each two-leg solution that arises in this penultimate step into a linear combination of zero-leg solutions. Consequently, the integration along Γ_l delivers an ultimate linear combination of the zero-leg solutions.

That the integration around Γ_r gives zero immediately implies that integration around Γ_l gives zero too. Because the latter integration equals a linear combination of the zero-leg solutions, we have constructed a sought linear dependence of $\mathcal{B}_N$.

Above, we noted that the integration around Γ_r delivers an s-leg solution when $\kappa \neq \kappa'$ and zero when $\kappa = \kappa'$. According to the proof of theorem II.25, the s-leg solution $F_0(\kappa)$ is recovered in this latter case as the limit of $(\kappa - \kappa')^{-1} F_0(\kappa)$ as $\kappa \to \kappa'$. Thus, we have proven the following theorem.

Theorem III.4. *Let $\kappa \in (0, 8)$, and suppose that conjecture II.16 is true. If κ is not an exceptional speed with $2 < q \leq N+1$, then each s-leg solution with $s \in \{3, \ldots, N\}$ equals a linear combination of $(s-1)$-leg solutions, and each two-leg solution equals a linear combination of zero-leg solutions. If κ is an exceptional speed (2.146) with $2 < q \leq N+1$, then each s-leg solution with $s \in \{q, \ldots, N\}$ equals a linear combination of $(s-1)$-leg solutions, each s-leg solution with $s \in \{3, \ldots, q-2\}$ equals a linear combination of $(s-1)$-leg solutions if $q > 4$, and each two-leg solution equals a linear combination of zero-leg solutions if $q > 3$.*

When $\kappa \neq \kappa'$, the s-leg solution $F_0(\kappa)$ with $s \geq q-1$ equals a linear combination of the elements of $\mathcal{B}_N$. If we multiply both sides of this equation by $(\kappa - \kappa')^{-1}$ before sending $\kappa \to \kappa'$, then the coefficients of the linear combination will blow up in the limit, spoiling the decomposition. This observation suggests the $s \geq q-1$ solutions are "cut off" from the $s < q-1$ solutions, as we state in the following theorem.

Theorem III.5. *Let $\kappa \in (0, 8)$, and suppose that conjecture II.16 is true. If κ is an exceptional speed (2.146) with $q > 2$, then no s-leg solution with $s \geq q-1$ equals a linear combination of elements of $\mathcal{B}_N$.*

Proof. We let κ' be an exceptional speed (2.146), and we let $F_0(\kappa)$ be an s-leg solution with $s \geq q-1$. First, we prove this theorem for the case where $s = N$ and the points $x_{N+1}, \ldots, x_{2N}$ are entwined by the sequence of $N-1$ nested Pochhammer contours. According to [69], there is a subset $\mathscr{B}_N^{(q)*} \subset \mathscr{B}_N^*$ with the following three properties:

1. The cardinality of $\mathscr{B}_N^{(q)*}$ equals the rank of the meander matrix $M_N(\kappa)$.

2. $\mathscr{B}_N^{(q)*}$ does not contain the element $[\mathscr{L}_{k_0}]$ whose diagram is the "rainbow diagram" [68] shown in figure 3.8.

3. The determinant of the Gram matrix $A(\kappa)$ for $\mathscr{B}_N^{(q)*}$, a minor of the meander matrix, is nonzero when $\kappa = \kappa'$.

We let $\mathscr{B}_N^{(q)*} = \{[\mathscr{L}_{k_1}], \ldots, [\mathscr{L}_{k_M}]\}$, and we let $\mathcal{B}_N^{(q)} := \{F_{k_1}, \ldots, F_{k_M}\}$. Then because $\det A(\kappa') \neq 0$, lemma II.17 implies that $\mathcal{B}_N^{(q)}$ is a linearly independent subset of $\mathcal{B}_N$ when $\kappa = \kappa'$. Also because $q \leq s+1$ and $s = N$, lemma II.22 implies that $\mathcal{B}_N$ is linearly dependent with rank M, so $\mathcal{B}_N^{(q)}$ is maximal.

If we assume that the theorem is false, then because $\mathcal{B}_N^{(q)}$ is a maximal linearly

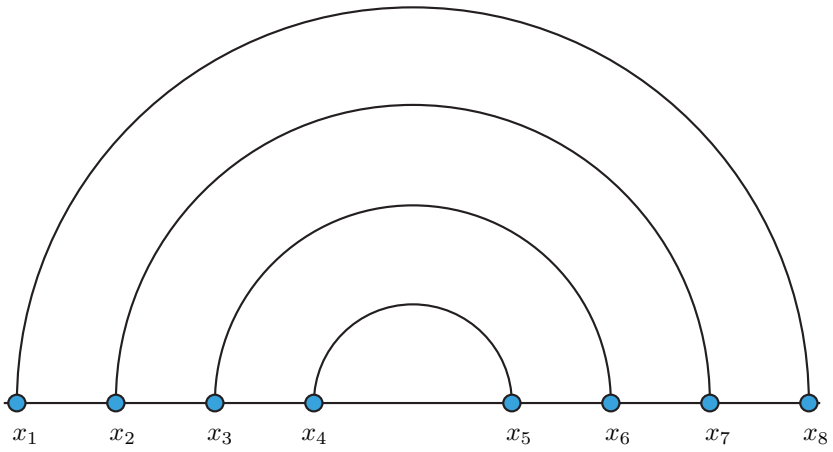

Figure 3.8: The $N = 4$ rainbow diagram.

independent subset of $\mathcal{B}_N$, there will exist nonzero constants c_k such that

$$F_0(\kappa') = \sum_{k\in\{k_1,\ldots,k_M\}} c_k F_k(\kappa'). \tag{3.13}$$

Now, the intervals $(x_1, x_2), \ldots, (x_{N-1}, x_N)$ are two-leg intervals of $F_0(\kappa)$. Consequently, every element of $\mathscr{B}_N^*$ whose diagram connects a pair of adjacent points among $x_1, \ldots, x_N$ annihilates $F_0(\kappa)$. The only diagram that does not meet this criterion is $[\mathscr{L}_{k_0}]$, which is not in $\mathscr{B}_N^{(q)*}$. Therefore, if we act on both sides of (3.13) with the elements of $\mathscr{B}_N^{(q)*}$, then we find the matrix equation $A(\kappa')c = 0$, where c is an M-dimensional vector whose coordinates are the coefficients c_k. Because $\det A(\kappa') \neq 0$, each c_k must equal zero, a contradiction. This proves the theorem in the case where $s = N$ and the points $x_{N+1}, \ldots, x_{2N}$ are entwined by the sequence of $N-1$ nested Pochhammer contours.

Next, suppose that the points $x_i, \ldots, x_{i+N-1}$ are entwined by the sequence of $N-1$ nested contours with $i \neq N+1$ (or $i \neq 1$, as the proof presented above holds for this case too). In this situation, $[\mathscr{L}_{k_0}]$ will not annihilate $F_0(\kappa)$. But as we reasoned earlier, all but one element $[\mathscr{L}_{k_0'}]$ of $\mathscr{B}_N^*$ will annihilate $F_0(\kappa)$, and it is apparent that the polygon diagram for $[\mathscr{L}_{k_0'}]$ will be some rotation of that for $[\mathscr{L}_{k_0}]$. If we apply this rotation to the polygon diagram of every element of the set $\mathscr{B}_N^{(q)*}$, then we generate a new set $\tilde{\mathscr{B}}_N^{(q)*} \subset \mathscr{B}_N^*$ that satisfies the three conditions listed above. From here, the proof proceeds as before.

Finally, suppose that $s < N$. Then $F_0(\kappa)$ will harbor $N - s$ charge-neutral pairs that may be eliminated through a sequence of $N-s$ limits in which each limit contracts one of the pairs away. If $F_0(\kappa')$ equals a linear combination of the elements of $\mathcal{B}_N$, then upon taking the sequence of limits, this equality becomes an equality between an s-leg solution in $\mathcal{S}_s$ and a linear combination of elements of $\mathcal{B}_s$. This contradicts the theorem for the proven case $s = N$. □

Theorem III.4 implies an important property of the minimal models: the confinement of their operator content to the Kac table. For example, suppose that κ equals the exceptional speed $\kappa_{q,q'}$ for q, q' coprime and $1 \leq q' < q \leq N+1$. These exceptional speeds belong to the dense phase, and their corresponding minimal models have central charge $c(\kappa_{q,q'}) = c_{q,q'}$. This includes all minimal models (p, p') with $p = q$. These minimal model are generated by the primary fields $\phi_{r,s+1}$ with $1 \leq r < q'$ and $0 \leq s < q-1$. In the dense phase, the s-leg operator is $\phi_{1,s+1}$, so the theory contains all s-leg operators with $s < q-1$, but it does not contain the $(q-1)$-leg operator. On the other hand, the likelihood of an *s-leg event* in which s distinct boundary arcs anchor to a point on the real axis is found from an s-leg solution essentially by fusing all s adjacent points within that solution's sequence of $s-1$ nested contours. Thus, the construction of an s-leg solution from the zero-leg solutions is equivalent to building linear combinations of the elements in $\mathcal{B}_N$ that isolate the s-leg channel from the fusion of s adjacent one-leg operators $\psi_1 = \phi_{1,2}$. The result is an s-leg solution. If the s-leg operator is (resp. is not) present in the theory, then this construction is (resp. is not) possible. This is precisely what we have observed for the exceptional speed $\kappa_{q,q'}$ in theorem III.4.

We can extend this observation to all of the other exceptional speeds $\kappa_{q,2mq\pm q'}$ with $m \in \mathbb{Z}^+$. These exceptional speeds belong to the dilute phase, and their corresponding minimal models have central charge $c(\kappa_{q,2mq\pm q'}) = c_{2mq\pm q',q}$. This includes all minimal models (p, p') with $p' = q$. These minimal model are generated by the primary fields $\phi_{r+1,s}$ with $0 \leq r < q-1$ and $1 \leq s < 2mq \pm q'$. In the dilute phase, the r-leg operator is $\phi_{r+1,1}$, and because the maximum r-index is $q-2$, the theory contains all r-leg operators with $r < q-1$, but it does not contain a $(q-1)$-leg operator. The connection between this fact and the linear dependence of $\mathcal{B}_N$ is argued exactly as in the previous paragraph.

Lemma II.22 shows that $\mathcal{B}_N$ is linearly dependent for all $N \geq q-1$ and is linearly

independent for all $N < q-1$, when κ is an exceptional speed. Now we intuitively understand why this should be true. When $N < q-1$, we lack a sufficient number of points to construct an $(q-1)$-leg solution that decouples from the rest of the simple solutions. We need at least $2(q-1)$ points, but only $2N$ are available.

We close this section with an interesting fact about s-leg solutions. To prove the following theorem by direct computation would be very difficult. This gives evidence of the power of lemma II.17.

Theorem III.6. *Let $\kappa \in (0,8)$, and suppose that conjecture II.16 is true. Then two s-leg solutions with identical charge-neutral pairs and whose sequence of nested Pochhammer contours entwine the same s points are proportional to each other, and any interval (x_i, x_{i+1}) whose two endpoints are among these s entwined points is a two-leg interval.*

Proof. We prove this lemma for the case $s = N$ first. Without loss of generality, we consider N-leg solutions with their nested Pochhammer contours entwining the points $x_{N+1}, \ldots, x_{2N}$. At first, there seem to be many. For one, we may endow any one point x_c among $x_{N-1}, \ldots, x_{2N}$ with the conjugate charge. And second, depending on which of these points is x_c, there may be more than one way to entwine the points $x_{N+1}, \ldots, x_{2N}$ together as described in definition III.3. However, all of these N-leg solutions share a common feature. For each, the intervals $(x_1, x_2), \ldots, (x_{N-1}, x_N)$ are two-leg intervals, so each is annihilated by every element of $\mathscr{B}_N^*$ except that element $[\mathscr{L}_{k_0}]$ whose half-plane diagram is the rainbow diagram in figure 3.8. Therefore, their images under the map v defined in lemma II.17 are proportional to each other, so by the same lemma, they are proportional to each other.

In fact, in the special case $s = N$, we can conclude something slightly stronger. Suppose that we "reflect" the arrangement of the previous paragraph across a vertical axis so that each N-leg solution is sent to another N-leg solution with its nested Pochhammer contours entwining the points $x_1, \ldots, x_N$. The same arguments show

that these new N-leg solutions are annihilated by every element of $\mathscr{B}_N^*$ except $[\mathscr{L}_{k_0}]$ too. Consequently, all of these N-leg solutions and all of those in the previous paragraph are proportional to each other, so the intervals $(x_{N+1}, x_{N+2}), \ldots, (x_{2N-1}, x_{2N})$ are two-leg intervals for the latter.

Finally, if $s < N$, we suppose that two s-leg solutions with identical charge-neutral pairs and whose sequence of nested contours entwine the same s points are not proportional to each other. That is, any arbitrary linear combination of these two solutions must equal another nonzero solution. Now we take the sequence of $N - s$ limits on both sides of this equality that eliminates the common charge-neutral pairs on the left side. As this sequence of limits only collapses identity intervals, the right side of this equality will go to something nonzero. The left side of this equality will go to a linear combination of two s-leg solutions in $\mathcal{S}_s$ whose sequence of nested Pochhammer contours entwine the same s points. We thus conclude that any linear combination of the two s-leg solutions under consideration and in $\mathcal{S}_s$ must not equal zero, but this contradicts the proven case $s = N$.

□

3.2 Exceptional speeds and the extended system

In this section, we exploit the connection between exceptional speeds and minimal models to predict the dimension of the solution space $\mathcal{R}_N$ of the complete infinite system of null-state PDEs and the Ward identities (2.2). We also examine the consequences of this prediction for certain specific models. Throughout this section, we will implicitly assume that conjecture II.16 is true.

Recall that, in the (p, p') minimal model, the Verma modules $V_{1,2}$ and $V_{2,1}$ each harbor an infinite tower of null-states in addition to their generic null-state at level two (section 1.2.6), and each null-state determines a set of $2N$ null-state PDEs that govern the $2N$-point function $\langle \psi_1(x_1) \ldots \psi_1(x_{2N}) \rangle$. We call the infinite collection of

all of these PDEs together with the Ward identities the *extended system,* and we define $\mathcal{R}_N$ to be the subset of $\mathcal{S}_N$ that solves the extended system.

Because of its explicit CFT construction via the Coulomb gas formalism, we expect that the elements of $\mathcal{B}_N$ will solve the extended system of the (p, p') minimal model, and even stronger, we posit that $\mathcal{R}_N = \operatorname{span} \mathcal{B}_N$. This supposition is motivated by the following reasoning.

First, we strengthen the discussion in the introduction of this chapter to show that $c(\kappa)$ is a minimal model central charge if and only if κ is an exceptional speed (2.146). In the introduction, we proved the "if" statement of this claim, so now we prove the "only if" statement. Simple algebra shows that $\kappa_{p,p'} = 4p/p'$ and $\kappa_{p',p} = 4p'/p$ are the speeds corresponding with the central charge $c_{p,p'}$ (3.2) of a minimal model. As usual, we take $1 \leq p' < p$ and p and p' coprime. Then first, $\kappa_{p,p'}$ is in the dense phase and is therefore an exceptional speed of the form $\kappa_{q,q'}$ with $1 \leq q' < q$ and q and q' coprime, so $q = p$ and $q' = p'$. Or second, $\kappa_{p',p}$ is in the dilute phase and is therefore an exceptional speed of the form $\kappa_{q,2mq\pm q'}$ with $1 \leq q' < q$, q and q' coprime, and $m \in \mathbb{Z}^+$. This implies that q and $2mq \pm q'$ are coprime, so $q = p'$. Also, $q' < p'$ must be the unique positive integer such that $p \mp q'$ is a positive multiple $2mp'$ of $2p'$ in either $(p - p', p - 1]$ or $[p + 1, p + p')$. Because p and p' are coprime and $(p-p', p+p')$ has length $2p'$, this interval contains a unique multiple of $2p'$ in it that is not p. Therefore, this unique integer must be in $(p-p', p-1] \cup [p+1, p+p')$, and this uniquely determines q', the sign, and thus m in the relation $2m = (p \mp q')/p'$. So in conclusion, each exceptional speed corresponds with a minimal model central charge, and each minimal model central charge corresponds with two exceptional speeds.

Next, if $\mathcal{B}_N$ solves the extended system, then because the extended system is contains the original system (2.1-2.2), we anticipate that the extended system imposes additional constraints on $\mathcal{B}_N$, causing it to perhaps exhibit some special property that would vanish when the central charge is perturbed from $c_{p,p'}$. In the previous

paragraph, we observed that the central charge is that of a minimal model (3.2) if and only if κ is an exceptional speed, so by lemma II.22, this linear dependence is likely the special property that we anticipate.

If our supposition that $\mathcal{R}_N = \operatorname{span} \mathcal{B}_N$ is true, then according to corollary II.24, the dimension of $\mathcal{R}_N$ is immediately given by the rank of the meander matrix (2.157). As we have shown above, there are two possible exceptional speeds that will go with $c_{p,p'}$. One is $\kappa_{q,q'}$ in the dense phase and with $q = p$, and the other is $\kappa_{q,2mq\pm q'}$ in the dilute phase and with $q = p'$. In the first (resp. second) case, $\mathcal{R}_N$ is the solution space of the extended system for the $2N$-point function of $\phi_{1,2}$ (resp. $\phi_{2,1}$) operators, and if it is spanned by $\mathcal{B}_N$, then its dimension is found by letting $q = p$ (resp. $q = p'$) in (2.157). In general, the dimensions of these two cases are different, and remarkably, neither depends on q'.

A direct proof of our supposition appears to be difficult. Not all of the null-state PDEs of the extended system are explicitly known, although they may be calculated by fusing Verma modules in a very tedious process described in [71]. Therefore, in lieu of a proof, we study a few explicit examples. Below, we let κ' denote the exceptional speed under consideration.

First, we examine cases with $N = 2$. The elements of $\mathcal{B}_2$ are given in (2.42-2.43). For generic κ, they are linearly independent, and suitable linear combinations give the two-leg solutions (2.40-2.41). The exceptional speeds are given by the roots of the meander matrix $\det M_2(\kappa)$ (2.153), which are κ' such that $n(\kappa') = n_{2,1}, n_{3,1}$, or $n_{3,2}$ (table 2.1). The meander matrix is

$$M_2(\kappa) = \begin{pmatrix} n^2 & n \\ n & n^2 \end{pmatrix}. \tag{3.14}$$

When $n = n_{2,1} = 0$, $M_2(\kappa')$ is the zero matrix and $\mathcal{B}_2 = \{0\}$, but both may be restored to rank two by dividing (2.42-2.43) by n before sending $\kappa \to \kappa'$. If $n = n_{3,1} = -1$,

then one element of $\mathcal{B}_2$ is the opposite of the other, and if $n = n_{3,2} = 1$, then both elements of $\mathcal{B}_2$ are equal. We examine the last scenario more closely.

First, we choose $n(\kappa') = n_{3,2} = 1$ and $\kappa' = \kappa_{3,2} = 6$ so that $(p, p') = (3, 2)$. In section 1.2.7, we identified this case with critical percolation. Because we are in the dense phase, $\psi_1 = \phi_{1,2}$, so the four-point function $\langle \psi_1(x_1) \dots \psi_1(x_4) \rangle$ obeys the $\phi_{1,2}$ null-state PDEs (2.1) with $N = 2$. But also when $\kappa' = 6$, $h_{1,2} = h_{1,1} = 0$, so $V_{1,2} \cong V_{1,1}$ also has a level-one null-state $\phi_{1,2}^{(-1)} := (L_{-1}\phi_{1,2}) = (L_{-1}\phi_{1,1})$. Therefore, $\langle \phi_{1,2}^{(-1)}(x_i)\phi_{1,2}(x_j)\phi_{1,2}(x_k)\phi_{1,2}(x_l) \rangle = 0$ for any one-to-one correspondence of indices i, j, k, and l with $1, 2, 3$, and 4. By factoring out the L_{-1} stress tensor mode via (1.93), we find that the four-point function must satisfy the $\phi_{1,1}$ null-state PDEs

$$\partial_{x_1} F = 0, \quad \partial_{x_2} F = 0, \quad \partial_{x_3} F = 0, \quad \partial_{x_4} F = 0, \tag{3.15}$$

and therefore be a constant. The level-one null-state tops an infinite tower of null-states in $V_{1,2}$, each a linear combination of stress tensor modes acting on $\phi_{1,2}$. Because $h_{1,2} = 0$, the constant term of each factored-out mode in (1.94) is zero, so the constant solution will solve the extended system. Thus $\mathcal{R}_2 = \mathbb{R}$. Knowing that $\mathcal{B}_2$ has rank one, we see that $\mathcal{B}_2 = \{1\}$ by inspecting the original system (2.1-2.2) with $\kappa = 6$. Thus, $\mathcal{R}_2 = \operatorname{span} \mathcal{B}_2$, confirming our supposition for this case.

In order to recover $\mathcal{S}_2$ from $\mathcal{R}_2$, we might "complete" $\mathcal{B}_2$ by adding a non-constant solution of the original system (2.1-2.2) to it, restoring its rank to two. This amounts to ignoring the PDEs of the extended system that are not in the original system (2.1-2.2). For example, we can include either of the two-leg solutions Π_1 or Π_2 in (2.40-2.41). By including Π_1, we directly add the two-leg family to the OPEs of $\phi_{1,2}(x_1)$ with $\phi_{1,2}(x_2)$ and $\phi_{1,2}(x_3)$ with $\phi_{1,2}(x_4)$ since (x_1, x_2) and (x_3, x_4) are two-leg intervals of Π_1. And since $\Pi_2 = 1 - \Pi_1$, we indirectly add the two-leg family to the OPEs of $\phi_{1,2}(x_1)$ with $\phi_{1,2}(x_4)$ and $\phi_{1,2}(x_2)$ with $\phi_{1,2}(x_3)$ as well. This amounts to

directly inserting the two-leg operator $\phi_{1,3}$ that is missing from the $(3,2)$ minimal model into it, and the result is a logarithmic CFT [72].

Next, we choose $n(\kappa') = n_{3,2} = 1$ and $\kappa' = \kappa_{3,4} = 3$ so that $(p,p') = (4,3)$. In section 1.2.7, we identified this case with the Ising model. Because we are in the dilute phase, $\psi_1 = \phi_{2,1}$, so the four-point function $\langle \psi_1(x_1) \dots \psi_1(x_4) \rangle$ will obey the $\phi_{2,1}$ null-state PDEs (2.1) with $N = 2$. But also when $\kappa' = 3$, $h_{2,1} = h_{1,3}$, so $V_{2,1} \cong V_{1,3}$. Because the $V_{1,3}$ Verma module harbors the level-three null-state [10]

$$(h_{1,3}+2)(L_{-3}\phi_{1,3}) - 2(L_{-1}L_{-2}\phi_{1,3}) + \frac{1}{(h_{1,3}+1)}(L_{-1}^3\phi_{1,3}), \tag{3.16}$$

the four-point function must also obey the four $\phi_{1,3}$ null-state PDEs (with $h_{1,3} = \kappa/2 - 1$ when $\kappa \leq 4$ (1.170)). For generic κ, these PDEs are

$$\left[\frac{2}{\kappa}\partial_i^3 + 2\sum_{j\neq i}^{4}\left(\frac{\partial_j}{x_j - x_i} - \frac{\kappa/2-1}{(x_j-x_i)^2}\right)\partial_i \right.$$
$$\left. - \left(\frac{\kappa}{2}-1\right)\sum_{j\neq i}^{4}\left(\frac{\partial_j}{(x_j-x_i)^2} - \frac{\kappa-2}{(x_j-x_i)^3}\right)\right] F = 0, \quad i = 1,\dots,4. \tag{3.17}$$

One can verify that the elements of $\mathcal{B}_2$ (2.42-2.43) satisfy (3.17) when $\kappa' = \kappa_{3,4} = 3$, but the functions Π_1 and Π_2 of (2.40-2.41) do not. The exclusion of the two-leg solutions from $\mathcal{R}_2$ implies that this solution space is at most one-dimensional, while $\mathcal{B}_2$ is exactly one-dimensional. In order for $\mathcal{R}_2$ to be one-dimensional, the two equal elements of $\mathcal{B}_2$ must solve the rest of the extended system. To show this directly is very difficult for the reasons that were mentioned above. But because the four-point function represents a nontrivial observable (to be argued in chapter four), we expect $\mathcal{R}_2$ to be one-dimensional when $\kappa' = \kappa_{3,2}$, so $\operatorname{span}\mathcal{B}_2 = \mathcal{R}_2$, confirming our supposition again.

As we have just observed in the case $\kappa' = 6$, the linear dependence that emerges in the $\kappa' = 3$ case is linked to the absence of the two-leg channel $\phi_{3,1}$ from the $(4,3)$

minimal model. The two-leg channel may be restored to all pairs of adjacent operators by ignoring the null-state PDEs of the extended system that are not in the original system (2.1-2.2). Similar conclusions can be made for the other exceptional speeds $\kappa_{3,6m\pm q'}$ with $m \in \mathbb{Z}^+$, which correspond with the O(n) loop fugacity $n = n_{3,q'} = (-1)^{q'}$ with $q' = 1, 2$.

Next, we survey some cases with $N \geq 2$. From (2.157), we can show that when $n(\kappa') = n_{3,q'}$ (so $\kappa' = \kappa_{3,q'}$ or $\kappa_{3,6m\pm q'}$ with $m \in \mathbb{Z}^+$) for $q' = 1, 2$,

$$\operatorname{rank} \mathcal{B}_N = C_N - d_N(3, q') = 1 \quad \text{for all } N \in \mathbb{Z}^+. \tag{3.18}$$

When $n(\kappa') = n_{3,1} = -1$, the k-th column of the meander matrix is $(-1)^{p_{k,k'}}$ times the k'-th column, where $p_{k,k'} = l_{m,k} - l_{m,k'}$ is the difference in the number of loops in the diagram for $[\mathscr{L}_m]F_k$ and in that for $[\mathscr{L}_m]F_{k'}$. (Interestingly, this difference does not depend on m.) Thus, $F_k = (-1)^{p_{k,k'}} F_{k'}$ for all $F_k, F_{k'} \in \mathcal{B}_N$. When $n(\kappa') = n_{3,2} = 1$, all of the entries of the meander matrix equal one, so all of the elements of $\mathcal{B}_N$ equal the same function F. Earlier, we argued that this function is a constant when $\kappa' = \kappa_{3,2} = 6$ and $N = 2$. This argument also shows that F is a constant when $\kappa' = 6$ and $N > 2$ too, and because $[\mathscr{L}_k]F = 1$, we conclude that this constant is one. Consideration of the explicit formula for F given by the product of (2.9) with the prefactor (2.144) leads to the indirect evaluation of the following C_N definite integrals:

$$\left| \int_{\Gamma_1} \cdots \int_{\Gamma_{N-1}} \left(\prod_{k=1}^{2N-1} \prod_{l=1}^{N-1} (x_k - u_l)^{-2/3} \right) \left(\prod_{p<q}^{N-1} (u_p - u_q)^{4/3} \right) du_{N-1} \ldots du_1 \right| = \frac{\Gamma(1/3)^{2N-2}}{\Gamma(2/3)^{N-1}} \prod_{i<j}^{2N-1} |x_i - x_j|^{1/3}. \tag{3.19}$$

Here, $\{\Gamma_m\}$ is one of C_N possible collections of nonintersecting simple contours in $\overline{\mathbb{H}}$, where both endpoints of each contour are at different points among $x_1, \ldots, x_{2N-1}$, and one endpoint of each contour carries an even index while the other carries an odd

index. (Exactly one point among $x_1, \ldots, x_{2N-1}$ is not the endpoint of a contour.) The absolute value sign in (3.19) merely eliminates a constant phase that could otherwise be eliminated by a prudent ordering of the differences in the factors of the integrand, as was noted in the discussion following the proof of lemma II.22. To prove (3.19) by working directly with the integral expression is very difficult if not impossible. This demonstrates the power of using the meander determinant in this special situation.

When $\kappa' = 6$, none of the PDEs in the extended system have a constant term since $h_{1,2} = 0$, so we explicitly see that $\mathcal{R}_N = \operatorname{span} \mathcal{B}_N$. This appears to be the only case where we can directly prove our supposition. In all of the other cases with $n(\kappa') = n_{3,q'}$ and $\kappa' < 8$, κ' has the form $\kappa_{3,6m\pm q'}$ and is in the dilute phase where the boundary one-leg operator is $\phi_{2,1}$. Here, the second null-state in the Verma module $V_{2,1}$ has Kac weight $h_{1,6m\pm q-1}$ which belongs to the first row of the conformal grid. The null-state PDEs that follow from this null-state are explicitly given by the Benoit-Saint-Aubin formula [67], so it is possible (in principle) to directly check that only multiples of the one element of $\mathcal{B}_N$ among those solutions in $\mathcal{S}_N = \operatorname{span} \mathcal{B}'_N$ (as constructed in the proof of theorem II.25) solve these additional PDEs. Thus, $\mathcal{R}_N$ is at most one-dimensional. Moreover, we expect $\mathcal{R}_N$ to not be $\{0\}$ since the $2N$-point function in it represents a nontrivial observable (to be argued in chapter four). If both of these statements are true, then we would have $\operatorname{span} \mathcal{B}_N = \mathcal{R}_N$.

Finally, we examine $n(\kappa') = n_{N+1,q'}$ with $q' \in \{1, \ldots, N\}$. These κ' are roots of $\det M_N(\kappa')$ with multiplicity $d_N(N+1, q') = 1$ (2.157), so $\operatorname{rank} \mathcal{B}_N = C_N - 1$. The roots of $n(\kappa') = n_{N+1,q'}$ are the dense phase speed $\kappa' = \kappa_{N+1,q'}$ with $q' < N+1$, corresponding to minimal model $(N+1, q')$ and the dilute phase speeds $\kappa_{N+1,2m(N+1)\pm q'}$, with $q' < N+1$ and $m \in \mathbb{Z}^+$, corresponding to minimal models $(2m(N+1) \pm q', N+1)$. In all cases, the first column or row of the Kac table truncates at the $(N-1)$-leg operator. According to theorem III.5, an N-leg solution cannot equal a linear combination of the elements of $\mathcal{B}_N$. There are N such N-leg

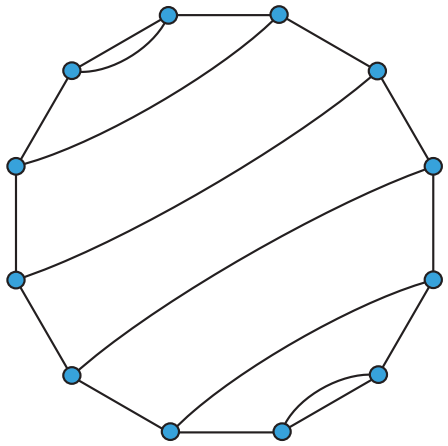

Figure 3.9: An s-leg solution with $s = N = 6$ is annihilated by all but one element $[\mathscr{L}_k]$ of $\mathscr{B}_N^*$. In the polygon diagram for $[\mathscr{L}_k]$, the interior arcs must connect antipodal vertices so that the diagram is some rotation of the twelve-gon shown here.

solutions $\{\Pi_1, \ldots, \Pi_N\}$, and the polygon diagram for the unique $[\mathscr{L}_k]$ that does not annihilate Π_k will connect antipodal vertices of the $2N$-sided polygon. By ignoring the null-state PDEs of the extended system that are not in the original system (2.1-2.2) and introducing a single N-leg solution into $\mathcal{B}_N$, we restore the rank of $\mathcal{B}_N$ to C_N. The inclusion of one of these solutions, say Π_1, in $\mathcal{B}_N$ will introduce the N-leg fusion channel to the two antipodal collections of N adjacent vertices connected by the arcs in the diagram for $[\mathscr{L}_1]$. Apparently, this inclusion also introduces the N-leg fusion channel to all other $N-1$ collections of N adjacent vertices. Interestingly, we do not need to insert $\Pi_2, \ldots, \Pi_N$ into $\mathcal{B}_N$ as well in order to introduce this channel into the other $N-1$ antipodal collections of N adjacent vertices that go around the polygon since $\mathcal{B}_N$ will have full rank after the first insertion.

3.3 Summary

We summarize the main results of this chapter. The exceptional speeds are in two-to-one correspondence with the central charges of the minimal models. In the (p, p') minimal model, the Kac operator fusion rules close under a finite set $\{\phi_{r,s} : 1 \leq r < p', 1 \leq s < p\}$. In particular, the dense (resp. dilute) $(p-1)$-leg operator

$\phi_{1,p}$ (resp. $(p'-1)$-leg operator $\phi_{p',1}$) is absent from the (p,p') minimal model. This absence is closely tied to the linear dependence of $\mathcal{B}_N$ when κ is an exceptional speed with $q \leq N+1$. In particular, theorem III.4 states that a $(q-1)$-leg solution cannot equal a linear combination of elements of $\mathcal{B}_N$ when κ is an exceptional speed of the form $\kappa_{q,q'}$ in the dense phase (resp. $\kappa_{q,2mq\pm q'}$ in the dilute phase). The central charge corresponding to this exceptional speed is that of a (p,p') minimal model with $p=q$ (resp. $p'=q$). Because a CFT description of a $(q-1)$-leg, or now a $(p-1)$-leg (resp. $(p'-1)$-leg), solution requires a $(p-1)$-leg (resp. $(p'-1)$-leg) operator, we have established the connection between the linear dependence of $\mathcal{B}_N$ when κ is an exceptional speed with $q \leq N+1$ and the first row (resp. column) operator truncation of the minimal models. We propose that the linear dependence of $\mathcal{B}_N$ is the result of $\mathcal{B}_N$ solving an *extended system* of null-state PDEs that arises as a special feature of the minimal models, and we give some examples of this phenomenon. We further suppose that $\mathcal{B}_N$ spans the solution space $\mathcal{R}_N$ of this extended system, and we use the meander determinant to thus compute the rank of $\mathcal{R}_N$ under this supposition.

CHAPTER IV

Partition functions and crossing formulas for critical systems in polygons

We consider a $2N$-sided polygon $\mathcal{P}$ whose interior harbors the continuum limit of a critical lattice model, in particular a Q-state Potts model with an FFBC. A boundary cluster anchors to each wired side of $\mathcal{P}$, and each boundary cluster may cross the interior of $\mathcal{P}$ and connect with other wired sides, forming a *crossing configuration* of at most N distinct boundary clusters that traverse the interior of $\mathcal{P}$. A *crossing formula* gives the probability that these boundary clusters will connect the wired sides of $\mathcal{P}$ in a certain topological crossing cofiguration.

Crossing formulas are simple examples of nonlocal observables that capture critical behavior. On a discrete, infinite lattice and below the critical point (for example, the critical FK bond activation probability for the Q-state Potts model), cluster diameters do not grow larger than a certain correlation length, while above the critical point, a cluster of infinite size will exist. By confining the continuum limit of the model to the interior of $\mathcal{P}$, we see that no boundary cluster may connect two different wired sides when the system temperature is below the critical point, but a single boundary cluster will connect all wired sides when the temperature is above the critical point. At the critical point, cluster sizes will saturate all length scales on a discrete, infinite lattice, so in the continuum limit, boundary clusters can connect the wired sides of $\mathcal{P}$

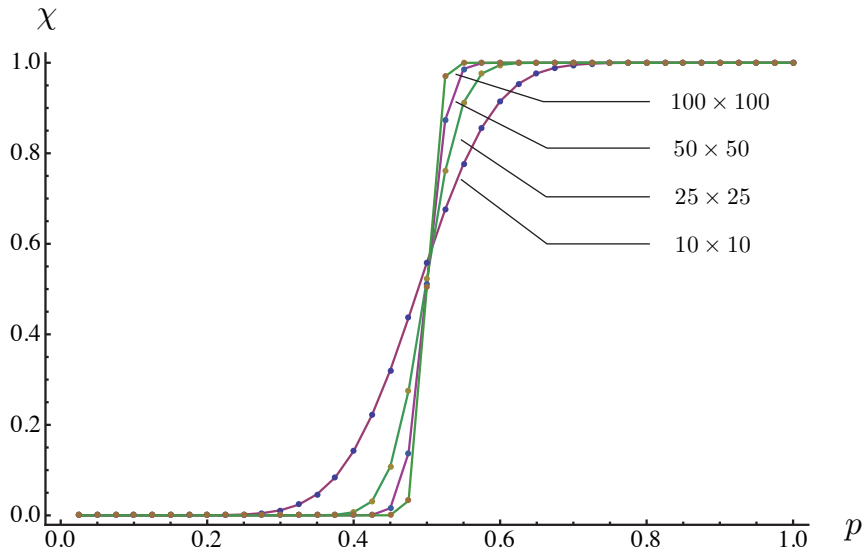

Figure 4.1: Crossing probability χ as a function of bond activation probability for percolation on a square lattice in a 10×10, 25×25, 50×50, and 100×100 square. We observe that χ approaches a step function that jumps at the critical probability $p_c = 0.5$ as the system size increases. This indicates the existence of a phase transition at $p = p_c$ in the thermodynamic limit of the system.

in many nontrivial crossing configurations (figures 4.1, 4.2). (All of these statements are true almost surely.) Thus, a crossing formula characterizes a (presumably unique) critical point of the system. Off of the critical point, the crossing formulas are trivial, but at the critical point, they are given by nontrivial, conformally invariant formulas that depend on the shape of $\mathcal{P}$.

The simplest critical lattice model that illustrates these points is percolation. The probability that a percolation cluster connects the left/right wired sides of a rectangle $\mathcal{R}$ as a function of the aspect ratio R is given by *Cardy's formula* [41]

$$\mathbb{P}\left\{\begin{array}{c}\text{left/right}\\ \text{crossing}\end{array}\right\} = \begin{cases} 0 & p < p_c \\ \dfrac{3\Gamma(2/3)}{\Gamma(1/3)^2}(1-m)^{1/3}\,{}_2F_1\left(\dfrac{1}{3},\dfrac{2}{3};\dfrac{4}{3}\,\middle|\,1-m\right) & p = p_c\,, \\ 1 & p > p_c \end{cases} \tag{4.1}$$

where p_c is the critical activation probability (which depends on microscopic details

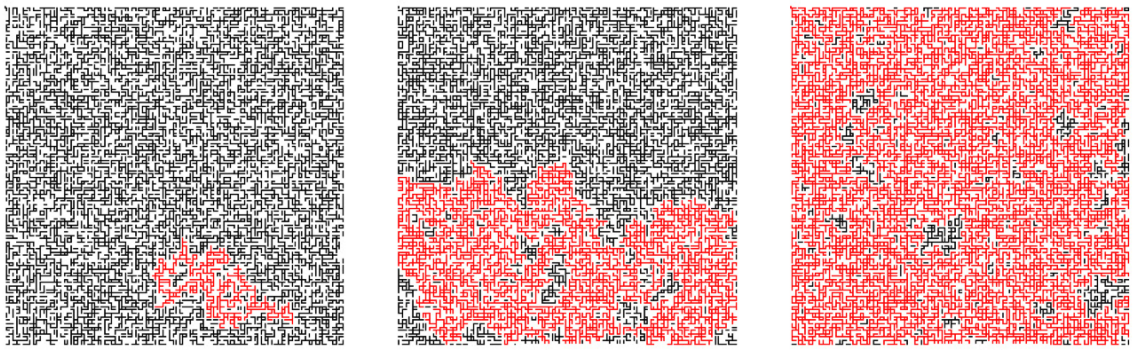

$p = 0.45$ $\quad$ $p = p_c = 0.5$ $\quad$ $p = 0.55$

Figure 4.2: Typical configurations for bond percolation on a large square lattice with the bond activation probability p slightly below, at, and slightly above the critical probability $p_c = 0.5$. Bonds belonging to the largest cluster are colored red.

such as the lattice type, the type (site-versus-bond) of percolation, etc.), and where m is related to the aspect ratio R (length divided by height) of the rectangle through $R = K(m)/K(1-m)$ with $K(m)$ the elliptic function of the first kind. We observe a phase transition at the critical point $p = p_c$. We note that when m goes to zero (resp. one), the aspect ratio goes to zero (resp. infinity), and the likelihood of a left/right crossing goes to one (resp. zero). Because our wiring scheme does not affect the statistics of the interior system in percolation, this crossing probability is actually the same for any choice of BC. This fact is not true in other models such as the Potts model, where the presence of a wired boundary affects the statistics of the bulk system. Nor is it true for critical percolation in polygons with more than two wired sides, as two wired sides may connect indirectly if their boundary clusters, while not touching in $\mathcal{P}$, touch a common third wired side.

Crossing formulas have other interpretations. For instance, we may interpret them as the probability that the boundary arcs, or the perimeters of the boundary clusters, connect the vertices of $\mathcal{P}$ pairwise in any one of the C_N possible BACs exemplified by the polygon diagrams for the elements of $\mathscr{B}_N^*$. This BAC interpretation of a crossing formula was proposed via multiple-SLE in [59], and we will frequently use it in this chapter. (BACs were defined in the discussion preceding (2.7), and $\mathscr{B}_N^*$ and

its polygon diagrams were defined in definitions II.10 and II.12.) In this chapter and in chapter five, we let λ denote a specified BAC, and in an abuse of notation, we also let λ denote the event of the specified BAC. We define the polygon diagram and the half-plane diagram for λ to be that of the element of $\mathscr{B}_N^*$ whose interior arcs connect the vertices of $\mathcal{P}$ as in the BAC event λ, and we let AC_N be the set of all C_N possible BAC events. In this chapter we index the elements of $\mathscr{B}_N^*$ so that $[\mathscr{L}_\lambda] \in \mathscr{B}_N^*$ and $\lambda \in \mathrm{AC}_N$ have identical diagrams.

Because they are among the simplest observables that capture critical behavior, crossing probabilities have interested researchers for some time. Crossing probabilities were shown to be the same for critical site and bond percolation on various lattices via computer simulation [73], supporting the assumption that these models belong to the same universality class. Shortly after, J. Cardy used CFT to predict the crossing formula (4.1) in [41] and showed that his prediction agrees with the measurements of previous computer simulations in [73]. The conformal invariance and other features of the crossing formula were further discussed in [42]. A rigorous proof of Cardy's formula for site percolation on the triangular lattice was discovered by S. Smirnov [16]. Critical Ising spin and FK cluster crossings for the rectangle with wired left/right sides were also computed by D. Bauer, M. Bernard, and K. Kytölä [59]. Moreover, critical percolation crossing formulas for a hexagon with an FFBC and alternating short/long sides were computed by J. Dubédat in [60], and more recently, this computation was extended to multiple-SLE curve connectivities for a hexagon of arbitrary shape and (almost) arbitrary κ by J. Simmons [74].

In this chapter, we use the results of chapters one and two to calculate crossing probabilities in an $2N$-sided polygon $\mathcal{P}$ with a specified FFBC. The derivation consists of several steps. In section 4.1, we construct partition functions and crossing formulas for a system with a specified FFBC among a set of C_N possibilities. These partition functions are linear combinations of crossing weights, which are essentially

un-normalized crossing probabilities. In section 4.2, we calculate the crossing weights in terms of the elements of $\mathcal{B}_N$ (definition II.20). In section 4.3, we uncover a relation between the partition functions that we construct in section 4.1 and the elements of $\mathcal{B}_N$ that further simplifies our crossing formulas. Finally in section 4.5, we conformally transform these formulas into functions of $2N-3$ variables that determine the shape of $\mathcal{P}$. (Actually, this transformation is trivial since crossing formulas are conformally invariant. Nonetheless, the universal partition functions that go into them are conformally covariant, so we include the details for completeness. This section is not completely necessary to understand the results of this chapter, but it will be helpful in the next chapter.) In section 4.6, we compare our crossing formula predictions for $Q = 1, 2, 3$ FK boundary clusters connecting the independently wired sides of a hexagon against high-precision computer simulation, finding excellent agreement.

The crossing formulas that we will derive, though explicit and exact for arbitrary N, have shortcomings. First, they are very complicated. Second, they are singular when the SLE speed κ is an exceptional speed (2.146), and their finite value as κ approaches an exceptional speed relies on the cancellation of many infinite quantities. Unfortunately, the most commonly studied models have SLE descriptions with κ an exceptional speed. However, more prudent choices of integration contours can often fix both of these problems, and we give examples of these better choices for the rectangle, the hexagon, and the octagon in section 4.4.

4.1 Partition functions for polygons with side-alternating free/fixed boundary conditions

We begin by deriving a loop representation for the random cluster partition function of a Q-state Potts model in a domain with a specified FFBC. Because of universality, the continuum limit of these partition functions are supposed to be independent

of the lattice we use, so we choose the infinite square lattice $a\mathbb{Z}^2$ intersecting $\overline{\mathbb{H}}$ with a small lattice spacing a. The points $x_1, \ldots, x_{2N}$ in the real axis host the free-to-fixed or fixed-to-free BCCs. In the discussion that follows, we describe our critical Potts model as residing in a $2N$-sided polygon $\mathcal{P}$ whose i-th vertex is the image of x_i under a conformal map taking the upper half-plane onto $\mathcal{P}$. For now, our system really resides in the upper half plane, but because these two domains are conformally equivalent, this detail is not relevant to the arguments that follow. Later in section 4.5, we will transform our results into results for a Potts model in $\mathcal{P}$.

In this chapter and in chapter five, we let ς denote a specified FFBC, and in an abuse of notation, we also let ς denote the event of the specified FFBC. Now we suppose that our system exhibits the specified FFBC event ς, and we recall equation (1.172) which gives the probability of observing the FFBC event ς with the i-th BCC occurring within distance ϵ_i from x_i:

$$\mathbb{P}(\varsigma) = Z_\varsigma / Z_f \tag{4.2}$$

$$\underset{\epsilon_i \to 0}{\sim} c_1^{2N} \epsilon_1^{2\theta_1} \ldots \epsilon_{2N}^{2\theta_1} \Upsilon_\varsigma, \quad \Upsilon_\varsigma := \langle \psi_1(x_1) \ldots \psi_1(x_{2N}) \rangle. \tag{4.3}$$

As indicated, we interpret this probability as the ratio of two partition functions Z_ς and Z_f. The partition function Z_ς (resp. Z_f) sums exclusively over samples in ς (resp. sums over all samples), and in the continuum limit, Z_ς and Z_f are infinite while their ratio is finite. We recall from chapter one that we call Υ_ς a "universal partition function."

In the discrete setting, Z_ς is a finite sum over FK-bond configurations $\{\beta\}$ exhibiting the FFBC event ς. At the critical point (1.27), the partition function (1.21) becomes (after dropping irrelevant factors)

$$Z_\varsigma = \sum_{\{\beta\}} Q^{N_{c,\varsigma} + N_\beta/2}, \tag{4.4}$$

where $N_{c,\varsigma}$ is the number of bond clusters in $\{\beta\}$ after we identify all boundary clusters that are mutually wired with each other in accordance with the FFBC event ς. (This identification ensures that, for example, we attribute a factor of Q instead of Q^2 to a pair of disjoint boundary clusters that are anchored to different sides of $\mathcal{P}$ that are mutually wired.)

We may also consider a partition function $Z_{(\lambda|\varsigma)}$ that sums exclusively over samples in the FFBC event ς and the BAC event λ. We have

$$Z_{(\lambda|\varsigma)} = \sum_{\{\beta\}} Q^{N_{c,\varsigma}+N_\beta/2} \mathbf{1}(\{\beta\} \in \lambda), \tag{4.5}$$

where $\mathbf{1}(\{\beta\} \in \lambda)$ is the indicator function on the event that $\{\beta\} \in \lambda$, and in the continuum setting, (4.5) becomes

$$\begin{aligned} \mathbb{P}(\lambda \cap \varsigma) &= Z_{(\lambda|\varsigma)}/Z_f \\ &\underset{\epsilon_i \to 0}{\sim} c_1^{2N} \epsilon_1^{2\theta_1} \dots \epsilon_{2N}^{2\theta_1} \Upsilon_{(\lambda|\varsigma)}(x_1, \dots, x_{2N}) \end{aligned} \tag{4.6}$$

for some universal partition function $\Upsilon_{(\lambda|\varsigma)}$.

We can decompose $\Upsilon_{(\lambda|\varsigma)}$ into the product of a factor that depends on ς and λ and a factor that only depends on λ by constructing a loop representation for (4.5), and this construction is possible for a certain collection of FFBC events. We define BC_N to be the collection of all FFBC events with the following two properties:

1. Either the index of the left endpoint of each wired interval (x_i, x_{i+1}) is even for all $\varsigma \in \mathrm{BC}_N$, or this index is odd for all $\varsigma \in \mathrm{BC}_N$.

2. There exists a crossing configuration that connects each collection of mutually wired sides and does not connect any pair of independently wired sides. This crossing configuration is unique for each element of BC_N, so we can represent each with a polygon diagram created by reflecting the boundary arcs of its

crossing configuration into the exterior of $\mathcal{P}$.

Each polygon diagram of an element in BC_N matches that of an element in $\mathcal{B}_N$, and because this correspondence is one-to-one, the cardinality of BC_N is C_N. In this chapter, we index the elements of $\mathcal{B}_N$ so that $F_\varsigma \in \mathcal{B}_N$ and $\varsigma \in \mathrm{BC}_N$ have identical diagrams.

The sets BC_2 and BC_3 contain all possible FFBC events for the rectangle and hexagon, but BC_4 does not contain all possible FFBC events for the octagon. For example, the FFBC with just the antipodal fixed sides of the octagon mutually wired does not have a crossing configuration that respects it. That is, there is no crossing configuration in the octagon that contains two disjoint boundary clusters with one connecting the top and bottom wired sides and the other connecting the left and right wired sides.

Now we construct a loop representation for (4.6). If ς is the unique FFBC event with all fixed sides wired independently of each other, then $N_{c,\varsigma} = N_c$ where N_c is the total number of clusters in bond configuration $\{\beta\}$, and a loop representation is given by (1.30). If any of the fixed sides are mutually wired with other fixed sides, then $N_{c,\varsigma}$ does not necessarily equal N_c since boundary clusters anchored to distinct but mutually wired sides should not be treated as distinct. A natural way to incorporate this effect is by reinterpreting the N exterior arcs of the diagram for ς as activated bonds inserted into the FK bond configuration of every event in ς [75]. These extra activated bonds connect the mutually wired sides so that they are constrained to exhibit the same state (figure 4.4). Let $\{\beta\,;\varsigma\}$ stand for this *augmented bond configuration*, or the bond configuration $\{\beta\}$ with these N extra activated bonds. Then the partition function (4.5) becomes

$$Z_{(\lambda|\varsigma)} = Q^{-N/2} \sum_{\{\beta\,;\varsigma\}} Q^{N_c+N_\beta/2} \mathbf{1}(\{\beta\} \in \lambda), \tag{4.7}$$

where the N_β (resp. N_c) is the number of bonds (resp. clusters) in the augmented bond configuration $\{\beta\,;\varsigma\}$, and where the factor of $Q^{-N/2}$ omits the superfluous factors that arise from the N exterior activated bonds. Now we can write a loop representation for this partition function similar to (1.30). The loops are closed medial lattice walks that trace the interior and exterior perimeter of every FK cluster (including the exterior perimeters of size-zero clusters, which are isolated lattice sites), and the Euler formula for planar graphs reads $N_l + N_s = 2N_c + N_\beta$, where N_s the total number of lattice sites and N_l is the total number of loops. Dropping a constant factor of n^{N_s}, we find the loop representation

$$Z_{(\lambda|\varsigma)} = n^{-N} \sum_{\{\beta\,;\varsigma\}} n^{N_l}\, \mathbf{1}(\{\beta\} \in \lambda), \quad n = \sqrt{Q}. \tag{4.8}$$

Under renormalization, (4.9) is supposed to flow onto the loop representation of a dense phase O(n)-model partition function with loop fugacity n. The loops in each term of the sum are either *bulk loops* that surround interior FK clusters or boundary loops that trace the perimeters of the boundary clusters (figures 4.3). We may decompose N_l into a sum $N_b + N_{\text{blk}}$ where N_b (resp. N_{blk}) equals the number of boundary loops (resp. bulk loops). The number of boundary loops is the same for any bond configuration $\{\beta\,;\varsigma\} \in \lambda$, so (4.9) becomes

$$Z_{(\lambda|\varsigma)} = n^{m_{\lambda,\varsigma}} \sum_{\{\beta\}} n^{N_{\text{blk}}} \mathbf{1}(\{\beta\} \in \lambda), \quad m_{\lambda,\varsigma} := N_b - N, \tag{4.9}$$

Because the fugacity factors for the boundary loops are factored out of the sum, the right side of (4.9) reverts back to a sum over bond configurations without the exterior activated bonds. Also, the sum may be viewed as a partition function for the system with boundary loops having fugacity one. Such a partition function clearly does not depend on our choice of FFBC event $\varsigma \in \text{BC}_N$, but it does depend on our choice of BAC event $\lambda \in \text{AC}_N$. We let Π_λ be the continuum limit version of this

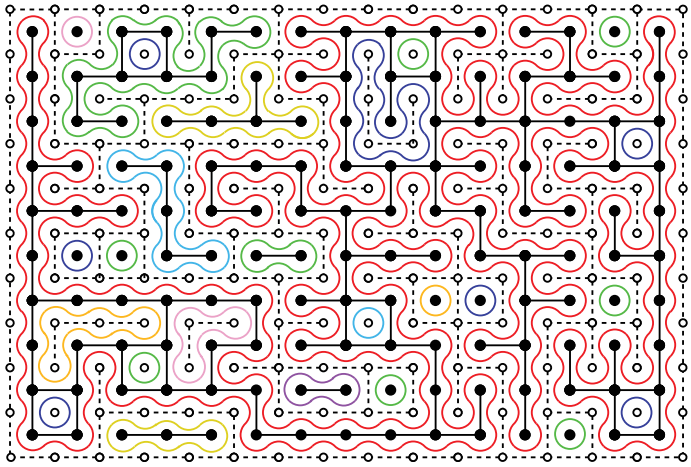

Figure 4.3: Bulk loops and boundary loops trace the inner faces and outer perimeters of the bond clusters. In the figure, boundary loops are red while bulk loops are any color but red.

partition function, we call it the *type-λ (half-plane) crossing weight*, and we define its polygon or half-plane diagram to be that of $\lambda \in \mathrm{AC}_N$. (Below, we will discover a more precise definition for a crossing weight that uses the formalism of chapter two.) The continuum limit version of (4.9) is then

$$\Upsilon_{(\lambda|\varsigma)} = n^{m_{\lambda,\varsigma}} \Pi_\lambda, \tag{4.10}$$

which may be inserted into (4.6). Summing over BACs gives a decomposition of Υ_ς into a linear combination of the crossing weights,

$$\Upsilon_\varsigma = \sum_{\lambda \in \mathrm{AC}_N} n^{m_{\lambda,\varsigma}} \Pi_\lambda, \tag{4.11}$$

which may be inserted into (4.2). The probability of the crossing event λ given the FFBC event ς is therefore

$$\chi_{(\lambda|\varsigma)}(x_1, \ldots, x_{2N}) := \mathbb{P}(\lambda \,|\, \varsigma) \tag{4.12}$$

$$= \frac{\Upsilon_{(\lambda|\varsigma)}}{\Upsilon_\varsigma} = \frac{n^{m_{\lambda,\varsigma}} \Pi_\lambda}{\sum_{\lambda' \in \mathrm{AC}_N} n^{m_{\lambda',\varsigma}} \Pi_{\lambda'}}. \tag{4.13}$$

Thus, the calculation of a crossing probability reduces to the calculation of the crossing weights Π_λ and the exponents $m_{\lambda,\varsigma}$. A more convenient version of this formula will be presented later.

A more formal definition of a crossing weight to be given below will show that each crossing weight solves the system (2.1-2.2) and therefore has the ansatz (2.4). Thus, the crossing formula depends only on the cross-ratios $\eta_1, \ldots, \eta_{2N-3}$, defined by

$$\eta_{i-1} := f(x_i), \quad i \in \{1, \ldots, 2N-3\}, \quad f(x) = \frac{(x - x_1)(x_{2N} - x_{2N-1})}{(x_{2N-1} - x_1)(x_{2N} - x)}, \tag{4.14}$$

and is therefore conformally invariant. (We note that $0 < \eta_1 < \eta_2 < \ldots < \eta_{2N-4} < \eta_{2N-3} < 1$.) So by replacing $x \mapsto f(x)$, we find

$$\chi_{(\lambda|\varsigma)}(x_1, \ldots, x_{2N}) = \chi_{(\lambda|\varsigma)}(0, \eta_1, \ldots, \eta_{2N-3}, 1, \infty). \tag{4.15}$$

We will write the right side of (4.15) as $\chi_{(\lambda|\varsigma)}(\eta_1, \ldots, \eta_{2N-3})$ when it is clear from context that we have dropped the three other variables at zero, one, and infinity.

The constant $m_{\lambda,\varsigma}$ can be calculated from a certain graph that follows from the polygon diagram for $[\mathscr{L}_\lambda]F_\varsigma$. To begin, we color the regions bounded by the boundary arcs and the wired (resp. free) sides of $\mathcal{P}$ black (resp. white), so that the boundary arcs divide the interior of $\mathcal{P}$ into adjacent black regions and white regions, and we identify each black region with a point to find a new planar graph $\mathcal{G}_{\lambda,\varsigma}$ (figure 4.7). This graph is the same for all augmented bond configurations $\{\beta; \varsigma\} \in \lambda$. The $2N$ edges of $\mathcal{G}_{\lambda,\varsigma}$ correspond to the exterior activated bonds, and the vertices of $\mathcal{G}_{\lambda,\varsigma}$ correspond to the black regions. To each internal face (resp. component) of $\mathcal{G}_{\lambda,\varsigma}$, we associate a loop that traces that face's interior (resp. that component's exterior) perimeter. This collection of loops corresponds one-to-one with the collection boundary loops of each configuration $\{\beta; \varsigma\} \in \lambda$. We let $\mathcal{I}_{\lambda,\varsigma}$ and $\mathcal{C}_{\lambda,\varsigma}$ be the set of internal faces and

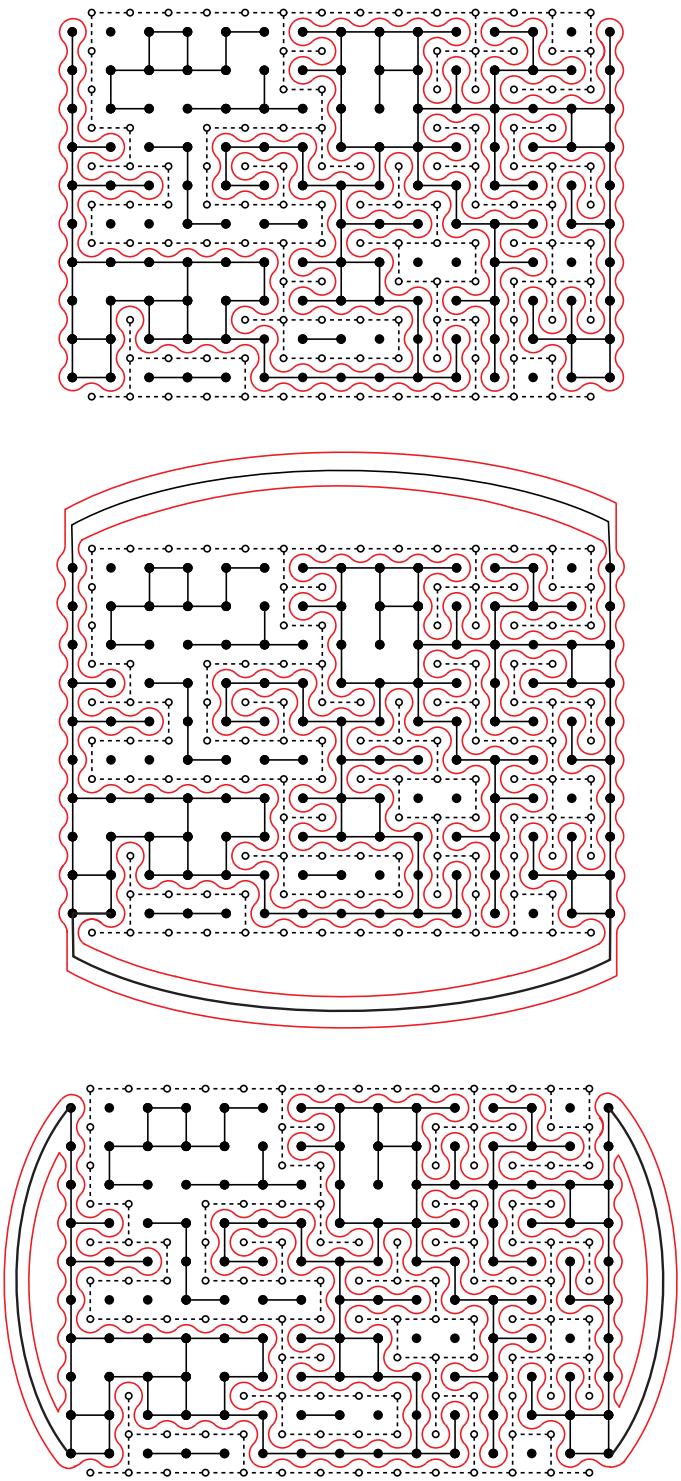

Figure 4.4: Boundary loops for a bond configuration in a rectangle without exterior bonds (top), with two horizontal exterior bonds (middle), and with two vertical exterior bonds (bottom). With the two exterior horizontal (resp. vertical bonds) included, the fixed left/right sides are always mutually (resp. independently) wired. The boundary arcs of all three rectangles connect the vertices horizontally in pairs. Thus, the top (resp. middle, resp. bottom) rectangle has one (resp. three, resp. three) boundary loop(s).

components of $\mathcal{G}_{\lambda,\varsigma}$ respectively. Then $N_b = |\mathcal{I}_{\lambda,\varsigma}| + |\mathcal{C}_{\lambda,\varsigma}|$, and from (4.9) we have

$$m_{\lambda,\varsigma} = |\mathcal{I}_{\lambda,\varsigma}| + |\mathcal{C}_{\lambda,\varsigma}| - N. \tag{4.16}$$

4.2 Crossing weights in polygons

In the discussion preceding (2.7) in chapter two, we predicted the dimension of the solution space of the system (2.1-2.2) by supposing that the space was spanned by a basis of C_N "partition functions," [59] where each function conditions the boundary arcs of the underlying multiple-SLE process to connect the vertices of $\mathcal{P}$ in a certain connectivity. Because Υ_ς solves this system, its decomposition (4.11) into a linear combination of the crossing weights suggests that the crossing weights are these partition functions. Therefore, we should be able to isolate the crossing weights in terms of the elements of $\mathcal{B}_N$.

We begin to isolate the crossing weights this way by using the following boundary condition argument. We recall from section 1.2.8 that (x_i, x_{i+1}) is a two-leg interval if the boundary arcs anchored to x_i and x_{i+1} are conditioned to not mutually connect and (x_i, x_{i+1}) is an identity interval if the mutual connectivity of the boundary arcs anchored to x_i and x_{i+1} is not conditioned (figure 1.17). By subtracting the two-leg family from the identity family (after correctly weighting these two families relative to each other), we condition these boundary arcs to mutually connect. In this situation, we call the mixed interval (x_i, x_{i+1}) a *zero-leg interval*, and we can use the crossing relation (1.152) to show that the boundary one-leg operators located at its endpoints exhibit the OPE

$$\psi_1(x_1)\psi_1(x_2) \underset{x_2 \to x_1}{\sim} C_{11}^0 (x_2 - x_1)^{-2\theta_1} \psi_0(x_1) - C_{11}^2 (x_2 - x_1)^{-2\theta_1 + \theta_2} \psi_2(x_1) \tag{4.17}$$

under its collapse, where C_{11}^0 (resp. C_{11}^2) is the boundary one-leg-one-leg-to-identity

(resp. one-leg-one-leg-to-two-leg) OPE coefficient.

The definition of a crossing weight implies that we know the type of each interval corresponding to a side of $\mathcal{P}$ for a given $\lambda \in \mathrm{AC}_N$. Each is either a two-leg interval or zero-leg interval. We also recall from chapter two that when a two-leg interval is collapsed, the crossing weight goes to zero, and when a zero-leg interval is collapsed, the boundary arc connecting its endpoints becomes a loop that lassos a region in the upper half-plane and anchors to the real axis at a single point. In the latter case, the area of the lassoed region is zero almost surely. Thus, the boundary arc contracts to a point as its zero-leg interval is collapsed, and the crossing weight for a $2N$-sided polygon goes to a crossing weight for a $(2N-2)$-sided polygon.

The ratio C_{11}^2/C_{11}^0 of the OPE coefficients appearing in (4.17) is fixed by the crossing relation (1.152) between the conformal blocks (summed over all possible free-to-fixed or fixed-to-free BCCs that can happen at each vertex of $\mathcal{P}$ in the event $\varsigma \in \mathrm{BC}_N$). (We note the double use of "crossing" in this section.) It is given by [48]

$$\frac{C_{11}^2}{C_{11}^0} = \sqrt{n(\kappa)\frac{\Gamma(12/\kappa-1)\Gamma(2-8/\kappa)}{\Gamma(8/\kappa)\Gamma(1-4/\kappa)}} = \sqrt{\frac{\Gamma(12/\kappa-1)\Gamma(4/\kappa)}{\Gamma(8/\kappa)\Gamma(1-4/\kappa)}}. \tag{4.18}$$

Because boundary loops have fugacity one in each sample contributing to a crossing weight, we must set $C_{11}^0 = 1$, in contrast with the convention in (1.157). We therefore

have the behavior for zero-leg and two-leg intervals (x_1, x_2),

$$\Pi_\lambda(x_1, \ldots, x_{2N}) \underset{x_2 \to x_1}{\sim} \left\{ \begin{array}{l} \left. \begin{array}{l} \sqrt{\dfrac{\Gamma(12/\kappa - 1)\Gamma(4/\kappa)}{\Gamma(8/\kappa)\Gamma(1 - 4/\kappa)}} \\ \qquad \times (x_2 - x_1)^{-2\theta_1 + \theta_2} \Xi_{\lambda,2}(x_1, \ldots, x_{2N}) \end{array} \right\} \text{two-leg} \\ \\ \left. \begin{array}{l} (x_2 - x_1)^{-2\theta_1} \Xi_{\lambda,0}(x_1, \ldots, x_{2N}) \\ \qquad - \sqrt{\dfrac{\Gamma(12/\kappa - 1)\Gamma(4/\kappa)}{\Gamma(8/\Gamma)\Gamma(1 - 4/\kappa)}} \\ \qquad \times (x_2 - x_1)^{-2\theta_1 + \theta_2} \Xi_{\lambda,2}(x_1, \ldots, x_{2N}) \end{array} \right\} \text{zero-leg} \end{array} \right. , \tag{4.19}$$

where $\Xi_{\lambda,0}$ and $\Xi_{\lambda,2}$ are analytic at $x_2 = x_1$, and where $\Xi_0(x_2, x_2, x_3, \ldots, x_{2N})$ is independent of x_2 and equals the crossing weight for the $(2N - 2)$-sided polygon whose half-plane diagram is identical to that for Π_λ but with x_1 and x_2 and the interior arc connecting them removed.

When N is sufficiently small, one can isolate the crossing weights in terms of elements of $\mathcal{B}_N$ by using (4.19) as boundary conditions. For example, we consider the case of the rectangle $\mathcal{R}$. Here, $N = 2$. The two crossing weights $\Pi_1 := \Pi_{\lambda_1}$ and $\Pi_2 := \Pi_{\lambda_2}$ sum exclusively over all samples with BAC event $\lambda_1 \cong \{x_1 \leftrightarrow x_4, x_2 \leftrightarrow x_3\}$ and $\lambda_2 \cong \{x_1 \leftrightarrow x_2, x_3 \leftrightarrow x_4\}$ respectively. (The notation "$a \leftrightarrow b$" indicates that vertices a and b of $\mathcal{R}$ are mutually connected by a boundary arc.) The intervals (x_1, x_2) and (x_3, x_4) must be two-leg intervals of Π_1 (resp. zero-leg intervals of Π_2) while (x_2, x_3) and (x_4, x_1) must be zero-leg intervals of Π_1 (resp. two-leg intervals of Π_2). By expanding the two elements of $\mathcal{B}_2$ (2.42, 2.43) in the limit that the length of these intervals go to zero and taking suitable linear combinations, we straightforwardly find the expressions (2.40, 2.41) for these crossing weights.

Unfortunately, the boundary conditions (4.19) are not sufficient to specify a particular BAC and isolate its crossing weight when N is sufficiently large. The sixteen-gon

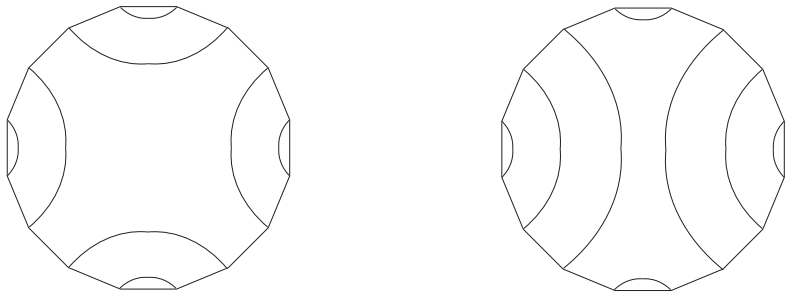

Figure 4.5: Two different BACs in a sixteen-gon with each side of the same interval type (zero-leg or two-leg).

in figure 4.5 shows that we need to specify these conditions for intervals corresponding to not just one side of $\mathcal{P}$ but to multiple adjacent sides too. Fortunately, the formalism of chapter two can be used to do this efficiently. We consider the action of some $[\mathscr{L}_\lambda]$ on the crossing weight $\Pi_{\lambda'}$. If $\lambda \neq \lambda'$, then the interior arcs in the half-plane diagrams for $[\mathscr{L}_\lambda]$ and $\Pi_{\lambda'}$ do not exhibit the same arc connectivity, $[\mathscr{L}_\lambda]$ eventually collapses a two-leg interval of some limit solution of Π_λ, and $[\mathscr{L}_\lambda]\Pi_\lambda$ is therefore zero. But if $\lambda = \lambda'$, then these diagrams do exhibit the same arc connectivity, $[\mathscr{L}_\lambda]$ only ever collapses zero-leg intervals of limit solutions of Π_λ, and $[\mathscr{L}_\lambda]\Pi_\lambda$ is therefore nonzero. Every zero-leg-interval collapse generates a crossing weight of a polygon with two fewer sides until we eventually reach the $N = 1$ crossing weight $\Pi_1 = (x_2 - x_1)^{-2\theta_1}$ (2.35) of the two-gon. Because $(x_2 - x_1)^{2\theta_1}\Pi_1 \to 1$ as $x_2 \to x_1$, we have $[\mathscr{L}_\lambda]\Pi_{\lambda'} = \delta_{\lambda,\lambda'}$, and because $\mathscr{B}^*_N$ spans $\mathcal{S}^*_N$ according to lemma II.27, we conclude that the set of crossing weights is dual to $\mathscr{B}^*_N$.

Definition IV.1. Suppose that $\kappa \in (0, 8)$ and that conjecture II.16 is true. Let $\mathscr{B}_N$ be the basis for $\mathcal{S}_N$ dual to the basis $\mathscr{B}^*_N$ for $\mathcal{S}^*_N$. We call the element of $\mathscr{B}_N$ dual to $[\mathscr{L}_\lambda]$ the *type-λ crossing weight*, and we denote it by Π_λ.

By exploiting the dual relationship between $\mathscr{B}_N$ and $\mathscr{B}^*_N$, it is easy to show that

the crossing weights are related to the solutions in $\mathcal{B}_N$ by

$$F_\varsigma = \sum_{\lambda \in \mathrm{AC}_N} ([\mathscr{L}_\lambda] F_\varsigma) \Pi_\lambda = \sum_{\lambda \in \mathrm{AC}_N} n^{l_{\lambda,\varsigma}} \Pi_\lambda \tag{4.20}$$

where $l_{\lambda,\varsigma}$ is the number of loops in the polygon diagram for $[\mathscr{L}_\lambda] F_\varsigma$ (with $\mathcal{P}$ deleted from the diagram). In terms of the meander matrix, this is

$$\begin{pmatrix} F_1 \\ \vdots \\ F_{C_N} \end{pmatrix} = M_N(\kappa) \begin{pmatrix} \Pi_1 \\ \vdots \\ \Pi_{C_N} \end{pmatrix}. \tag{4.21}$$

With the elements of $\mathcal{B}_N$ explicitly defined in definition II.20, we must simply invert (4.21) to find all C_N crossing weights.

While this method works for arbitrarily large N, it does have drawbacks. First, we cannot invert $M_N(\kappa)$ when κ equals any of the exceptional speeds κ' in (2.146) with $q \leq N+1$ since $\det M_N(\kappa')$ is zero. This is unfortunate since most lattice models correspond with one of these speeds. We can circumvent this issue by inverting (4.21) at $\kappa = \kappa' + \epsilon$ and sending $\epsilon \to 0$. This limit exists and is not zero since Π_λ is always an element of a basis for $\mathcal{S}_N$. Unfortunately, computing this limit directly is very awkward as we must rely on the cancellation of infinite quantities in order to arrive with a finite crossing weight. Second, we have expressed our crossing weights as linear combinations of all C_N solutions in $\mathcal{B}_N$, each solution containing a complicated $(N-1)$-fold integral. Although $\mathcal{B}_N$ is the simplest basis to use for proving the results in chapter two, it does not give the simplest expressions for the crossing weights.

Often, we can find simpler expressions for the crossing weights through a careful selection of integration contours. For example, when $N = 2$, the method outlined

above gives

$$\begin{pmatrix} \Pi_1 \\ \Pi_2 \end{pmatrix} = \frac{1}{n^2(n^2-1)} \begin{pmatrix} n^2 & -n \\ -n & n^2 \end{pmatrix} \begin{pmatrix} F_1 \\ F_2 \end{pmatrix}, \tag{4.22}$$

where $F_1, F_2 \in \mathcal{B}_2$ are given in (2.42, 2.43). But Π_1 and Π_2 are also given by (2.40) and (2.41) respectively. (We can show that both formulas are the same by using Cauchy's theorem.) The latter choice is better because it does not accrue canceling infinite quantities when $\kappa \to \kappa'$ with $n(\kappa') = \pm 1$. (We recall that the limit of F_1/n and F_2/n as $\kappa \to \kappa'$ with $n(\kappa') = 0$ is finite. Thus, the $n = 0$ case does not raise concern.) Also, with a single integral expression, the latter choice is simpler than (4.22) which includes a linear combination of two integrals. This advantage becomes significant when N is large and the numerical evaluation of many $(N-1)$-fold Coulomb-gas integrals becomes very time consuming. We will show how to construct simpler formulas for crossing weights when $N = 2, 3$, and 4 in section 4.4.

4.3 The polygon crossing formula

Having devised a method for calculating explicit formulas for all crossing weights in $\mathscr{B}_N$, the probability of observing the crossing event $\lambda \in \mathrm{AC}_N$ conditioned on the FFBC event $\varsigma \in \mathrm{BC}_N$ can be computed from formula (4.12). This formula is inconvenient because of the need to calculate the exponents $m_{\lambda,\varsigma}$ and all C_N crossing weights Π_λ, which is tedious when N is large. Both of these tasks are dramatically simplified after we observe a special relation between Υ_ς and F_ς.

To anticipate the forthcoming result, we consider the rectangle $\mathcal{R}$ ($N = 2$) with wired left/right sides. We let λ_1 (resp. λ_2) be the BAC event $\{x_1 \leftrightarrow x_4, x_2 \leftrightarrow x_3\}$ (resp. $\{x_1 \leftrightarrow x_2, x_3 \leftrightarrow x_4\}$), we let ς_1 (resp. ς_2) be the FFBC event in which the left side (x_4, x_1) and right side (x_2, x_3) of $\mathcal{R}$ are independently (resp. mutually) wired, and we let $\Upsilon_k := \Upsilon_{\varsigma_k}, F_k := F_{\varsigma_k}$, and $\Pi_k := \Pi_{\lambda_k}$. From (4.11) and (4.16), we immediately

find that

$$\Upsilon_1 = n^2\Pi_1 + n\Pi_2, \tag{4.23}$$

$$\Upsilon_2 = \Pi_1 + n\Pi_2. \tag{4.24}$$

We see that these decompositions are correct for the following reasons. In the BAC event λ_1, the two distinct boundary clusters, one anchored to the left side of $\mathcal{R}$ and the other anchored to the right side, are each surrounded by a loop that is counted with fugacity one in Π_1. To restore the fugacity of both loops to n, we must multiply Π_1 by n^2. In the BAC event λ_2, one crossing boundary cluster connecting the left and right sides is surrounded by a single loop that is counted with fugacity one in Π_2. To restore its fugacity to n, we must multiply Π_2 by n. This justifies (4.23). In (4.24), the coefficients are argued in the same way except for one modification. In the BAC event λ_1, $n^2\Pi_1$ sums exclusively over events in which the disjoint left and right boundary clusters independently exhibit any one of the Q spin states for Q^2 possible combinations. But if these sides were mutually wired, then this term should include only events in which the disjoint left and right boundary clusters exhibit the same state for Q possibilities. To reconcile this difference, we must divide $n^2\Pi_1$ by $Q = n^2$. In the BAC event λ_2, this modification is not necessary since a crossing boundary cluster always connects the left and right sides. This justifies (4.24).

In chapter two, we noted a similar decomposition of the elements of $\mathcal{B}_2$ in terms of the crossing weights. It is (2.44)

$$F_1 = n^2\Pi_1 + n\Pi_2, \qquad F_2 = n\Pi_1 + n^2\Pi_2. \tag{4.25}$$

Comparing (2.44) with (4.25), we find

$$F_1 = \Upsilon_1, \quad F_2 = n\Upsilon_2. \tag{4.26}$$

That is, the elements of $\mathcal{B}_2$ equal the universal partition functions modulo a factor that depends on the FFBC event. If this is true for all $N \geq 2$, then we may replace Υ_ς with F_ς in the denominator of the crossing formula (4.12). To do this poses a major advantage since a single element F_ς of $\mathcal{B}_N$ is much easier to calculate than is the universal partition function Υ_ς, the latter being a linear combination of all crossing weights which are in turn linear combinations of the elements of $\mathcal{B}_N$. We will show that this supposition is true, and more precisely that

$$F_\varsigma = n^{l_{\vartheta,\varsigma}-1}\Upsilon_\varsigma, \tag{4.27}$$

where $\vartheta \in \mathrm{AC}_N$ is the particular BAC event with the two endpoints of every free interval mutually connected by a boundary arc, and where $l_{\lambda,\varsigma}$ is again the number of loops in the polygon diagram for $[\mathscr{L}_\lambda]F_\varsigma$ (with $\mathcal{P}$ deleted from the diagram). In an abuse of terminology, we will call these loops *boundary loops.* This definition of a boundary loop is different from that given in section 4.1. (In the earlier definition, the number of boundary loops equaled $m_{\lambda,\varsigma} + N$ (4.16), and in the current definition, the number of boundary loops equals $l_{\lambda,\varsigma}$.)

Now we prove (4.27). Comparing (4.11) with (4.20), we see that F_ς and Υ_ς are proportional only if the difference of the exponents

$$d_{\lambda,\varsigma} := l_{\lambda,\varsigma} - m_{\lambda,\varsigma} = l_{\lambda,\varsigma} - (|\mathcal{I}_{\lambda,\varsigma}| + |\mathcal{C}_{\lambda,\varsigma}| - N) \tag{4.28}$$

is a number d_ς independent of λ, so $F_\varsigma = n^{d_\varsigma}\Upsilon_\varsigma$. To show that this is true, we use this following fact. We can pass from any interior arc connectivity in $\mathcal{P}$ to any other interior arc connectivity in $\mathcal{P}$ by exchanging a finite number of pairs of interior arcs in a suitable progression. By *exchanging*, we mean the following process. We consider the k-th interior arc connectivity diagram, corresponding with the BAC event $\lambda_k \in \mathrm{AC}_N$. If the interior arcs γ_1 and γ_2 connect the vertices $\{a, b\}$ and $\{c, d\}$

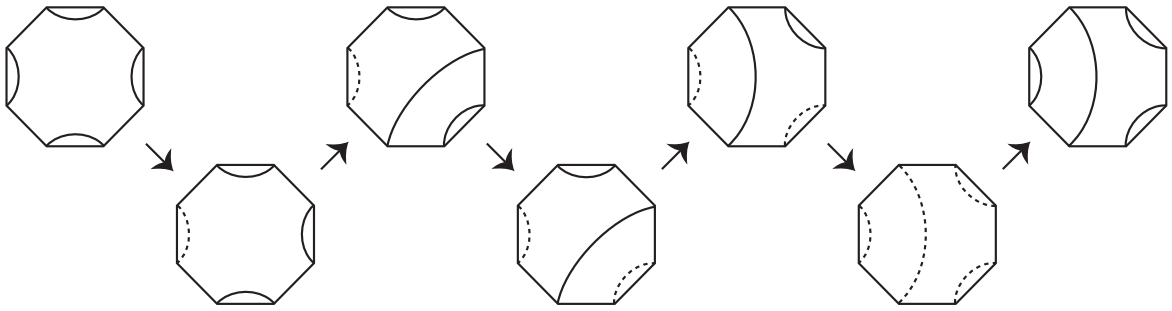

Figure 4.6: An illustration of the sequence of arc exchanges that take us from the k_ϑ-th arc connectivity to the arc connectivity of the top right octagon. Upward (resp. downward) pointing arrows indicate an arc exchange (deletion), and the last upward pointing arrow indicates that we have restored all deleted arcs to arrive with our target arc connectivity.

of $\mathcal{P}$ respectively and are not separated by other arcs, then they may be replaced with non-intersecting interior arcs γ_1' and γ_2' that connect either vertices $\{a, d\}$ and $\{b, c\}$ respectively or vertices $\{a, c\}$ and $\{b, d\}$ respectively, (Only one of these choices will allow γ_1' and γ_2' to not intersect.) This replacement takes us from the k-th arc connectivity to some other, say the k'-th, arc connectivity, and we say that the arcs γ_1 and γ_2 have *exchanged* to form arcs γ_1' and γ_2'.

To prove the claim of the previous paragraph, it suffices to show that we can go from the k_ϑ-th arc connectivity, corresponding to the BAC event $\vartheta \in \mathrm{AC}_N$, to any other, say the k-th, arc connectivity through a sequence of exchanges since such a process is reversible. (We recall that in the k_ϑ-th arc connectivity, the endpoints of each free side of $\mathcal{P}$ are joined by a common interior arc.) We begin by deleting all M interior arcs common to both the k_ϑ-th and the k-th arc connectivity to arrive with the k_ϑ-th and the k_0-th arc connectivities respectively in the $2(N-M)$-gon $\mathcal{P}_0$. Next, we exchange an adjacent pair of arcs in the k_ϑ-th connectivity of $\mathcal{P}_0$ to create two new arcs, one of which γ mutually connects two endpoints of a side of $\mathcal{P}_0$ in the k_0-th arc connectivity of $\mathcal{P}_0$. (Topological considerations show that such a γ always exists.) Then we delete the shared arc γ from both connectivities to arrive with the k_ϑ-th and the k_1-th arc connectivities respectively in the $2(N-M-1)$-gon $\mathcal{P}_1$. We repeat this process of exchanging followed by deleting until all arcs have been deleted.

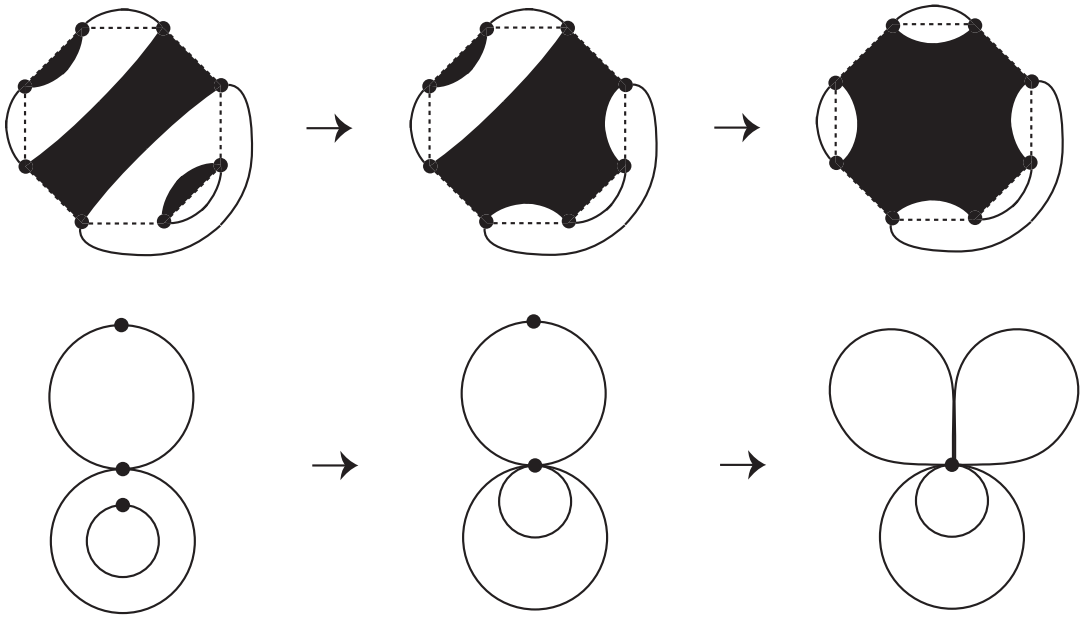

Figure 4.7: The three topologically distinct BACs (boundaries of black regions) in an octagon with diagonal sides wired. The same FFBC (i.e., exterior arcs) is shown for all three octagons, and the corresponding graph $\mathcal{G}_{\lambda,\varsigma}$ appears beneath each octagon. Boundary arcs are exchanged through white (resp. black) regions as we move leftwards (resp. rightwards). In each column, the difference between the number of boundary loops in the top row minus the sum of the number of internal faces and components in the graph in the bottom row is always negative two.

Now if we restore all of the deleted arcs to the (now trivial) k_ϑ-th arc connectivity in the zero-gon, then we find the k-th arc connectivity in the original $2N$-sided polygon $\mathcal{P}$, as desired. An illustration of this process is presented in figure 4.6.

Now we return to proving that $d_{\lambda,\varsigma}$ is independent of λ. By the results of the previous paragraphs, it suffices to check that $d_{\lambda,\varsigma}$ does not change when two boundary arcs are exchanged. To this end, we consider the diagram for $[\mathscr{L}_\lambda]F_\varsigma$, which contains $l_{\lambda,\varsigma}$ boundary loops. The exchanging of two boundary arcs changes their respective boundary loops in one of two ways. First, if the boundary arcs belong to different boundary loops, then this exchange will join two distinct boundary loops into one, decreasing $l_{\lambda,\varsigma}$ by one (figure 4.7). This exchange will also alter the graph $\mathcal{G}_{\lambda,\varsigma}$, defined in the discussion preceding (4.16). If the two original boundary arcs are separated by a black region (resp. white region), then the number of internal faces

$|\mathcal{I}_{\lambda,\varsigma}|$ (resp. components $|\mathcal{C}_{\lambda,\varsigma}|$) of $\mathcal{G}_{\lambda,\varsigma}$ will decrease by one. Thus, $d_{\lambda,\varsigma}$ does not change (figure 4.7). Second, if the boundary arcs belong to the same boundary loop, then this exchange will split the boundary loop into two boundary loops with one nested inside of the other, increasing $l_{\lambda,\varsigma}$ by one (figure 4.7). Again, this exchange will also alter $\mathcal{G}_{\lambda,\varsigma}$. If the two original boundary arcs are separated by a black region (resp. white region), then the number of components $|\mathcal{C}_{\lambda,\varsigma}|$ (resp. internal faces $|\mathcal{I}_{\lambda,\varsigma}|$) of $\mathcal{G}_{\lambda,\varsigma}$ will increase by one. Thus, $d_{\lambda,\varsigma}$ does not change (figure 4.7). We conclude that $d_{\lambda,\varsigma}$ is a number d_ς independent of λ.

The most straightforward way to calculate d_ς is by examining the graph $\mathcal{G}_{\vartheta,\varsigma}$. Again, in the BAC event ϑ, the endpoints of each free side of $\mathcal{P}$ are mutually connected by a boundary arc. We let $\mathcal{E}_\varsigma$ and $\mathcal{V}_{\lambda,\varsigma}$ be the set of edges and the set of vertices of $\mathcal{G}_{\lambda,\varsigma}$ respectively. It is easy to see that $\mathcal{G}_{\vartheta,\varsigma}$ is comprised of $|\mathcal{C}_{\vartheta,\varsigma}| = 1$ component, $|\mathcal{V}_{\vartheta,\varsigma}| = 1$ vertex, and $|\mathcal{E}_\varsigma| = N$ edges. (The right column of figure 4.7 illustrates $\mathcal{G}_{\vartheta,\varsigma}$ for a particular ς and with $N = 4$.) Then by Euler's formula for planar graphs, which says that

$$|\mathcal{C}_{\vartheta,\varsigma}| + |\mathcal{E}_\varsigma| = |\mathcal{I}_{\vartheta,\varsigma}| + |\mathcal{V}_{\vartheta,\varsigma}|, \tag{4.29}$$

it follows that $\mathcal{G}_{\vartheta,\varsigma}$ has $|\mathcal{I}_{\vartheta,\varsigma}| = N$ internal faces. From (4.28) we therefore have

$$F_\varsigma = n^{d_\varsigma}\Upsilon_\varsigma, \quad d_\varsigma = d_{\vartheta,\varsigma} = l_{\vartheta,\varsigma} - (|\mathcal{I}_{\vartheta,\varsigma}| + |\mathcal{C}_{\vartheta,\varsigma}| - N) \tag{4.30}$$

$$= l_{\vartheta,\varsigma} - 1. \tag{4.31}$$

This proves (4.27).

We may use this result to simplify the crossing formula (4.12). By multiplying the numerator and denominator of this formula by $n^{l_{\vartheta,\varsigma}-1}$, we find that the probability of the crossing event $\lambda \in \mathrm{AC}_N$ conditioned on the FFBC event $\varsigma \in \mathrm{BC}_N$ is

$$\chi_{(\lambda|\varsigma)} = \frac{n^{l_{\lambda,\varsigma}}\Pi_\lambda}{F_\varsigma}, \tag{4.32}$$

where the functions and variables that appear in this formula are given as follows.

- The BAC event $\lambda \in \mathrm{AC}_N$ (defined in the introduction of this chapter) is represented by a diagram of N non-intersecting interior arcs inscribed in $\mathcal{P}$ that join its vertices pairwise in the same connectivity as the boundary arcs of any sample in λ.

- The FFBC event $\varsigma \in \mathrm{BC}_N$ (defined in section 4.1) is represented by a diagram of N non-intersecting exterior arcs that connect the vertices of $\mathcal{P}$ pairwise. There exists a unique crossing event $\lambda' \in \mathrm{AC}_N$ that connects each collection of mutually wired sides of ς and does not connect any pair of independently wired sides. The exterior arcs are created by reflecting the boundary arcs of the diagram for λ' into the exterior of $\mathcal{P}$.

- $l_{\lambda,\varsigma}$ is the number of loops formed by joining the interior arcs in the diagram for λ with the exterior arcs in the diagram for ς at the vertices of $\mathcal{P}$ and deleting $\mathcal{P}$ from the diagram that results.

- n is the loop fugacity of the O(n) model, given by $n(\kappa) = -2\cos(4\pi/\kappa)$, with κ the SLE speed.

- The partition function F_ς is given by (2.9)

$$
\begin{aligned}
&F_\varsigma(\{\Gamma_m\} \,|\, x_1, \ldots, x_{2N}) := \\
&n(\kappa)^N \frac{\Gamma(2-8/\kappa)^N}{\Gamma(1-4/\kappa)^{2N}} \prod_{i<j}^{2N-1} (x_i - x_j)^{2/\kappa} \prod_{i=1}^{2N-1} (x_{2N} - x_i)^{1-6/\kappa} \\
&\times \mathcal{I}_{N-1}\left(\beta_{kl} = \left\{ \begin{array}{ll} -4/\kappa & i \neq 2N \\ 12/\kappa - 2 & i = 2N \end{array} \right\}; \gamma_{pq} = \frac{8}{\kappa} \;\middle|\; \{\Gamma_m\} \middle| x_1, \ldots, x_{2N}\right),
\end{aligned}
\tag{4.33}
$$

where $\mathcal{I}_M, M \in \mathbb{Z}^+$ is the M-fold complex-contour integral

$$\mathcal{I}_M(\{\beta_{kl}\};\{\gamma_{pq}\}\,|\,\{\Gamma_m\}_{m=1}^M\,|\,x_1,\ldots,x_{2N}) := \\ \times \int_{\Gamma_1}\ldots\int_{\Gamma_M}\left(\prod_{k=1}^{2N}\prod_{l=1}^{M}(x_k-u_l)^{\beta_{ij}}\right)\left(\prod_{p<ql}^{M}(u_p-u_q)^{\gamma_{kl}}\right)du_M\ldots du_1. \quad (4.34)$$

Here, x_i is the pre-image of the i-th vertex of $\mathcal{P}$ under a conformal map taking the upper half-plane onto $\mathcal{P}$, and $x_i < x_j$ when $i < j$. Also, the collection $\{\Gamma_m\}$ of integration contours consists of $N-1$ non-intersecting simple curves that connect the points x_i pairwise just as their images as vertices of $\mathcal{P}$ are connected in the diagram for ς. There is one exception to this statement. No integration contour connects the point x_{2N} with the point to which it is joined by an arc in the diagram for ς.

- The crossing weight is given by $\Pi_\lambda = [M_N^{-1}]_{\lambda,\varsigma}F_\varsigma$, where the λ,ς-th entry of the $C_N \times C_N$ "meander matrix" M_N equals $n^{l_{\lambda,\varsigma}}$ [68]. M_N^{-1} does not exist when κ is an exceptional speed (2.146). However, the limit of Π_λ as κ approaches an exceptional speed exists, and we use this limit in this case.

To finish, we technically must conformally map the upper half-plane onto the interior of $\mathcal{P}$ in order to obtain the true crossing formulas $\chi^{\mathcal{P}}_{(\lambda|\varsigma)}$ for $\mathcal{P}$. We call the map that accomplishes this task f. But because the partition functions $Z_{(\lambda|\varsigma)}$ and Z_ς are conformally invariant, the crossing formula must also be conformally invariant. That is, we must have

$$\chi^{\mathcal{P}}_{(\lambda|\varsigma)}(w_1,\ldots,w_{2N}) = \chi_{(\lambda|\varsigma)}(x_1,\ldots,x_{2N}), \quad (4.35)$$

where $w_i = f(x_i)$ is the i-th vertex of $\mathcal{P}$. There are some subtleties that we have overlooked related to the failure of f to be conformal at the vertices of $\mathcal{P}$ where the BCCs reside. Ultimately, these details will not spoil conformal invariance, and (4.35)

remains true. We will examine these details further in section 4.5.

We can extend our results beyond FK cluster connectivities to probabilities of multiple-SLE arc connectivities, as we noted in the introduction of chapter two. We recall that a multiple-SLE process is driven in part by a "partition function" Z, which is any solution of the system (2.1-2.2). Assuming that conjecture II.16 is true, the results of chapter two imply that we may decompose Z into a sum over crossing weights:

$$Z = \sum_{\lambda \in \mathrm{AC}_N} c_\lambda \Pi_\lambda. \tag{4.36}$$

As previously argued, we expect that the curves of a multiple-SLE process in $\mathcal{P}$ driven by the solution Π_λ will join pairwise as in the BAC event λ. Now, conjecturing the existence of C_N such crossing weights Π_λ, [59] argues that if we drive the multiple-SLE process by the partition function (4.36), then the probability that the boundary arcs connect as in the BAC event λ is

$$\mathbb{P}(\lambda \,|\, \{c_{\lambda'}\}_{\lambda' \in \mathrm{AC}_N}) = \frac{c_\lambda \Pi_\lambda}{\sum_{\lambda' \in \mathrm{AC}_N} c_{\lambda'} \Pi_{\lambda'}}. \tag{4.37}$$

The authors of [59] pose the question of calculating all of the C_N crossing weights Π_λ. In this chapter, we propose an answer by giving explicit formulas for all of them.

The connection with multiple-SLE extends into the dilute phase. Because $\kappa \leq 4$ in this phase, we must replace each integration contour of $F_\varsigma \in \mathcal{B}_N$ connecting two points, say x_i and x_j, with the Pochhammer contour $\mathscr{P}(x_i, x_j)$ so that all of the integrals in the crossing formula (4.32) converge.

Because the crossing formula extends into the dilute phase, (4.32) gives crossing probabilities for Potts model spin clusters too. In the dilute phase, the one-leg operator $\phi_{2,1}$ induces a BCC from fixed to, say, spin a, to free but excluding spin a, and then it sums over all Q possible spins. In this case, the wired sides are automatically constrained to be mutually wired, so the only admissible FFBC event is $\vartheta \in \mathrm{BC}_N$,

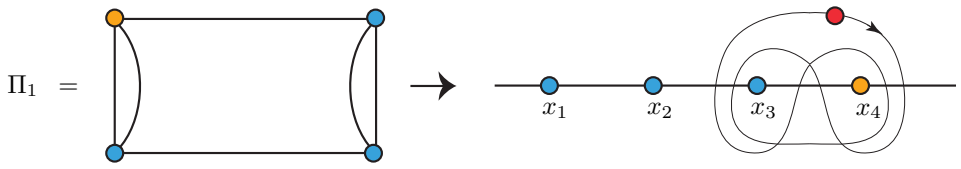

Figure 4.8: The one topologically distinct BAC in the rectangle and its corresponding integration contour choice. The bottom-left vertex of the rectangle is sent to the leftmost point on the real axis, and moving counterclockwise around the rectangle corresponds to moving rightwards along the real axis.

where the endpoints of every free side are connected by an exterior arc. Another way to see this fact is by immersing the system in $\mathcal{P}$ in a sea of spin a sites if a is the state of the wired sides. The partition function for the immersed system equals that of the original system to within an irrelevant constant, and the boundary arcs of the immersed system are the perimeters of the spin a boundary clusters. These boundary arcs close into boundary loops through external arcs that pass just outside the free sides. This external arc connectivity is exactly that of ϑ, so all of our samples must lie in the FFBC event ϑ.

4.4 Crossing weights in rectangles, hexagons, and octagons

In this section, we derive alternative formulas for the crossing weights of the rectangle, the hexagon, and the octagon that are simpler than those prescribed by (4.21) and are typically not singular when κ equals an exceptional speed (2.146) with $q \leq N + 1$. Each crossing weight necessarily has the form (2.9), so for each BAC event $\lambda \in \mathrm{AC}_N$, we must simply select the integration contours and normalize the result so that $[\mathscr{L}_\lambda]\Pi_\lambda = 1$. The hexagon crossing formulas of this section were originally discovered by J. Simmons in presently unpublished work [74]. Throughout this section, we let $\Pi_k := \Pi_{\lambda_k}$ for some indexed BAC event $\lambda_k \in \mathrm{AC}_N$.

4.4.1 Crossing weights in rectangles

There are $C_2 = 2$ possible BACs in a rectangle $\mathcal{R}$. Both connectivities are topologically identical, so we only compute the weight Π_1 for the vertical connectivity λ_1 (figure 4.8). The other can be found by rotating $\mathcal{R}$.

The vertices of $\mathcal{R}$ in figure 4.8 are sent to real numbers so that moving counterclockwise around $\mathcal{R}$ corresponds to moving rightward along the real axis, and the bottom-left vertex is sent to x_1. From the figure, we see that Π_1 is a two-leg solution. According to section 3.1, we must therefore entwine x_3 and x_4 with a Pochhammer contour $\Gamma_1 = \mathscr{P}(x_3, x_4)$, and according to (1.195), the Pochhammer contour may be replaced by an integration along $[x_3, x_4]$ when $\kappa > 4$. With the proper normalization, the result is (2.40). The weight Π_2 for the horizontal BAC event λ_2 is given in (2.41).

Earlier, we wrote Π_2 in terms of a hypergeometric function (2.37-2.38), and now we note that this formula reduces to Cardy's formula (4.1) when $\kappa = 6$, as it must since this speed captures critical percolation. (The cross-ratio $\eta = x_{21}x_{43}/x_{31}x_{42}$ is equivalent to the modular parameter m in Cardy's formula.)

4.4.2 Crossing weights in hexagons

There are $C_3 = 5$ possible BACs in a hexagon $\mathcal{H}$, and they can be grouped into the two topologically distinct classes shown in figure 4.9. We compute one weight per class as the others can be found by rotating $\mathcal{H}$.

The vertices of $\mathcal{H}$ in figure 4.9 are sent to real numbers so that moving counterclockwise around $\mathcal{H}$ corresponds to moving rightward along the real axis, and the bottom-left vertex is sent to x_1. From the top hexagon in the figure, we see that Π_1 is a three-leg solution. According to section 3.1, we must entwine x_5 and x_6 with a Pochhammer contour $\Gamma_1 = \mathscr{P}(x_5, x_6)$, and we must entwine Γ_1 and x_4 with a second Pochhammer contour Γ_2 to arrive with Π_1.

When $\kappa > 4$, we can decompose the double integral in Π_1 into a linear combination

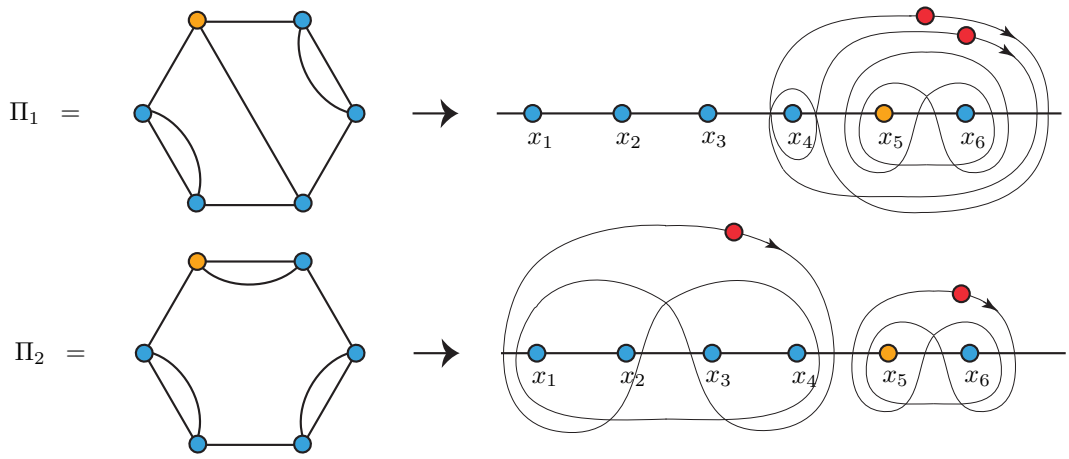

Figure 4.9: The two topologically distinct BACs in the hexagon and their corresponding integration contour choices. The bottom-left vertex of the hexagon is sent to the leftmost point on the real axis, and moving counterclockwise around the hexagon corresponds to moving rightwards along the real axis.

of double integrals that integrate along the individual sides of $\mathcal{H}$. The result is simplest if we place the one conjugate charge at x_5. For $i, j \in \{1, \dots, 6\}$ with $i \neq j$, we let

$$I_{ij} := \left| \mathcal{I}_2 \left(\beta_{mn} = \begin{cases} -4/\kappa & m \neq 5 \\ 12/\kappa - 2 & m = 5 \end{cases}; \gamma_{pq} = \frac{8}{\kappa} \begin{vmatrix} [x_{i-1}, x_i] \\ [x_{j-1}, x_j] \end{vmatrix} \middle| x_1, \dots, x_6 \right) \right|, \tag{4.38}$$

where the Coulomb gas integral $\mathcal{I}_M$ is defined in (2.10). The absolute value sign eliminates a phase that is independent of $x_1, \dots, x_6$. We note that $I_{ij} = I_{ji}$ by Fubini's theorem. Now if we momentarily suppose that u_1 is frozen at a specific location in (x_5, x_6), then the integration along Γ_2 decomposes into (figure 4.10)

$$\begin{aligned} &e^{4\pi i/\kappa} J_{x_4}^{x_5} + e^{-8\pi i/\kappa} J_{x_5}^{u_1} + e^{-16\pi i/\kappa} J_{u_1}^{x_6} - e^{-28\pi i/\kappa} J_{x_4}^{x_5} - e^{-16\pi i/\kappa} J_{x_5}^{u_1} - e^{-8\pi i/\kappa} J_{u_1}^{x_6} \\ &+ e^{-36\pi i/\kappa} J_{x_4}^{x_5} + e^{-24\pi i/\kappa} J_{x_5}^{u_1} + e^{-16\pi i/\kappa} J_{u_1}^{x_6} - e^{-4\pi i/\kappa} J_{x_4}^{x_5} - e^{-16\pi i/\kappa} J_{x_5}^{u_1} - e^{-24\pi i/\kappa} J_{u_1}^{x_6}. \end{aligned} \tag{4.39}$$

Here, J_a^b is the magnitude of the integrand of I_{ij} with u_1 frozen at a location in (x_5, x_6)

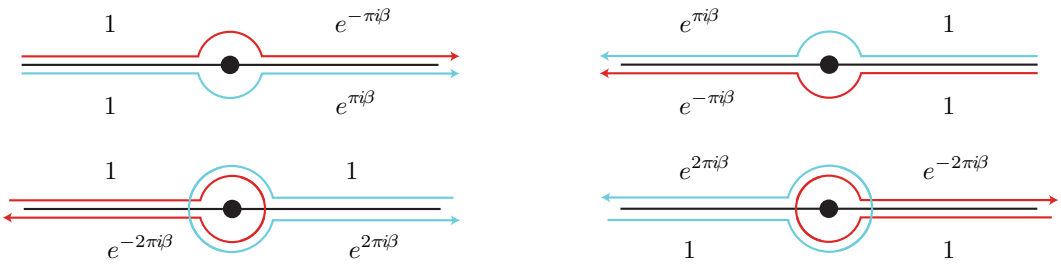

Figure 4.10: A summary of the phase factors accrued as an integration contour winds either $\pm\pi$ or $\pm 2\pi$ radians around a branch point with monodromy factor $e^{2\pi i\beta}$.

and with u_2 integrated from a to b. This may also be written as

$$2i \sin\left(\frac{4\pi}{\kappa}\right)(1 - e^{-32\pi i/\kappa})J^{x_5}_{x_4} + (e^{-8\pi i/\kappa} - 2e^{-16/\pi i/\kappa} + e^{-24\pi i/\kappa})(J^{u_1}_{x_5} - J^{x_6}_{u_1}). \quad (4.40)$$

Now, the integrations of $J^{u_1}_{x_5}$ and $J^{x_6}_{u_1}$ with respect to u_1 from x_5 to x_6 are equal. Thus, by integrating u_1 along $[x_5, x_6]$, we find that (figure 4.11)

$$\mathcal{I}_2(\Gamma_1, \Gamma_2) \propto I_{56}. \quad (4.41)$$

The correct normalization is found by multiplying the right side by $(x_4 - x_3)^{6/\kappa - 1}$, sending $x_4 \to x_3$, and requiring that we recover the rectangle crossing weight Π_1 with $x_3 \mapsto x_5$ and $x_4 \mapsto x_6$ in the limit. We thus find

$$\Pi_1 = n^2 I_{56} \prod_{\substack{i<j \\ i,j\neq 5}}^{6} |x_j - x_i|^{2/\kappa} \prod_{i\neq 5}^{6} |x_5 - x_i|^{1-6/\kappa}. \quad (4.42)$$

Next, we calculate the crossing weight Π_2 for the BAC event λ_2. We rely on techniques explained in section 1.2.9 to determine the appropriate contours. The bottom hexagon in figure 4.9 illustrates λ_2, and we see that $(x_1, x_2), (x_3, x_4)$ and (x_5, x_6) must be two-leg intervals. Before we introduce any contours, we also see that x_5 is the endpoint of two adjacent identity intervals since it bears the conjugate charge. To convert (x_5, x_6) into a two-leg interval, we entwine x_5 and x_6 with a Pochhammer

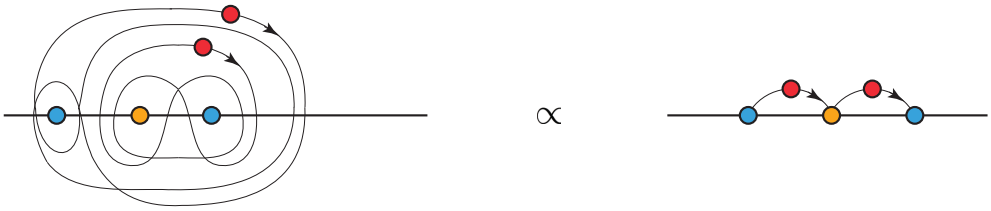

Figure 4.11: Integration around the nested pair of Pochhammer contours shown on the left is proportional to performing the first integration along the right interval and the second integration along the left interval.

contour Γ_1. On the other hand, (x_1, x_2) and (x_3, x_4) are already two-leg intervals since neither of their endpoints bear the conjugate charge. To preserve this feature, we require Γ_2 to not cross these intervals. Next, $(x_6, x_1), (x_2, x_3)$ and (x_4, x_5) must be zero-leg intervals. Prior to choosing Γ_2, (x_2, x_3) is a two-leg interval, and to convert it into a zero-leg interval, we let Γ_2 cross (x_2, x_3). The simplest way to satisfy these requirements is by entwining (x_1, x_2) and (x_3, x_4) with a Pochhammer contour Γ_2. This choice is consistent with the requirement that we find a two-leg operator when we send $x_2, \ldots, x_4 \to x_1$ since the net charge of this fusion is $-4\alpha_-/2 + \alpha_- = \alpha^-_{1,3}$.

When $\kappa > 4$, we can decompose Π_2 into a linear combination of the I_{ij}. As we observed earlier, Γ_1 can be replaced by an integration over $[x_5, x_6]$. If we make this replacement and decompose the integration along Γ_2 into integrations along $[x_1, x_2], [x_2, x_3]$, and $[x_3, x_4]$, then we find

$$\begin{aligned}\mathcal{I}_2(\Gamma_1, \Gamma_2) \propto\ & e^{4\pi i/\kappa} I_{25} + e^{8\pi i/\kappa} I_{35} + e^{12\pi i/\kappa} I_{45} - e^{20\pi i/\kappa} I_{25} - e^{24\pi i/\kappa} I_{35} - e^{20\pi i\kappa} I_{45} \\ & + e^{12\pi i/\kappa} I_2 + e^{8\pi i/\kappa} I_{35} + e^{4\pi i\kappa} I_{45} - e^{-4\pi i/\kappa} I_{25} - e^{-8\pi i/\kappa} I_{35} - e^{-4\pi i/\kappa} I_{45}, \quad (4.43)\end{aligned}$$

which may also be written as (figure 4.12)

$$\mathcal{I}_2(\Gamma_1, \Gamma_2) \propto (e^{4\pi i/\kappa} - e^{20\pi i/\kappa} + e^{12\pi i/\kappa} - e^{-4\pi i/\kappa})[I_{26} + I_{46} - nI_{36}]. \quad (4.44)$$

The correct normalization is found by multiplying the right side by $(x_3 - x_2)^{6/\kappa - 1}$,

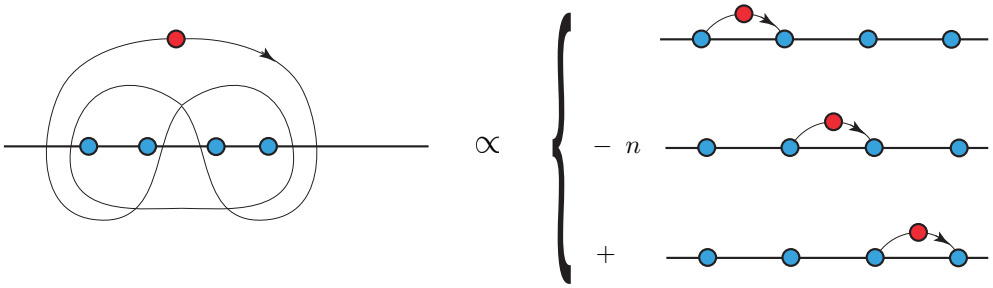

Figure 4.12: The decomposition of the integration along the left Pochhammer contour for the hexagon crossing weight Π_2 (figure 4.9).

sending $x_3 \to x_2$, and requiring that we recover the rectangle crossing weight Π_1 with $x_2 \mapsto x_4, x_3 \mapsto x_5$, and $x_4 \mapsto x_6$ in the limit. We thus find

$$\Pi_2 = \frac{n^2}{n^2-2}[nI_{36} - I_{26} - I_{46}] \prod_{\substack{i<j \\ i,j\neq 5}}^{6} |x_j - x_i|^{2/\kappa} \prod_{i\neq 5}^{6} |x_5 - x_i|^{1-6/\kappa}. \tag{4.45}$$

4.4.3 Crossing weights in octagons

There are $C_4 = 14$ possible BACs in an octagon $\mathcal{O}$, and they can be grouped into the three topologically distinct class shown in figure 4.13. We compute one weight per class as the others can be found by rotating $\mathcal{O}$.

The vertices of $\mathcal{O}$ in figure 4.9 are sent to real numbers so that moving counterclockwise around $\mathcal{O}$ corresponds to moving rightward along the real axis, and the bottom-left vertex is sent to x_1. From the top octagon in the figure, we see that Π_1 is a four-leg solution. According to section 3.1, we must entwine x_7 and x_8 with a Pochhammer contour Γ_1, we must entwine Γ_1 and x_6 with a second Pochhammer contour Γ_2, and we must entwine Γ_2 and x_5 with a third Pochhammer contour Γ_3 to arrive with Π_1.

When $\kappa > 4$, we can decompose the triple integral in Π_1 into a linear combination triple integrals along the individual sides of $\mathcal{O}$. For this purpose, we will use the

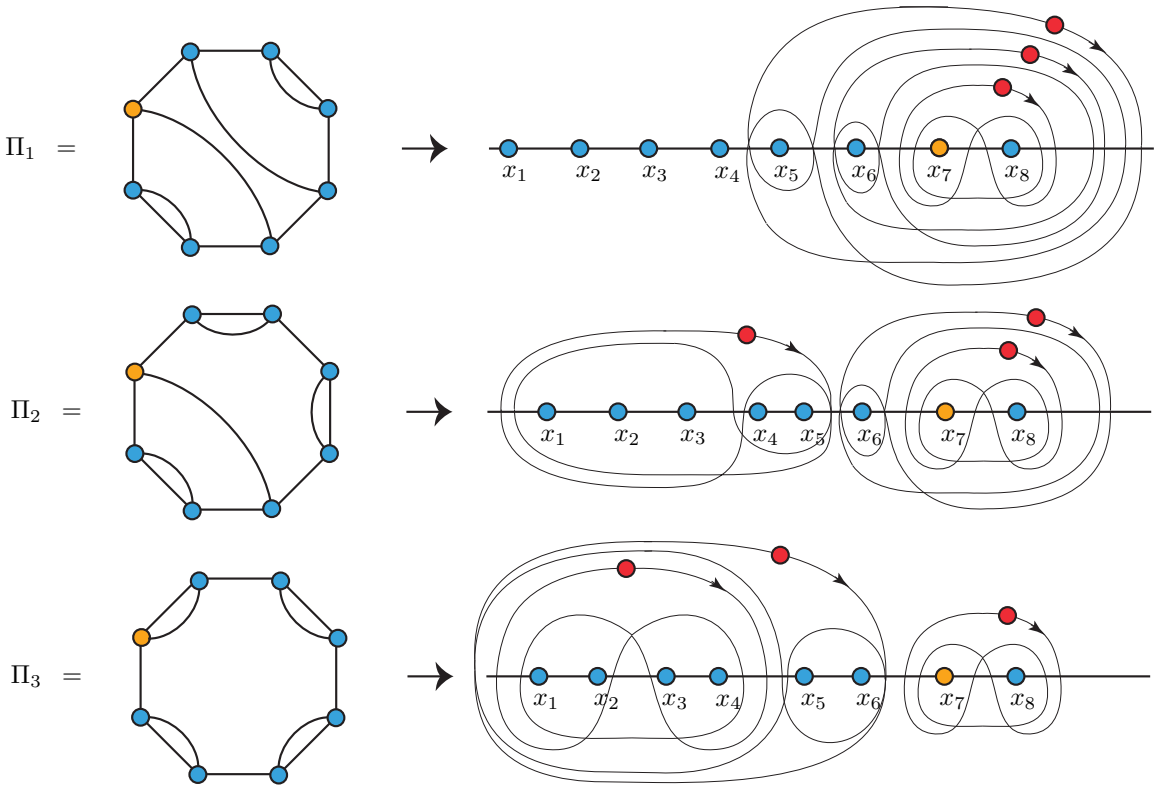

Figure 4.13: The three topologically distinct BACs in the octagon and their corresponding integration contour choices. The bottom-left vertex of the octagon is sent to the leftmost point on the real axis, and moving counterclockwise around the octagon corresponds to moving rightwards along the real axis.

integral

$$I_{ijk} := \left| \mathcal{I}_3 \left(\beta_{mn} = \left\{ \begin{array}{ll} -4/\kappa & m \neq 7 \\ 12/\kappa - 2 & m = 7 \end{array} \right\}; \gamma_{pq} = \frac{8}{\kappa} \left| \begin{array}{l} [x_{i-1}, x_i] \\ [x_{j-1}, x_j] \\ [x_{k-1}, x_k] \end{array} \right| x_1, \ldots, x_8 \right) \right|, \tag{4.46}$$

defined for $i, j, k \in \{1, \ldots, 8\}$, $i \neq j \neq k$. Again, the absolute value sign eliminates a phase that is independent of $x_1, \ldots, x_8$. We note that I_{ijk} is invariant under permutation of its indices by Fubini's theorem. We will also use I_{iik}, defined by

$$I_{iik} := |\mathcal{I}_3([x_{i-1}, u_2], [x_{i-1}, x_i], [x_{k-1}, x_k])|, \tag{4.47}$$

where u_2 is the integration variable that is integrated along $[x_{i-1}, x_i]$. As we observed in the case of the hexagon, the double integration over the nested pair $\Gamma_2 \times \Gamma_1$ can be replaced by a double integration along $[x_6, x_7] \times [x_7, x_8]$. If we momentarily suppose that u_1 and u_2 are frozen at specific locations in (x_7, x_8) and (x_6, x_7) respectively, then the integration along Γ_3 decomposes into

$$+e^{4\pi i/\kappa} J^{x_6}_{x_5} + e^{8\pi i/\kappa} J^{u_2}_{x_6} + J^{x_7}_{u_2} + e^{-12\pi i/\kappa} J^{u_1}_{x_7} + e^{-20\pi i/\kappa} J^{x_8}_{u_1} \tag{4.48}$$

$$-e^{-36\pi i/\kappa} J^{x_6}_{x_5} - e^{-40\pi i/\kappa} J^{u_2}_{x_6} - e^{-32\pi i/\kappa} J^{x_7}_{u_2} - e^{-20\pi i/\kappa} J^{u_1}_{x_7} - e^{-12\pi i/\kappa} J^{x_8}_{u_1} \tag{4.49}$$

$$+e^{-44\pi i/\kappa} J^{x_6}_{x_5} + e^{-48\pi i/\kappa} J^{u_2}_{x_6} + e^{-40\pi i/\kappa} J^{x_7}_{u_2} + e^{-28\pi i/\kappa} J^{u_1}_{x_7} + e^{-20\pi i/\kappa} J^{x_8}_{u_1} \tag{4.50}$$

$$-e^{-4\pi i/\kappa} J^{x_6}_{x_5} - J^{u_2}_{x_6} - e^{-8\pi i/\kappa} J^{x_7}_{u_2} - e^{-20\pi i/\kappa} J^{u_1}_{x_7} - e^{-28\pi i/\kappa} J^{x_8}_{u_1}, \tag{4.51}$$

where J^b_a is the magnitude of the integrand of I_{ijk} with u_1 and u_2 frozen at locations in (x_7, x_8) and (x_6, x_7) respectively and with u_3 integrated from a to b. This can also be written as

$$\begin{aligned} 2i \sin\left(\frac{4\pi}{\kappa}\right) [&(1 - e^{-40\pi i/\kappa}) J^{x_6}_{x_5} + (1 - e^{-40\pi i/\kappa})(e^{4\pi i/\kappa} + e^{-4/\pi i/\kappa}) J^{u_2}_{x_6} \\ &+ (e^{-4\pi i/\kappa} - e^{-36/\pi i/\kappa})(J^{x_7}_{u_2} - J^{u_2}_{x_6}) + (e^{-16\pi i/\kappa} - e^{-24/\pi i/\kappa})(J^{u_1}_{x_7} - J^{x_8}_{u_1})]. \end{aligned} \tag{4.52}$$

Now, the integrations of $J^{u_1}_{x_7}$ and $J^{x_8}_{u_1}$ (reps. $J^{x_7}_{u_2}$ and $J^{u_2}_{x_6}$) with respect to u_1 (resp. u_2) from x_7 to x_8 (resp. x_6 to x_7) are equal. Thus, by integrating u_1 and u_2 along $[x_7, x_8]$ and $[x_6, x_7]$ respectively, we find that (figure 4.14)

$$\mathcal{I}_3(\Gamma_1, \Gamma_2, \Gamma_3) \propto \mathcal{I}_3([x_6, x_7], [x_7, x_8], \Gamma_3) \tag{4.53}$$

$$\propto I_{678} - n I_{778}. \tag{4.54}$$

The correct normalization is found by multiplying the right side by $(x_5 - x_4)^{6/\kappa - 1}$, sending $x_5 \to x_4$, and requiring that we recover the hexagon crossing weight Π_1 with

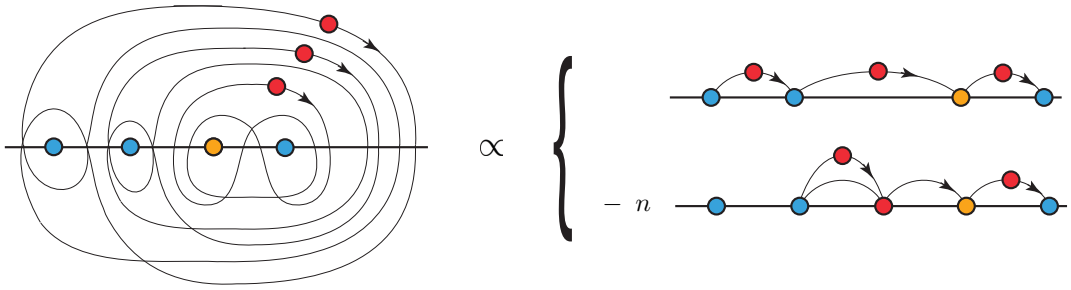

Figure 4.14: Integration around the three nested Pochhammer contours shown on the left is proportional to the difference of the two integrations shown on the right.

$x_4 \mapsto x_6, x_5 \mapsto x_7, x_6 \mapsto x_8$ in the limit. We thus find

$$\Pi_1 = n^3(I_{678} - nI_{778}) \prod_{\substack{i<j \\ i,j\neq 7}}^{8} |x_j - x_i|^{2/\kappa} \prod_{i\neq 7}^{8} |x_7 - x_i|^{1-6/\kappa}. \tag{4.55}$$

The second crossing weight is more complicated. From figure 4.13, we see that $(x_1, x_2), (x_2, x_3), (x_4, x_5), (x_6, x_7)$, and (x_7, x_8) must be two-leg intervals. Prior to choosing contours, (x_6, x_7) and (x_7, x_8) start as identity intervals in (2.9), and in order to convert them into two-leg intervals, we choose Γ_1 and Γ_2 as in Π_1. Next, $(x_1, x_2), (x_2, x_3)$ and (x_4, x_5) start as two-leg intervals, and to preserve this, Γ_3 must not cross any of them. On the other hand, (x_3, x_4) and (x_5, x_6) must be zero-leg intervals of Π_2. Because they start as two-leg intervals, a contour must cross them in order to convert them into zero-leg intervals. In particular, Γ_3 must cross (x_3, x_4). The simplest way to satisfy these requirements is by entwining $[x_1, x_3]$ and $[x_4, x_5]$ with a Pochhammer contour Γ_3. This choice is consistent with the requirement that we find a three-leg operator when we send $x_2, \dots x_5 \to x_1$ since the net charge of this fusion is $-5\alpha_-/2 + \alpha_- = \alpha^-_{1,4}$.

When $\kappa > 4$, we can decompose Π_2 into a linear combination of the I_{ijk}. As we observed earlier, the integration over $\Gamma_2 \times \Gamma_1$ can be replaced by a double integration over $[x_6, x_7] \times [x_7, x_8]$. If we decompose the integration along Γ_3 into integrations

along $[x_1, x_2], \ldots, [x_4, x_5]$, then we find

$$\begin{aligned}
\mathcal{I}_3(\Gamma_1, \Gamma_2, \Gamma_3) \quad \propto \quad & e^{4\pi i/\kappa} I_{278} + e^{8\pi i/\kappa} I_{378} + e^{12\pi i/\kappa} I_{478} + e^{16\pi i/\kappa} I_{578} && (4.56)\\
& - e^{20\pi i/\kappa} I_{278} - e^{24\pi i/\kappa} I_{378} - e^{28\pi i/\kappa} I_{478} - e^{24\pi i/\kappa} I_{578} && (4.57)\\
& + e^{12\pi i/\kappa} I_{278} + e^{8\pi i/\kappa} I_{378} + e^{4\pi i/\kappa} I_{478} + I_{578} && (4.58)\\
& - e^{-4\pi i/\kappa} I_{278} - e^{-8\pi i/\kappa} I_{378} - e^{-12\pi i/\kappa} I_{478} - e^{-8\pi i/\kappa} I_{578}. && (4.59)
\end{aligned}$$

After factoring out a common phase of $e^{8\pi i/\kappa}$, we can rewrite this as

$$\mathcal{I}_3(\Gamma_1, \Gamma_2, \Gamma_3) \propto e^{8\pi i/\kappa}(n^2-4)[n(I_{278} - nI_{378}) + (n^2-1)(nI_{478} - I_{578})]. \qquad (4.60)$$

The correct normalization is found by multiplying the right side by $(x_4 - x_3)^{6/\kappa - 1}$, sending $x_4 \to x_3$, and requiring that we recover the hexagon crossing weight Π_1 with $x_3 \mapsto x_5, x_4 \mapsto x_6, x_5 \mapsto x_7$, and $x_6 \mapsto x_8$ in the limit. We thus find

$$\begin{aligned}
\Pi_2 = \frac{n^3}{n^4 - 3n^2 + 1}[n(I_{278} - nI_{378}) + (n^2-1)(nI_{478} - I_{578})] \\
\times \prod_{\substack{i<j \\ i,j\neq 7}}^{8} |x_j - x_i|^{2/\kappa} \prod_{i\neq 7}^{8} |x_7 - x_i|^{1-6/\kappa}. \qquad (4.61)
\end{aligned}$$

The third crossing weight is the most complicated. To begin, we choose Γ_1 as in Π_1 and Π_2 to convert (x_7, x_8) into a two-leg interval. Next, $(x_1, x_2), (x_3, x_4)$, and (x_5, x_6) must be two-leg intervals, and because they start off as such in (2.9), neither Γ_2 nor Γ_3 can cross these intervals. Moreover, $(x_8, x_1), (x_2, x_3), (x_4, x_5)$ and (x_6, x_7) must be zero-leg intervals, but because they start as two-leg intervals, an integration contour must cross each of them to convert them into two-leg intervals. In particular, Γ_2 or Γ_3 must cross (x_2, x_3) and (x_4, x_5). To satisfy these requirements, we entwine $[x_1, x_2]$ and $[x_3, x_4]$ with a Pochhammer contour Γ_2, and we entwine $[x_5, x_6]$ and Γ_2 with a Pochhammer contour Γ_3. This choice is consistent with the requirement that

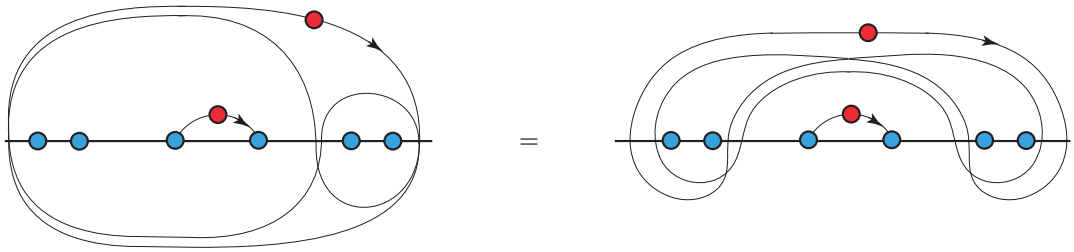

Figure 4.15: We decompose the nested Pochhammer contour for the octagon crossing weight Π_3 into three integrations, one of which is shown on the left. Using identity (3.3), we may deform the outer Pochhammer contour so that it does not contain any of these three integrations, as shown on the right.

we find a two-leg operator when we send $x_2, \ldots, x_6 \to x_1$ since the net charge of this fusion is $-6\alpha_-/2 + 2\alpha_- = \alpha_{1,3}^-$. We also note a second option to entwine $[x_3, x_4]$ and $[x_5, x_6]$ with a Pochhammer contour Γ_2 and entwine $[x_1, x_2]$ and Γ_2 with another Pochhammer contour Γ_3. Using lemma II.17, we can show that both options are the same to within a constant.

Now we decompose Π_3 into a linear combination of the I_{ijk}. The decomposition for Γ_2 was done in (4.44), and we found three terms (figure 4.12). The first term integrates along $[x_1, x_2]$, the second integrates along $[x_2, x_3]$, and the last integrates along $[x_3, x_4]$. Using identity (3.3), we can deform Γ_3 around each of these integrations so that Γ_3 entwines $[x_5, x_6]$ with $[x_3, x_4]$, with x_1 and x_4, and with $[x_1, x_2]$ in the first, second, and third terms respectively (figure 4.15). Thus Γ_3 can be decomposed in the same way as Γ_2 in each term, giving nine terms total. Using the identity shown in figure 4.16, we find the decomposition

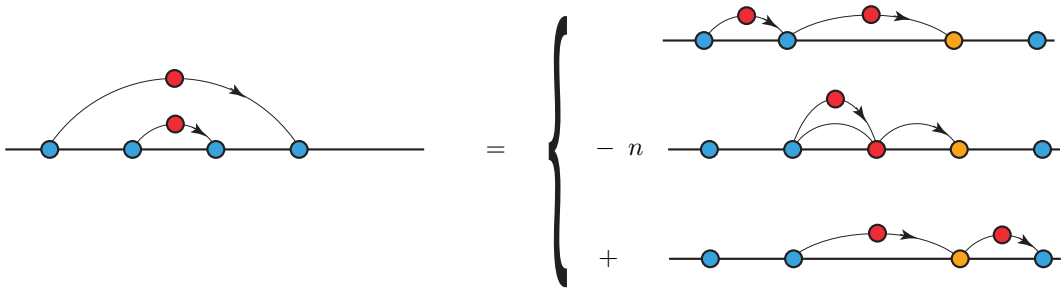

Figure 4.16: The pair of nested integration contours shown on the left decomposes into the sum of integrations shown on the right.

$$\mathcal{I}_3(\Gamma_1,\Gamma_2,\Gamma_3) \propto I_{468} - nI_{458} + n^2 I_{448} - 2nI_{348} + 2I_{248} \\ - nI_{368} + n^2 I_{358} + n^2 I_{338} - nI_{238} + I_{268} - nI_{258}. \quad (4.62)$$

The correct normalization is found by multiplying the right side by $(x_3 - x_2)^{6/\kappa-1}$, sending $x_3 \to x_2$, and requiring that we recover the hexagon crossing weight Π_2 with $x_2 \mapsto x_4, \ldots, x_6 \mapsto x_8$ in the limit. We thus find

$$\Pi_3 = \prod_{\substack{i<j \\ i,j\neq 7}}^{8} |x_j - x_i|^{2/\kappa} \prod_{i\neq 7}^{8} |x_7 - x_i|^{1-6/\kappa} \\ \times \frac{n^3}{(n^2-2)^2}[I_{468} - nI_{458} + n^2 I_{448} - 2nI_{348} + 2I_{248} \\ - nI_{368} + n^2 I_{358} + n^2 I_{338} - nI_{238} + I_{268} - nI_{258}]. \quad (4.63)$$

Occasionally, simpler expressions can be found by working with collections of solutions in which the conjugate charge not always located at the same vertex. Also, we could consider special cases with extra symmetry, such as regular polygons, that require many of these integrals to be equal. These strategies may simplify the crossing-weight formulas that we have encountered, but beyond the octagon where these calculations become extremely cumbersome, they give limited help. For this reason, we will not pursue them here.

4.5 Transforming the universal partition functions

In this section, we transform our crossing partition functions into partition functions for the appropriate $2N$-sided polygon, but before we address polygons, we consider more general simply connected domains. The Riemann mapping theorem guarantees the existence of a conformal bijection f from the upper half-plane onto a simply connected domain $\mathcal{D} \neq \mathbb{C}$. We further suppose that f extends to and bijectively sends

the extended real axis onto $\partial\mathcal{D}$ and is conformal at each BCC (in the sense of sending infinitesimal half-disks onto infinitesimal half-disks). If $\mathcal{D} = \mathbb{H}$, then for a given BAC event $\lambda \in \mathrm{AC}_N$ and FFBC event $\varsigma \in \mathrm{BC}_N$, we have (4.6)

$$Z_{(\lambda|\varsigma)}/Z_f \underset{\epsilon_i \to 0}{\sim} c_1^{2N} \epsilon_1^{\theta_1} \dots \epsilon_{2N}^{\theta_1} \Upsilon_{(\lambda|\varsigma)}, \tag{4.64}$$

where x_i marks the center of the disk of radius ϵ_i that contains the i-th BCC along the real axis. If $\mathcal{D}$ is some other domain and f is as described above, then under this mapping, $\epsilon_i \mapsto \delta_i(w_i) = |\partial f(x_i)|\epsilon_i$ where $w_i = f(x_i)$. To compensate this change, $\Upsilon_{(\lambda|\varsigma)}$ transforms covariantly (1.146),

$$\Upsilon^{\mathcal{D}}_{(\lambda|\varsigma)}(w_1, \dots, w_{2N}) = |\partial f(x_1)|^{-\theta_1} \dots |\partial f(x_{2N})|^{-\theta_1} \Upsilon_{(\lambda|\varsigma)}(x_1, \dots, x_{2N}), \tag{4.65}$$

so that $Z_{(\lambda|\varsigma)}$ is invariant under the transformation:

$$Z^{\mathcal{D}}_{(\lambda|\varsigma)}(w_1, \dots, w_{2N})/Z_f = Z_{(\lambda|\varsigma)}(x_1, \dots, x_{2N})/Z_f. \tag{4.66}$$

For the domain $\mathcal{D}$, we now have

$$Z^{\mathcal{D}}_{(\lambda|\varsigma)}/Z_f \underset{\delta_i(w_i) \to 0}{\sim} c_1^{2N} \delta_1(w_1)^{\theta_1} \dots \delta_{2N}(w_{2N})^{\theta_1} \Upsilon^{\mathcal{D}}_{(\lambda|\varsigma)}. \tag{4.67}$$

The free partition function Z_f does not depend on $x_1, \dots, x_{2N}$ as its BC is free, so it does not transform.

The partition function $Z^{\mathcal{D}}_{(\lambda|\varsigma)}$ is unnatural because the radii $\delta_i(w_i)$ are not constant but depend on the centers of their respective disks. A more natural partition function to use is (4.67) with each $\delta_i(w_i)$ replaced by a fixed, small number δ_i so that we can confine each BCC to a uniformly small segment in $\partial\mathcal{D}$. This modifies $Z^{\mathcal{D}}_{(\lambda|\varsigma)}$ to a new

partition function $\mathcal{Z}^{\mathcal{D}}_{(\lambda|\varsigma)}$ given by

$$\mathcal{Z}^{\mathcal{D}}_{(\lambda|\varsigma)}/Z_f \underset{\delta_i\to 0}{\sim} c_1^{2N}\delta_1^{\theta_1}\dots\delta_{2N}^{\theta_1}\Upsilon^{\mathcal{D}}_{(\lambda|\varsigma)}. \tag{4.68}$$

The partition function $\mathcal{Z}^{\mathcal{D}}_{\varsigma}$ follows from a similar modification of $Z^{\mathcal{D}}_{\varsigma}$ and is found by summing $\mathcal{Z}^{\mathcal{D}}_{(\lambda|\varsigma)}$ over all BAC events $\lambda \in \mathrm{AC}_N$.

Now we may propose the following more natural definition of a crossing probability for $\mathcal{D}$:

$$\chi^{\mathcal{D}}_{(\lambda|\varsigma)} := \mathcal{Z}^{\mathcal{D}}_{(\lambda|\varsigma)}/\mathcal{Z}^{\mathcal{D}}_{\varsigma}. \tag{4.69}$$

We see that, with this definition, the crossing probability is indeed conformally invariant:

$$\chi^{\mathcal{D}}_{(\lambda|\varsigma)} := \frac{\mathcal{Z}^{\mathcal{D}}_{(\lambda|\varsigma)}}{\mathcal{Z}^{\mathcal{D}}_{\varsigma}} = \frac{Z_{(\lambda|\varsigma)}}{Z_{\varsigma}} = \chi_{(\lambda|\varsigma)}. \tag{4.70}$$

More generally, we have $\chi^{\mathcal{D}_1}_{(\lambda|\varsigma)} = \chi^{\mathcal{D}_2}_{(\lambda|\varsigma)}$ for any two simply connected domains $\mathcal{D}_1$ and $\mathcal{D}_2$ that are images of respective conformal bijections $f_1 : \mathbb{H} \to \mathcal{D}_1$ and $f_2 : \mathbb{H} \to \mathcal{D}_2$ that satisfy the requirements described above. Apparently, the adjustment of $Z^{\mathcal{D}}_{(\lambda|\varsigma)}$ to $\mathcal{Z}^{\mathcal{D}}_{(\lambda|\varsigma)}$ does not affect our crossing formula. However, this adjustment will be relevant to the calculation of pinch-point densities in the next chapter. For this reason, we mention it here.

Now we suppose that f does not does not conformally extend to the BCCs on the real axis but that it does conformally extend to a deleted neighborhood of each BCC. We have in mind that $\mathcal{D}$ is simply connected and its boundary is smooth except at a finite number of corner points, and if w_i is located at a corner point, then $|\partial f(x_i)|$ is infinite or zero. In this event, the radius $\delta_i(w_i)$ is infinite or zero, and the asymptotic statement $\delta_i(w_i) \to 0$ in (4.67) has no meaning. The replacement $\delta_i(w_i) \mapsto \delta_i$ would seem to remedy this fact. However, the product $\delta_1(w_1)^{\theta_1}\dots\delta_{2N}(w_{2N})^{\theta_1}\Upsilon^{\mathcal{D}}_{(\lambda|\varsigma)}$ is already finite and nonzero, a quality that such a replacement would spoil. Instead, we remedy this problem by proposing an appropriate redefinition of the universal

partition function.

Before we propose the redefinition, we note that the crossing formula (4.32) is not affected by the situation in which some or all BCCs occur at corner points. Indeed, (4.70) remains true as we let w_i approach a corner point due to the cancellation of the identical derivative factors appearing in the numerator and denominator. For this reason, what follows may seem superfluous, and if we simply wish to prove the invariance of the crossing formula, then this is true. But because universal partition functions are physically relevant in their own, we propose a good redefinition of them for these cases anyway. This is the main point of this section.

Now we propose a redefinition of the universal partition functions to accommodate the cases where the BCCs occur at corner points. We specialize to the situation where $\mathcal{D}$ is a $2N$-sided polygon $\mathcal{P}$ with w_i the i-th vertex. In this situation, f is the Schwarz-Christoffel transformation [32]

$$f(z) = a \int_{x_1}^{z} (x_1 - \zeta)^{\phi_1/\pi - 1} \dots (x_{2N} - \zeta)^{\phi_{2N}/\pi - 1} \, d\zeta + b, \tag{4.71}$$

where ϕ_i is the interior angle of $\mathcal{P}$ at the i-th vertex, x_i is the preimage of w_i, and a and b are unspecified complex constants that determine the position, size, and orientation of $\mathcal{P}$ in the complex plane. The failure of f to be conformal at x_i is manifested by the behavior of its derivative as a point $x_i' > x_i$ approaches x_i. We can express this behavior as a function of the difference $w_i' - w_i$, where $w_i' = f(x_i')$ is slightly shifted away from w_i along the side $[w_i, w_{i+1}]$ of $\mathcal{P}$. That is,

$$w_i' - w_i = \varepsilon_i \exp i \left(\arg(a) + \sum_{j=1}^{i} (\pi - \phi_j) \right), \tag{4.72}$$

for some very small $\varepsilon_i > 0$. Now, w_i' is given by

$$w_i' = f(x_i') = w_i + a \int_{x_i}^{x_i'} (x_1 - \zeta)^{\phi_1/\pi - 1} \dots (x_{2N} - \zeta)^{\phi_{2N}/\pi - 1} \, d\zeta, \tag{4.73}$$

and by introducing the substitution $\zeta(t) = (1-t)x_i + x_i' t$, we immediately find the asymptotic behavior

$$w_i' = f(x_i') \underset{\varepsilon_i \to 0}{\sim} w_i + \frac{a\pi}{\phi_i}(x_i - x_i')^{\phi_i/\pi} \prod_{j \neq i} (x_j - x_i)^{\phi_j/\pi - 1}. \tag{4.74}$$

After isolating $x_i' - x_i$ in terms of $w_i' - w_i$, we can use (4.74) to write $|\partial f(x_i')|$ to leading order in ε_i. We have

$$|\partial f(x_i')| \underset{\varepsilon_i \to 0}{\sim} \left(\frac{|a|\pi}{\phi_i}\right)^{\pi/\phi_i} \left(\frac{\phi_i}{\pi}\varepsilon_i^{1-\pi/\phi_i}\right) \prod_{j \neq i} |x_j - x_i|^{\phi_j/\phi_i - \pi/\phi_i}. \tag{4.75}$$

As we expect, the derivative blows up or vanishes as $\varepsilon_i \to 0$ when $\phi_i \neq \pi$.

Now we use (4.75) to give a proper redefinition of $\Upsilon^{\mathcal{P}}_{(\lambda|\varsigma)}$. The product on the right side of (4.64) evaluated at $x_1', \ldots, x_{2N}'$ may be written as

$$\delta_1 (w_1')^{\theta_1} \ldots \delta_{2N} (w_{2N}')^{\theta_1} \Upsilon^{\mathcal{P}}_{(\lambda|\varsigma)}(w_1', \ldots, w_{2N}'), \tag{4.76}$$

where, as usual, we have used the covariant transformation rule (4.65) and also $\delta_i(w_i') = \epsilon_i |\partial f(x_i')|$. Next, we make the replacement

$$\delta_i(w_i) = |\partial f(x_i)| \epsilon_i \quad \longrightarrow \quad \tilde{\delta}_i(w_i) = \epsilon_i \lim_{\varepsilon_i \to 0} |\partial f(x_i')| \left(\frac{\pi}{\phi_i}\varepsilon_i^{\pi/\phi_i - 1}\right), \tag{4.77}$$

and we also make the replacement

$$\begin{aligned} &\Upsilon^{\mathcal{P}}_{(\lambda|\varsigma)}(w_1, \ldots, w_{2N}) = |\partial f(x_1)|^{-\theta_1} \ldots |\partial f(x_{2N})|^{-\theta_1} \Upsilon_{(\lambda|\varsigma)}(x_1, \ldots, x_{2N}) \\ \longrightarrow \quad &\tilde{\Upsilon}^{\mathcal{P}}_{(\lambda|\varsigma)}(w_1, \ldots, w_{2N}) = \lim_{\varepsilon_i \to 0} \left(\frac{\phi_1}{\pi}\varepsilon_1^{1-\pi/\phi_1}\right)^{\theta_1} |\partial f(x_1')|^{-\theta_1} \ldots \\ &\qquad \ldots \left(\frac{\phi_{2N}}{\pi}\varepsilon_{2N}^{1-\pi/\phi_{2N}}\right)^{\theta_1} |\partial f(x_{2N}')|^{-\theta_1} \Upsilon_{(\lambda|\varsigma)}(x_1', \ldots, x_{2N}'). \end{aligned} \tag{4.78}$$

Thus, $\tilde{\delta}_i$ and $\tilde{\Upsilon}^{\mathcal{P}}_{(\lambda|\varsigma)}$ are both finite and nonzero as $\varepsilon_i \to 0$, and furthermore

$$\lim_{\varepsilon_i \to 0} \delta_1 (w_1')^{\theta_1} \dots \delta_{2N} (w_{2N}')^{\theta_1} \Upsilon^{\mathcal{P}}_{(\lambda|\varsigma)}(w_1', \dots, w_{2N}') \\ = \tilde{\delta}_1(w_1) \dots \tilde{\delta}_{2N}(w_{2N}) \tilde{\Upsilon}^{\mathcal{P}}_{(\lambda|\varsigma)}(w_1, \dots, w_{2N}). \quad (4.79)$$

(In the limit, we are sending all ε_i to zero simultaneously.) Now we replace the right side of (4.67) with the right side of (4.79), and because each $\tilde{\delta}_i(w_i)$ is finite and nonzero, we may replace each with a number δ_i to obtain the regularized version of (4.68) in the limit $\varepsilon_i \to 0$:

$$\tilde{\mathcal{Z}}^{\mathcal{P}}_{(\lambda|\varsigma)}/Z_f \underset{\delta_i \to 0}{\sim} c_1^{2N} \delta_1^{\theta_1} \dots \delta_{2N}^{\theta_1} \tilde{\Upsilon}^{\mathcal{P}}_{(\lambda|\varsigma)}. \quad (4.80)$$

The regularized universal partition function $\tilde{\Upsilon}^{\mathcal{P}}_{(\lambda|\varsigma)}$ may also be expressed in terms of *corner operators* [45, 76]. For a polygon $\mathcal{P}$ with a vertex at the boundary point w, we define the corner operator $\phi_h^c(w)$ associated with the boundary primary operator $\phi_h(w)$ of conformal weight h by

$$\phi_h^c(w) = \lim_{\varepsilon \to 0} \left(\frac{\phi}{\pi} \varepsilon^{1-\pi/\phi} \right)^h \phi_h(w + \varepsilon). \quad (4.81)$$

Then the replacement in (4.78) is equivalent to replacing all boundary one-leg operators ψ_1 with *corner one-leg operators* ψ_1^c in the correlation function for $\Upsilon^{\mathcal{P}}_{(\lambda|\varsigma)}$:

$$\Upsilon^{\mathcal{P}}_{(\lambda|\varsigma)} = \langle \psi_1(w_1) \dots \psi_1(w_{2N}) \rangle_{\mathcal{P}} \quad \longrightarrow \quad \tilde{\Upsilon}^{\mathcal{P}}_{(\lambda|\varsigma)} = \langle \psi_1^c(w_1) \dots \psi_1^c(w_{2N}) \rangle_{\mathcal{P}}. \quad (4.82)$$

Using (4.78), we write an explicit expression for the regularized universal partition function when all $2N$ interior angles of $\mathcal{P}$ equal $\phi = (N-1)\pi/N$. We typically choose

the parameters for the map (4.71)

$$a = \frac{\phi}{\pi c} x^{1-\phi/\pi} e^{-i(\pi-\phi)}, \quad b = 0, \quad x_1 = 0, \quad x_2 = m_1, \quad \ldots \tag{4.83}$$

$$\ldots, \quad x_{2N-2} = m_{2N-3}, \quad x_{2N-1} = 1, \quad x_{2N} = x \to \infty, \tag{4.84}$$

where c is some unspecified real constant. With these choices, the interior of $\mathcal{P}$ resides in the upper half-plane, x_1 is sent to zero, and the bottom side $[w_1, w_2]$ of $\mathcal{P}$ sits flush against the real axis. From (4.73), we find that as we send $\varepsilon_i \to 0$,

$$x'_1 \sim (c\varepsilon_1)^{N/(N-1)} \prod_j m_j^{1/(N-1)}, \tag{4.85}$$

$$x'_i \sim m_{i-1} + (c\varepsilon_i)^{N/(N-1)} \prod_{j \neq i} |m_j - m_i|^{1/(N-1)}, \quad i = 2, \ldots, 2N-2, \tag{4.86}$$

$$x'_{2N-1} \sim 1 + (c\varepsilon_{2N-1})^{N/(N-1)} \prod_j (1 - m_j)^{1/(N-1)}, \tag{4.87}$$

$$x'_{2N} \sim (c\varepsilon_{2N})^{-N/(N-1)}. \tag{4.88}$$

Because x_{2N} has been sent to infinity, the last point $x'_{2N} < 0$ is not found from (4.73). Instead, by substituting $\zeta(t) = x'_{2N}/t$ into the map (4.71) with parameter choices (4.83-4.84), we find (4.88). By direct substitution into $\partial f(z)$, we also find that

$$|\partial f(x'_{2N})| \underset{\varepsilon_{2N} \to 0}{\sim} c^{N/(N-1)} \varepsilon_{2N}^{2N/(N-1)} \left(\frac{\phi}{\pi} \varepsilon_{2N}^{1-\pi/\phi} \right), \quad \phi = (N-1)\pi/N. \tag{4.89}$$

If we synthesize these results together in (4.78), then we arrive at the following expression for the regularized universal partition function $\tilde{\Upsilon}_{(\lambda|\varsigma)}$ in the equiangular $2N$-sided polygon:

$$\tilde{\Upsilon}^{\mathcal{P}}_{(\lambda|\varsigma)}(m_1, \ldots, m_{2N-3}) = \left[\prod_i m_i \prod_{i<j} (m_j - m_i) \prod_i (1 - m_i) \right]^{(1-6/\kappa)/(N-1)}$$

$$\times\, c^{N(1-6/\kappa)/(N-1)} \lim_{x \to \infty} x^{6/\kappa - 1} \Upsilon_{(\lambda|\varsigma)}(0, m_1, \ldots, m_{2N-3}, 1, x). \tag{4.90}$$

It is evident from the ansatz (2.4) that the limit in (4.90) exists. We may also define a regularized crossing weight $\tilde{\Pi}_k^{\mathcal{P}}$ related to its half-plane version Π_λ as in (4.90) so that (4.10) becomes $\tilde{\Upsilon}_{(\lambda|\varsigma)}^{\mathcal{P}} = n^{m_{\lambda,\varsigma}} \tilde{\Pi}_\lambda^{\mathcal{P}}$. Finally, we can sum over all BAC events $\lambda \in \mathrm{AC}_N$ to find that the adjusted universal partition function $\tilde{\Upsilon}_\varsigma^{\mathcal{P}}$ is related to its half-plane version Υ_ς through (4.90) too.

Now we can propose the following more natural definition of a crossing probability for the $2N$-sided polygon $\mathcal{P}$:

$$\chi_{(\lambda|\varsigma)}^{\mathcal{P}}(w_1, \ldots, w_{2N}) := \frac{\tilde{\mathcal{Z}}_{(\lambda|\varsigma)}^{\mathcal{P}}}{\tilde{\mathcal{Z}}_\varsigma^{\mathcal{P}}} = \frac{\tilde{\Upsilon}_{(\lambda|\varsigma)}^{\mathcal{P}}}{\tilde{\Upsilon}_\varsigma^{\mathcal{P}}}. \tag{4.91}$$

We immediately observe that this new crossing formula equals its half-plane version, as we predicted:

$$\begin{aligned} \chi_{(\lambda|\varsigma)}^{\mathcal{P}}(w_1, \ldots, w_{2N}) &= \frac{\tilde{\Upsilon}_{(\lambda|\varsigma)}^{\mathcal{P}}(m_1, \ldots, m_{2N-3})}{\tilde{\Upsilon}_\varsigma^{\mathcal{P}}(m_1, \ldots, m_{2N-3})} && (4.92) \\ &= \frac{\Upsilon_{(\lambda|\varsigma)}(0, m_1, \ldots, m_{2N-3}, 1, \infty)}{\Upsilon_\varsigma(0, m_1, \ldots, m_{2N-3}, 1, \infty)} && (4.93) \\ &= \chi_{(\lambda|\varsigma)}(0, m_1, \ldots, m_{2N-3}, 1, \infty). && (4.94) \end{aligned}$$

Because $x_1 = 0, x_2 = m_1, \ldots, x_{2N-2} = m_{2N-3}, x_{2N-1} = 1, x_{2N} = \infty$, the cross-ratio η_i, defined in (4.14), equals the parameter m_i. The set of $2N-3$ numbers $\{m_1, \ldots, m_{2N-3}\}$ control the relative side-lengths of $\mathcal{P}$, but they do not control the location, size, or orientation of $\mathcal{P}$ in the complex plane. Thus, the crossing formula is unchanged when we translate, rotate, or dilate $\mathcal{P}$, a fact that must be true in order for it to be conformally invariant.

4.6 Simulation results for crossings in hexagons

In this section, we present computer simulation measurements of the crossing probabilities for an equiangular hexagon harboring a critical Q-state Potts model

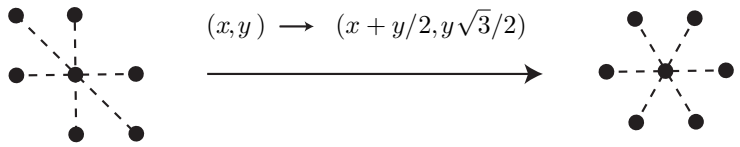

Figure 4.17: The transformation from a square lattice to a triangular lattice. Dotted lines connect the centermost site with its nearest neighbors.

on a triangular lattice with $Q = 1, 2, 3$. We create the triangular lattice from a square lattice as shown in figure 4.17. Our simulations sampled thirty-three hexagons with their bottom and top-left/right (resp. top and bottom-left/right) sides wired (resp. free) and with their side-lengths alternating between two lengths ℓ and ℓ'. In each hexagon, we generated $3,276,800$ samples.

We generate a hexagon $\mathcal{H}$ with the properties described above as the image of the upper half-plane under the conformal mapping (4.71, 4.83-4.84) with $c = 1$. This map is (figure 4.18)

$$f(z) = \frac{2}{3} \int_0^z \zeta^{-1/3}(m_1 - \zeta)^{-1/3}(m_2 - \zeta)^{-1/3}(m_3 - \zeta)^{-1/3}(1 - \zeta)^{-1/3}\, d\zeta \tag{4.95}$$

with $0 < m_1 < m_2 < m_3 < 1 < \infty$ the preimages of the vertices $w_1, \ldots, w_6$ of $\mathcal{P}$. We further have

$$m_1 = \frac{m_2^2}{1 - m_2 + m_2^2}, \quad m_3 = \frac{m_2}{1 - m_2 + m_2^2} \tag{4.96}$$

so that the side-length alternates between two values. We number the vertices of $\mathcal{H}$ starting with the bottom-left endpoint as vertex one and proceeding counterclockwise, so that the first vertex is $w_1 = f(0) = 0$, the second vertex is $w_2 = f(m_1) > 0$,

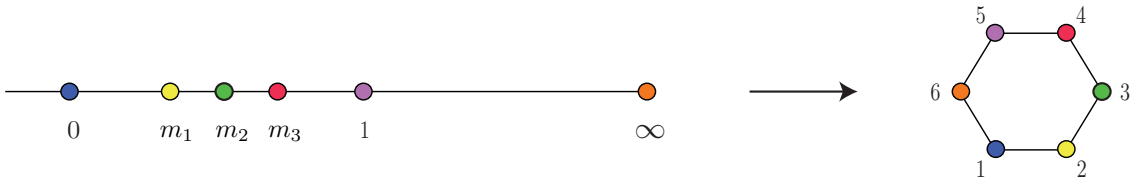

Figure 4.18: The transformation of the upper half-plane to the interior of the rectangle and the hexagon and our enumeration of the vertices of either shape.

the third vertex is $w_3 = f(m_2) \in \mathbb{H}$, etc. Thus, the length of the bottom side is $\ell = w_2 > 0$, and the equation $f(m_1) = \ell$ puts all $\ell \in (0, \infty)$ in one-to-one relation with all $m_1 \in (0, 1)$. We plot our crossing-probability measurements as a function of the ratio

$$R := \frac{\ell}{\ell'} = \frac{f(m_1)}{|f(m_2) - f(m_1)|}. \tag{4.97}$$

We enumerate three of the possible crossing configurations in figure 4.19 so that the k-th configuration corresponds with the BAC event λ_k. In general there are five distinct crossing configurations. However, when the side-length of the hexagon alternates, the probabilities of the three configurations that are some rotation of the $k = 1$ arc connectivity are equal by symmetry. This leaves the three crossing configurations shown in figure 4.19.

In our simulations, we independently wired the bottom and top-left/right sides of each hexagon. The exterior arc connectivity for this FFBC is created from the third hexagon in figure 4.19 by reflecting the boundary arcs from the inside to the outside. So according to our labeling scheme, we are conditioning on the FFBC event ς_3.

Throughout this section, we write $\chi_{(k|k')} := \chi_{(\lambda_k|\varsigma_{k'})}$ for some indexed BAC event $\lambda_k \in \mathrm{AC}_N$ and some indexed FFBC event $\varsigma_{k'} \in \mathrm{BC}_N$. The probabilities $\chi^{\mathcal{H}}_{(1|3)}$ and $\chi^{\mathcal{H}}_{(2|3)}$ of the first two configurations are given by (4.32, 4.94), with the crossing weights given by (4.42) and (4.45) respectively. The probability $\chi^{\mathcal{H}}_{(3|3)}$ of the third configuration is found by rotating the crossing weight Π_2 (i.e., replacing $x_{i+1} \mapsto x_i$, where $x_7 := x_1$). Altogether, we have

$$\chi^{\mathcal{H}}_{(1|3)} = \frac{n^2\Pi_1}{F_3} = \frac{n^4 I_{56}}{I_{24}}, \tag{4.98}$$

$$\chi^{\mathcal{H}}_{(2|3)} = \frac{n\Pi_2}{F_3} = \frac{n^3(nI_{36} - I_{26} - I_{46})}{(n^2-2)I_{24}}, \tag{4.99}$$

$$\chi^{\mathcal{H}}_{(3|3)} = \frac{n^3\Pi_3}{F_3} = \frac{n^5(nI'_{41} - I'_{31} - I'_{51})}{(n^2-2)I_{24}}. \tag{4.100}$$

Figure 4.19: The BACs of the three crossing configurations in a hexagon with alternating side-length. The exterior arc connectivities indicate that the bottom and top-left/right sides are wired in each hexagon.

Here, the I_{ij} and I'_{ij} are given by

$$I_{56} = \left| \int_{m_3}^{1} \int_{1}^{\infty} \dots \, du_1 \, du_2 \right|, \qquad I_{24} = \left| \int_{0}^{m_1} \int_{m_2}^{m_3} \dots \, du_1 \, du_2 \right|, \tag{4.101}$$

$$I_{36} = \left| \int_{m_1}^{m_2} \int_{1}^{\infty} \dots \, du_1 \, du_2 \right|, \qquad I_{26} = \left| \int_{0}^{m_1} \int_{1}^{\infty} \dots \, du_1 \, du_2 \right|, \tag{4.102}$$

$$I_{46} = \left| \int_{m_2}^{m_3} \int_{1}^{\infty} \dots \, du_1 \, du_2 \right|, \qquad I'_{41} = \left| \int_{m_2}^{m_3} \int_{-\infty}^{0} \dots \, du_1 \, du_2 \right|, \tag{4.103}$$

$$I'_{31} = \left| \int_{m_1}^{m_2} \int_{-\infty}^{0} \dots \, du_1 \, du_2 \right|, \qquad I'_{51} = \left| \int_{m_3}^{1} \int_{-\infty}^{0} \dots \, du_1 \, du_2 \right|, \tag{4.104}$$

with the integrand of the I_{ij} being

$$(u_2 - u_1)^{8/\kappa} \prod_{i=1,2} u_i^{-4/\kappa} (u_i - 1)^{12/\kappa - 2} \prod_{j=1}^{3} (u_i - m_j)^{-4/\kappa} \tag{4.105}$$

and with the integrand of the I'_{ij} being

$$(u_2 - u_1)^{8/\kappa} \prod_{i=1,2} u_i^{-4/\kappa} (u_i - 1)^{-4/\kappa} \prod_{j=1}^{3} (u_i - m_j)^{-4/\kappa}. \tag{4.106}$$

In the Q-state Potts model with $Q \in \{1, 2, 3, 4\}$, the function $\chi^{\mathcal{H}}_{(k|3)}$ equals the probability that the FK boundary clusters connect the independently wired sides of the hexagon as in the k-th crossing configuration (or BAC) shown in figure 4.19 conditioned on the independent wiring FFBC event. We tested this prediction by sampling FK clusters of the $Q = 1, 2, 3$ Potts models on the triangular lattice, which

corresponded with the dense phase SLE speeds $\kappa = 6, 16/3$, and $24/5$ respectively (table 1.1), and tracking the frequency of each crossing configuration. We found very good agreement with our measurements. (Actually, we only sampled percolation hull-walks in the case $Q = 1$ since this case corresponds with percolation. Details are presented in the following section.)

In addition, the function $\chi^{\mathcal{H}}_{(k|\varsigma)}$ equals the probability that the Potts model spin boundary clusters connect the wired sides of the hexagon as in the k-th crossing configuration shown in figure 4.19. Here, ς must be the mutual-wiring boundary condition event, as explained in the last paragraph of section 4.3, and this is the FFBC event ς_2 according to figure 4.19. Furthermore, the SLE speeds of the spin cluster interfaces belong to the dilute phase (table 1.1), so the integrals in (4.101-4.104) diverge. We can remedy this problem by replacing the simple integration contours with Pochhammer contours, but because the integrals that follow are difficult to evaluate numerically, we did not test these cases.

4.6.1 Critical percolation

The FK clusters of the $Q = 1$ Potts model are bond percolation clusters. Because site percolation and bond percolation belong to the same universality class, probabilities of like crossing configurations for either model should be equal. Assuming this fact, we sampled site percolation clusters on the triangular lattice instead of bond percolation clusters since the former is easier to simulate.

In site percolation on the triangular lattice, each lattice site is activated or deactivated with critical probability $p_c = 1/2$. Because nearest-neighbor sites do not interact, it is sufficient for our simulations to only sample the boundary cluster perimeters (boundary arcs) in order to measure the probability of each crossing event.

We describe the generation of each sample. It starts with the state of each site in $\mathcal{H}$ or the boundary of $\mathcal{H}$ undecided, except for the states of the sites in the wired sides

of $\mathcal{H}$, which start as activated. This is the independent-wiring boundary condition. Then a walk, called a *site-percolation hull-walk*, is performed to create a boundary cluster perimeter in $\mathcal{H}$. Each step of the hull-walk takes us from a site z in $\mathcal{H}$ to a nearest neighbor of z in $\mathcal{H}$. We perform two hull-walks in each sample. The first walk begins at the left endpoint w_1 of the bottom wired side and considers a first step in the $\vec{v}_1$ direction pointing into the adjacent free side. Before taking that step, the neighboring site onto which it would step is activated or deactivated with probability p_c or $1 - p_c$ respectively. If it is activated, then the walk steps onto that site. If it is deactivated, then the walk rotates its direction by $-\pi/3$ radians, considers a first step in that new direction, and the process repeats. Because the bottom side is wired, a first step is eventually taken. Now, after the $(i-1)$-th step, the walk considers an i-th step in the $\vec{v}_i$ direction rotated $\pi/3$ radians from the $\vec{v}_{i-1}$ direction of its previous step. The nearest-neighboring site in the $\vec{v}_i$ direction was either activated or deactivated by this process earlier, or is activated or deactivated now with probability p_c or $1-p_c$ respectively. If it is activated, then the walk takes its i-th step onto this site. If it is deactivated, then the walk rotates its direction by $-\pi/3$ radians and considers a next step in this new direction. The walk follows the same process to determine if it will step in this new direction or turn $-\pi/3$ radians again, and the process repeats until a next step is taken. Ultimately, the walk will take an i-th step, although this step may cause the walk to backtrack on its path. To keep the walk from leaving the system, we surround the boundary of $\mathcal{H}$ with a ring of deactivated sites off of which the hull-walk reflects.

We note three important facts concerning the hull-walk described in the previous paragraph. First, the walk never becomes trapped with no possible next step. Second, the walk never forms a loop that it traces an infinite number of times. Third, a hull-walk starting at an odd (resp. even) vertex of $\mathcal{H}$ will eventually reach an even (resp. odd) vertex. This is a feature of a hexagon with a FFBC.

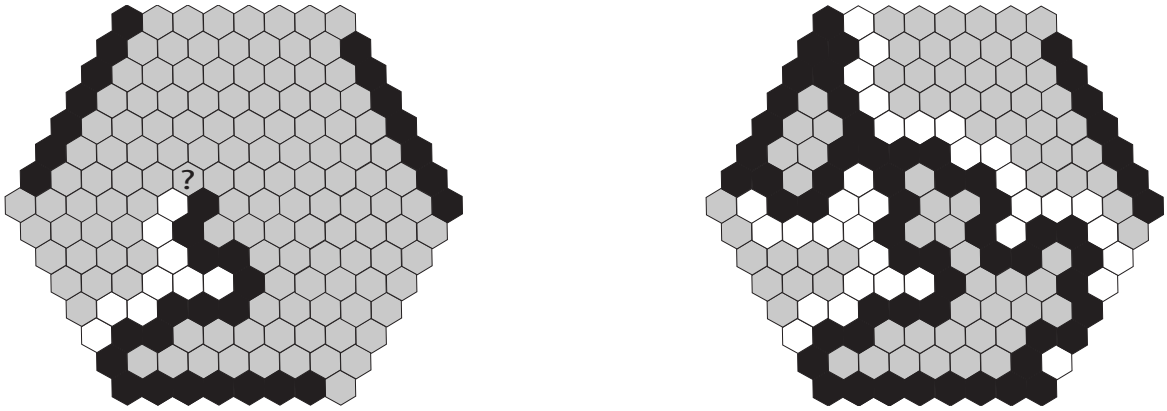

Figure 4.20: A hull-walk starting from the first vertex of the hexagon and deciding its twelfth step (left hexagon), and a complete sample exhibiting the $k = 1$ BAC. Black (resp. white, resp. gray) sites are activated (resp. deactivated, resp. undecided).

The first hull-walk starts at the first vertex w_1 of the hexagon, so it eventually touches an even vertex. When it reaches this vertex, we end the first hull-walk, we begin a second hull-walk from vertex five (top-left), and we end the second hull-walk when it touches an even vertex that is necessarily not the end of the first hull-walk. When the second hull-walk ends, we have two boundary arcs, and each connects an odd vertex with an even vertex. Because the third hull-walk would necessarily connect the remaining two vertices, we know the BAC, and thus the crossing configuration, of the sample without performing the third walk. By tallying the number of each type of BAC that we observe and dividing by the total number of samples, we find the measured probability of each BAC for a specified side-length ratio R.

We chose the side-lengths of each hexagon so that a long side and a short side are comprised of about 2048 lattice sites altogether. (In our simulations, side-length was defined to be the total number of lattice points within that side excluding the right endpoint, which was considered to be a member of the adjacent side.) We considered thirty-three different side-lengths, with the length of the wired sides in the i-th choice equaling

$$\ell_i = \left\lfloor \frac{2048}{5} + \frac{i}{32}\left(\frac{8192}{5} - \frac{2048}{5}\right)\right\rfloor, \quad i \in \{0, \ldots, 32\}, \tag{4.107}$$

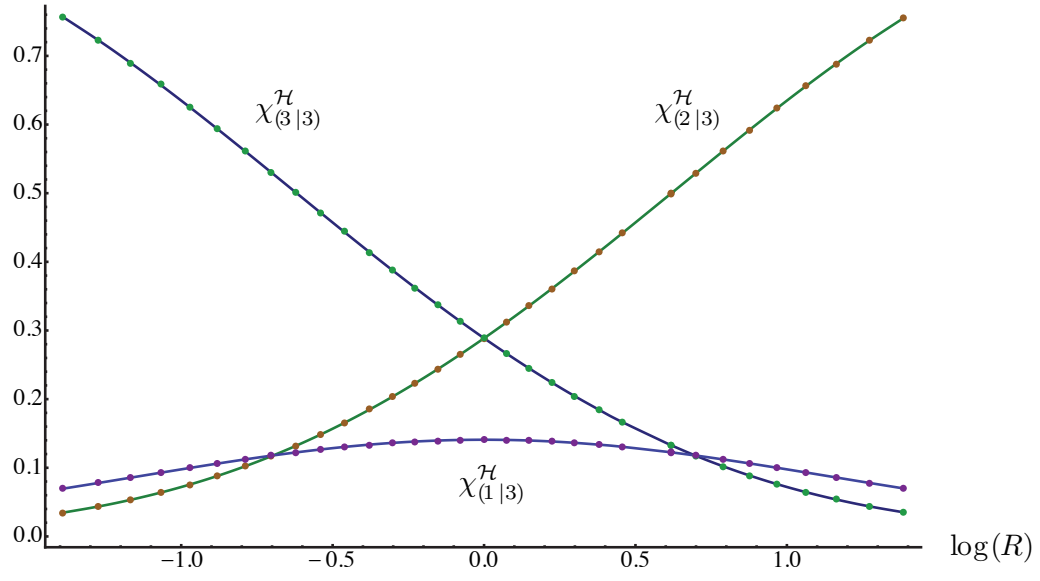

Figure 4.21: Crossing probabilities versus $\log R$, with R the ratio of the wired side-length to the free side-length, for critical site percolation on the triangular lattice in a hexagon. Note that $\chi_{(2|3)}$ and $\chi_{(3|3)}$ are reflections of each other about $\log(R) = 0$ and that $\chi_{(1|3)}$ is symmetric about this same axis.

and the length of the free sides equaling $2048 - \ell_i \approx \ell_{32-i}$. With this choice, the ℓ_i were approximately uniformly distributed between ℓ_0 and ℓ_{32}, and $R_0 \approx 1/4, R_{16} = 1$, and $R_{32} \approx 4$ where $R_i := \ell_i/(2048 - \ell_i)$ is the ratio of the side-lengths.

In figure 4.21, we plot the three crossing formulas $\chi^{\mathcal{H}}_{(1|3)}, \chi^{\mathcal{H}}_{(2|3)}$, and $\chi^{\mathcal{H}}_{(3|3)}$ versus $\log(R)$ (solid curves) with our measurements of the probability of these crossing events (points). The figure shows excellent agreement with our predictions. The $\log(R)$-values of the data points increase from $\log(R_0) \approx -\log(4)$ on the far left to $\log(R_{32}) \approx \log(4)$ on the far right. The double integrals in these crossing formulas were evaluated by using the "NIntegrate" function in Mathematica (version 8) with the "Method" option set to "MultiPeriodic." Table 5.3 presents the average error and the standard deviation of the error from this average.

Figure 4.21 suggests that $\chi^{\mathcal{H}}_{(2|3)}$ and $\chi^{\mathcal{H}}_{(3|3)}$ are reflections of each other about the $(\log(R) = 0)$-axis (i.e., $\chi^{\mathcal{H}}_{(2|3)}(R) = \chi^{\mathcal{H}}_{(3|3)}(1/R)$), and that $\chi^{\mathcal{H}}_{(1|3)}$ is an even function of $\log(R)$ (i.e., $\chi^{\mathcal{H}}_{(1|3)}(R) = \chi^{\mathcal{H}}_{(1|3)}(1/R)$). To explain this symmetry, we consider lining

the free sides of $\mathcal{H}$ with a collection of deactivated sites just outside of $\mathcal{H}$. (In a very large system, this has a negligible affect on the shape of $\mathcal{H}$.) If we do this, then the statistics of the activated sites in $\mathcal{H}$ with side-length ratio R are the same as the statistics of the deactivated sites with side-length ratio $1/R$. This explains the identity.

The simulation results presented in the following section will show that these symmetries are unique to percolation among the random cluster models. Because the addition of any collection of conditioned sites placed behind a free side of $\mathcal{H}$ will interact with that free side and affect the statistics of the model when $Q \neq 1$, the argument of the preceding paragraph cannot be used in these cases. We therefore do not expect our $Q \neq 1$ Potts model simulation results to exhibit these identities for FK clusters, and indeed our data, presented in figure 4.23 below, does not.

Avg. error	$\chi_{(1\|3)}$	$\chi_{(2\|3)}$	$\chi_{(3\|3)}$
FK $Q=1$	1.42×10^{-5}	6.67×10^{-5}	8.92×10^{-5}
FK $Q=2$	-4.411×10^{-4}	1.9984×10^{-3}	3.2274×10^{-3}
FK $Q=3$	-7.924×10^{-4}	3.9962×10^{-3}	1.9474×10^{-3}

Std. dev.	$\chi_{(1\|3)}$	$\chi_{(2\|3)}$	$\chi_{(3\|3)}$
FK $Q=1$	4.13×10^{-5}	2.591×10^{-4}	4.273×10^{-4}
FK $Q=2$	6.22×10^{-5}	4.5270×10^{-3}	5.0539×10^{-3}
FK $Q=3$	1.326×10^{-4}	6.7855×10^{-3}	4.0168×10^{-3}

Table 4.1: The error (theory minus simulation) averaged over $\log(R)$, and the standard deviation of the error from that average, of the data displayed in figures 4.21, 4.23, and 4.24.

4.6.2 Critical Q-state Potts model: $Q = 2, 3$

We used the Swendsen-Wang (SW) algorithm [77] to sample FK clusters in the critical Q-state Potts models. This algorithm is born from the random cluster representation of the Potts model (1.21). Beginning with a random collection of spins on the lattice, we update to a new sample by activating or deactivating the bonds be-

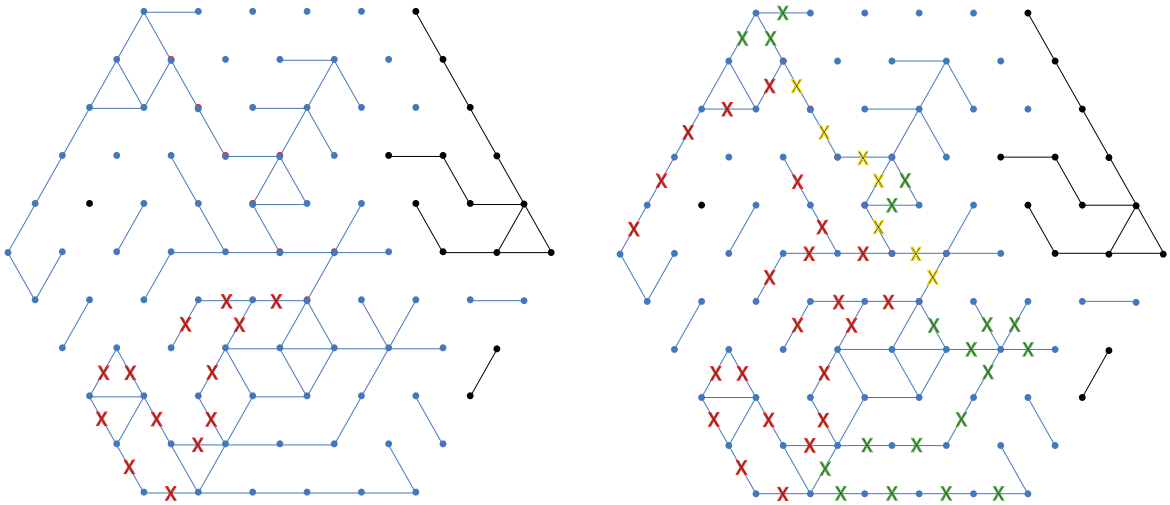

Figure 4.22: Hull-walks along the outer perimeter of a boundary Ising FK cluster. Spin $+$ (resp. $-$) sites and the FK bonds between them are colored blue (resp. black). The left figure shows the partially complete first hull-walk, with each step marked by an orange "$\times$," and the right figure shows the complete first (resp. second) hull-walk, with each step marked with an orange (resp. green) "$\times$." Each step common to both hull-walks is marked by a yellow "$\times$."

tween nearest-neighbor sites of like spin. Each bond is activated (resp. deactivated) with critical probability p_c^{tri} (1.28) (resp. $1 - p_c^{\text{tri}}$), except for those bonds within a wired boundary which are always activated to maintain the fixed BC on that side. Each cluster of activated bonds is an FK cluster by definition. After each bond is activated or deactivated, we choose an FK cluster and a spin σ_0 from among the Q possibilities with uniform probability, and we update the spin of each site in the FK cluster to σ_0. We repeat this process for each FK cluster (including those of size zero) so that all spins are updated. Thus, we generate a new sample from the original. After repeating this update procedure many times, the simulation eventually starts to sample spin configurations according to the Boltzman distribution.

After each update, we checked the BAC of the new sample to determine the crossing configuration that it exhibits. We took the boundary arcs to be the activated bonds that comprise the perimeter of an FK boundary cluster. To determine how they connect the vertices of $\mathcal{H}$ pairwise in a given sample, we performed two hull-walks. The first hull-walk started at the center of the activated bond in the bottom

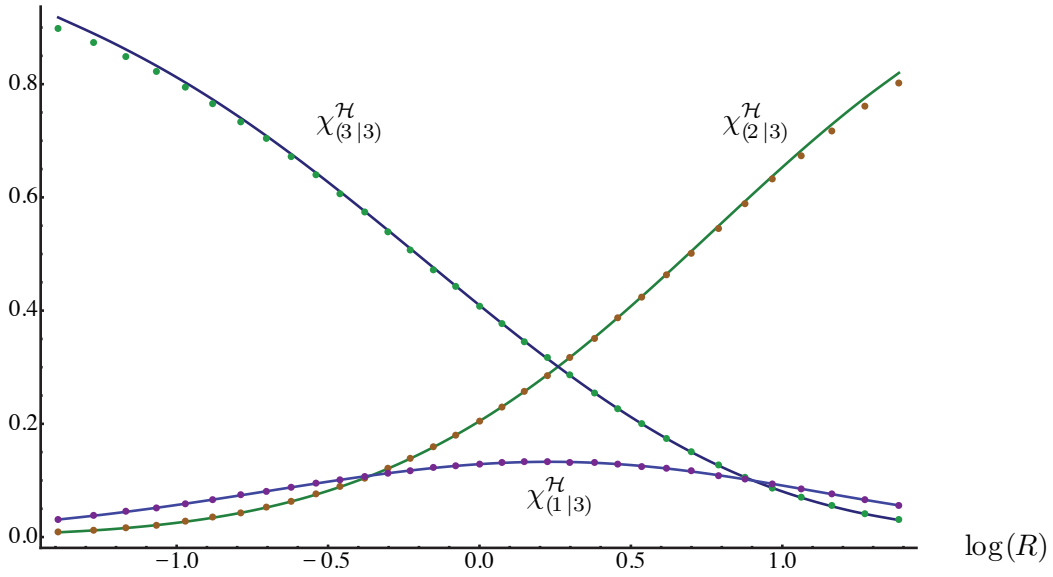

Figure 4.23: Crossing probabilities versus $\log R$, with R the ratio of the wired side-length to the free side-length, for critical $Q = 2$ FK clusters on the triangular lattice in a hexagon.

wired side and with the left endpoint at the first vertex of $\mathcal{H}$, and it stepped along the midpoints of the activated bonds that form the perimeter of the FK boundary cluster anchored to the bottom wired side (figure 4.22). The walk eventually stepped onto the midpoint of an activated bond in a wired side and with an endpoint at an even vertex of $\mathcal{H}$, and when this happened, we ended the walk. Then we started a second walk from the midpoint of the activated bond in the top-left wired side of $\mathcal{H}$ with an endpoint at vertex five, and we ended the walk when it stepped onto the midpoint of an activated bond in a wired side and with an endpoint at an even vertex of $\mathcal{H}$. Knowing the endpoints of these two hull-walks was sufficient to determine the BAC, and thus the crossing configuration, of the sample without performing the third walk. By tallying the number of each type of BAC that was observed and dividing by the total number of samples, we found the measured probability of each BAC for a specified ratio R.

We chose the side-lengths of each hexagon so that a long side and a short side comprised of about 2048 lattice sites altogether. Actually, only every other lattice

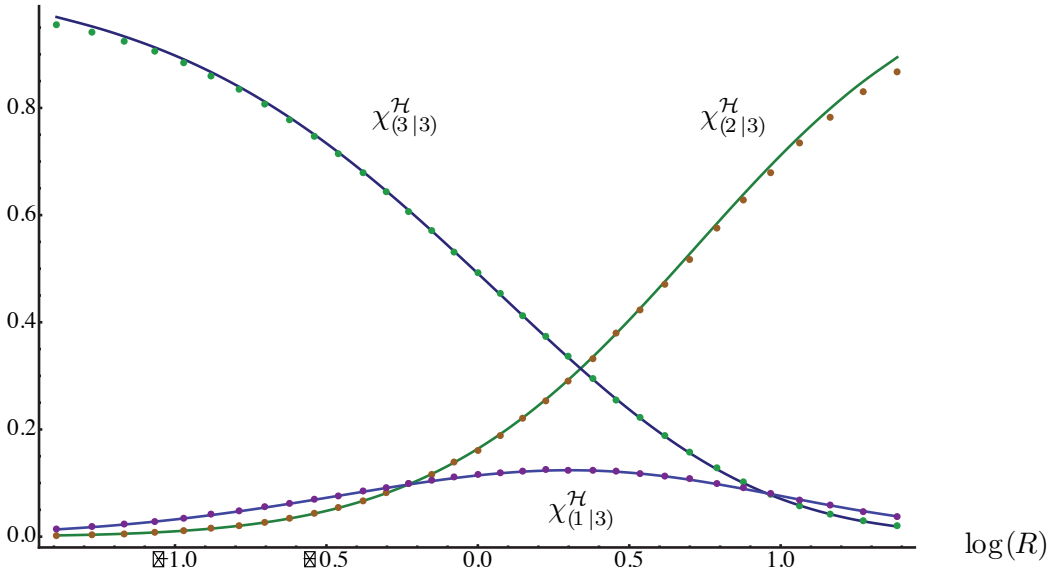

Figure 4.24: Crossing probabilities versus $\log R$, with R the ratio of the wired side-length to the free side-length, for critical $Q = 3$ FK clusters on the triangular lattice in a hexagon.

site was physical in the sense that it harbored a Potts model spin variable. All of the other lattice sites fell on the midpoints of the FK bonds connecting the physical lattice sites, and each harbored a variable that equaled zero (resp. one) if its FK bond was deactivated (resp. activated). Thus, our lattice size and side-lengths were effectively half of those used for percolation. In order to create this setup, we needed all side-lengths of $\mathcal{H}$ to be even. Thirty-three different side-lengths were considered. The length of the wired sides in the i-th choice was

$$\ell_i = 2\left\lfloor \frac{1}{2}\left(\frac{2048}{5} + \frac{i}{32}\left(\frac{8192}{5} - \frac{2048}{5}\right)\right)\right\rfloor, \quad i \in \{0, \ldots, 32\}. \tag{4.108}$$

and the length of the free sides was $2048 - \ell_i \approx \ell_{32-i}$. With this choice, the ℓ_i were approximately uniformly distributed between ℓ_0 and ℓ_{32}, and $R_0 \approx 1/4, R_{16} = 1$, and $R_{32} \approx 4$ where $R_i := \ell_i/(2048 - \ell_i)$ is the ratio of the side-lengths.

In figure 4.23 (resp. figure 4.24), we plot the three $Q = 2$ (resp. $Q = 3$) FK cluster crossing formulas $\chi^{\mathcal{H}}_{(1|3)}, \chi^{\mathcal{H}}_{(2|3)}$, and $\chi^{\mathcal{H}}_{(3|3)}$ versus $\log(R)$ (solid curves) with our measurements of the probability of these crossing events (points), and we observe

excellent agreement with our predictions. The explanation of this figure is the same as for figure 4.21. Table 5.3 presents the average error and the standard deviation of the error from this average. We note from figure 4.23 (resp. figure 4.24) that the difference between the prediction for $\chi^{\mathcal{H}}_{(2|3)}$ (resp. $\chi^{\mathcal{H}}_{(3|3)}$) and the simulation results is larger when R is large (resp. small), but we do not offer an explanation since it is not clear if this is a finite-size effect or a consequence of the numerical evaluation of the double integral in the crossing formulas.

4.7 Summary

We summarize the main results of this chapter. The elements of the basis $\mathcal{B}_N$ (definition II.20) are interpreted as universal partition functions for a continuum limit critical lattice model in a $2N$-sided polygon with a certain FFBC among those in the collection BC_N (defined in section 4.1). In particular, $F_\varsigma \in \mathcal{B}_N$ is the universal partition function summing exclusively over samples in the FFBC event ς. Universal partition functions summing exclusively over the intersection of the FFBC event ς and the BAC event λ are given by $n^{l_{\lambda,\varsigma}}\Pi_\lambda$, where $l_{\lambda,\varsigma}$ equals the number of loops created by fusing the exterior arcs of the diagram for F_ς with the interior arcs of the diagram for $[\mathscr{L}_\lambda]$, with n given by (1.155), and where the *type-λ crossing weight* Π_λ is the element of $\mathcal{S}_N$ dual to $[\mathscr{L}_\lambda] \in \mathscr{B}^*_N$. Thus, the probability of observing the BAC event λ conditioned on the FFBC event ς is given by the *crossing formula* $n^{l_{\lambda,\varsigma}}\Pi_\lambda/F_\varsigma$. This result is predictive rather than rigorous, and we confirm this prediction via computer simulation for the case of an equiangular hexagon with independently wired sides and with a side-length that alternates between two possibilities as we move around it. Our simulations sampled FK clusters in the $Q = 1, 2, 3$ Potts model ($\kappa = 6$, $16/3$, and $24/5$ respectively), and our measurements show very good agreement with our predictions.

CHAPTER V

Cluster pinch-point densities for critical systems in polygons

We consider critical bond percolation on a very fine square lattice inside of a rectangle $\mathcal{R}$ with wired left and right sides. Of intrinsic interest to the system are bonds whose activation or deactivation will respectively join or disconnect the percolation boundary cluster anchored to the left side of $\mathcal{R}$ from that anchored to the right side. Such a bond that connects them is an example of a *red bond* [78]. Red bonds inherit their name from the following scenario. If we suppose that only activated bonds conduct electricity and the wired left and right sides are attached to opposite leads of a battery, then an activated red bond carries the total current, and its deactivation stops the flow of current. Red bonds carry similar significance in other physical scenarios modeled by percolation. Many of their properties have been studied before, first in context with cluster ramification [79]. The average number of red bonds weighted by cluster size was measured in [78], and the fractal dimension of the set of red bonds is predicted in [27, 80], and measured in [81]. Further fragmentation properties of percolation clusters are considered in [82]. In this chapter, we calculate the density (i.e., frequency of occurrence) of red bonds at a given bulk point $w \in \mathcal{R}$ and some generalizations which we now explore.

In percolation, red bonds are marked by pinch points, or bulk points where distinct

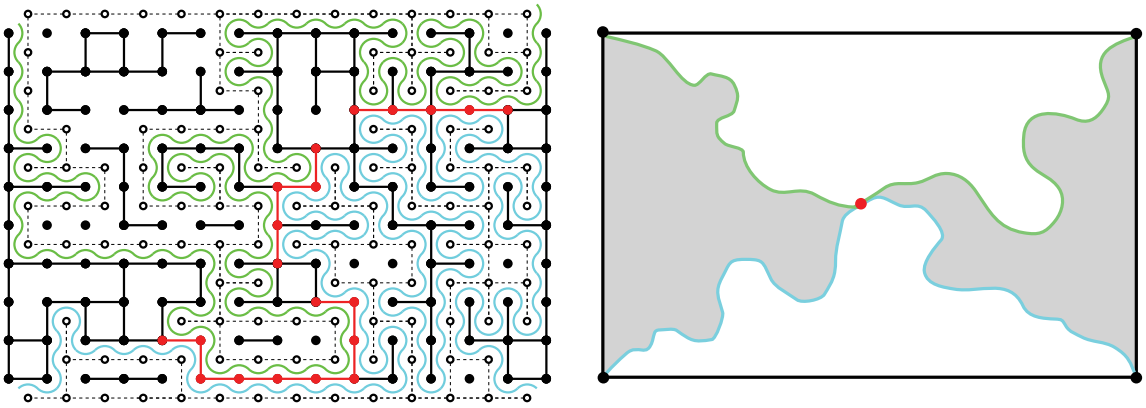

Figure 5.1: A percolation configuration with the red bonds, or two-pinch-points (colored red) and the boundary arcs connecting the vertices of the rectangle pairwise (colored green and blue). The left illustration is a sample in the discrete setting while the right figure only shows the (filled) boundary clusters of a sample in the continuum limit.

percolation clusters touch. We consider the two boundary arcs of the percolating system in $\mathcal{R}$. At the center w of a red bond, the two boundary arcs pass very close to each other, separated there by only the red bond (figure 5.1). In the continuum limit, four distinct boundary arcs appear to emanate from w, each ending at a different vertex of $\mathcal{R}$. In reality, these four curves are not distinct but join pairwise at (or pass very close to) w to form two boundary arcs. Each boundary cluster is pinched into a narrow channel between an adjacent pair of boundary arcs, and they touch each other at (or pass very close to) w where the tips of these channels meet (or almost meet). Thus, we call w a *pinch point* [83] (figure 5.1). The detail of whether or not the red bond at w is activated is lost in the continuum limit where, formally speaking, bonds do not exist but their clusters do. But the location of the red bond remains. It is marked by the pinch point at w. Thus, the continuum limit of the density of red bonds in $\mathcal{R}$ equals the density of pinch points between the left and right boundary clusters in $\mathcal{R}$.

The connection between red bonds and pinch points generalizes the problem of computing the red bond density in $\mathcal{R}$ to computing the pinch-point density involving s boundary clusters in a $2N$-sided polygon $\mathcal{P}$. In particular, we suppose that $\mathcal{P}$

harbors critical percolation in its interior and exhibits a specified FFBC. We define an *s-pinch point* to be a bulk point $w \in \mathcal{P}$ where s distinct boundary clusters touch. In the continuum limit, $2s$ boundary arcs emanate from w, each ending at a different vertex of $\mathcal{P}$ (figure 5.1). Clearly, we must have $1 \leq s \leq N$ since at most N distinct boundary clusters can anchor to the wired sides of $\mathcal{P}$. When $s = 1$ we define a one-pinch point to be a bulk point touched by just one of the boundary arcs. As the continuum limit is approached, the density of pinch-point events decays as a power law of the shrinking lattice spacing (section 5.2.2). This power, with other scaling exponents, is determined in [27, 83]. (For $2N$-sided polygons with $N > 2$, the density of red bonds is still dominated by pinch points involving two clusters in the large system limit, since s-pinch points with $s > 2$ occur much less often, as discussed in section 5.3.)

We obtain another generalization by considering the statistics of the boundary arcs, which, as mentioned in the introduction of chapter two, fluctuate in $\mathcal{P}$ with the law of multiple-SLE. In these terms, an s-pinch point is a bulk point $w \in \mathcal{P}$ where s distinct multiple-SLE curves touch (or pass very near each other). In particular, a one-pinch point is a bulk point on (or very near) one of these curves (figure 5.2), and the problem of calculating its density generalizes the same problem for when there is one SLE curve. The latter was originally solved in [50]. In our generalization, the regions that a boundary arc can explore in $\mathcal{P}$ are influenced by the presence of the other boundary arcs, so a one-pinch point can be interpreted as measuring the repulsion between the various boundary arcs. In the case of percolation, this "repulsion" is not felt until the boundary arcs actually collide due to the locality property of SLE with $\kappa = 6$ [15].

As we have observed, the range $\kappa \in (0, 8)$ describes boundary arcs in many interesting critical lattice models, including those of the Q-state Potts model for $Q \leq 4$. As in percolation, an s-pinch point is still a bulk point where s distinct boundary

clusters touch in the Q-state Potts model, but now there are two different types of clusters to consider: FK clusters and spin clusters. In section 1.2.8, we saw that boundary arcs of the former type are multiple-SLE curves with speed κ in the dense phase and related to Q through [8]

$$Q = n(\kappa)^2 = 4\cos^2(4\pi/\kappa), \quad \kappa \in (4, 8), \tag{5.1}$$

while boundary arcs of the latter type are multiple-SLE curves with the dual speed $\hat{\kappa} = 16/\kappa$ in the dilute phase and κ related to Q through (5.1). Scaling exponents and fractal dimensions associated with pinch points are found in [80]. The generalization of red bonds from percolation to other models is also considered in [81].

In this chapter, we calculate various continuum limit pinch-point densities in the rectangle $\mathcal{R}$ and in the hexagon $\mathcal{H}$ (and for $s = N$ in any $2N$-sided polygon) with a specified FFBC and for arbitrary $\kappa \in (0, 8)$, but before we begin, we refine our definition of a pinch point. We let the event Λ contain all samples in which exactly s distinct boundary arcs, each with both endpoints among $2s$ specified vertices of $\mathcal{P}$, pass within a small distance δ from a specified point $w \in \mathcal{P}$ and the other boundary arcs join the remaining vertices of $\mathcal{P}$ in some particular connectivity. Then for a specified FFBC event $\varsigma \in \mathrm{BC}_N$, the *type-$\Lambda$ s-pinch-point density* $\rho^{\mathcal{P}}_{(\Lambda|\varsigma)}(w)$ is the probability of the pinch-point event Λ conditioned on the FFBC event ς, and it equals the ratio of the (continuum limit) partition function $\tilde{\mathcal{Z}}^{\mathcal{P}}_{(\Lambda|\varsigma)}$ summing exclusively over samples in $\Lambda \cap \varsigma$ divided by the partition function $\tilde{\mathcal{Z}}^{\mathcal{P}}_{\varsigma}$ summing exclusively over samples in ς.

Our goal is to study the asymptotic behavior of $\rho^{\mathcal{P}}_{(\Lambda|\varsigma)}(w)$ as $\delta \to 0$. The asymptotic behavior of the partition functions $\tilde{\mathcal{Z}}^{\mathcal{P}}_{(\Lambda|\varsigma)}$ is supposed to be a natural generalization

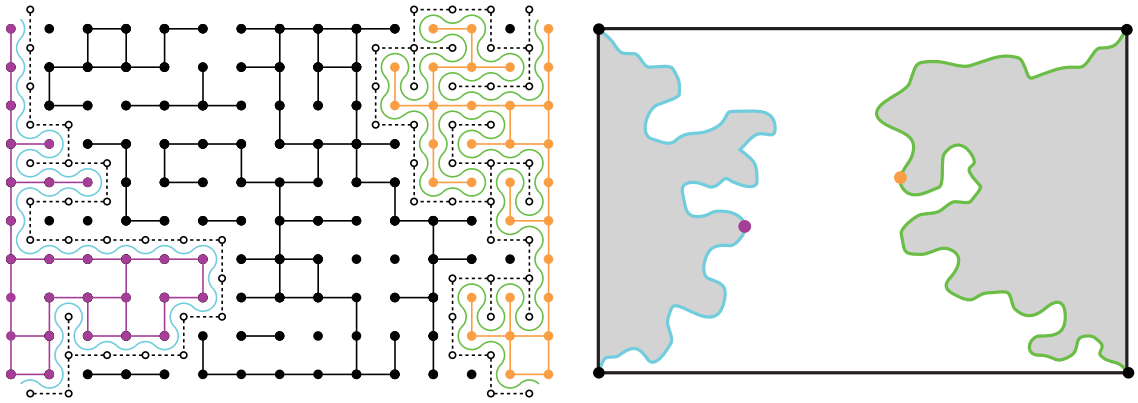

Figure 5.2: An illustration of one-pinch-point events on the perimeters of the boundary clusters (orange and purple) in the discrete (left) and continuum (right) settings.

of that of $\tilde{\mathcal{Z}}^{\mathcal{P}}_{(\lambda|\varsigma)}$ in (4.80) with λ a specified BAC event. This generalization is

$$\tilde{\mathcal{Z}}^{\mathcal{P}}_{(\Lambda|\varsigma)}/Z_f \underset{\delta,\delta_i\to 0}{\sim} c_1^{2N} C_s^2 \delta_1^{\theta_1} \dots \delta_{2N}^{\theta_1} \delta^{2\Theta_s} \tilde{\Upsilon}^{\mathcal{P}}_{(\Lambda|\varsigma)}, \tag{5.2}$$

$$\tilde{\mathcal{Z}}^{\mathcal{P}}_{\varsigma}/Z_f \underset{\delta_i\to 0}{\sim} c_1^{2N} \delta_1^{\theta_1} \dots \delta_{2N}^{\theta_1} \tilde{\Upsilon}^{\mathcal{P}}_{\varsigma}, \tag{5.3}$$

where Z_f is the free partition function, where the functions $\tilde{\Upsilon}^{\mathcal{P}}_{(\Lambda|\varsigma)}$ and $\tilde{\Upsilon}^{\mathcal{P}}_{\varsigma}$ are universal partition functions given by $(2N+2)$-point and $2N$-point correlation functions respectively, where θ_1 is the boundary one-leg weight (1.169), and where Θ_s is the *bulk* $2s$*-leg weight*, a new scaling exponent to be explicitly given below and associated with the s-pinch-point event. Also, c_1 is the nonuniversal scaling coefficient associated with the boundary one-leg operator ψ_1, C_s is a nonuniversal scaling coefficient associated with the s-pinch-point event, and the i-th BCC occurs within distance δ_i from the i-th vertex w_i of $\mathcal{P}$. Then the density $\rho^{\mathcal{P}}_{(\Lambda|\varsigma)}$ behaves as

$$\rho^{\mathcal{P}}_{(\Lambda|\varsigma)} = \tilde{\mathcal{Z}}^{\mathcal{P}}_{(\Lambda|\varsigma)}/\tilde{\mathcal{Z}}^{\mathcal{P}}_{\varsigma} \tag{5.4}$$

$$\underset{\delta\to 0}{\sim} C_s^2 \delta^{2\Theta_s} \tilde{\Upsilon}^{\mathcal{P}}_{(\Lambda|\varsigma)}/\tilde{\Upsilon}^{\mathcal{P}}_{\varsigma}. \tag{5.5}$$

The function $\tilde{\Upsilon}^{\mathcal{P}}_{\varsigma}$ was determined in chapter four for any FFBC event $\varsigma \in \mathrm{BC}_N$. Thus, determining the behavior of $\rho^{\mathcal{P}}_{(\Lambda|\varsigma)}$ to within a constant amounts to determining $\tilde{\Upsilon}^{\mathcal{P}}_{(\Lambda|\varsigma)}$.

The organization of this chapter is as follows. In section 5.1, we equate the universal partition function $\tilde{\Upsilon}^{\mathcal{P}}_{(\Lambda|\varsigma)}$ with a bulk-boundary CFT correlation function of certain primary operators, and we find a formula for it using the Coulomb gas formalism. Also in this section, we calculate the N-pinch-point weight (defined below) of a $2N$-sided polygon, and we find that it is completely algebraic. In section 5.2, we compute various s-pinch-point densities in the rectangle ($N = 2$) and in the hexagon ($N = 3$). We find that the formulas for the $(N-1)$-pinch-point densities are given by algebraic factors times Lauricella functions of cross-ratios of (the half-plane conformal images of) the bulk point w and the vertices w_i of $\mathcal{P}$. In section 5.3, we compare some of our predictions with high-precision simulations of percolation and Ising FK clusters inside of a rectangle and a regular hexagon and find very good agreement.

The research presented in this chapter is also presented in our preprint [84].

5.1 Conformal field theory description

In the continuum limit, $\tilde{\Upsilon}^{\mathcal{P}}_{(\Lambda|\varsigma)}$ is a correlation function of appropriate CFT primary operators that are chosen as follows. To alternate the BC on the sides of $\mathcal{P}$ from free to fixed, we insert a corner one-leg operator $\psi^c_1(w_i)$ at each vertex w_i of $\mathcal{P}$ into the correlation function. Corner operators are defined in (4.81). The collection of $2N$ corner one-leg operators introduces N non-crossing boundary arcs that connect the

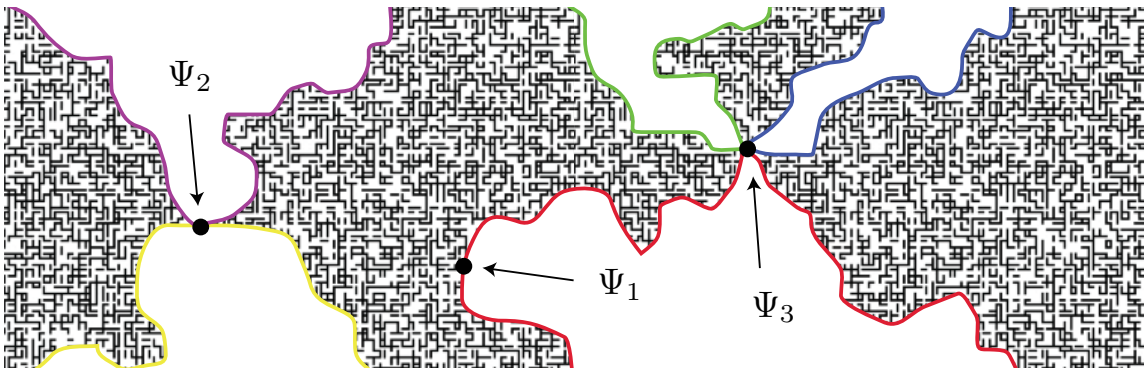

Figure 5.3: An s-pinch-point event is induced by the insertion of a bulk $2s$-leg operator.

vertices $w_1, \ldots, w_{2N}$ pairwise in one of C_N possible connectivities (figure 4.9), with C_N the N-th Catalan number and given by (2.7). Now to generate an s-pinch point at $w \in \mathcal{P}$, we require s of these arcs to touch at (or come very close to) this point. One may view this as the event in which $2s$ distinct boundary arcs emanate from w, which is conditioned by the insertion of a spinless bulk $2s$-leg operator $\Psi_s(w, \bar{w})$ into the correlation function [23, 83] (figure 5.3). Hence, $\tilde{\Upsilon}^{\mathcal{P}}_{(\Lambda|\varsigma)}$ is given by the $(2N+2)$-point function

$$\tilde{\Upsilon}^{\mathcal{P}}_{(\Lambda|\varsigma)} = \langle \psi_1^c(w_1)\psi_1^c(w_2)\ldots\psi_1^c(w_{2N-1})\psi_1^c(w_{2N})\Psi_s(w,\bar{w})\rangle_{\mathcal{P}}. \tag{5.6}$$

The half-plane version of this correlation function is

$$\begin{aligned} \Upsilon_{(\Lambda|\varsigma)} &= \langle \psi_1(x_1)\psi_1(x_2)\ldots\psi_1(x_{2N-1})\psi_1(x_{2N})\Psi_s(z,\bar{z})\rangle_{\mathbb{H}} & (5.7)\\ &= \langle \psi_1(x_1)\psi_1(x_2)\ldots\psi_1(x_{2N-1})\psi_1(x_{2N})\Psi_s(z)\Psi_s(\bar{z})\rangle_{\mathbb{C}}, & (5.8) \end{aligned}$$

where we have used Cardy's method of images, discussed in section 1.2.8, to rewrite the half-plane correlation function on the right side of (5.7) as the whole-plane correlation function (5.8). First, we will focus on calculating $\Upsilon_{(\Lambda|\varsigma)}$, and later in section 5.2.3, we will transform $\Upsilon_{(\Lambda|\varsigma)}$ to $\tilde{\Upsilon}^{\mathcal{P}}_{(\Lambda|\varsigma)}$.

In the multiple-SLE picture, the bulk $2s$-leg operator conditions $2s$ of the $2N$ available multiple-SLE curves to grow from their respective origin points at the vertices of $\mathcal{P}$ towards the common bulk point $w \in \mathcal{P}$ until they join pairwise very near w in any one of C_s possible connectivities, where C_s is the s-th Catalan number (2.7). The s-pinch-point event Λ, defined above, contains all samples exhibiting any one of these C_s connectivities near the pinch-point. Each is equally likely, and the i-th connectivity will imply a certain number p_i of boundary loops in the system that depends on the specified FFBC event ς. By factoring out the fugacity factors associated with

the boundary loops, we may write $\Upsilon_{(\Lambda|\varsigma)}$ in the form

$$\Upsilon_{(\Lambda|\varsigma)} = (n^{p_1} + \ldots + n^{p_{C_s}})\Pi_\Lambda. \tag{5.9}$$

Here, Π_Λ is called the *(half-plane) type-Λ pinch-point weight*, and it bears the same partition function interpretation as $\Upsilon_{(\Lambda|\varsigma)}$, but with the boundary loops having fugacity one. This interpretation is analogous with that of the type-λ crossing weight in chapter four.

The bulk $2s$-leg and boundary s-leg operators Ψ_s and ψ_s are primary operators of a boundary CFT in the upper half-plane. The highest-weight vector of their Verma modules respectively belongs to the $(0, s)$ and $(1, s+1)$ (resp. $(s, 0)$ and $(s+1, 1)$) positions of the Kac table in the dense phase (resp. dilute phase) of SLE [23]. Their respective conformal weights Θ_s (for both holomorphic and antiholomorphic sector of Ψ_s) and θ_s in terms of the SLE speed κ therefore follow from (1.170) and are

$$\Theta_s = \frac{16s^2 - (\kappa-4)^2}{16\kappa}, \quad \theta_s = \frac{s(2s+4-\kappa)}{2\kappa}. \tag{5.10}$$

As demonstrated in section 1.2.6, CFT translates the reducibility of the $V_{1,2}$ (resp. $V_{2,1}$) Verma module associated with each boundary one-leg operator into the following semi-elliptic system of $2N$ PDEs that govern the correlation function (5.7), or equivalently, the pinch-point weight Π_Λ:

$$\left[\frac{\kappa}{4}\partial_i^2 + \sum_{j\neq i}^{2N}\left(\frac{\partial_j}{x_j - x_i} - \frac{\theta_1}{(x_j-x_i)^2}\right) + \frac{\partial_z}{z-x_i} - \frac{\Theta_s}{(z-x_i)^2} + \frac{\partial_{\bar{z}}}{\bar{z}-x_i} - \frac{\Theta_s}{(\bar{z}-x_i)^2}\right]\Pi_\Lambda = 0, \quad i \in \{1,\ldots,2N\}. \tag{5.11}$$

The domain of Π_Λ is

$$\Omega_0 := \{(x_1,\ldots,x_{2N},z,\bar{z}) \,:\, x_1 < \ldots < x_{2N}, z \in \mathbb{H}, \bar{z} \in \mathbb{H}^*\}, \tag{5.12}$$

and we always set $\bar{z} = z^*$ at the end of our calculations. In addition, the three Ward identities (1.54) ensure that Π_Λ is conformally covariant such that each x_i has scaling weight θ_1 and z and $\bar{z}$ have respective holomorphic and antiholomorphic weight Θ_s:

$$\left[\partial_z + \partial_{\bar{z}} + \sum_{i=1}^{2N} \partial_{x_i}\right] \Pi_\Lambda = 0 \tag{5.13}$$

$$\left[z\partial_z + \bar{z}\partial_{\bar{z}} + 2\Theta_s + \sum_{i=1}^{2N} (x_i \partial_{x_i} + \theta_1)\right] \Pi_\Lambda = 0 \tag{5.14}$$

$$\left[z^2\partial_z + \bar{z}^2\partial_{\bar{z}} + 2\Theta_s(z+\bar{z}) + \sum_{i=1}^{2N} (x_i^2 \partial_i + 2\theta_1 x_i)\right] \Pi_\Lambda = 0. \tag{5.15}$$

The Ward identities restrict Π_Λ to a conformally covariant ansatz which may be chosen as

$$\Pi_\Lambda(x_1, \ldots, x_{2N}; z, \bar{z}) = |z - \bar{z}|^{-2\Theta_s} \prod_{i=1}^{N} (x_{2i} - x_{2i-1})^{-2\theta_1} G(\eta_2, \ldots, \eta_{2N-2}; \mu, \nu) \tag{5.16}$$

with

$$\eta_i := \frac{(x_i - x_1)(x_{2N} - x_{2N-1})}{(x_{2N-1} - x_1)(x_{2N} - x_i)}, \quad i = 2, \ldots, 2N-2, \tag{5.17}$$

$$\mu := \frac{(z - x_1)(x_{2N} - x_{2N-1})}{(x_{2N-1} - x_1)(x_{2N} - z)}, \quad \nu := \frac{(\bar{z} - x_1)(x_{2N} - x_{2N-1})}{(x_{2N-1} - x_1)(x_{2N} - \bar{z})}, \tag{5.18}$$

where $\{\eta_2, \ldots, \eta_{2N-2}, \mu, \nu\}$ is a maximal set of independent cross-ratios that can be formed from the points $x_1, \ldots, x_{2N}, z, \bar{z}$ and G is an analytic function of $x_1, \ldots, x_{2N}$ thanks to the analyticity theorem for elliptic PDEs [64]. This ansatz reduces the number of variables in the problem from $2N + 2$ to $2N - 1$. A standard approach that takes advantage of this reduction is to transform (5.11) into a system of PDEs governing $x_{2N}^{2\theta_1}\Pi_\Lambda$ and take the limit

$$\{x_1, x_2, \ldots x_{2N-2}, x_{2N-1}, x_{2N}, z, \bar{z}\} \to \{0, \eta_2, \ldots, \eta_{2N-2}, 1, \infty, \mu, \nu\}. \tag{5.19}$$

This gives a system of $2N$ PDEs governing the unknown function G from which we

can glean information, ideally exact solutions. Because we mainly consider the cases $N = 1, 2$ and 3 in this chapter, we use the following notation throughout:

$$\eta := \eta_2, \quad \tau := \eta_3, \quad \sigma := \eta_4. \tag{5.20}$$

We can explicitly solve (5.11-5.15) in the case $s = N = 1$ (i.e., the two-gon). In this one-pinch-point event, a boundary arc γ connecting x_1 with x_2 passes some very small distance ϵ from the specified point $z \in \mathbb{H}$. We denote the corresponding pinch-point weight by Π_{12}. Substituting the ansatz

$$\Pi_{12}(x_1, x_2; z, \bar{z}) = |z - \bar{z}|^{-2\Theta_1}(x_2 - x_1)^{-2\theta_1} G(\upsilon), \qquad \upsilon := \frac{(x_1 - z)(x_2 - \bar{z})}{(x_1 - \bar{z})(x_2 - z)} \tag{5.21}$$

(slightly modified from (5.16)) into (5.11) yields a second-order, linear, homogeneous differential equation in G. The general solution is

$$F(x_1, x_2; z, \bar{z}) = \frac{(x_2 - x_1)^{-2\theta_1+\theta_2}|z - \bar{z}|^{-2\Theta_1+\theta_2}}{|x_1 - z|^{8/\kappa-1}|x_2 - z|^{8/\kappa-1}} \times \left[c_1 + c_2\, \beta\left(\frac{4}{\kappa}, 1 - \frac{8}{\kappa} \;\middle|\; \frac{(x_1 - z)(x_2 - \bar{z})}{(x_1 - \bar{z})(x_2 - z)}\right)\right], \tag{5.22}$$

where β is the incomplete beta function, c_1 and c_2 are arbitrary real constants, and the weights θ_1, θ_2, and Θ_1 are given in (5.10). We argue that $c_2 = 0$ in our application by letting $z \to x \in \mathbb{R}\backslash\{x_1, x_2\}$. Because the boundary arc γ is conditioned to touch z, γ will touch the real axis at x in this limit, and two boundary arcs will emanate from

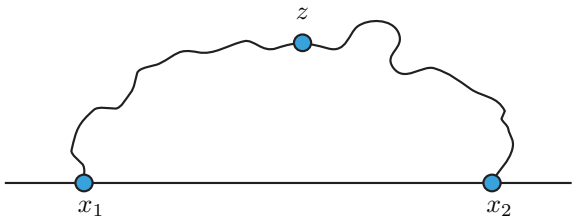

Figure 5.4: The one-pinch-point configuration in the upper half-plane. Note that the limits $x_2 \to x_1$ and $z \to x \in \mathbb{R} \setminus \{x_1, x_2\}$ each generate a boundary two-leg operator.

x. Thus, the bulk operator $\Psi_1(z)$ must fuse with its image $\Psi_1(\bar{z})$ to create a boundary two-leg operator $\psi_2(x)$ to leading order. Or instead suppose that x_2 approaches x_1. Then in this limit, the two endpoints of γ touch at x_1, and the boundary operators $\psi_1(x_1)$ and $\psi_1(x_2)$ fuse to create $\psi_2(x_1)$ to leading order as well (figure 5.4). In both cases, $\upsilon \to 1$. Because

$$\beta(a, b \,|\, \upsilon) \underset{\upsilon \to 1}{\sim} b^{-1}(1-\upsilon)^b \quad \text{if } b < 0, \tag{5.23}$$

and because $b = -\theta_2 < 0$ for $\kappa < 8$ (5.10), we see that

$$F(x_1, x_2; z, \bar{z}) \underset{\upsilon \to 1}{\sim} \frac{(x_2 - x_1)^{-2\theta_1 + \theta_2} |z - \bar{z}|^{-2\Theta_1 + \theta_2}}{|x_1 - z|^{8/\kappa - 1} |x_2 - z|^{8/\kappa - 1}} \times \left[c_1 - \frac{c_2}{\theta_2} \left(\frac{(x_2 - x_1)(z - \bar{z})}{(x_1 - \bar{z})(x_2 - z)} \right)^{-\theta_2} \right]. \tag{5.24}$$

To ensure that the bulk-image or boundary-boundary fusion has the two-leg channel at leading order, the second term in the brackets must be absent. Thus, $c_2 = 0$, and we find the one-pinch-point weight for an SLE connecting the real points x_1 and x_2:

$$\Pi_{12}(x_1, x_2; z, \bar{z}) = \frac{(x_2 - x_1)^{2/\kappa} |z - \bar{z}|^{(8-\kappa)^2/8\kappa}}{|x_1 - z|^{8/\kappa - 1} |x_2 - z|^{8/\kappa - 1}}. \tag{5.25}$$

If we put $x_1 = 0$ and $x_2 = \infty$ as in the usual setup for SLE, then we have

$$\lim_{x_2 \to \infty} x_2^{2\theta_1} \Pi_{12}(0, x_2, z, \bar{z}) = |z - \bar{z}|^{\kappa/8 - 1} \sin \arg(z)^{8/\kappa - 1} \tag{5.26}$$

$$\asymp \epsilon^{-2\Theta_1} \mathbb{P}\{\mathcal{B}(\epsilon, z) \cap \gamma \neq \emptyset\}, \quad \kappa \in (0, 8), \tag{5.27}$$

where $\mathbb{P}\{\mathcal{B}(\epsilon, z) \cap \gamma \neq \emptyset\}$ is the probability that γ intersects a ball $\mathcal{B}(\epsilon, z)$ centered at z of small radius ϵ. Equation (5.27) is rigorously proven in [50]. This rigorous result is supposed to be stronger by the formalism presented in this thesis. Namely, it is

expected to be

$$\mathbb{P}\{\mathcal{B}(\epsilon, z) \cap \gamma \neq \emptyset\} \underset{\epsilon \to 0}{\sim} \epsilon^{2\Theta_1} |z - \bar{z}|^{\kappa/8-1} \sin \arg(z)^{8/\kappa - 1}. \tag{5.28}$$

This is equivalent to the prediction (5.2) when $N = 1$. Note that $\Theta_1 > 0$ for $\kappa < 8$, so this probability goes to zero as $\epsilon \to 0$ as it must. Below, we will compute this pinch-point weight with another method.

As we have observed this example, it is generally true that the set of pinch-point densities span a proper subspace of the solution space of the system (5.11-5.15). This follows from the result (5.128) in the appendix 5.4.

The system (5.11-5.15) is very difficult to solve directly when $N > 1$, but fortunately the Coulomb gas formalism (section 1.2.9) provides a tractable approach to finding solutions. To this end, we write a chiral operator representation for (5.8). Adopting dense phase notation conventions, we represent $\psi_1(x_i)$ by the chiral operator $V^-_{1,2}(x_i)$, and we represent $\Psi_s(z, \bar{z})$ by the *vertex operator* $V^+_{0,s}(z)\bar{V}^+_{0,s}(\bar{z})$. The correlation function now has total charge

$$2N\alpha^-_{1,2} + 2\alpha^+_{0,s} = 2\alpha_0 + (s - N)\alpha_-, \tag{5.29}$$

which equals $2\alpha_0$ only if $N = s$.

We momentarily restrict our attention to the case $s = N$, where the correlation function is neutral. Here, (1.178) gives an explicit, algebraic formula for the upper half-plane N-pinch-point weight in a $2N$-sided polygon:

$$\Pi_{N\text{-pinch point}}(x_1, \ldots, x_{2N}; z, \bar{z}) = |z - \bar{z}|^{(4N+4-\kappa)^2/8\kappa} \times \prod_{i<j}^{2N} (x_j - x_i)^{2/\kappa} \prod_{i=1}^{2N} |z - x_i|^{1-4(N+1)/\kappa}. \tag{5.30}$$

The bulk point z is connected to all boundary points x_i hosting the BCCs via the N

boundary arcs that touch at z. We note that (5.30) is identical to (5.25) when $N = 1$, as it must be.

Next, we consider the cases with $s < N$. In order for the total charge (5.29) of the correlation function to equal $2\alpha_0$, we must insert $N - s$ Q_- screening operators, leading to the following modified $(2N + 2)$-point function:

$$\oint_{\Gamma_1} \dots \oint_{\Gamma_{N-s}} \langle V^-_{1,2}(x_1) \dots V^-_{1,2}(x_{2N}) V^+_{0,s}(z) V^+_{0,s}(\bar{z}) V_-(u_1) \dots V_-(u_{N-s}) \rangle \, du_1 \dots \, du_{N-s}. \tag{5.31}$$

What remains is to determine a collection of closed, non-intersecting integration contours $\{\Gamma_m\}_{m=1}^{N-s}$ appropriate for a particular type-Λ pinch-point event. The simplest closed contour along which an integration is nonzero is a closed Pochhammer contour entwining only a pair among the branch points $x_1, \dots, x_{2N}, z$, and $\bar{z}$ of the integrand, as shown figure 1.20. Throughout this chapter, we take each Γ_m to be such a Pochhammer contour. We may use (1.178) to write out the integrand of (5.31). After including a useful prefactor, we find that (5.31) is

$$\begin{aligned}
&\left(\prod_{m=1}^{N-s} \frac{n(\kappa)\Gamma(2 - 8/\kappa)}{4 \exp \pi i(\beta_{1m} - \beta_{2m}) \sin \pi\beta_{1m} \sin \pi\beta_{2m} \Gamma(1 - 4/\kappa)^2} \right) \\
&\times |z - \bar{z}|^{(\kappa - 4s - 4)^2/8\kappa} \left(\prod_{i<j}^{2N} (x_j - x_i)^{2/\kappa} \right) \left(\prod_{i=1}^{2N} |z - x_i|^{(\kappa - 4s - 4)/\kappa} \right) \\
&\times \oint_{\Gamma_1} \dots \oint_{\Gamma_{N-s}} \left(\prod_{k=1}^{2N} \prod_{l=1}^{N-s} (x_k - u_l)^{-4/\kappa} \right) \left(\prod_{p<q\leq}^{N-s} (u_p - u_q)^{8/\kappa} \right) \\
&\times \left(\prod_{m=1}^{N-s} (z - u_m)^{(4s+4-\kappa)/\kappa} (\bar{z} - u_m)^{(4s+4-\kappa)/\kappa} \right) du_1 \dots du_{N-s}.
\end{aligned} \tag{5.32}$$

Here, $e^{2\pi i \beta_{1m}}$ and $e^{2\pi i \beta_{2m}}$ are the monodromy factors (relative to u_m) of the two branch points entwined by the m-th contour, $n(\kappa)$ is the O(n) model loop fugacity (1.155), and we choose the branch of the logarithm with $\arg z \in [-\pi, \pi)$ for all $z \in \mathbb{C}$ so that each branch cut is parallel to the real axis. Every pinch-point weight Π_Λ will be some

linear combination of functions of the form (5.32), with each term using a different set of contours $\{\Gamma_m\}$. A proof that (5.32) solves the system (5.11-5.15) is given in section 5.4.

Now we explain convenience of the prefactor in (5.32). A first reason involves the limit $x_{i+1} \to x_i$ that sends the $2N$-sided polygon to a $(2N-2)$-sided polygon. In most of our formulas, each Pochhammer contour will entwine a pair of the points among $x_1, \ldots, x_{2N}$. After multiplying the half-plane weight Π_Λ by $(x_{i+1} - x_i)^{2\theta_1}$ and taking this limit, this product goes to either zero or an s-pinch-point density in a $(2N-2)$-gon. Meanwhile, one can show that (5.32) goes to either zero or the same expression except with all factors containing x_i, x_{i+1}, and u_{N-s} omitted, the u_{N-s} integration omitted, a factor of $\beta(-4/\kappa, -4/\kappa)^{-1} = \Gamma(2-8/\kappa)/\Gamma(1-4/\kappa)^2$ and $[4\sin^2(4\pi/\kappa)]^{-1}$ omitted (with $\beta(a,b)$ the Euler beta function), and possibly a fugacity factor $n(\kappa)$ omitted. So to within a factor of $n(\kappa)$, we retain the same normalization as in the $2N$-sided polygon with $N \mapsto N-1$. A second reason is to ensure that (5.32) is finite and nonzero when $\kappa = 8/m$ for some even, positive integer m, and a third reason involves replacing each Pochhammer contour with a simple curve (figure 1.20) in the dense phase. Both matters were considered in the discussion surrounding (2.162).

5.2 Pinch-point densities

In this section, we calculate the explicit formula for the type-Λ s-pinch-point density $\rho^{\mathcal{P}}_{(\Lambda|\varsigma)}$ conditioned on the FFBC event ς for various Λ and $1 \le s \le N$ in either a rectangle $\mathcal{R}$ ($N = 2$) or a hexagon $\mathcal{H}$ ($N = 3$). We proceed in four steps. First we compute the half-plane pinch-point weight Π_Λ. Second, we construct from Π_Λ the universal partition function $\Upsilon_{(\Lambda|\varsigma)}$ that sums exclusively over the event $\varsigma \cap \Lambda$. Third, we transform $\Upsilon_{(\Lambda|\varsigma)}$ into the universal partition function $\tilde{\Upsilon}^{\mathcal{P}}_{(\Lambda|\varsigma)}$ with the appropriate polygon $\mathcal{P}$ for its domain. Fourth, we divide $\tilde{\Upsilon}^{\mathcal{P}}_{(\Lambda|\varsigma)}$ by the universal partition function $\tilde{\Upsilon}^{\mathcal{P}}_{\varsigma}$ that sums exclusively over the FFBC event ς to obtain formulas for pinch-point

densities in $\mathcal{R}$ or $\mathcal{H}$.

5.2.1 Half-plane pinch-point weights

N=2, s=2 and N=3, s=3: First, we consider the two-pinch-point weight Π_{1234} for $N = 2$ and the three-pinch-point weight Π_{123456} for $N = 3$. The subscripts on each weight indicates the indices of the points x_i that are connected to the pinch point. The weights are given by (5.30) with $N = 2$ and $N = 3$ respectively, and both may be expressed in the covariant form (5.16) which we will find convenient later. We find that the $(s = N = 2)$-pinch-point density is

$$\begin{aligned}\Pi_{1234}(x_1,\dots,x_4;z,\bar{z}) &= [(x_2-x_1)(x_4-x_3)]^{1-6/\kappa}|z-\bar{z}|^{\kappa/8-6/\kappa-1}\\ &\times \eta^{8/\kappa-1}(1-\eta)^{2/\kappa}|\mu-\nu|^{24/\kappa-2}[\mu\nu(\eta-\mu)(\eta-\nu)(1-\mu)(1-\nu)]^{1/2-6/\kappa},\end{aligned} \tag{5.33}$$

and the $(s = N = 3)$-pinch-point density is

$$\begin{aligned}\Pi_{123456}(x_1,\dots,x_6;z,\bar{z}) &= [(x_2-x_1)(x_4-x_3)(x_6-x_5)]^{1-6/\kappa}|z-\bar{z}|^{\kappa/8-16/\kappa-1}\\ &\times [\eta(\sigma-\tau)]^{8/\kappa-1}[\tau\sigma(\tau-\eta)(\sigma-\eta)(1-\eta)(1-\tau)(1-\sigma)]^{2/\kappa}|\mu-\nu|^{48/\kappa-3}\\ &\times [\mu\nu(\eta-\mu)(\eta-\nu)(\tau-\mu)(\tau-\nu)(\sigma-\mu)(\sigma-\nu)(1-\mu)(1-\nu)]^{1/2-8/\kappa},\end{aligned} \tag{5.34}$$

where the cross-ratios $\eta, \tau, \sigma, \mu, \nu$ are defined in (5.17, 5.20). The correct normalization of these pinch-point weights depends on bulk-boundary fusion coefficients, but because it is not needed for our purposes, we ignore it in this chapter.

Before we calculate s-pinch-point weights for $s < N$, we comment on the normalizations of these weights too. When $s < N$, almost all samples in the s-pinch-point event Λ will have at least one interval (x_i, x_{i+1}) with its endpoints mutually connected by a boundary arc that does not pass near the pinch-point. The fugacity of this boundary arc is one since we are working with pinch-point weights, so when we

collapse this interval, we must recover an s-pinch-point weight in a system with BCCs at the remaining $2(N-1)$ points on the real axis. Continuing this process until no such intervals remain, we eventually reach an s-pinch-point weight in a system with BCCs at the remaining $2s$ points on the real axis. The weight of this event is given by (5.30) with $N = s$. Therefore, the s-pinch-point weights with $s < N$ are normalized so that they equal the s-pinch-point weight with $N = s$ when all of the intervals whose touching boundary arcs do not pass near the pinch-point are collapsed.

N=2, s=1: Next, we consider one-pinch-point events with $N = 2$ boundary arcs. Here, one boundary arc γ_1 connects the points x_i and x_j with a bulk point $w \in \mathbb{H}$ while the other γ_2 connects the remaining points x_k and x_l. The weight $\Pi_{ij:kl}$ of this event is given by (5.32) with $N = 2$ and $s = 1$.

The formula for $\Pi_{ij:kl}$ has a single contour integral, and the contour $\Gamma_{ij:kl}$ is chosen so that the chiral operators exhibit specific fusion rules that depend on which vertices are connected to z through γ_1. For example, we consider $\Pi_{23:41}$ (figure 5.5). If we let z approach a point x in the segment (x_1, x_2), then γ_1 must touch (x_1, x_2) at x in this limit, which is equivalent to placing a boundary two-leg operator $\psi_2(x)$ there. Therefore the bulk operator $\Psi_1(z)$ must fuse with its image $\Psi_1(\bar{z})$ to give $\psi_2(x)$ to leading order. Now, when the two chiral operators $V^+_{0,1}(z)$ and $V^+_{0,1}(\bar{z})$ fuse, their product is a boundary chiral operator with charge $2\alpha^+_{0,1} = \alpha^+_{1,3}$ which carries the weight θ_2 of a boundary two-leg operator as required (5.10). The same is true of the intervals (x_2, x_3) and (x_3, x_4).

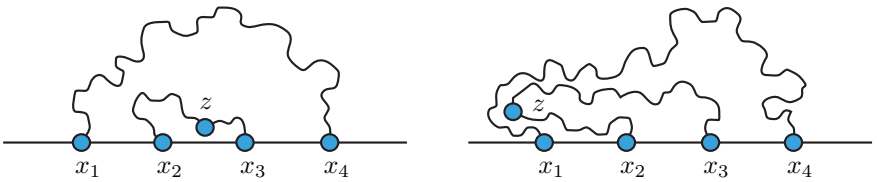

Figure 5.5: The configuration $\Pi_{23:41}$. The left (resp. right) figure shows that a boundary two-leg (resp. four-leg) operator is generated when z approaches the intervals $(x_1, x_2), (x_2, x_3)$, and (x_3, x_4) (resp. the interval (x_4, x_1)).

Next, we let z and $\bar{z}$ approach a point x in the interval (x_4, x_1). Because γ_2 links x_1 with x_4, topological considerations show that both γ_1 and γ_2 must touch (x_4, x_1) at x in this limit (figure 5.5). Therefore the leading operator of the ensuing bulk-image fusion must be a boundary four-leg operator. Above, we saw that the total charge of the bulk-image pair equals that of a boundary two-leg operator. But if we add the screening charge α_-, this total charge becomes $2\alpha^+_{0,1} + \alpha_- = \alpha^+_{1,5}$, which is that of a chiral operator with the desired boundary four-leg weight θ_4 (5.10). The screening charge is pulled in with the bulk-image fusion only if $\Gamma_{23:41}$ contracts to a point in the process. Thus, $\Gamma_{23:41}$ must be a simple curve starting at $\bar{z}$ and ending at z.

In order for $\Pi_{23:41}$ to be a continuous function of z and $\bar{z}$, each point of $\Gamma_{23:41}$ must reside on the same Riemann sheet of the integrand, so $\Gamma_{23:41}$ can only cross the real axis through a specific segment (x_i, x_{i+1}). (Here, $x_5 := x_1$.) This segment must be (x_4, x_1) in order to ensure that $\Gamma_{23:41}$ contracts to a point when we let z and $\bar{z}$ approach a point in (x_4, x_1). This choice creates another desired effect. In the event of a bulk-image fusion over $(x_1, x_4) \setminus \{x_2, x_3\}$, $\Gamma_{23:41}$ does not contract to a point, the screening charge is not drawn in, and an undesired boundary four-leg operator in (x_1, x_4), which would contradict the assertions of the previous paragraph, is not produced.

By cyclically permuting the indices, we find four one-pinch-point weights:

$$\{\Pi_{12:34}, \Pi_{23:41}, \Pi_{34:12}, \Pi_{41:23}\}. \tag{5.35}$$

Each weight is given by (5.32) with $N = 2, s = 1$, and $\Gamma_{ij:kl}$ a simple curve connecting z with $\bar{z}$ and crossing the real axis only through (x_k, x_l). In the formula for each weight, we order the differences in the factors of the integrand so that the branch cuts do not intersect $\Gamma_{ij:kl}$ and the integrand restricted to $\Gamma_{ij:kl}$ is therefore a continuous function of $x_1, \ldots, x_4, z, \bar{z}$, and $u := u_1$.

It is useful to decompose these one-pinch-point weights (5.35) into a linear combination of the integrals (with $x_5 := z$ and $x_6 := \bar{z}$)

$$I_i := \beta(-4/\kappa, -4/\kappa)^{-1} \int_{x_{i-1}}^{x_i} du\, \mathcal{N}\left[\prod_{j=1}^{4}(x_j - u)^{-4/\kappa} \times\ (x_5 - u)^{8/\kappa-1}(x_6 - u)^{8/\kappa-1}\right], \quad i \in \{1, \ldots, 6\}, \quad (5.36)$$

for the purpose of explicitly showing that these weights are real (or at least share a common phase) as they must be for physical reasons and for expressing them in terms of Lauricella functions. Just as in chapter two, the operator "$\mathcal{N}$" orders the differences in the factors of the integrand so that I_i is real. (I_1 is a sum of integrations from $x_0 := x_6$ to ∞ and from $-\infty$ to x_1.) Because $\arg(z) \in [-\pi, \pi)$ for $z \in \mathbb{C}$, the integrand has a branch cut that starts at each x_j with $j < i$ (resp. $j \geq i$) and points leftward (resp. rightward) along the real axis. For simplicity, we momentarily suppose that x_5 and x_6 are real as we decompose each one-pinch-point weight into a linear combination of the various I_i times algebraic factors. For example, we can use figure 5.6 to find the decomposition

$$\Pi_{12:34} = A\left[2i \sin\left(\frac{4\pi}{\kappa}\right) I_5 + e^{4\pi i/\kappa} I_6\right](x_5 - x_6)^{\kappa/8+8/\kappa-2} \times \prod_{i<j}^{4}(x_j - x_i)^{2/\kappa} \prod_{i=1}^{4}(x_5 - x_i)^{1/2-4/\kappa}(x_6 - x_i)^{1/2-4/\kappa}. \quad (5.37)$$

The proportionality constant A will be determined below. Now, to show that the one-pinch-point weights are real, we seek a basis of integrals for the span of $\{I_1, \ldots, I_6\}$ that are real when $x_5 = z$ and $x_6 = \bar{z}$. Integrating the screening charge along a contour parallel to and immediately above (resp. below) the real axis gives the $-$

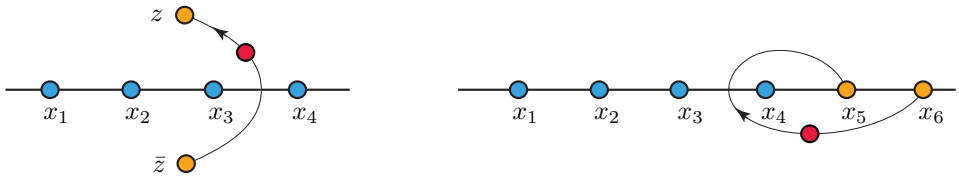

Figure 5.6: The contour used for the one-pinch-point weight $\Pi_{12:34}$. To facilitate calculation, we at times place z and $\bar{z}$ at adjacent locations x_5, x_6 respectfully on the real axis as in the right figure. (In each figure of this chapter, a blue (resp. orange, resp. red) circle marks a point of charge $\alpha^-_{1,2}$ (resp. $\alpha^+_{0,s}$, resp. α_-) in the dense phase.)

(resp. +) branch of the linear relation

$$I_1 + e^{\pm 4\pi i/\kappa} I_2 + e^{\pm 8\pi i/\kappa} I_3 + e^{\pm 12\pi i/\kappa} I_4 + e^{\pm 16\pi i/\kappa} I_5 - e^{\pm 8\pi i/\kappa} I_6 = 0, \tag{5.38}$$

which allows us to write I_5 and I_6 in terms of $I_1, \ldots, I_4$. Then because the integral

$$\mathcal{I}_1 := \beta(-4/\kappa, -4/\kappa)^{-1} \int_{x_4}^{x_1} du\, \mathcal{N} \Bigg[(z-u)^{8/\kappa - 1} (\bar{z}-u)^{8/\kappa - 1} \times \prod_{j=1}^{4} (u - x_i)^{-4/\kappa} \Bigg] = I_5 - e^{8\pi i/\kappa} I_6 + I_1 \tag{5.39}$$

is real when $x_5 = z$ and $x_6 = \bar{z}$, we find a real basis $\{\mathcal{I}_1, \mathcal{I}_2 := I_2, \mathcal{I}_3 := I_3, \mathcal{I}_4 := I_4\}$ for the span of $\{I_i\}_{i=1}^6$. We anticipate that the coefficients found from decomposing the $\Pi_{ij:kl}$ over this basis will share a common phase.

However, it is more useful for our purposes (of calculating one-pinch point weights for the hexagon later) to compute this decomposition via a different approach in which the four integrals $\mathcal{I}_i$ arise naturally as conformal blocks. We consider the one-pinch-point weight $\Pi_{12}(x_1, x_2; z, \bar{z})$, given by $\langle \psi_1(x_1)_{[2]} \psi_1(x_2) \Psi_1(z)_{[2]} \Psi_1(\bar{z}) \rangle$. Here, the bracketed subscript between a pair of operators indicates the unique fusion channel propagating between that pair, so $[s]$ indicates the s-leg channel for $s > 0$ and the identity channel for $s = 0$. To increase N form one to two, we insert the charge-neutral collection $\int_{x_3}^{x_4} du\, V^-_{1,2}(x_3) V^-_{1,2}(x_4) V_-(u)$ with $x_2 < x_3 < x_4$ into the chiral

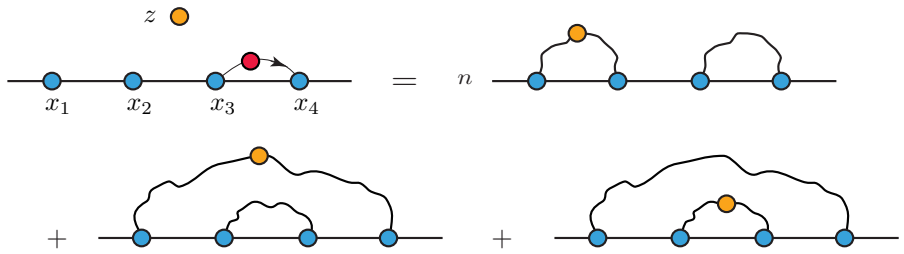

Figure 5.7: The decomposition of (5.40) into a linear combination of the weights $\Pi_{12:34}, \Pi_{41:23}$, and $\Pi_{23:41}$ as given in (5.42).

operator representation of this four-point function. We find

$$\langle \psi_1(x_1)_{[2]}\psi_1(x_2)\psi_1(x_3)_{[0]}\psi_1(x_4)\Psi_1(z)_{[2]}\Psi_1(\bar{z})\rangle \\ = nJ(x_1,\dots x_4;z,\bar{z})\,\mathcal{I}_4(x_1,\dots x_4;z,\bar{z}), \quad (5.40)$$

where the function J is given by (5.32) with $N=2$ and $s=1$:

$$J(x_1,\dots,x_4;z,\bar{z}) := |z-\bar{z}|^{\kappa/8+8/\kappa-2}\prod_{i<j}^{4}(x_j-x_i)^{2/\kappa}\prod_{i=1}^{4}|z-x_i|^{1-8/\kappa}. \quad (5.41)$$

The new pair of boundary one-leg operators at x_3 and x_4 fuse through only the identity channel because the screening charge is integrated along a simple curve connecting x_3 with x_4. The original boundary one-leg operators at x_1 and x_2 still fuse through only the two-leg channel. Three of the four one-pinch-point events $(ij{:}kl)$ are consistent with these fusion rules, (12:34), (41:23), and (23:41), so (5.40) must be a linear combination of the pinch-point weights $\Pi_{12:34}, \Pi_{41:23}$, and $\Pi_{23:41}$ with the coefficients shown below (figure 5.7):

$$\Pi_{41:23} + n\Pi_{12:34} + \Pi_{23:41} = nJ(x_1,\dots x_4;z,\bar{z})\,\mathcal{I}_4(x_1,\dots x_4;z,\bar{z}). \quad (5.42)$$

As usual, n is the loop fugacity (1.155) of the O(n) model.

The coefficients of the linear combination on the left side of (5.42) are found in the

following way. First, to find the coefficient of $\Pi_{12:34}$, we send $x_4 \to x_3$ on both sides of (5.42). (We always implicitly multiply by $(x_j - x_i)^{6/\kappa-1}$ before sending $x_j \to x_i$ so that the limit exists. This is the usual convention for collapsing intervals that we used in chapters two, three, and four.) Then $\Pi_{41:23}, \Pi_{23:41} \to 0$ while $\Pi_{12:34} \to \Pi_{12}$ (5.25), and $nJ \times \mathcal{I}_4 \to n\Pi_{12}$. This justifies the coefficient of n that dresses $\Pi_{12:34}$ in (5.42). Next, to find the coefficient of $\Pi_{41:23}$, we send $x_3 \to x_2$. On the left side of (5.42), $\Pi_{12:34}, \Pi_{23:41} \to 0$ while $\Pi_{41:23} \to \Pi_{14}$, or really Π_{12} with $x_2 \mapsto x_4$. On the right side, we use (5.38) to write $nJ \times \mathcal{I}_4$ as a linear combination of $nJ \times I_1, nJ \times I_3, nJ \times I_5$, and $nJ \times I_6$. (These are the four $nJ \times I_i$ that have either both or neither bounds of integration among $\{x_2, x_3\}$. Again, $x_5 = z$ and $x_6 = \bar{z}$ as usual.) All of the integrals in this combination except $nJ \times I_3$ vanish in this limit, while $nJ \times I_3$ goes to $n\Pi_{12}$. Because $nJ \times I_3$ carries a coefficient of n^{-1} in this linear combination, the right side of (5.42) becomes Π_{12} with $x_2 \mapsto x_4$. This justifies the coefficient of one that dresses $\Pi_{12:34}$ in (5.42). The same reasoning gives the coefficient of one for $\Pi_{23:41}$ in (5.42).

Cyclically permuting the indices in (5.42) gives three more equations relating the four one-pinch-point weights (5.35) to the four integrals $\mathcal{I}_i$. Upon inverting these equations to isolate the weights, we find

$$\Pi_{ij:kl} = J\left[\frac{2\,\mathcal{I}_j + (n^2-2)\,\mathcal{I}_l - n\,\mathcal{I}_i - n\,\mathcal{I}_k}{n^2-4}\right]. \tag{5.43}$$

For each index i, we can multiply $J \times \mathcal{I}_i$ by $(x_2 - x_1)^{6/\kappa-1}(x_4 - x_3)^{6/\kappa-1}|z - \bar{z}|^{1-\kappa/8}$ to arrive with a function G_i that depends only on cross-ratios η, μ, and ν, according to (5.16). After making the replacement $(x_1, x_2, x_3, x_4, z, \bar{z}) \mapsto (0, \eta, 1, \infty, \mu, \nu)$, we find

$$\begin{aligned} G_1(\eta,\mu,\nu) &= \frac{(\eta|\mu-\nu|)^{8/\kappa-1}(1-\eta)^{2/\kappa}}{(\mu\nu(\eta-\mu)(\eta-\nu)(1-\mu)(1-\nu))^{4/\kappa-1/2}} \qquad (5.44)\\ &\times\ F_D\left(1-\frac{4}{\kappa};\frac{4}{\kappa},1-\frac{8}{\kappa},1-\frac{8}{\kappa};2-\frac{8}{\kappa}\,\middle|\,1-\eta,1-\mu,1-\nu\right),\\ G_2(\eta,\mu,\nu) &= \frac{(\mu\nu|\mu-\nu|^2)^{4/\kappa-1/2}(1-\eta)^{2/\kappa}}{((\eta-\mu)(\eta-\nu)(1-\mu)(1-\nu))^{4/\kappa-1/2}} \qquad (5.45) \end{aligned}$$

$$
\begin{aligned}
&\times \quad F_D\left(1-\frac{4}{\kappa};\frac{4}{\kappa},1-\frac{8}{\kappa},1-\frac{8}{\kappa};2-\frac{8}{\kappa}\,\middle|\,\eta,\frac{\eta}{\mu},\frac{\eta}{\nu}\right),\\
G_3(\eta,\mu,\nu) &= \frac{(\eta^2(1-\mu)(1-\nu)|\mu-\nu|^2)^{4/\kappa-1/2}}{(\mu\nu(\eta-\mu)(\eta-\nu))^{4/\kappa-1/2}(1-\eta)^{6/\kappa-1}} \qquad (5.46)\\
&\times \quad F_D\left(1-\frac{4}{\kappa};\frac{4}{\kappa},1-\frac{8}{\kappa},1-\frac{8}{\kappa};2-\frac{8}{\kappa}\,\middle|\,1-\eta,\frac{1-\eta}{1-\mu},\frac{1-\eta}{1-\nu}\right),\\
G_4(\eta,\mu,\nu) &= \frac{(\eta|\mu-\nu|)^{8/\kappa-1}(1-\eta)^{2/\kappa}}{(\mu\nu(\eta-\mu)(\eta-\nu)(1-\mu)(1-\nu))^{4/\kappa-1/2}} \qquad (5.47)\\
&\times \quad F_D\left(1-\frac{4}{\kappa};\frac{4}{\kappa},1-\frac{8}{\kappa},1-\frac{8}{\kappa};2-\frac{8}{\kappa}\,\middle|\,\eta,\mu,\nu\right).
\end{aligned}
$$

We have expressed each G_i in terms of the Lauricella function F_D, defined as [85]

$$
\begin{aligned}
F_D(a,b_1,\ldots,b_m,c\,|\,x_1,\ldots,x_m) &:= \frac{\Gamma(a)}{\Gamma(c)\Gamma(c-a)}\\
&\times \int_0^1 t^{a-1}(1-t)^{c-a-1}(1-x_1t)^{-b_1}\ldots(1-x_mt)^{-b_m}\,dt, \qquad (5.48)
\end{aligned}
$$

by writing the integration variable u of $\mathcal{I}_i$ as the following Möbius transformation of the integration variable t in (5.48):

$$
i=1: \quad u=\frac{t-1}{t}, \qquad (5.49)
$$

$$
i=2: \quad u=\eta\,t, \qquad (5.50)
$$

$$
i=3: \quad u=1-(1-\eta)t, \qquad (5.51)
$$

$$
i=4: \quad u=\frac{1}{t}. \qquad (5.52)
$$

These transformations are chosen so that each F_D has $m=3$ arguments with the first argument between zero and one and the last two arguments being complex conjugates of each other. This choice ensures that each F_D is real. Thus, the $\Pi_{ij:kl}$, expressed in the covariant form (5.16), are

$$\Pi_{ij:kl}(x_1,\ldots,x_4;z,\bar{z}) = [(x_2-x_1)(x_4-x_3)]^{1-6/\kappa}|z-\bar{z}|^{\kappa/8-1} \times \left[\frac{2G_j+(n^2-2)G_l-nG_i-nG_k}{n^2-4}\right](\eta,\mu,\nu), \quad (5.53)$$

with η, μ, ν, and n defined in (5.17, 5.18, 5.20, 1.155) respectively. We note that our normalization in (5.53) ensures that $(x_l - x_k)^{2\theta_1}\Pi_{ij:kl} \to \Pi_{ij}$ (5.25) as $x_l \to x_k$. Now, if we let κ approach $4/m$ with $m \in \mathbb{Z}^+$ so that $n \to \pm 2$, then Π_{ij} remains finite. Thus (5.53) must be finite when $n = \pm 2$, though showing this explicitly appears to be difficult. Comparing (5.53) with (5.37), we find that $A = -in/\sqrt{4-n^2}$.

N=3, s=2: Next, we consider two-pinch-point events with $N = 3$ boundary arcs. Here, two boundary arcs γ_1 and γ_2, with endpoints respectively at $x_i, x_j \in \mathbb{R}$ and $x_k, x_l \in \mathbb{R}$, touch at a bulk point z, and the remaining boundary arc γ_3 has endpoints at x_m and x_n. We note that this setup restricts the allowed BACs to those in which γ_3 does not separate γ_1 from γ_2, so x_m and x_n must be adjacent. The weight $\Pi_{ijkl:mn}$ of this event is given by (5.32) with $N = 3$ and $s = 2$. By cyclically permuting the indices, we find six such two-pinch-point configurations.

The formula for $\Pi_{ijkl:mn}$ contains a single contour integral $\Gamma_{ijkl:mn}$ that is determined via the same reasoning that was used for the case $N = 2$ and $s = 1$ above. We summarize the argument. The two-pinch-point event is conditioned by the insertion of a bulk four-leg operator $\Psi_2(z)$. Topological considerations (as can be understood upon examining figure 5.8) show that fusing this operator with its image across any interval (x_a, x_b) with $(a, b) \neq (m, n)$ (resp. $(a, b) = (m, n)$) must, to leading order, give rise to a boundary four-leg (resp. six-leg) operator ψ_4 (resp. ψ_6). Because $2\alpha^+_{0,2} = \alpha^+_{1,5}$ is the charge of a chiral operator with the boundary four-leg weight θ_4, this requirement is already satisfied when $(a, b) \neq (m, n)$. If $\Gamma_{ijkl:mn}$ is a simple curve with endpoints at z and $\bar{z}$ and crossing the real axis only through (x_m, x_n), then the screening charge is drawn into a bulk-image fusion across this interval, shifting the product to a chiral operator with net charge $2\alpha^+_{0,2} + \alpha_- = \alpha^+_{1,7}$. This operator has the desired

boundary six-leg weight θ_6 (5.10).

To express the two-pinch-point weights in terms of Lauricella functions, we write them as linear combinations of the six real integrals

$$\mathcal{K}_i := \beta(-4/\kappa,-4/\kappa)^{-1}\int_{x_{i-1}}^{x_i} du\,\mathcal{N}\Bigg[(z-u)^{12/\kappa-1}(\bar{z}-u)^{12/\kappa-1} \times\prod_{j=1}^{6}(u-x_j)^{-4/\kappa}\Bigg], \quad i=1,\ldots,6. \quad (5.54)$$

(As before, the operator "$\mathcal{N}$" orders the differences in the factors of the integrand so that the integrand is real, and $\mathcal{K}_1$ is integrated from $x_0 := x_6$ to ∞ and then from $-\infty$ to x_1.) To proceed, we consider the two-pinch-point weight Π_{1234}. Inserting the charge-neutral collection $\int_{x_5}^{x_6} du\, V_{1,2}^-(x_5)V_{1,2}^-(x_6)V_-(u)$ into the chiral representation of its six-point function $\langle\psi_1(x_1)_{[2]}\psi_1(x_2)\psi_1(x_3)_{[2]}\psi_1(x_4)\Psi_1(z)_{[4]}\Psi_1(\bar{z})\rangle$ with $x_4<x_5<x_6$ gives the conformal block

$$\langle\psi_1(x_1)_{[2]}\psi_1(x_2)\psi_1(x_3)_{[2]}\psi_1(x_4)\psi_1(x_5)_{[0]}\psi_1(x_6)\Psi_1(z)_{[4]}\Psi_1(\bar{z})\rangle = nL(x_1,\ldots,x_6;z,\bar{z})\,\mathcal{K}_6(x_1,\ldots,x_6;z,\bar{z}), \quad (5.55)$$

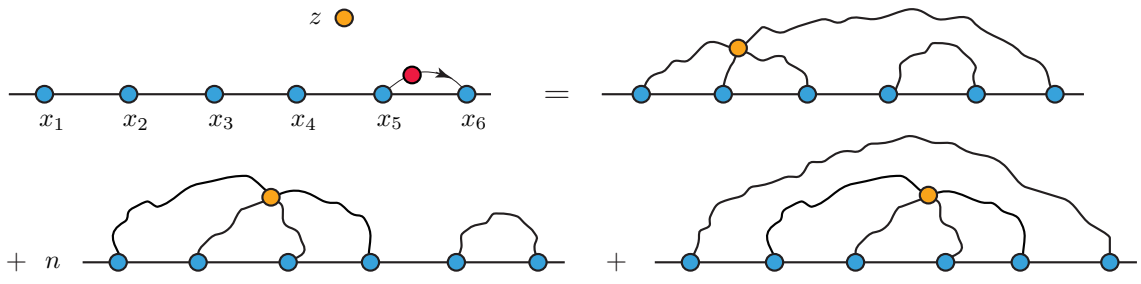

Figure 5.8: The decomposition of (5.55) into a linear combination of the weights $\Pi_{6123:45}, \Pi_{1234:56}$, and $\Pi_{2345:61}$, as given in (5.57).

where the pre-factor L is given by (5.32) with $N = 3$ and $s = 2$:

$$L(x_1, \ldots, x_6; z, \bar{z}) := |z - \bar{z}|^{\kappa/8+18/\kappa-3} \prod_{i<j}^{6} (x_j - x_i)^{2/\kappa} \prod_{i=1}^{6} |z - x_i|^{1-12/\kappa}. \tag{5.56}$$

After following the reasoning that led to (5.42), we find (figure 5.8)

$$\Pi_{6123:45} + n\Pi_{1234:56} + \Pi_{2345:61} = nL(x_1, \ldots, x_6; z, \bar{z})\, \mathcal{K}_6(x_1, \ldots, x_6; z, \bar{z}). \tag{5.57}$$

Another five equations relating the six weights with the six integrals $\mathcal{K}_i$ may be found by cyclically permuting the indices in (5.57). These equations may be simultaneously solved to give

$$\Pi_{ijkl:mn} = nL \left[\frac{(2 - n^2)(\mathcal{K}_i + \mathcal{K}_m) + n(\mathcal{K}_j + \mathcal{K}_l) - 2\,\mathcal{K}_k + (n^3 - 3n)\mathcal{K}_n}{(n^2 - 4)(n^2 - 1)} \right]. \tag{5.58}$$

(We note the double use of n as an index and the loop fugacity of the O(n) model.) To finish, we seek a form for the weights that expresses the $\mathcal{K}_i$ in terms of Lauricella functions and exhibits the conformally covariant ansatz of (5.16). To this end, we define the function

$$\begin{aligned} H_i(x_1, \ldots, x_6; z, \bar{z}) &:= [(x_2 - x_1)(x_4 - x_3)(x_6 - x_5)]^{2\theta_1} |z - \bar{z}|^{2\Theta_2} L \times \mathcal{K}_i & (5.59) \\ &= [(x_2 - x_1)(x_4 - x_3)]^{6/\kappa-1} |z - \bar{z}|^{1+6/\kappa-\kappa/8} L' \times \mathcal{K}'_i, & (5.60) \end{aligned}$$

with L and $\mathcal{K}_i$ adjusted to respective quantities L' and $\mathcal{K}'_i$ that are finite in the limit $x_6 \to \infty$:

$$\begin{aligned} L'(x_1, \ldots, x_6; z, \bar{z}) &:= (x_6 - x_5)^{2/\kappa-1} L, & (5.61) \\ \mathcal{K}'_i(x_1, \ldots, x_6; z, \bar{z}) &:= (x_6 - x_5)^{4/\kappa} \mathcal{K}_i. & (5.62) \end{aligned}$$

According to (5.16), H_i is strictly a function of the cross-ratios η, τ, σ, μ, and ν. After making the replacement $(x_1, x_2, x_3, x_4, x_5, x_6, z, \bar{z}) \mapsto (0, \eta, \rho, \sigma, 1, \infty, \mu, \nu)$, we find

$$\begin{aligned} H_i(\eta,\tau,\sigma,\mu,\nu) &= \mathcal{K}'_i(\eta,\tau,\sigma,\mu,\nu) \\ &\times [\eta(\sigma-\tau)]^{8/\kappa-1}[\tau\sigma(\tau-\eta)(\sigma-\eta)(1-\eta)(1-\tau)(1-\sigma)]^{2/\kappa}|\mu-\nu|^{24/\kappa-2} \\ &\times [\mu\nu(\mu-\eta)(\nu-\eta)(\mu-\tau)(\nu-\tau)(\mu-\sigma)(\nu-\sigma)(\mu-1)(\nu-1)]^{1/2-6/\kappa}, \end{aligned} \tag{5.63}$$

with each $\mathcal{K}'_i(\eta,\tau,\sigma,\mu,\nu) := \mathcal{K}'_i(0,\eta,\tau,\sigma,1,\infty;\mu,\nu)$ finite and equaling a Lauricella function F_D times algebraic prefactors:

$$\mathcal{K}'_1(\eta,\tau,\sigma,\mu,\nu) = F_D\left(\{\chi_j\}\,\middle|\, 1-\eta, 1-\tau, 1-\sigma, 1-\mu, 1-\nu\right), \tag{5.64}$$

$$\mathcal{K}'_2(\eta,\tau,\sigma,\mu,\nu) = \eta^{1-8/\kappa}\tau^{-4/\kappa}\sigma^{-4/\kappa}\mu^{12/\kappa-1}\nu^{12/\kappa-1}F_D\left(\{\chi_j\}\,\middle|\, \eta, \frac{\eta}{\tau}, \frac{\eta}{\sigma}, \frac{\eta}{\mu}, \frac{\eta}{\nu}\right), \tag{5.65}$$

$$\begin{aligned} \mathcal{K}'_3(\eta,\tau,\sigma,\mu,\nu) &= \eta^{1-8/\kappa}\tau^{4/\kappa-1}(\tau-\eta)^{1-8/\kappa}(\sigma-\eta)^{-4/\kappa}(1-\eta)^{-4/\kappa} \\ &\times (\mu-\eta)^{12/\kappa-1}(\nu-\eta)^{12/\kappa-1}F_D\left(\{\chi_j\}\,\middle|\, 1-\frac{\eta}{\tau}, \frac{\sigma(\tau-\eta)}{\tau(\sigma-\eta)}, \right. \\ &\qquad \left. \frac{\tau-\eta}{\tau(1-\eta)}, \frac{\mu(\tau-\eta)}{\tau(\mu-\eta)}, \frac{\nu(\tau-\eta)}{\tau(\nu-\eta)}\right), \end{aligned} \tag{5.66}$$

$$\begin{aligned} \mathcal{K}'_4(\eta,\tau,\sigma,\mu,\nu) &= \tau^{-4/\kappa}(\tau-\eta)^{1-8/\kappa}(\sigma-\eta)^{4/\kappa-1} \\ &\times (\sigma-\tau)^{1-8/\kappa}(1-\tau)^{-4/\kappa}(\mu-\tau)^{12/\kappa-1}(\nu-\tau)^{12/\kappa-1} \\ &\times F_D\left(\{\chi_j\}\,\middle|\, \frac{\sigma-\tau}{\sigma-\eta}, \frac{\eta(\sigma-\tau)}{\tau(\sigma-\eta)}, \frac{(1-\eta)(\sigma-\tau)}{(1-\tau)(\sigma-\eta)}, \right. \\ &\qquad \left. \frac{(\mu-\eta)(\sigma-\tau)}{(\mu-\tau)(\sigma-\eta)}, \frac{(\nu-\eta)(\sigma-\tau)}{(\nu-\tau)(\sigma-\eta)}\right), \end{aligned} \tag{5.67}$$

$$\begin{aligned} \mathcal{K}'_5(\eta,\tau,\sigma,\mu,\nu) &= (1-\eta)^{-4/\kappa}(1-\tau)^{-4/\kappa}(1-\mu)^{12/\kappa-1}(1-\nu)^{12/\kappa-1} \\ &\times (1-\sigma)^{1-8/\kappa}F_D\left(\{\chi_j\}\,\middle|\, 1-\sigma, \frac{1-\sigma}{1-\eta}, \frac{1-\sigma}{1-\tau}, \frac{1-\sigma}{1-\mu}, \frac{1-\sigma}{1-\nu}\right), \end{aligned} \tag{5.68}$$

$$\mathcal{K}'_6(\eta,\tau,\sigma,\mu,\nu) = F_D\left(\{\chi_j\}\,\middle|\, \eta, \tau, \sigma, \mu, \nu\right).$$

Again, we have expressed each $\mathcal{K}'_i$ in terms of F_D by writing its integration variable

u as the following Möbius transformation of the integration variable t in (5.48):

$$i = 1: \quad u = \frac{t-1}{t}, \tag{5.69}$$

$$i = 2: \quad u = \eta\, t, \tag{5.70}$$

$$i = 3: \quad u = \frac{\eta\tau}{\tau - (\tau-\eta)t}, \tag{5.71}$$

$$i = 4: \quad u = \frac{\eta(\sigma-\tau)t - \tau(\sigma-\eta)}{(\sigma-\tau)t - (\sigma-\eta)}, \tag{5.72}$$

$$i = 5: \quad u = 1 - (1-\sigma)t, \tag{5.73}$$

$$i = 6: \quad u = \frac{1}{t}. \tag{5.74}$$

The transformations are chosen so that the first three arguments of each F_D is between zero and one and the last two arguments are complex conjugates. This choice ensures that each F_D is real. Each F_D uses the same set of seven parameters:

$$\{\chi_j\}_{j=1}^{7} = \left\{1 - \frac{4}{\kappa}; \frac{4}{\kappa}, \frac{4}{\kappa}, \frac{4}{\kappa}, 1 - \frac{12}{\kappa}, 1 - \frac{12}{\kappa}; 2 - \frac{8}{\kappa}\right\}. \tag{5.75}$$

Combining (5.58) and (5.59), we find that each weight is given by the conformally covariant formula

$$\begin{aligned}\Pi_{ijkl:mn}(x_1,\ldots,x_6;z,\bar{z}) &= (n^2-4)^{-1}(n^2-1)^{-1} \\ &\times [(x_2-x_1)(x_4-x_3)(x_6-x_5)]^{1-6/\kappa}|z-\bar{z}|^{\kappa/8-6/\kappa-1} \\ &\times [n(2-n^2)(H_i+H_m) + n^2(H_j+H_l) \\ &\qquad - 2nH_k + n^2(n^2-3)H_n](\eta,\tau,\sigma,\mu,\nu),\end{aligned} \tag{5.76}$$

with each H_i explicitly given among (5.63-5.69), η, τ, σ, μ, and ν given by (5.17, 5.20), and n given by (1.155). We note that our normalization in (5.58) ensures that $(x_n - x_m)^{2\theta_1}\Pi_{ijkl:mn} \to \Pi_{ijkl}$ (5.33) as $x_n \to x_m$. Upon letting κ approach the zeros $4/m$ and $12/(3m \pm 1)$, with $m \in \mathbb{Z}^+$, of the denominator of (5.76) in this relation, Π_{ijkl}

remains finite, so (5.76) must be finite when $n = \pm 2, \pm 1$, although this seems to be very difficult to prove directly.

N=3, s=1: Last, we consider one-pinch-point events with $N = 3$ boundary arcs. Here, a boundary arc γ_1 connects x_i, x_j and z, another γ_2 connects x_k and x_l, and the last γ_3 connects x_m and x_n. We denote the half-plane weight of this event by $\Pi_{ij:kl:mn}$, and it is given by (5.32) with $N = 3$ and $s = 1$. This formula contains a double contour integral, and the contours must not intersect in order to guarantee a solution of the system of null-state PDEs (figure 2.1). According to the discussion preceding (2.7), there are $C_3 = 5$ possible BACs, and in each, z may touch any one of the three boundary arcs to give a total of fifteen possible one-pinch-point events.

Now we associate certain choices of integration contours with particular linear combinations of these configurations. In the previously considered cases with one screening charge, we noted that a half-plane pinch-point weight with a simple contour connecting z with $\bar{z}$ by crossing a specified interval (x_a, x_b) corresponds to a specified pinch-point event, and now we investigate to what extent this remains true in our present situation with two screening charges. We suppose that γ_1 connects x_1, x_2, and z. Then $x_3, \ldots, x_6$ are connected pairwise by the two remaining boundary arcs in one of two possible ways. In both cases, topological considerations show that fusion of the bulk two-leg operator $\Psi_1(z)$ with its image across intervals (x_3, x_4) or (x_5, x_6) must

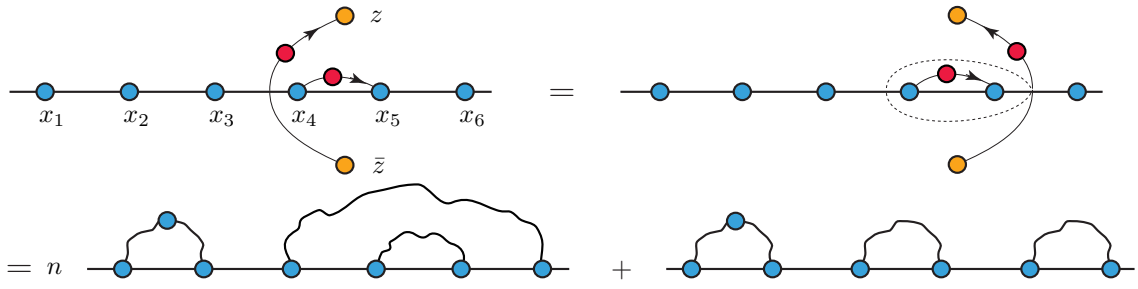

Figure 5.9: The decomposition of the integral in (5.77) into a linear combination of the weights $\Pi_{12:34:56}$ and $\Pi_{12:36:45}$. The contour Γ_{12} connecting z with $\bar{z}$ in the top-left figure can be deformed into the contour that is a vertical reflection of Γ_{12} plus the dashed contour in the top-right figure. According to (3.3), integration along the dashed contour gives zero.

give rise to a boundary four-leg operator to leading order. Hence, we choose the first contour Γ_{12} to be a simple curve connecting z and $\bar{z}$ and crossing the real axis only through (x_3, x_4). A natural choice for the second contour would be the same as for the first but crossing (x_5, x_6) instead, yet this is not allowed because the contours would then intersect at z and $\bar{z}$. Suppose that the second contour is $[x_4, x_5]$ instead. Identity (3.3) allows us to deform Γ_{12} into a simple curve crossing the real axis only through (x_5, x_6), so a bulk-image fusion across (x_5, x_6) will produce a boundary four-leg operator there as well (figure 5.9). The formula that follows from these contour choices sum over both possible boundary arc connectivities between $x_3, \ldots, x_6$. Their relative coefficients can be found in the usual way. Thus, we have from (5.32) with $N = 3$ and $s = 1$ that

$$\Pi_{12:34:56} + n\Pi_{12:36:45} = \frac{n|z-\bar{z}|^{\kappa/8+8/\kappa-2}}{i\beta(-4/\kappa,-4/\kappa)^2\sqrt{4-n^2}} \times \prod_{i<j}^{6}(x_j-x_i)^{2/\kappa}\prod_{i=1}^{6}|z-x_i|^{1-8/\kappa}\int_{\Gamma_{12}}\int_{x_4}^{x_5} du_1\,du_2\,\mathcal{N}\Big[\ \ldots\ \Big]. \quad (5.77)$$

The normalization follows form requiring the we recover the two-pinch-point weight $\Pi_{12:34}$ with $x_6 \mapsto x_4$ upon sending $x_5 \to x_4$. The ellipsis stands for the rest of the integrand in (5.32). Although this density is a natural observable, the left side is not a single one-pinch-point configuration. Cyclic permutation of the indices generates only five more equations involving just twelve of the fifteen possible weights. One of the missing weights is $\Pi_{14:23:56}$, and the other two missing weights are generated by rotating the hexagon.

In order to isolate all fifteen weights, we pursue our usual second strategy of splicing charge-neutral pairs into simpler correlation functions. We begin the one-pinch-point weight $\Pi_{12}(x_i, x_j; z, \bar{z})$, given by $\langle \psi_1(x_i)_{[0]}\psi_1(x_j)\Psi_1(z)_{[2]}\Psi_1(\bar{z})\rangle$. We insert into its chiral representation a first charge-neutral collection $\int_{x_k}^{x_l} V_{1,2}^-(x_k)V_{1,2}^-(x_l)$ $V_-(u_1)\,du_1$, chosen so that x_k and x_l are not separated within the real axis by x_i and

	$M \times \mathcal{K}_{12;34}$	$M \times \mathcal{K}_{12;45}$	$M \times \mathcal{K}_{12;56}$	$M \times \mathcal{K}_{12;63}$
	0	0	0	0
	0	n	n^2	n
	n^2	n	0	n
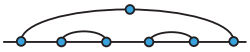	0	1	1	1
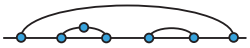	1	n	1	0
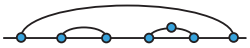	1	0	1	0
	0	n	n	1
	0	1	n	1
	n	1	0	1
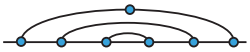	n	1	0	1
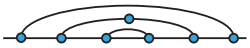	n	1	0	1
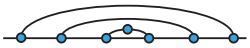	0	1	n	1
	0	0	0	0
	n	n^2	n	0
	n	0	n	n^2

Table 5.1: The $M \times \mathcal{K}_{kl;mn}$ (columns) may be decomposed into linear combinations of the fifteen one-pinch-point densities (rows). (Relative) coefficients for four of the fifteen decompositions are shown in this table.

x_j, and then a second collection $\int_{x_m}^{x_n} V_{1,2}^-(x_m)V_{1,2}^-(x_n)V_-(u_2)\,du_2$, chosen so that x_m and x_n are not separated within the real axis by x_i, x_j, x_k, or x_l. We find fifteen distinct conformal blocks, each with $n = m+1$ and $k = l+1$ (i.e., the inserted boundary arcs are not nested) or $k = l+3$ (i.e., the inserted boundary arcs are nested) (The case $n = 7$ or $k = 7, 8, 9$ is identified with $n = 1$ or $k = 1, 2, 3$ respectively). Each block has the form

$$\langle \psi_1(x_i)_{[2]}\psi_1(x_j)\psi_1(x_k)_{[0]}\psi_1(x_l)\psi_1(x_m)_{[0]}\psi_1(x_n)\Psi_1(z)_{[2]}\Psi_1(\bar{z})\rangle$$
$$= n^2 M(x_1,\ldots,x_6;z,\bar{z})\,\mathcal{K}_{kl;mn}(x_1,\ldots,x_6;z,\bar{z}), \quad (5.78)$$

where $\mathcal{K}_{kl;mn}$ is the real-valued integral

$$\mathcal{K}_{kl;mn} := \beta(-4/\kappa,-4/\kappa)^{-2}\int_{x_k}^{x_l}\int_{x_m}^{x_n} du_1\,du_2\,\mathcal{N}\Bigg[(u_1-z)^{8/\kappa-1}(u_1-\bar{z})^{8/\kappa-1}$$
$$\times\,(u_2-z)^{8/\kappa-1}(u_2-\bar{z})^{8/\kappa-1}(u_2-u_1)^{8/\kappa}\prod_{i=1}^{6}(u_1-x_i)^{-4/\kappa}(u_2-x_i)^{-4/\kappa}\Bigg], \quad (5.79)$$

and where M follows from (5.32):

$$M(x_1,\ldots,x_6;z,\bar{z}) := |z-\bar{z}|^{\kappa/8+8/\kappa-2}\prod_{i<j}^{6}(x_j-x_i)^{2/\kappa}\prod_{i=1}^{6}|z-x_i|^{1-8/\kappa}. \quad (5.80)$$

The $\mathcal{K}_{kl;mn}$ can be decomposed into linear combinations of the fifteen crossing weights in the usual way. This decomposition is shown for four of the $\mathcal{K}_{kl;mn}$ in the top row of table 5.1, and the other eleven are found by cyclically permuting the indices. We thus find an invertible system of fifteen equations with the fifteen weights as unkowns. The formulas that follow from this inversion are complicated, and we leave their further investigation to the interested reader.

5.2.2 Half-plane universal partition functions

In this section, we construct half-plane universal partition functions $\Upsilon_{(\Lambda|\varsigma)}$ from the weights computed in section 5.2.3. We complete these calculations only for the cases $N = 2$ and 3. However, the method is clearly generalizable to polygons with more sides.

For simplicity, our language will suggest that we have conformally mapped the upper half-plane onto the interior of a $2N$-sided polygon $\mathcal{P}$ so that the vertices are numbered counterclockwise in ascending order starting with the bottom-left vertex,

the i-th vertex w_i is the image of x_i, and $\mathcal{P}$ will have a bottom side $[w_1, w_2]$ sitting flush against the real axis (figure 5.13). However, we will postpone the actual implementation of this mapping to the next subsection because of subtleties that arise with the use of corner one-leg operators.

Also, we enumerate the five possible BACs as in figure 5.10 for $N = 2$ and 3, and we enumerate the five possible exterior arc connectivities, or FFBCs, identically to the BACs after reflecting the interior arcs into exterior arcs that are outside of $\mathcal{P}$.

In order to write a formula for $\Upsilon_{(\Lambda|\varsigma)}$, we need to know the number of boundary loops present in the system. Throughout this section, we use the second definition of "boundary loops" given in chapter four. These are the boundary loops formed by joining the exterior arcs in the diagram for the FFBC event $\varsigma \in \mathrm{BC}_N$ with the interior arcs in the diagram for the BAC event $\lambda \in \mathrm{AC}_N$. The number of boundary loops is denoted by $l_{\lambda,\varsigma}$. We recall that these boundary loops are not the same as the physical boundary loops induced by, for example, treating those exterior arcs as fictional bonds in the Q-state Potts model. The difference d_ς in the number of boundary loops between the second and first definitions is given by (4.30) and does

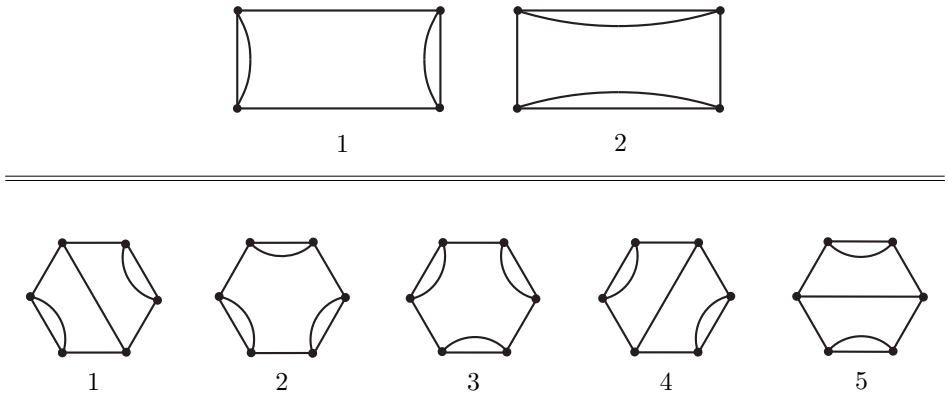

Figure 5.10: An illustration of the labeling that we will use for the boundary arc connectivities of $\mathcal{R}$ and $\mathcal{H}$.

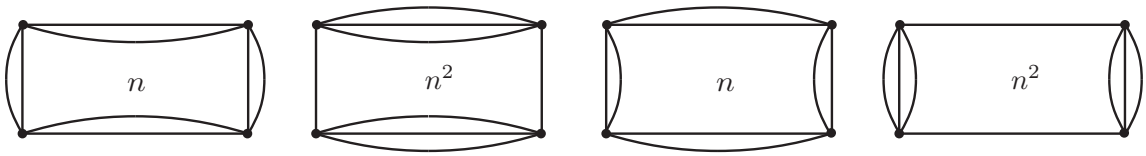

Figure 5.11: The four boundary loop configurations for $\mathcal{R}$. Each boundary loop contributes a factor of n.

not depend on Λ. Thus, the universal partition functions $\Upsilon_{(\Lambda|\varsigma)}$ is given by

$$\Upsilon_{(\Lambda|\varsigma)} = n^{-d_\varsigma} \sum_{\substack{\lambda \in \mathrm{AC}_N \\ \lambda \cap \Lambda \neq \emptyset}} n^{l_{\lambda,\varsigma}} \Pi_\Lambda. \tag{5.81}$$

The extra factor of n^{-d_ς} will have no bearing since it appears in the numerator and denominator of (5.5) and thus cancels with itself. But to be technically correct, we include it anyway. This factor is given in (4.30).

First, we sum (5.81) for pinch-point events in the rectangle $\mathcal{R}$ with the left/right sides wired. With $N = 2$, there are two possible FFBC events, and they are enumerated according to figure 5.10. Thus, ς_1 is the independent wiring event and ς_2 is the mutual wiring event. Both FFBC events are possible in the dense phase while only the latter is possible in the dilute phase. If Λ is a specified one-pinch-point event, then the boundary arcs connect in exactly one way, so there is only one term in the sum (5.81). From figure 5.11, we find (with $d_k := d_{\varsigma_k}$)

$$\left.\begin{array}{ll} \Upsilon_{(12:34|1)} = n^{-d_1+1}\Pi_{12:34} & \Upsilon_{(34:12|1)} = n^{-d_1+1}\Pi_{34:12} \\ \Upsilon_{(41:23|1)} = n^{-d_1+2}\Pi_{41:23} & \Upsilon_{(23:41|1)} = n^{-d_1+2}\Pi_{23:41} \end{array}\right\} \quad \begin{array}{l}\text{independently} \\ \text{wired,}\end{array} \tag{5.82}$$

$$\left.\begin{array}{ll} \Upsilon_{(12:34|2)} = n^{-d_2+2}\Pi_{12:34} & \Upsilon_{(34:12|2)} = n^{-d_2+2}\Pi_{34:12} \\ \Upsilon_{(41:23|2)} = n^{-d_2+1}\Pi_{41:23} & \Upsilon_{(23:41|2)} = n^{-d_2+1}\Pi_{23:41} \end{array}\right\} \quad \begin{array}{l}\text{mutually} \\ \text{wired,}\end{array} \tag{5.83}$$

with the one-pinch-point half-plane weight $\Pi_{ij:kl}$ and the loop fugacity n given in (5.53) and (1.155) respectively. Also d_ς is given by (4.30), so $d_1 = 0$ and $d_2 = 1$. If Λ is the two-pinch-point event, then the tips of the four multiple-SLE curves, each

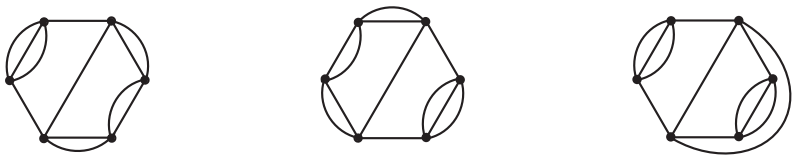

Figure 5.12: Three possible exterior arc connectivities (equivalently three FFBCs) of $\mathcal{H}$ out of five possibilities. Left to right, there are two, two, and three boundary loops, giving rise to fugacity factors n^2, n^2, n^3 respectively.

anchored to a different corner of $\mathcal{R}$, are conditioned to evolve towards a common specified bulk point $w \in \mathcal{R}$. As these tips approach w, they are equally likely to connect vertically or horizontally, so there are two terms in the sum (5.81). For the mutual wiring and independent wiring events, we respectively find

$$\Upsilon_{(1|1234)} = n^{-d_1}(n+n^2)\Pi_{1234}, \quad \Upsilon_{(2|1234)} = n^{-d_2}(n+n^2)\Pi_{1234}, \tag{5.84}$$

with the two-pinch-point half-plane weight Π_{1234} and the loop fugacity n given in (5.33) and (1.155) respectively. Again, $d_1 = 0$ and $d_2 = 1$.

Next, we sum (5.81) for pinch-point events in the hexagon $\mathcal{H}$ with the bottom and top left/right sides wired. When $N = 3$, there are five possible FFBCs. They are enumerated according to figure 5.10, so ς_3 is the independent wiring event, ς_2 is the mutual wiring event, and ς_1 (resp. ς_4, resp. ς_5) is the event with the bottom and top-left (resp. bottom and top-right, resp. top-left and top-right) sides mutually wired and the remaining fixed side independently wired. We call ς_1, ς_4, and ς_5 a *mixed FFBC*. As usual, only the mutual wiring event is possible in the dilute phase. If Λ is a specified one-pinch-point event, then there is only one term in the sum (5.81) since the exterior arcs connect with the boundary arcs to form the same number $p \in \{1, 2, 3\}$ of boundary loops for each sample Λ (figure 5.12). Therefore,

$$\Upsilon_{(ij:kl:mn|\varsigma)} = n^{-d_\varsigma + p}\Pi_{ij:kl:mn} \tag{5.85}$$

with the loop fugacity n and d_ς given in (1.155) and (4.30) respectively, and the half-plane weight $\Pi_{ij:kl:mn}$ given by inverting the system of equations that is partly shown in table 5.1. If Λ is a specified two-pinch-point event, then there are two terms in the sum (5.81) since the two boundary arcs touching at the two-pinch-point can be separated into two nonintersecting boundary arcs in two ways. The first and second way will have p_1 and p_2 boundary loops respectively, with $\{p_1, p_2\} = \{1, 2\}$ or $\{2, 3\}$. Therefore,

$$\Upsilon_{(ijkl:mn|\varsigma)} = n^{-d_\varsigma}(n^{p_1} + n^{p_2})\Pi_{ijkl:mn}, \tag{5.86}$$

with the two-pinch-point half-plane weight $\Pi_{ijkl:mn}$, the loop fugacity n, and d_ς given in (5.76, 1.155, 4.30) respectively. If Λ is the three-pinch-point event, then there are five terms in the sum (5.81) since the three boundary arcs touching at the three-pinch-point can be separated into any of the five possible BACs shown in figure (5.10). We therefore find

$$\Upsilon_{(123456|\varsigma)} = n^{-d_\varsigma}(n + 3n^2 + n^3)\Pi_{123456}, \quad \begin{cases} \varsigma \text{ the independently wired} \\ \text{or the mutually wired FFBC,} \end{cases} \tag{5.87}$$

$$\Upsilon_{(123456|\varsigma)} = n^{-d_\varsigma}(2n + 2n^2 + n^3)\Pi_{123456}, \quad \varsigma \text{ a mixed FFBC,} \tag{5.88}$$

with the three-pinch-point half-plane weight Π_{123456}, the loop fugacity n, and d_ς given in (5.34, 1.155, 4.30) respectively.

There are many possible combinations of pinch-point configurations Λ and FFBCs events $\varsigma \in \mathrm{BC}_N$ for the hexagon. We give explicit formulas for type-Λ pinch-point densities for a few different Λ and with the independent wiring event ς_3. (The exponent d_3 is zero.) Except for the three-pinch-point density, which is too rare to accurately measure, these results are verified via simulation in section 5.3. First, the following combination sums exclusively over samples with a specified one-pinch-point

w on a boundary arc connecting vertex one with vertex two:

$$\Upsilon_{(12:34:56|3)} + n^2\Upsilon_{(12:36:45|3)} = n^3[\Pi_{12:34:56} + n\Pi_{12:36:45}]. \tag{5.89}$$

The linear combination on the left side is chosen so that the right side is given by (5.77). Next, the universal partition function for a two-pinch point between two boundary arcs that connect vertices w_6, w_1, w_2, and w_3 of the hexagon is given by (5.86). We find

$$\Upsilon_{(6123:45|3)} = (n + n^2)\Pi_{6123:45}, \tag{5.90}$$

with n and $\Pi_{6123:45}$ given in (1.155) and (5.105) respectfully. Finally, the three-pinch-point partition function $\Upsilon_{(123456|3)}$ is already given in (5.87).

5.2.3 Transforming the universal partition functions

In this section, we transform the universal partition functions to functions with the appropriate $2N$-sided polygons for their domains. Most of the main points and calculations are done in section 4.5, and we use those results here. The FFBC events of BC_N are labeled as in the previous section (see figure 5.10).

Let $Z^{\mathcal{D}}_{(\Lambda|\varsigma)}$ be the partition function for the system in a simply connected domain $\mathcal{D}$ with a smooth boundary and with the invariance relation

$$Z^{\mathcal{D}}_{(\Lambda|\varsigma)}(w_1, \ldots, w_{2N}; w) = Z_{(\Lambda|\varsigma)}(x_1, \ldots, x_{2N}; z), \tag{5.91}$$

where f is a conformal bijection taking the upper half-plane onto $\mathcal{D}$, $w_i = f(x_i) \in \partial\mathcal{D}$ and $w = f(x)$. As the upper half-plane partition function $Z_{(\Lambda|\varsigma)}$ has the asymptotic behavior

$$Z_{(\Lambda|\varsigma)}/Z_f \underset{\epsilon_i,\epsilon\to 0}{\sim} C_s^2 c_1^{2N} \epsilon_1^{\theta_1} \ldots \epsilon_{2N}^{\theta_1} \epsilon^{2\Theta_s} \Upsilon_{(\Lambda|\varsigma)}, \tag{5.92}$$

$Z^{\mathcal{D}}_{(\Lambda|\varsigma)}$ will have the asymptotic behavior

$$Z^{\mathcal{D}}_{(\Lambda|\varsigma)}/Z_f \underset{\delta_i,\delta\to 0}{\sim} c_1^{2N}\delta_1(w_1)^{\theta_1}\dots\delta_{2N}(w_{2N})^{\theta_1}\delta(w)^{2\Theta_s}\Upsilon^{\mathcal{D}}_{(\Lambda|\varsigma)}, \tag{5.93}$$

with $\delta_i = \epsilon_i|\partial f(x_i)|, \delta = \epsilon|\partial f(x)|$, and with

$$\Upsilon^{\mathcal{D}}_{(\Lambda|\varsigma)} := |\partial f(x_1)|^{-\theta_1}\dots|\partial f(x_{2N})|^{-\theta_1}|\partial f(z)|^{-2\Theta_s}\Upsilon_{(\Lambda|\varsigma)}. \tag{5.94}$$

In section 4.5, we argued that, although conformally invariant, the pinch-point density given by $Z^{\mathcal{D}}_{(\Lambda|\varsigma)}/Z^{\mathcal{D}}_{\varsigma}$ is unnatural because the disk size $\delta(w)$ (resp. $\delta_i(w_i)$) containing the pinch-point (resp. i-th BCC) varies with its location w in $\mathcal{D}$ (resp. w_i in $\partial\mathcal{D}$). Indeed, when we measured some of the pinch-point densities via computer simulation (see section 5.3), we naturally counted a sample as an s-pinch-point event at $w \in \mathcal{D}$ if s distinct boundary arcs passed within zero or one lattice spacings of w (depending on the lattice) regardless of the location of w in $\mathcal{D}$. To this end, it is natural to replace

$$Z^{\mathcal{D}}_{(\Lambda|\varsigma)} \quad\longrightarrow\quad \mathcal{Z}^{\mathcal{D}}_{(\Lambda|\varsigma)} \underset{\delta_i,\delta\to 0}{\sim} c_1^{2N}\delta_1^{\theta_1}\dots\delta_{2N}^{\theta_1}\delta^{2\Theta_s}\Upsilon^{\mathcal{D}}_{(\Lambda|\varsigma)} \tag{5.95}$$

with δ and each δ_i independent of w and w_i respectively.

Now we suppose that the boundary of $\mathcal{D}$ is smooth except at a finite number of corner points $w_1,\dots,w_{2N} \in \partial\mathcal{D}$. We have in mind the case that $\mathcal{D}$ is an equiangular $2N$-sided polygon $\mathcal{P}$ with vertices $w_1,\dots,w_{2N}$, near which the $2N$ BCCs occur. Then to replace $\delta(w)$ with δ as prescribed above is valid as long as w is sufficiently far from the vertices, but to replace the other $\delta_i(w_i)$ with δ_i is not valid since the derivative of f is either infinite or zero at the vertices. According to section 4.5, we must instead replace

$$Z^{\mathcal{P}}_{(\Lambda|\varsigma)} \quad\longrightarrow\quad \tilde{\mathcal{Z}}^{\mathcal{P}}_{(\Lambda|\varsigma)} \underset{\delta_i,\delta\to 0}{\sim} c_1^{2N}\delta_1^{\theta_1}\dots\delta_{2N}^{\theta_1}\delta^{2\Theta_s}\tilde{\Upsilon}^{\mathcal{D}}_{(\Lambda|\varsigma)}, \tag{5.96}$$

where $\tilde{\Upsilon}^{\mathcal{P}}_{(\Lambda|\varsigma)}$ is the correlation function (5.6) using corner one-leg operators at the

vertices of $\mathcal{P}$.

First, we transform the $N = 2$ half-plane universal partition functions into functions with the rectangle $\mathcal{R}$ for their domains (figure 5.13). The rectangle will have aspect ratio R and vertices $w_1 = 0, w_2 = R, w_3 = R + i$, and $w_4 = i$. The interior angles are $\phi = \pi/2$, so (4.78) gives

$$\tilde{\Upsilon}^{\mathcal{R}}_{(\Lambda|\varsigma)} = \langle \psi_1^c(0)\psi_1^c(R)\psi_1^c(R+i)\psi_1^c(i)\Psi_s(z,\bar{z})\rangle_{\mathcal{R}} = \lim_{\varepsilon_j \to 0} (16\varepsilon_1\varepsilon_2\varepsilon_3\varepsilon_4)^{-\theta_1} \times \langle \psi_1(\varepsilon_1)\psi_1(R+i\varepsilon_2)\psi_1(R+i-\varepsilon_3)\psi_1(i-i\varepsilon_4)\Psi_s(z,\bar{z})\rangle_{\mathcal{R}}. \quad (5.97)$$

We use the Schwarz-Christoffel map f of (4.71) with parameters (4.83-4.84), $m := m_1$, and $c = K'(m) := K(1-m)$ where K is the elliptic function of the first kind. This map sends $(x_1, x_2, x_3, x_4) \mapsto (0, m, 1, \infty)$. Here, m is the modular parameter of the transformation, related to the aspect ratio R (length divided by height) of $\mathcal{R}$ through

$$R = K(m)/K'(m), \quad m = \left(\frac{\vartheta_4(0, e^{-\pi R})}{\vartheta_3(0, e^{-\pi R})}\right)^4, \quad (5.98)$$

where ϑ_3 and ϑ_4 are the Jacobi theta functions of the third and fourth kinds respectively. Using the covariance rule (5.94), we have

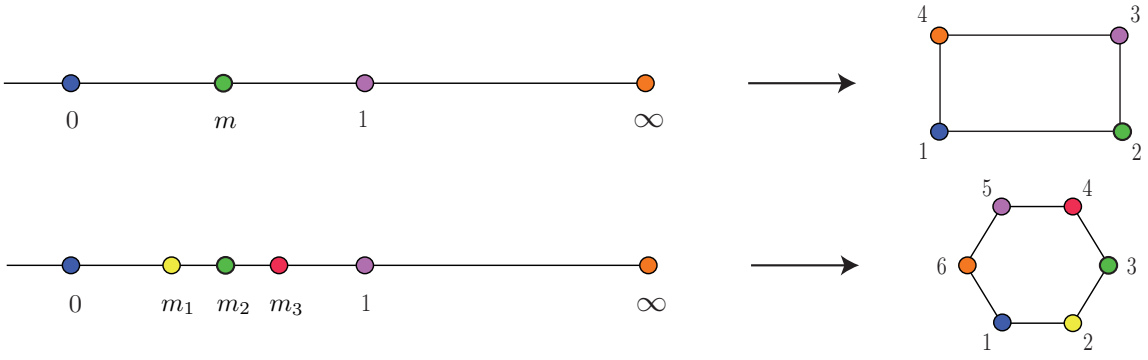

Figure 5.13: The transformation of the upper half-plane to the interior of the rectangle and the hexagon and our enumeration of the vertices of either shape.

$$\tilde{\Upsilon}^{\mathcal{R}}_{(\Lambda|\varsigma)}(m;z,\bar{z}) = |\partial f(z)|^{-2\Theta_s} \lim_{\varepsilon_j\to 0}(16\varepsilon_1\varepsilon_2\varepsilon_3\varepsilon_4)^{-\theta_1} \times \prod_{j=1}^{4} |\partial f(x'_j)|^{-\theta_1} \Upsilon_{(\Lambda|\varsigma)}(x'_1,x'_2,x'_3,x'_4;z,\bar{z}), \quad (5.99)$$

with $x'_1,\ldots,x'_4$ given in (4.85-4.88). Using the inverse of the transformation f, given by $z = f^{-1}(w) = m\,\mathrm{sn}(w\,K'\,|\,m)^2$ with "sn" the Jacobi sine function, we find

$$\tilde{\Upsilon}^{\mathcal{R}}_{(\Lambda|\varsigma)}(m;w) = |2mK'\mathrm{sn}(wK'\,|\,m)\mathrm{cn}(wK'\,|\,m)\mathrm{dn}(wK'\,|\,m)|^{[16s^2-(\kappa-4)^2]/8\kappa} \times n^{-d_\varsigma}[m(1-m)]^{6/\kappa-1}K'^{24/\kappa-4} \lim_{x\to\infty} x^{6/\kappa-1}\Upsilon_{(\Lambda|\varsigma)}(0,m,1,x;z,\bar{z}). \quad (5.100)$$

We note that $\eta \to m$ as $\varepsilon_1,\ldots,\varepsilon_4 \to 0$.

The expression for the universal partition function $\tilde{\Upsilon}^{\mathcal{R}}_{\varsigma}$ in the rectangle was computed in section 4.5, and it is given by (4.90) with $N = 2$. Using the Euler integral definition of the hypergeometric function, we find that they are given by

$$\tilde{\Upsilon}^{\mathcal{R}}_{1}(m) = n^{-d_1+2}K'(m)^{24/\kappa-4}\,{}_2F_1\left(2-\frac{12}{\kappa},1-\frac{4}{\kappa};2-\frac{8}{\kappa}\,\middle|\,1-m\right), \quad (5.101)$$

$$\tilde{\Upsilon}^{\mathcal{R}}_{2}(m) = n^{-d_2+2}K'(m)^{24/\kappa-4}\,{}_2F_1\left(2-\frac{12}{\kappa},1-\frac{4}{\kappa};2-\frac{8}{\kappa}\,\middle|\,m\right). \quad (5.102)$$

In accordance with our conventions, $\tilde{\Upsilon}^{\mathcal{R}}_{1}$ (resp. $\tilde{\Upsilon}^{\mathcal{R}}_{2}$) corresponds to a rectangle with independently (resp. mutually) wired sides. We recall that $d_1 = 0$ while $d_2 = 1$.

Next we transform the $N = 3$ half-plane universal partition functions into functions with their domain the hexagon $\mathcal{H}$ with vertices $w_1 = 0, w_2 > 0$, $w_3,\ldots,w_6$ in the upper half-plane, and interior angles $\phi = 2\pi/3$ (figure 5.13). Equation (4.78) says

$$\tilde{\Upsilon}^{\mathcal{H}}_{(\Lambda|\varsigma)} = \langle\psi^c_1(w_1)\psi^c_1(w_2)\psi^c_1(w_3)\psi^c_1(x_4)\psi^c_1(w_5)\psi^c_1(w_6)\Psi_s(w,\bar{w})\rangle_{\mathcal{H}} = \lim_{\varepsilon_j\to 0}\left(\frac{729\sqrt{\varepsilon_1\varepsilon_2\varepsilon_3\varepsilon_4\varepsilon_5\varepsilon_6}}{64}\right)^{-\theta_1}\left\langle\prod_{j=1}^{6}\psi_1(w_j+\varepsilon_j e^{(j-1)\pi i/3})\Psi_s(w,\bar{w})\right\rangle_{\mathcal{H}}. \quad (5.103)$$

We use the Schwarz-Christoffel map f given by (4.71) with parameters (4.83-4.84) and $c = 1$. (The parameter c sets the length of the side $[w_1, w_2]$.) Using the covariance rule (5.94), we have

$$\tilde{\Upsilon}^{\mathcal{H}}_{(\Lambda|\varsigma)}(m_1, m_2, m_3; w) = |\partial f(z)|^{-2\Theta_s} \lim_{\varepsilon_j \to 0} \left(\frac{729\sqrt{\varepsilon_1\varepsilon_2\varepsilon_3\varepsilon_4\varepsilon_5\varepsilon_6}}{64} \right)^{-\theta_1} \times \prod_{j=1}^{6} |\partial f(x'_j)|^{-\theta_1} \Upsilon_{(\Lambda|\varsigma)}(x'_1, x'_2, x'_3, x'_4, x'_5, x'_6; z, \bar{z}), \quad (5.104)$$

with $x'_1, \ldots, x'_6$ given in (4.85-4.88). This becomes (with $z = f^{-1}(w)$)

$$\begin{aligned} \tilde{\Upsilon}^{\mathcal{H}}_{(\Lambda|\varsigma)}(m_1, m_2, m_3; w) &= n^{-d_\varsigma} |27z(m_1 - z)(m_2 - z)(m_3 - z)(1 - z)/8|^{[16s^2 - (\kappa-4)^2]/24\kappa} \\ &\times [(m_2 - m_1)(m_3 - m_1)(m_3 - m_2)(1 - m_1)(1 - m_2)(1 - m_3)]^{(6-\kappa)/2\kappa} \\ &\times [m_1 m_2 m_3]^{(6-\kappa)/2\kappa} \lim_{x \to \infty} x^{6/\kappa - 1} \Upsilon_{(\Lambda|\varsigma)}(0, m_1, m_2, m_3, 1, x; z, \bar{z}). \end{aligned} \quad (5.105)$$

We note that $(\eta, \tau, \sigma) \to (m_1, m_2, m_3)$ as $\varepsilon_1, \ldots, \varepsilon_6 \to 0$.

The expression for the universal partition function $\tilde{\Upsilon}^{\mathcal{H}}_{\varsigma}$ in the hexagon was computed in section 4.5, and it is given by (4.90) with $N = 3$. There are five half-plane universal partition functions Υ_ς, and each is proportional to an element of $\mathcal{B}_3$ (4.27). We will only consider the function Υ_3 with the sides $(x_1, x_2), (x_3, x_4)$, and (x_5, x_6) independently wired. In this case, $d_3 = 0$, so $\Upsilon_3 = F_3$. We therefore have

$$\begin{aligned} \tilde{\Upsilon}^{\mathcal{H}}_{3}(m_1, m_2, m_3) &= n^3 \beta(-4/\kappa, -4/\kappa)^{-2} [m_1 m_2 m_3]^{(10-\kappa)/2\kappa} \\ &\times [(m_2 - m_1)(m_3 - m_1)(m_3 - m_2)(1 - m_1)(1 - m_2)(1 - m_3)]^{(10-\kappa)/2\kappa} \\ &\times \int_0^{m_1} \int_{m_2}^{m_3} \mathcal{N} \Big[\prod_{i=1}^{2} u_i(1 - u_i) \prod_{j=1}^{3} (m_j - u_i) \Big]^{-4/\kappa} (u_2 - u_1)^{8/\kappa} \, du_2 \, du_1. \end{aligned} \quad (5.106)$$

5.2.4 Pinch-point densities in polygons

In this section, we give the general formula for pinch-point densities and explicit expressions for some of these densities in the rectangle $\mathcal{R}$ ($N = 2$) and in the hexagon $\mathcal{H}$ ($N = 3$). The type-Λ pinch-point event is defined in the introduction of this chapter, and the FFBC event $\varsigma \in \mathrm{BC}_N$ is defined in section 4.1. The type-Λ pinch-point density $\rho^{\mathcal{P}}_{(\Lambda|\varsigma)}$ in the polygon $\mathcal{P}$ with the FFBC event $\varsigma \in \mathrm{BC}_N$ behaves as

$$\rho^{\mathcal{P}}_{(\Lambda|\varsigma)}(w) = \tilde{\mathcal{Z}}^{\mathcal{P}}_{(\Lambda|\varsigma)}/\tilde{\mathcal{Z}}^{\mathcal{P}}_{\varsigma} \tag{5.107}$$

$$\underset{\delta\to 0}{\sim} C_s^2 \delta^{2\Theta_s} \tilde{\Upsilon}^{\mathcal{P}}_{(\Lambda|\varsigma)}/\tilde{\Upsilon}^{\mathcal{P}}_{\varsigma}, \tag{5.108}$$

with the bulk s-leg exponent Θ_s given by (5.10) and with the universal partition functions $\tilde{\Upsilon}^{\mathcal{P}}_{(\Lambda|\varsigma)}$ and $\tilde{\Upsilon}_{\varsigma}$ computed in section 5.2.3 for the rectangle and the hexagon. Also, $1 \le s \le N$ necessarily.

Now we examine some particular pinch-point density formulas for the rectangle and the hexagon. First, we summarize some details pertaining to the case $N = 2$. The rectangle $\mathcal{R}$ is generated by conformally mapping the upper half-plane onto the domain

$$\mathcal{R} = \{w \in \mathbb{C} \,:\, 0 < \mathrm{Re}(w) < R,\ 0 < \mathrm{Im}(w) < 1\} \tag{5.109}$$

via the Schwarz-Christoffel f transformation sending $(0, m, 1, \infty)$ to the vertices $(0, R, R + i, i)$ of $\mathcal{R}$,

$$f(z) = \frac{1}{2K'} \int_0^{\zeta} \zeta^{-1/2}(m - \zeta)^{-1/2}(1 - \zeta)^{-1/2}\, d\zeta, \tag{5.110}$$

where $K'(m) = K(1 - m)$ with $K(m)$ the complete elliptic function of the first kind, and where the aspect ratio R equals $K(m)/K'(m)$. The vertices of $\mathcal{R}$ are labeled one through four starting with the bottom-left vertex and proceeding counterclockwise. By convention, we wire the left and right sides of $\mathcal{R}$, and the set BC_N contains two

FFBC events, the independent wiring event ς_1 and the mutual wiring event ς_2.

Next, we summarize the details pertaining to the case $N = 3$. The upper half-plane is mapped onto the hexagon $\mathcal{H}$ via the following Schwarz-Christoffel transformation sending $(0, m_1, m_2, m_3, 1, \infty)$ to the vertices $(w_1 = 0, w_2 > 0, w_3, \ldots, w_6)$ of $\mathcal{H}$:

$$f(z) = \frac{2}{3} \int_0^{\zeta} \zeta^{-1/3}(m_1 - \zeta)^{-1/3}(m_2 - \zeta)^{-1/3}(m_3 - \zeta)^{-1/3}(1 - \zeta)^{-1/3}\, d\zeta. \qquad (5.111)$$

The vertices of $\mathcal{H}$ are labeled one through six starting with the bottom-left vertex and proceeding counterclockwise. By convention, we wire the bottom, the top-left, and the top-right sides of $\mathcal{H}$, and the set BC_N contains five FFBC events, the independent wiring event ς_3, the mutual wiring event ς_1, and the three mixed wiring events ς_2, ς_4, and ς_5.

Explicit formulas for pinch-point densities in $\mathcal{R}$ and $\mathcal{H}$ with independently wired sides are presented on the following pages.

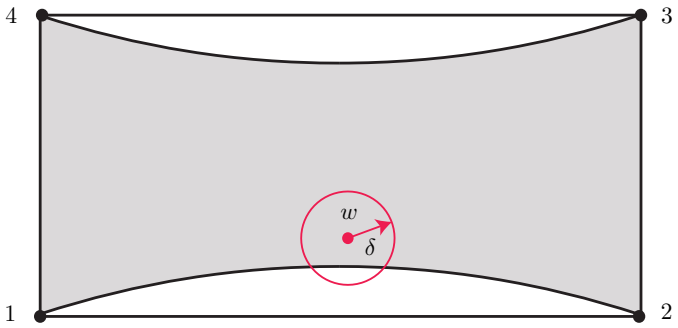

Figure 5.14: Illustration of the type-$(12:34)$ pinch-point configuration in the rectangle. The boundary cluster is shaded gray.

The density of type-$(12:34)$ one-pinch-points in the rectangle $\mathcal{R}$ with the left/right sides independently wired is

$$\begin{aligned}\rho^{\mathcal{R}}_{(1|12:34)}(m;w) \underset{\delta\to 0}{\sim} C_1^2\delta^{1-\kappa/8}&\left[\frac{(1-m)^{6/\kappa-1}}{{}_2F_1(2-\frac{12}{\kappa},1-\frac{4}{\kappa};2-\frac{8}{\kappa}\,|\,1-m)}\right]\\ &\times\left[\frac{\mathrm{Im}[\,\mathrm{sn}(w\,K'\,|\,m)^2]}{K'|\mathrm{sn}(wK'\,|\,m)\mathrm{cn}(wK'\,|\,m)\mathrm{dn}(wK'\,|\,m)|}\right]^{\kappa/8-1}\\ &\times\left[\frac{2G_2+(n^2-2)G_4-nG_1-nG_3}{n(n^2-4)}\right](m,z,\bar z)\,.\end{aligned} \tag{5.112}$$

The G_i are given in (5.44-5.47), and n is given in (1.155). The density $\rho^{\mathcal{R}}_{(2|12:34)}$ with the left/right sides mutually wired is found by replacing the argument of the hypergeometric function with $1-m$ in (5.112) and multiplying by n.

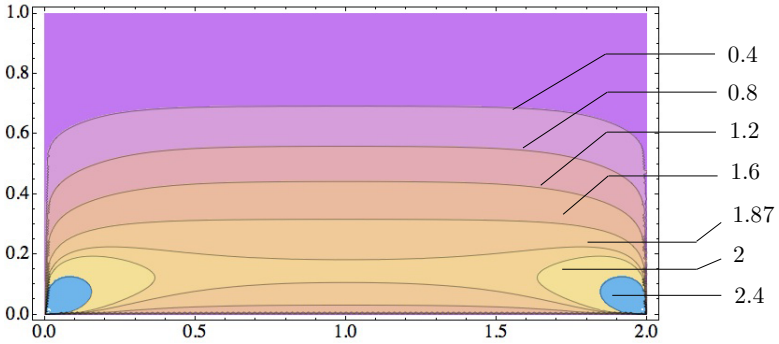

Figure 5.15: Contour plot of Ising FK cluster one-pinch-point density $\rho^{\mathcal{R}}_{(1|12:34)}$.

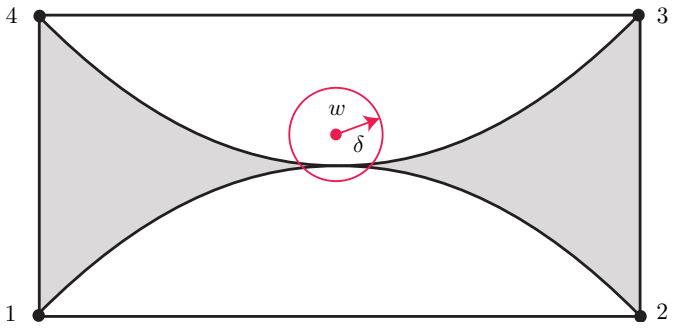

Figure 5.16: Illustration of the two-pinch-point configuration in the rectangle. Boundary clusters are shaded gray.

The density of two-pinch-points in the rectangle $\mathcal{R}$ with the left/right sides independently wired is

$$\rho^{\mathcal{R}}_{(1|1234)}(m;w) \underset{\delta\to 0}{\sim} C_2^2\delta^{6/\kappa-\kappa/8+1}\left[\frac{2^{24/\kappa-2}K'^{6/\kappa-\kappa/8+1}(n^{-1}+1)[m(1-m)]^{8/\kappa-1}}{{}_2F_1(2-\frac{12}{\kappa},1-\frac{4}{\kappa};2-\frac{8}{\kappa}\,|\,1-m)}\right] \times\left[\frac{\mathrm{Im}\,[\mathrm{sn}(wK'\,|\,m)^2]}{|\mathrm{sn}(wK'\,|\,m)\mathrm{cn}(wK'\,|\,m)\mathrm{dn}(wK'\,|\,m)|}\right]^{\kappa/8+18/\kappa-3}. \quad (5.113)$$

The density $\rho^{\mathcal{R}}_{(2|12:34)}$ with the left/right sides mutually wired is found by replacing the argument of the hypergeometric function with $1-m$ in (5.113).

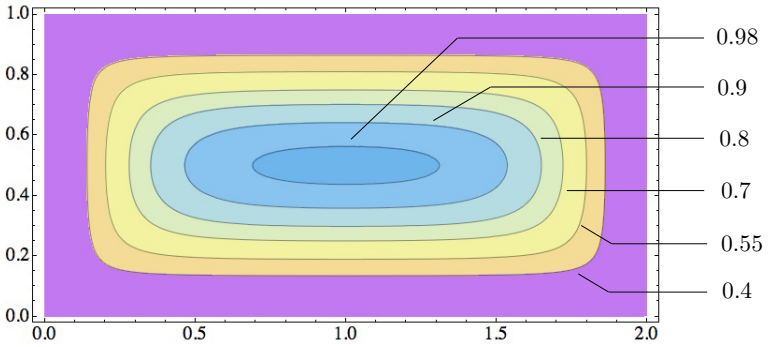

Figure 5.17: Contour plot of Ising FK cluster two-pinch-point density $\rho^{\mathcal{R}}_{(1|1234)}$.

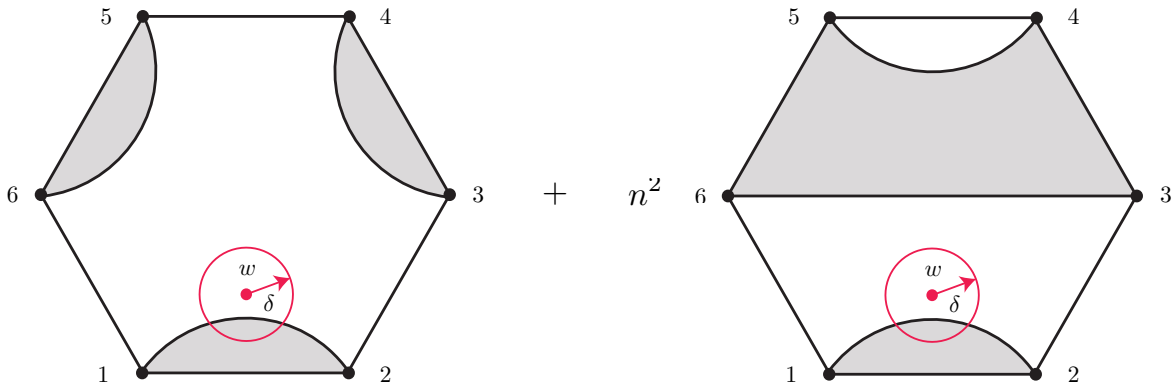

Figure 5.18: Illustration of the type-(12 : 34 : 56) one-pinch-point configuration plus n^2 times the (12 : 36 : 45) one-pinch-point configuration in the hexagon. Boundary clusters are shaded gray.

Equation (5.89) is a combination of one-pinch-point densities in the hexagon $\mathcal{H}$ with the bottom and top-left/right sides independently wired (figure 5.18). We have

$$[\rho^{\mathcal{H}}_{(12:34:56|3)} + n^2\rho^{\mathcal{H}}_{(12:36:45|3)}](m_1, m_2, m_3; w) \underset{\delta\to 0}{\sim} C_1^2\delta^{1-\kappa/8}n(4-n^2)^{-1/2}|z-\bar{z}|^{\kappa/8+8/\kappa-2}$$
$$\times\,|27z(m_1-z)(m_2-z)(m_3-z)(1-z)/8|^{1/3-\kappa/24}\frac{|I_1(m_1,m_2,m_3;z,\bar{z})|}{I_2(m_1,m_2,m_3)}. \quad (5.114)$$

Here, I_1 is

$$I_1(m_1,m_2,m_3;z,\bar{z}) := \int_\Gamma\int_{m_3}^1 \mathcal{N}\left[\prod_{i=1,2}(u_i-z)^{8/\kappa-1}(u_i-\bar{z})^{8/\kappa-1}\right.$$
$$\left.\times(u_2-u_1)^{8/\kappa}\prod_{i=1,2}u_i^{-4/\kappa}(1-u_i)^{-4/\kappa}\prod_{j=1}^{3}(m_j-u_i)^{-4/\kappa}\right]du_1\,du_2 \quad (5.115)$$

with the contour Γ starting at $\bar{z}$, crossing the real axis through either (m_2, m_3) or $(1,\infty)$, and ending at z. One can show that I_1 is purely imaginary. Also, I_2 is

$$I_2(m_1,m_2,m_3) := \int_0^{m_1}\int_{m_2}^{m_3}\mathcal{N}\Big[\prod_{i=1,2}u_i^{-4/\kappa}(1-u_i)^{-4/\kappa}\prod_{j=1,2,3}(m_j-u_i)^{-4/\kappa}\Big]$$
$$\times\,(u_2-u_1)^{8/\kappa}\,du_2\,du_1. \quad (5.116)$$

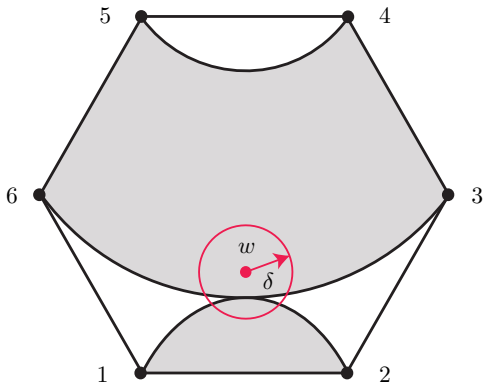

Figure 5.19: Illustration of the type-(6123 : 45) two-pinch-point configuration in the hexagon. Boundary clusters are shaded gray.

The density of two-pinch-points in the hexagon $\mathcal{H}$ with the top and bottom-left/right sides independently wired is

$$\begin{aligned}
&\rho^{\mathcal{H}}_{(6123:45|3)}(m_1,m_2,m_3;w) \underset{\delta\to 0}{\sim} \\
&\quad C_2^2\delta^{6/\kappa-\kappa/8+1}(n^{-1}+1)\beta(-4/\kappa,-4/\kappa)^2|z-\bar{z}|^{\kappa/8-6/\kappa-1}I_2(m_1,m_2,m_3)^{-1} \\
&\quad\times \frac{[m_1(m_3-m_2)]^{1-6/\kappa}|27z(m_1-z)(m_2-z)(m_3-z)(1-z)/8|^{1/3-\kappa/24+2/\kappa}}{[m_1m_2m_3(m_2-m_1)(m_3-m_1)(m_3-m_2)(1-m_1)(1-m_2)(1-m_3)]^{2/\kappa}} \\
&\quad\times \left[\frac{(2-n^2)(H_6+H_4)+nH_1-2H_2+nH_3+n(n^2-3)H_5}{(n^2-4)(n^2-1)}\right](m_1,m_2,m_3;z,\bar{z}),
\end{aligned} \tag{5.117}$$

where I_2 is given in (5.116) and the H_i are given in (5.63, 5.64-5.69).

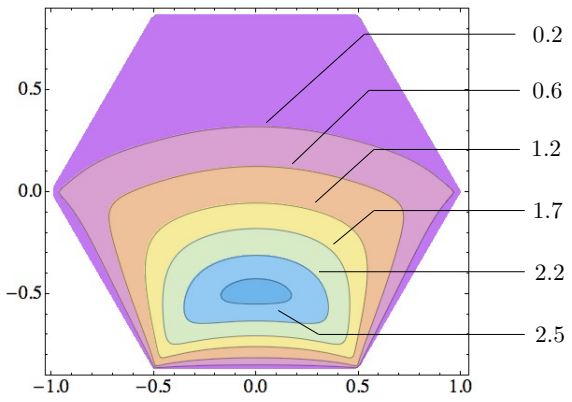

Figure 5.20: Contour plot of Ising FK cluster two-pinch-point density $\rho^{\mathcal{H}}_{(3|6123:45)}$

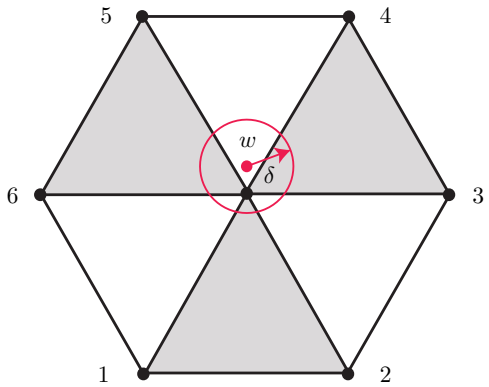

Figure 5.21: Illustration of the three-pinch-point configuration in the hexagon. Boundary clusters are shaded gray.

The density of three-pinch-points in the hexagon $\mathcal{H}$ with the top and bottom-left/right sides independently wired is

$$\begin{aligned}\rho^{\mathcal{H}}_{(6123:45|3)}(m_1,m_2,m_3;w) \underset{\delta\to 0}{\sim} C_3^2\delta^{16/\kappa-\kappa/8+1}(27/8)^{16/3\kappa-\kappa/24-1/3}(n^{-2}+3n^{-1}+1)\\ \times|z(m_1-z)(m_2-z)(m_3-z)(1-z)|^{4/3-\kappa/24-32/3\kappa}\\ \times|z-\bar{z}|^{\kappa/8+32/\kappa-4}\beta(-4/\kappa,-4/\kappa)^2 I_2(m_1,m_2,m_3)^{-1},\end{aligned} \tag{5.118}$$

where I_2 is given in (5.116).

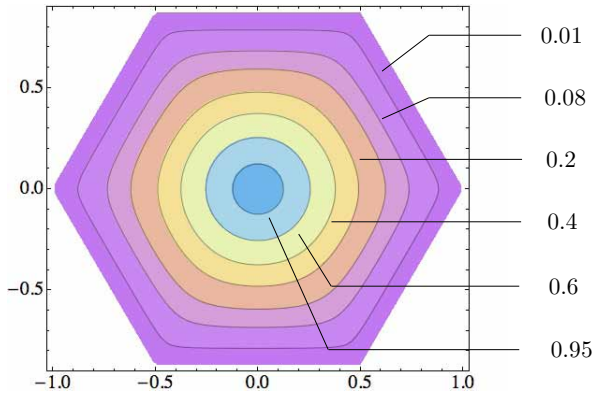

Figure 5.22: Contour plot of Ising FK cluster two-pinch-point density $\rho^{\mathcal{H}}_{(3|123456)}$.

5.3 Simulation results

In this section, we present simulation results that verify our predicted pinch-point densities $\rho^{\mathcal{R}}_{(12:34|1)}$ and $\rho^{\mathcal{R}}_{(1234|1)}$ (5.112, 5.113) for the rectangle and $\rho^{\mathcal{H}}_{(12:34:56|3)} + n^2\rho^{\mathcal{H}}_{(12:36:45|3)}$ and $\rho^{\mathcal{H}}_{(6123:45|3)}$ (5.114, 5.117) for the hexagon. We simulated critical bond percolation on a 2000×1000 square lattice (aspect ratio $R = 2$) in a rectangle $\mathcal{R}$ and critical site percolation on a triangular lattice in a regular hexagon $\mathcal{H}$ inscribed in a 2000×2000 rhombus. Using the SW algorithm [77], we also sampled critical Ising FK clusters on the same lattices in $\mathcal{R}$ and $\mathcal{H}$. We independently wired the left/right sides of $\mathcal{R}$ and independently wired the bottom and top left/right sides of $\mathcal{H}$, leaving all other sides free. Our simulation results show good agreement with our predictions. We used Mathematica (version 8) to evaluate all Coulomb gas integrals that appear in our analytic predictions, and we used the Schwarz-Christoffel toolbox [86] for MATLAB to numerically perform the transformation from the upper half-plane to the interior of $\mathcal{H}$.

To approximate the continuum limit of these critical models, we used very large lattices in our simulations. This suppressed the frequency of each s-pinch-point event at every lattice site, so we generated many samples in order to compensate this effect. Overall, about sixteen months of computer time (with about a 2 GHz processor) were used to sample percolation clusters in $\mathcal{R}$ and $\mathcal{H}$ and Ising FK clusters in $\mathcal{R}$. Over thirty-two months of computer time were used to sample Ising FK clusters in $\mathcal{H}$.

As usual, we number the vertices of $\mathcal{R}$ and $\mathcal{H}$ counterclockwise, starting with the left vertex of the bottom side of either polygon as vertex one. In this section, we also shift the hexagon so that its center coincides with the origin.

5.3.1 The rectangle

To measure the density of percolation pinch points ($\kappa = 6$), we simulated critical bond percolation on the square lattice in $\mathcal{R}$. One-pinch points are bonds inside

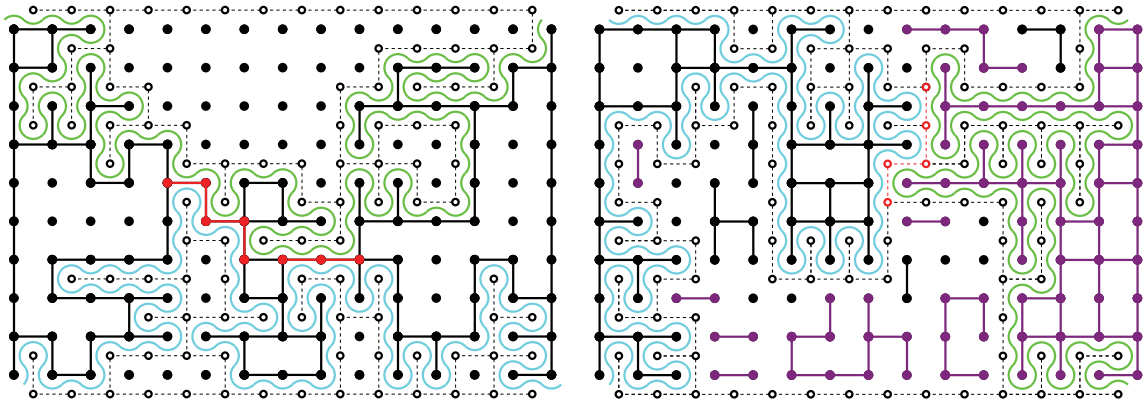

Figure 5.23: Typical percolation (left) and Ising FK (right) cluster and hull-walk samples in $\mathcal{R}$ generated by our simulations. Two-pinch points are colored red. We note that for percolation (left), our simulation only generates bonds that comprise the boundary clusters' perimeters.

$\mathcal{R}$ and on the perimeter of a boundary cluster, and two-pinch points are red bonds whose activation or deactivation respectively connects or disconnects the left and right boundary clusters. Because pinch points occur only on a boundary cluster perimeters, our simulations only sampled these perimeters via percolation hull-walks on the medial lattice [28]. They did not generate entire percolation bond configurations.

We performed two hull-walks to generate the two boundary cluster perimeters in $\mathcal{R}$ (figure 5.23). Hull-walks were defined in section 1.1.3. The first (resp. second) walk starts at the medial lattice site $a/2$ units below vertex one (resp. above vertex three), where a is the lattice spacing. One walk ends at the medial lattice site $a/2$ units below vertex two, and the other ends at $a/2$ units above vertex four. Each step of the walk is located at the midpoint of a bond, and at each step we decide to activate or deactivate that bond with critical bond activation probability $p_c^{\text{sqr}} = 1/2$. If the bond is activated, then the walk turns right. Otherwise it turns left. Each site that is visited by either hull-walk is a one-pinch point, and each site that is visited by both hull-walks is a two-pinch point, or red bond. (Actually, one-pinch-point events and two-pinch-point events at $z \in \mathcal{R}$ are mutually exclusive according to our definitions. However, our method counts a two-pinch point as a one-pinch

point of both hull walks too. This miscounting is insignificant though because the ratio of the two-pinch-point density to any one-pinch-point density vanishes as the system size increases, or equivalently, as the lattice spacing a goes to zero with power $a^{2(\Theta_2-\Theta_1)} = a^{6/\kappa}$.)

When all of the hull-walks finish, we note how they connect the vertices of $\mathcal{R}$ and bin one-pinch-point events accordingly. If they connect vertex one with vertex two and vertex three with vertex four (resp. vertex one with vertex four and vertex two with vertex three) to create a horizontal (resp. vertical) crossing, then one-pinch-point events on the first and second hull-walks contribute to $\rho^{\mathcal{R}}_{(12:34|1)}$ and $\rho^{\mathcal{R}}_{(34:12|1)}$ (resp. $\rho^{\mathcal{R}}_{(41:23|1)}$ and $\rho^{\mathcal{R}}_{(23:41|1)}$) respectively. Two-pinch-point events did not need to be sorted this way, although it is interesting to note that the red bonds are activated (resp. deactivated) in the event of a horizontal (resp. vertical) crossing. After generating about 2×10^8 samples, we tallied the number of each kind of pinch-point event at each site in an array and divide the total by the corresponding array value at the center of $\mathcal{R}$ to eliminate the nonuniversal constant and scaling factor appearing in (5.112, 5.113). With this normalization scheme, our measured densities always equal one at the center of $\mathcal{R}$.

Our percolation pinch-point simulation results are compared with our theory predictions for $\rho^{\mathcal{R}}_{(12:34|1)}$ and $\rho^{\mathcal{R}}_{(1234|1)}$ (respectively (5.112) and (5.113) with $\kappa = 6$) in figure 5.24. In the figure, $\mathcal{R}$ has been centered at $(1, 0.5)$ and rescaled to have length two and height one, and we have fixed y to $0.1, 0.2, 0.3, 0.4$, and 0.5. The top plot shows the density $\rho^{\mathcal{R}}_{(12:34|1)}$ of points touched by the hull-walk connecting vertices one and two. The left/right peaks of the top curve in the figure show that these events are most likely to occur near vertices one and two, and this is expected because these vertices are connected by the hull-walk. The bottom plot shows the density $\rho^{\mathcal{R}}_{(1234|1)}$ of two-pinch points, or red bonds. Our results show that these events are most likely to occur near the center of $\mathcal{R}$, and this is expected because there is more room in the

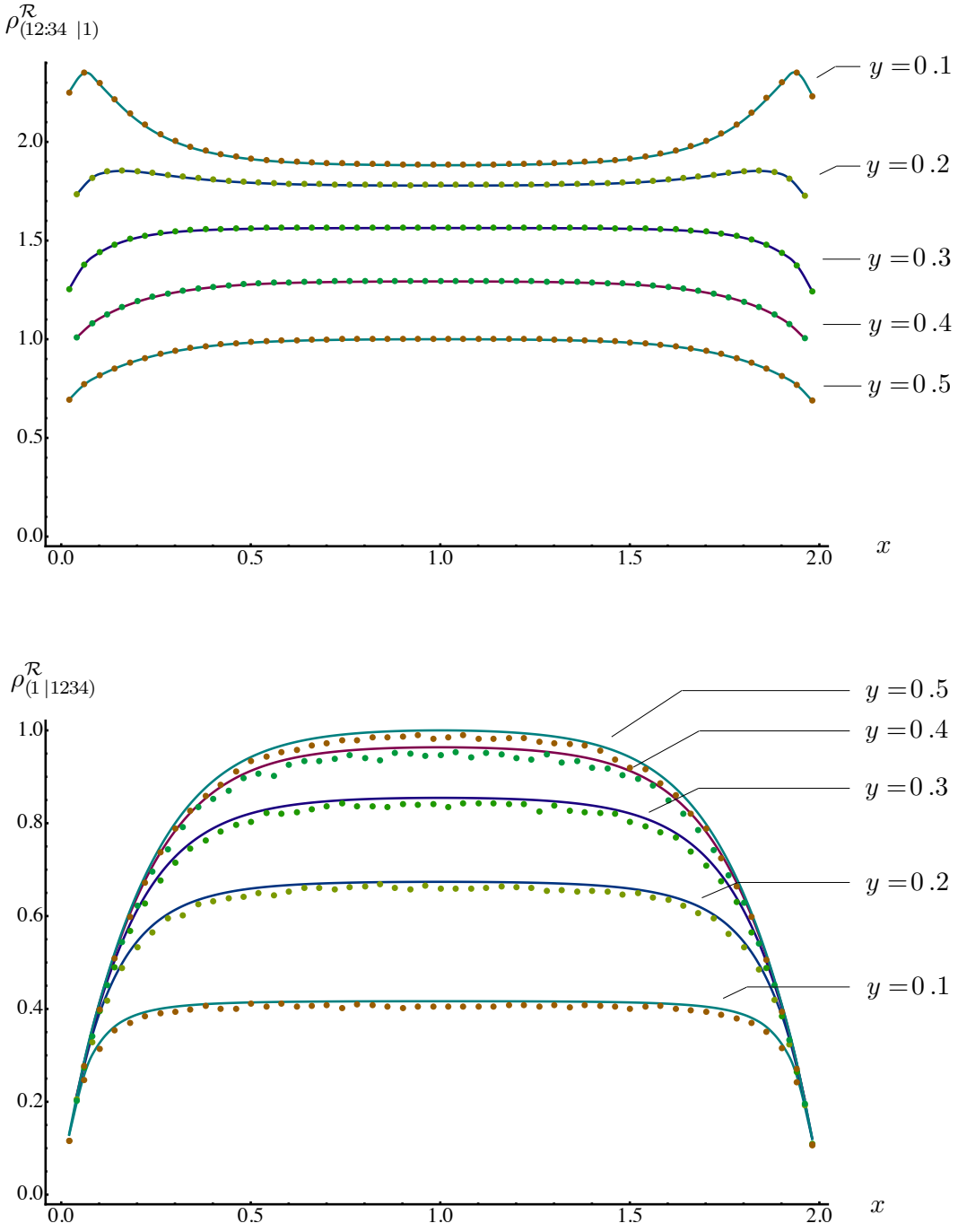

Figure 5.24: Density of percolation one-pinch-points $\rho_{12:34}$ (top) and two-pinch-points ρ_{1234} (bottom) versus x in a 2000×1000 rectangle rescaled to 2×1. Both densities are normalized to equal one at the center of $\mathcal{R}$.

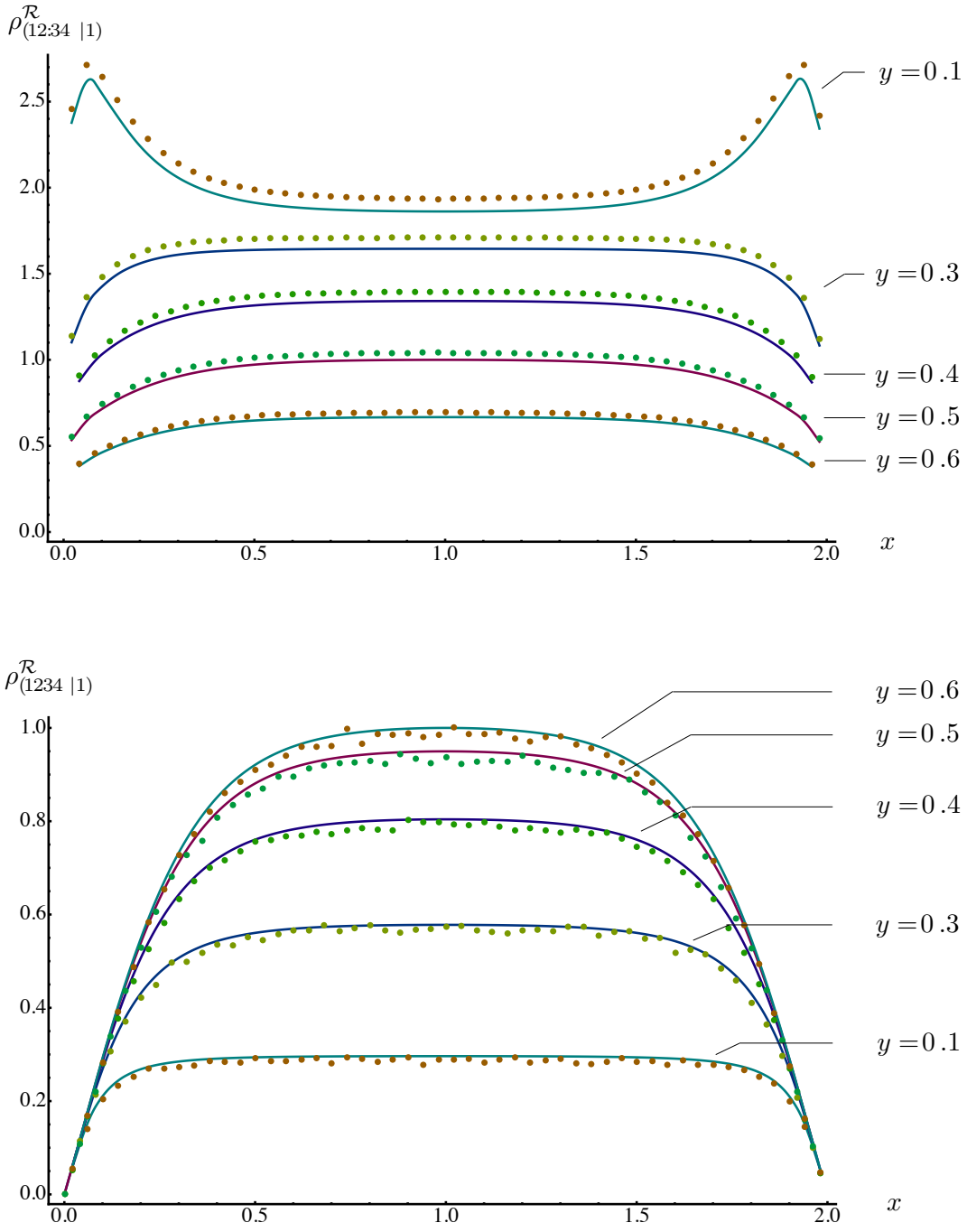

Figure 5.25: Density of Ising FK one-pinch points $\rho_{(1|12:34)}$ (top) and two-pinch-points $\rho_{(1|1234)}$ (bottom) versus x in a 2000×1000 rectangle rescaled to 2×1. Both densities are normalized to equal one at the center of $\mathcal{R}$.

center of $\mathcal{R}$ for the hull-walks to collide. Errors averaged over x and the standard deviation from this average are shown in table 5.2.

To measure the density of Ising FK pinch points ($\kappa = 16/3$), we generated about 4×10^8 samples of critical Ising FK clusters on the square lattice in $\mathcal{R}$ via the SW algorithm, described in section 4.6, with critical bond activation probability $p_c = \sqrt{2}/(1+\sqrt{2})$ (1.27). In each sample, the left/right sides of $\mathcal{R}$ were independently wired. That is, all FK bonds of either side were activated and necessarily the same color as the other bonds in its boundary cluster, but the bond color of the left boundary cluster was allowed to differ from that of the right. The perimeters of the boundary clusters anchored to these wired sides were explored via the hull-walk used for percolation to detect the pinch points (without ever activating or deactivating FK bonds during the walk) (figure 5.23). One-pinch-point events and two-pinch-point events were detected by the hull-walk in the same way as in bond percolation. However, we note that the "red bond definition" of a two-pinch point in percolation does not have a perfect analog with FK clusters. If two boundary FK clusters of different colors are separated by a single unactivated bond, we cannot activate this bond and join the clusters, so such a bond is not "red" according to the definition of a "spin red bond" in [81]. (Although, the fractal properties of the set of spin red bonds and the set of two-pinch-point bonds is the same since the Q colors of the Q-state Potts model are distributed uniformly across the FK clusters.)

Our Ising pinch-point simulation results are compared with our theory predictions for $\rho^{\mathcal{R}}_{(12:34|1)}$ and $\rho^{\mathcal{R}}_{(1234|1)}$ (respectively (5.112) and (5.113) with $\kappa = 16/3$) in figure 5.25. Explanations and noteable features of these two plots are the same as in figure 5.24, except that y is fixed to 0.1, 0.3, 0.4, 0.5, and 0.6. In addition, we note that our measurements of the one-pinch-point density consistently exceeded our predictions by a small amount that increased as y decreased. We suspect that this is a finite-size effect that may be reduced by sampling from a larger system. A similar effect was

observed for the simulations in [75].

Avg. error	$y = 0.1$	$y = 0.2$	$y = 0.3$	$y = 0.4$	$y = 0.5$	$y = 0.6$
Perc. $s = 1$	-0.004	0.023	-0.003	0.012	-0.002	–
Perc. $s = 2$	0.010	0.012	0.014	0.014	0.014	–
Ising $s = 1$	-0.080	–	-0.062	-0.048	-0.036	-0.346
Ising $s = 2$	0.008	–	0.009	0.012	0.014	0.046

Std. dev.	$y = 0.1$	$y = 0.2$	$y = 0.3$	$y = 0.4$	$y = 0.5$	$y = 0.6$
Perc. $s = 1$	0.002	0.026	0.002	0.025	0.000	–
Perc. $s = 2$	0.003	0.003	0.003	0.005	0.004	–
Ising $s = 1$	0.008	–	0.006	0.013	0.006	0.042
Ising $s = 2$	0.004	–	0.006	0.005	0.007	0.034

Table 5.2: The error (theory minus simulation) averaged over x, and the standard deviation of the error from that average, of the data displayed in figures 5.24 and 5.25.

5.3.2 The hexagon

To measure the density of percolation pinch points, we generated about 6.56×10^8 samples of critical site percolation (site activation probability $p_c = 1/2$) on the triangular lattice in $\mathcal{H}$. Again, because pinch-point events occur on the perimeters of the three boundary clusters, our simulations sampled only these perimeters via three distinct site-percolation hull-walks on the triangular lattice (left picture in figure 5.26). These hull-walks are described in section 4.6. The first, second, and third hull-walks respectively started at vertices one, three, and five and in the direction pointing into the adjacent free side of $\mathcal{H}$. Each hull-walk ended at an even vertex, and no two hull-walks could end at the same vertex. The finished hull-walk actually consists of two juxtaposed paths of neighboring activated and deactivated sites. We will call the former (resp. latter) path the *inner* (resp. *outer) boundary arc* of the boundary cluster (figure 5.26). A path, called a *smart kinetic walk*, passes between these juxtaposed paths with each step on the dual (honeycomb) lattice [56].

Pinch-point events were counted in almost the same way as with the simulations for the rectangle. Each point on the inner boundary arc is a one-pinch point, activated

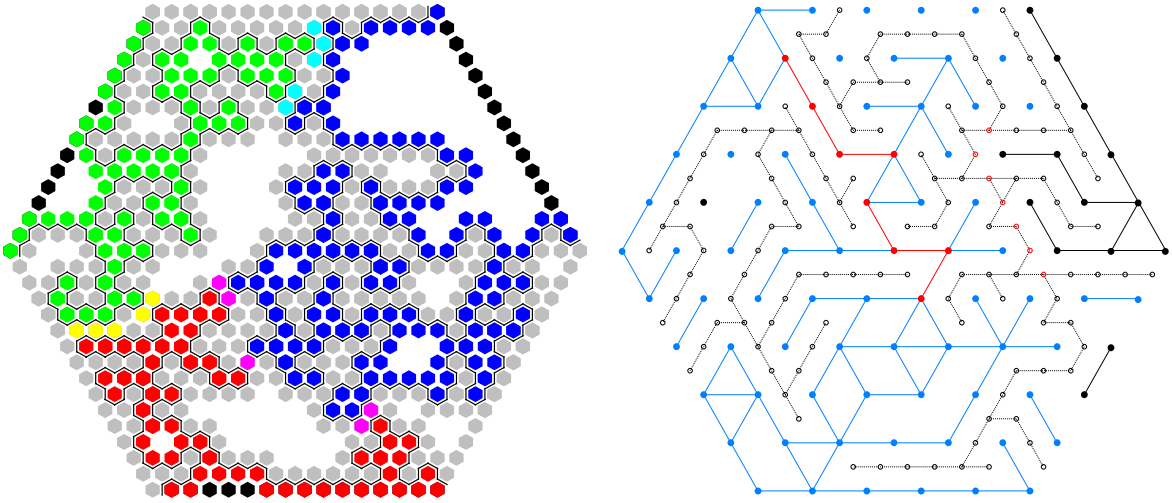

Figure 5.26: Typical percolation (left) and Ising FK (right) cluster samples $\mathcal{H}$ generated by our simulations. In the left illustration, black, red, blue, and green (resp. gray, yellow, pink, light blue, resp. white) sites are activated (resp. deactivated, resp. undecided), black paths are smart kinetic walks, red, blue, and green (resp. gray) sites form the inner (resp. outer) boundary arc of a boundary cluster, and yellow, pink, and light blue sites are two-pinch points. In the right illustration, red sites and centers of red bonds are two-pinch points.

(resp. deactivated) sites shared between two inner or outer boundary arcs are two-pinch points, and activated (resp. deactivated) sites shared between three inner or outer hulls are three-pinch points. Again, although one-pinch-point, two-pinch-point, and three-pinch-point events are technically mutually exclusive, we also counted three-pinch-point events as two-pinch-point events and two-pinch-point events as one-pinch-point events in our simulations, knowing that this over-counting has a negligible effect on our results.

Our percolation pinch-point simulation results are compared with our theory predictions for $\rho^{\mathcal{H}}_{(12:34:56|3)} + \rho^{\mathcal{H}}_{(12:36:45|3)}$ and $\rho^{\mathcal{H}}_{(6123:45|3)}$ (respectively (5.114) and (5.117) with $\kappa = 6$) in figure 5.27. (Three-pinch-point events were so rare that we could not generate enough samples to verify our three-pinch-point density prediction (5.118).) In the figure, $\mathcal{H}$ has been centered at the origin, rescaled to have side-length one, and oriented as in figure 5.26, and we have fixed y to $-0.69, -0.52, -0.31$, and -0.03. The top plot shows the density $\rho^{\mathcal{H}}_{(12:34:56|3)} + \rho^{\mathcal{H}}_{(12:36:45|3)}$ of one-pinch points touched by the hull-walk connecting vertices one and two. (This density includes all such events

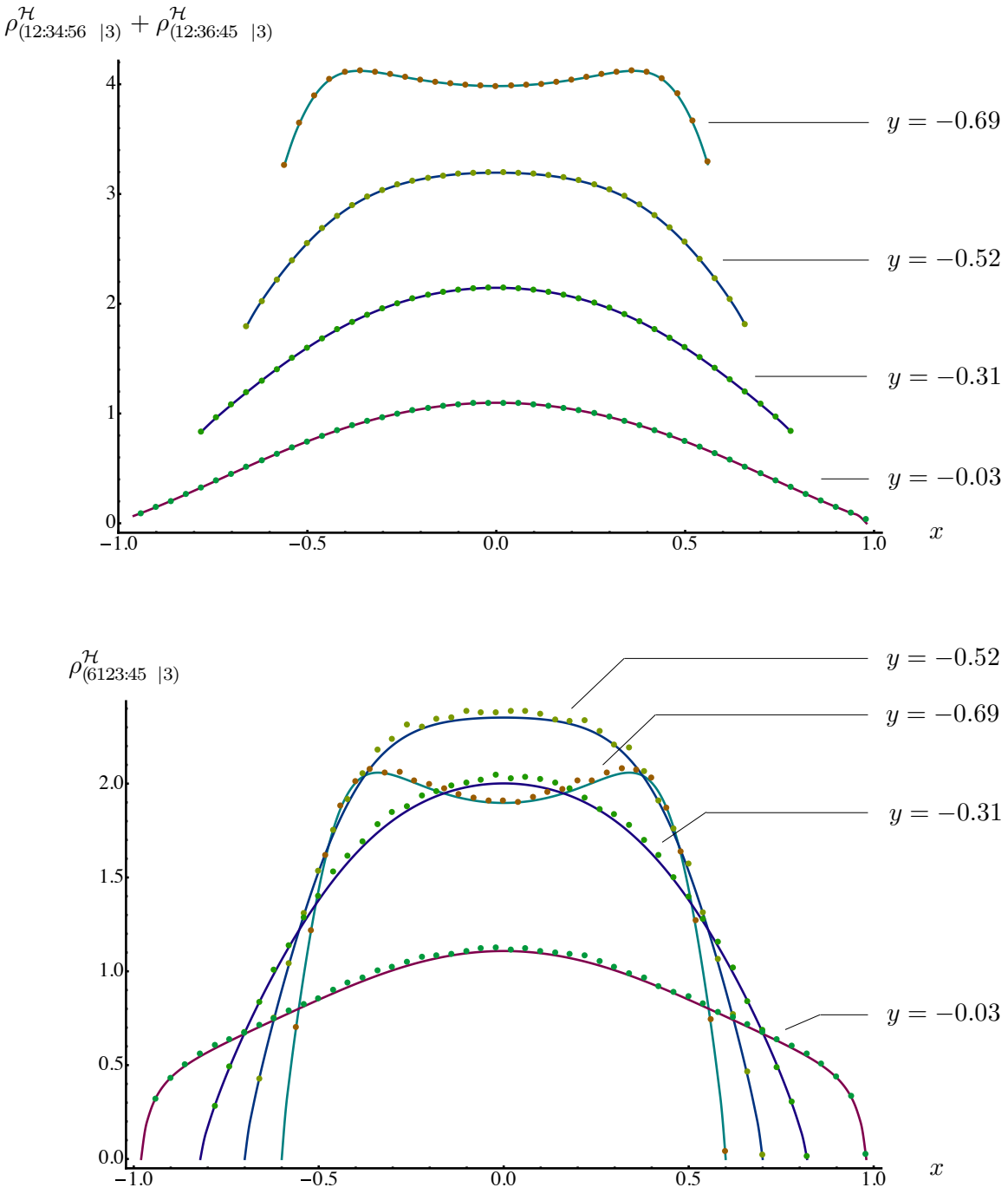

Figure 5.27: Density of percolation one-pinch points (top) and two-pinch points (bottom) versus x in a regular hexagon inscribed in 2000×2000 rhombus and adjusted to have side-length 1 and center at the origin. Both densities are normalized to one at the center of $\mathcal{H}$.

without regard to how the other two walks connect vertices three through six.) As expected, this density is greatest near vertices one and two which are connected by the hull-walk. The right plot shows the density $\rho^{\mathcal{H}}_{(6123:45|3)}$ of two-pinch points, or sites touched by a hull-walk connecting vertices one and two and another hull walk connecting vertices three and six. This density grows at first as we move from the bottom side of $\mathcal{H}$ towards its center, as expected, and then it diminishes as the center is approached. This diminishing is also expected since $\rho^{\mathcal{H}}_{(6123:45|3)}$ is greatest below the center of the rectangle conformally equivalent to $\mathcal{H}$ with vertices one, two, three, and six, and the image of this point in $\mathcal{H}$ is below the origin and on the y-axis.

To measure the density of Ising FK pinch points, we generated 5.68×10^8 samples of critical Ising FK clusters on the triangular lattice in $\mathcal{H}$ via the SW algorithm. The critical probability of FK bond activation on the triangular lattice is $p_c = (\sqrt{3} - 1)/\sqrt{3} \approx 0.42265$ (1.28). In each sample, the perimeters of the three FK boundary clusters were explored via the same hull-walk used in section 4.6 to detect FK cluster crossing events in the hexagon. The steps of this walk constitute the inner boundary arc. We also tracked the activated dual bonds that form the outer boundary arc that traces the inner boundary arc. The s-pinch-point events were identified with intersections between s distinct inner or outer boundary arcs in the same way as with percolation (figure 5.26).

Our Ising FK cluster pinch-point simulation results are compared with our theory predictions for $\rho^{\mathcal{H}}_{(12:34:56|3)} + 2\rho^{\mathcal{H}}_{(12:36:45|3)}$ and $\rho^{\mathcal{H}}_{(6123:45|3)}$ (respectively (5.114) and (5.117) with $\kappa = 16/3$) in figure 5.28. (Again, three-pinch-point events were so rare that we could not generate enough samples to reasonably verify our three-pinch-point density prediction (5.118).) Explanations and noticeable features of these two plots are the same as in figure 5.27. The top plot shows the density $\rho^{\mathcal{H}}_{(12:34:56|3)} + 2\rho^{\mathcal{H}}_{(12:36:45|3)}$ of one-pinch points touched by the hull-walk connecting vertices one and two. The factor of two arises from the factor of n^2 in (5.114) and because $n = \sqrt{2}$ when $\kappa = 16/3$.

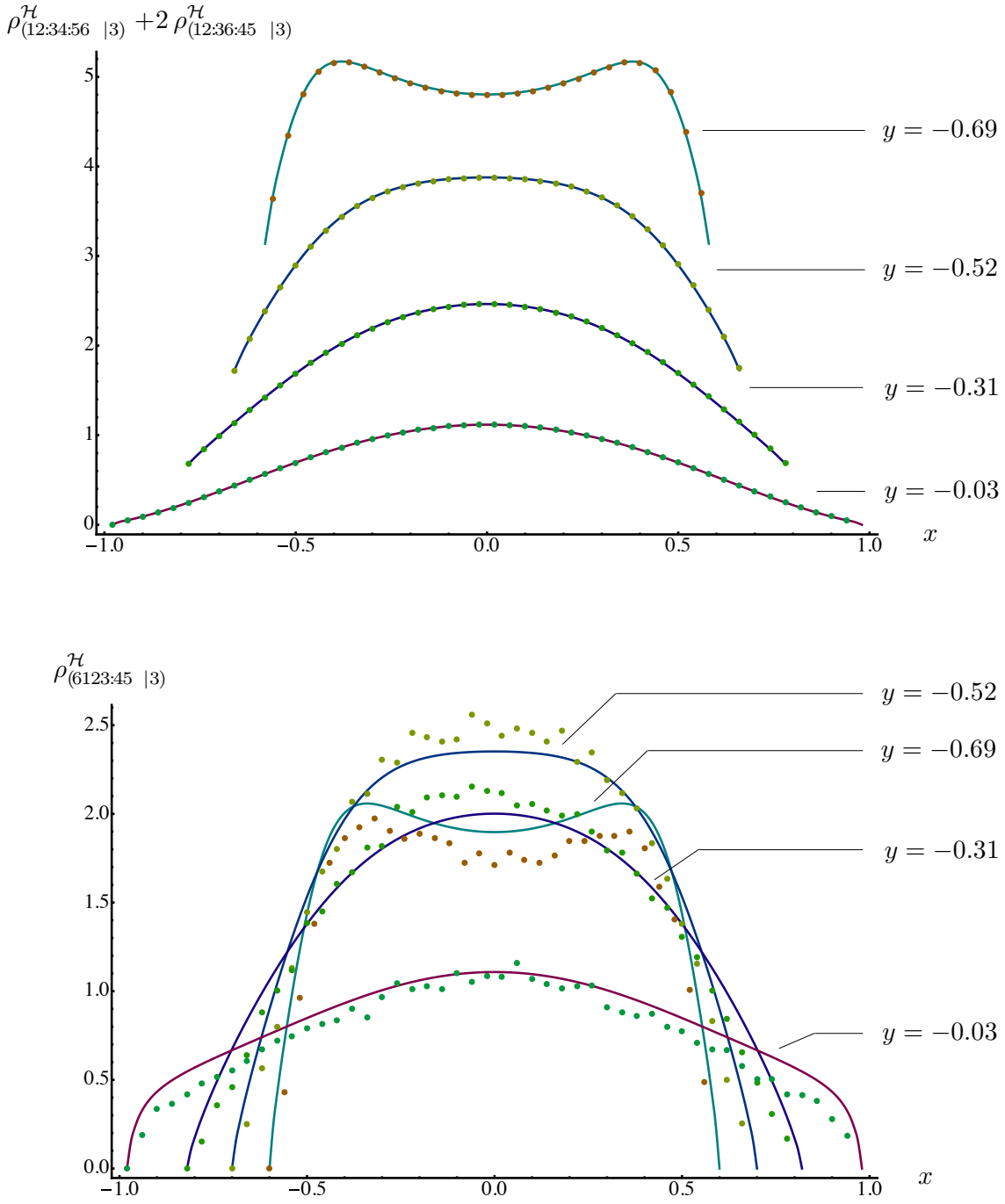

Figure 5.28: Density of Ising FK one-pinch points (top) and two-pinch points (bottom) versus x in a regular hexagon inscribed in 2000×2000 rhombus and adjusted to have side-length one and center at the origin. Both densities are normalized to one at the center of $\mathcal{H}$.

This factor may seem unnatural, but omitting it considerably worsens the agreement of prediction and simulation. Thus, the agreement we find a non-trivial verification of our prediction for the relative coefficients between the two densities in (5.114). We note that this one-pinch-point density deviates from our prediction by much less than that in the rectangle. The deviations of our two-pinch-point simulation results from our prediction (5.117) with $\kappa = 16/3$ are larger than those for percolation. This may be understood as follows. The two-pinch-point density scales as $a^{2\Theta_2}$ as the lattice spacing a goes to zero. For percolation ($\kappa = 6$), the power is 5/4, but for Ising FK clusters ($\kappa = 16/3$), the power increases to 35/24. Thus on a very large lattice, the frequency of Ising FK two-pinch-point events are suppressed even more than the percolation two-pinch-point events. Indeed, this is what have observed. We expect that more samples would lessen the deviation. However, such simulations would require very considerable computer resources.

Avg. error	$y = -0.69$	$y = -0.52$	$y = -0.31$	$y = -0.03$
Perc. $s = 1$	-0.005	-0.004	-0.003	-0.002
Perc. $s = 2$	-0.017	-0.024	-0.024	-0.013
Ising $s = 1$	0.006	0.001	-0.000	-0.000
Ising $s = 2$	0.140	-0.002	0.005	0.068

Std. dev.	$y = -0.69$	$y = -0.52$	$y = -0.31$	$y = -0.03$
Perc. $s = 1$	0.004	0.004	0.003	0.002
Perc. $s = 2$	0.011	0.015	0.013	0.006
Ising $s = 1$	0.006	0.006	0.004	0.002
Ising $s = 2$	0.052	0.114	0.107	0.045

Table 5.3: The error (theory minus simulation) averaged over x, and the standard deviation of the error from that average, of the data displayed in figures 5.27 and 5.28.

5.4 A solution space of the system (5.11-5.15)

We demonstrate that the Coulomb gas solution (5.32) solves the null-state PDEs (5.11) and the Ward identities (5.13-5.15). This calculation closely resembles the proof

of lemma II.2. Throughout this section, we use the dense phase conventions for our Kac charge and screening charge notations (1.190), we modify the notation of (5.32) by letting $x_{2N+1} = z, x_{2N+2} = \bar{z}$, and $x_{2N+2+i} := u_i$, and we assume that $s < N$. When $s = N$, (5.32) reduces to (5.30), and because this formula is purely algebraic, it is easy to directly verify that it solves the system. As usual, $x_1 < x_2 < \ldots < x_{2N-1} < x_{2N}$.

To begin, we consider the function

$$\Phi(\, x_1, \ldots, x_{2N+2+M}) = \prod_{i<j}^{2N+2+M} (x_j - x_i)^{2\alpha_i \alpha_j}. \tag{5.119}$$

Our strategy is to choose the α_i (i.e., the charges of the chiral operators) such that for $1 \leq i \leq 2N$,

$$\begin{aligned}\Bigg[\frac{\kappa}{4}\partial_i^2 + \sum_{j\neq i}^{2N}\left(\frac{\partial_j}{x_j - x_i} - \frac{\theta_1}{(x_j - x_i)^2}\right) + \frac{\partial_{2N+1}}{x_{2N+1} - x_i} \\ + \frac{\partial_{2N+2}}{x_{2N+2} - x_i} - \frac{\Theta_s}{(x_{2N+1} - x_i)^2} - \frac{\Theta_s}{(x_{2N+2} - x_i)^2}\Bigg]\Phi = \sum_{k=2N+3}^{2N+2+M} \partial_k(\, \ldots\,),\end{aligned} \tag{5.120}$$

where we recognize the differential operator of the null-state PDE centered on x_i on the left side of (5.120), and then integrate $x_{2N+3}, \ldots, x_{2N+2+M}$ on both sides of (5.120) around nonintersecting closed contours $\Gamma_1, \ldots, \Gamma_M$ such as Pochhammer contours entwining pairs of the points $x_1, \ldots, x_{2N+2}$ (figure 1.20). Integration on the right side gives zero. On the left side, the integrand is a smooth function of $x_1, \ldots, x_{2N+M+2}$ because the contours do not intersect. Thus, we may commute each differentiation with each integration to find that the M-fold integral $\oint \Phi$ solves the system (5.11).

With some algebra, we find that for any choice of $\{h_j\}, \{\alpha_j\}$, $M \in \mathbb{Z}^+$, and $1 \leq i \leq 2N$,

$$\left[\frac{\kappa}{4}\partial_i^2 + \sum_{j\neq i}^{2N+2+M}\left(\frac{\partial_j}{x_j-x_i} - \frac{h_j}{(x_j-x_i)^2}\right)\right]\Phi$$
$$= \left[\sum_{\substack{j,k\neq i\\ j\neq k}}^{2N+2+M} \frac{\alpha_j\alpha_k(\kappa\alpha_i^2-1)}{(x_j-x_i)(x_k-x_i)} + \sum_{j\neq i}^{2N+2+M} \frac{\alpha_i\alpha_j(\kappa\alpha_i\alpha_j-\kappa/2+2)-h_j}{(x_j-x_i)^2}\right]\Phi. \quad (5.121)$$

If we set $h_j = \theta_1$ for $1 \leq j \leq 2N$, $h_j = \Theta_s$ for $j = 2N+1, 2N+2$, and $h_j = 1$ for $j > 2N+2$ (the conformal weight of the $V_\pm$ chiral operators that generate screening operators (1.187)), then for $1 \leq i \leq 2N$, we can write (5.121) as

$$\left[\frac{\kappa}{4}\partial_i^2 + \sum_{j\neq i}^{2N}\left(\frac{\partial_j}{x_j-x_i} - \frac{\theta_1}{(x_j-x_i)^2}\right)\right.$$
$$\left. + \frac{\partial_{2N+1}}{x_{2N+1}-x_i} + \frac{\partial_{2N+2}}{x_{2N+2}-x_i} - \frac{\Theta_s}{(x_{2N+1}-x_i)^2} - \frac{\Theta_s}{(x_{2N+2}-x_i)^2}\right]\Phi$$
$$= \left[\sum_{\substack{j,k\neq i\\ j\neq k}}^{2N+2+M} \frac{\alpha_j\alpha_k(\kappa\alpha_i^2-1)}{(x_j-x_i)(x_k-x_i)} + \sum_{j\neq i}^{2N+2+M} \frac{\alpha_i\alpha_j(\kappa\alpha_i\alpha_j-\kappa/2+2)-h_j}{(x_j-x_i)^2}\right]\Phi$$
$$+ \sum_{k=2N+3}^{2N+2+M}\partial_k\left(-\frac{\Phi}{x_k-x_i}\right). \quad (5.122)$$

Next, we choose a particular $i \in \{1,\ldots,2N\}$. If we set

$$\alpha_i = \alpha_{1,2}^- = 1/\sqrt{\kappa}, \qquad \alpha_j = \alpha_0 \pm \sqrt{\alpha_0 + h_j}, \quad j \neq i, \quad (5.123)$$

then the term in brackets on the right side of (5.122) vanishes, giving the desired form (5.120). In order to satisfy (5.123) for all $1 \leq i \leq 2N$, we need

$$\alpha_j = \alpha_{1,2}^- \qquad 1 \leq j \leq 2N, \quad (5.124)$$
$$\alpha_j = \alpha_{0,s}^\pm \qquad 2N+1 \leq j \leq 2N+2, \quad (5.125)$$
$$\alpha_j = \alpha_\pm \qquad 2N+3 \leq j \leq 2N+2+M. \quad (5.126)$$

Explicit formulas for (5.124-5.126) are given by (1.190). If we make this choice, then $\oint \Phi$ solves the $2N$ null-state equations.

To finish, we choose M and the signs of the square roots in (5.125,5.126) so that the total charge $\sum_j \alpha_j$ equals $2\alpha_0$ and $\oint \Phi$ therefore solves the Ward identities. We suppose that m_+ (resp. m_-) of the screening charges equal α_+ (resp. α_-) with $m_+ + m_- = M$ necessarily. Then the total charge is

$$\begin{aligned} 2\alpha_0 = \sum_j \alpha_j &= 2N\alpha_{1,2}^- + \alpha_{0,s}^\pm + \alpha_{0,s}^\pm + m_+\alpha_+ + m_-\alpha_- \\ &= -N\alpha_- + \alpha_+ + (1 \pm s)\alpha_-/2 + (1 \pm s)\alpha_-/2 + m_+\alpha_+ + m_-\alpha_- \\ &= \begin{cases} (m_+ + 1)\alpha_+ + (-N + s + m_- + 1)\alpha_- & ++ \\ (m_+ + 1)\alpha_+ + (-N - s + m_- + 1)\alpha_- & -- \\ (m_+ + 1)\alpha_+ + (-N + m_- + 1)\alpha_- & +- \end{cases} . \end{aligned} \tag{5.127}$$

The $++$ (resp. $--$) case corresponds to using the $+$ (resp. $-$) sign for both $\alpha_{0,s}$, and the $+-$ case corresponds to using the $+$ sign for one of the $\alpha_{0,s}$ and the $-$ sign for the other. In order for these expressions to equal $2\alpha_0$, we need the coefficients of α_+ and α_- in (5.127) to equal one. Therefore, $m_+ = 0$ and $m_- = M$, so all M screening charges use the $-$ sign. The number of screening charges is thus given by

$$M = \begin{cases} N - s & ++ \\ N + s & -- \\ N & +- \end{cases} . \tag{5.128}$$

The $++$ case is used exclusively in this chapter since it apparently contains all of the pinch-point densities when $N = 1, 2$, and 3. We anticipate that the $++$ case contains all pinch-point densities for all $N \in \mathbb{Z}^+$. Moreover, we see that these solutions span

a subspace of a larger solution space containing all cases in (5.128) (among possibly more solutions).

5.5 Summary

We summarize the main results of this chapter. The half-plane weight Π_Λ of the type-Λ s-pinch-point configuration is given by (5.53, 5.33) for the cases $N = 2$ and $s = 1$ and 2 and is given by (5.77, 5.76, 5.34) for the cases $N = 3$ and $s = 1, 2$, and 3 also for various pinch-point events Λ. After specifying a particular FFBC event ς, we construct the universal partition function $\Upsilon_{(\Lambda|\varsigma)}$ that sums exclusively over the event $\Lambda \cap \varsigma$, and we transform it into a universal partition function with the rectangle $\mathcal{R}$ or the hexagon $\mathcal{H}$ for its domain. The results are (5.100) and (5.105) respectively. Then to within nonuniversal factors, the type-Λ pinch-point density $\rho^{\mathcal{P}}_{(\Lambda|\varsigma)}$ is found by dividing the transformed universal partition function by the partition function $\tilde{\Upsilon}_\varsigma$ of chapter four. This prediction agrees well with measurements by simulation that sampled one-pinch-point and two-pinch-point events between critical percolation and Ising FK boundary clusters in rectangles and hexagons with independently wired sides.

APPENDICES

APPENDIX A

Holomorphic and antiholomorphic coordinates

This section of the appendix supplements chapter one of this thesis. Its purpose is to give a more complete explanation of holomorphic versus antiholomorphic complex coordinates and of the treatment of $\bar{z}$ not as the complex conjugate of z (this is denoted by z^* in this thesis) but as a number independent of z. These matters are important to much of the material presented in chapter one where we witnessed the "decoupling" of the holomorphic and antiholomorphic sectors of a CFT defined on the complex plane. This phenomenon follows from properties of holomorphic and antiholomorphic functions on $\mathbb{C}^2$.

A.1 Holomorphic and antiholomorphic coordinates

Let $f : \mathcal{D} \to \mathbb{C}$ be a function of one complex variable $z = x + iy$ defined on a domain $\mathcal{D} \subset \mathbb{C}$. We can write $f(z) = u(x, y) + iv(x, y)$ with $u : \mathbb{R}^2 \to \mathbb{R}$ and $v : \mathbb{R}^2 \to \mathbb{R}$. Necessary and sufficient conditions for the differentiability of f are for first partial derivatives of u and v to exist and satisfy the Cauchy-Riemann equations:

$$\partial_x u = \partial_y v \quad \partial_y u = -\partial_x v. \tag{A.1}$$

If f satisfies these conditions at z, then the derivative of f at z is defined and equals

$$D_z f(z) = \partial_x f(z) = -i\partial_y f(z). \tag{A.2}$$

In this situation, we say that f is *complex-differentiable at* z. A major theorem in the theory of functions of one complex variable is that a function f is complex-differentiable at z if and only if it is analytic at z, and typically the term "analytic" is used in place of "complex-differentiable." If f is complex-differentiable at every $z \in \mathbb{C}$, then we say that f is *complex-differentiable*.

There is an interesting interpretation of complex-differentiability that introduces the idea of holomorphic and antiholomorphic coordinates. Let $\bar{z} := x - iy$ be the complex conjugate of z (for now), so that

$$z = x + iy, \quad \bar{z} = x - iy \quad \Longleftrightarrow \quad x = \frac{z + \bar{z}}{2}, \quad y = \frac{z - \bar{z}}{2i}. \tag{A.3}$$

If we momentarily think of z and $\bar{z}$ as independent variables, then the chain rule gives

$$\partial_z f(z) = \frac{1}{2}[\partial_x f(z) - i\partial_y f(z)] = D_z f(z) \tag{A.4}$$

$$\partial_{\bar{z}} f(z) = \frac{1}{2}[\partial_x f(z) + i\partial_y f(z)] = 0. \tag{A.5}$$

The last identity is proven by inserting $f = u + iv$ and using the Cauchy-Riemann equations (A.1). To say that f depends on z but does not depend on $\bar{z}$ is a natural interpretation of (A.4-A.5), but such an interpretation is meaningless since z and $\bar{z}$ depend on each other.

We can give certain meaning to this interpretation by promoting x and y to complex variables ξ and ψ so that the variables $z := \xi + i\psi$ and $\bar{z} := \xi - i\psi$ are independent. This construction is inspired by the following fact. If $g : \mathbb{R} \to \mathbb{R}$ is such

that the principal value of the integrals

$$u_1(x,y) = \frac{1}{\pi}\int_{-\infty}^{\infty} g(s)\frac{y}{(x-s)^2+y^2}\,ds, \tag{A.6}$$

$$u_2(x,y) = \frac{1}{\pi}\int_{-\infty}^{\infty} g(s)\frac{x-s}{(x-s)^2+y^2}\,ds, \tag{A.7}$$

exist for all $(x,y) \in \mathbb{R}^2$, then the function $f = u_1 + iu_2$ is the unique complex-differentiable function whose real part equals g on the real axis. We can verify this by checking that $u := u_1$ and $v := u_2$ satisfy the Cauchy-Riemann equations (A.1). (To match our previous notation, we set $u := u_1$ and $v := u_2$. We will find both of these notations useful below.) Thus, we extend the real function g to a complex-differentiable function $f = u + iv$.

Now we repeat this extension a second time. We promote the functions $u = u_1$ and $v = u_2$ to functions with domain $\mathbb{C} \times \mathbb{R}$ by promoting x to a complex variable $\xi := x + ix'$, and we suppose that the principal values of the integrals

$$u_{j1}(x,x';y) = \frac{1}{\pi}\int_{-\infty}^{\infty} u_j(s,y)\frac{x'}{(x-s)^2+x'^2}\,ds, \tag{A.8}$$

$$u_{j2}(x,x';y) = \frac{1}{\pi}\int_{-\infty}^{\infty} u_j(s,y)\frac{x-s}{(x-s)^2+x'^2}\,ds, \tag{A.9}$$

exist. By construction u' and v' are each complex-differentiable functions of ξ. Let f' be f but with $u_j \mapsto (u_{j1} + iu_{j2})$. We write

$$u' := u_{11} + iu_{12}, \quad v' = u_{21} + iu_{22} \tag{A.10}$$

so that u' and v', with y fixed, are complex-valued extensions of the original functions u and v and

$$f'(x,x';y) = u'(x,x';y) + iv'(x;x',y) \tag{A.11}$$

$$= \quad [u_{11} - u_{22} + i(u_{12} + u_{21})](x, x'; y). \tag{A.12}$$

Then we can use the Cauchy-Riemann equations (A.1) to verify that the function $f'(x, x'; y)$ is a complex-differentiable function of $x + iy$ and ξ.

Now we repeat this extension a last time. We promote the functions u' and v' to functions with domain $\mathbb{C} \times \mathbb{C}$ by promoting y to a complex variable $\psi := y + iy'$, and we suppose that the principal values of the integrals

$$u_{jk1}(x, x'; y, y') = \frac{1}{\pi} \int_{-\infty}^{\infty} u_{jk}(x, x'; s) \frac{y'}{(y - s)^2 + y'^2}\, ds, \tag{A.13}$$

$$u_{jk2}(x, x'; y, y') = \frac{1}{\pi} \int_{-\infty}^{\infty} u_{jk}(x, x'; s) \frac{y - s}{(y - s)^2 + y'^2}\, ds, \tag{A.14}$$

exist. By construction, u'' and v'' are each complex-differentiable functions of ξ and ψ. Let f'' be f' but with $u_{jk} \mapsto (u_{jk1} + iu_{jk2})$. We write

$$u'' = (u_{111} + iu_{112}) + i(u_{121} + iu_{122}), \quad v'' = (u_{211} + iu_{212}) + i(u_{221} + iu_{222}) \tag{A.15}$$

so that u'' and v'', with x and x' fixed, are complex extensions of u' and v' and

$$\begin{aligned} f''(x, x'; y, y') &= u''(x, x'; y, y') + iv''(x, x'; y, y') \\ &= [(u_{111} - u_{221} - u_{122} - u_{212}) + i(u_{112} - u_{222} + u_{121} + u_{211})](x, x'; y, y'). \end{aligned} \tag{A.16}$$

Then we can use the Cauchy-Riemann equations (A.1) to verify that the function $f'' = u'' + iv''$ is a complex-differentiable function of $x + iy$ and ξ and ψ.

We have promoted the complex-differentiable function f of one variable $z = x + iy$ to a function $f'' : \mathbb{C}^2 \to \mathbb{C}$ of two complex variables ξ and ψ. We have also shown that f'' is a complex-differentiable function of $x + iy$, and it is apparent that $f''(x, 0; y, 0) = f(x, y)$ (i.e., $f(z)$ with $z = x + iy$).

By construction, u'' and v'' and therefore f'' are complex-differentiable functions

of ξ and ψ, so we can differentiate f'' with respect to the coordinates $z = \xi + i\psi$ and $\bar{z} = \xi = i\psi$. By using the relation

$$(z, \bar{z}) = (\xi + i\psi, \xi - i\psi) \quad \Longleftrightarrow \quad (\xi, \psi) = \left(\frac{z + \bar{z}}{2}, \frac{z + \bar{z}}{2i} \right) \tag{A.17}$$

with $\xi := x + ix'$, $\psi = y + iy'$ and x, x', y, and $y' \in \mathbb{R}$ and writing $\partial := \partial_z$ and $\bar{\partial} := \partial_{\bar{z}}$, we find

$$\begin{aligned}
\partial f'' &= \frac{1}{2}(\partial_\xi - i\partial_\psi) f'' && \text{(A.18)} \\
&= \frac{1}{2}(\partial_x u + i\partial_x v) - \frac{i}{2}(\partial_y u + i\partial_y v), && \text{(A.19)} \\
\bar{\partial} f'' &= \frac{1}{2}(\partial_\xi + i\partial_\psi) f'' && \text{(A.20)} \\
&= \frac{1}{2}(\partial_x u + i\partial_x v) + \frac{i}{2}(\partial_y u + i\partial_y v). && \text{(A.21)}
\end{aligned}$$

Because f'' is also a complex-differentiable function of $x + iy$, we can use the Cauchy-Riemann equations (A.1) to conclude that

$$\begin{aligned}
\partial f'' &= \partial_x u + i\partial_x v = \partial_x f'' = -i\partial_y f'', && \text{(A.22)} \\
\bar{\partial} f'' &= 0. && \text{(A.23)}
\end{aligned}$$

The first line shows that a derivative with respect to z is equivalent to a derivative with respect to x or iy.

If a complex function $f'' : \mathbb{C}^2 \to \mathbb{C}$ satisfies (A.22-A.23) at the point $(z, \bar{z}) \in \mathbb{C}^2$, then we say that f'' is *holomorphic at* $(z, \bar{z})$, and we call z (resp. $\bar{z}$) the *holomorphic* (resp. *antiholomorphic*) coordinate. The coordinate representation $(z, \bar{z})$ of a point in $\mathbb{C}^2$ may be replaced by the representation (ξ, ψ) defined through (A.17). These coordinates, sometimes called *space-time coordinates*, may be written as $\xi = x + ix'$ and $\psi = y + iy'$ for $x, y, x', y' \in \mathbb{R}$. In either set of coordinates, we may define the

real surface

$$S = \{(z, \bar{z}) \in \mathbb{C}^2 \,:\, \bar{z} = z^*\} = \{(\xi, \psi) \in \mathbb{C} \,:\, x' = y' = 0\}. \tag{A.24}$$

Here and in the rest of this appendix, z^* denotes the complex conjugate of z.

Our construction shows that if f is complex-differentiable at $z \in \mathbb{C}$, then under appropriate conditions, there exists a function $f'' : \mathbb{C}^2 \to \mathbb{C}$ holomorphic at $(z, \bar{z}) \in \mathbb{C}^2$ whose restriction to the real surface equals f. In an abuse of terminology, we say that f is *holomorphic at* z if it is complex-differentiable at z. When we restrict to the real surface, equations (A.22-A.23) become (A.2, A.5), and this gives meaning to the interpretation of f as independent of $\bar{z}$ (in a neighborhood of z).

Also in chapter one, we sometimes invoke the function $\bar{f}'' = u - iv$ with u'' and v'' defined in (A.15). This function is not the complex conjugate of f'' since u'' and v'' may be complex. Repeating the calculations that led to (A.22-A.23), we find

$$\partial \bar{f}'' = 0 \tag{A.25}$$

$$\bar{\partial} \bar{f}'' = \partial_x u - i\partial_x v = \partial_x \bar{f}'' = -i\partial_y \bar{f}''. \tag{A.26}$$

If a function $\bar{f}'' : \mathbb{C}^2 \to \mathbb{C}$ satisfy (A.25-A.26) at the point $(z, \bar{z}) \in \mathbb{C}^2$, we say that $\bar{f}''$ is *antiholomorphic at* $(z, \bar{z}) \in \mathbb{C}^2$. We note that when restricted to the real surface, $\bar{f}$ is the complex conjugate of the function f used above.

A.2 Holomorphic tensors and space-time tensors

In this section, we briefly describe the transformation of space-time coordinates to holomorphic coordinates for vectors and tensors. We let $x \in \mathbb{C}^2$ with space-time coordinates $x^0 = \xi, x^1 = \psi$ and holomorphic coordinates $x^0 = z$ and $x^1 = \bar{z}$. Throughout this section, we use the Greek labels μ, ν for space-time indices and α, β

for holomorphic indices. We can use the relation (A.17) to convert between these indices, and we have the contravariant rule

$$x^\alpha = h^\alpha{}_\mu\, x^\mu, \quad \Longleftrightarrow x^\mu = (h^{-1})^\mu{}_\alpha\, x^\alpha, \tag{A.27}$$

with h the tensor

$$h^\alpha{}_\mu = \begin{pmatrix} 1 & i \\ 1 & -i \end{pmatrix}, \quad (h^{-1})^\mu{}_\alpha = \frac{1}{2}\begin{pmatrix} 1 & 1 \\ -i & i \end{pmatrix}. \tag{A.28}$$

The conversion rule (A.27) may be generalized in the usual way for multiple tensor indices. For example, if $g^{\alpha\beta}$ is a tensor, then

$$g^{\alpha\beta} = h^\alpha{}_\mu h^\beta{}_\nu g^{\mu\nu}, \quad g^{\mu\nu} = (h^{-1})^\mu{}_\alpha (h^{-1})^\nu{}_\beta g^{\alpha\beta}. \tag{A.29}$$

In particular, if $g^{\mu\nu}$ is the metric tensor for the Euclidean metric, that is $g^{\mu\nu} = \delta^{\mu\nu}$, then we have the following metric tensor in holomorphic indices:

$$g^{\alpha\beta} = \begin{pmatrix} 0 & 2 \\ 2 & 0 \end{pmatrix}, \quad (g^{-1})_{\alpha\beta} = \begin{pmatrix} 0 & \frac{1}{2} \\ \frac{1}{2} & 0 \end{pmatrix}. \tag{A.30}$$

So far, we have given rules for conversion between two types of contravariant indices. To convert a holomorphic index from covariant to contravariant, we use the usual rule

$$x^\alpha = g^{\alpha\beta} x_\beta, \quad x_\alpha = (g^{-1})_{\alpha\beta} x^\beta, \tag{A.31}$$

which leads to the relation $x^\alpha = 2x_{\beta\neq\alpha}$. This is the holomorphic version of the trivial rule $x^\mu = x_\mu$. Finally, we can use these relations to uncover the covariant version of

conversion rule (A.27):

$$x_\mu = x^\mu = (h^{-1})^\mu{}_\alpha \, x^\alpha = (h^{-1})^\mu{}_\alpha \, g^{\alpha\beta} \, x_\beta = (k^{-1})_\mu{}^\beta x_\beta, \tag{A.32}$$

with $k^{-1} := h^{-1} g$ so that

$$k_\alpha{}^\mu = \frac{1}{2} \begin{pmatrix} 1 & -i \\ 1 & i \end{pmatrix}, \quad (k^{-1})_\mu{}^\alpha = \frac{1}{2} \begin{pmatrix} 1 & 1 \\ i & -i \end{pmatrix}. \tag{A.33}$$

Thus, we have the conversion rule

$$x_\alpha = k_\alpha{}^\mu \, x_\mu, \quad \Longleftrightarrow x_\mu = (k^{-1})^\mu{}_\alpha \, x_\alpha. \tag{A.34}$$

Using these identities, we can transform usual space-time (i.e., cartesian) covariant and contravariant transformation rules for tensor components to rules that work with holomorphic/antiholomorphic coordinates. For example, one can now show that if ϕ is the component of a tensor with covariant indices $\alpha = 0, \beta = 1$ or $\alpha = 1, \beta = 0$ component of a tensor, then under a holomorphic/antiholomorphic pair of maps $f, \bar{f}$, it will transform as

$$\phi(z, \bar{z}) \mapsto \phi'(z', \bar{z}') = \partial f(z) \bar{\partial} \bar{f}(\bar{z}) \phi(z, \bar{z}). \tag{A.35}$$

In the next section, we will derive a generalization of this rule.

These conversion rules will be used in the next section of the appendix. There, we will contrast the phenomenon of conformal invariance in more-than-two dimensions to that in two-dimensions. In so doing, we will work with space-time indices in more-than-two dimensions, and we will work with holomorphic indices in two dimensions to exploit their notational convenience. The identities presented in this section will allow us to convert between these two settings.

APPENDIX B

A motivation of the conformal covariance transformation law

This section of the appendix supplements chapter one of this thesis, and its purpose is to motivate the transformation rule (1.48) for quasi-primary fields in CFT. Throughout this section, we let ϕ be a smooth field (i.e., scalar, spinor, vector) on $\mathbb{R}^d$, we let f be a smooth, invertible transformation taking a subdomain of $\mathbb{R}^d$ into $\mathbb{R}^d$, and we let $x' = f(x)$. Then f induces a transformation on ϕ, sending it to a new field ϕ' for which x' is its argument. The transformation rule is written as

$$\phi \mapsto \phi', \qquad \phi'(x') = \mathcal{F}[\phi](x) = \mathcal{F}[\phi] \circ f^{-1}(x'). \tag{B.1}$$

The transformation $\mathcal{F}$ accounts for orientation change and other effects on the field ϕ induced by f, and it depends on the point x in general. The field ϕ is called a *scalar field* if $\mathcal{F}$ is the identity for any smooth f. In this case, (B.1) reads $\phi'(x') = \phi(x)$.

Suppose that the transformation f is infinitesimal within some subdomain $\Omega \subset \mathbb{R}^d$ and determined by a set of infinitesimal parameters $\{\omega_a\}$ there. For example, if $f : \mathbb{R}^3 \to \mathbb{R}^3$ is a rotation, then this set consists of three infinitesimal Euler angles, and Ω is a ball of sufficiently small radius centered at the origin. If we expand (B.1) to first order in the infinitesimal parameters near zero, then we find that f has the

following infinitesimal effect at $x \in \Omega$:

$$x^\mu \mapsto x'^\mu = x^\mu + \epsilon^\mu(x), \qquad \epsilon^\mu(x) = \omega_a \frac{\delta x^\mu}{\delta \omega_a}, \tag{B.2}$$

$$\phi \mapsto \phi' = \phi \circ f^{-1} + \delta\mathcal{F}[\phi] \circ f^{-1}, \qquad \delta\mathcal{F}[\phi] = \omega_a \frac{\delta \mathcal{F}[\phi]}{\delta \omega_a}, \tag{B.3}$$

$$= \phi - \epsilon^\mu \partial_\mu \phi + \delta\mathcal{F}[\phi]. \tag{B.4}$$

The *generator* G_a of the infinitesimal transformation is defined in terms of the variation of the field $\delta\phi = \phi' - \phi$:

$$G_a[\phi] := -i\frac{\delta x^\mu}{\delta \omega_a}\partial_\mu \phi + i\frac{\delta \mathcal{F}[\phi]}{\delta \omega_a}, \qquad \Longrightarrow \qquad -i\omega_a G_a[\phi] = \delta\phi. \tag{B.5}$$

A transformation $f : \mathbb{R}^d \to \mathbb{R}^d$ is *conformal* at x is it preserves the metric tensor there to within a local scale factor and is conformal in $\Omega \subset \mathbb{R}^d$ if it is conformal at every point in Ω. (In two dimensions, this definition reduces to the definition for conformality that is given in section 1.1.4.) One can show that when $d > 2$, a transformation $x \mapsto f(x) = x + \epsilon(x)$ that is infinitesimal and conformal in Ω has the following expansion to first order in its infinitesimal parameters:

$$\epsilon^\mu(x) = a^\mu + \omega^\mu{}_\nu\,(x^\nu - \xi^\nu) + b(x^\mu - \xi^\mu) + [2(x^\mu - \xi^\mu)x\cdot c - c^\mu |x-\xi|^2], \quad x, \xi \in \Omega. \tag{B.6}$$

Here, the infinitesimal real parameters are $a^\mu, b, \omega^\mu{}_\nu, c_\nu$, and ξ is some reference point in Ω. The first, second, and third term signifies a translation, rotation about ξ, and dilation about ξ respectively, and the last term signifies a SCT, which is in inversion about ξ followed by an translation followed by another inversion about ξ. The rotation tensor $\omega^{\mu\nu}$ in two dimensions is given in terms of the rotation angle θ by

$$\omega^{\mu\nu} = \begin{pmatrix} 0 & -\theta \\ \theta & 0 \end{pmatrix}. \tag{B.7}$$

It is evident from (B.6) that a transformation that is infinitesimal in Ω cannot be infinitesimal over all of $\mathbb{R}^d$ unless $b, \omega^\mu{}_\nu$, and c_ν are all zero. In the following discussion, we assume that the infinitesimal parameters are so small that zero is in Ω and we can choose $\xi = 0$.

The generator corresponding with each of these four transformations may be computed for a scalar field ($\delta\mathcal{F}[\phi] = 0$) via (B.5). These generators, which we generically label as $\mathcal{G}_a$, are given in table B.1. Their commutation relations generate the conformal Lie algebra:

$$[\mathcal{D}, \mathcal{P}_\mu] = i\mathcal{P}_\mu \tag{B.8}$$

$$[\mathcal{D}, \mathcal{K}_\mu] = -i\mathcal{K}_\mu \tag{B.9}$$

$$[\mathcal{K}_\mu, \mathcal{P}_\nu] = 2i(\eta_{\mu\nu}\mathcal{D} - \mathcal{L}_{\mu\nu}) \tag{B.10}$$

$$[\mathcal{K}_\rho, \mathcal{L}_{\mu\nu}] = i(\eta_{\rho\mu}\mathcal{K}_\nu - \eta_{\rho\nu}\mathcal{K}_\mu) \tag{B.11}$$

$$[\mathcal{P}_\rho, \mathcal{L}_{\mu\nu}] = i(\eta_{\rho\mu}\mathcal{P}_\nu - \eta_{\rho\nu}\mathcal{P}_\mu) \tag{B.12}$$

$$[\mathcal{L}_{\mu\nu}, \mathcal{L}_{\rho\sigma}] = i(\eta_{\nu\rho}\mathcal{L}_{\mu\sigma} + \eta_{\mu\sigma}\mathcal{L}_{\nu\rho} - \eta_{\mu\rho}\mathcal{L}_{\nu\sigma} - \eta_{\nu\sigma}\mathcal{L}_{\mu\rho}). \tag{B.13}$$

Here, the metric tensor $\eta_{\mu\nu}$ is the identity matrix $\delta_{\mu\nu}$. Furthermore, we can use the Hausdorff lemma,

$$e^{-A}Be^{A} = B + [B, A] + \frac{1}{2}[[B, A], A] + \ldots, \tag{B.14}$$

$\delta\mathcal{F}[\phi] = 0$	ω_a	$\epsilon^\mu(x)$	$\mathcal{G}_a$
translation	a^μ	a^μ	$\mathcal{P}_\mu = -i\partial_\mu$
rotation	$\omega_{\mu\nu}$	$\frac{\omega_{\rho\nu}}{2}(\eta^{\rho\mu}x^\nu - \eta^{\nu\mu}x^\rho)$	$\frac{1}{2}\mathcal{L}_{\mu\nu}(x) = \frac{i}{2}(x_\mu\partial_\nu - x_\nu\partial_\mu)$
dilation	b	bx^μ	$\mathcal{D}(x) = -ix^\nu\partial_\nu$
SCT	c^μ	$2x_\nu b^\nu x^\mu - b^\mu\lvert x\rvert$	$\mathcal{K}_\mu(x) = -i(2x_\mu x^\nu\partial_\nu - \lvert x\rvert^2\partial_\mu)$

Table B.1: The infinitesimal parameters, the infinitesimal coordinate variation, and the generator for a scalar field corresponding to each of the four types of infinitesimal conformal transformations in more than two dimensions.

to show that each generator may be mapped from zero to some $x \in \Omega$ via conjugation by the translation operator $\exp(ix^\rho \mathcal{P}_\rho)$:

$$\mathcal{G}_a(x) = e^{ix^\rho \mathcal{P}_\rho} \mathcal{G}_a(0) e^{-ix^\rho \mathcal{P}_\rho}. \tag{B.15}$$

To show this, we keep only terms with first derivatives in the series (B.14) and take care to evaluate the commutators before setting the argument of $\mathcal{G}_a$ to zero on the right side of (B.15).

We let the elements of $S = \{P_\mu, L_{\mu\nu}, D, K_\mu\}$ respectively be, from left to right, the generators of infinitesimal translations, rotations, dilations, and SCTs of a field ϕ where $\delta\mathcal{F}[\phi]$ may be nonzero except for translations, and we let G_a be a generic label for an element of S. Because S must also generate the conformal Lie algebra, it elements will obey the commutation relations (B.8-B.13) with $\mathcal{G}_a \mapsto G_a$ for each generator. If we further suppose that each G_a may be translated via conjugation (B.15), then we can use (B.14) to calculate each generator $G_a(x)$ in terms of $\mathcal{G}_a(x)$ and $G_a(0)$. Furthermore, we can use this result to calculate the field variation, which equals $\delta\mathcal{F} = -i\omega_a(G_a - \mathcal{G}_a)$ according to (B.5). The results are given in table B.2.

We can use (B.8-B.10) and the Jacobi identity to show that $[D(0), L_{\mu\nu}(0)] = 0$. If we employ an irreducible representation of the sub-algebra generated by the collection $\{L_{\mu\nu}(0)\}$, then this commutation relation and Schur's lemma imply that $D(0)$ must be a multiple of the identity matrix. We take $D(0) = -i\Delta$ (supposing that Δ is real), and we call Δ the *scaling weight* of the field ϕ. The commutation relation (B.9) evaluated at zero then implies that $K_\mu(0) = 0$.

From (B.6), we observe that an infinitesimal conformal transformation in $d > 2$ dimensions has a finite number of degrees of freedom. However, we find considerably less restriction in two dimensions. Indeed, one can show that if a transformation $z \mapsto f(z) = z + \epsilon(z)$ is infinitesimal and conformal on $\Omega \subset \mathbb{C}$, then ϵ is analytic on

	$G_a(x)$	$\delta\mathcal{F}(x)$
translation	$P_\mu = \mathcal{P}_\mu$	0
rotation	$L_{\mu\nu}(x) = L_{\mu\nu}(0) + \mathcal{L}_{\mu\nu}(x)$	$-\frac{i}{2}\omega^{\mu\nu}L_{\mu\nu}(0)$
dilation	$D(x) = D(0) + \mathcal{D}(x)$	$-ibD(0)$
SCT	$K_\mu(x) = K_\mu(0) + 2x_\mu D(0) - x^\nu L_{\mu\nu}(0) + \mathcal{K}_\mu(x)$	$-ic^\mu[K_\mu(0) + 2x_\mu D(0) - 2x^\nu L_{\mu\nu}(0)]$

Table B**.2:** The generator and the field variation of a non-scalar field that accompany the four types of infinitesimal conformal transformations.

Ω. Thus $\epsilon(z)$ has a power series expansion at each $\zeta \in \Omega$, so

$$\epsilon(z) = a + (b + i\theta)(z - \zeta) + c(z - \zeta)^2 + \ldots, \quad z, \zeta \in \Omega, \tag{B.16}$$

where $a, c \in \mathbb{C}$ and $b, \theta \in \mathbb{R}$ are infinitesimal. Also, the antiholomorphic version $\bar{z} \mapsto \bar{f}(\bar{z}) = \bar{z} + \bar{\epsilon}(\bar{z})$ is

$$\bar{\epsilon}(\bar{z}) = \bar{a} + (b - i\theta)(\bar{z} - \bar{\zeta}) + \bar{c}(\bar{z} - \bar{\zeta})^2 + \ldots, \quad \bar{z}, \bar{\zeta} \in \bar{\Omega}. \tag{B.17}$$

Such an infinitesimal transformation has an infinite number of degrees of freedom captured by the coefficients of the terms in the series. We note that in two dimensions, the first three terms of (B.16, B.17) agree with (B.6) when written in space-time coordinates with $(\zeta, \bar{\zeta}) \mapsto \xi$ with the barred coordinates equaling the complex conjugates of the corresponding unbarred coordinates. We also note that this transformation is infinitesimal on all of $\mathbb{C}$ only if all but the zeroth order term are present. This is an example of Liouville's theorem. (Because the holomorphic and antiholomorphic sectors are essentially the same, we will omit explicit reference to the latter for now.)

If we further require that f is a global conformal transformation that is infinitesimal in Ω, that is, of the form

$$f(z) = \frac{(1 + b'/2)(z - \zeta) + a'}{-c'(z - \zeta) + 1 - b'/2}, \quad z, \zeta \in \Omega \tag{B.18}$$

with $a', b', c' \in \mathbb{C}$ infinitesimal, then the expansion (B.16) terminates at second order, just as it did in $d > 2$ dimensions for *any* transformation that is conformal and infinitesimal in Ω:

$$\epsilon(z) = f(z) - z \approx a' + b'(z - \zeta) + c'(z - \zeta)^2, \quad z, \zeta \in \Omega. \tag{B.19}$$

We will focus on this special case for now. As usual, the zeroth and second order terms capture translation and SCTs respectively, while the first order term captures both rotation and dilation by virtue of the fact that b' is complex.

Next, we derive a useful identity for the variation of the field ϕ under a global conformal transformation that is infinitesimal in Ω. (We suppose that zero is in Ω, and we set $\zeta = 0$.) Because $L_{\alpha\beta}(0)$ is antisymmetric, we may write $L_{\alpha\beta}(0) = -\varepsilon_{\alpha\beta} S$, where S is a spin operator acting on some space of states in analogy with quantum mechanics. We suppose that ϕ is an eignevector of the spin operator, with eigenvalue s called the *spin* of the field ϕ, and $\varepsilon_{\alpha\beta}$ is the antisymmetric tensor in complex coordinates:

$$\varepsilon^{\alpha\beta} = -2i \begin{pmatrix} 0 & 1 \\ -1 & 0 \end{pmatrix}, \qquad \varepsilon_{\alpha\beta} = \frac{i}{2} \begin{pmatrix} 0 & 1 \\ -1 & 0 \end{pmatrix}. \tag{B.20}$$

By summing the contribution of each type of conformal transformation to the total variation $\delta\mathcal{F}(z)$ (the right columns of table (B.2)) and substituting $L_{\alpha\beta}(0) = s\varepsilon_{\alpha\beta}, D(0) = -i\Delta, K_\alpha(0) = 0$, we find

$$\delta\mathcal{F}[\phi](z) = \left[\frac{is}{2}\omega^{\alpha\beta}\varepsilon_{\alpha\beta} - b\Delta - 2c^\alpha(\Delta z_\alpha + isz^\beta\varepsilon_{\alpha\beta})\right]\phi \tag{B.21}$$

for the infinitesimal variation of the field ϕ in response to the global conformal transformation (B.6) that is infinitesimal at z. In holomorphic coordinates and with $\xi = 0$,

this transformation is

$$\epsilon^\alpha(z) = a^\alpha + \omega^\alpha{}_\beta\, z^\beta + bz^\alpha + (2z^\alpha z^\beta c_\beta - c^\alpha z^\beta z_\beta), \quad z \in \Omega. \tag{B.22}$$

By exploiting the fact that $\eta_{\alpha\beta}$ and $\omega_{\alpha\beta}$ are respectively symmetric and antisymmetric, we can rewrite the transformation law (B.21) as

$$\delta\mathcal{F}[\phi] = -2h^{\alpha\beta}\phi\partial_\beta\epsilon_\alpha = -h\phi\partial\epsilon - \bar{h}\phi\partial\bar{\epsilon} \tag{B.23}$$

(now we are showing the antiholomorphic contribution too), where $h^{\alpha\beta}$ is the tensor

$$h^{\alpha\beta} = \frac{1}{2}\left(\eta^{\alpha\beta}\Delta - i\varepsilon^{\alpha\beta}s\right) = \frac{1}{2}\begin{pmatrix} 0 & \Delta - s \\ \Delta + s & 0 \end{pmatrix}, \tag{B.24}$$

and $h := h^{10}$ (resp. $\bar{h} := h^{01}$) is called the *holomorphic* (resp. *antiholomorphic*) *conformal weight* of the field ϕ. From (B.4), we thus find the total variation in the field under a global conformal transformation that is infinitesimal in Ω:

$$\delta\phi(z,\bar{z}) := \phi'(z,\bar{z}) - \phi(z,\bar{z}), \quad z \in \Omega. \tag{B.25}$$

$$= -\epsilon\partial\phi(z,\bar{z}) - \bar{\epsilon}(\bar{z})\bar{\partial}\phi(z,\bar{z}) - h\phi(z,\bar{z})\partial\epsilon(z) - \bar{h}\phi(z,\bar{z})\bar{\partial}\bar{\epsilon}(\bar{z}). \tag{B.26}$$

If the field has zero holomorphic and antiholomorphic weights, then $\mathcal{F}$ is the identity, and $\phi'(z',\bar{z}') = \phi(z,\bar{z})$. In this case, (B.26) reduces to the generic transformation law found by expanding $\delta\phi(z) = \phi(z'-\epsilon) - \phi(z)$ to first order in ϵ:

$$\delta\phi = -\epsilon\partial\phi - \bar{\epsilon}\bar{\partial}\phi \tag{B.27}$$

In the more general case where ϵ (resp. $\bar{\epsilon}$) has a Laurent expansion $\epsilon(z) = \sum_k \epsilon_k(z -$

$\zeta)^{k+1}$ (resp. $\bar{\epsilon}(\bar{z}) = \sum_k \bar{\epsilon}_k(\bar{z} - \bar{\zeta})^{k+1}$), we may write (B.27) as

$$\delta\phi(z,\bar{z}) = \sum_n (\epsilon_n \ell_n(\zeta)\phi(z,\bar{z}) + \bar{\epsilon}_n \bar{\ell}_n(\bar{\zeta})\phi(z,\bar{z})), \tag{B.28}$$

where

$$\ell_n(\zeta) = -(z-\zeta)^{n+1}\partial, \quad \bar{\ell}_n(\bar{\zeta}) = -(\bar{z}-\bar{\zeta})^{n+1}\bar{\partial}. \tag{B.29}$$

The generators $\ell_n, \bar{\ell}_n$ obey the Witt algebra:

$$[\ell_n, \ell_m] = (n-m)\ell_{n+m}, \quad [\bar{\ell}_n, \bar{\ell}_m] = (n-m)\bar{\ell}_{n+m}, \quad [\ell_n, \bar{\ell}_m] = 0. \tag{B.30}$$

The sub-aglebra generated by $\{\ell_{-1}, \ell_0, \ell_1\}$ (and its antiholomorphic counterpart) are generators of infinitesimal global conformal transformations. $\ell_{-1}, \bar{\ell}_{-1}$ and $\ell_1, \bar{\ell}_1$ generate translations and SCTs respectively, while the combinations $\ell_0 + \bar{\ell}_0$ and $i(\ell_0 - \bar{\ell}_0)$ generate dilations and rotations.

Now we use (B.26) to motivate a transformation rule for ϕ under a non-infinitesimal global conformal map. It is easy to show that the rule

$$\phi'(z',\bar{z}') = \partial f(z)^{-h} \bar{\partial}\bar{f}(\bar{z})^{-\bar{h}} \phi(z,\bar{z}), \tag{B.31}$$

is equivalent to (B.26) to first order in $\epsilon, \partial\epsilon$. If a field transforms as in (B.31), then we say that ϕ is *conformally covariant at z (resp.$\bar{z}$) with holomorphic weight h (resp. antiholomorphic weight $\bar{h}$).*

We argue heuristically that for global conformal f, (B.31) is the unique transformation rule that reduces to (B.26) if f is infinitesimal. Suppose that we divide f into a composition of M uniformly (in some sense) infinitesimal global conformal transformations $f_1, \ldots, f_M$ so that $f = f_M \circ \ldots \circ f_1$. Let $z_m = f_m \circ \ldots \circ f_1(z)$ and $z' = f_M(z_{M-1}) = f(z)$. Then be repeatedly applying the transformation law (B.31),

we find that to leading order

$$\phi'(z',\bar{z}') = \partial f_M(z_{M-1})^{-h}\ldots\partial f_1(z)^{-h}\bar{\partial}\bar{f}_M(\bar{z}_{M-1})^{-\bar{h}}\ldots\bar{\partial}\bar{f}_1(\bar{z})^{-\bar{h}}\phi(z,\bar{z}) \quad \text{(B.32)}$$

$$= \partial f(z)^{-h}\bar{\partial}\bar{f}(\bar{z})^{-\bar{h}}\phi(z,\bar{z}). \quad \text{(B.33)}$$

By increasing M, we decrease the error in (B.32) that arises from lower order terms until we have the exact result (B.31). A field that transforms according to (B.31) under a global conformal transformation is called a *quasi-primary field,* while a field that transforms as in (B.31) at an point z where f is just conformal is called a *primary field.* By definition, a primary field is quasi-primary, but a quasi-primary field may not be primary. The transformation rule (B.33) can be understood as a generalization of the conventional covariant tensor transformation rule (A.35). The former reduces to the latter in the case that ϕ is a spinless field with scaling weight two.

BIBLIOGRAPHY

BIBLIOGRAPHY

[1] F Y Wu. The Potts model. *Rev. Mod. Phys.*, 54:235–268, 1982.

[2] H E Stanley. Dependence of critical properties on dimensionality of spins. *Phys. Rev. Lett.*, 20:598–592, 1968.

[3] M Henkel. *Conformal Invariance and Critical Phenomena*. Springer-Verlag, Berlin Heidelberg, 1999.

[4] R Baxter. *Exactly Solved Models in Statistical Mechanics*. Academic Press Inc., 1982.

[5] H Nishimori and O Geraldo. *Elements of Phase Transitions and Critical Phenomena*. Oxford University Press, Great Clarendon Street, Oxford, OX2 6DP, 2011.

[6] G Grimmett. *Percolation*. Springer-Verlag, New York, 1989.

[7] H Duminil-Copin, C Hongler, and P Nolin. Connection probabilities and RSW-type bounds for the FK Ising model. *Comm. Pure and Applied Math.*, 64:1165–1198, 2011.

[8] H Duminil-Copin and S Smirnov. Conformal invariance of lattice models. *preprint, arXiv:1109.1549v1*, 2011.

[9] S Smirnov. Towards conformal invariance of 2D lattice models. *Proc. Int. Congr. Math.*, 2:1421–1451, 2006.

[10] A A Belavin, A M Polyakov, and A B Zamolodchikov. Infinite conformal symmetry in two-dimensional quantum field theory. *Nucl. Phys. B*, 241:333–380, 1984.

[11] P Di Francesco, R Mathieu, and D Sénéchal. *Conformal Field Theory*. Springer-Verlag, New York, 1997.

[12] M Schottenloher. *A Mathematical Introduction to Conformal Field Theory*. Springer-Verlag, Berlin Heidelberg, 2008.

[13] G Moore and N Seiberg. Classical and conformal field theory. *Comm. Math. Phys.*, 123:177–254, 1989.

[14] S Rohde and O Schramm. Basic properties of SLE. *Annals Math.*, 161:879–920, 2005.

[15] W Kager, B Nienhuis, and L P Kadanoff. A guide to stochastic Loewner evolution and its applications. *J. Stat. Phys.*, 115:1149–1229, 2004.

[16] S Smirnov. Critical percolation in the plane. *C. R. Acad. Sci. Paris Sr. I Math.*, 333:239–244, 2001. preprint, arXiv:0909.4499v1.

[17] C N Yang. The spontaneous magnetization of a two-dimensional Ising model. *Phys. Rev.*, 85:808–816, 1952.

[18] C N Yang and T D Lee. Statistical theory of equations of state and phase transitions. II. lattice gas and Ising model. *Phys. Rev.*, 87:410–419, 1952.

[19] L Onsager. Crystal statistics. I. A two-dimensional model with an order-disorder transition. *Phys. Rev.*, 65:117–149, 1944.

[20] D Kim and R I Joseph. Exact transition temperature of the Potts model with Q states per site for the triangular and honeycomb lattices. *J. Phys. C: Solid State Phys.*, 7:L167–L169, 1974.

[21] H A Kramers and G H Wannier. Statistics of the Two-Dimensional Ferromagnet. Part I. *Phys. Rev.*, 60:252–262, 1941.

[22] B Nienhuis. Critical behavior of two-dimensional spin models and charge asymmetry in the Coulomb gas. *J. Stat. Phys.*, 34:731–761, 1984.

[23] I Rushkin, E Bettelheim, I A Gruzberg, and P Wiegmann. Critical curves in conformally invariant statistical systems. *J. Phys. A Math Theor.*, 40:2165–2195, 2007.

[24] C M Fortuin and P W Kasteleyn. On the random cluster model I. introduction and relation to other models. *Physica D*, 57:536–564, 1972.

[25] R Baxter. Potts model at the critical temperature. *J. Phys. C: Solid State Phys.*, 6:L445–L448, 1973.

[26] R B Potts. *Proc. Camb. Phil. Soc.*, 48:106–109, 1952.

[27] H Saleur and B Duplantier. Exact determination of the percolation hull exponent in two dimensions. *Phys. Rev. Letters*, 58:2325–2328, 1987.

[28] R M Ziff. Hull-generating walks. *Physica D*, 38:377–383, 1998.

[29] S Sheffield. Exploration trees and conformal loop ensembles. *preprint, arXiv:math/0609167v2*, 2006.

[30] O Schramm, S Sheffield, and D B Wilson. Conformal radii for conformal loop ensembles. *Commun. Math. Phys.*, 288:43–53, 2009.

[31] J Cardy. Conformal Invariance. In C Domb and J L L Lebowitz, editors, *Phase Transitions and Critical Phenomena*, volume 11. Academic Press Inc., London, 1976.

[32] L V Ahlfors. *Complex analysis: an introduction to the theory of analytic functions of one complex variable*. McGraw-Hill, 1979.

[33] I A Gruzberg. Stochastic geometry of critical curves, Schramm-Löwner evolutions, and conformal field theory. *J. Phys. A*, 39:12601–12656, 2006.

[34] P Ginsparg. Applied conformal field theory. In *Fields, Strings and Critical Phenomena, (Les Houches, Session XLIX)*. North-Holland, 1989.

[35] V G Kac and A K Raina. *Bombay lectures on highest-weight representations of infinite dimensional Lie algebras*. World Scientific, 1987.

[36] D Friedan, Z Qiu, and S Shenker. Conformal invariance, unitarity, and critical exponents in two dimensions. *Phys. Rev. Lett.*, 52:1575–1578, 1984.

[37] V G Knizhnik, A M Polyakov, and A B Zamolodchikov. Fractal structure of 2d quantum gravity. *Mod. Phys. Lett.*, A3:819, 1988.

[38] D Friedan, Z Qiu, and S Shenker. Superconformal invariance in two dimensions and the tricritical Ising model. *Phys. Lett.*, 151B:1–15, 1984.

[39] V S Dotsenko. Critical behavior and associated conformal algebra of the Z_3 Potts model. *Nucl. Phys.*, B235:54–74, 1984.

[40] B Nienhuis, E K Riedel, and M Schick. Magnetic exponents of the two-dimensional Q-state Potts model. *J. Phys. A: Math. Gen.*, 13:L189–L192, 1980.

[41] J Cardy. Critical percolation in finite geometries. *J. Phys. A Math Gen.*, 25:L201–L206, 1992.

[42] R Langlands, P Pouliot, and Yvan Saint-Aubin. Conformal invariance in two-dimensional percolation. *Bull. Amer. Math. Soc.*, 30:1–61, 1994.

[43] R P Langlands, M A Lewis, and Y Saint-Aubin. Universality and conformal invariance for the Ising model in domains with boundary. *J. Stat. Phys.*, 98:131–244, 2000.

[44] S Smirnov. Conformal invariance in random cluster models. I. Holomorphic fermions in the Ising model. *Ann. Math.*, 172:1435–1467, 2010.

[45] J Cardy. Conformal invariance and surface critical behavior. *Nucl. Phys. B*, 240:514–532, 1984.

[46] J Cardy. Boundary conditions, fusion rules, and the Verlinde formula. *Nucl. Phys. B*, 324:581–596, 1989.

[47] J J H Simmons. *Applications of Conformal Field Theory to Problems in 2D Percolation*. PhD thesis, University of Maine, 2007.

[48] J J H Simmons and P Kleban. First column boundary operator product expansion coefficients. *preprint, arXiv:0712.3575v2*, 2008.

[49] G Lawler. *Conformally Invariant Processes in the Plane*. American Mathematical Society, 2005.

[50] V Beffara. The dimensions of the SLE curves. *Annals of Probability*, 36:1421–1452, 2008.

[51] G Lawler. A self-avoiding walk. *Duke Math. J.*, 47:655–694, 1980.

[52] G Lawler, O Schramm, and W Werner. Conformal invariance of planar loop-erased random walks and uniform spanning trees. *Ann. Prob.*, 32:939–995, 2004.

[53] G Madra and G Slade. *The Self-Avoiding Walk*. Birkhäuser, Boston, 1996.

[54] G Lawler, O Schramm, and W Werner. On the scaling limit of planar self-avoiding walk. In M L Lapidus and M V Frankenhuysen, editors, *Fractal geometry and applications: a jubilee of Benoît Mandelbrot, Part 2*, 2002.

[55] O Schramm and S Sheffield. The harmonic explorer and its convergence to SLE_4. *Ann. Prob.*, 33:2127–2148, 2005.

[56] A Weinrib and S A Trugman. A new kinetic walk and percolation perimeters. *Phys. Rev. B*, 31:2993–2997, 1985.

[57] M Bauer and D Bernard. Conformal field theories of stochastic Löwner evolutions. *Commun. Math. Phys.*, 239:493–521, 2003.

[58] M Bauer and D Bernard. 2D growth processes: SLE and Loewner chains. *Phys. Rept.*, 432:115–221, 2006.

[59] M Bauer, D Bernard, and K Kytölä. Multiple Schramm-Löwner evolutions and statistical mechanics martingales. *J. Stat. Phys.*, 120:1125, 2005.

[60] J Dubédat. Commutation relations for SLE. *Comm. Pure Applied Mathematics*, 60:1792–1847, 2007.

[61] V S Dotsenko and V A Fateev. Four-point correlation functions and the operator algebra in 2D conformal invariant theories with central charge $c \leq 1$. *Nucl. Phys. B*, 251:691–673, 1985.

[62] V S Dotsenko and V A Fateev. Conformal algebra and multipoint correlation functions in 2D statistical models. *Nucl. Phys. B*, 240:312–348, 1984.

[63] S Sheffield. Gaussian free fields for mathematicians. *preprint, arXiv:math/0312099v3*, 2006.

[64] L Bers and M Schechter. Elliptic Equations. In *Partial Differential Equations*, 1957.

[65] G Folland. *Fourier Analysis and its Applications*. Brooks/Cole Publishing Comapny, 1992.

[66] D Gilbarg and N S Trudinger. *Elliptic Partial Differential Equations of Second Order*. Springer-Verlag, New York, 1983.

[67] L Benoit and Y Saint-Aubin. Degenerate conformal field theories and explicit expressions for some null vectors. *Phys. Lett. B*, 215:517–522, 1988.

[68] P Di Francesco, O Golinelli, and E Guitter. Meanders and the Temperley-Lieb algebra. *Commun. Math. Phys*, 186:1–59, 1997.

[69] P Di Francesco. Truncated Meanders. In N Jing and K Misra, editors, *Recent Developments in Quantum Affine Algebras and Related Topics*. American Mathematical Society, 1999.

[70] V Gurarie. Logarithmic operators in conformal field theory . *Nucl. Phys. B*, 410:535–549, 1993.

[71] M Bauer and P Di Francesco. Covariant differential equations and singular vectors in Virasoro representations. *Nucl. Phys. B*, 362:515–562, 1991.

[72] Pierre Mathieu and David Ridout. From percolation to logarithmic conformal field theory. *Phys. Lett. B*, 657:120–129, 2007.

[73] R P Langlands, C Pichet, Ph Pouliot, and Y Saint-Aubin. On the universality of crossing probabilities in two-dimensional percolation. *J. Stat. Phys.*, 67:553–574, 1992.

[74] J J H Simmons. Conformal crossing probabilites in hexagons. In preparation.

[75] J J H Simmons, P Kleban, S M Flores, and R M Ziff. Cluster densities at 2-D critical points in rectangular geometries. *J. Phys. A Math Theor.*, 44:385002, 2011.

[76] J J H Simmons and P Kleban. Complete conformal field theory solution of a chiral six-point correlation function. *J. Phys. A Theor.*, 44:315403, 2011.

[77] R S Swendsen and J S Wang. Nonuniversal critical dynamics in monte carlo simulations. *Phys. Rev. Letters*, 58:86–88, 1987.

[78] R Pike and H E Stanley. Order propagation near the percolation threshold. *J. Phys. A. Math Gen.*, 14:L169–L177, 1981.

[79] H E Stanley. Cluster shapes at the percolation threshold: an effective cluster dimensionality and its connection with critical-point exponents. *J. Phys. A Math Gen.*, 10:L211–L220, 1977.

[80] A Coniglio. Fractal structure of Ising and Potts clusters: exact results. *Phys. Rev. Letters*, 62:3054–3057, 1989.

[81] Y Saint-Aubin, P A Pearce, and J Rasmussen. Geometric exponents, SLE and logarithmic minimal models. *J. Stat. Mech. Theory and Experiment*, 10:P02028, 2009.

[82] B F Edwards, M F Gyure, and M Ferer. Exact enumeration and scaling for fragmentation of percolation clusters. *Phys. Rev. A.*, 46:6252–6264, 1992.

[83] B Duplantier. Two-dimensional fractal geometry, critical phenomena and conformal invariance. *Physics Reports (Review Section of Physics Letters)*, pages 229–257, 1989.

[84] S M Flores, P Kleban, and R M Ziff. Cluster pinch-point densities in polygons. *preprint, arXiv:1201.6405v1*, 2012.

[85] H Exton. *Multiple Hypergeometric Functions and Applications.* Wiley, New York, 1976.

[86] T A Driscoll and L N Trefethen. *Schwarz-Christoffel Mapping.* Cambridge University Press, 2002.